Final Annual Report

"Functional Studies on Glutathione S-Transferases (GSTs) from *Anopheles dirus* a Thai Malaria Vector" TRF BRG/47/80021

Associate Professor Albert J. Ketterman Ph.D. et al.

August 2007

TRF BRG/47/80021

Final Annual Report

"Functional Studies on Glutathione S-Transferases (GSTs) from *Anopheles dirus* a Thai Malaria Vector"

1. Assoc. Prof. Albert J. Ketterman	Institute of Molecular Biology and Genetics (IMBG), Mahidol University, Salaya Campus
2. Dr. Rungrutai Udomsinprasert	IMBG, Mahidol University
3. Dr. Ardcharaporn Vararattanavech	IMBG, Mahidol University
4. Dr. Jantana Wongsantichon	IMBG, Mahidol University
5. Pakorn Winayanuwattikun	IMBG, Mahidol University
6. Gulsiri Charoensilp	IMBG, Mahidol University
7. Chonticha Saisawang	IMBG, Mahidol University
8. Juthamart Piromjitpong	IMBG, Mahidol University
9. Mashamon Mitprasat	IMBG, Mahidol University
10.Piya Temviriyanukul	IMBG, Mahidol University
11.Tassanee Lerksuthirat	IMBG, Mahidol University

Funded by the Thailand Research Fund (TRF)

Acknowledgements

The progress achieved for the last three years on this project was possible because of the efforts and contributions from the following people:

Institute of Molecular Biology and Genetics, Mahidol University

Research Assistants:
Juthamart Piromjitpong
Suthasinee Somyong

Post-doctoral Researchers:
Dr. Rungrutai Udomsinprasert
Dr. Ardcharaporn Vararattanavech
Dr. Jantana Wongsantichon

Ph.D. Students:
Rungrutai Udomsinprasert (now completed; funded by the Royal Golden Jubilee).
Pakorn Winayanuwattikun (now completed; funded by the Royal Golden Jubilee).
Ardcharaporn Vararattanavech (now completed; funded by the Royal Golden Jubilee).
Jantana Wongsantichon (now completed; funded by the Royal Golden Jubilee).
Gulsiri Charoensilp (now completed; funded by the Royal Golden Jubilee).
Chonticha Saisawang (funded by the Royal Golden Jubilee).

M.Sc. Students:
Juthamart Piromjitpong (now completed)
Mashamon Mitprasat (now completed)
Piya Temviriyanukul (now completed)
Tassanee Lerksuthirat

Dept of Biochem/Center Excell Protein Structure and Function, Mahidol University
Dr. J.Yuvaniyama

Maejo University
Dr. S. Pongjareankit

Chiang Mai University
Dr. L. Prapanthadara
Dr. J. Wongtrakul.

University of Western Australia, Australia
Dr. M.A. Bogoyevitch

Australian National University
Dr. A.J. Oakley

Abstracts

The aim of this project is to characterize functional relationships for the amino acids that can affect substrate specificity as well as protein-protein interactions in glutathione S-transferases. We have published fourteen papers in the last three years for a total Impact Factor of 43.633 (2005 Impact Factors). Reprints of these fourteen papers are included in the appendix. For the sake of simplicity we only present the three Biochemical Journal (2005 Impact Factor 4.224) papers published in 2007. Therefore this Final Annual Report consists of three papers that have been published and the format is of separate studies, one from each paper. These studies involve characterization of structural amino acid residues that also appear to modulate enzymatic properties such as substrate and inhibitor specificity. Each study utilizes one of the enzymes and its crystal structure obtained from the research previously funded by the TRF. This report therefore describes on-going structure function studies.

บทคัดย่อ

งานวิจัยนี้มุ่งศึกษาความสำคัญของกรดอะมิโนที่มีต่อหน้าที่ของเอนไซม์กลูตาไธโอน เอส-ทรานสเฟอเรส โดยศึกษาผลกระทบต่อความจำเพาะเจาะจงกับสารตั้งต้น รวมทั้งการมีปฏิสัมพันธ์กับโปรตีนอื่นๆ ในช่วงสามปีที่ผ่านมา ได้มีผลงานตีพิมพ์ทั้งสิ้น 14 บทความด้วยค่า Impact Factor รวม 43.633 (ค่า Impact Factor ปี 2548) เพื่อความเรียบง่ายของรายงานประจำปีฉบับนี้ จึงได้นำเสนอในรูปแบบของบทความ 3 เรื่อง จาก 3 การศึกษาวิจัยที่แตกต่างกันซึ่งได้ตีพิมพ์ในปี 2550 การศึกษานี้ได้จำแนกกรดอะมิโนที่มีผลต่อโครงสร้างของเอนไซม์ และพบว่ากรดอะมิโนเหล่านี้มีส่วนในการควบคุมคุณสมบัติทางจลนศาสตร์ อันได้แก่ความจำเพาะเจาะจงกับสารตั้งต้นและกับตัวยับยั้งปฏิกิริยาด้วย แต่ละการศึกษาใช้เอนไซม์และโครงร่างผลึกของเอนไซม์ที่ได้จากการวิจัยก่อนหน้านี้ ซึ่งได้รับการสนับสนุนจาก สกว. รายงานฉบับนี้จึงเป็นความก้าวหน้าของการศึกษาดังกล่าว

Executive Summary

We have published fourteen papers in the last three years for a total 2005 impact factor of 43.633. For the sake of simplicity we only present the three Biochemical Journal (2005 Impact Factor 4.224) papers published this year (2007) in this Final Annual Report. Therefore this Final Annual Report consists of three papers that have been published and the format is of separate studies, one from each paper.

The present study characterized conserved residues in a GST (glutathione S-transferase) in the active-site region that interacts with glutathione. This region of the active site is near the glycine moiety of glutathione and consists of a hydrogen bond network. In the GSTD (Delta class GST) studied, adGSTD4-4, the network consisted of His38, Met39, Asn47, Gln49, His50 and Cys51. In addition to contributing to glutathione binding, this region also had major effects on enzyme catalysis, as shown by changes in kinetic parameters and substrate specific activity. The results also suggest that the electron distribution of this network plays a role in stabilization of the ionized thiol of glutathione as well as impacting on the catalytic rate-limiting step. This area constitutes a second glutathione active site network involved in glutathione ionization distinct from a network previously observed interacting with the glutamyl end of glutathione. This second network also appears to be functionally conserved inGSTs. In the present study, His50 is the key basic residue stabilized by this network as shown by up to a 300-fold decrease in *k*cat and 5200-fold decrease in *k*cat/*K*m for glutathione. Although these network residues have a minor role in structural integrity, the replaced residues induced changes in active site topography as well as generating positive co-operativity towards glutathione. Moreover, this network at the glycinemoiety ofGSH (glutathione) also contributed to the 'base-assisted deprotonationmodel' forGSHionization. Taken together, the results indicate a critical role for the functionally conserved basic residue His50 and this hydrogen bond network in the active site.

In *Anopheles dirus* glutathione transferaseD3-3, position 64 is occupied by a functionally conserved glutamate residue, which interacts directly with the γ -glutamate moiety of GSH (glutathione) as part of an electron-sharing network present in all soluble GSTs (glutathione transferases). Primary sequence alignment of all GST classes suggests that Glu64 is one of a few residues that is functionally conserved in the GST superfamily. Available crystal structures as well as consideration of the property of the equivalent residue at position 64, acidic or polar, suggest that the GST electron-sharing motif can be divided into two types. Electrostatic interaction between the GSH glutamyl and carboxylic Glu64, as well as with Arg66 and Asp100, was observed to extend the electron-sharing motif identified previously. Glu64 contributes to the catalytic function of this motif and the 'base-assisted deprotonation' that are essential for GSH ionization during catalysis. Moreover, this residue also appears to affect multiple steps in the enzyme catalytic strategy, including binding of GSH, nucleophilic attack by thiolate at the electrophilic centre and product formation, probably through active-site packing effects. Replacement with non-functionally-conserved amino acids alters initial packing or folding by favouring aggregation during heterologous expression. Thermodynamic and reactivation *in vitro* analysis indicated that Glu64 also contributes to the initial folding pathway and overall structural stability. Therefore Glu64 also appears to impact upon catalysis through roles in both initial folding and structural maintenance.

GSTs (glutathione transferases) are multifunctional widespread enzymes. Currently there are 13 identified classes within this family. Previously most structural characterization has been

reported for mammalian Alpha, Mu and Pi class GSTs. In the present study we characterize two enzymes from the insect-specific Delta class, adGSTD3-3 and adGSTD4-4. These two proteins are alternatively spliced products from the same gene and have very similar tertiary structures. Several major contributions to the dimer interface area can be separated into three regions: conserved electrostatic interactions in region 1, hydrophobic interactions in region 2 and an ionic network in region 3. The four amino acid side chains studied in region 1 interact with each other as a planar rectangle. These interactions are highly conserved among theGST classes, Delta, Sigma and Theta. The hydrophobic residues in region 2 are not only subunit interface residues but also active site residues. Overall these three regions provide important contributions to stabilization and folding of the protein. In addition, decreases in yield aswell as catalytic activity changes, suggest that the mutations in these regions can disrupt the active site conformation which decreases binding affinity, alters kinetic constants and alters substrate specificity. Several of these residues have only a slight effect on the initial folding of each subunit but have more influence on the dimerization process as well as impacting upon appropriate active site conformation. The results also suggest that even splicing products from the same gene may have specific features in the subunit interface area that would preclude heterodimerization.

Keywords: *Anopheles dirus*, glutathione transferase (GST), subunit interface, conserved active-site residue, enzyme catalysis, electron sharing network, structural integrity.

Objectives:

The aim of this project is to characterize functional relationships for the amino acids that can affect substrate specificity as well as protein-protein interactions in glutathione S-transferases from the Thai malaria vector *Anopheles dirus*. We will obtain new GSTs from different classes as well as enzyme sequence variants generated by site-directed mutagenesis for kinetic characterization studies. The available crystal structures in my laboratory and these new protein forms will yield data that will increase our understanding of the mechanism of GSTs in their role in resistance to insecticides. We will also continue studying the protein-protein interactions of the GSTs and the Jun N-terminal kinase (JNK) pathway proteins. This will provide information on other physiological functions of GSTs and will increase our understanding of the interaction and regulation of proteins *in vivo*. This GST-JNK interaction is important as the JNK pathway has been shown to be involved in cell growth, cell differentiation, the cell stress response and apoptosis or cell death.

To achieve this goal the project entails continuing several aspects of the research previously funded by the Thailand Research Fund. These aspects include the following:

1. To continue to obtain new recombinant GST enzymes for kinetic characterization studies including enzyme sequence variants generated by site-directed mutagenesis.
2. To continue to obtain more GST crystal structures and to use the now available *An. dirus* GST crystal structures to provide a basis for understanding the mechanism of GSTs in their role in resistance to insecticides.
3. To continue studying the protein-protein interactions of the GSTs and the JNK kinase pathway proteins.

We have published fourteen papers in the last three years for a total 2005 impact factor of 43.633. For the sake of simplicity we only present the three Biochemical Journal (2005 Impact Factor 4.224) papers published this year (2007) in this Final Annual Report. Therefore this Final Annual Report consists of three papers that have been published and the format is of separate studies, one from each paper.

A functionally conserved basic residue in glutathione S-transferases interacts with the glycine moiety of glutathione and is pivotal for enzyme catalysis

Ardcharaporn VARARATTANAVECH and Albert J. KETTERMAN[1]

Institute of Molecular Biology and Genetics, Mahidol University, Salaya Campus, 25/25 Putthamonthol Road 4, Salaya, Nakon Pathom 73170, Thailand

The present study characterized conserved residues in a GST (glutathione S-transferase) in the active-site region that interacts with glutathione. This region of the active site is near the glycine moiety of glutathione and consists of a hydrogen bond network. In the GSTD (Delta class GST) studied, adGSTD4-4, the network consisted of His^{38}, Met^{39}, Asn^{47}, Gln^{49}, His^{50} and Cys^{51}. In addition to contributing to glutathione binding, this region also had major effects on enzyme catalysis, as shown by changes in kinetic parameters and substrate specific activity. The results also suggest that the electron distribution of this network plays a role in stabilization of the ionized thiol of glutathione as well as impacting on the catalytic rate-limiting step. This area constitutes a second glutathione active site network involved in glutathione ionization distinct from a network previously observed interacting with the glutamyl end of glutathione. This second network also appears to be functionally conserved in GSTs. In the present study, His^{50} is the key basic residue stabilized by this network as shown by up to a 300-fold decrease in k_{cat} and 5200-fold decrease in k_{cat}/K_m for glutathione. Although these network residues have a minor role in structural integrity, the replaced residues induced changes in active site topography as well as generating positive co-operativity towards glutathione. Moreover, this network at the glycine moiety of GSH (glutathione) also contributed to the 'base-assisted deprotonation model' for GSH ionization. Taken together, the results indicate a critical role for the functionally conserved basic residue His^{50} and this hydrogen bond network in the active site.

Key words: base-assisted deprotonation model, conserved active-site residue, Delta class GST, enzyme catalysis, glutathione S-transferase (GST), glycine moiety of glutathione (GSH).

INTRODUCTION

GSTs (glutathione S-transferases; EC 2.5.1.18) are intracellular proteins, which are widely distributed in nature, being found in most aerobic eukaryotes and prokaryotes [1,2]. GSTs are polymorphic with most organisms possessing a genetic capacity to encode multiple isoforms of various classes [3,4]. The enzymes are an integral part of the phase II detoxification mechanism being involved in xenobiotic metabolism as well as protection against peroxide damage. GSTs catalyse reactions with a very broad range of structurally diverse electrophilic substrates (e.g. alkylhalides, arylhalides, lactones, epoxides, quinones, esters and activated alkenes) [4–6]. This enzyme family therefore displays a wide range of catalytic functions while retaining a high specificity towards the thiol substrate glutathione (GSH). The GSH conjugation by GST increases the solubility of the target molecule, thus facilitating the excretion of the molecule from the organism.

All cytosolic GSTs have very similar three-dimensional structures and the active site pocket is very similar in the G-site (GSH-binding site) [7–9]. The N-terminal domain of GST adopts a $\beta\alpha\beta\alpha\beta\beta\alpha$ topology that contributes most of the contacts to GSH and is called the G-site. The crystal structures of GSTs show that most of the active site residues involved in the binding and activation of GSH are found within the N-terminus; hence this region of the protein is therefore highly conserved between GSTs [7,8,10]. The C-terminal domain is all α-helical providing some of the contacts to the hydrophobic binding site that lies adjacent to the G-site.

Substrate conjugation of electrophilic xenobiotics involves its nucleophilic attack at the ionized thiol of GSH in the active site. A conserved tyrosine (for Alpha, Mu and Pi classes) or serine (for Theta and Delta classes) residue within hydrogen-bonding distance of the thiol of GSH has been shown to be of primary importance in facilitating GSH deprotonation as well as stabilization of the ionized GSH by hydrogen-bonding [10–14]. In addition, conserved residues that interact directly with the glutamyl moiety of GSH, for example Ser^{65}, Arg^{66} and Ile^{52} in GSTD (Delta class GST) have also been implicated in critical roles in the catalytic mechanism, involvement in GSH binding, GSH thiol ionization, as well as structural integrity [15–17]. Therefore the residues interacting with the other end of GSH, the glycine moiety (His^{38}, Met^{39}, Asn^{47}, Gln^{49}, His^{50} and Cys^{51}) were of interest (Figure 1) [18]. His^{38} and His^{50} interact directly with the glycine carboxylic group of GSH [19]. Both histidines appear to be assisted or stabilized by dipole–dipole interaction with Met^{39}. Moreover, a hydrogen bond network in the G-site near the glycine moiety of GSH, involving several residues (His^{50}, Asn^{47}, Gln^{49} and Cys^{51}) and GSH, is proposed to be essential to electron distribution for enzyme catalysis. To investigate the roles of these residues, mutagenesis studies were performed and the engineered enzymes characterized by kinetic constants, substrate specific activity, pK_a determination and rate-limiting step determination in addition to physical properties.

Abbreviations used: CDNB, 1-chloro-2,4-dinitrobenzene; DCNB, 1,2-dichloro-4-nitrobenzene; EA, ethacrynic acid; FDNB, 1-fluoro-2,4-dinitrobenzene; G-site, GSH (glutathione)-binding site; GST, glutathione S-transferase; GSTD, Delta class GST; hGSTP1-1, human GSTP1-1; PNBC, *p*-nitrobenzyl chloride; PNPBr, *p*-nitrophenethyl bromide; ZmGST1, *Zea mays* (maize) GST1.

[1] To whom correspondence should be addressed (email albertketterman@yahoo.com).

COLOUR

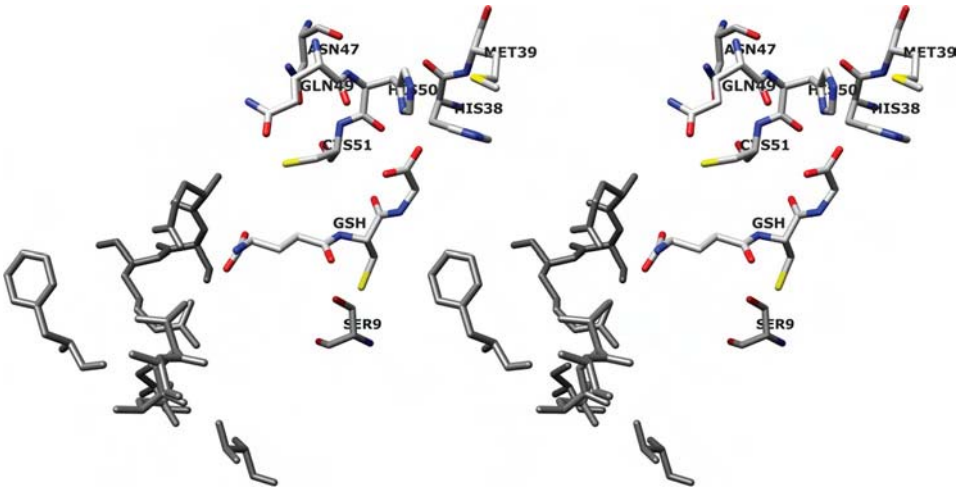

Figure 1 Stereoview of conserved G-site residues that directly interact with the glycine moiety of GSH and generate a hydrogen bond network

His[38] and His[50] interact directly with the glycine carboxylic group of GSH and are assisted or stabilized by dipole–dipole interaction with Met[39]. A hydrogen bond network in the G-site is formed by several residues (His[50], Asn[47], Gln[49] and Cys[51]) and GSH. The previously identified electron-sharing network at the glutamyl end of GSH is shown in grey [16]. The image was produced using the UCSF Chimera package from the Resource for Biocomputing, Visualization, and Informatics at the University of California, San Francisco, CA, U.S.A. (http://www.cgl.ucsf.edu/chimera) (supported by National Institutes of Health grant P41 RR-01081) [18].

MATERIALS AND METHODS

Site directed mutagenesis

The engineered enzymes were generated using Stratagene's QuikChange® site-directed mutagenesis protocol. The primers used were designed based on the sequence of the *adGSTD4* wild-type gene (GenBank® accession number AF273040). Full-length DNA sequencing in both directions was performed to confirm the engineered clones.

Protein expression and purification

After transformation of the engineered plasmids into *Escherichia coli* BL21(DE3)pLysS, protein expression was performed. The recombinant adGSTD4-4 engineered enzymes and wild-type were purified either by glutathione affinity chromatography according to the manufacturer's instructions (Amersham Biosciences) or by cation exchanger (SP-XL) followed by hydrophobic interaction chromatography (phenyl-Sepharose) as described previously [19]. The purified enzymes (in 50 mM potassium phosphate, pH 6.5) were stored in 50 % (v/v) glycerol at −20 °C until used. The concentrations of the proteins were determined by Bio-Rad protein reagent (Bio-Rad) by using BSA as the standard protein and the purity of the proteins was observed by SDS/PAGE.

Kinetic parameters determination

Kinetic experiments were performed as previously described [20]. Kinetic constants were determined by varying the CDNB (1-chloro-2,4-dinitrobenzene) concentration (0.031–3.0 mM) while GSH was held constant at a saturating concentration and by varying GSH concentrations (0.25–20 mM) at a saturating concentration of CDNB. The standard GST assay was performed using 3 mM CDNB and 10 mM GSH for adGSTD4-4 wild-type. The rate of conjugation between GSH and CDNB was monitored by continuously measuring change in absorbance at 340 nm for 1 min using a SpectraMax 250 at 25–27 °C. A molar absorption coefficient (ε) of 9.6 $mM^{-1} \cdot cm^{-1}$ was used to convert the absorbance to moles [21]. Steady-state kinetics followed Michaelis–Menten kinetics except where stated. With evidence of co-operativity upon GSH binding, demonstrated by a sigmoidal curve instead of a hyperbolic curve on a Michaelis–Menten plot, a Hill equation (eqn 1) was used to fit the experimental kinetic data on the plot. $K_{0.5}$ is the substrate concentration that gives the rate of reaction at half of V_{max}, similar to the K_m value for non-co-operative binding ($h = 1$).

$$Y = V/V_{max} = [S]^h/(K_{0.5} + [S]^h) \quad (1)$$

$$\log[Y/(1-Y)] = h \log[S] - \log K_{0.5} \quad (2)$$

A sigmoidal Hill equation was practically transformed into a linear rate equation (eqn 2), where Y is the fractional saturation; h is the Hill coefficient; and $K_{0.5}$ is an averaged binding constant at $Y = 0.5$. A Hill plot, a plot between $\log[Y/(1–Y)]$ and $\log[S]$, was employed to determine the degree of co-operativity by the slope of the plot that yields the Hill coefficient (h) [22]. Catalytic constant (k_{cat}) and the catalytic efficiency (k_{cat}/K_m) were calculated on an active site basis using the subunit molecular mass of each enzyme. Maximal velocity (V_{max}) and Michaelis constant (K_m) were determined by nonlinear regression software analysis (GraphPad Prism version 5.00 for Windows; GraphPad Software, San Diego, CA, U.S.A.; http://www.graphpad.com). One-way ANOVA with Dunnett's multiple comparison post test was performed with wild-type as control using GraphPad Prism 5.

Specific activity determination

The specific activities towards several GST substrates were determined as previously described [23]. All measurements were performed at 25–27 °C in 0.1 M potassium phosphate buffer (pH 6.5 or 7.5). The GST activities were measured with glutathione and five hydrophobic substrates: CDNB, DCNB (1,2-dichloro-4-nitrobenzene), EA (ethacrynic acid), PNPBr (*p*-nitrophenethyl bromide) and PNBC (*p*-nitrobenzyl chloride). Specific activities were calculated according to the molar absorption coefficient for each substrate [21].

pH dependence of kinetic parameters

The pH dependence of k_{cat}/K_m^{CDNB} was obtained by performing kinetic measurements in the following buffers: 0.1 M sodium

Table 1 Steady-state kinetic constants using GSH and CDNB as GST substrates

The units of V_{max}, k_{cat}, K_m and k_{cat}/K_m are μmol · min^{-1} · mg of protein^{-1}, s^{-1}, mM and s^{-1} · mM^{-1} respectively. *These engineered GSTs showed positive co-operativity upon GSH binding with Hill coefficient (h) shown. The value shown is $K_{0.5}$, obtained from the Hill equation, which is the substrate concentration that gives the rate of reaction at half of V_{max} [22]. [a]Some of these values have been previously reported and are shown for purposes of comparison [19,20]. One-way ANOVA with Dunnett's multiple comparison test was performed with wild-type as control; statistical significance is shown by † for $P < 0.05$, ‡ for $P < 0.01$ and § for $P < 0.001$.

			CDNB		GSH		
Enzyme	V_{max}	k_{cat}	K_m	k_{cat}/K_m	K_m	k_{cat}/K_m	h
Wild-type[a]	62.45 ± 1.24	26.13	0.50 ± 0.02	51.84	0.50 ± 0.10	52.06	0.91 ± 0.02
H38A[a]	36.4 ± 1.12§	15.26	1.25 ± 0.12§	12.21	15.8 ± 1.19§	0.97	–
H38E[a]	14.91 ± 0.44§	6.23	0.92 ± 0.11§	6.76	8.32 ± 0.22*§	0.74	1.83 ± 0.01§
H38F[a]	9.71 ± 0.43§	4.06	0.98 ± 0.09§	4.14	35.26 ± 0.86§	0.12	–
H38D	4.61 ± 0.12§	1.93	0.71 ± 0.01†	2.71	15.90 ± 0.21§	0.12	–
H38K	5.54 ± 0.12§	2.32	0.71 ± 0.08†	3.27	23.50 ± 1.21§	0.10	–
M39A	25.56 ± 0.96§	10.70	0.79 ± 0.06§	13.50	6.32 ± 0.34*§	1.69	1.72 ± 0.12§
M39F	38.56 ± 1.72§	16.14	0.50 ± 0.02	32.22	2.18 ± 0.09†	5.75	–
N47A	0.225 ± 0.003§	0.09	0.67 ± 0.06	0.13	11.50 ± 0.51§	0.01	–
Q49A	43.28 ± 0.96§	18.11	0.74 ± 0.06‡	24.47	5.58 ± 0.46*§	3.24	1.64 ± 0.04§
Q49E	49.75 ± 1.36§	20.82	0.49 ± 0.05	42.49	2.87 ± 0.09*§	7.26	1.51 ± 0.03§
H50A[a]	6.46 ± 0.26§	2.70	1.10 ± 0.15§	2.45	7.34 ± 0.21§	0.37	–
H50E[a]	0.21 ± 0.01§	0.09	0.81 ± 0.04§	0.11	12.34 ± 0.36§	0.01	–
H50Y[a]	0.87 ± 0.02§	0.36	0.83 ± 0.06§	0.43	12.57 ± 0.73§	0.03	–
H50K	8.14 ± 0.03§	3.40	0.69 ± 0.06†	4.95	6.77 ± 0.27*§	0.45	1.54 ± 0.06§
H50F	1.44 ± 0.03§	0.60	0.76 ± 0.01‡	0.79	6.43 ± 0.38§	0.09	–
C51A	19.64 ± 0.65§	8.22	0.82 ± 0.04§	10.01	6.40 ± 0.12*§	1.28	1.57 ± 0.08§
C51D	2.16 ± 0.07§	0.91	1.30 ± 0.08§	0.7	16.94 ± 0.69*§	0.05	1.40 ± 0.03§

acetate buffers (from pH 5.0 to 5.5) and 0.1 M potassium phosphate buffer (from pH 6.0 to 8.5). Increments of pH were 0.5 and control experiments showed no discontinuities from buffer types. The pK_a values of bound GSH were obtained by fitting the data to the equation $y = y^{lim}/(1 + 10^{pKa-pH})$ as previously described [13]. The program GraphPad Prism 5 was used for nonlinear fit of the data to the sigmoidal dose–response (variable slope) equation.

Fluoride/chloride leaving group substitution

A diagnostic test in evaluating the rate-limiting step in nucleophilic aromatic substitution reactions is the effect of different leaving groups on kinetic parameters [13]. The second order kinetic constants at pH 6.5 for the spontaneous reaction of GSH with CDNB and FDNB (1-fluoro-2,4-dinitrobenzene) were determined by kinetic measurement by using CDNB or FDNB as co-substrate as previously described [24]. The ratios of the catalytic constants ($k_{cat}^{FDNB}/k_{cat}^{CDNB}$) were determined.

Effect of viscosity on the kinetic parameters

The dependence of the steady-state kinetic parameters on relative viscosity was observed by performing kinetics measurements in the presence of varying glycerol concentrations. The range of relative viscosities (η/η^0) was between 1.53 and 4.43. The slope of the plots for relative catalytic constant (k_{cat}^0/k_{cat}) versus relative viscosity (η/η^0) was determined. Viscosity values (η) at 25 °C were calculated as described previously [25].

Thermal stability assay

The enzymes at 0.1 mg/ml in 0.1 M phosphate buffer (pH 6.5) containing 1 mM EDTA and 5 mM dithiothreitol were incubated at 45 °C for various times and then activity was measured in the standard GST assay. The data were plotted as log percentage of remaining activity versus pre-incubation time. The half-life ($t_{½}$) of the enzyme at 45 °C was calculated from the slope of the plot using the equations: Slope = k/2.3, $k = 0.693/t_{½}$.

Intrinsic fluorescence measurement

There are two tryptophan residues in each monomer of adGSTD4-4: Trp^{64} and Trp^{191}. The intrinsic fluorescence from Trp^{64}, which is exposed to solvent at the base of the G-site, can be used to monitor the active site conformation indirectly. The intrinsic fluorescence of adGSTD4-4 was measured in a single-photon counting spectrofluorimeter. Excitation was at 295 nm and emission was scanned from 300 to 450 nm. In these experiments, a number of samples containing 0.1 mg/ml GST in 0.1 M potassium phosphate buffer (pH 6.5) were prepared similarly for the wild-type and engineered enzymes. The wavelength that gives the maximum fluorescence intensity (λ_{max}) and fluorescence intensity at λ_{max} were observed. The experimental data was corrected both for dilution and for inner filter effects.

RESULTS

Enzymatic characterization

Michaelis–Menten analysis was performed using nonlinear regression to determine steady-state kinetic constants (Table 1). The kinetic constants showed the residue changes of His^{38}, His^{50}, Met^{39}, Asn^{47}, Cys^{51} and Gln^{49} impacted upon catalysis. The engineered G-site residue enzymes showed only small changes in K_m^{CDNB}, whereas remarkably lower affinities towards GSH were shown (greater K_m^{GSH}) compared with wild-type. Positive co-operativity for GSH binding was observed for several engineered enzymes that displayed deviation of steady-state kinetics from a Michaelis–Menten hyperbolic to a sigmoidal curve response. The extent of positive co-operativity is shown by Hill coefficients (h) ranging from 1 (no co-operativity) to 2 (full co-operativity) for a dimeric enzyme with two active sites. Positive co-operativity was observed for H38E, M39A, H50K, C51A, C51D, Q49A and GA49E as determined by Hill coefficients ranging from 1.40 to 1.83, suggesting that the changed residues altered the movement of α2-helix and its flanking region to influence the induced-fit mechanism.

Table 2 Substrate-specific activity of the engineered enzymes compared to the wild-type

The substrates used were 3 mM CDNB, 1 mM DCNB, 0.1 mM PNPBr, 0.1 mM PNBC and 0.2 mM EA. The reactions were performed at a constant GSH concentration (appropriate for each enzyme). [a]Some of these values have been previously reported and are shown for purposes of comparison [19,20]. One-way ANOVA with Dunnett's multiple comparison test was performed with wild-type as control; statistical significance is shown by † for $P < 0.05$, ‡ for $P < 0.01$ and § for $P < 0.001$.

	Specific activity (μmol · min^{-1} · mg^{-1})				
Enzyme	CDNB	DCNB	EA	PNPBr	PNBC
Wild-type[a]	52.50 ± 0.52	0.035 ± 0.006	0.286 ± 0.062	0.074 ± 0.012	0.064 ± 0.002
H38A[a]	21.70 ± 0.20§	0.037 ± 0.001	0.146 ± 0.016§	0.040 ± 0.004§	0.013 ± 0.002§
H38E[a]	11.21 ± 0.24§	< 0.001	0.191 ± 0.026§	< 0.008	< 0.005
H38F[a]	3.76 ± 0.09§	< 0.001	0.230 ± 0.019†	< 0.005	< 0.003
H38D	2.33 ± 0.07§	< 0.001	0.111 ± 0.011§	< 0.001	< 0.003
H38K	2.02 ± 0.07§	< 0.001	0.165 ± 0.007§	< 0.003	< 0.002
M39A	18.84 ± 0.66§	0.012 ± 0.001§	0.183 ± 0.011§	< 0.005	< 0.003
M39F	28.67 ± 0.71§	0.043 ± 0.002†	0.166 ± 0.010§	0.029 ± 0.008§	0.065 ± 0.009
N47A	0.13 ± 0.01§	< 0.001	0.079 ± 0.001§	< 0.001	< 0.001
Q49A	33.36 ± 0.92§	0.023 ± 0.002‡	0.244 ± 0.012	0.050 ± 0.002§	0.044 ± 0.001‡
Q49E	41.76 ± 0.60§	0.032 ± 0.001	0.244 ± 0.020	0.020 ± 0.001§	0.048 ± 0.003‡
H50A[a]	3.80 ± 0.10§	0.015 ± 0.007§	0.146 ± 0.050§	0.012 ± 0.002§	0.016 ± 0.007§
H50E[a]	0.15 ± 0.01§	< 0.001	0.026 ± 0.004§	< 0.005	< 0.005
H50Y[a]	0.47 ± 0.01§	< 0.001	0.064 ± 0.008§	< 0.008	< 0.005
H50K	6.28 ± 0.04§	0.007 ± 0.001§	0.053 ± 0.020§	< 0.007	< 0.004
H50F	0.93 ± 0.03§	< 0.001	0.077 ± 0.005§	< 0.001	< 0.001
C51A	15.44 ± 0.58§	0.009 ± 0.001§	0.046 ± 0.001§	0.019 ± 0.001§	< 0.001
C51D	1.24 ± 0.03§	< 0.001	0.080 ± 0.004§	< 0.002	< 0.001

Although Met[39] interacts directly with GSH interacting residues, His[38] and His[50], the contribution to catalytic function is through the effect on GSH binding. The results suggest that the effect is mostly through a packing rearrangement that includes any perturbation of the orientation of His[38] or His[50]. Rearrangement of active site residues is elicited by M39A to accommodate the decreased volume as well as the lack of dipole–dipole interaction with the histidines. This condition also appears to engender flexibility to this region, which is shown by positive co-operativity for GSH binding with a Hill coefficient of 1.72 ± 0.12 (Table 1).

The GSH interaction was decreased for all His[38] engineered enzymes as shown by an increase in K_m^{GSH} of 17–71-fold. In addition, positive co-operativity for GSH was observed for H38E with a Hill coefficient (h) of 1.83 ± 0.01.

There is a hydrogen bond network in the GST active site that is adjacent to the GSH glycine moiety. This network is formed by several residues, Asn[47], Gln[49] and Cys[51], as well as His[50], with the latter directly interacting with GSH. His[50] replacements not only decreased binding affinity to GSH (ranging from 13- to 25-fold) but also impacted upon catalytic rates as shown by k_{cat} values that decreased from 13 to 0.3 % of the wild-type enzyme k_{cat} values. The N47A change displayed several large effects on the enzyme, one on enzyme catalysis with the enzyme having only 0.3 % k_{cat} of the wild-type, and another on GSH binding with a 23-fold increase in K_m^{GSH}. Gln[49] and Cys[51] interaction is through their main-chain nitrogens and oxygens. Changes in these residues showed intermediate effects on catalysis except for C51D, which had a k_{cat} only 3.5 % of wild-type. However, the changes in these residues all showed a major impact on GSH binding with increased K_m^{GSH} values from 6- to 34-fold. The results suggest that a packing rearrangement occurred. This rearrangement also enabled subunit–subunit communication as shown by the observed positive co-operativity upon GSH binding (Table 1).

Substrate specific activity was affected for all the engineered enzymes to varying degrees (Table 2). For example, most of the enzymes exhibited less effect on activity for EA. This suggests that the binding mode and the orientation of this substrate are different from the other substrates. Both GSH and hydrophobic substrate-binding sites are located in the same active site pocket of GSTs, therefore it is not surprising that changes in the G-site residues can perturb the hydrophobic substrate site.

It has been proposed that many steps occur in the GST catalytic mechanism including GSH ionization through thiol deprotonation, substrate conjugation by nucleophilic attack of the thiolate at the electrophilic centre, product formation and product release from the active site [13,26–28]. The overall velocity of the enzyme-catalysed reaction is affected by most of the engineered residues, although to different extents. Therefore several steps in the catalytic pathway were studied to determine the roles of the engineered residues.

pH dependence of kinetic constants

The pK_a values of ionized GSH (enzyme-bound GSH) were calculated from plots of k_{cat}/K_m^{CDNB} versus pH for the wild-type and engineered enzymes (Table 3; Figure 2). The apparent pK_a for wild-type is approx. 6.0. The pK_a values of ionized GSH in the engineered enzymes varied, with the greatest effect shown by H50A which increased it by almost 1 pH unit. GSH ionization is considered to be an important step in the catalytic mechanism of GST that generates the thiolate anion (intermediate deprotonated form of GSH) for conjugation with the electrophilic substrate. This kinetically relevant ionization of GSH has been shown to be reflected in pH dependence for k_{cat}/K_m^{CDNB} [13]. Several reports have shown that residues located near the cysteine thiol and glutamyl α-carboxylate of GSH contribute to promoting and stabilizing the anionic glutathione thiol group [13,27–31]. However, this is the first report of involvement of the GSH glycine moiety in GSH ionization.

Meisenheimer complex formation

Meisenheimer complex or σ-complex intermediate, is generated during a nucleophilic aromatic substitution reaction. Leaving group effects on enzyme catalysis can be used to determine

Table 3 The pK_a value of ionized GSH in the active site of wild-type and engineered enzymes

The effect of pH on k_{cat}/k_m^{CDNB} was obtained by measuring kinetic constants using various pH buffers of 0.1 M sodium acetate buffers (from pH 5.0 to 5.5) and 0.1 M potassium phosphate buffer (from pH 6.0 to 8.5). The pK_a values of ionized GSH (GSH-bound enzyme) were determined. n.d., Not determined (low activity precluded measurement). One-way ANOVA with Dunnett's multiple comparison test was performed with wild-type as control; statistical significance is shown by § for $P < 0.001$. See Figure 2 for a plot of the experimental data.

Enzyme	pK_a (ionized GSH)
Wild-type	6.00 ± 0.05
H38A	6.10 ± 0.02
M39A	6.52 ± 0.05§
N47A	n.d.
Q49A	6.23 ± 0.05§
H50A	6.92 ± 0.06§
C51A	6.22 ± 0.03§
C51D	6.42 ± 0.03§

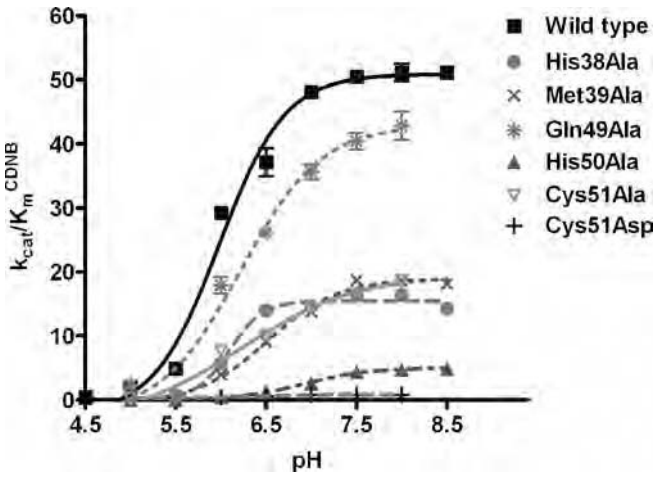

Figure 2 Plot of the data to determine the pK_a value of ionized GSH in the active site of wild-type and engineered enzymes

The effect of pH on k_{cat}/k_m^{CDNB} was obtained by measuring kinetic constants using various pH buffers of 0.1 M sodium acetate buffers (from pH 5.0 to 5.5) and 0.1 M potassium phosphate buffer (from pH 6.0 to 8.5). The pK_a values of ionized GSH (GSH-bound enzyme) were determined (see Table 3). The results are presented as means ± S.D. from at least three independent experiments.

whether the rate-limiting step of the reaction is σ-complex formation. The substitution of a more electronegative leaving group concomitant with an increase in the rate constant of the spontaneous reaction with glutathione is a signal that the σ-complex formation is a rate-limiting step [13]. Therefore the influence on the catalytic constant of the chlorine leaving group of CDNB replaced with fluorine was examined (Table 4).

Although the wild-type enzyme was insensitive, several of the engineered enzymes demonstrated sensitivity to the halogen leaving group, particularly H50A, C51D and D47A, with increased ratio values of 19-, 27- and 18-fold respectively. The catalytic efficiency (k_{cat}/K_m) of the engineered enzymes showed a different sensitivity to the nature of the leaving group, suggesting that an alteration of the relative catalytic-centre activity is a consequence of changes in the rate of σ-complex formation rather than changes in binding affinity towards the different substrate

Table 4 Effect of fluoride/chloride leaving group substitution on the rate of catalysis

The ratio of catalytic rates for the conjugation reaction catalysed by wild-type and engineered GSTs using GSH and CDNB or FDNB as co-substrates. One-way ANOVA with Dunnett's multiple comparison test was performed with wild-type as control; statistical significance is shown by † for $P < 0.05$, ‡ for $P < 0.01$ and § for $P < 0.001$.

	Leaving group effect	
Enzyme	$k_{cat}^{FDNB}/k_{cat}^{CDNB}$	$(k_{cat}/K_m)^{FDNB}/(k_{cat}/K_m)^{CDNB}$
Wild-type	1.76 ± 0.01	20.59 ± 1.02
H38A	3.11 ± 0.21	14.12 ± 0.84†
M39A	8.29 ± 0.95§	32.45 ± 3.72§
N47A	18.09 ± 0.90§	29.65 ± 1.32‡
Q49A	2.63 ± 0.08	26.29 ± 1.77†
Q49E	1.50 ± 0.08	24.95 ± 1.21
H50A	18.57 ± 0.41§	16.55 ± 1.59
C51A	2.93 ± 0.05	30.31 ± 2.85§
C51D	26.75 ± 0.99§	44.71 ± 4.15§

Table 5 Viscosity effect on kinetic constants and free energy changes of wild-type and engineered enzymes

The effect of viscosity on kinetic constants was assayed by using 0.1 M potassium phosphate buffer (pH 6.5) with various glycerol concentrations. The slope of a reciprocal plot of the relative catalytic constant (k_{cat}^0/k_{cat}) versus relative viscosity (η/η^0) was determined. n.d., Not determined (low activity precluded measurement); $\Delta\Delta G$ (the difference in the free energy changes for the formation of the transition states in the wild-type and engineered enzymes) is calculated from the equation: $\Delta\Delta G = -RT \ln(k_{cat}/K_m^{CDNB})_{engineered}/(k_{cat}/K_m^{CDNB})_{wild-type}$. One-way ANOVA with Dunnett's multiple comparison test was performed with wild-type as control; statistical significance is shown by § for $P < 0.001$.

Enzyme	Slope	$\Delta\Delta G$ (kJ/mol)
Wild-type	0.959 ± 0.036	–
H38A	0.485 ± 0.019§	3.58 ± 0.033
M39A	0.430 ± 0.031§	3.33 ± 0.132
N47A	n.d.	14.8 ± 0.222
Q49A	0.797 ± 0.036§	1.86 ± 0.105
H50A	0.005 ± 0.001§	7.56 ± 0.095
C51A	1.11 ± 0.010§	4.08 ± 0.125
C51D	0.051 ± 0.007§	10.7 ± 0.201

leaving groups. The results suggest that the process of σ-complex intermediate formation is affected by the disruption of the hydrogen bond network to GSH which affected the overall velocity of the enzyme-catalysed reaction. It is possible that the residue changes caused incorrect orientation of the GSH thiol or of the His^{50} side chain, which then disturbs the conjugation process of the thiolate anion with the electrophilic substrate. Additionally, the results strongly support that the hydrogen bond network contributes to both the GSH ionization process and σ-complex intermediate formation. This contribution appears to stabilize the His^{50} residue as shown by the changes in pK_a and the greater effect of the leaving group on the catalytic constants of C51D but not C51D.

Viscosity effect on kinetic constants

The viscosity effect was studied to determine if the rate-limiting step of the reaction is physical or chemical. The slope of the reciprocal plot of inverse relative catalytic constant (k_{cat}^0/k_{cat}) versus relative medium viscosity (η/η^0) was determined (Table 5). A slope near unity gives a proportional decrease in rate constant with increasing viscosity of the solution and shows a physical

Table 6 Thermal stability of wild-type and engineered adGSTD4-4 at 45 °C

The remaining GST activity was measured after incubating the enzyme at various time points at 45 °C. n.d., Not determined (low activity precluded measurement). [a]Some of these values have been previously reported and are shown for purposes of comparison [19,20]. One-way ANOVA with Dunnett's multiple comparison test was performed with wild-type as control; statistical significance is shown by ‡ for $P < 0.01$ and § for $P < 0.001$.

Enzyme	Half-life at 45 °C (min)
Wild-type[a]	15.32 ± 0.31
H38A[a]	15.33 ± 0.88§
H38E[a]	40.17 ± 1.26§
H38F[a]	19.33 ± 0.59§
H38D	15.18 ± 1.67
H38K	14.07 ± 0.73
M39A	4.71 ± 0.16§
M39F	4.72 ± 0.23§
N47A	n.d.
Q49A	15.19 ± 1.06§
Q49E	25.19 ± 1.37§
H50A[a]	25.81 ± 1.99§
H50E[a]	15.31 ± 0.54
H50Y[a]	20.79 ± 0.34§
H50K	11.99 ± 0.51§
H50F	27.07 ± 0.82§
C51A	14.86 ± 0.64
C51D	18.18 ± 1.01‡

step is rate-determining, whereas a slope of zero indicates that a chemical reaction step is rate limiting [32,33].

Wild-type enzyme displayed a linear dependence with a slope of approx. 1.0 suggesting that a physical step of the reaction that includes product release and/or structural transition is rate limiting. The engineered enzymes exhibited viscosity effects on k_{cat} to different degrees. H50A and C51D were viscosity-independent with a slope approaching zero. These engineered enzymes changed the rate-limiting step of the reaction to a chemical step that includes GSH ionization step and σ-complex formation as described above, whereas partial dependence on a diffusion barrier and other viscosity-dependent motions were observed for the remaining enzymes that displayed viscosity effects with intermediate values ($0 < \text{slope} < 1$).

Also displayed in Table 5 is $\Delta\Delta G$, which is shown to illustrate the differences in the free energy changes for the formation of the transition states in the wild-type and engineered enzymes, as calculated at 25 °C from the equation below [34]:

$$\Delta\Delta G = -RT \ln \left(k_{cat}/K_m^{CDNB}\right)_{mutant} / \left(k_{cat}/K_m^{CDNB}\right)_{wild\text{-}type}.$$

H50A, D47A and C51D have a greater $\Delta\Delta G$ (7.562, 14.842 and 10.671 kJ/mol respectively) compared with other engineered enzymes (ranging from 1.860 to 4.075 kJ/mol) indicating that upon disruption of the hydrogen bond network, the enzymes require more energy than the wild-type enzyme to form and stabilize the transition state.

Characterization of physical properties

The stability of the proteins was determined in comparison with the adGSTD4-4 wild-type (Table 6). In general, the engineered His[38], His[50], Asn[47], Cys[51] and Gln[49] proteins exhibited comparable stabilities to the wild-type, indicating a minor role of these residues in structural maintenance. However, H38E increased stability of the enzyme 2.6-fold, suggesting that a conformational change occurred which also is supported by the observed positive co-operativity. Met[39] appears to play a role in structural integrity as shown by 3-fold decreased enzyme stability for both the alanine and phenylalanine changes. However, the initial folding processes of the enzymes were observed to yield comparable refolding rates to the wild-type (results not shown). These results suggest that the Met[39] dipole–dipole interaction and positioning of His[38] and His[50] in a suitable conformation impact not only the kinetic properties but also enzyme stability.

The intrinsic fluorescence of tryptophan was used as an indicator of changes in tertiary structure (Figure 3). The λ_{max} of tryptophan fluorescence in the engineered enzymes was slightly different from wild-type with a red shift in the range of 1–4 nm indicating a different polarity in tryptophan environments. In addition, differences in fluorescence intensity between wild-type and engineered enzymes were observed. This result suggests that there are minor conformational disturbances in the active site topography, which affect orientations of tryptophan and/or its neighbouring residues thereby modulating the quenching and tryptophan exposure to the electrophilic environment. For example, the active site topology changes that generated the positive co-operativity in H50K also yielded the lowest fluorescence intensity among the His[50] engineered enzymes (~44 % of wild-type). Moreover, the conformational change induced by glutamic acid residue replacement of His[38] also gave a 2-fold increase in enzyme stability, increased intrinsic fluorescence intensity to 197 % of wild-type, modulated GSH binding and enzyme catalysis as well as yielding the observed positive co-operativity towards GSH.

DISCUSSION

The G-site residues interacting directly with cysteine and glutamyl moieties of GSH have been shown in several studies to contribute to GST catalytic mechanisms including GSH binding, catalysis, GSH ionization as well as rate-limiting step determination [10–14]. In the present study, we have examined the significant contributions of GST residues that interact with the GSH glycine moiety as well as identification of a hydrogen bond network. The network consists of His[38], Met[39], Asn[47], Gln[49], His[50] and Cys[51] and contributes to catalysis through multiple processes including GSH ionization, nucleophilic substitution, product formation and product dissociation.

The kinetic studies demonstrated that the engineered residues greatly impacted the enzyme's ability to interact with GSH. Moreover, the engineered enzymes of His[38], Met[39], His[50], Cys[51] and Gln[49] have shown strong positive co-operativity upon binding of GSH. However, the positive co-operativity was not observed for the engineered enzymes of residues interacting with the other moieties of GSH [11–13,15]. Therefore it can be suggested that the residues interacting with the GSH glycine moiety are not only involved in GSH interaction but also control the motion of a flexible region of GST. Upon binding of GSH in the active site, these GST residues induce an active site conformational change for the induced-fit mechanism. These residues are on the loops on either side of α2-helix which connects the helix to β2-sheet and β3-sheet. These loops would serve as hinges for the movement of α2-helix.

In the present study, changes of the active-site residues generated positive co-operativity between two subunits, a finding similar to that obtained in previous studies in which the subunit interface had been changed or where changes in highly flexible regions, for example Gly[41], Cys[47] and Lys[54] of hGSTP1-1 (human GSTP1-1) [33,35] or Asn[49] and Gln[53] of maize GST1 [36,37],

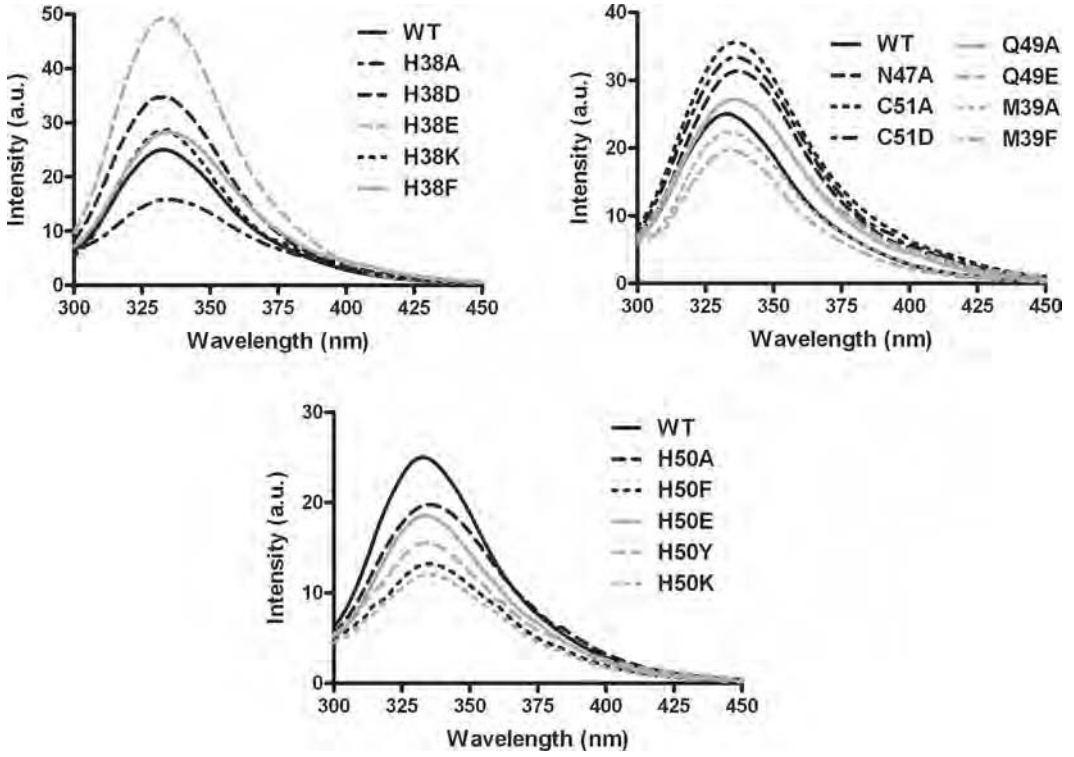

Figure 3 The maximum emission wavelength (λ_{max}) and intrinsic fluorescence intensity at λ_{max} of tryptophan fluorescence of wild-type and the engineered enzymes

Excitation was at 295 nm and emission was scanned from 300 to 450 nm. Samples ($n = 3$) contained 0.1 mg/ml protein in 0.1 M potassium phosphate buffer (pH 6.5). Percent intensity change compared with wild-type enzyme was measured at fluorescence λ_{max} averaged over three scans corrected for dilution and inner filter effects.

had been made. It has been proposed that the conformational transitions generate two different binding modes upon GSH binding: low-affinity and high-affinity conformations, which are related to positive co-operativity observed [5,38,39]. The binding of GSH to the first active site stabilizes the low-affinity conformation of the enzyme which then becomes the high-affinity conformational state. Positive co-operativity upon GSH binding observed in His^{38}, Met^{39}, His^{50}, Cys^{51} and Gln^{49} engineered enzymes may be relevant to this conformational transition concept. These residues are located in a highly flexible region; therefore the residue changes would alter the flexibility of the α2-helix to fit GSH in the active site, which may then generate two different conformational transition states upon GSH binding.

Both His^{38} and His^{50} interact directly with the glycine carboxylate of GSH. The functional groups at positions 38 and 50 are significant in size, volume and polarity for GSH binding and enzyme catalysis. However, His^{50} contributes more to the GSH activation process and enzyme catalysis in which the full function is achieved by the synergistic action with the hydrogen bond network residues (Asn^{47}, Gln^{49} and Cys^{51}). The disruption of the hydrogen bond network, for the engineered enzymes of His^{50}, Asn^{47} and Cys^{51}, showed progressively decreased k_{cat} values to more than 90 %. Moreover, several aspects of the GST catalytic mechanism were altered by H50A. H50A decreased the enzyme's ability to lower the pK_a of the GSH thiol group up to 1 pH unit; this large an effect has been observed for mutations of the conserved serine/tyrosine residue interacting with the GSH thiol group [13,40–42]. Additionally, the rate-limiting step of the H50A is fully switched from a physical step to a chemical step as determined by fluoride/chloride leaving group and viscosity effect on the kinetic constants. As the important His^{50} is still present, lesser effects were observed for the engineered enzymes of Gln^{49} and Cys^{51} for minor disruptions of the stabilizing hydrogen bond network.

The results strongly support that His^{50} is a key residue in the hydrogen bond network which functions as a proton acceptor as well as controls the electron distribution in the active site to promote ionization and stabilization of the GSH thiolate anion. The His^{50} residue contributes to precise residue and substrate orientations, GSH ionization, σ-complex intermediate formation and the release of product from the active site. The regulation of the electrostatic field in the active site by positively charged residues has also been reported in several studies [15,43,44].

The changes in catalytic efficiency are also related to differences in free energy changes for the formation of transition states in the engineered and wild-type enzymes as determined by $\Delta\Delta G$ [34]. The greater value of $\Delta\Delta G$ refers to a decrease in the stabilization of transition state compared with wild-type in which the enzyme utilizes more energy to stabilize its transition state. Moreover, the stabilization of transition state contributes to multiple mechanisms in enzyme-catalysed reactions. $\Delta\Delta G$ values are increased up to 7.562, 14.84 and 10.666 kJ/mol for H50A, D47A and C51D respectively in which the hydrogen bond network is strongly disrupted, indicative of the incomplete pre-organized environment for enhancing catalysis along the reaction pathway of the engineered enzymes [45]. Therefore it can be noted that the network of hydrogen bonds is also required for the organization inside the enzyme molecule to provide stabilization of the transition state.

The positively charged residue position 50 appears to be highly conserved or functionally conserved across GST classes by histidine, lysine or arginine located at the equivalent structural

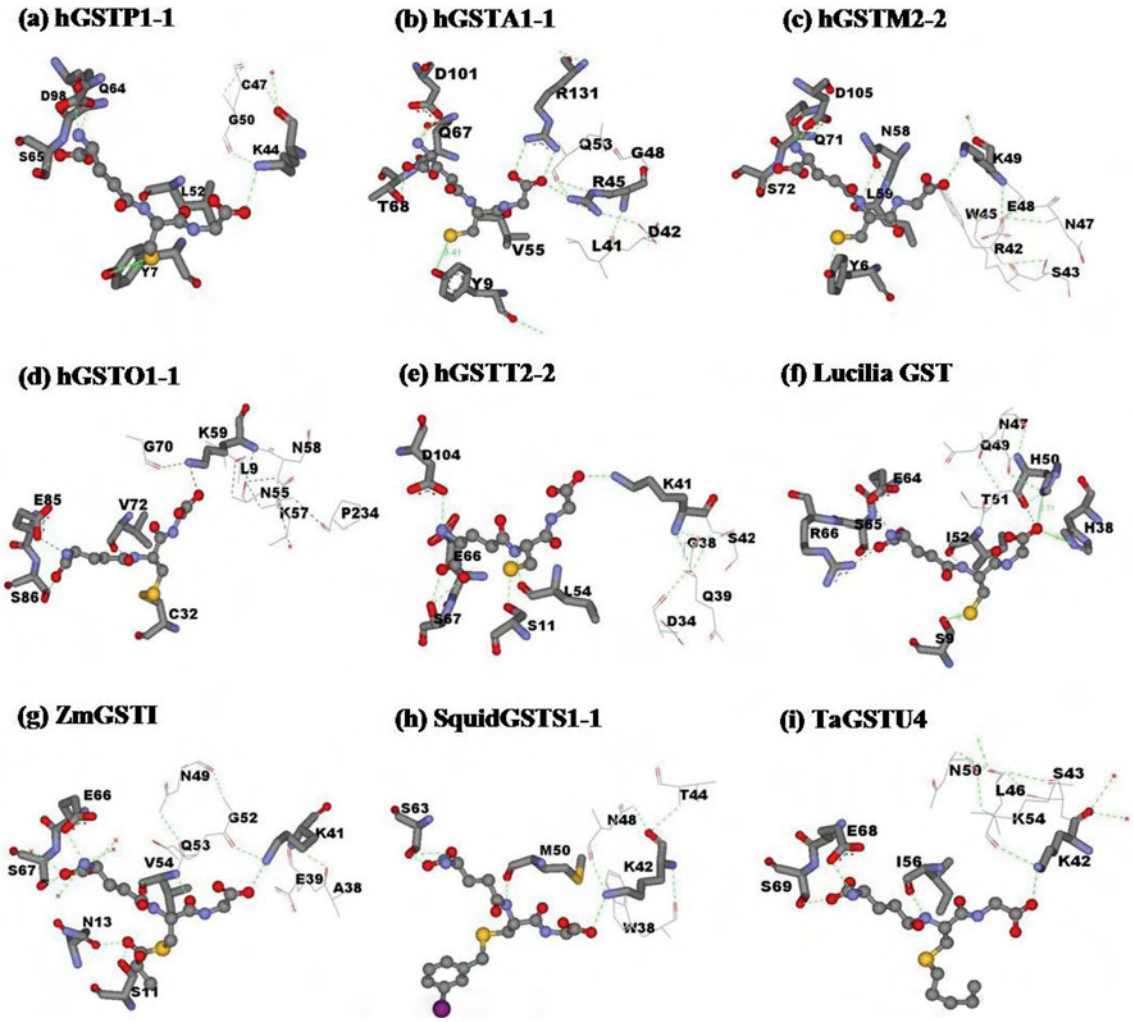

COLOUR

Figure 4 Conserved G-site residues that directly interact with the glycine moiety of GSH and generate a hydrogen bond network in several GST classes

The conserved G-site residues are shown by stick models, while line models represent the hydrogen bond network residues at the glycine moiety of GSH. GSH or GSH analogues are illustrated in ball-and-stick; GSH (**a**, **b**, **c**, **d**, **e**, **f**), lactoylglutathione (**g**), iodobenzylglutathione (**h**) and *S*-hexyl-GSH (**i**). Green dotted lines represent hydrogen-bond interactions. PDB code numbers: hGSTP1-1 (PDB id 8GSS), hGSTA1-1 (PDB id 1PKW), hGSTM2-2 (PDB id 1XW5), hGSTO1-1 (PDB id 1EEM), hGSTT2-2 (PDB id 1LJR), Lucilia GST [7], ZmGST1 (PDB id 1AXD), squid GSTS1-1 (PDB id 2GSQ) and TaGSTU4 [*Triticum aestivum* (wheat) GSTU4; PDB id 1GWC]. The Figure was created with Accelrys DS ViewerPro 5.0.

position. This conserved residue is in hydrogen bonding distance to the glycine carboxylate moiety of GSH which is stabilized by a hydrogen bond network of surrounding residues (Figure 4) for example Lys[40] in PtGSTU1 [*Pinus tabulaeformis* (Chinese hard pine) GSTU1], Lys[41] in ZmGST1 [*Zea mays* (maize) GST1], Lys[44] in hGSTP1-1, Lys[41] in hGSTT2-2, Lys[59] in hGSTO1-1, Lys[49] in hGSTM2-2, Lys[42] in squid GSTS1-1, Lys[45] in Sj26GST [26 kDa GST from *Schistosoma japonicum* (oriental blood-fluke)] and Arg[45] in hGSTA1-1. However, the feature of two positively charged histidines, His[38] and His[50], interacting with the glycine carboxylate moiety of GSH is a unique trait for insect GSTDs. His[38] is responsible for GSH binding, whereas His[50] contributes to several steps of the enzyme-catalysed reaction from GSH interaction to the release of product from the active site.

For the GSH activation mechanism of Alpha, Mu and Pi GST isoenzymes, it has been described that the thiol proton is quantitatively released into solution after the thiolate anion is formed [46,47]. In contrast with GSTD, which behaves differently, the thiol proton is captured by at least an internal base residue at high pH value [46,47]. The present study shows that His[50] is also a candidate for the thiol proton acceptor in addition to the residues at the γ-glutamyl portion of GSH reported previously [15,31]. Moreover, the overall velocity of His[50] engineered enzymes is progressively restricted; therefore it can be assumed that the thiol proton released must be accepted first by the active site residues, e.g. His[50], before a new cycle of the reaction can initiate.

The 'base-assisted deprotonation model' is an alternative model that describes the mechanism of GST enzymes in GSH ionization process. This model has been implicated in several studies of the glutamyl α-carboxylate of GSH acting as a catalytic base, involved in the thiol proton acceptance from the GSH thiol group [15,16,31,46]. In the present study, we addressed the contribution of the glycine moiety of GSH for GSH ionization in which this end of GSH is involved in proton acceptance by providing a counter ion from the charged His[50] which is stabilized by the hydrogen bond network.

In conclusion, the present study revealed a critical role for residues located at the glycine moiety of GSH in catalytic rate determination. This area constitutes a second G-site network involved in GSH ionization distinct from the network previously

reported interacting with the glutamyl end of GSH [16,17]. This second network also appears to be functionally conserved in GSTs (Figure 4). In the present study, we showed that His^{50} is a central residue in the hydrogen bond network to GSH with the protonated imidazole ring of His^{50} being stabilized by the network. His^{50} plays important roles in several processes of the enzyme mechanism. Moreover, this network at the glycine moiety of GSH also contributed to the 'base-assisted deprotonation model' for GSH ionization.

This work was funded by the TRF (Thailand Research Fund). A.V. was supported by a Royal Golden Jubilee Ph.D. Scholarship.

REFERENCES

1 Sheehan, D., Meade, G., Foley, V. M. and Dowd, C. A. (2001) Structure, function and evolution of glutathione transferases: implications for classification of non-mammalian members of an ancient enzyme superfamily. Biochem. J. **360**, 1–16

2 Ketterer, B. (2001) A bird's eye view of the glutathione transferase field. Chem. Biol. Interact. **138**, 27–42

3 Mannervik, B., Awasthi, Y. C., Board, P. G., Hayes, J. D., Di Ilio, C., Ketterer, B., Listowsky, I., Morgenstern, R., Muramatsu, M., Pearson, W. R. et al. (1992) Nomenclature for human glutathione transferases. Biochem. J. **282**, 305–306

4 Hayes, J. D., Flanagan, J. U. and Jowsey, I. R. (2005) Glutathione transferases. Annu. Rev. Pharmacol. Toxicol. **45**, 51–88

5 Mannervik, B. and Danielson, U. H. (1988) Glutathione transferases – structure and catalytic activity. CRC Crit. Rev. Biochem. **23**, 283–337

6 Armstrong, R. N. (1997) Structure, catalytic mechanism, and evolution of the glutathione transferases. Chem. Res. Toxicol. **10**, 2–18

7 Wilce, M. C. J., Board, P. G., Feil, S. C. and Parker, M. W. (1995) Crystal structure of a theta-class glutathione transferase. EMBO J. **14**, 2133–2143

8 Dirr, H., Reinemer, P. and Huber, R. (1994) X-ray crystal structures of cytosolic glutathione S-transferases. Implications for protein architecture, substrate recognition and catalytic function. Eur. J. Biochem. **220**, 645–661

9 Rossjohn, J., Feil, S. C., Wilce, M. C. J., Sexton, J., Spithill, T. W. and Parker, M. W. (1997) Crystallization, structural determination and analysis of a novel parasite vaccine candidate: *Fasciola hepatica* glutathione S-transferase. J. Mol. Biol. **273**, 857–872

10 Stenberg, G., Board, P. G., Carlberg, I. and Mannervik, B. (1991) Effects of directed mutagenesis on conserved arginine residues in a human class Alpha glutathione transferase. Biochem. J. **274**, 549–555

11 Liu, S., Zhang, P., Ji, X., Johnson, W. W., Gilliland, G. L. and Armstrong, R. N. (1992) Contribution of tyrosine 6 to the catalytic mechanism of isoenzyme 3-3 of glutathione S-transferase. J. Biol. Chem. **267**, 4296–4299

12 Kolm, R. H., Sroga, G. E. and Mannervik, B. (1992) Participation of the phenolic hydroxyl group of Tyr-8 in the catalytic mechanism of human glutathione transferase P1-1. Biochem. J. **285**, 537–540

13 Caccuri, A. M., Antonini, G., Nicotra, M., Battistoni, A., Lo Bello, M., Board, P. G., Parker, M. W. and Ricci, G. (1997) Catalytic mechanism and role of hydroxyl residues in the active site of theta class glutathione S-transferases. Investigation of Ser-9 and Tyr-113 in a glutathione S-transferase from the Australian sheep blowfly, *Lucilia cuprina*. J. Biol. Chem. **272**, 29681–29686

14 Tan, K.-L., Chelvanayagam, G., Parker, M. W. and Board, P. G. (1996) Mutagenesis of the active site of the human Theta-class glutathione transferase GSTT2-2: catalysis with different substrates involves different residues. Biochem. J. **319**, 315–321

15 Winayanuwattikun, P. and Ketterman, A. J. (2004) Catalytic and structural contributions for glutathione binding residues in a Delta class glutathione S-transferase. Biochem. J. **382**, 751–757

16 Winayanuwattikun, P. and Ketterman, A. J. (2005) An electron-sharing network involved in the catalytic mechanism is functionally conserved in different glutathione transferase classes. J. Biol. Chem. **280**, 31776–31782

17 Winayanuwattikun, P. and Ketterman, A. J. (2007) Glutamate 64, a newly identified residue of the functionally conserved electron-sharing network contributes to catalysis and structural integrity of glutathione transferases. Biochem. J. **402**, 339–348

18 Pettersen, E. F., Goddard, T. D., Huang, C. C., Couch, G. S., Greenblatt, D. M., Meng, E. C. and Ferrin, T. E. (2004) UCSF chimera – a visualization system for exploratory research and analysis. J. Comput. Chem. **25**, 1605–1612

19 Vararattanavech, A. and Ketterman, A. (2003) Multiple roles of glutathione binding-site residues of glutathione S-transferase. Protein Peptide Lett. **10**, 441–448

20 Vararattanavech, A., Prommeenate, P. and Ketterman, A. J. (2006) The structural roles of a conserved small hydrophobic core in the active site and an ionic bridge in domain I of Delta class glutathione S-transferase. Biochem. J. **393**, 89–95

21 Habig, W. H., Pabst, M. J. and Jakoby, W. B. (1974) Glutathione S-transferases. The first enzymatic step in mercapturic acid formation. J. Biol. Chem. **249**, 7130–7139

22 Segel, I. H. (1993) Enzyme Kinetics, Behavior and Analysis of Rapid Equilibrium and Steady-state Enzyme Systems, John Wiley and Sons, New York

23 Jirajaroenrat, K., Pongjaroenkit, S., Krittanai, C., Prapanthadara, L. and Ketterman, A. J. (2001) Heterologous expression and characterization of alternatively spliced glutathione *S*-transferases from a single *Anopheles* gene. Insect Biochem. Mol. Biol. **31**, 867–875

24 Caccuri, A. M., Ascenzi, P., Lo Bello, M., Federici, G., Battistoni, A., Mazzetti, P. and Ricci, G. (1994) Are the steady state kinetics of glutathione transferase always dependent on the deprotonation of the bound glutathione? New insights in the kinetic mechanism of GST P1-1. Biochem. Biophys. Res. Commun. **200**, 1428–1434

25 Wolf, A. V., Brown, M. G. and Prentiss, P. G. (1985) Handbook of Chemistry and Physics, CRC Press, Boca Raton, FL

26 Armstrong, R. N., Rife, C. and Wang, Z. (2001) Structure, mechanism and evolution of thiol transferases. Chem. Biol. Interact. **133**, 167–169

27 Caccuri, A. M., Ascenzi, P., Antonini, G., Parker, M. W., Oakley, A. J., Chiessi, E., Nuccetelli, M., Battistoni, A., Bellizia, A. and Ricci, G. (1996) Structural flexibility modulates the activity of human glutathione transferase P1-1. Influence of a poor co-substrate on dynamics and kinetics of human glutathione transferase. J. Biol. Chem. **271**, 16193–16198

28 Caccuri, A. M., Lo Bello, M., Nuccetelli, M., Rossi, P., Antonini, G., Federici, G. and Ricci, G. (1998) Proton release upon glutathione binding to glutathione transferase P1-1: kinetic analysis of a multistep glutathione binding process. Biochemistry **37**, 3028–3034

29 Armstrong, R. N. (1997) Structure, catalytic mechanism, and evolution of the glutathione transferases. Chem. Res. Toxicol. **10**, 2–18

30 Gustafsson, A., Pettersson, P. L., Grehn, L., Jemth, P. and Mannervik, B. (2001) Role of the glutamyl α-carboxylate of the substrate glutathione in the catalytic mechanism of human glutathione transferase A1-1. Biochemistry **40**, 15835–15845

31 Widersten, M., Björnestedt, R. and Mannervik, B. (1996) Involvement of the carboxyl groups of glutathione in the catalytic mechanism of human glutathione transferase A1-1. Biochemistry **35**, 7731–7742

32 Johnson, W. W., Liu, S., Ji, X., Gilliland, G. L. and Armstrong, R. N. (1993) Tyrosine 115 participates both in chemical and physical steps of the catalytic mechanism of a glutathione S-transferase. J. Biol. Chem. **268**, 11508–11511

33 Ricci, G., Caccuri, A. M., Lo Bello, M., Rosato, N., Mei, G., Nicotra, M., Chiessi, E., Mazzetti, A. P. and Federici, G. (1996) Structural flexibility modulates the activity of human glutathione transferase P1-1. Role of helix 2 flexibility in the catalytic mechanism. J. Biol. Chem. **271**, 16187–16192

34 Dirr, H. W., Little, T., Kuhnert, D. C. and Sayed, Y. (2005) A conserved N-capping motif contributes significantly to the stabilization and dynamics of the C-terminal region of class alpha glutathione transferases. J. Biol. Chem. **280**, 19480–19487

35 Lo Bello, M., Nuccetelli, M., Chiessi, E., Lahm, A., Mazzetti, A. P., Parker, M. W., Tramontano, A., Federici, G. and Ricci, G. (1998) Mutations of Gly to Ala in human glutathione transferase P1-1 affect helix 2 (G-site) and induce positive cooperativity in the binding of glutathione. J. Mol. Biol. **284**, 1717–1725

36 Labrou, N. E., Mello, L. V. and Clonis, Y. D. (2001) Functional and structural roles of the glutathione-binding residues in maize (*Zea mays*) glutathione S-transferase I. Biochem. J. **358**, 101–110

37 Labrou, N. E., Mello, L. V. and Clonis, Y. D. (2001) The conserved Asn49 of maize glutathione *S*-transferase I modulates substrate binding, catalysis and intersubunit communication. Eur. J. Biochem. **268**, 3950–3957

38 Principato, G. B., Danielson, U. H. and Mannervik, B. (1988) Relaxed thiol substrate specificity of glutathione transferase effected by a non-substrate glutathione derivative. FEBS Lett. **231**, 155–158

39 Jemth, P. and Mannervik, B. (1999) Fast product formation and slow product release are important features in a hysteretic reaction mechanism of glutathione transferase T2-2. Biochemistry **38**, 9982–9991

40 Wang, J., Barycki, J. J. and Colman, R. F. (1996) Tyrosine 8 contributes to catalysis but is not required for activity of rat liver glutathione S-transferase, 1-1. Protein Sci. **5**, 1032–1042

41 Gustafsson, A., Etahadieh, M., Jemth, P. and Mannervik, B. (1999) The C-terminal region of human glutathione transferase A1-1 affects the rate of glutathione binding and the ionization of the active-site Tyr9. Biochemistry **38**, 16268–16275

42 Labrou, N. E., Rigden, D. J. and Clonis, Y. D. (2003) Engineering the pH-dependence of kinetic parameters of maize glutathione *S*-transferase I by site-directed mutagenesis. Biomol. Eng. **21**, 61–66

43 Patskovsky, Y. V., Patskovska, L. N. and Listowsky, I. (2000) The enhanced affinity for thiolate anion and activation of enzyme-bound glutathione is governed by an arginine residue of human Mu class glutathione S-transferases. J. Biol. Chem. **275**, 3296–3304
44 Björnestedt, R., Tardioli, S. and Mannervik, B. (1995) The high activity of rat glutathione transferase 8-8 with alkene substrates is dependent on a glycine residue in the active site. J. Biol. Chem. **270**, 29705–29709
45 Garcia-Viloca, M., Gao, J., Karplus, M. and Truhlar, D. G. (2004) How enzymes work: analysis by modern rate theory and computer simulations. Science **303**, 186–195
46 Caccuri, A. M., Antonini, G., Board, P. G., Parker, M. W., Nicotra, M., Lo Bello, M., Federici, G. and Ricci, G. (1999) Proton release on binding of glutathione to Alpha, Mu and Delta class glutathione transferases. Biochem. J. **344**, 419–425
47 Caccuri, A. M., Antonini, G., Board, P. G., Flanagan, J., Parker, M. W., Paolesse, R., Turella, P., Federici, G., Lo Bello, M. and Ricci, G. (2001) Human glutathione transferase T2-2 discloses some evolutionary strategies for optimization of substrate binding to the active site of glutathione transferases. J. Biol. Chem. **276**, 5427–5431

Received 27 March 2007/22 May 2007; accepted 24 May 2007
Published as BJ Immediate Publication 24 May 2007, doi:10.1042/BJ20070422

BJ www.biochemj.org

BJ Structure

Biochem. J. (2007) **402**, 339–348 (Printed in Great Britain) doi:10.1042/BJ20061253

Glutamate-64, a newly identified residue of the functionally conserved electron-sharing network contributes to catalysis and structural integrity of glutathione transferases

Pakorn WINAYANUWATTIKUN and Albert J. KETTERMAN[1]

Institute of Molecular Biology and Genetics, Mahidol University, Salaya Campus, Nakhon Pathom 73170, Thailand

In *Anopheles dirus* glutathione transferase D3-3, position 64 is occupied by a functionally conserved glutamate residue, which interacts directly with the γ-glutamate moiety of GSH (glutathione) as part of an electron-sharing network present in all soluble GSTs (glutathione transferases). Primary sequence alignment of all GST classes suggests that Glu^{64} is one of a few residues that is functionally conserved in the GST superfamily. Available crystal structures as well as consideration of the property of the equivalent residue at position 64, acidic or polar, suggest that the GST electron-sharing motif can be divided into two types. Electrostatic interaction between the GSH glutamyl and carboxylic Glu^{64}, as well as with Arg^{66} and Asp^{100}, was observed to extend the electron-sharing motif identified previously. Glu^{64} contributes to the catalytic function of this motif and the 'base-assisted deprotonation' that are essential for GSH ionization during catalysis. Moreover, this residue also appears to affect multiple steps in the enzyme catalytic strategy, including binding of GSH, nucleophilic attack by thiolate at the electrophilic centre and product formation, probably through active-site packing effects. Replacement with non-functionally-conserved amino acids alters initial packing or folding by favouring aggregation during heterologous expression. Thermodynamic and reactivation *in vitro* analysis indicated that Glu^{64} also contributes to the initial folding pathway and overall structural stability. Therefore Glu^{64} also appears to impact upon catalysis through roles in both initial folding and structural maintenance.

Key words: active-site residue, *Anopheles dirus*, catalytic mechanism, electron sharing network, glutathione transferase, structural integrity.

INTRODUCTION

GSTs (glutathione transferases; EC 2.5.1.18) are a superfamily of enzymes that contribute towards diverse cellular processes ranging from detoxification to control of gene expression [1–4]. The enzymes generally catalyse nucleophilic attack of the GSH (glutathione) sulfhydryl group to an electrophilic centre of a number of endogenous and xenobiotic compounds [1,5,6]. Conjugation of GSH to such organic molecules enhances solubility, thus facilitating their eventual elimination [5–7]. This reaction is an early step along the mercapturic acid pathway in which hydrophobic compounds are inactivated and eliminated from an organism [8]. Based on amino acid identity, substrate specificities and immunological cross-reactivity, cytosolic GSTs are currently divided into at least 12 distinct evolutionary classes, namely Alpha, Mu, Pi, Theta, Sigma, Zeta, Omega, Phi, Tau, Delta, Epsilon and Beta [6,9–15]. In addition, the number of members identified in this enzyme superfamily is increasing due to the massive growth of genomic information, which includes a number of unclassified GSTs [16].

All cytosolic GSTs adopt the same highly conserved tertiary structure [17]. GSTs are dimeric proteins (with a molecular mass of about 50 kDa) assembled from identical or structurally related subunits. Each subunit is characterized by two distinct domains and an active site. However, each active site is only fully functional when amino acid residues from both subunits are present in the final dimeric structure. The active-site of GSTs consists of two adjacent regions. The first region is the G-site (GSH binding site), formed mostly by the N-terminal domain (domain I), which adopts an α/β topology that binds GSH as the thiol substrate [7]. The second region is the non-polar H-site (hydrophobic substrate binding site), generated primarily by the C-terminal domain (domain II), which is an all-helical structure that provides structural elements for recognition of a wide range of hydrophobic co-substrates [7]. Although GSTs possess a high specificity for GSH as the nucleophile, the enzymes exhibit broad specificity with regard to structurally diverse hydrophobic substrates [17]. The catalytic strategy of GSTs for the nucleophilic substitution reaction can be divided into several steps: binding of substrates to the enzyme active site, activation of GSH by thiol deprotonation, nucleophilic attack by thiolate at the electrophilic centre, product formation and product release [18–20].

The roles of several active-site residues and functional groups of GSH have been studied intensively and a potential model has been proposed to describe deprotonation of the GSH thiol group which enhances the nucleophilicity of the reaction [20–24]. The hydroxyl group of the conserved tyrosine/serine residue at the G-site of GSTs (i.e. Tyr^{8} for Pi, Tyr^{9} for Alpha, Tyr^{6} for Mu and Ser^{9} for Delta classes) is within hydrogen-bonding distance of the thiol group of the bound GSH, and is required for correct orientation and stabilization of the deprotonated thiol anion. The deprotonated anionic GSH results from subtraction of a thiol proton by the glutamyl α-carboxylate of GSH, which acts as a catalytic base in the base-assisted deprotonation model with assistance from an electron-sharing network. The functionally conserved electron-sharing network is characterized by an ionic

Abbreviations used: adGSTD3-3, *Anopheles dirus* glutathione transferase Delta class homodimer of subunit 3; CDNB, 1-chloro-2,4-dinitrobenzene; DTT, dithiothreitol; FDNB, 1-fluoro-2,4-dinitrobenzene; GdmCl, guanidinium chloride; GSH, glutathione; G-site, GSH binding site; GST, glutathione transferase; PtGSTU1-1, plant Tau class GST.

[1] To whom correspondence should be addressed (email frakt@mahidol.ac.th).

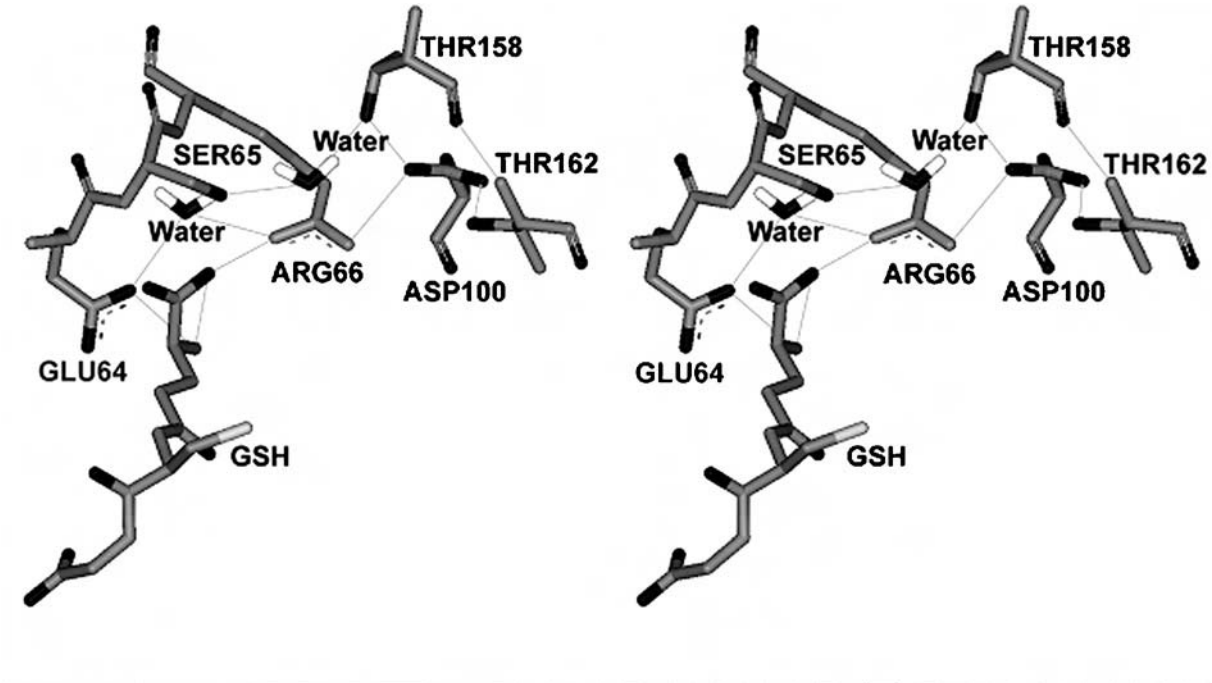

NCBI Seq ID	GST class	Source	Isoform																											
AAG38505	Delta	*A.dirus*	3	52	I	P	T	L	V	D	N	-	G	F	A	L	W	E	S	R	A	I	C	T	Y	L	A	E	K	Y	G
NP_000844.1	Theta	*H.sapiens*	1	54	V	P	A	L	K	D	G	-	D	F	T	L	T	E	S	V	A	I	L	L	Y	L	T	R	K	Y	K
AH004172.1	Omega	*H.sapiens*	1	72	V	P	V	L	E	N	S	Q	G	Q	L	I	Y	E	S	A	I	T	C	E	Y	L	D	E	A	Y	P
CAC94005.1	Tau	*T.aestivum*	1	59	V	P	V	L	I	H	N	-	G	R	P	V	C	E	S	L	L	I	L	E	Y	L	D	D	A	V	G
CAD29575.1	Phi	*T.aestivum*	1	55	I	P	A	F	Q	D	G	-	D	L	L	L	F	E	S	R	A	I	A	R	Y	V	L	R	K	Y	K
P15214	Beta	*P.mirabilis*	1	52	V	P	V	L	Q	L	D	N	G	D	I	L	T	E	G	V	A	I	V	Q	Y	L	A	D	L	K	P
NP_611323.1	Epsilon	*D.melanogaster*	1	57	V	P	M	L	D	D	N	-	G	T	F	I	W	D	S	H	A	I	A	A	Y	L	V	D	K	Y	A
A37378	Pi	*H.sapiens*	1	53	L	P	K	F	Q	D	G	-	D	L	T	L	Y	Q	S	N	T	I	L	R	H	L	G	R	T	L	G
NP_665683.1	Alpha	*H.sapiens*	1	55	V	P	M	V	E	I	D	-	G	M	K	L	V	Q	T	R	A	I	L	N	Y	I	A	S	K	Y	N
P46088	Sigma	*O.sloani*	1	51	M	P	V	L	D	I	D	-	G	T	K	M	S	Q	S	M	C	I	A	R	H	L	A	R	E	F	G
NP_000552	Mu	*H.sapiens*	1	60	L	P	Y	L	I	D	G	-	A	H	K	I	T	Q	S	N	A	I	L	C	Y	I	A	R	K	H	N
O43708	Zeta	*H.sapiens*	1	59	V	P	T	L	K	I	D	-	G	I	T	I	H	Q	S	L	A	I	I	E	Y	L	E	E	T	R	P

Figure 1 Newly identified extension of an electron-sharing network in adGSTD3-3

The electron-sharing network is an ionic interaction between negatively charged and positively charged residues stabilized by a network of hydrogen-bonds. The stereo view of corresponding three-dimensional structure of the electron-sharing network is shown in the upper panel. The lines show the putative electron movement pathway with distances between 2.5 and 3.0 Å. The lower panel shows the sequence alignment of amino acid residues in Delta, Theta, Omega, Tau, Phi, Beta, Epsilon, Pi, Alpha, Sigma, Mu and Zeta class GSTs. The newly identified functionally conserved glutamate, aspartate and glutamine in the electron-sharing network are identified by an arrow.

bridge interaction between the negatively charged glutamyl α-carboxylate of GSH, a positively charged residue and a negatively charged residue, forming a resonance motif stabilized by a network of hydrogen-bonds with surrounding residues. The network is distributed among multiple interacting amino acids that collectively provide a network function. This conserved motif's contribution to the base-assisted deprotonation is essential for the GSH ionization step of catalysis.

The functionally conserved glutamate residue, Glu^{64} in adGSTD3-3 (*Anopheles dirus* GST Delta class homodimer of subunit 3) is located in the same region as the electron-sharing network (Figure 1). Initial characterization of the electron-sharing network has provided further insight into this motif [25]. The carboxylic group of Glu^{64} interacts directly with the glutamyl α-amino group of GSH. Moreover, by observing the configuration of the GSH glutamyl α-carboxylate, the GSH glutamyl α-amino, Glu^{64} and the electron-sharing network, it is now possible to extend this conserved motif, which is maintained in all GSTs. The aim of the present paper was to ascertain the validity of Glu^{64} function in the electron-sharing network. We have observed previously [25] that alanine replacement of Glu^{64} caused the enzyme to be expressed in an insoluble form. This suggested that Glu^{64} is a critical residue involved in tertiary structure or initial folding of the enzyme. Therefore the contribution of this residue to structural maintenance and initial folding was also examined. The results of the present paper indicate that Glu^{64} is a part of the functionally conserved electron-sharing network and has roles both in catalysis as well as structural folding and maintenance.

MATERIALS AND METHODS

Site-directed mutagenesis

The plasmid pET3a-adgstD3, described previously [26], was used as the template to generate the single point mutations via PCR-based site-directed mutagenesis. The functionally conserved active-site residue Glu^{64} was replaced by an alanine, leucine, valine, lysine, glutamine, asparagine or aspartate residue by using

PCR primers based on the wild-type *adgstD3* gene sequence (Genbank accession number AF273039). Mutants were screened randomly by restriction enzyme digestion analysis. Mutant plasmids could be distinguished from the wild-type template by digestion with restriction enzymes corresponding to the restriction recognition site introduced by the mutagenic primers. The full-length GST coding sequence carrying E64A, E64L, E64V, E64K, E64Q, E64D and E64N mutations were verified by the dideoxy chain termination method.

Heterologous expression and purification

The proteins were expressed from the pET3a-adgstD3 vector in *Escherichia coli* BL21 (DE3) pLysS cells. The cells were grown to $D_{600} = 0.5$ and expression was induced by addition of 0.1 mM isopropyl β-D-thiogalactoside. Following a 3 h induction, cells were collected by centrifugation at 10000 ***g*** for 20 min at 4 °C and lysed by sonication using an Ultrasonic processor XL (Misonix) at power level 3 for 10 s, paused for 1 min and repeated three times at 4 °C. The soluble recombinant GST proteins were purified by GSTrap™ affinity chromatography (Amersham Biosciences) or *S*-hexylglutathione agarose (Sigma–Aldrich) affinity chromatography. The protein concentration was determined by the Bradford method [27] using BSA as a standard.

Steady-state kinetics

Steady-state kinetics were studied for wild-type and mutant enzymes at varying concentrations of CDNB (1-chloro-2,4-dinitrobenzene) and GSH in 0.1 M phosphate buffer pH 6.5. The reaction was monitored at 340 nm, ε 9600 $M^{-1}cm^{-1}$. Apparent kinetic constants, k_{cat}, K_m and k_{cat}/K_m were determined by fitting the collected data to a Michaelis–Menten equation by non-linear regression analysis using GraphPad Prism (GraphPad software).

pH dependence of kinetic constants

The pH dependence of k_{cat}/K_m^{CDNB} was obtained as stated above by recording the enzymatic reaction in the following buffers: 0.1 M sodium acetate buffers (from pH 5.0 to 5.5) and 0.1 M potassium phosphate buffer (from pH 6.0 to 8.5). The pH was altered in increments of 0.5, and control experiments showed no discontinuities from buffer types. pK_a values were obtained by fitting the data to eqn (1) [20]:

$$y = y_{lim}/(1 + 10^{pKa-pH}) \quad (1)$$

Fluoride/chloride leaving group replacement

The second order kinetic constants at pH 6.5 for the spontaneous reaction of GSH with CDNB and FDNB (1-fluoro-2,4-dinitrobenzene) and the catalytic-centre activities at pH 6.5 for adGSTD3-3 with CDNB and FDNB as co-substrates were obtained as described previously [28].

Viscosity effect on the kinetic parameters

The effect of viscosity on kinetic parameters was obtained by using 0.1 M potassium phosphate buffer pH 6.5 with various glycerol concentrations. Viscosity values (η) at 25 °C were calculated as described previously [29].

Structural studies

A Jasco J-714 spectropolarimeter was used for CD measurements in the far-UV region from 190–260 nm. Spectra were recorded using 0.3 mg/ml of protein in 2-mm path length cuvettes. Intrinsic fluorescence emission spectra were measured with a Jasco FP-6300 spectrofluorimeter. The excitation wavelength was 295 nm and the λ_{max} and the fluorescence intensity of emission spectra were analysed at a protein concentration of 0.2 mg/ml.

Kinetics of thermal denaturation

Heat inactivation of the wild-type and Glu[64] mutant enzymes was monitored at different temperatures. Enzymes (40 μM) were incubated in 0.1 mM potassium phosphate buffer pH 6.5, 1 mM EDTA and 5 mM DTT (dithiothreitol). The inactivation time-courses were determined by withdrawing suitable aliquots at different time points to assay the remaining activity using the first time point as 100 % native protein. An equation describing a single exponential decay with a rate constant of thermal unfolding k_u was fitted to the data according to eqn (2) [30]:

$$-\ln(\%\text{native}/100\%) = k_u t \quad (2)$$

The free-energy of activation of thermal unfolding (ΔG_u) was calculated according to Eyring theory as eqn (3) [30]:

$$\ln k_u = \ln\frac{K k_b T}{h} - \frac{\Delta G_u}{RT} \quad (3)$$

where k_b is the Boltzmann constant; T, absolute temperature Kelvin; h, Plank's constant; R, the gas constant; and K is the transmission factor, which was set to unity. The difference of free-energy of activation of the thermal denaturation between wild-type (wt) and each mutant (mut) protein ($\Delta\Delta G_u$) was calculated according to eqn (4) [30]:

$$\Delta\Delta G_u = \Delta G_u^{wt} - \Delta G_u^{mut} = -RT \times \ln\left(k_u^{wt}/k_u^{mut}\right) \quad (4)$$

Substitution of Equation 5:

$$\Delta G_u = \Delta H_u - T\Delta S_u \quad (5)$$

into eqn (3) yields eqn (6):

$$\ln\frac{k_u}{T} = \ln\frac{K \times k_b}{h} - \frac{\Delta H_u}{R} \times \frac{1}{T} + \frac{\Delta S_u}{R} \quad (6)$$

Both activation enthalpy ΔH_u and entropy ΔS_u were determined from the temperature dependence of k_u.

Temperature dependence of refolding *in vitro*

The *in vitro* refolding of the wild-type and Glu[64] mutant enzymes were monitored at different temperatures. Enzyme (20 μM) was first denatured in 4 M GdmCl (guanidinium chloride) in renaturation buffer (0.2 M potassium phosphate buffer, 1 mM EDTA and 5 mM DTT, pH 7.0) at room temperature (25 °C) for 30 min and then rapidly diluted (defining time 0) 1:40 (v/v) into renaturation buffer at 18, 25 and 33 °C. The final GdmCl concentration was 0.1 M during refolding. All refolding experiments were carried out by rapid addition of the denatured enzyme to renaturation buffer. The recovery of activity of the proteins was monitored as a function of time by withdrawal of appropriate aliquots of the renaturation mixture and immediately assaying for activity at 25 °C. Refolding rate constants were determined by nonlinear regression analysis of the experimental data by using SigmaPlot 2001 for Windows version 7.0 (SPSS). The refolding rates of all variants were independent, in the range 10 to 30 μM, of the protein concentration. At greater enzyme concentrations all

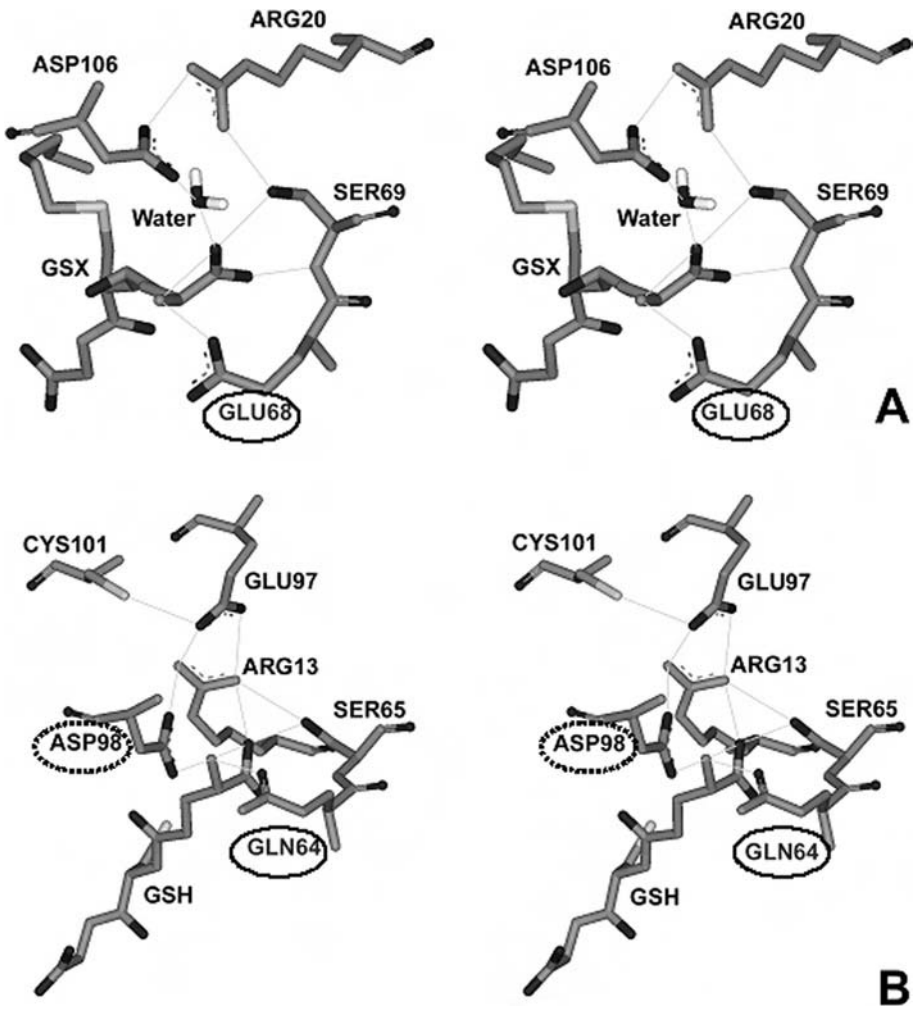

Figure 2 Stereo views of examples of electron-sharing networks for type I (A) and type II (B) of GSTs

Categorization is based on properties of the equivalent amino acid at position 64 and configuration of the electron-sharing network. (**A**) Electron-sharing network type I is composed of only one conserved acidic amino acid (circled), which forms an ionic interaction. Wheat Tau GSTI (PDB accession number 1GWC). (**B**) Electron-sharing network type II contains two strictly conserved polar and acidic residues (circled by solid and dotted lines respectively), which participate in an ionic bridge interaction. Human Pi hGSTP1-1 (PDB accession number 1PKW).

variants were characterized by reduced refolding yield. The values reported represent the means for three different experimental data sets. Under these conditions, an equation describing a single exponential reaction can be fitted to the data:

$$F(\mathrm{t}) = A[1 - \exp(-k_{\mathrm{ref}})] + B \quad (7)$$

where $F(\mathrm{t})$ is the activity at time t; A, the amplitude; k_{ref}, the rate constant; and B, the reactivation value at time 0 [31]. The effect of mutation on the energy of the transition state of folding can be calculated using transition-state theory in a similar manner to that reported by Jackson et al. [32]. The stability of the transition state of a mutant protein relative to that of the wild-type is calculated from:

$$\Delta\Delta G_{\mathrm{ref}} = -RT \times \ln\left(k_{\mathrm{ref}}{}^{\mathrm{wt}} / k_{\mathrm{ref}}{}^{\mathrm{mut}}\right) \quad (8)$$

where $\Delta\Delta G_{\mathrm{ref}}$ is the difference in energy of the transition state of folding relative to the unfolded state between wild-type (wt) and mutant (mut) proteins and k_{ref}, the rate constants of refolding [32].

RESULTS AND DISCUSSION

A functionally conserved electron-sharing network can be observed in the same region for all GSTs, but with slightly different residue positions [22]. However, a primary sequence alignment of the known GST classes suggests that Glu^{64} is one of a few residues that is functionally conserved in the GST superfamily. Observation of available crystal structures; adGSTD3-3, hGSTP1-1 (human Pi GST1), hGSTA1-1 (human Alpha GST1), rGSTM1-1 (rat Mu GST1), hGSTO1-1 (human Omega GST1), hGSTT2-2 (human Theta GST2), squid Sigma GST and wheat Tau GST, as well as consideration of the property of the equivalent residue at position 64, acidic or polar, suggests that the GST electron-sharing motif can be divided into two types (Figure 2). Electron-sharing network type I, consisting of GSTs from Delta, Theta, Omega, Pi and Tau classes, contain an acidic amino acid (glutamate or aspartate) at this position. The equivalent residue is the only amino acid in an acceptable distance range to form an ionic interaction between its own negatively charged side chain and the positively charged GSH glutamyl α-amino (Figure 2A). On the other hand, electron-sharing network type II GSTs from the Alpha, Mu, Pi and Sigma classes have a polar amino acid (glutamine) side-chain

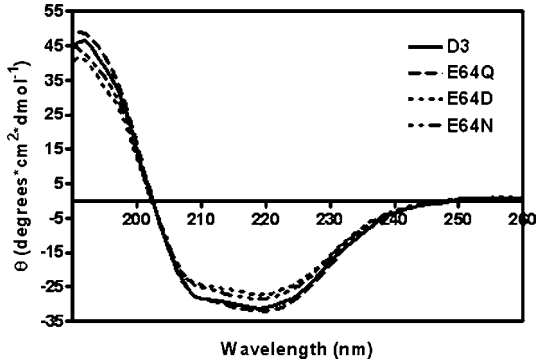

Figure 3 Far-UV CD spectra of adGSTD3-3 and mutants

CD spectra were measured in far-UV region from 190–260 nm. Spectra were recorded at a protein concentration of 0.3 mg/ml with cuvettes with a 2-μm path-length. D3, wild-type adGSTD3-3.

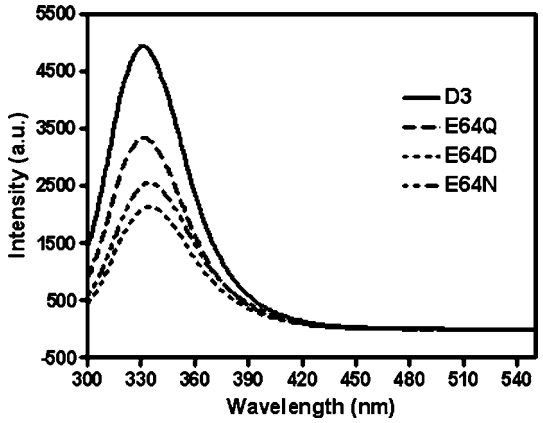

Figure 4 Intrinsic fluorescence spectra of wild-type and mutant adGSTD3-3

Intrinsic fluorescence emission spectra were measured with the excitation wavelength 295 nm. The λ_{max} and the fluorescence intensity of emission spectra were analysed at a protein concentration of 0.2 mg/ml. The λ_{max} are 331 nm for wild-type (D3), 332 nm for E64Q, 335 nm for E64D and 334 nm for E64N. The intensity is shown in arbitrary units. The results are means $\pm$ S.D. for experiments performed in triplicate.

that interacts directly with the GSH glutamyl α-amino. In addition, type II networks have a strictly conserved acidic amino acid (Asp[98] in the Pi class, Asp[101] in the Alpha class, Asp[105] in the Mu class and Asp[97] in the Sigma class) that participates in an ionic interaction (Figure 2B). In the Pi class GSTs, replacement of this acidic residue (Asp[98] with asparagine) was shown to increase the pK_a for GSH by approx. 0.5 pH unit [33]. These results suggest the importance of a negative charge involvement with the positively charged GSH glutamyl α-amino to fulfil the function of the electron-sharing network in the ionization process [33]. Dividing the electron-sharing network into two types is supported by studies of binding, activation and ionization of GSH, including the fate of the thiol proton in Pi, Alpha, Mu and Delta class GSTs [23]. It has been reported that GST classes Pi, Alpha and Mu, which are classified as electron-sharing network type II GSTs, display similarities in the multi-step mechanism for binding of the substrate and also yield a similar fate for the thiol proton. The Delta class GST, which we propose belongs to electron-sharing network type I, shows a difference in proton extrusion that implies a different activation mechanism for GSH. Moreover, the modality of proton output is also preserved in Pi, Alpha and Mu class enzymes. This mechanistic difference suggests that Delta GST is distantly related to Pi, Alpha and Mu GSTs in evolutionary terms.

To investigate the role of the functionally conserved Glu[64] residue in adGSTD3-3, this residue was replaced with seven amino acids; alanine, leucine, valine, lysine, glutamine, aspartate or asparagine. Evidence suggested that the replacements were temperature-sensitive therefore protein expression was performed at 18, 25 and 37 °C. The E64A, E64L, E64V and E64K mutants were expressed as insoluble proteins at all temperatures. Attempts at refolding these four proteins were unsuccessful. The yields of the E64Q, E64D and E64N mutants were less than wild-type and clearly decreased with increasing temperature (results not shown). This probably reflects the fact that the E64Q, E64D and E64N molecules fail to achieve the native folding at near physiological temperatures. Therefore, proteins expressed at the more permissive temperature of 18 °C were utilized in this study.

In the present study, a structural role for Glu[64] for stability and folding was examined. The similarity of the far-UV CD spectra of all the Glu[64] mutants indicated that the secondary structure content of the proteins are essentially unaffected by the mutations (Figure 3). The intrinsic fluorescence spectra show differences between the wild-type and all of the Glu[64] mutants (Figure 4). The spectra of the Glu[64] mutants were slightly red-shifted compared with the wild-type protein (λ_{max} at 331 nm) to give a λ_{max} at 332 nm for E64Q, 335 nm for E64D and 334 nm for E64N. The normalized intensities of the fluorescence of the mutants were slightly less than that of the wild-type. Changes in amino acid side-chains around Trp[63] resulted in an alteration in fluorescence intensity, and a red-shifted spectrum is observed as the protein unfolds to random coil [34]. Consequently, the differences in both λ_{max} and fluorescence intensity suggest that the mutation of Glu[64] causes the tryptophan residue to be more exposed to the solvent. Heat inactivation of wild-type and Glu[64] mutants was performed at different temperatures (Figure 5). Furthermore, the E64Q and E64N mutants were much more unstable than the wild-type or E64D mutant. It is important to note that the single Glu[64] replacement with polar residues (glutamine and asparagine) became unstable at a lower temperature than the negatively charged residues (wild-type and E64D) and their inactivation generated the formation of protein aggregates under the experimental conditions used. Thermal denaturation of all variants was irreversible, showing that inactivation kinetics could not be used to determine thermodynamic parameters at equilibrium. However, making use of the temperature dependence of the unfolding rate, the application of Eyring formalism provides the thermodynamic parameters of the activation barrier of the thermal denaturation [30]. The heat inactivation of all variants is described by straight lines in an Eyring plot. This indicates that the temperature dependence of both the unfolding activation enthalpy (ΔH) and activation entropy (ΔS) is negligible. The temperature dependence of ΔG is reflected in the slope of the linear fit, dependent on ΔH. Table 1 summarizes the kinetic and thermodynamic constants for the activation barrier of thermal denaturation for the wild-type and Glu[64] mutant enzymes. The large energy changes of Glu[64] mutants compared with the wild-type ($\Delta\Delta H$) are almost completely compensated for by an accompanying reduction in ΔS (that is, $\Delta\Delta S$). At 42 °C, this corresponds to lower values of the unfolding free-energy for all the Glu[64] mutant enzymes ($\Delta\Delta G$). The Glu[64] mutants were remarkably more destabilized than the wild-type enzyme, especially for the polar amino acids glutamine and asparagine (Table 1). This corresponds to an unfolding free-energy difference ($\Delta\Delta G$) for the polar amino acid replacements compared with the wild-type, being greater

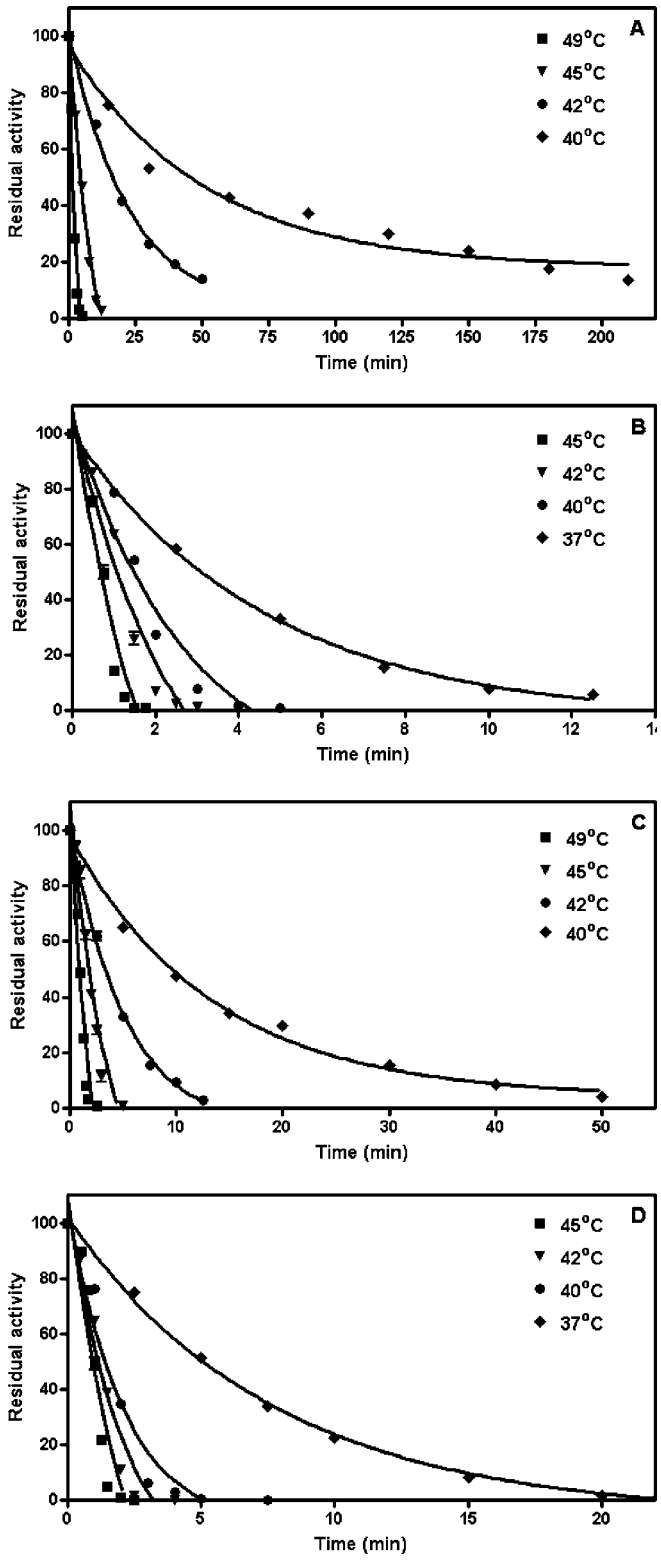

Figure 5 Thermal stability of wild-type adGSTD3-3 (A), E64Q (B), E64D (C) and E64N (D) mutants at different temperatures

Each enzyme (40 μM) was incubated at various temperatures in 0.1 M potassium phosphate buffer, pH 6.5, 1 mM EDTA and 5 mM DTT. Appropriate aliquots from an incubation mixture were assayed at 25 °C to monitor residual activity. The lines represent fits according to eqn (2), as described in the Materials and methods section.

than with the acidic residue aspartate. The Gibbs free-energy for the unfolding process of wild-type and Glu^{64} mutants were comparable, with general estimations of Gibbs free-energy for small globular proteins based on the summation of increments of the different stabilizing forces that give values in the range 42–84 kJ/mol [35]. Due to the large decrease in activation enthalpy ($\Delta\Delta H$, 131–220 kJ/mol), the destabilizing effects of the Glu^{64} mutants were clearly significant to the structural properties of the enzymes. In addition the magnitude of $T\Delta\Delta S$ at 42 °C, which is the energy difference from decreases in the entropy of the thermal unfolding pathway (198.4, 126.0 and 211.0 kJ/mol for E64Q, E64D and E64N respectively), indicates that major changes in the conformational freedom characterizes the denaturation of the wild-type protein compared with those occurring during the thermal inactivation of the Glu^{64} mutants [36]. This means that the wild-type adGSTD3-3, because it is more rigid than the Glu^{64} mutants, tolerates larger perturbations of its structure before the unfolding transition state is reached. The replacement of polar amino acids, both glutamine and asparagine, give greater values of all thermodynamic constants than for the acidic amino acids glutamate and aspartate. This data suggests that the negatively charged residue forming an ionic bridge interaction in this position plays an essential role for the overall stability of the protein. Recent studies proposed that Glu^{64} is a critical residue involved in the determination of the direction of the polypeptide chain during folding [25]. One consequence of replacing Glu^{64} with other amino acid residues results in a completely impaired folding property (for E64A, E64L, E64V and E64K) or temperature-sensitive folding (for E64Q, E64D and E64N). To test this hypothesis, reactivation yields of adGSTD3-3 and its mutants at different temperatures were determined. The denaturant 4 M GdmCl was sufficient to completely unfold 20 μM enzyme, as shown by CD spectrum (results not shown). The reactivation yields of the Glu^{64} mutants were very different from the wild-type protein at increasing temperatures of refolding (Table 2 and Figure 6). The reactivation yield of the wild-type enzyme was unaffected by temperatures from 18–33 °C, whereas the yield of the mutants, although to different extents, decreased markedly with increasing temperature. All data sets were fit to a single exponential equation for the refolding kinetics (Figure 6). At each temperature, as shown in Table 2, the temperature-dependent refolding rates show a similar tendency in the wild-type and Glu^{64} mutants that was expected, that is, the enzymes refold at higher temperature more rapidly than at lower temperature. The refolding rates of both E64Q and E64D mutants were slightly different from the wild-type at all temperatures. These differences in refolding rates reflect changes in free-energy of activation of folding for a mutation. Estimated free-energy values ($\Delta\Delta G_{ref}$) at 18 °C that were significantly different from zero indicate that interactions of the residue at position 64 toward neighbouring residues are present in the transition state of the reactivation process. The *in vitro* refolding experiments suggest that the thermal stability of the final structure of the mutants reflects differences in the conformational properties of a productive folding intermediate. Reactivation *in vitro* of all Glu^{64} mutants was thermosensitive, and so the refolding yields of the Glu^{64} mutants, although to different extents, decreased markedly with increasing temperature. The analysis of the reactivation at 18 °C indicates that amino acid replacement of Glu^{64} destabilizes the transition of folding. It should be noted that a single exponential equation could be fitted to refolding data for all adGSTD3-3 variants indicating that no significant amount of intermediate is accumulated during the reactivation of wild-type and variants, and that none of the mutations had a major change on the refolding pathway. Upon

Table 1 Kinetic and thermodynamic parameters for the activation barrier of thermal denaturation for wild-type and Glu^{64} mutants of adGSTD3-3

Enzyme	k_u (min^{-1})	$k_u/k_{u,wt}$*	ΔG_u* (kJ/mol)	$\Delta\Delta G_u$ (kJ/mol)	ΔH_u† (kJ/mol)	$\Delta\Delta H_u$† (kJ/mol)	ΔS_u† (kJ/mol · K)	$\Delta\Delta S_u$† (kJ/mol · K)
Wild-type	0.040 ± 0.001	1	85.69 ± 0.09	0	439.00 ± 4.90	0	1.120 ± 0.015	0
E64Q	1.583 ± 0.028	39.58	76.08 ± 0.05	9.63	231.38 ± 13.02	207.62	0.490 ± 0.041	0.630
E64D	0.256 ± 0.008	6.40	80.85 ± 0.08	4.86	307.51 ± 1.28	131.49	0.720 ± 0.004	0.400
E64N	1.590 ± 0.045	39.75	76.07 ± 0.08	9.64	218.52 ± 10.92	220.48	0.450 ± 0.035	0.670

* From denaturation kinetics at 42 °C according to eqns 2 and 4.
† From temperature dependence of thermal unfolding (Eyring plot) according to eqn 6.

Table 2 Kinetics of the reactivation and percentage recovery of wild-type adGSTD3-3 and Glu^{64} mutants during refolding at different temperatures and changes in free energy of the transition state of folding at 18 °C

Statistics performed using one-way ANOVA and Tukey–Kramer multiple comparisons test. Values significantly different from wild-type are shown by * $P < 0.001$. Nd, not determined, low enzymatic activity precluded performing this experiment.

	18 °C		25 °C		37 °C		
Enzyme	k_{ref} (min^{-1})	% recovery	k_{ref} (min^{-1})	% recovery	k_{ref} (min^{-1})	% recovery	$\Delta\Delta G_{ref}$ at 18 °C (kJ/mol)
Wild-type	0.169 ± 0.020	60.9 ± 0.4	0.518 ± 0.053	35.1 ± 3.4	0.957 ± 0.027	35.1 ± 0.6	0
E64Q	0.074 ± 0.003	63.8 ± 0.7	0.289 ± 0.004	40.0 ± 0.3	1.073 ± 0.124	10.6 ± 0.3	−1.987 ± 0.371*
E64D	0.059 ± 0.005	93.0 ± 6.5	0.242 ± 0.024	57.7 ± 1.1	0.981 ± 0.030	34.5 ± 1.3	−2.521 ± 0.129*
E64N	Nd	Nd	Nd	Nd	Nd	Nd	Nd

mutation of adGSTD3-3, rate constants decreased for all mutants (Table 2). This is because the removal of the negative charge or size decrease of the side-chain at this position destabilized the transition state and thereby increased the activation energy for folding. In particular, the $\Delta\Delta G_{ref}$ value for E64D is greater than E64Q, suggesting that the functional group size is important for the Glu^{64} position, which contributes to stabilizing the transition state. Previous investigations of the equivalent residue, Glu^{66}, in PtGSTU1-1 (plant Tau class GST) demonstrated that alanine replacement made the enzyme unstable at 50 °C, retaining only about 15 % of its activity compared with 95 % for the wild-type enzyme [37]. In contrast, the reactivation yield of E66A was 2-fold greater than the wild-type. The effect of the mutation at this equivalent residue in PtGSTU1-1 was less than found in adGSTD3-3, an insect Delta class GST. This result might be explained by data for Glu^{64} in adGSTD4-4, an alternatively spliced product derived from the same gene as adGSTD3-3. Glu^{64} is not only located at the dimeric interface of the enzyme, but has also been identified as a 'lock' residue in the Delta class specific 'lock-and-key clasp' motif, which is not found in plant Tau class GST [38]. The lock-and-key motif, including the Delta class specific lock-and-key clasp motif, is located at the intersubunit interface and plays a crucial role in the structural stability of dimeric GSTs [39,40]. These data therefore confirm a critical structural role for the functionally conserved Glu^{64} residue for both overall protein stability and initial folding process.

Steady-state kinetic constants were obtained with various concentrations of GSH and CDNB substrate. Michaelis–Menten kinetic analysis was performed using non-linear regression (Table 3). All of the mutations showed significantly increased K_m values for GSH. Individually, the mutants; E64Q, E64D and E64N had values 26-, 34- and 29-fold greater than wild-type. Conversely, no significant changes were found in the K_m values for CDNB substrate when compared with the wild-type enzyme. The differences in k_{cat} values with CDNB observed for E64D and E64N decreased approximately 1.5- and 25-fold respectively. The kinetic studies of soluble Glu^{64} mutant enzymes demonstrated that replacement with a glutamine residue, a similar size and property functional group, preserved the catalytic activity, whereas replacement with the slightly smaller amino acids aspartate and asparagine reduced k_{cat}, especially the arparagine replacement, which nearly abolished enzyme activity. This suggests that the volume of the amino acid at this position affects packing of the active-site, which directly impacts upon enzyme catalysis. However, all the mutants showed a substantially lower affinity (greater K_m) towards GSH indicating that the Glu^{64} position impacts upon the binding of GSH possibly through active-site rearrangement. Catalytic efficiency can be related to the difference in free-energy change for formation of transition states in the mutant and wild-type enzymes ($\Delta\Delta G$), as calculated from eqn (9) [41]:

$$\Delta\Delta G = -RT \times \ln\left(k_{cat}/K_m^{GSH}\right)_{mut}/\left(k_{cat}/K_m^{GSH}\right)_{wt} \quad (9)$$

These calculated values are 8.03 kJ/mol for E64Q, 9.94 kJ/mol for E64D and 16.33 kJ/mol for E64N at 25 °C, indicative of a decreased stabilization of the transition state for the Glu^{64} mutations. Stabilization of the transition state may occur through a pre-organized active-site contributing to catalysis through multiple mechanisms: binding interaction with GSH, activation of GSH by thiol deprotonation or nucleophilic attack at the electrophilic centre (σ-bond formation) by the thiolate. Deficiency in the pre-organized environment (the changes that occur along the reaction pathway from reactants to the transition state) would decrease the rate of catalysis by incompletely providing a stabilization of the transition state [42]. Therefore, the effect on the rate-limiting step in the catalytic mechanism was examined. The pH dependence of k_{cat}/K_m^{CDNB} reflects a kinetically relevant ionization of the GST–GSH complex. Therefore, an apparent pK_a value of 6.36 was determined for the wild-type adGSTD3-3. To differentiate the influence of the functional group of Glu^{64} on the GSH thiol ionization, the pK_a values for Glu^{64} mutants were measured by this kinetic approach (Table 3). An increased pK_a for bound GSH of approx. 0.6 and 1 pH unit greater than that found for wild-type were observed for the E64Q and E64N mutants. It has been shown previously that a crucial function of the electron-sharing

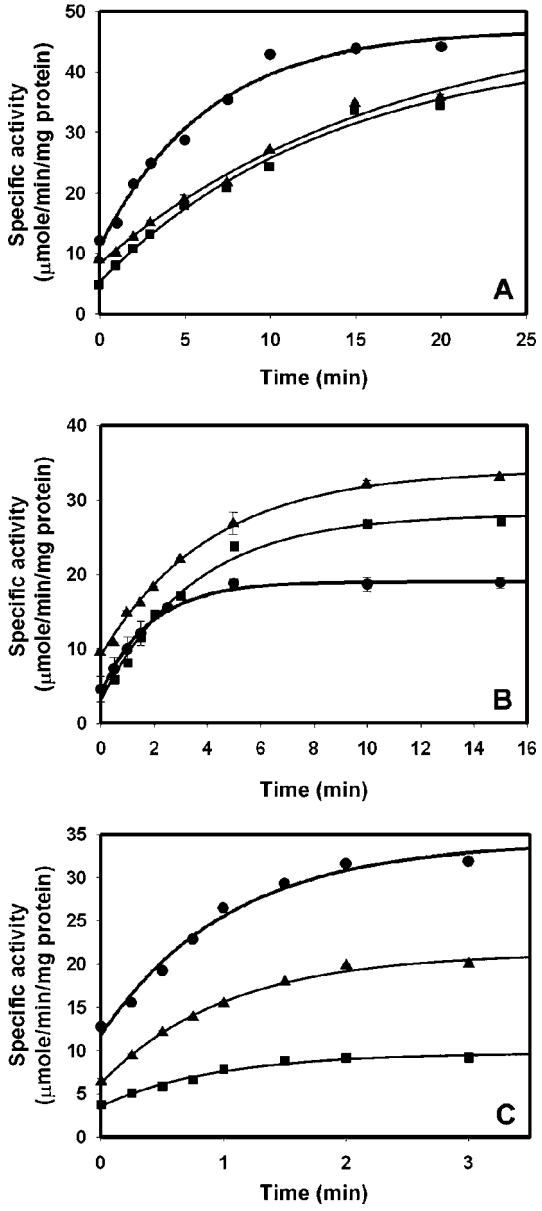

Figure 6 Kinetics of reactivation of wild-type adGSTD3-3 (●), E64Q (■) and E64D (▲) during refolding at different temperatures: 18 °C (A), 25 °C (B) and 33 °C (C)

Purified enzyme (20 μM), heterologously expressed at 18 °C, was first denatured in 4 M GdmCl for 30 min. This denaturant concentration was sufficient to completely unfold the proteins, as indicated by the loss of secondary structure shown by CD. Successive aliquots of unfolded enzyme were diluted (defining time 0) 1:40 into renaturation buffer at the different temperatures. The final GdmCl concentration was 0.1 M during the refolding. Appropriate aliquots from this incubation mixture were immediately assayed for catalytic activity at 25 °C.

network is to lower the pK_a of the thiol group of the bound GSH [22]. Our results show that Glu^{64} replacement with the polar amino acids glutamine and asparagine increased the pK_a values by about 0.5–1.0 pH unit. This consequence appears to be due to the deletion of the negative charge, resulting in loss of ionic interaction within the electron-sharing network. This is supported by the replacement of the critical glutamate residue with the negatively charged aspartate, which has no affect on the ionization process. Therefore, an acidic amino acid in this position is essential to form an ionic interaction to fulfil the function of the electron-sharing network in the ionization process. However, the formation of a σ-complex intermediate in the enzyme-catalysed reaction was affected by the replacement with glutamine and aspartate. It is well established that the bimolecular nucleophilic substitution reactions proceed through a σ-complex intermediate [43]. Thus, the rate-limiting formation of a spontaneous σ-complex intermediate can be increased by replacement of chlorine in the CDNB molecule with the more electronegative fluorine. The ratio of the catalytic rate of GSH with FDNB and CDNB was comparable to the ratio of the second-order rate constants for a spontaneous uncatalysed reaction. That is, $k_{cat}^{FDNB}/k_{cat}^{CDNB} = 40$ is similar to $k_c^{FDNB}/k_c^{CDNB} = 47$, which indicates that the σ-complex formation is the rate-limiting step. Although the $k_{cat}^{FDNB}/k_{cat}^{CDNB}$ of all Glu^{64} mutants reflected varying insensitivity to the nature of the leaving group, there were two mutants E64Q and E64D that exhibited significant differences in the catalytic efficiency (k_{cat}/K_m) (Table 4). For the E64N mutant, it appears that an alteration of the relative turn-over number is a consequence of changes in binding affinity towards different substrate leaving groups rather than a reflection of the rate of σ-complex formation. Differences in relative catalytic efficiency (k_{cat}/K_m) for the fluoride/chloride leaving group replacement may not strongly support the idea that the rate-determining step to σ-complex formation for E64Q and E64D was changed. Although it appears that transition state stability of the enzyme–intermediate complex, influenced by electron density and distribution in the σ-complex, was partially altered by these two amino acid replacements [43,44].

Table 3 Steady-state kinetic constants and pK_a values for the thiol group of GSH of wild-type and mutants of adGSTD3-3 for the CDNB conjugation reaction at pH 6.5 and 25 °C

The enzyme activities were measured at various concentrations of CDNB and GSH in 0.1 M phosphate buffer pH 6.5. The pK_a was obtained by using 0.1 M sodium acetate buffers (from pH 5.0 to 5.5) and 0.1 M potassium phosphate buffer (from pH 6.0 to 8.5).The reaction was monitored at 340 nm, ε 9600 $M^{-1}cm^{-1}$. Statistics were performed using one-way ANOVA and Tukey–Kramer multiple comparisons test. Values significantly different from wild-type are shown by * $P < 0.001$. The wild-type values have been reported previously [25].

Enzyme	k_{cat} (s^{-1})	K_m^{GSH} (mM)	K_m^{CDNB} (mM)	k_{cat}/K_m^{GSH} (s^{-1}/mM)	k_{cat}/K_m^{CDNB} (s^{-1}/mM)	pK_a
Wild-type	35.4	0.27 ± 0.05	0.14 ± 0.01	131	246	6.36 ± 0.11
E64Q	36.3	7.10 ± 0.28*	0.43 ± 0.03	5.11	83.6	6.97 ± 0.14*
E64D	21.6	9.12 ± 0.20*	0.28 ± 0.01	2.37	75.8	6.42 ± 0.12
E64N	1.4	7.89 ± 0.19*	0.33 ± 0.01	0.18	4.4	7.37 ± 0.07*

Table 4 Effect of fluoride/chloride leaving group substitution on the rate of catalysis

The ratios of kinetic constants for the conjugation reaction catalyzed by adGSTD3-3 enzymes for GSH with CDNB or FDNB as co-substrates were calculated at pH 6.5. Statistics performed using one-way ANOVA and Tukey–Kramer multiple comparisons test. Values significantly different from wild-type are shown by * $P < 0.001$. The wild-type values have been reported previously [25].

Enzyme	$k_{cat}^{FDNB}/k_{cat}^{CDNB}$	$(k_{cat}/K_m)^{FDNB}/(k_{cat}/K_m)^{CDNB}$
Wild-type	2.40 ± 0.08	6.72 ± 0.34
E64Q	6.97 ± 0.24*	14.36 ± 1.22*
E64D	8.40 ± 0.08*	10.31 ± 0.38*
E64N	5.92 ± 0.05*	6.58 ± 0.05

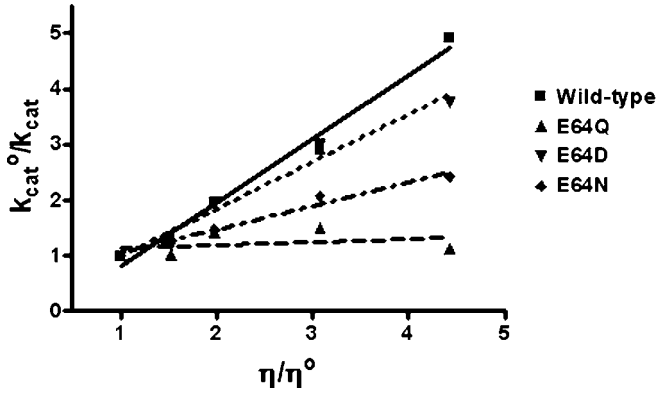

Figure 7 Viscosity effect on kinetic parameters of wild-type adGSTD3-3 and mutant enzymes

The effect of viscosity on kinetic constants was assayed by using 0.1 M potassium phosphate buffer, pH 6.5, with various glycerol concentrations. Dependence of the reciprocal of the relative turn-over number (k_{cat}^{o}/k_{cat}) on the relative viscosity (η/η^{o}) for CDNB as a co-substrate. The experiment was performed in triplicate and the lines were calculated by linear regression analysis. The slopes of the linear regression lines are 1.14 ± 0.01 for wild-type, 0.05 ± 0.01 for E64Q, 0.85 ± 0.01 for E64D and 0.42 ± 0.02 for E64N.

The effect of viscosity on kinetic parameters was examined to elucidate the rate-limiting step in the catalytic reaction. A decrease in the rate constant with increasing medium viscosity should reflect the weight of diffusion events on catalysis [45]. It would indicate that the rate-limiting step is related to diffusion-controlled motions of the protein or the dissociation of the product. A plot of the reciprocal of the relative catalytic constant (k_{cat}^{o}/k_{cat}) against the relative viscosity (η/η^{o}) should be linear. The slope should be equal to unity when the product release or structural transition is limited by a strictly diffusional barrier. If the slope approaches zero either the chemistry or another non-diffusion barrier is rate-limiting. For wild-type adGSTD3-3, a plot of the inverse relative rate constant (k_{cat}^{o}/k_{cat}) versus the relative viscosity (η/η_{o}) gives a linear dependence with a slope (1.14 ± 0.01) very close to unity (Figure 7). In contrast the E64Q mutant enzyme yields plots that are fully viscosity independent, with a slope approaching zero (0.05 ± 0.01). The other mutants, E64D and E64N, exhibited k_{cat} values with different degrees of viscosity dependence compared with the wild-type enzyme. The viscosity experiment showed that the rate-limiting step catalysed by adGSTD3-3 is a non-physical step (Figure 7). However, structural alterations in the Glu[64] mutants decreased the viscosity effects on the enzyme to intermediate values ($0 < \text{slope} < 1$), especially for the replacement with the polar residues glutamine and asparagine. This indicates that the rate-limiting step is not strictly dependent on a diffusion barrier or other viscosity-dependent motions and that conformational changes of the engineered proteins contribute to the rate-limiting step [45]. This suggests that the structural flexibility of functionally important regions of the engineered enzymes have been altered. Previously, we have observed [22] that changing the residues in the electron-sharing network can influence the topology of the active-site, which affects both the catalytic mechanism as well as the structural maintenance of the enzyme. The results of the present study demonstrate that the functionally conserved Glu[64], which is now identified as being part of the electron-sharing network, impacts upon enzyme catalysis not only through its negative charge but also through structural effects.

In conclusion, the results of the present paper, as well as the high level of functional conservation of the residue at position 64 among all classes of GSTs supports the hypothesis that Glu[64] is part of a functionally conserved electron-sharing network. The present paper now extends the network identified previously to include three critical residues that form ionic bridge interactions. These are between a negatively charged/polar active site residue (glutamate, aspartate or glutamine), a positively charged GSH glutamyl α-amino, a negatively charged GSH glutamyl α-carboxylate, a positively charged active-site residue (primarily arginine) and a negatively charged active-site residue (glutamate or aspartate) stabilized by hydrogen-bonding networks with surrounding residues (serine, threonine and/or water mediated contact). Glu[64] in the electron-sharing network contributes to the function of this motif and the base-assisted deprotonation model which are essential for the GSH ionization process in the catalytic mechanism. However, this residue also appears to affect additional steps in the enzyme catalytic strategy including binding of GSH to the enzyme active site, nucleophilic attack by thiolate at the electrophilic centre and product formation. Therefore, the Glu[64] position also appears to impact upon catalysis through roles in both initial folding and structural maintenance.

This work was supported by the Thailand Research Fund. P.W. was supported by a Royal Golden Jubilee Scholarship and a scholarship from the Senior Research Fellowship of Professor Emeritus Sakol Panyim.

REFERENCES

1 Sheehan, D., Meade, G., Foley, V. M. and Dowd, C. A. (2001) Structure, function and evolution of glutathione transferases: implications for classification of non-mammalian members of an ancient enzyme superfamily. Biochem. J. **360**, 1–16
2 Cho, S.-G., Lee, Y. H., Park, H.-S., Ryoo, K., Kang, K. W., Park, J., Eom, S.-J., Kim, M. J., Chang, T.-S., Choi, S.-Y. et al. (2001) Glutathione *S*-transferase Mu modulates the stress-activated signals by suppressing apoptosis signal-regulating kinase 1. J. Biol. Chem. **276**, 12749–12755
3 Gate, L., Majumdar, R. S., Lunk, A. and Tew, K. D. (2004) Increased myeloproliferation in glutathione *S*-transferase π deficient mice is associated with a deregulation of JNK and janus kinase/STAT. J. Biol. Chem. **279**, 8608–8616
4 Ronai, Z. (2001) Coordinated regulation of stress kinases by GSTp. Chem. Biol. Interact. **133**, 285–286
5 Hayes, J. D. and Pulford, D. J. (1995) The glutathione S-transferase supergene family: regulation of GST and the contribution of the isoenzymes to cancer chemoprotection and drug resistance. CRC Crit. Rev. Biochem. Mol. Biol. **30**, 445–600
6 Mannervik, B. and Danielson, U. H. (1988) Glutathione transferases: structure and catalytic activity. CRC Crit. Rev. Biochem. **23**, 283–337
7 Armstrong, R. N. (1997) Structure, catalytic mechanism, and evolution of the glutathione transferases. Chem. Res. Toxicol. **10**, 2–18
8 Habig, W. H., Pabst, M. J. and Jakoby, W. B. (1974) Glutathione *S*-transferases. The first enzymatic step in mercapturic acid formation. J. Biol. Chem. **249**, 7130–7139
9 Ahmad, H., Wilson, D. E., Fritz, R. R., Singh, S. V., Medh, R. D., Nagle, G. T., Awasthi, Y. C. and Kurosky, A. (1990) Primary and secondary structural analyses of glutathione S-transferase π from human placenta. Arch. Biochem. Biophys. **278**, 398–408
10 Board, P., Baker, R. T., Chelvanayagam, G. and Jermiin, L. S. (1997) Zeta, a novel class of glutathione transferases in a range of species from plants to humans. Biochem. J. **328**, 929–935
11 Mannervik, B., Ålin, P., Guthenberg, C., Jensson, H., Tahir, M. K., Warholm, M. and Jörnvall, H. (1985) Identification of three classes of cytosolic glutathione transferase common to several mammalian species: correlation between structural data and enzymatic properties. Proc. Natl. Acad. Sci. U.S.A. **82**, 7202–7206
12 Mannervik, B., Awasthi, Y. C., Board, P. G., Hayes, J. D., Di Ilio, C., Ketterer, B., Listowsky, I., Morgenstern, R., Muramatsu, M., Pearson, W. R. et al. (1992) Nomenclature for human glutathione transferases. Biochem. J. **282**, 305–306
13 Meyer, D. J., Coles, B., Pemble, S. E., Gilmore, K. S., Fraser, G. M. and Ketterer, B. (1991) Theta, a new class of glutathione transferases purified from rat and man. Biochem. J. **274**, 409–414
14 Motoyama, N. and Dauterman, W. C. (1978) Molecular weight, subunits, and multiple forms of glutathione S-transferase from the house fly. Insect Biochem. **8**, 337–348

15 Pemble, S. E. and Taylor, J. B. (1992) An evolutionary perspective on glutathione transferases inferred from class-Theta glutathione transferase cDNA sequences. Biochem. J. **287**, 957–963
16 Ding, Y., Ortelli, F., Rossiter, L. C., Hemingway, J. and Ranson, H. (2003) The *Anopheles gambiae* glutathione transferase supergene family: annotation, phylogeny and expression profiles. BMC Genomics **4**, 35–50
17 Wilce, M. C. J. and Parker, M. W. (1994) Structure and function of glutathione S-transferases. Biochim. Biophys. Acta **1205**, 1–18
18 Armstrong, R. N., Rife, C. and Wang, Z. (2001) Structure, mechanism and evolution of thiol transferases. Chem. Biol. Interact. **133**, 167–169
19 Caccuri, A. M., Ascenzi, P., Antonini, G., Parker, M. W., Oakley, A. J., Chiessi, E., Nuccetelli, M., Battistoni, A., Bellizia, A. and Ricci, G. (1996) Structural flexibility modulates the activity of human glutathione transferase P1-1. Influence of a poor co-substrate on dynamics and kinetics of human glutathione transferase. J. Biol. Chem. **271**, 16193–16198
20 Caccuri, A. M., Antonini, G., Nicotra, M., Battistoni, A., Lo Bello, M., Board, P. G., Parker, M. W. and Ricci, G. (1997) Catalytic mechanism and role of hydroxyl residues in the active site of theta class glutathione S-transferases. Investigation of Ser-9 and Tyr-113 in a glutathione S-transferase from the Australian sheep blowfly, *Lucilia cuprina*. J. Biol. Chem. **272**, 29681–29686
21 Gustafsson, A., Pettersson, P. L., Grehn, L., Jemth, P. and Mannervik, B. (2001) Role of the glutamyl α-carboxylate of the substrate glutathione in the catalytic mechanism of human glutathione transferase A1-1. Biochemistry **40**, 15835–15845
22 Winayanuwattikun, P. and Ketterman, A. J. (2005) An electron-sharing network involved in the catalytic mechanism is functionally conserved in different glutathione transferase classes. J. Biol. Chem. **280**, 31776–31782
23 Caccuri, A. M., Antonini, G., Board, P. G., Parker, M. W., Nicotra, M., Lo Bello, M., Federici, G. and Ricci, G. (1999) Proton release on binding of glutathione to Alpha, Mu and Delta class glutathione transferases. Biochem. J. **344**, 419–425
24 Tan, K.-L., Chelvanayagam, G., Parker, M. W. and Board, P. G. (1996) Mutagenesis of the active site of the human Theta-class glutathione transferase GSTT2-2: catalysis with different substrates involves different residues. Biochem. J. **319**, 315–321
25 Winayanuwattikun, P. and Ketterman, A. J. (2004) Catalytic and structural contributions for glutathione binding residues in a delta class glutathione S-transferase. Biochem. J. **382**, 751–757
26 Jirajaroenrat, K., Pongjaroenkit, S., Krittanai, C., Prapanthadara, L. and Ketterman, A. J. (2001) Heterologous expression and characterization of alternatively spliced glutathione *S*-transferases from a single *Anopheles* gene. Insect Biochem. Mol. Biol. **31**, 867–875
27 Bradford, M. M. (1976) A rapid and sensitive method for the quantitation of microgram quantities of protein utilizing the principle of protein-dye binding. Anal. Biochem. **72**, 248–254
28 Caccuri, A. M., Ascenzi, P., Lo Bello, M., Federici, G., Battistoni, A., Mazzetti, P. and Ricci, G. (1994) Are the steady state kinetics of glutathione transferase always dependent on the deprotonation of the bound glutathione? New insights in the kinetic mechanism of GST P1-1. Biochem. Biophys. Res. Commun. **200**, 1428–1434
29 Wolf, A. V., Brown, M. G. and Prentiss, P. G. (1985) Handbook of Chemistry and Physics, CRC Press, Boca Raton
30 Kong, G. K. W., Polekhina, G., McKinstry, W. J., Parker, M. W., Dragani, B., Aceto, A., Paludi, D., Principe, D. R., Mannervik, B. and Stenberg, G. (2003) Contribution of glycine 146 to a conserved folding module affecting stability and refolding of human glutathione transferase P1-1. J. Biol. Chem. **278**, 1291–1302
31 Stenberg, G., Dragani, B., Cocco, R., Principe, D. R., Mannervik, B. and Aceto, A. (2001) A conserved 'hydrophobic staple motif' plays a crucial role in the refolding of human glutathione transferase P1-P1. Chem. Biol. Interact. **133**, 49–50
32 Jackson, S. E., el Masry, N. and Fersht, A. R. (1993) Structure of the hydrophobic core in the transition state for folding of chymotrypsin inhibitor 2: a critical test of the protein engineering method of analysis. Biochemistry **32**, 11270–11278
33 Widersten, M., Kolm, R. H., Björnestedt, R. and Mannervik, B. (1992) Contribution of five amino acid residues in the glutathione binding site to the function of human glutathione transferase P1-1. Biochem. J. **285**, 377–381
34 Dirr, H. W. and Wallace, L. A. (1999) Role of the C-terminal helix 9 in the stability and ligandin function of class a glutathione transferase A1-1. Biochemistry **38**, 15631–15640
35 Jones, M. N. (1979) In Biochemical Thermodynamics (Studies in Modern Thermodynamics). (Jones, M. N., ed.), pp. 75–115, Elsevier, Oxford
36 Haynie, D. T. (2001) Statistical thermodynamics. In Biological thermodynamics, pp. 185–222, Cambridge University Press, Cambridge
37 Zeng, Q.-Y. and Wang, X.-R. (2005) Catalytic properties of glutathione-binding residues in a τ class glutathione transferase (PtGSTU1) from *Pinus tabulaeformis*. FEBS Lett. **579**, 2657–2662
38 Wongsantichon, J. and Ketterman, A. J. (2006) An intersubunit lock-and-key 'clasp' motif in the dimer interface of delta class glutathione transferase. Biochem. J. **394**, 135–144
39 Sayed, Y., Wallace, L. A. and Dirr, H. W. (2000) The hydrophobic lock-and-key intersubunit motif of glutathione transferase A1-1: implications for catalysis, ligandin function and stability. FEBS Lett. **465**, 169–172
40 Stenberg, G., Abdalla, A.-M. and Mannervik, B. (2000) Tyrosine 50 at the subunit interface of dimeric human glutathione transferase P1-1 is a structural key residue for modulating protein stability and catalytic function. Biochem. Biophys. Res. Commun. **271**, 59–63
41 Dirr, H. W., Little, T., Kuhnert, D. C. and Sayed, Y. (2005) A conserved N-capping motif contributes significantly to the stabilisation and dynamics of the C-terminal region of class alpha glutathione transferases. J. Biol. Chem. **280**, 19480–19487
42 Garcia-Viloca, M., Gao, J., Karplus, M. and Truhlar, D. G. (2004) How enzymes work: analysis by modern rate theory and computer simulations. Science **303**, 186–195
43 Chen, W.-J., Graminski, G. F. and Armstrong, R. N. (1988) Dissection of the catalytic mechanism of isozyme 4–4 of glutathione S-transferase with alternative substrates. Biochemistry **27**, 647–654
44 Graminski, G. F., Zhang, P., Sesay, M. A., Ammon, H. L. and Armstrong, R. N. (1989) Formation of the 1-(*S*-glutathionyl)-2,4,6-trinitrocyclohexadienate anion at the active site of glutathione *S*-transferase: evidence for enzymic stabilization of σ-complex intermediates in nucleophilic aromatic substitution reactions. Biochemistry **28**, 6252–6258
45 Johnson, W. W., Liu, S., Ji, X., Gilliland, G. L. and Armstrong, R. N. (1993) Tyrosine 115 participates both in chemical and physical steps of the catalytic mechanism of a glutathione S-transferase. J. Biol. Chem. **268**, 11508–11511

Received 16 August 2006/19 October 2006; accepted 14 November 2006
Published as BJ Immediate Publication 14 November 2006, doi:10.1042/BJ20061253

BJ www.biochemj.org

BJ Structure

Biochem. J. (2007) **401**, 635–644 (Printed in Great Britain) doi:10.1042/BJ20060603

Differences in the subunit interface residues of alternatively spliced glutathione transferases affects catalytic and structural functions

Juthamart PIROMJITPONG, Jantana WONGSANTICHON and Albert J. KETTERMAN[1]

Institute of Molecular Biology and Genetics, Mahidol University, Salaya Campus, Nakhon Pathom 73170, Thailand

GSTs (glutathione transferases) are multifunctional widespread enzymes. Currently there are 13 identified classes within this family. Previously most structural characterization has been reported for mammalian Alpha, Mu and Pi class GSTs. In the present study we characterize two enzymes from the insect-specific Delta class, adGSTD3-3 and adGSTD4-4. These two proteins are alternatively spliced products from the same gene and have very similar tertiary structures. Several major contributions to the dimer interface area can be separated into three regions: conserved electrostatic interactions in region 1, hydrophobic interactions in region 2 and an ionic network in region 3. The four amino acid side chains studied in region 1 interact with each other as a planar rectangle. These interactions are highly conserved among the GST classes, Delta, Sigma and Theta. The hydrophobic residues in region 2 are not only subunit interface residues but also active site residues. Overall these three regions provide important contributions to stabilization and folding of the protein. In addition, decreases in yield as well as catalytic activity changes, suggest that the mutations in these regions can disrupt the active site conformation which decreases binding affinity, alters kinetic constants and alters substrate specificity. Several of these residues have only a slight effect on the initial folding of each subunit but have more influence on the dimerization process as well as impacting upon appropriate active site conformation. The results also suggest that even splicing products from the same gene may have specific features in the subunit interface area that would preclude heterodimerization.

Key words: *Anopheles dirus*, glutathione transferase (GST), hydrophobic interaction, subunit interface.

INTRODUCTION

GSTs (glutathione transferases; EC 2.5.1.18) are a supergene family of multifunctional enzymes which are widely distributed in nature and found in most aerobic eukaryotes and prokaryotes. The dimeric cytosolic GSTs catalyse reactions with a broad range of substrates and play an essential role in detoxification of endogenous and xenobiotic compounds [1,2]. The dimerization of the GSTs not only contributes to stabilization of the subunit tertiary structure, but also allows for the construction of a fully functional active site [3]. Although tertiary structures of all classes of GSTs are similar, dimerization is highly specific and is thought to occur only between subunits within the same class [4,5].

The structural features at the dimer interface of the GSTs suggest at least two major subunit interaction areas [6]. The first area is the predominantly hydrophobic interaction at the outer ends of the interface called a hydrophobic 'lock-and-key' (also referred to as a 'ball-and-socket') motif which is formed by the insertion of an aromatic residue from domain I of one subunit into a 'lock' of five residues of domain II in the other subunit [6–9]. The second major subunit interaction area is the symmetry axis interactions at the 2-fold axis of the protein which show highly conserved electrostatic interactions at one edge of the subunit interface and a variety of interactions along the interface depending on the GST class. The *Anopheles dirus* mosquito is an important malaria vector in South East Asia. From an *A. dirus* genomic library, a 7.5 kb fragment containing the adgst1AS1 gene (*A. dirus* alternatively spliced GST gene) was identified [10]. This gene contains six exons that encode four Delta class GSTs, adGSTD1-1, 2-2, 3-3 and 4-4, which possess 61–77 % amino acid identity compared among themselves. Previously these proteins had been named adGST1-1, 1-2, 1-3 and 1-4, according to insect GST nomenclature in use (that is, insect class 1-protein 1, 2, 3 and 4 respectively). However, to be in alignment with a proposed universal GST nomenclature, the proteins were renamed adGSTD1-1, adGSTD2-2, adGSTD3-3 and adGSTD4-4 respectively [11,12]. The subunit number remains the same, since subunits were enumerated as they were initially discovered, 'D' refers to GST Delta class and '4-4' refers to the homodimeric isoenzyme. These four GSTs share an untranslated exon 1 and a translated exon 2 coding for 45 amino acids at the N-terminus but vary between four different exon 3 sequences (exons 3A–3D). The arrangement of each exon is similar to the aggst1α gene from *A. gambiae,* the major malaria vector in Africa, with approx. 79 % nucleotide identity for the two genes [13]. In *A. dirus*, although four splice products are encoded from the same gene, the enzymes possess distinct enzyme kinetic properties for substrates, inhibitors, including insecticides, as well as physical properties such as stability [14,15]. Although two splice products, adgstD3-3 (PDB accession number: 1JLV) and adgstD4-4 (PDB accession number: 1JLW), have very similar tertiary structures when aligned, the amino acid identity is only 68 % [16].

When compared with human Alpha, Mu and Pi classes, the dimer interfaces of both Delta class isoenzymes are more extensively hydrophilic. Although lacking the previously identified hydrophobic 'lock-and-key' motif (a conserved motif in human Alpha, Mu and Pi classes), the Delta class does possess a 'Clasp' motif with a similar function [17]. In addition to this motif, there are nine amino acids making major contributions to the interactions within this interface area, which can be separated into three regions: conserved electrostatic interactions in region

Abbreviations used: ANS, 8-anilino-1-naphthalene sulfonate; CDNB, 1-chloro-2,4-dinitrobenzene; DCNB, 1,2-dichloro-4-nitrobenzene; EA, ethacrynic acid; GST, glutathione transferase; PNBC, p-nitrobenzyl chloride; PNPB, p-nitrophenethyl bromide.

[1] To whom correspondence should be addressed (email albertketterman@yahoo.com).

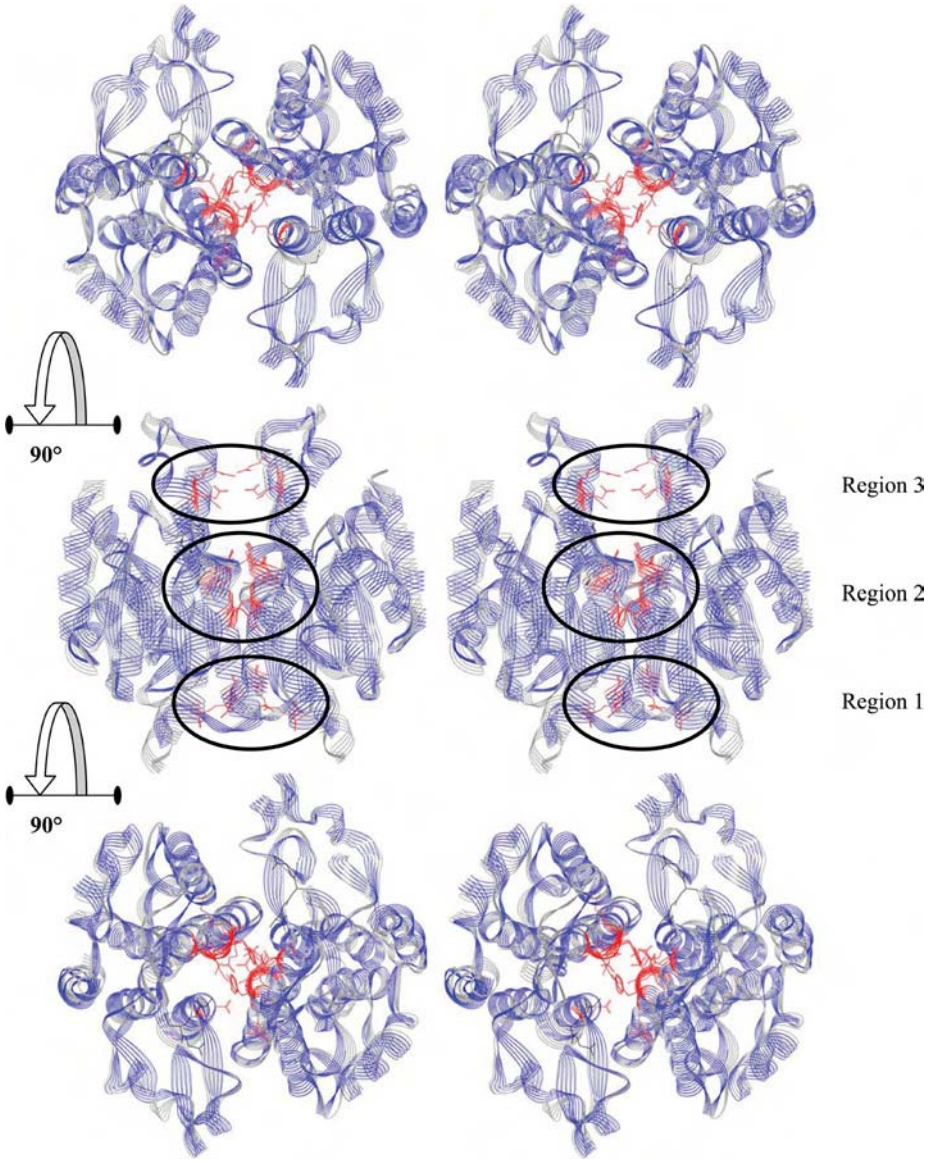

Figure 1 The three regions of the interface characterized in the present study

The two GST proteins are carbon backbone aligned with the adGSTD3-3 secondary structure wire ribbon shown in blue and the adGSTD4-4 secondary structure ribbon shown in grey. The GSH in the two active sites is shown as a black stick; the residues engineered in the present study are shown in red. The top panel is a stereo view looking at the 2-fold axis from the side opposite to the active sites. The middle panel shows the proteins rotated 90°, to show the position of the studied interface residues down the length of α-helices 3 and 4. The bottom panel shows the proteins rotated a further 90° and looking down upon the 2-fold axis on to the active sites. The Figure was created using Accelrys DS ViewerPro 5.0.

1, hydrophobic interactions in region 2 and an ionic network in region 3 (Figure 1).

The conserved electrostatic interactions in region 1 of the subunit interface are formed by two amino acid residues from one subunit (a glutamate residue in α-helix 3 and an arginine residue in α-helix 4) interacting with the same two amino acids from the other subunit. These interactions are of interest because the four amino acid side chains interact with each other as a planar rectangle with distances of 3.83–4.26 Å (1Å = 0.1 nm). These interactions are highly conserved among the GST classes, Delta, Sigma and Theta, however at present there are no reports of these interactions for any of the three GST classes. In adGSTD4-4, each arginine residue not only interacts with both of the negatively charged Glu^{75} residues in both subunits, but also forms cation–π interactions with the aromatic ring of Tyr^{89} and an ionic interaction with the carboxy group of Pro^{90}. In adGSTD3-3, the equivalent residues to Glu^{75} and Arg^{96} of adGSTD4-4 are Glu^{74} and Arg^{90}. These residues also form the same planar rectangle arrangement within adGSTD3-3 and are stabilized in a similar manner by interactions with Tyr^{83} and Pro^{84} (Tyr^{89} and Pro^{90} in adGSTD4-4). Therefore as the motif appears to be highly conserved in both proteins it was only studied in adGSTD4-4. In addition, these interactions appear to be highly conserved among the insect GST classes. Therefore the aim of the present study was to determine whether the inter- and intra-subunit electrostatic interactions of these residues are important contributions that help to maintain tertiary and quaternary structures.

Region 2 at the subunit interface shows the most variation in amino acid residues at equivalent positions between the two isoenzymes, Tyr^{98}, Met^{101} and Gly^{102} of adGSTD3-3 and Phe^{104},

Val[107] and Ala[108] of adGSTD4-4 respectively. These residues are of interest because they are not only subunit interface residues but also active site residues with several of them involved in both active sites of the dimeric enzyme. Therefore the amino acids at the equivalent positions of the two isoenzymes were studied by switching the amino acids of the two proteins; Y98F, M101V, G102A and Y98F/M101V/G102A of adGSTD3-3 and F104Y, V107M, A108G and F104Y/V107M/A108G of adGSTD4-4.

The last region is the hydrophilic area in region 3 of the subunit interface, Asp[110] of adGSTD3-3 and Glu[116] of adGSTD4-4. Not only are these subunit interface residues, but these two equivalent positions also are involved in the active site as part of the H-site (hydrophobic substrate-binding site). For adGSTD4-4, Glu[116] forms hydrogen bonds with Arg[134] in both inter- and intra-subunit interactions; however, these interactions do not appear in adGSTD3-3. For adGSTD3-3, there are hydrogen bonds only in the same subunit between Asp[110] and the highly conserved residue Glu[106]. To study the influence of the ionic network in region 3 of the subunit interface and whether it impacts upon the catalytic activity and stability of the enzymes, mutations at the equivalent positions of these two isoenzymes were generated, that is, D110A of adGSTD3-3 and E116A of adGSTD4-4.

MATERIALS AND METHODS

Site-directed mutagenesis and protein purification

The adGSTD3-3 and adGSTD4-4 plasmid DNA templates were prepared from previous constructs [14]. The construction of the mutants was based on the Stratagene QuikChange® site-directed mutagenesis kit using *pfu* DNA polymerase. The expression constructs of recombinant plasmid that were obtained were sequenced at least twice and transformed into *Escherichia coli* BL21DE3plysS. The soluble recombinant GSTs were purified by GSTrap affinity chromatography (Amersham Phamacia) as previously described [14]. After purification, proteins were homogeneous as judged by SDS/PAGE, and the protein concentration was determined using the Bradford protein reagent with bovine serum albumin as a standard [18].

Catalytic activity and kinetic studies

Steady-state kinetics were studied at various concentrations of CDNB (1-chloro-2,4-dinitrobenzene) and GSH in 0.1 M phosphate buffer (pH 6.5). The reaction was monitored at 340 nm, $\varepsilon = 9600\ M^{-1} \cdot cm^{-1}$. Apparent kinetic parameters, k_{cat}, K_m and k_{cat}/K_m were determined by fitting the collected data to a Michaelis–Menten equation by non-linear regression analysis using GraphPad Prism version 4 (GraphPad software; www.graphpad.com) [19,20]. Specific activities of the enzymes were determined with five different substrates; CDNB, DCNB (1,2-dichloro-4-nitrobenzene), EA (ethacrynic acid), PNPB (p-nitrophenethyl bromide) and PNBC (p-nitrobenzyl chloride) as previously described [21]. Specific activities reported are the means ± S.D. from at least three independent experiments. One-way ANOVA with Dunnett's post test was performed using GraphPad InStat version 3.06 for Windows (GraphPad software; www.graphpad.com).

Structural studies

Enzymes at 0.1 mg/ml final concentration were incubated at 45 °C. Inactivation time courses were determined by withdrawing suitable aliquots at different time points for an assay of remaining activity to calculate the half-life of the enzyme [22]. Data are the means ± S.D. from at least three independent experiments.

Spectroscopic properties of wild-type and mutant proteins were measured for evidence of conformational changes. Intrinsic fluorescence emission spectra were measured at an excitation wavelength of 295 nm and λ_{max} and fluorescence intensity of emission spectra were analysed at a protein concentration of 0.2 mg/ml [23].

A refolding experiment was performed with enzymes first being denatured in 4 M guanidinium chloride in renaturation buffer [0.2 M phosphate, 1 mM EDTA and 5 mM dithiothreitol (pH 7.0)] at room temperature (25 °C) for 1 h and then rapidly diluted (defining time zero) 1:40 into renaturation buffer. Therefore the final guanidinium chloride concentration was 0.1 M during refolding. Recovered activity was monitored as a function of time by withdrawal of appropriate aliquots of renaturation mixture and immediately assaying for activity. Refolding rate constants were determined by non-linear regression analysis using a single exponential equation [23].

The ANS (8-anilino-1-naphthalenesulfonate) binding assay was monitored using a PerkinElmer Luminescence spectrometer LS50B. ANS [200 μM in 0.1 M sodium phosphate buffer (pH 6.5)] was added to a final concentration of 2 μM enzyme in a 400 μl reaction mixture [24]. The spectrum of ANS in phosphate buffer (pH 6.5) was subtracted from the spectrum of protein-binding ANS. A total of three scans each for blank and sample were recorded and averaged for each enzyme. Reported spectra are the means from at least three independent experiments. Enzyme activity measurements in the presence of ANS were assessed immediately after adding ANS by using the standard reaction assay.

RESULTS AND DISCUSSION

The investigations of GST dimerization performed in mammalian GSTs indicated that the subunit interactions are a significant source of stabilization not only for the association of subunits but also for tertiary structures of the individual subunits [9,25,26]. In the present study, most mutations gave similar purification yields as the wild-type with the exception of the E75A and R96A mutants of adGSTD4-4, which had yields approx. 2 and 0.4 % of the wild-type respectively. As the proteins were expressed in similar amounts, it appears that the alteration of these residues disrupts the intra-subunit interaction between helix 3 and helix 4 which impacts upon the active site architecture thereby affecting binding to the affinity matrix.

Both adGSTD3-3 and adGSTD4-4 have two tryptophan residues in each subunit that are located in β-sheet 4 in domain I and α-helix 7 in domain II. The tryptophan residue located in β-sheet 4 in domain I (Trp[63]) is in close proximity to the active site, with an involvement in sequestering the substrate glutathione, as well as being in the subunit interface. This makes it a sensitive fluorescence probe to monitor conformational changes at/near the active site. The normalized fluorescence spectra of adGSTD3-3 and adGSTD4-4 wild-type compared with the mutants were obtained to study the effect of mutations on the enzyme tertiary structure (Figure 2). The results showed that although every mutant had the same λ_{max} as the wild-type, several mutants presented differences in the normalized intensities of fluorescence, implying that the mutations caused significant conformational changes in the environment of the tryptophan residues located near the subunit interface and the mutation site. The mutants also had different intensities from their wild-type especially R96A, with the intensity of fluorescence decreased by approx. 66 %. This finding suggests that there are significant conformational changes in the tryptophan residue neighbourhood that distinguish the final structure of the mutant from that of the wild-type. This decrease

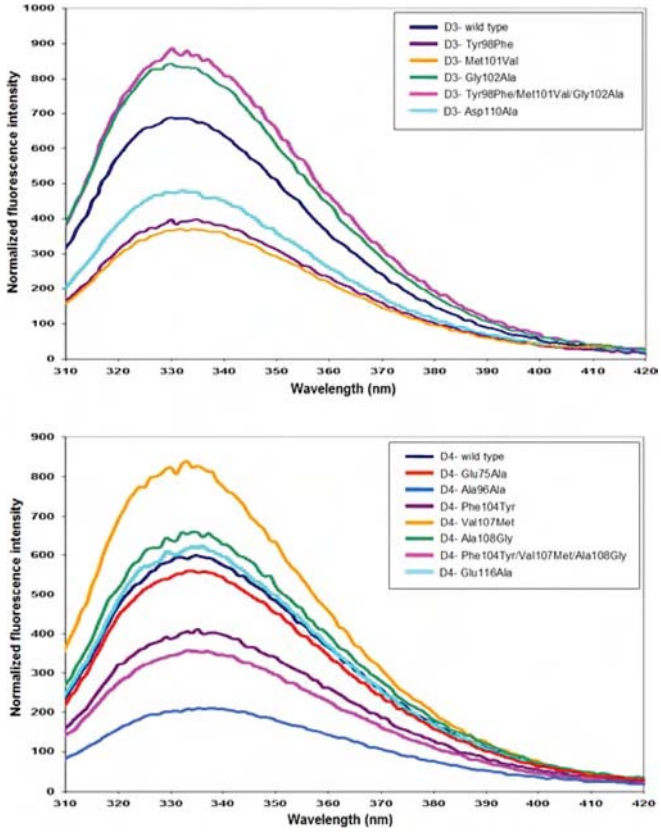

Figure 2 Normalized intrinsic tryptophan residue fluorescence spectra of the adGSTD3-3 and adGSTD4-4 (wild-type) and the recombinant mutant GSTs

The same colour represents the equivalent position. The data are means of three independent experiments.

demonstrates that movements have occurred in the tryptophan residues or in the surrounding fluorescence quenching groups.

The half-life of the enzymes corresponds to the time of incubation when there is 50 % remaining activity (Table 1). The conserved cation–π interaction residue, Arg[96], and the conserved electrostatic interaction residue, Glu[75], have important roles in stabilizing enzyme structure as shown by a much decreased stability for R96A and E75A of approx. 15- and 7.4-fold respectively. For region 2, several mutants possessed similar stability as the wild-type enzymes. However, there were three mutants which had very different thermal stabilities. Two of the mutations were at an equivalent position, adGSTD3-3 Gly[102] and adGSTD4-4 Ala[108]. Replacement of a glycine residue by an alanine residue in adGSTD3-3 at this position caused decreases of about 8-fold in half-life, whereas a glycine residue substitution of adGSTD4-4 showed an increase in half-life of about 4.7-fold. The other mutant that showed stability changes was the V104M protein which decreased the half-life by approx. 3-fold. For region 3, the half-life of D110A of adGSTD3-3 was similar to the wild-type. However, the equivalent adGSTD4-4 mutation E116A disrupted the charge–charge network and showed a 64 % decreased stability for the enzyme. The results showed that the positively charged residue at the edge of the subunit interface of adGSTD4-4 participates in stabilizing the enzyme structure while the equivalent residue of adGSTD3-3 appeared to have only a minor contribution.

Three mutations in adGSTD4-4, E75A, R96A and V107M, did not recover activity after being unfolded by 4 M guanidinium chloride (Table 1). This implies that these residues play a critical role in the folding process of the enzymes. For the remaining mutants, the refolding rate constants were similar. The activity recovered illustrates the ability of the enzymes to recover their appropriate active site conformation for catalytic activity. After unfolding, the enzymes were able to recover activity ranging from 19 % to 94 %. To study the influence of mutations on protein folding and to assess whether the changes affected tertiary folding of each subunit or dimerization of the two subunits, intrinsic tryptophan residue fluorescence spectroscopy was performed. The fluorescence spectra of native, unfolded and refolded enzymes were monitored to compare the tertiary structure of the proteins in each state (Figures 3 and 4). The λ_{max} values of the native (335 nm) and the unfolded form (355 nm) of the protein were observed for every enzyme. The data showed that the enzymes were refolded in a similar manner as the native form, as shown by similar λ_{max} values, including the E75A, R96A and V107M mutants, although

Table 1 Half-life, refolding rate constants, activity recovered (%) and the effect of ANS on CDNB specific activity of the adGSTD3-3 and adGSTD4-4 (wild-type) and the recombinant engineered GSTs

The data are means ± S.D. for at least three independent experiments. One-way ANOVA with Dunnett's post test was performed to show statistical significance with $*P < 0.05$ and $\dagger P < 0.01$. D3 and D4 indicate adGSTD3-3 and adGSTD4-4 respectively. Inside parentheses the numbers indicate the subunit interface region: 1 is region 1, 2 is region 2 and 3 is region 3; and the same lowercase letter indicates an equivalent residue position for the two GST isoenzymes. nd, not detectable.

Enzymes	Half-life (min)	Refolding rate constant (min^{-1})	Activity recovered (%)	Inhibition by ANS (%)
D3-wild-type	2.71 ± 0.35	0.87 ± 0.09	56.9 ± 0.23	24.6 ± 1.41
D3-Y98F (2/a)	3.12 ± 0.33	0.58 ± 0.05†	66.1 ± 2.83*	13.1 ± 0.54†
D3-M101V (2/b)	2.77 ± 0.43	0.42 ± 0.05†	40.5 ± 1.93†	11.9 ± 0.80†
D3-G102A (2/c)	0.34 ± 0.03†	0.38 ± 0.07†	94.4 ± 5.77†	13.7 ± 2.66†
D3-Y98F/M101V/G102A (2/d)	1.88 ± 0.01*	0.31 ± 0.03†	85.8 ± 4.39†	18.4 ± 0.65†
D3-D110A (3/e)	2.21 ± 0.24	0.58 ± 0.11†	80.5 ± 3.48†	23.4 ± 1.83
D4-wild-type	14.0 ± 1.70	0.59 ± 0.03	19.7 ± 0.70	18.4 ± 1.20
D4-G75A(1)	1.89 ± 0.13†	nd	0.00	22.5 ± 0.82
D4-R96A(1)	0.91 ± 0.07†	nd	0.00	18.8 ± 3.89
D4-F104Y (2/a)	17.1 ± 1.76*	0.28 ± 0.02†	23.5 ± 0.51	31.9 ± 1.96†
D4-V107M (2/b)	4.76 ± 0.15†	nd	0.00	25.4 ± 1.41†
D4-A108G (2/c)	65.4 ± 1.45†	0.32 ± 0.04†	69.6 ± 7.55†	32.8 ± 1.03†
D4-F104Y/V107M/A108G (2/d)	16.7 ± 1.23	0.60 ± 0.10	25.0 ± 0.18	21.1 ± 1.83
D4-E116A (3/e)	5.16 ± 0.93†	0.68 ± 0.11	9.93 ± 0.68*	17.3 ± 2.05

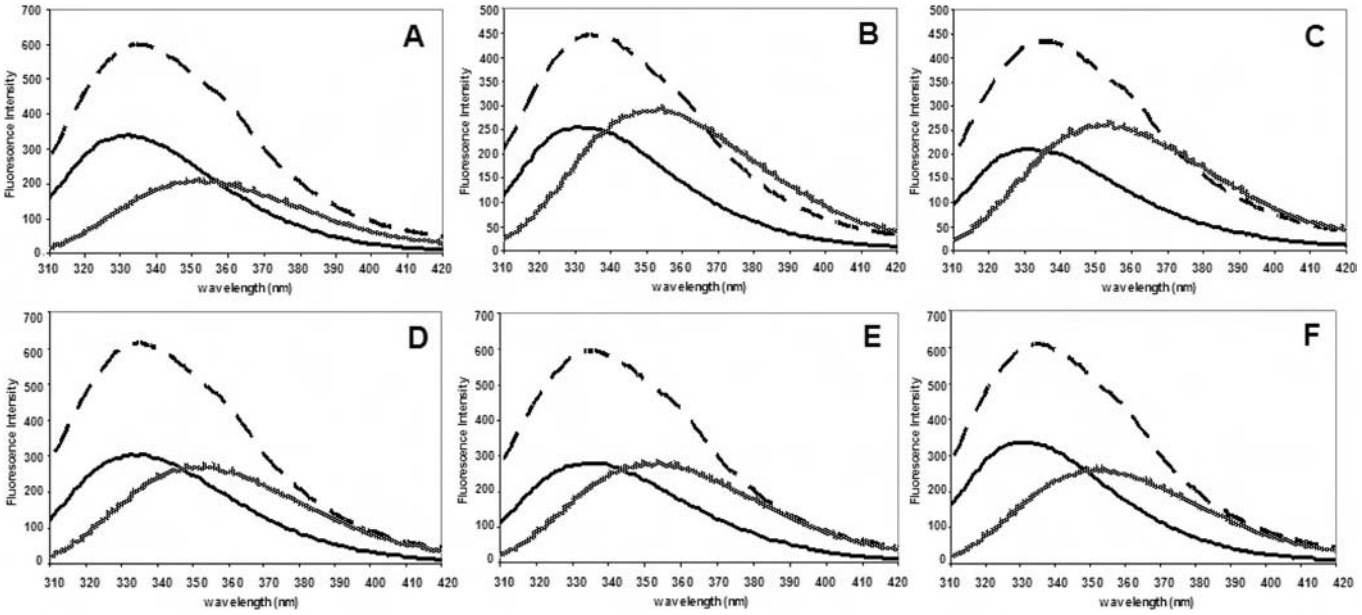

Figure 3 Normalized intrinsic tryptophan residue fluorescence spectra compared with the native, refolded and unfolded forms of the adGSTD3-3 (wild-type) and the recombinant mutant GSTs

(**A**) Wild-type, (**B**) Y98F, (**C**) M101V, (**D**) G102A, (**E**) Y98F/M101V/G102A and (**F**) D110A. The data are means for at least three independent experiments. Solid line, native form; dashed line, refolded form; and hashed line, unfolded form of the enzyme.

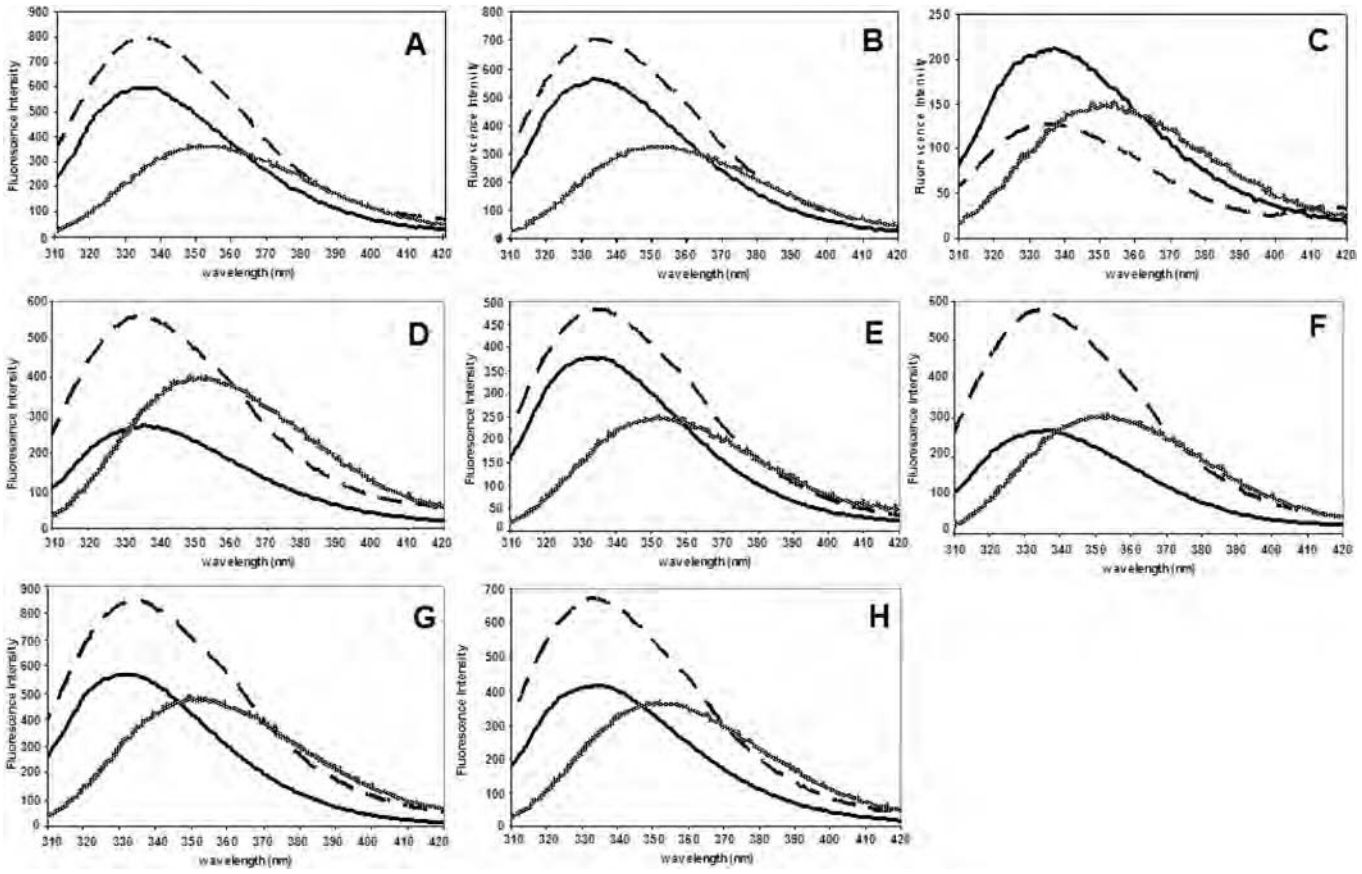

Figure 4 Normalized intrinsic tryptophan residue fluorescence spectra compared with the native, refolded and unfolded forms of the adGSTD4-4 (wild-type) and the recombinant mutant GSTs

(**A**) Wild-type, (**B**) G75A, (**C**) R96A, (**D**) F104Y, (**E**) V107M, (**F**) A108G, (**G**) F104Y/V107M/A108G and (**H**) E116A. The data are means for at least three independent experiments. Solid line, native form; dashed line, refolded form; and hashed line, unfolded form of the enzyme.

these enzymes could not recover catalytic activity. As shown by the similar patterns of the adGSTD3-3 mutant spectra, the mutations did not affect the tertiary folding of each subunit but influenced the dimerization process, which is necessary to achieve an appropriate active site conformation. Therefore both catalytic and structural data suggest that the single mutation of Gly^{102} and the triple mutation had significant effects on the dimerization of the enzymes by increasing the activity recovered from 56.9 % for wild-type to approx. 94.4 % and 85.8 % for the two proteins respectively (Table 1). In both catalytic and structural experiments, the refolding data showed that loss of the conserved electrostatic interactions, E75A and R96A, and the hydrophobic residue, V107M, had a dramatic effect on the dimerization process, which is critical to formation of the complete active site pocket. The results for the Arg^{96} position indicated that not only does this residue have a critical role in the dimerization process, but it is also important for the protein folding pathway of each monomeric subunit.

The anionic dye ANS has been shown to bind in the solvent-exposed cleft in the subunit interface of class Alpha and Pi enzymes [27–29]. Therefore ANS was utilized as a probe to monitor the appearance/disappearance of hydrophobic patches or surfaces on the proteins that were undergoing structural changes. When ANS was bound to the proteins the fluorescence was enhanced, accompanied by a blue shift in its emission maximum from 514 nm (free ANS in buffer) to 498 nm for adGSTD3-3 and 482 nm for wild-type adGSTD4-4, indicating that the polarity of the binding site had become more hydrophobic, with decreasing polarity the greater the blue shift.

When compared with the wild-type proteins, there was no change in the emission maximum wavelength of ANS bound to all mutants (Figure 5). For the ANS fluorescence intensity, which reflects the degree of solvent quenching of ANS bound to the protein, the adGSTD4-4 mutants showed variations in the amount of ANS bound, except E75A, which showed a similar intensity to the wild-type. However, there was no relative intensity change for the adGSTD3-3 mutants. The results showed that the residue substitutions of adGSTD4-4 with the adGSTD3-3 amino acids had a dramatic effect at the subunit interface, much more than for adGSTD3-3.

To study the impact of ANS on the enzyme conformation, the enzyme activity in the presence and absence of ANS was measured using the standard reaction assay. The results showed that for the mutants, ANS molecules can bind and alter the active site architecture in a manner similar to the wild-type (Table 1). It implied that differences in ANS spectra intensities in Figure 5 occurred only from an alteration of a hydrophobic patch at the subunit-binding site.

In general, the engineered enzyme reactions followed Michaelis–Menten kinetics as did the wild-type except for E75A, F104Y and E116A of adGSTD4-4 which showed positive co-operativity upon substrate binding. Positive co-operativity is shown by a sigmoidal velocity curve which reflects the substrate binding in the first active site, that then facilitates a second substrate molecule binding in the second active site by increasing the binding affinity of the vacant binding site [30]. For CDNB, two of the enzymes had significantly different Hill coefficients (shown by one-way ANOVA with Dunnett's post test) compared with wild-type enzyme [Hill coefficients for wild-type 1.08 ± 0.08 versus E75A 1.79 ± 0.03 ($P < 0.01$) and E116A 1.40 ± 0.20 ($P < 0.05$)]. For GSH only F104Y had a significantly different Hill coefficient (shown by one-way ANOVA with Dunnett's post test) compared with wild-type enzyme [Hill coefficients for wild-type 1.06 ± 0.14 versus F104Y 2.01 ± 0.09 ($P < 0.01$)]. These data show that two of the mutant enzymes, E75A and F104Y, had very strong positive co-operativity, with the Hill coefficients approaching the number of substrate-binding sites. In addition, comparison of the kinetic constants of the mutants with the wild-type values showed that the residue changes affected additional enzymatic properties (Table 2). These effects on the active site were also reflected in changes in substrate specificity with changes in the equivalent residue position showing different effects on the two isoforms (Table 3). For example, D110A activity was significantly decreased with CDNB and DCNB in adGSTD3-3 but E116A activity was significantly increased with CDNB and showed no significant activity with DCNB in adGSTD4-4. For another position, M101V in adGSTD3-3 equivalent to V107M in adGSTD4-4, both enzymes showed significant decreases in activity with CDNB. However, the adGSTD4-4 enzyme showed significant increases in activity with DCNB and EA, whereas the adGSTD3-3 enzyme showed a significant decrease with DCNB and no significant change with EA.

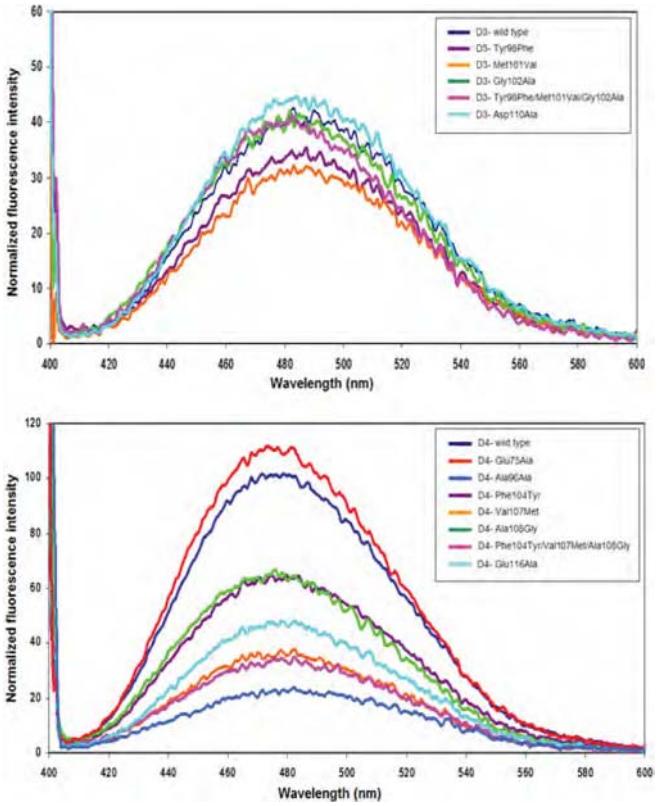

Figure 5 ANS binding spectra of the adGSTD3-3 and adGSTD4-4 (wild-type) and the recombinant mutant GSTs

The same colour represents the equivalent position. The spectra were measured immediately after addition of ANS. As ANS fluorescence is quenched by water, alteration of the fluorescence intensity of protein-bound ANS is highly dependent upon its accessibility to water. The data are means for at least three independent experiments.

The insect GST class Delta has a conserved planar rectangular electrostatic motif formed by four amino acid residues from different helices of both subunits (Glu^{75} in α-helix 3 and Arg^{96} in α-helix 4) (Figure 6). These interactions are highly conserved among GST classes Delta, Sigma and Theta. This is the first report of these interactions for any of these three classes. To study the function of this motif two mutants were generated, E75A and R96A, which break the conserved electrostatic interactions and ionic network at the dimer interface of adGSTD4-4. The results showed that the motif provides an important contribution

Table 2 Yield of purification and kinetic parameters of the adGSTD3-3 and adGSTD4-4 (wild-type) and the recombinant engineered GSTs

The data are means ± S.D. for at least three independent experiments. One-way ANOVA with Dunnett's post test was performed to show statistical significance with $*P < 0.05$ and $\dagger P < 0.01$. D3 and D4 indicate adGSTD3-3 and adGSTD4-4 respectively. Inside parentheses the numbers indicate the subunit interface region: 1 is region 1, 2 is region 2 and 3 is region 3; and the same lowercase letter indicates an equivalent residue position for the two GST isoenzymes.

Enzymes	CDNB k_{cat} (s^{-1})	CDNB K_m (mM)	CDNB k_{cat}/K_m ($mM^{-1}•s^{-1}$)	GSH K_m (mM)	GSH k_{cat}/K_m ($mM^{-1}•s^{-1}$)	Purification yield (%)
D3-wild-type	39.2	0.15 ± 0.01	258	0.29 ± 0.04	114	53.7
D3-Y98F (2/a)	24.9†	0.12 ± 0.01	213	0.47 ± 0.05	53.1	49.2
D3-M101V (2/b)	26.0†	0.72 ± 0.06†	36.3	1.04 ± 0.06†	25.0	60.0
D3-G102A (2/c)	23.5†	0.37 ± 0.02†	63.3	2.94 ± 0.38†	7.99	47.6
D3-Y98F/M101V/G102A (2/d)	40.7	0.28 ± 0.03†	147	1.12 ± 0.07†	36.7	58.3
D3-D110A (3/e)	51.7†	0.49 ± 0.07†	106	0.54 ± 0.04	95.8	34.3
D4-wild-type	22.5	0.63 ± 0.09	35.7	0.67 ± 0.05	33.6	61.3
D4-G75A (1)	23.3	8.26 ± 2.63†	2.82	0.54 ± 0.06	43	5.5
D4-R96A (1)	16.2†	0.80 ± 0.06	22.0	1.08 ± 0.02	15.0	1.4
D4-F104Y (2/a)	15.5†	0.52 ± 0.03	29.8	24.01 ± 2.94†	0.65	42.2
D4-V107M (2/b)	13.7†	1.6 ± 0.08	8.56	0.76 ± 0.11	18.0	60.0
D4-A108G (2/c)	26.8	0.87 ± 0.07	26.8	0.73 ± 0.12	36.7	59.2
D4-F104Y/V107M/A108G (2/d)	32.5†	0.72 ± 0.04	45.2	0.25 ± 0.02	130	59.2
D4- E116A (3/e)	46.1†	1.55 ± 0.01	29.7	1.24 ± 0.06	37.1	37.1

Table 3 Specific activities of the adGSTD3-3 and adGSTD4-4 (wild-type) and the recombinant engineered GSTs

The data are means ± S.D. for at least three independent experiments. One-way ANOVA with Dunnett's post test was performed to show statistical significance with $*P < 0.05$ and $\dagger P < 0.01$. The substrate concentrations used were 1 mM CDNB for adGSTD3 and 3 mM CDNB for adGSTD4, 1 mM DCNB, 0.1 mM PNBC, 0.1 mM PNPB and 0.2 mM EA. D3 and D4 indicate adGSTD3-3 and adGSTD4-4 respectively. Inside parentheses the numbers indicate the subunit interface region: 1 is region 1, 2 is region 2 and 3 is region 3; and the same lowercase letter indicates an equivalent residue position for the two GST isoenzymes. nd is not detectable.

Enzymes	Specific Activity (μmol/min/mg) CDNB	DCNB	EA	PNPB	PNBC
D3-wild-type	85.3 ± 3.23	0.25 ± 0.01	0.10 ± 0.05	nd	0.13 ± 0.01
D3-Y98F (2/a)	46.9 ± 6.38†	0.23 ± 0.03	0.03 ± 0.01*	nd	0.05 ± 0.00†
D3-M101V (2/b)	41.1 ± 0.81†	0.05 ± 0.01†	0.08 ± 0.02	nd	0.09 ± 0.00†
D3-G102A (2/c)	46.8 ± 0.25†	0.08 ± 0.01†	nd	nd	0.05 ± 0.00†
D3-Y98F/M101V/G102A (2/d)	84.8 ± 5.47	0.21 ± 0.01*	0.15 ± 0.01	nd	0.08 ± 0.00†
D3-D110A (3/e)	71.6 ± 2.69†	0.16 ± 0.01†	0.01 ± 0.01†	0.03 ± 0.01	0.07 ± 0.01†
D4-wild-type	48.0 ± 1.98	0.03 ± 0.00	0.27 ± 0.00	0.06 ± 0.01	0.03 ± 0.01
D4-E75A (1)	36.6 ± 5.03†	0.06 ± 0.01	0.12 ± 0.01	0.02 ± 0.01	0.06 ± 0.00
D4-R96A (1)	26.0 ± 0.13†	0.27 ± 0.04†	0.18 ± 0.01	0.23 ± 0.02	nd
D4-F104Y (2/a)	28.5 ± 2.24†	0.06 ± 0.01	0.14 ± 0.01	0.05 ± 0.01	0.11 ± 0.05
D4-V107M (2/b)	22.0 ± 2.29†	0.08 ± 0.004*	2.06 ± 0.29†	0.31 ± 0.08	nd
D4-A108G (2/c)	55.3 ± 2.07	0.06 ± 0.02	0.32 ± 0.01	nd	0.08 ± 0.02
D4-F104Y/V107M/A108G (2/d)	53.8 ± 1.43	0.05 ± 0.01	0.02 ± 0.00*	nd	0.04 ± 0.01
D4- E116A (3/e)	56.3 ± 6.83*	0.06 ± 0.01	0.01 ± 0.01*	0.04 ± 0.01	0.04 ± 0.01

to the stabilization and folding of the protein. The mutants were expressed in both inclusion and soluble forms, with the R96A mutant mostly being expressed as an inclusion body. This evidence and the results from the refolding assay (Table 1; Figures 3 and 4) indicated that the folding process was altered by the mutations. In addition, decreases in yield as well as catalytic activity changes (Table 2), suggest that the mutations disrupt the active site conformation which decreases binding affinity, alters kinetic constants and substrate specificities.

Although both Glu^{75} and Arg^{96} are located in the same area, in the present study region 1 of the subunit interface, there is a conserved amino acid sequence around Arg^{96} which forms a pocket around the arginine residue. Arg^{96} is stabilized by several highly conserved residues in a cation–π interaction with Tyr^{89} and Pro^{90}, whereas Glu^{75} does not have amino acids surrounding it, except Arg^{96}, as it is located within a hole in the subunit interface edge (Figure 6). Therefore substitution of an alanine residue for Arg^{96} appears to have more impact on the tertiary and quaternary structure of the protein compared with Glu^{75}, as shown by decreases in the fluorescence intensities of both intrinsic tryptophan spectroscopy (Figure 2) and the ANS binding assay (Figure 5). This also suggests that there are significant conformational changes in amino acid side chains near the subunit interface and the mutation site. However, disappearance of the salt bridges with the loss of either Glu^{75} or Arg^{96} affected both initial protein folding, as shown in the refolding experiment, and the protein stability as shown by decreased half-life. Although Arg^{96} is not located in the active site pocket, structural changes that occurred due to this mutation also affected the active site conformation, probably through packing effects (Tables 2 and 3).

Region 2 of the subunit interface, which shows the most variation in amino acid residues at the equivalent positions between adGSTD3-3 and adGSTD4-4, is of interest because the residues are not only in the interface but also in the active site,

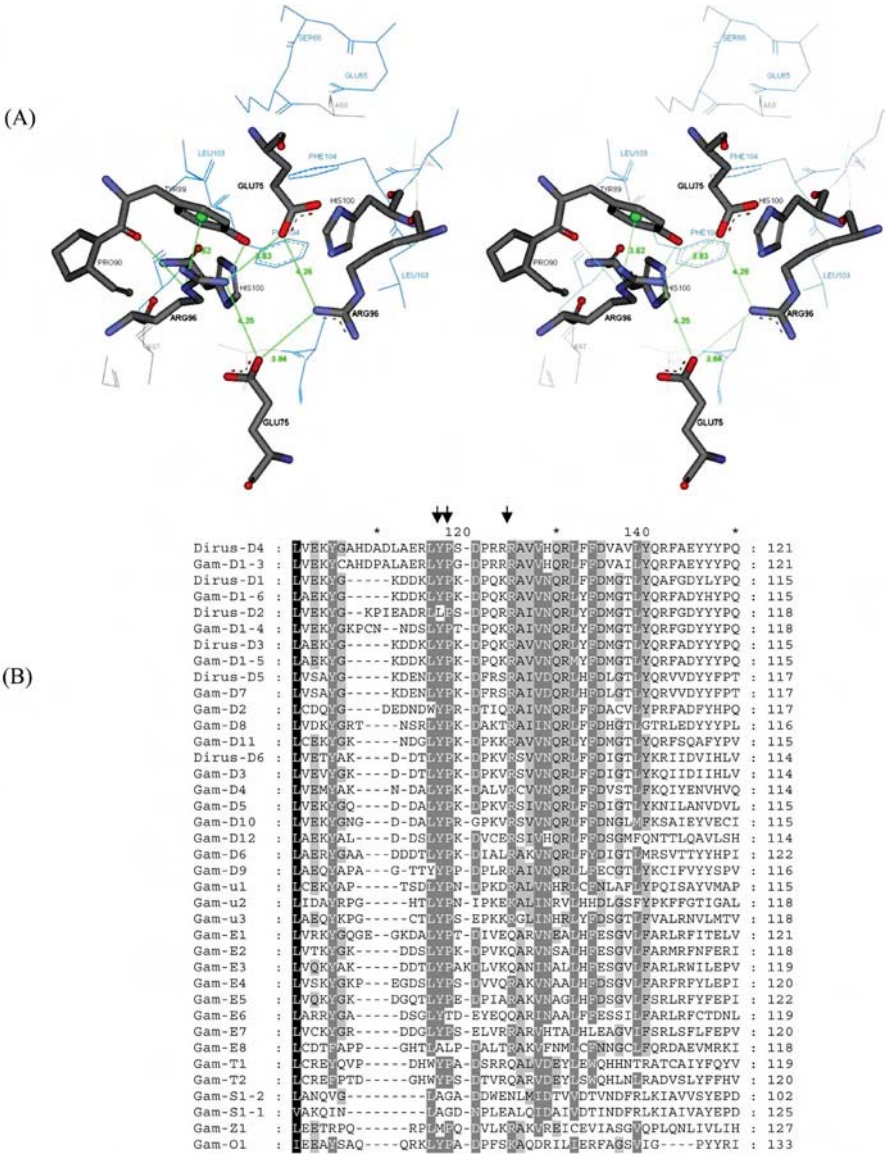

Figure 6 Conserved electrostatic interaction in region 1 of the subunit interface

(**A**) The planar rectangle electrostatic interaction of Glu^{75} and Arg^{96} from both subunits. Distances between the charged atoms are shown in Å. Also shown are the conserved anion–cation–π interactions between Tyr^{89}, Pro^{90} and Arg^{96}. (**B**) Amino acid alignment of insect GST classes. Dirus is *A. dirus* and Gam is *A. gambiae*. The arrows point to the highly conserved tyrosine, proline and arginine residues. D is Delta, u is unclassified, E is Epsilon, T is Theta, S is Sigma, Z is Zeta and O is Omega GST class. GenBank® accession numbers: adGSTD1 (AF273041), adGSTD2 (AF273038), adGSTD3 (AF273039), adGSTD4 (AF273040), adGSTD5 (AF251478), adGSTD6 (AY014406), agGSTD1-3 (Protein ID AAC79992), agGSTD1-4 (Protein ID AAC79994), agGSTD1-5 (Protein ID AAC79993), agGSTD1-6 (Protein ID AAC79995), agGSTD2 (Z71480), agGSTD3 (AF513638), agGSTD4 (AF513635), agGSTD5 (AF513634), agGSTD6 (AF513636), agGSTD7 (AF071161), agGSTD8 (AF316637), agGSTD9 (AY255857), agGSTD10 (AF515527), agGSTD11 (AF513637), agGSTD12 (AF316638), agGSTu1 (AF515521), agGSTu2 (AF515523), agGSTu3 (AF515524), agGSTE1 (AF316635), agGSTE2 (AF316636), agGSTE3 (AY070234), agGSTE4 (AY070254), agGSTE5 (AY070255), agGSTE6 (AY070256), agGSTE7 (AF491816), agGSTE8 (AY070257), agGSTT1 (AF515526), agGSTT2 (AF515525), agGSTS1-1 (L07880), agGSTS1-2 (AF513639), agGSTZ1 (AF515522), agGSTO1 (AY255856). agGSTD6 and agGSTD9 were suggested to be pseudogenes [33]. The Figure in (**A**) was created using Accelrys DS ViewerPro 5.0.

with several residues involved in both active sites of the dimer. The effects of the different hydrophobic amino acids at the equivalent positions of the two isoenzymes were studied by switching the equivalent amino acids with the amino acid from the other protein; that is, Y98F, M101V, G102A and Y98F/M101V/G102A for adGSTD3-3 and F104Y, V107M, A108G and F104Y/V107M/A108G for adGSTD4-4. The refolding experiments demonstrated that every enzyme could be refolded, although the activity recovered varied (Table 1). This indicates that the mutations have only a slight effect on the initial folding of each subunit but have more influence on the dimerization process through subunit interface conformation, as well as other structural aspects which impact upon appropriate active site conformation. When comparing the two isoforms adGSTD3-3 and adGSTD4-4, in terms of changes in catalytic activity, the mutations affected the proteins in different ways for the equivalent residues, as shown in Table 2. The crystal structures show that all selected equivalent positions are located in the active site pocket suggesting that the whole electrostatic field in the active site pocket was disturbed by the mutations, which thereby altered catalytic parameters of the enzymes. Moreover, these residues are also located at the interface of the two active

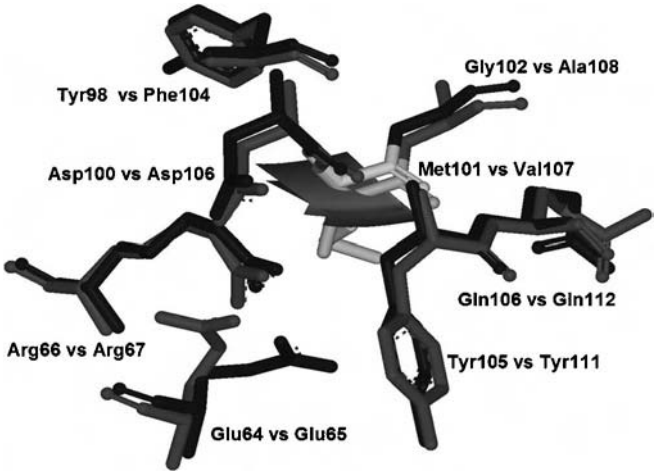

Figure 7 In region 2 the amino acid milieu of adGSTD3-Met[101] and adGSTD4-Val[107]

The dark grey represents adGSTD3-3 and medium grey is adGSTD4-4. The Figure was created using Accelrys DS ViewerPro 5.0.

site areas which provide different substrate-binding sites for GSH and the hydrophobic substrate. Therefore these positions would allow the residues to influence binding of both substrates as shown by the K_m values.

The first sphere milieu of the equivalent positions, Met[101] of adGSTD3-3 and Val[107] of adGSTD4-4, consists of seven amino acids of which only two residues are different between the two isoforms, adGSTD3-3 Tyr[98] compared with adGSTD4-4 Phe[104] and adGSTD3-3 Gly[102] compared with adGSTD4-4 Ala[108] (Figure 7). However, the triple mutations which changed all three amino acids at these equivalent positions to the amino acid of the other isoform, showed that they had only a slight effect on the half-life. Steric interactions and van der Waals forces are important interactions for the stability of proteins [31,32]. The side chain size of the three amino acids at these equivalent positions had a major impact on subunit interface packing, with differences between the two splice forms, especially Met[101] and Gly[102] of adGSTD3-3 and Val[107] and Ala[108] of adGSTD4-4. Although the amino acids possess similar properties, the packing effects were great enough to alter the protein and enzyme properties.

From the conserved electrostatic interactions in region 1 to the hydrophobic area in region 2 of the subunit interface, every residue appears to contribute to either maintaining structure or subunit binding. The last area to be examined was the hydrophilic area in region 3 of the subunit interface, Asp[110] of adGSTD3-3 and Glu[116] of adGSTD4-4. Both mutations, D110A of adGSTD3-3 and G116A of adGSTD4-4, affected catalysis as shown by changes in both specific activity and kinetic constants. The equivalent residue in the human Alpha class A1-1 is Glu[104] whereas in the human Pi class GST it is a polar Ser[105]. In insects, the acidic residue appears to be conserved within the Delta class, however in the Epsilon class it is generally an aromatic amino acid and in the other insect classes, such as Sigma, Theta and Zeta, the residue is hydrophobic. This residue therefore appears to be conserved within a class and would contribute to class specific dimerization motifs. Additionally, in adGSTD4-4 the Glu[116] interacts with Arg[134] in a similar fashion to Glu[75] and Arg[96] in region 1 (Figure 8). That is, electrostatic interactions occur between the two residues within the same subunit as well as with the identical residues from the other subunit. So in adGSTD4-4 but not in adGSTD3-3 similar intra- and inter-subunit electrostatic interactions occur in both regions 1 and 3 of the subunit interface. In adGSTD3-3 the equivalent residue to Arg[134] is Asn[126] and so, because of the shorter side chains of the Asp[110] and the Asn[126], the distances preclude electrostatic interaction across the subunits.

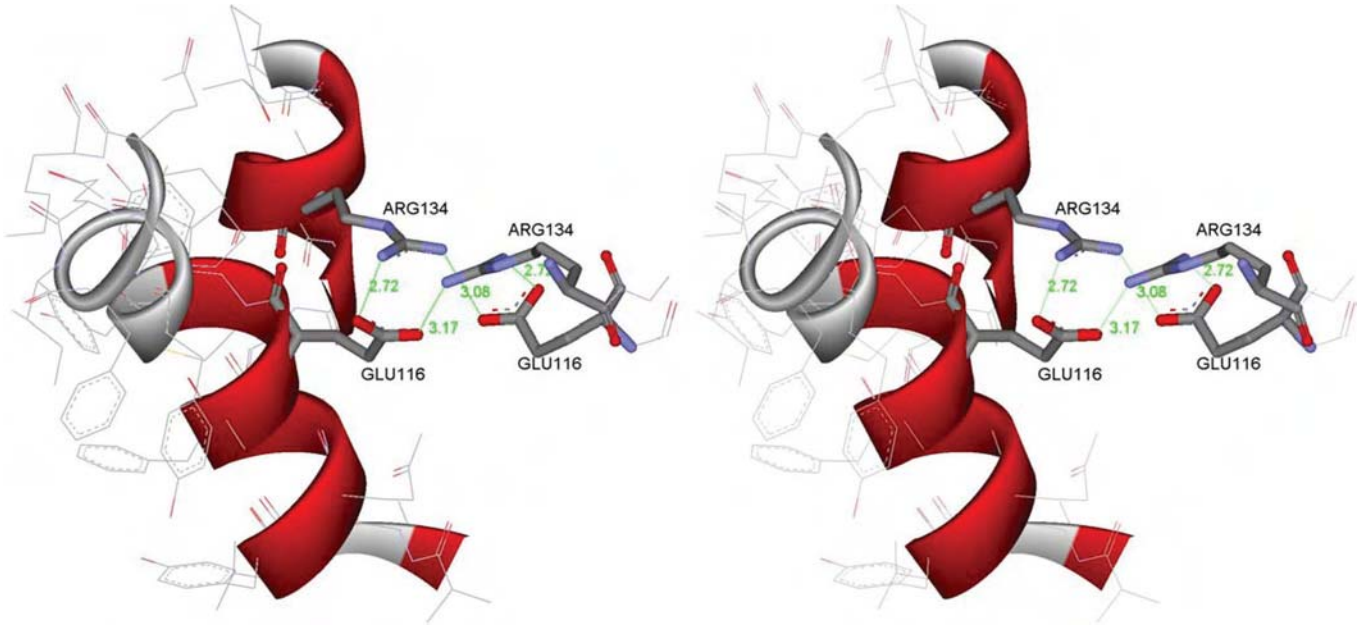

Figure 8 The electrostatic interaction in region 3 of Glu[116] and Arg[134] in adGSTD4-4

The two residues from each subunit are in proximity to interact electrostatically with each other as well as with the same residues from the other subunit. For the first subunit parts of α-helices 4 and 5, containing Glu[116] and Arg[134] respectively, are shown. For clarity only Glu[116] and Arg[134] from the second subunit are shown. Distances between the charged atoms are shown in Å. The Figure was created using Accelrys DS ViewerPro 5.0.

In conclusion, the conserved electrostatic interactions between the charged residues from α-helix 3 and α-helix 4 show important roles for protein folding, stabilization and dimerization of the alternatively spliced enzymes. However, the subunit interface region with the most variation in amino acid residues at equivalent positions between adGSTD3-3 and adGSTD4-4 showed that although the mutations did not alter the overall protein folding, the enzyme properties were changed, especially the catalytic activity, thermal stability and subunit interface. Even highly conservative amino acid replacements changed the protein properties. The results suggest that even splicing products from the same gene may have specific features in the subunit interface area that would preclude heterodimerization.

This work was funded by the TRF (Thailand Research Fund). J. P. held a DPST (Development and Promotion of Science and Technology Talent) scholarship. J. W. was supported by a Royal Golden Jubilee scholarship.

REFERENCES

1 Ketterer, B. (2001) A bird's eye view of the glutathione transferase field. Chem.-Biol. Interact. **138**, 27–42
2 Hayes, J. D., Flanagan, J. U. and Jowsey, I. R. (2005) Glutathione transferases. Annu. Rev. Pharmacol. Toxicol. **45**, 51–88
3 Luo, J.-K., Hornby, J. A. T., Wallace, L. A., Chen, J., Armstrong, R. N. and Dirr, H. W. (2002) Impact of domain interchange on conformational stability and equilibrium folding of chimeric class μ glutathione transferases. Protein Sci. **11**, 2208–2217
4 Hornby, J. A. T., Luo, J.-K., Stevens, J. M., Wallace, L. A., Kaplan, W., Armstrong, R. N. and Dirr, H. W. (2000) Equilibrium folding of dimeric class μ glutathione transferases involves a stable monomeric intermediate. Biochemistry **39**, 12336–12344
5 Luo, J.-K., Hornby, J. A. T., Armstrong, R. N. and Dirr, H. W. (2001) Equilibrium unfolding and enzyme kinetics of chimeric Mu class glutathione transferases. Chem.-Biol. Interact. **133**, 58–59
6 Sinning, I., Kleywegt, G. J., Cowan, S. W., Reinemer, P., Dirr, H. W., Huber, R., Gilliland, G. L., Armstrong, R. N., Ji, X., Board, P. G. et al. (1993) Structure determination and refinement of human Alpha class glutathione transferase A1-1, and a comparison with the Mu and Pi class enzymes. J. Mol. Biol. **232**, 192–212
7 Ji, X., Zhang, P., Armstrong, R. N. and Gilliland, G. L. (1992) The three-dimensional structure of a glutathione S-transferase from the Mu gene class: structural analysis of the binary complex of isoenzyme 3-3 and glutathione at 2.2 Å resolution. Biochemistry **31**, 10169–10184
8 Reinemer, P., Dirr, H. W., Ladenstein, R., Huber, R., Lo Bello, M., Federici, G. and Parker, M. W. (1992) Three-dimensional structure of class π glutathione S-transferase from human placenta in complex with S-hexylglutathione at 2.8 Å resolution. J. Mol. Biol. **227**, 214–226
9 Hornby, J. A. T., Codreanu, S. G., Armstrong, R. N. and Dirr, H. W. (2002) Molecular recognition at the dimer interface of a class Mu glutathione transferase: role of a hydrophobic interaction motif in dimer stability and protein function. Biochemistry **41**, 14238–14247
10 Pongjaroenkit, S., Jirajaroenrat, K., Boonchauy, C., Chanama, U., Leetachewa, S., Prapanthadara, L. and Ketterman, A. J. (2001) Genomic organization and putative promotors of highly conserved glutathione S-transferases originating by alternative splicing in *Anopheles dirus*. Insect Biochem. Mol. Biol. **31**, 75–85
11 Chelvanayagam, G., Parker, M. W. and Board, P. G. (2001) Fly fishing for GSTs: a unified nomenclature for mammalian and insect glutathione transferases. Chem.-Biol. Interact. **133**, 256–260
12 Wongsantichon, J., Harnnoi, T. and Ketterman, A. J. (2003) A sensitive core region in the structure of glutathione S-transferases. Biochem. J. **373**, 759–765
13 Ranson, H., Collins, F. and Hemingway, J. (1998) The role of alternative mRNA splicing in generating heterogeneity within the *Anopheles gambiae* class I glutathione S-transferase family. Proc. Natl. Acad. Sci. U.S.A. **95**, 14284–14289
14 Jirajaroenrat, K., Pongjaroenkit, S., Krittanai, C., Prapanthadara, L. and Ketterman, A. J. (2001) Heterologous expression and characterization of alternatively spliced glutathione S-transferases from a single *Anopheles* gene. Insect Biochem. Mol. Biol. **31**, 867–875
15 Ketterman, A. J., Prommeenate, P., Boonchauy, C., Chanama, U., Leetachewa, S., Promtet, N. and Prapanthadara, L. (2001) Single amino acid changes outside the active site significantly affect activity of glutathione S-transferases. Insect Biochem. Mol. Biol. **31**, 65–74
16 Oakley, A. J., Harnnoi, T., Udomsinprasert, R., Jirajaroenrat, K., Ketterman, A. J. and Wilce, M. C. J. (2001) The crystal structures of glutathione S-transferases isozymes 1-3 and 1-4 from *Anopheles dirus* species B. Protein Sci. **10**, 2176–2185
17 Wongsantichon, J. and Ketterman, A. J. (2006) An intersubunit lock-and-key 'Clasp' motif in the dimer interface of Delta class glutathione transferase. Biochem. J. **394**, 135–144
18 Bradford, M. M. (1976) A rapid and sensitive method for the quantitation of microgram quantities of protein utilizing the principle of protein–dye binding. Anal. Biochem. **72**, 248–254
19 Prapanthadara, L., Koottathep, S., Promtet, N., Hemingway, J. and Ketterman, A. J. (1996) Purification and characterization of a major glutathione S-transferase from the mosquito *Anopheles dirus* (species B). Insect Biochem. Mol. Biol. **26**, 277–285
20 Udomsinprasert, R. and Ketterman, A. J. (2002) Expression and characterization of a novel class of glutathione S-transferase from *Anopheles dirus*. Insect Biochem. Mol. Biol. **32**, 425–433
21 Habig, W. H., Pabst, M. J. and Jakoby, W. B. (1974) Glutathione S-transferases: the first enzymatic step in mercapturic acid formation. J. Biol. Chem. **249**, 7130–7139
22 Vararattanavech, A. and Ketterman, A. (2003) Multiple roles of glutathione binding-site residues of glutathione S-transferase. Protein Pept. Lett. **10**, 441–448
23 Stenberg, G., Dragani, B., Cocco, R., Mannervik, B. and Aceto, A. (2000) A conserved 'hydrophobic staple motif' plays a crucial role in the refolding of human glutathione transferase P1-1. J. Biol. Chem. **275**, 10421–10428
24 Stevens, J. M., Hornby, J. A. T., Armstrong, R. N. and Dirr, H. W. (1998) Class Sigma glutathione transferase unfolds via a dimeric and a monomeric intermediate: impact of subunit interface on conformational stability in the superfamily. Biochemistry **37**, 15534–15541
25 Dirr, H. (2001) Folding and assembly of glutathione transferases. Chem.-Biol. Interact. **133**, 19–23
26 Sayed, Y., Wallace, L. A. and Dirr, H. W. (2000) The hydrophobic lock-and-key intersubunit motif of glutathione transferase A1-1: implications for catalysis, ligandin function and stability. FEBS Lett. **465**, 169–172
27 Sluis-Cremer, N., Naidoo, N. and Dirr, H. (1996) Class-Pi glutathione S-transferase is unable to regain its native conformation after oxidative inactivation by hydrogen peroxide. Eur. J. Biochem. **242**, 301–307
28 Sayed, Y., Hornby, J. A. T., Lopez, M. and Dirr, H. (2002) Thermodynamics of the ligandin function of human class Alpha glutathione transferase A1-1: energetics of organic anion ligand binding. Biochem. J. **363**, 341–346
29 Sluis-Cremer, N., Naidoo, N. N., Kaplan, K. H., Manoharan, T. H., Fahl, W. E. and Dirr, H. W. (1996) Determination of a binding site for a nonsubstrate ligand in mammalian cytosolic glutathione S-transferases by means of fluorescence-resonance energy transfer. Eur. J. Biochem. **241**, 484–488
30 Segel, I. H. (1993) Enzyme kinetics, Behavior and Analysis of Rapid Equilibrium and Steady State Enzyme Systems. John Wiley & Sons, New York
31 Otzen, D. E., Rheinnecker, M. and Fersht, A. R. (1995) Structural factors contributing to the hydrophobic effect: the partly exposed hydrophobic minicore in chymotrypsin inhibitor 2. Biochemistry **34**, 13051–13058
32 Xu, J., Baase, W. A., Baldwin, E. and Matthews, B. W. (1998) The response of T4 lysozyme to large-to-small substitutions within the core and its relation to the hydrophobic effect. Protein Sci. **7**, 158–177
33 Ding, Y., Ortelli, F., Rossiter, L. C., Hemingway, J. and Ranson, H. (2003) The *Anopheles gambiae* glutathione transferase supergene family: annotation, phylogeny and expression profiles. BMC Genomics **4**, 35–50

Received 24 April 2006/21 August 2006; accepted 29 August 2006
Published as BJ Immediate Publication 29 August 2006, doi:10.1042/BJ20060603

Future Plans

We will continue to perform structure function studies to increase our understanding of which amino acid residues affect enzyme specificity. We are also interested in determining the mechanism of how the elucidated amino acids contribute to the observed specificity.

Publications

We have published fourteen papers in the last three years for a total 2005 impact factor of 43.633. For the sake of simplicity we only present the three Biochemical Journal (2005 Impact Factor 4.224) papers published this year (2007; publications 1-3 in the list below) in this Final Annual Report. The complete reprints of all fourteen papers are included in the appendix.

1. Vararattanavech, A. and **Ketterman**, A.J. (2007) A functionally conserved basic residue in glutathione transferases interacts with the glycine moiety of glutathione and is pivotal for enzyme catalysis. *Biochem. J.* Immediate Publication **DOI (Digital Object Identifier): 10.1042/BJ20070422,** In press. (2005 Impact Factor 4.224)
2. Winayanuwattikun, P. and **Ketterman**, A.J. (2007) Glutamate 64, a newly identified residue of the functionally conserved electron-sharing network contributes to catalysis and structural integrity of glutathione transferases. *Biochem. J.* **402**, 339-348. (2005 Impact Factor 4.224)
3. Piromjitpong, J., Wongsantichon, J. and **Ketterman**, A.J. (2007) Differences in the subunit interface residues of alternatively spliced glutathione transferases affects catalytic and structural functions. *Biochem. J.* **401,** 635-644. (2005 Impact Factor 4.224)
4. Wongsantichon, J., Yuvaniyama, J. and **Ketterman**, A.J. (2006) Crystallization and preliminary X-ray crystallographic analysis of a highly stable mutant V107A of glutathione transferase from *Anopheles dirus* in complex with glutathione. *Acta Crys. F* **62**, 310-312. (No impact factor)
5. Laohavechvanich, P., Kangsadalampai, K., Tirawanchai, N. and **Ketterman**, A.J. (2006) Effect of different Thai traditional processing of various hot chili peppers on urethane-induced somatic mutation and recombination in *Drosophila melanogaster*: assessment of the role of glutathione transferase activity. *Food Chem. Toxicol.* **44**, 1348-1354. (2005 Impact Factor 2.047)
6. Charoensilp, G., Vararattanavech, A., Leelapat, P., Prapanthadara, L. and **Ketterman**, A.J. (2006) Characterization of *Anopheles dirus* glutathione transferase Epsilon 4. *ScienceAsia* **32**, 159-165. (No impact factor)
7. Wongsantichon, J. and **Ketterman**, A.J. (2006) An Intersubunit Lock-and-Key 'Clasp' Motif in the Dimer Interface of Delta Class Glutathione Transferase. *Biochem. J.* **394,** 135-144. (2005 Impact Factor 4.224)
8. Vararattanavech, A., Prommeenate, P. and **Ketterman**, A.J. (2006) The structural roles of a conserved small hydrophobic core in the active site and an ionic bridge in domain I of delta class glutathione transferase. *Biochem. J.* **393,** 89-95. (2005 Impact Factor 4.224)
9. Bogoyevitch, M.A., Barr, R.K., **Ketterman**, A.J. (2005) Peptide inhibitors of protein kinases – discovery, characterisation and use. *Biochim. Biophys. Acta - Proteins & Proteomics* **1754**, 79-99. (2005 Impact Factor 2.980)
10. Winayanuwattikun, P. and **Ketterman**, A.J. (2005) An electron-sharing network involved in the catalytic mechanism is functionally conserved in different glutathione transferase classes. *J. Biol. Chem.* **280**, 31776-31782. (2005 Impact Factor 5.854)
11. Wongsantichon, J. and **Ketterman**, A.J. (2005) [6] Alternative Splicing Of Glutathione S-Transferases. Edited by Helmut Sies and Lester Packer. **In** *Methods in Enzymology,* "Phase II: Conjugation Enzymes, Glutathione Transferases and Transport Systems". Vol. **401**, 100-116. Elsevier Inc., San Diego. (2005 Impact Factor 1.695)
12. Udomsinprasert, R., Pongjaroenkit, S., Wongsantichon, J., Oakley, A.J., Prapanthadara, L., Wilce, M.C.J. and **Ketterman**, A.J. (2005) Identification, characterization and structure of a new delta class glutathione transferase isoenzyme. *Biochem. J.* **388**, 763-771. (2005 Impact Factor 4.224)
13. Wongtrakul, J., Sramala, I., Prapanthadara, L. and **Ketterman**, A.J. (2005) Intra-subunit residue interactions from the protein surface to the active site of glutathione S-transferase AdGSTD3-3 impact on structure and enzyme properties. *Insect Biochem. Molec. Biol.* **35,** 197-205**.** (2005 Impact Factor 2.733)
14. Bogoyevitch, M.A., Boehm, I., Oakley, A., **Ketterman**, A.J. and Barr, R.K. (2004) Targeting the JNK MAPK cascade for inhibition: basic science and therapeutic potential. *Biochim. Biophys Acta* **1697**, 89-101. (2005 Impact Factor 2.980)

Professional Invitations
Within the last 3 years, I have been invited to join the Panel of Editorial Advisers for the *Biochemical Journal* (http://www.biochemj.org/bj/bjedavpanel.htm). I have also been a co-author on the top downloaded paper of BBA Proteins and Proteomics in 2005 (**Publications** Paper 14). I have been an invited speaker at the 17th FAOBMB Symposium/2nd IUBMB Special Meeting/7th S-IMBN Conference on "Genomics and Health in the 21st Century". 22-26 November 2004, Bangkok, Thailand. Session R: Protein Expression, Structure and Function. IL-C11 Structural studies on glutathione S-transferases from *Anopheles dirus*.

Collaborations Domestic and International
I have several working collaborations. One collaboration is with Dr. L. Prapanthadara at the Research Institute for Health Sciences, Chiangmai University. Dr. Prapanthadara is involved with the enzyme characterization studies and also in supplying my laboratory with *An. dirus* mosquitoes. I have two collaborations with my former PhD students who have now completed, Dr. Saengtong Pongjareankit and Dr. Jeerang Wongtrakul. Both have now returned to their universities, Maejo and Chiangmai University. Another collaboration within Thailand is with Dr. Jirundon Yuvaniyama at the Department of Biochemistry and Center for Excellence in Protein Structure and Function, Faculty of Science, Mahidol University. Dr. Yuvaniyama has been involved in helping us to obtain new GST structures. An overseas collaboration is with Dr. Marie A. Bogoyevitch in the Cell Signalling Laboratory, Department of Biochemistry, University of Western Australia. The collaboration with Dr. Bogoyevitch is investigating the GST interactions with the MAP kinase pathways. The second overseas collaboration is with Dr. Aaron J. Oakley in the Biological Chemistry Section of the Research School of Chemistry at the Australian National University. Dr. Oakley is a crystallographer and is currently crystallizing and elucidating the tertiary structure of the *An. dirus* recombinant GSTs that we are studying. We have also now formed a new collaboration with Assoc. Prof. Robert Robinson at the Institute of Molecular and Cell Biology, Proteos, Singapore. Dr. Robinson is also a crystallographer and is helping us to obtain new GST structures.

Collaborations within Institute
We have formed a scientific support network consisting of the following four ajarns and their respective groups (at this time this includes 30 people): Drs. G. Katzenmeier, C. Angsuthanasombat, A. Ketterman, and C. Krittanai.

Problems
There are no unusual problems.

Comments and Suggestions
It would be helpful to receive the next funding budget quickly.

Appendix

Reprints of the fourteen papers published in the last three years.

A functionally conserved basic residue in glutathione S-transferases interacts with the glycine moiety of glutathione and is pivotal for enzyme catalysis

Ardcharaporn VARARATTANAVECH and Albert J. KETTERMAN[1]

Institute of Molecular Biology and Genetics, Mahidol University, Salaya Campus, 25/25 Putthamonthol Road 4, Salaya, Nakon Pathom 73170, Thailand

The present study characterized conserved residues in a GST (glutathione S-transferase) in the active-site region that interacts with glutathione. This region of the active site is near the glycine moiety of glutathione and consists of a hydrogen bond network. In the GSTD (Delta class GST) studied, adGSTD4-4, the network consisted of His^{38}, Met^{39}, Asn^{47}, Gln^{49}, His^{50} and Cys^{51}. In addition to contributing to glutathione binding, this region also had major effects on enzyme catalysis, as shown by changes in kinetic parameters and substrate specific activity. The results also suggest that the electron distribution of this network plays a role in stabilization of the ionized thiol of glutathione as well as impacting on the catalytic rate-limiting step. This area constitutes a second glutathione active site network involved in glutathione ionization distinct from a network previously observed interacting with the glutamyl end of glutathione. This second network also appears to be functionally conserved in GSTs. In the present study, His^{50} is the key basic residue stabilized by this network as shown by up to a 300-fold decrease in k_{cat} and 5200-fold decrease in k_{cat}/K_m for glutathione. Although these network residues have a minor role in structural integrity, the replaced residues induced changes in active site topography as well as generating positive co-operativity towards glutathione. Moreover, this network at the glycine moiety of GSH (glutathione) also contributed to the 'base-assisted deprotonation model' for GSH ionization. Taken together, the results indicate a critical role for the functionally conserved basic residue His^{50} and this hydrogen bond network in the active site.

Key words: base-assisted deprotonation model, conserved active-site residue, Delta class GST, enzyme catalysis, glutathione S-transferase (GST), glycine moiety of glutathione (GSH).

INTRODUCTION

GSTs (glutathione S-transferases; EC 2.5.1.18) are intracellular proteins, which are widely distributed in nature, being found in most aerobic eukaryotes and prokaryotes [1,2]. GSTs are polymorphic with most organisms possessing a genetic capacity to encode multiple isoforms of various classes [3,4]. The enzymes are an integral part of the phase II detoxification mechanism being involved in xenobiotic metabolism as well as protection against peroxide damage. GSTs catalyse reactions with a very broad range of structurally diverse electrophilic substrates (e.g. alkylhalides, arylhalides, lactones, epoxides, quinones, esters and activated alkenes) [4–6]. This enzyme family therefore displays a wide range of catalytic functions while retaining a high specificity towards the thiol substrate glutathione (GSH). The GSH conjugation by GST increases the solubility of the target molecule, thus facilitating the excretion of the molecule from the organism.

All cytosolic GSTs have very similar three-dimensional structures and the active site pocket is very similar in the G-site (GSH-binding site) [7–9]. The N-terminal domain of GST adopts a $\beta\alpha\beta\alpha\beta\beta\alpha$ topology that contributes most of the contacts to GSH and is called the G-site. The crystal structures of GSTs show that most of the active site residues involved in the binding and activation of GSH are found within the N-terminus; hence this region of the protein is therefore highly conserved between GSTs [7,8,10]. The C-terminal domain is all α-helical providing some of the contacts to the hydrophobic binding site that lies adjacent to the G-site.

Substrate conjugation of electrophilic xenobiotics involves its nucleophilic attack at the ionized thiol of GSH in the active site. A conserved tyrosine (for Alpha, Mu and Pi classes) or serine (for Theta and Delta classes) residue within hydrogen-bonding distance of the thiol of GSH has been shown to be of primary importance in facilitating GSH deprotonation as well as stabilization of the ionized GSH by hydrogen-bonding [10–14]. In addition, conserved residues that interact directly with the glutamyl moiety of GSH, for example Ser^{65}, Arg^{66} and Ile^{52} in GSTD (Delta class GST) have also been implicated in critical roles in the catalytic mechanism, involvement in GSH binding, GSH thiol ionization, as well as structural integrity [15–17]. Therefore the residues interacting with the other end of GSH, the glycine moiety (His^{38}, Met^{39}, Asn^{47}, Gln^{49}, His^{50} and Cys^{51}) were of interest (Figure 1) [18]. His^{38} and His^{50} interact directly with the glycine carboxylic group of GSH [19]. Both histidines appear to be assisted or stabilized by dipole–dipole interaction with Met^{39}. Moreover, a hydrogen bond network in the G-site near the glycine moiety of GSH, involving several residues (His^{50}, Asn^{47}, Gln^{49} and Cys^{51}) and GSH, is proposed to be essential to electron distribution for enzyme catalysis. To investigate the roles of these residues, mutagenesis studies were performed and the engineered enzymes characterized by kinetic constants, substrate specific activity, pK_a determination and rate-limiting step determination in addition to physical properties.

Abbreviations used: CDNB, 1-chloro-2,4-dinitrobenzene; DCNB, 1,2-dichloro-4-nitrobenzene; EA, ethacrynic acid; FDNB, 1-fluoro-2,4-dinitrobenzene; G-site, GSH (glutathione)-binding site; GST, glutathione S-transferase; GSTD, Delta class GST; hGSTP1-1, human GSTP1-1; PNBC, *p*-nitrobenzyl chloride; PNPBr, *p*-nitrophenethyl bromide; ZmGST1, *Zea mays* (maize) GST1.

[1] To whom correspondence should be addressed (email albertketterman@yahoo.com).

COLOUR

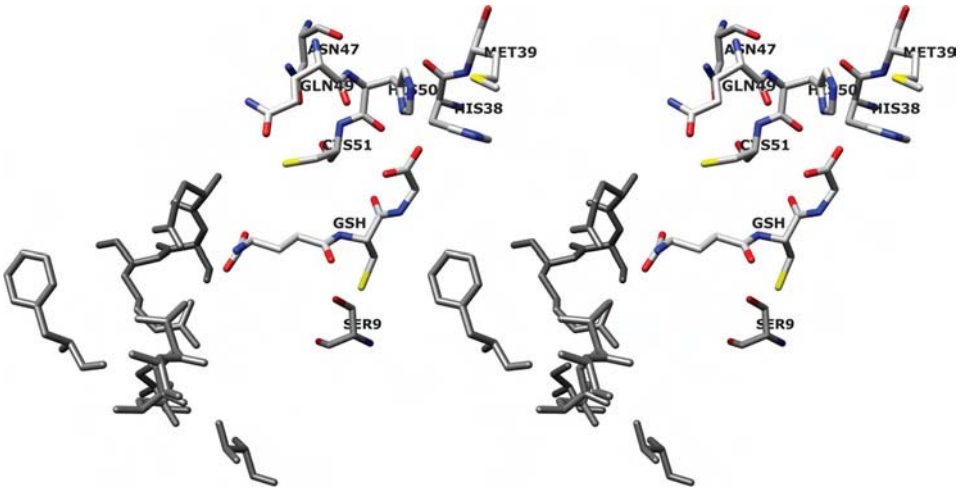

Figure 1 Stereoview of conserved G-site residues that directly interact with the glycine moiety of GSH and generate a hydrogen bond network

His[38] and His[50] interact directly with the glycine carboxylic group of GSH and are assisted or stabilized by dipole–dipole interaction with Met[39]. A hydrogen bond network in the G-site is formed by several residues (His[50], Asn[47], Gln[49] and Cys[51]) and GSH. The previously identified electron-sharing network at the glutamyl end of GSH is shown in grey [16]. The image was produced using the UCSF Chimera package from the Resource for Biocomputing, Visualization, and Informatics at the University of California, San Francisco, CA, U.S.A. (http://www.cgl.ucsf.edu/chimera) (supported by National Institutes of Health grant P41 RR-01081) [18].

MATERIALS AND METHODS

Site directed mutagenesis

The engineered enzymes were generated using Stratagene's QuikChange® site-directed mutagenesis protocol. The primers used were designed based on the sequence of the *adGSTD4* wild-type gene (GenBank® accession number AF273040). Full-length DNA sequencing in both directions was performed to confirm the engineered clones.

Protein expression and purification

After transformation of the engineered plasmids into *Escherichia coli* BL21(DE3)pLysS, protein expression was performed. The recombinant adGSTD4-4 engineered enzymes and wild-type were purified either by glutathione affinity chromatography according to the manufacturer's instructions (Amersham Biosciences) or by cation exchanger (SP-XL) followed by hydrophobic interaction chromatography (phenyl-Sepharose) as described previously [19]. The purified enzymes (in 50 mM potassium phosphate, pH 6.5) were stored in 50 % (v/v) glycerol at −20 °C until used. The concentrations of the proteins were determined by Bio-Rad protein reagent (Bio-Rad) by using BSA as the standard protein and the purity of the proteins was observed by SDS/PAGE.

Kinetic parameters determination

Kinetic experiments were performed as previously described [20]. Kinetic constants were determined by varying the CDNB (1-chloro-2,4-dinitrobenzene) concentration (0.031–3.0 mM) while GSH was held constant at a saturating concentration and by varying GSH concentrations (0.25–20 mM) at a saturating concentration of CDNB. The standard GST assay was performed using 3 mM CDNB and 10 mM GSH for adGSTD4-4 wild-type. The rate of conjugation between GSH and CDNB was monitored by continuously measuring change in absorbance at 340 nm for 1 min using a SpectraMax 250 at 25–27 °C. A molar absorption coefficient (ε) of 9.6 $mM^{-1} \cdot cm^{-1}$ was used to convert the absorbance to moles [21]. Steady-state kinetics followed Michaelis–Menten kinetics except where stated. With evidence of co-operativity upon GSH binding, demonstrated by a sigmoidal curve instead of a hyperbolic curve on a Michaelis–Menten plot, a Hill equation (eqn 1) was used to fit the experimental kinetic data on the plot. $K_{0.5}$ is the substrate concentration that gives the rate of reaction at half of V_{max}, similar to the K_m value for non-co-operative binding ($h = 1$).

$$Y = V/V_{max} = [S]^h/(K_{0.5} + [S]^h) \quad (1)$$

$$\log[Y/(1-Y)] = h \log[S] - \log K_{0.5} \quad (2)$$

A sigmoidal Hill equation was practically transformed into a linear rate equation (eqn 2), where Y is the fractional saturation; h is the Hill coefficient; and $K_{0.5}$ is an averaged binding constant at $Y = 0.5$. A Hill plot, a plot between $\log[Y/(1–Y)]$ and $\log[S]$, was employed to determine the degree of co-operativity by the slope of the plot that yields the Hill coefficient (h) [22]. Catalytic constant (k_{cat}) and the catalytic efficiency (k_{cat}/K_m) were calculated on an active site basis using the subunit molecular mass of each enzyme. Maximal velocity (V_{max}) and Michaelis constant (K_m) were determined by nonlinear regression software analysis (GraphPad Prism version 5.00 for Windows; GraphPad Software, San Diego, CA, U.S.A.; http://www.graphpad.com). One-way ANOVA with Dunnett's multiple comparison post test was performed with wild-type as control using GraphPad Prism 5.

Specific activity determination

The specific activities towards several GST substrates were determined as previously described [23]. All measurements were performed at 25–27 °C in 0.1 M potassium phosphate buffer (pH 6.5 or 7.5). The GST activities were measured with glutathione and five hydrophobic substrates: CDNB, DCNB (1,2-dichloro-4-nitrobenzene), EA (ethacrynic acid), PNPBr (*p*-nitrophenethyl bromide) and PNBC (*p*-nitrobenzyl chloride). Specific activities were calculated according to the molar absorption coefficient for each substrate [21].

pH dependence of kinetic parameters

The pH dependence of k_{cat}/K_m^{CDNB} was obtained by performing kinetic measurements in the following buffers: 0.1 M sodium

Table 1 Steady-state kinetic constants using GSH and CDNB as GST substrates

The units of V_{max}, k_{cat}, K_m and k_{cat}/K_m are μmol · min^{-1} · mg of protein^{-1}, s^{-1}, mM and s^{-1} · mM^{-1} respectively. *These engineered GSTs showed positive co-operativity upon GSH binding with Hill coefficient (h) shown. The value shown is $K_{0.5}$, obtained from the Hill equation, which is the substrate concentration that gives the rate of reaction at half of V_{max} [22]. [a]Some of these values have been previously reported and are shown for purposes of comparison [19,20]. One-way ANOVA with Dunnett's multiple comparison test was performed with wild-type as control; statistical significance is shown by † for $P < 0.05$, ‡ for $P < 0.01$ and § for $P < 0.001$.

			CDNB		GSH		
Enzyme	V_{max}	k_{cat}	K_m	k_{cat}/K_m	K_m	k_{cat}/K_m	h
Wild-type[a]	62.45 ± 1.24	26.13	0.50 ± 0.02	51.84	0.50 ± 0.10	52.06	0.91 ± 0.02
H38A[a]	36.4 ± 1.12§	15.26	1.25 ± 0.12§	12.21	15.8 ± 1.19§	0.97	–
H38E[a]	14.91 ± 0.44§	6.23	0.92 ± 0.11§	6.76	8.32 ± 0.22*§	0.74	1.83 ± 0.01§
H38F[a]	9.71 ± 0.43§	4.06	0.98 ± 0.09§	4.14	35.26 ± 0.86§	0.12	–
H38D	4.61 ± 0.12§	1.93	0.71 ± 0.01†	2.71	15.90 ± 0.21§	0.12	–
H38K	5.54 ± 0.12§	2.32	0.71 ± 0.08†	3.27	23.50 ± 1.21§	0.10	–
M39A	25.56 ± 0.96§	10.70	0.79 ± 0.06§	13.50	6.32 ± 0.34*§	1.69	1.72 ± 0.12§
M39F	38.56 ± 1.72§	16.14	0.50 ± 0.02	32.22	2.18 ± 0.09†	5.75	–
N47A	0.225 ± 0.003§	0.09	0.67 ± 0.06	0.13	11.50 ± 0.51§	0.01	–
Q49A	43.28 ± 0.96§	18.11	0.74 ± 0.06‡	24.47	5.58 ± 0.46*§	3.24	1.64 ± 0.04§
Q49E	49.75 ± 1.36§	20.82	0.49 ± 0.05	42.49	2.87 ± 0.09*§	7.26	1.51 ± 0.03§
H50A[a]	6.46 ± 0.26§	2.70	1.10 ± 0.15§	2.45	7.34 ± 0.21§	0.37	–
H50E[a]	0.21 ± 0.01§	0.09	0.81 ± 0.04§	0.11	12.34 ± 0.36§	0.01	–
H50Y[a]	0.87 ± 0.02§	0.36	0.83 ± 0.06§	0.43	12.57 ± 0.73§	0.03	–
H50K	8.14 ± 0.03§	3.40	0.69 ± 0.06†	4.95	6.77 ± 0.27*§	0.45	1.54 ± 0.06§
H50F	1.44 ± 0.03§	0.60	0.76 ± 0.01‡	0.79	6.43 ± 0.38§	0.09	–
C51A	19.64 ± 0.65§	8.22	0.82 ± 0.04§	10.01	6.40 ± 0.12*§	1.28	1.57 ± 0.08§
C51D	2.16 ± 0.07§	0.91	1.30 ± 0.08§	0.7	16.94 ± 0.69*§	0.05	1.40 ± 0.03§

acetate buffers (from pH 5.0 to 5.5) and 0.1 M potassium phosphate buffer (from pH 6.0 to 8.5). Increments of pH were 0.5 and control experiments showed no discontinuities from buffer types. The pK_a values of bound GSH were obtained by fitting the data to the equation $y = y^{lim}/(1 + 10^{pKa-pH})$ as previously described [13]. The program GraphPad Prism 5 was used for nonlinear fit of the data to the sigmoidal dose–response (variable slope) equation.

Fluoride/chloride leaving group substitution

A diagnostic test in evaluating the rate-limiting step in nucleophilic aromatic substitution reactions is the effect of different leaving groups on kinetic parameters [13]. The second order kinetic constants at pH 6.5 for the spontaneous reaction of GSH with CDNB and FDNB (1-fluoro-2,4-dinitrobenzene) were determined by kinetic measurement by using CDNB or FDNB as co-substrate as previously described [24]. The ratios of the catalytic constants ($k_{cat}^{FDNB}/k_{cat}^{CDNB}$) were determined.

Effect of viscosity on the kinetic parameters

The dependence of the steady-state kinetic parameters on relative viscosity was observed by performing kinetics measurements in the presence of varying glycerol concentrations. The range of relative viscosities (η/η^0) was between 1.53 and 4.43. The slope of the plots for relative catalytic constant (k_{cat}^0/k_{cat}) versus relative viscosity (η/η^0) was determined. Viscosity values (η) at 25 °C were calculated as described previously [25].

Thermal stability assay

The enzymes at 0.1 mg/ml in 0.1 M phosphate buffer (pH 6.5) containing 1 mM EDTA and 5 mM dithiothreitol were incubated at 45 °C for various times and then activity was measured in the standard GST assay. The data were plotted as log percentage of remaining activity versus pre-incubation time. The half-life ($t_{½}$) of the enzyme at 45 °C was calculated from the slope of the plot using the equations: Slope $= k/2.3$, $k = 0.693/t_{½}$.

Intrinsic fluorescence measurement

There are two tryptophan residues in each monomer of adGSTD4-4: Trp^{64} and Trp^{191}. The intrinsic fluorescence from Trp^{64}, which is exposed to solvent at the base of the G-site, can be used to monitor the active site conformation indirectly. The intrinsic fluorescence of adGSTD4-4 was measured in a single-photon counting spectrofluorimeter. Excitation was at 295 nm and emission was scanned from 300 to 450 nm. In these experiments, a number of samples containing 0.1 mg/ml GST in 0.1 M potassium phosphate buffer (pH 6.5) were prepared similarly for the wild-type and engineered enzymes. The wavelength that gives the maximum fluorescence intensity (λ_{max}) and fluorescence intensity at λ_{max} were observed. The experimental data was corrected both for dilution and for inner filter effects.

RESULTS

Enzymatic characterization

Michaelis–Menten analysis was performed using nonlinear regression to determine steady-state kinetic constants (Table 1). The kinetic constants showed the residue changes of His^{38}, His^{50}, Met^{39}, Asn^{47}, Cys^{51} and Gln^{49} impacted upon catalysis. The engineered G-site residue enzymes showed only small changes in K_m^{CDNB}, whereas remarkably lower affinities towards GSH were shown (greater K_m^{GSH}) compared with wild-type. Positive co-operativity for GSH binding was observed for several engineered enzymes that displayed deviation of steady-state kinetics from a Michaelis–Menten hyperbolic to a sigmoidal curve response. The extent of positive co-operativity is shown by Hill coefficients (h) ranging from 1 (no co-operativity) to 2 (full co-operativity) for a dimeric enzyme with two active sites. Positive co-operativity was observed for H38E, M39A, H50K, C51A, C51D, Q49A and GA49E as determined by Hill coefficients ranging from 1.40 to 1.83, suggesting that the changed residues altered the movement of α2-helix and its flanking region to influence the induced-fit mechanism.

Table 2 Substrate-specific activity of the engineered enzymes compared to the wild-type

The substrates used were 3 mM CDNB, 1 mM DCNB, 0.1 mM PNPBr, 0.1 mM PNBC and 0.2 mM EA. The reactions were performed at a constant GSH concentration (appropriate for each enzyme). [a]Some of these values have been previously reported and are shown for purposes of comparison [19,20]. One-way ANOVA with Dunnett's multiple comparison test was performed with wild-type as control; statistical significance is shown by † for $P < 0.05$, ‡ for $P < 0.01$ and § for $P < 0.001$.

	Specific activity (μmol · min^{-1} · mg^{-1})				
Enzyme	CDNB	DCNB	EA	PNPBr	PNBC
Wild-type[a]	52.50 ± 0.52	0.035 ± 0.006	0.286 ± 0.062	0.074 ± 0.012	0.064 ± 0.002
H38A[a]	21.70 ± 0.20§	0.037 ± 0.001	0.146 ± 0.016§	0.040 ± 0.004§	0.013 ± 0.002§
H38E[a]	11.21 ± 0.24§	< 0.001	0.191 ± 0.026§	< 0.008	< 0.005
H38F[a]	3.76 ± 0.09§	< 0.001	0.230 ± 0.019†	< 0.005	< 0.003
H38D	2.33 ± 0.07§	< 0.001	0.111 ± 0.011§	< 0.001	< 0.003
H38K	2.02 ± 0.07§	< 0.001	0.165 ± 0.007§	< 0.003	< 0.002
M39A	18.84 ± 0.66§	0.012 ± 0.001§	0.183 ± 0.011§	< 0.005	< 0.003
M39F	28.67 ± 0.71§	0.043 ± 0.002†	0.166 ± 0.010§	0.029 ± 0.008§	0.065 ± 0.009
N47A	0.13 ± 0.01§	< 0.001	0.079 ± 0.001§	< 0.001	< 0.001
Q49A	33.36 ± 0.92§	0.023 ± 0.002‡	0.244 ± 0.012	0.050 ± 0.002§	0.044 ± 0.001‡
Q49E	41.76 ± 0.60§	0.032 ± 0.001	0.244 ± 0.020	0.020 ± 0.001§	0.048 ± 0.003‡
H50A[a]	3.80 ± 0.10§	0.015 ± 0.007§	0.146 ± 0.050§	0.012 ± 0.002§	0.016 ± 0.007§
H50E[a]	0.15 ± 0.01§	< 0.001	0.026 ± 0.004§	< 0.005	< 0.005
H50Y[a]	0.47 ± 0.01§	< 0.001	0.064 ± 0.008§	< 0.008	< 0.005
H50K	6.28 ± 0.04§	0.007 ± 0.001§	0.053 ± 0.020§	< 0.007	< 0.004
H50F	0.93 ± 0.03§	< 0.001	0.077 ± 0.005§	< 0.001	< 0.001
C51A	15.44 ± 0.58§	0.009 ± 0.001§	0.046 ± 0.001§	0.019 ± 0.001§	< 0.001
C51D	1.24 ± 0.03§	< 0.001	0.080 ± 0.004§	< 0.002	< 0.001

Although Met[39] interacts directly with GSH interacting residues, His[38] and His[50], the contribution to catalytic function is through the effect on GSH binding. The results suggest that the effect is mostly through a packing rearrangement that includes any perturbation of the orientation of His[38] or His[50]. Rearrangement of active site residues is elicited by M39A to accommodate the decreased volume as well as the lack of dipole–dipole interaction with the histidines. This condition also appears to engender flexibility to this region, which is shown by positive co-operativity for GSH binding with a Hill coefficient of 1.72 ± 0.12 (Table 1).

The GSH interaction was decreased for all His[38] engineered enzymes as shown by an increase in K_m^{GSH} of 17–71-fold. In addition, positive co-operativity for GSH was observed for H38E with a Hill coefficient (h) of 1.83 ± 0.01.

There is a hydrogen bond network in the GST active site that is adjacent to the GSH glycine moiety. This network is formed by several residues, Asn[47], Gln[49] and Cys[51], as well as His[50], with the latter directly interacting with GSH. His[50] replacements not only decreased binding affinity to GSH (ranging from 13- to 25-fold) but also impacted upon catalytic rates as shown by k_{cat} values that decreased from 13 to 0.3 % of the wild-type enzyme k_{cat} values. The N47A change displayed several large effects on the enzyme, one on enzyme catalysis with the enzyme having only 0.3 % k_{cat} of the wild-type, and another on GSH binding with a 23-fold increase in K_m^{GSH}. Gln[49] and Cys[51] interaction is through their main-chain nitrogens and oxygens. Changes in these residues showed intermediate effects on catalysis except for C51D, which had a k_{cat} only 3.5 % of wild-type. However, the changes in these residues all showed a major impact on GSH binding with increased K_m^{GSH} values from 6- to 34-fold. The results suggest that a packing rearrangement occurred. This rearrangement also enabled subunit–subunit communication as shown by the observed positive co-operativity upon GSH binding (Table 1).

Substrate specific activity was affected for all the engineered enzymes to varying degrees (Table 2). For example, most of the enzymes exhibited less effect on activity for EA. This suggests that the binding mode and the orientation of this substrate are different from the other substrates. Both GSH and hydrophobic substrate-binding sites are located in the same active site pocket of GSTs, therefore it is not surprising that changes in the G-site residues can perturb the hydrophobic substrate site.

It has been proposed that many steps occur in the GST catalytic mechanism including GSH ionization through thiol deprotonation, substrate conjugation by nucleophilic attack of the thiolate at the electrophilic centre, product formation and product release from the active site [13,26–28]. The overall velocity of the enzyme-catalysed reaction is affected by most of the engineered residues, although to different extents. Therefore several steps in the catalytic pathway were studied to determine the roles of the engineered residues.

pH dependence of kinetic constants

The pK_a values of ionized GSH (enzyme-bound GSH) were calculated from plots of k_{cat}/K_m^{CDNB} versus pH for the wild-type and engineered enzymes (Table 3; Figure 2). The apparent pK_a for wild-type is approx. 6.0. The pK_a values of ionized GSH in the engineered enzymes varied, with the greatest effect shown by H50A which increased it by almost 1 pH unit. GSH ionization is considered to be an important step in the catalytic mechanism of GST that generates the thiolate anion (intermediate deprotonated form of GSH) for conjugation with the electrophilic substrate. This kinetically relevant ionization of GSH has been shown to be reflected in pH dependence for k_{cat}/K_m^{CDNB} [13]. Several reports have shown that residues located near the cysteine thiol and glutamyl α-carboxylate of GSH contribute to promoting and stabilizing the anionic glutathione thiol group [13,27–31]. However, this is the first report of involvement of the GSH glycine moiety in GSH ionization.

Meisenheimer complex formation

Meisenheimer complex or σ-complex intermediate, is generated during a nucleophilic aromatic substitution reaction. Leaving group effects on enzyme catalysis can be used to determine

Table 3 The pK_a value of ionized GSH in the active site of wild-type and engineered enzymes

The effect of pH on k_{cat}/k_m^{CDNB} was obtained by measuring kinetic constants using various pH buffers of 0.1 M sodium acetate buffers (from pH 5.0 to 5.5) and 0.1 M potassium phosphate buffer (from pH 6.0 to 8.5). The pK_a values of ionized GSH (GSH-bound enzyme) were determined. n.d., Not determined (low activity precluded measurement). One-way ANOVA with Dunnett's multiple comparison test was performed with wild-type as control; statistical significance is shown by § for $P < 0.001$. See Figure 2 for a plot of the experimental data.

Enzyme	pK_a (ionized GSH)
Wild-type	6.00 ± 0.05
H38A	6.10 ± 0.02
M39A	6.52 ± 0.05§
N47A	n.d.
Q49A	6.23 ± 0.05§
H50A	6.92 ± 0.06§
C51A	6.22 ± 0.03§
C51D	6.42 ± 0.03§

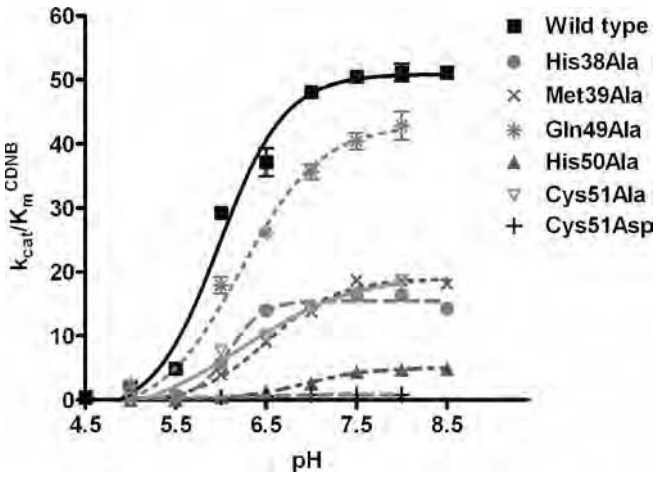

Figure 2 Plot of the data to determine the pK_a value of ionized GSH in the active site of wild-type and engineered enzymes

The effect of pH on k_{cat}/k_m^{CDNB} was obtained by measuring kinetic constants using various pH buffers of 0.1 M sodium acetate buffers (from pH 5.0 to 5.5) and 0.1 M potassium phosphate buffer (from pH 6.0 to 8.5). The pK_a values of ionized GSH (GSH-bound enzyme) were determined (see Table 3). The results are presented as means ± S.D. from at least three independent experiments.

whether the rate-limiting step of the reaction is σ-complex formation. The substitution of a more electronegative leaving group concomitant with an increase in the rate constant of the spontaneous reaction with glutathione is a signal that the σ-complex formation is a rate-limiting step [13]. Therefore the influence on the catalytic constant of the chlorine leaving group of CDNB replaced with fluorine was examined (Table 4).

Although the wild-type enzyme was insensitive, several of the engineered enzymes demonstrated sensitivity to the halogen leaving group, particularly H50A, C51D and D47A, with increased ratio values of 19-, 27- and 18-fold respectively. The catalytic efficiency (k_{cat}/K_m) of the engineered enzymes showed a different sensitivity to the nature of the leaving group, suggesting that an alteration of the relative catalytic-centre activity is a consequence of changes in the rate of σ-complex formation rather than changes in binding affinity towards the different substrate leaving groups. The results suggest that the process of σ-complex intermediate formation is affected by the disruption of the hydrogen bond network to GSH which affected the overall velocity of the enzyme-catalysed reaction. It is possible that the residue changes caused incorrect orientation of the GSH thiol or of the His[50] side chain, which then disturbs the conjugation process of the thiolate anion with the electrophilic substrate. Additionally, the results strongly support that the hydrogen bond network contributes to both the GSH ionization process and σ-complex intermediate formation. This contribution appears to stabilize the His[50] residue as shown by the changes in pK_a and the greater effect of the leaving group on the catalytic constants of C51D but not C51D.

Table 4 Effect of fluoride/chloride leaving group substitution on the rate of catalysis

The ratio of catalytic rates for the conjugation reaction catalysed by wild-type and engineered GSTs using GSH and CDNB or FDNB as co-substrates. One-way ANOVA with Dunnett's multiple comparison test was performed with wild-type as control; statistical significance is shown by † for $P < 0.05$, ‡ for $P < 0.01$ and § for $P < 0.001$.

	Leaving group effect	
Enzyme	$k_{cat}^{FDNB}/k_{cat}^{CDNB}$	$(k_{cat}/K_m)^{FDNB}/(k_{cat}/K_m)^{CDNB}$
Wild-type	1.76 ± 0.01	20.59 ± 1.02
H38A	3.11 ± 0.21	14.12 ± 0.84†
M39A	8.29 ± 0.95§	32.45 ± 3.72§
N47A	18.09 ± 0.90§	29.65 ± 1.32‡
Q49A	2.63 ± 0.08	26.29 ± 1.77†
Q49E	1.50 ± 0.08	24.95 ± 1.21
H50A	18.57 ± 0.41§	16.55 ± 1.59
C51A	2.93 ± 0.05	30.31 ± 2.85§
C51D	26.75 ± 0.99§	44.71 ± 4.15§

Table 5 Viscosity effect on kinetic constants and free energy changes of wild-type and engineered enzymes

The effect of viscosity on kinetic constants was assayed by using 0.1 M potassium phosphate buffer (pH 6.5) with various glycerol concentrations. The slope of a reciprocal plot of the relative catalytic constant (k_{cat}^0/k_{cat}) versus relative viscosity (η/η^0) was determined. n.d., Not determined (low activity precluded measurement); $\Delta\Delta G$ (the difference in the free energy changes for the formation of the transition states in the wild-type and engineered enzymes) is calculated from the equation: $\Delta\Delta G = -RT\ln(k_{cat}/K_m^{CDNB})_{engineered}/(k_{cat}/K_m^{CDNB})_{wild-type}$. One-way ANOVA with Dunnett's multiple comparison test was performed with wild-type as control; statistical significance is shown by § for $P < 0.001$.

Enzyme	Slope	$\Delta\Delta G$ (kJ/mol)
Wild-type	0.959 ± 0.036	–
H38A	0.485 ± 0.019§	3.58 ± 0.033
M39A	0.430 ± 0.031§	3.33 ± 0.132
N47A	n.d.	14.8 ± 0.222
Q49A	0.797 ± 0.036§	1.86 ± 0.105
H50A	0.005 ± 0.001§	7.56 ± 0.095
C51A	1.11 ± 0.010§	4.08 ± 0.125
C51D	0.051 ± 0.007§	10.7 ± 0.201

Viscosity effect on kinetic constants

The viscosity effect was studied to determine if the rate-limiting step of the reaction is physical or chemical. The slope of the reciprocal plot of inverse relative catalytic constant (k_{cat}^0/k_{cat}) versus relative medium viscosity (η/η^0) was determined (Table 5). A slope near unity gives a proportional decrease in rate constant with increasing viscosity of the solution and shows a physical

Table 6 Thermal stability of wild-type and engineered adGSTD4-4 at 45 °C

The remaining GST activity was measured after incubating the enzyme at various time points at 45 °C. n.d., Not determined (low activity precluded measurement). [a]Some of these values have been previously reported and are shown for purposes of comparison [19,20]. One-way ANOVA with Dunnett's multiple comparison test was performed with wild-type as control; statistical significance is shown by ‡ for $P < 0.01$ and § for $P < 0.001$.

Enzyme	Half-life at 45 °C (min)
Wild-type[a]	15.32 ± 0.31
H38A[a]	15.33 ± 0.88§
H38E[a]	40.17 ± 1.26§
H38F[a]	19.33 ± 0.59§
H38D	15.18 ± 1.67
H38K	14.07 ± 0.73
M39A	4.71 ± 0.16§
M39F	4.72 ± 0.23§
N47A	n.d.
Q49A	15.19 ± 1.06§
Q49E	25.19 ± 1.37§
H50A[a]	25.81 ± 1.99§
H50E[a]	15.31 ± 0.54
H50Y[a]	20.79 ± 0.34§
H50K	11.99 ± 0.51§
H50F	27.07 ± 0.82§
C51A	14.86 ± 0.64
C51D	18.18 ± 1.01‡

step is rate-determining, whereas a slope of zero indicates that a chemical reaction step is rate limiting [32,33].

Wild-type enzyme displayed a linear dependence with a slope of approx. 1.0 suggesting that a physical step of the reaction that includes product release and/or structural transition is rate limiting. The engineered enzymes exhibited viscosity effects on k_{cat} to different degrees. H50A and C51D were viscosity-independent with a slope approaching zero. These engineered enzymes changed the rate-limiting step of the reaction to a chemical step that includes GSH ionization step and σ-complex formation as described above, whereas partial dependence on a diffusion barrier and other viscosity-dependent motions were observed for the remaining enzymes that displayed viscosity effects with intermediate values ($0 < \text{slope} < 1$).

Also displayed in Table 5 is $\Delta\Delta G$, which is shown to illustrate the differences in the free energy changes for the formation of the transition states in the wild-type and engineered enzymes, as calculated at 25 °C from the equation below [34]:

$$\Delta\Delta G = -RT \ln \left(k_{cat}/K_m^{CDNB}\right)_{mutant} / \left(k_{cat}/K_m^{CDNB}\right)_{wild\text{-}type}.$$

H50A, D47A and C51D have a greater $\Delta\Delta G$ (7.562, 14.842 and 10.671 kJ/mol respectively) compared with other engineered enzymes (ranging from 1.860 to 4.075 kJ/mol) indicating that upon disruption of the hydrogen bond network, the enzymes require more energy than the wild-type enzyme to form and stabilize the transition state.

Characterization of physical properties

The stability of the proteins was determined in comparison with the adGSTD4-4 wild-type (Table 6). In general, the engineered His[38], His[50], Asn[47], Cys[51] and Gln[49] proteins exhibited comparable stabilities to the wild-type, indicating a minor role of these residues in structural maintenance. However, H38E increased stability of the enzyme 2.6-fold, suggesting that a conformational change occurred which also is supported by the observed positive co-operativity. Met[39] appears to play a role in structural integrity as shown by 3-fold decreased enzyme stability for both the alanine and phenylalanine changes. However, the initial folding processes of the enzymes were observed to yield comparable refolding rates to the wild-type (results not shown). These results suggest that the Met[39] dipole–dipole interaction and positioning of His[38] and His[50] in a suitable conformation impact not only the kinetic properties but also enzyme stability.

The intrinsic fluorescence of tryptophan was used as an indicator of changes in tertiary structure (Figure 3). The λ_{max} of tryptophan fluorescence in the engineered enzymes was slightly different from wild-type with a red shift in the range of 1–4 nm indicating a different polarity in tryptophan environments. In addition, differences in fluorescence intensity between wild-type and engineered enzymes were observed. This result suggests that there are minor conformational disturbances in the active site topography, which affect orientations of tryptophan and/or its neighbouring residues thereby modulating the quenching and tryptophan exposure to the electrophilic environment. For example, the active site topology changes that generated the positive co-operativity in H50K also yielded the lowest fluorescence intensity among the His[50] engineered enzymes (~44 % of wild-type). Moreover, the conformational change induced by glutamic acid residue replacement of His[38] also gave a 2-fold increase in enzyme stability, increased intrinsic fluorescence intensity to 197 % of wild-type, modulated GSH binding and enzyme catalysis as well as yielding the observed positive co-operativity towards GSH.

DISCUSSION

The G-site residues interacting directly with cysteine and glutamyl moieties of GSH have been shown in several studies to contribute to GST catalytic mechanisms including GSH binding, catalysis, GSH ionization as well as rate-limiting step determination [10–14]. In the present study, we have examined the significant contributions of GST residues that interact with the GSH glycine moiety as well as identification of a hydrogen bond network. The network consists of His[38], Met[39], Asn[47], Gln[49], His[50] and Cys[51] and contributes to catalysis through multiple processes including GSH ionization, nucleophilic substitution, product formation and product dissociation.

The kinetic studies demonstrated that the engineered residues greatly impacted the enzyme's ability to interact with GSH. Moreover, the engineered enzymes of His[38], Met[39], His[50], Cys[51] and Gln[49] have shown strong positive co-operativity upon binding of GSH. However, the positive co-operativity was not observed for the engineered enzymes of residues interacting with the other moieties of GSH [11–13,15]. Therefore it can be suggested that the residues interacting with the GSH glycine moiety are not only involved in GSH interaction but also control the motion of a flexible region of GST. Upon binding of GSH in the active site, these GST residues induce an active site conformational change for the induced-fit mechanism. These residues are on the loops on either side of α2-helix which connects the helix to β2-sheet and β3-sheet. These loops would serve as hinges for the movement of α2-helix.

In the present study, changes of the active-site residues generated positive co-operativity between two subunits, a finding similar to that obtained in previous studies in which the subunit interface had been changed or where changes in highly flexible regions, for example Gly[41], Cys[47] and Lys[54] of hGSTP1-1 (human GSTP1-1) [33,35] or Asn[49] and Gln[53] of maize GST1 [36,37],

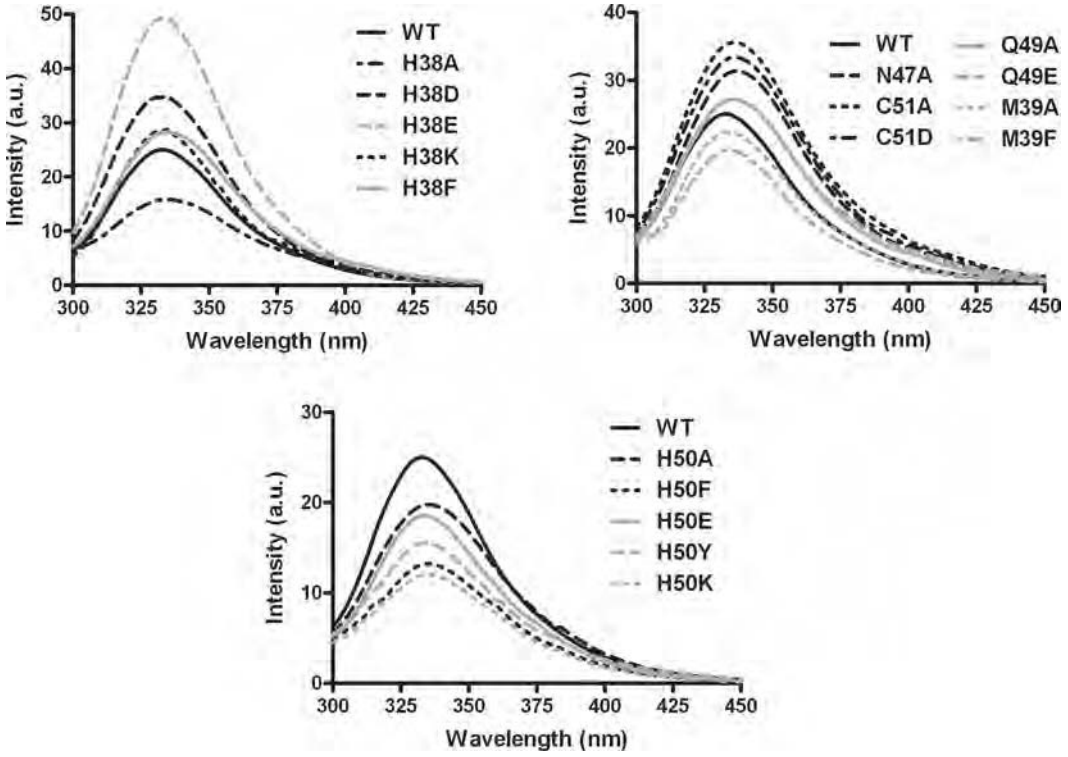

Figure 3 The maximum emission wavelength (λ_{max}) and intrinsic fluorescence intensity at λ_{max} of tryptophan fluorescence of wild-type and the engineered enzymes

Excitation was at 295 nm and emission was scanned from 300 to 450 nm. Samples ($n = 3$) contained 0.1 mg/ml protein in 0.1 M potassium phosphate buffer (pH 6.5). Percent intensity change compared with wild-type enzyme was measured at fluorescence λ_{max} averaged over three scans corrected for dilution and inner filter effects.

had been made. It has been proposed that the conformational transitions generate two different binding modes upon GSH binding: low-affinity and high-affinity conformations, which are related to positive co-operativity observed [5,38,39]. The binding of GSH to the first active site stabilizes the low-affinity conformation of the enzyme which then becomes the high-affinity conformational state. Positive co-operativity upon GSH binding observed in His^{38}, Met^{39}, His^{50}, Cys^{51} and Gln^{49} engineered enzymes may be relevant to this conformational transition concept. These residues are located in a highly flexible region; therefore the residue changes would alter the flexibility of the α2-helix to fit GSH in the active site, which may then generate two different conformational transition states upon GSH binding.

Both His^{38} and His^{50} interact directly with the glycine carboxylate of GSH. The functional groups at positions 38 and 50 are significant in size, volume and polarity for GSH binding and enzyme catalysis. However, His^{50} contributes more to the GSH activation process and enzyme catalysis in which the full function is achieved by the synergistic action with the hydrogen bond network residues (Asn^{47}, Gln^{49} and Cys^{51}). The disruption of the hydrogen bond network, for the engineered enzymes of His^{50}, Asn^{47} and Cys^{51}, showed progressively decreased k_{cat} values to more than 90 %. Moreover, several aspects of the GST catalytic mechanism were altered by H50A. H50A decreased the enzyme's ability to lower the pK_a of the GSH thiol group up to 1 pH unit; this large an effect has been observed for mutations of the conserved serine/tyrosine residue interacting with the GSH thiol group [13,40–42]. Additionally, the rate-limiting step of the H50A is fully switched from a physical step to a chemical step as determined by fluoride/chloride leaving group and viscosity effect on the kinetic constants. As the important His^{50} is still present, lesser effects were observed for the engineered enzymes of Gln^{49} and Cys^{51} for minor disruptions of the stabilizing hydrogen bond network.

The results strongly support that His^{50} is a key residue in the hydrogen bond network which functions as a proton acceptor as well as controls the electron distribution in the active site to promote ionization and stabilization of the GSH thiolate anion. The His^{50} residue contributes to precise residue and substrate orientations, GSH ionization, σ-complex intermediate formation and the release of product from the active site. The regulation of the electrostatic field in the active site by positively charged residues has also been reported in several studies [15,43,44].

The changes in catalytic efficiency are also related to differences in free energy changes for the formation of transition states in the engineered and wild-type enzymes as determined by $\Delta\Delta G$ [34]. The greater value of $\Delta\Delta G$ refers to a decrease in the stabilization of transition state compared with wild-type in which the enzyme utilizes more energy to stabilize its transition state. Moreover, the stabilization of transition state contributes to multiple mechanisms in enzyme-catalysed reactions. $\Delta\Delta G$ values are increased up to 7.562, 14.84 and 10.666 kJ/mol for H50A, D47A and C51D respectively in which the hydrogen bond network is strongly disrupted, indicative of the incomplete pre-organized environment for enhancing catalysis along the reaction pathway of the engineered enzymes [45]. Therefore it can be noted that the network of hydrogen bonds is also required for the organization inside the enzyme molecule to provide stabilization of the transition state.

The positively charged residue position 50 appears to be highly conserved or functionally conserved across GST classes by histidine, lysine or arginine located at the equivalent structural

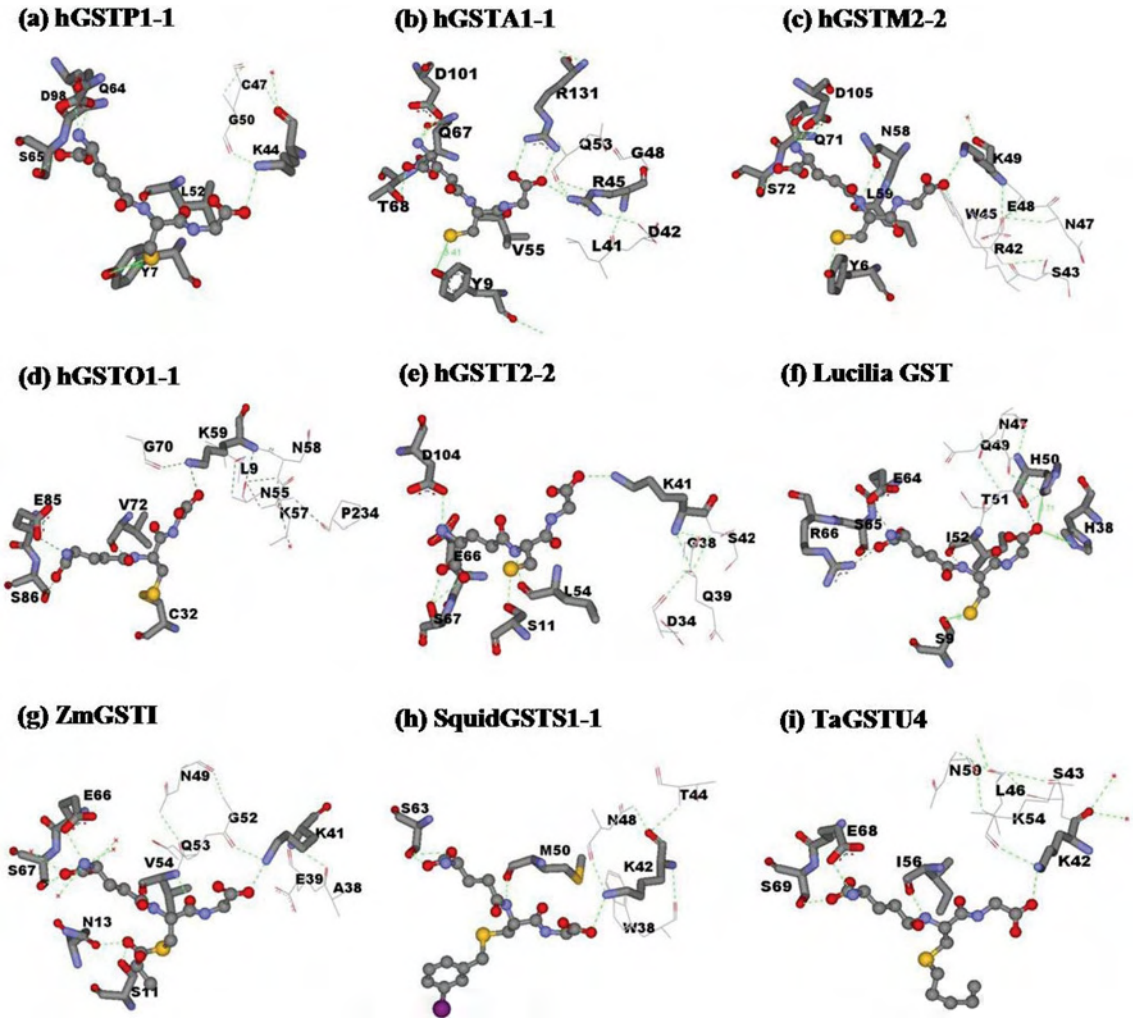

COLOUR

Figure 4 Conserved G-site residues that directly interact with the glycine moiety of GSH and generate a hydrogen bond network in several GST classes

The conserved G-site residues are shown by stick models, while line models represent the hydrogen bond network residues at the glycine moiety of GSH. GSH or GSH analogues are illustrated in ball-and-stick; GSH (**a**, **b**, **c**, **d**, **e**, **f**), lactoylglutathione (**g**), iodobenzylglutathione (**h**) and *S*-hexyl-GSH (**i**). Green dotted lines represent hydrogen-bond interactions. PDB code numbers: hGSTP1-1 (PDB id 8GSS), hGSTA1-1 (PDB id 1PKW), hGSTM2-2 (PDB id 1XW5), hGSTO1-1 (PDB id 1EEM), hGSTT2-2 (PDB id 1LJR), Lucilia GST [7], ZmGST1 (PDB id 1AXD), squid GSTS1-1 (PDB id 2GSQ) and TaGSTU4 [*Triticum aestivum* (wheat) GSTU4; PDB id 1GWC]. The Figure was created with Accelrys DS ViewerPro 5.0.

position. This conserved residue is in hydrogen bonding distance to the glycine carboxylate moiety of GSH which is stabilized by a hydrogen bond network of surrounding residues (Figure 4) for example Lys[40] in PtGSTU1 [*Pinus tabulaeformis* (Chinese hard pine) GSTU1], Lys[41] in ZmGST1 [*Zea mays* (maize) GST1], Lys[44] in hGSTP1-1, Lys[41] in hGSTT2-2, Lys[59] in hGSTO1-1, Lys[49] in hGSTM2-2, Lys[42] in squid GSTS1-1, Lys[45] in Sj26GST [26 kDa GST from *Schistosoma japonicum* (oriental blood-fluke)] and Arg[45] in hGSTA1-1. However, the feature of two positively charged histidines, His[38] and His[50], interacting with the glycine carboxylate moiety of GSH is a unique trait for insect GSTDs. His[38] is responsible for GSH binding, whereas His[50] contributes to several steps of the enzyme-catalysed reaction from GSH interaction to the release of product from the active site.

For the GSH activation mechanism of Alpha, Mu and Pi GST isoenzymes, it has been described that the thiol proton is quantitatively released into solution after the thiolate anion is formed [46,47]. In contrast with GSTD, which behaves differently, the thiol proton is captured by at least an internal base residue at high pH value [46,47]. The present study shows that His[50] is also a candidate for the thiol proton acceptor in addition to the residues at the γ-glutamyl portion of GSH reported previously [15,31]. Moreover, the overall velocity of His[50] engineered enzymes is progressively restricted; therefore it can be assumed that the thiol proton released must be accepted first by the active site residues, e.g. His[50], before a new cycle of the reaction can initiate.

The 'base-assisted deprotonation model' is an alternative model that describes the mechanism of GST enzymes in GSH ionization process. This model has been implicated in several studies of the glutamyl α-carboxylate of GSH acting as a catalytic base, involved in the thiol proton acceptance from the GSH thiol group [15,16,31,46]. In the present study, we addressed the contribution of the glycine moiety of GSH for GSH ionization in which this end of GSH is involved in proton acceptance by providing a counter ion from the charged His[50] which is stabilized by the hydrogen bond network.

In conclusion, the present study revealed a critical role for residues located at the glycine moiety of GSH in catalytic rate determination. This area constitutes a second G-site network involved in GSH ionization distinct from the network previously

reported interacting with the glutamyl end of GSH [16,17]. This second network also appears to be functionally conserved in GSTs (Figure 4). In the present study, we showed that His^{50} is a central residue in the hydrogen bond network to GSH with the protonated imidazole ring of His^{50} being stabilized by the network. His^{50} plays important roles in several processes of the enzyme mechanism. Moreover, this network at the glycine moiety of GSH also contributed to the 'base-assisted deprotonation model' for GSH ionization.

This work was funded by the TRF (Thailand Research Fund). A.V. was supported by a Royal Golden Jubilee Ph.D. Scholarship.

REFERENCES

1 Sheehan, D., Meade, G., Foley, V. M. and Dowd, C. A. (2001) Structure, function and evolution of glutathione transferases: implications for classification of non-mammalian members of an ancient enzyme superfamily. Biochem. J. **360**, 1–16

2 Ketterer, B. (2001) A bird's eye view of the glutathione transferase field. Chem. Biol. Interact. **138**, 27–42

3 Mannervik, B., Awasthi, Y. C., Board, P. G., Hayes, J. D., Di Ilio, C., Ketterer, B., Listowsky, I., Morgenstern, R., Muramatsu, M., Pearson, W. R. et al. (1992) Nomenclature for human glutathione transferases. Biochem. J. **282**, 305–306

4 Hayes, J. D., Flanagan, J. U. and Jowsey, I. R. (2005) Glutathione transferases. Annu. Rev. Pharmacol. Toxicol. **45**, 51–88

5 Mannervik, B. and Danielson, U. H. (1988) Glutathione transferases – structure and catalytic activity. CRC Crit. Rev. Biochem. **23**, 283–337

6 Armstrong, R. N. (1997) Structure, catalytic mechanism, and evolution of the glutathione transferases. Chem. Res. Toxicol. **10**, 2–18

7 Wilce, M. C. J., Board, P. G., Feil, S. C. and Parker, M. W. (1995) Crystal structure of a theta-class glutathione transferase. EMBO J. **14**, 2133–2143

8 Dirr, H., Reinemer, P. and Huber, R. (1994) X-ray crystal structures of cytosolic glutathione S-transferases. Implications for protein architecture, substrate recognition and catalytic function. Eur. J. Biochem. **220**, 645–661

9 Rossjohn, J., Feil, S. C., Wilce, M. C. J., Sexton, J., Spithill, T. W. and Parker, M. W. (1997) Crystallization, structural determination and analysis of a novel parasite vaccine candidate: *Fasciola hepatica* glutathione S-transferase. J. Mol. Biol. **273**, 857–872

10 Stenberg, G., Board, P. G., Carlberg, I. and Mannervik, B. (1991) Effects of directed mutagenesis on conserved arginine residues in a human class Alpha glutathione transferase. Biochem. J. **274**, 549–555

11 Liu, S., Zhang, P., Ji, X., Johnson, W. W., Gilliland, G. L. and Armstrong, R. N. (1992) Contribution of tyrosine 6 to the catalytic mechanism of isoenzyme 3-3 of glutathione S-transferase. J. Biol. Chem. **267**, 4296–4299

12 Kolm, R. H., Sroga, G. E. and Mannervik, B. (1992) Participation of the phenolic hydroxyl group of Tyr-8 in the catalytic mechanism of human glutathione transferase P1-1. Biochem. J. **285**, 537–540

13 Caccuri, A. M., Antonini, G., Nicotra, M., Battistoni, A., Lo Bello, M., Board, P. G., Parker, M. W. and Ricci, G. (1997) Catalytic mechanism and role of hydroxyl residues in the active site of theta class glutathione S-transferases. Investigation of Ser-9 and Tyr-113 in a glutathione S-transferase from the Australian sheep blowfly, *Lucilia cuprina*. J. Biol. Chem. **272**, 29681–29686

14 Tan, K.-L., Chelvanayagam, G., Parker, M. W. and Board, P. G. (1996) Mutagenesis of the active site of the human Theta-class glutathione transferase GSTT2-2: catalysis with different substrates involves different residues. Biochem. J. **319**, 315–321

15 Winayanuwattikun, P. and Ketterman, A. J. (2004) Catalytic and structural contributions for glutathione binding residues in a Delta class glutathione S-transferase. Biochem. J. **382**, 751–757

16 Winayanuwattikun, P. and Ketterman, A. J. (2005) An electron-sharing network involved in the catalytic mechanism is functionally conserved in different glutathione transferase classes. J. Biol. Chem. **280**, 31776–31782

17 Winayanuwattikun, P. and Ketterman, A. J. (2007) Glutamate 64, a newly identified residue of the functionally conserved electron-sharing network contributes to catalysis and structural integrity of glutathione transferases. Biochem. J. **402**, 339–348

18 Pettersen, E. F., Goddard, T. D., Huang, C. C., Couch, G. S., Greenblatt, D. M., Meng, E. C. and Ferrin, T. E. (2004) UCSF chimera – a visualization system for exploratory research and analysis. J. Comput. Chem. **25**, 1605–1612

19 Vararattanavech, A. and Ketterman, A. (2003) Multiple roles of glutathione binding-site residues of glutathione S-transferase. Protein Peptide Lett. **10**, 441–448

20 Vararattanavech, A., Prommeenate, P. and Ketterman, A. J. (2006) The structural roles of a conserved small hydrophobic core in the active site and an ionic bridge in domain I of Delta class glutathione S-transferase. Biochem. J. **393**, 89–95

21 Habig, W. H., Pabst, M. J. and Jakoby, W. B. (1974) Glutathione S-transferases. The first enzymatic step in mercapturic acid formation. J. Biol. Chem. **249**, 7130–7139

22 Segel, I. H. (1993) Enzyme Kinetics, Behavior and Analysis of Rapid Equilibrium and Steady-state Enzyme Systems, John Wiley and Sons, New York

23 Jirajaroenrat, K., Pongjaroenkit, S., Krittanai, C., Prapanthadara, L. and Ketterman, A. J. (2001) Heterologous expression and characterization of alternatively spliced glutathione *S*-transferases from a single *Anopheles* gene. Insect Biochem. Mol. Biol. **31**, 867–875

24 Caccuri, A. M., Ascenzi, P., Lo Bello, M., Federici, G., Battistoni, A., Mazzetti, P. and Ricci, G. (1994) Are the steady state kinetics of glutathione transferase always dependent on the deprotonation of the bound glutathione? New insights in the kinetic mechanism of GST P1-1. Biochem. Biophys. Res. Commun. **200**, 1428–1434

25 Wolf, A. V., Brown, M. G. and Prentiss, P. G. (1985) Handbook of Chemistry and Physics, CRC Press, Boca Raton, FL

26 Armstrong, R. N., Rife, C. and Wang, Z. (2001) Structure, mechanism and evolution of thiol transferases. Chem. Biol. Interact. **133**, 167–169

27 Caccuri, A. M., Ascenzi, P., Antonini, G., Parker, M. W., Oakley, A. J., Chiessi, E., Nuccetelli, M., Battistoni, A., Bellizia, A. and Ricci, G. (1996) Structural flexibility modulates the activity of human glutathione transferase P1-1. Influence of a poor co-substrate on dynamics and kinetics of human glutathione transferase. J. Biol. Chem. **271**, 16193–16198

28 Caccuri, A. M., Lo Bello, M., Nuccetelli, M., Rossi, P., Antonini, G., Federici, G. and Ricci, G. (1998) Proton release upon glutathione binding to glutathione transferase P1-1: kinetic analysis of a multistep glutathione binding process. Biochemistry **37**, 3028–3034

29 Armstrong, R. N. (1997) Structure, catalytic mechanism, and evolution of the glutathione transferases. Chem. Res. Toxicol. **10**, 2–18

30 Gustafsson, A., Pettersson, P. L., Grehn, L., Jemth, P. and Mannervik, B. (2001) Role of the glutamyl α-carboxylate of the substrate glutathione in the catalytic mechanism of human glutathione transferase A1-1. Biochemistry **40**, 15835–15845

31 Widersten, M., Björnestedt, R. and Mannervik, B. (1996) Involvement of the carboxyl groups of glutathione in the catalytic mechanism of human glutathione transferase A1-1. Biochemistry **35**, 7731–7742

32 Johnson, W. W., Liu, S., Ji, X., Gilliland, G. L. and Armstrong, R. N. (1993) Tyrosine 115 participates both in chemical and physical steps of the catalytic mechanism of a glutathione S-transferase. J. Biol. Chem. **268**, 11508–11511

33 Ricci, G., Caccuri, A. M., Lo Bello, M., Rosato, N., Mei, G., Nicotra, M., Chiessi, E., Mazzetti, A. P. and Federici, G. (1996) Structural flexibility modulates the activity of human glutathione transferase P1-1. Role of helix 2 flexibility in the catalytic mechanism. J. Biol. Chem. **271**, 16187–16192

34 Dirr, H. W., Little, T., Kuhnert, D. C. and Sayed, Y. (2005) A conserved N-capping motif contributes significantly to the stabilization and dynamics of the C-terminal region of class alpha glutathione transferases. J. Biol. Chem. **280**, 19480–19487

35 Lo Bello, M., Nuccetelli, M., Chiessi, E., Lahm, A., Mazzetti, A. P., Parker, M. W., Tramontano, A., Federici, G. and Ricci, G. (1998) Mutations of Gly to Ala in human glutathione transferase P1-1 affect helix 2 (G-site) and induce positive cooperativity in the binding of glutathione. J. Mol. Biol. **284**, 1717–1725

36 Labrou, N. E., Mello, L. V. and Clonis, Y. D. (2001) Functional and structural roles of the glutathione-binding residues in maize (*Zea mays*) glutathione S-transferase I. Biochem. J. **358**, 101–110

37 Labrou, N. E., Mello, L. V. and Clonis, Y. D. (2001) The conserved Asn49 of maize glutathione *S*-transferase I modulates substrate binding, catalysis and intersubunit communication. Eur. J. Biochem. **268**, 3950–3957

38 Principato, G. B., Danielson, U. H. and Mannervik, B. (1988) Relaxed thiol substrate specificity of glutathione transferase effected by a non-substrate glutathione derivative. FEBS Lett. **231**, 155–158

39 Jemth, P. and Mannervik, B. (1999) Fast product formation and slow product release are important features in a hysteretic reaction mechanism of glutathione transferase T2-2. Biochemistry **38**, 9982–9991

40 Wang, J., Barycki, J. J. and Colman, R. F. (1996) Tyrosine 8 contributes to catalysis but is not required for activity of rat liver glutathione S-transferase, 1-1. Protein Sci. **5**, 1032–1042

41 Gustafsson, A., Etahadieh, M., Jemth, P. and Mannervik, B. (1999) The C-terminal region of human glutathione transferase A1-1 affects the rate of glutathione binding and the ionization of the active-site Tyr9. Biochemistry **38**, 16268–16275

42 Labrou, N. E., Rigden, D. J. and Clonis, Y. D. (2003) Engineering the pH-dependence of kinetic parameters of maize glutathione *S*-transferase I by site-directed mutagenesis. Biomol. Eng. **21**, 61–66

43 Patskovsky, Y. V., Patskovska, L. N. and Listowsky, I. (2000) The enhanced affinity for thiolate anion and activation of enzyme-bound glutathione is governed by an arginine residue of human Mu class glutathione S-transferases. J. Biol. Chem. **275**, 3296–3304
44 Björnestedt, R., Tardioli, S. and Mannervik, B. (1995) The high activity of rat glutathione transferase 8-8 with alkene substrates is dependent on a glycine residue in the active site. J. Biol. Chem. **270**, 29705–29709
45 Garcia-Viloca, M., Gao, J., Karplus, M. and Truhlar, D. G. (2004) How enzymes work: analysis by modern rate theory and computer simulations. Science **303**, 186–195
46 Caccuri, A. M., Antonini, G., Board, P. G., Parker, M. W., Nicotra, M., Lo Bello, M., Federici, G. and Ricci, G. (1999) Proton release on binding of glutathione to Alpha, Mu and Delta class glutathione transferases. Biochem. J. **344**, 419–425
47 Caccuri, A. M., Antonini, G., Board, P. G., Flanagan, J., Parker, M. W., Paolesse, R., Turella, P., Federici, G., Lo Bello, M. and Ricci, G. (2001) Human glutathione transferase T2-2 discloses some evolutionary strategies for optimization of substrate binding to the active site of glutathione transferases. J. Biol. Chem. **276**, 5427–5431

Received 27 March 2007/22 May 2007; accepted 24 May 2007
Published as BJ Immediate Publication 24 May 2007, doi:10.1042/BJ20070422

BJ www.biochemj.org

BJ Structure

Biochem. J. (2007) **402**, 339–348 (Printed in Great Britain) doi:10.1042/BJ20061253

Reprint 2 339

Glutamate-64, a newly identified residue of the functionally conserved electron-sharing network contributes to catalysis and structural integrity of glutathione transferases

Pakorn WINAYANUWATTIKUN and Albert J. KETTERMAN[1]

Institute of Molecular Biology and Genetics, Mahidol University, Salaya Campus, Nakhon Pathom 73170, Thailand

In *Anopheles dirus* glutathione transferase D3-3, position 64 is occupied by a functionally conserved glutamate residue, which interacts directly with the γ-glutamate moiety of GSH (glutathione) as part of an electron-sharing network present in all soluble GSTs (glutathione transferases). Primary sequence alignment of all GST classes suggests that Glu^{64} is one of a few residues that is functionally conserved in the GST superfamily. Available crystal structures as well as consideration of the property of the equivalent residue at position 64, acidic or polar, suggest that the GST electron-sharing motif can be divided into two types. Electrostatic interaction between the GSH glutamyl and carboxylic Glu^{64}, as well as with Arg^{66} and Asp^{100}, was observed to extend the electron-sharing motif identified previously. Glu^{64} contributes to the catalytic function of this motif and the 'base-assisted deprotonation' that are essential for GSH ionization during catalysis. Moreover, this residue also appears to affect multiple steps in the enzyme catalytic strategy, including binding of GSH, nucleophilic attack by thiolate at the electrophilic centre and product formation, probably through active-site packing effects. Replacement with non-functionally-conserved amino acids alters initial packing or folding by favouring aggregation during heterologous expression. Thermodynamic and reactivation *in vitro* analysis indicated that Glu^{64} also contributes to the initial folding pathway and overall structural stability. Therefore Glu^{64} also appears to impact upon catalysis through roles in both initial folding and structural maintenance.

Key words: active-site residue, *Anopheles dirus*, catalytic mechanism, electron sharing network, glutathione transferase, structural integrity.

INTRODUCTION

GSTs (glutathione transferases; EC 2.5.1.18) are a superfamily of enzymes that contribute towards diverse cellular processes ranging from detoxification to control of gene expression [1–4]. The enzymes generally catalyse nucleophilic attack of the GSH (glutathione) sulfhydryl group to an electrophilic centre of a number of endogenous and xenobiotic compounds [1,5,6]. Conjugation of GSH to such organic molecules enhances solubility, thus facilitating their eventual elimination [5–7]. This reaction is an early step along the mercapturic acid pathway in which hydrophobic compounds are inactivated and eliminated from an organism [8]. Based on amino acid identity, substrate specificities and immunological cross-reactivity, cytosolic GSTs are currently divided into at least 12 distinct evolutionary classes, namely Alpha, Mu, Pi, Theta, Sigma, Zeta, Omega, Phi, Tau, Delta, Epsilon and Beta [6,9–15]. In addition, the number of members identified in this enzyme superfamily is increasing due to the massive growth of genomic information, which includes a number of unclassified GSTs [16].

All cytosolic GSTs adopt the same highly conserved tertiary structure [17]. GSTs are dimeric proteins (with a molecular mass of about 50 kDa) assembled from identical or structurally related subunits. Each subunit is characterized by two distinct domains and an active site. However, each active site is only fully functional when amino acid residues from both subunits are present in the final dimeric structure. The active-site of GSTs consists of two adjacent regions. The first region is the G-site (GSH binding site), formed mostly by the N-terminal domain (domain I), which adopts an α/β topology that binds GSH as the thiol substrate [7]. The second region is the non-polar H-site (hydrophobic substrate binding site), generated primarily by the C-terminal domain (domain II), which is an all-helical structure that provides structural elements for recognition of a wide range of hydrophobic co-substrates [7]. Although GSTs possess a high specificity for GSH as the nucleophile, the enzymes exhibit broad specificity with regard to structurally diverse hydrophobic substrates [17]. The catalytic strategy of GSTs for the nucleophilic substitution reaction can be divided into several steps: binding of substrates to the enzyme active site, activation of GSH by thiol deprotonation, nucleophilic attack by thiolate at the electrophilic centre, product formation and product release [18–20].

The roles of several active-site residues and functional groups of GSH have been studied intensively and a potential model has been proposed to describe deprotonation of the GSH thiol group which enhances the nucleophilicity of the reaction [20–24]. The hydroxyl group of the conserved tyrosine/serine residue at the G-site of GSTs (i.e. Tyr^{8} for Pi, Tyr^{9} for Alpha, Tyr^{6} for Mu and Ser^{9} for Delta classes) is within hydrogen-bonding distance of the thiol group of the bound GSH, and is required for correct orientation and stabilization of the deprotonated thiol anion. The deprotonated anionic GSH results from subtraction of a thiol proton by the glutamyl α-carboxylate of GSH, which acts as a catalytic base in the base-assisted deprotonation model with assistance from an electron-sharing network. The functionally conserved electron-sharing network is characterized by an ionic

Abbreviations used: adGSTD3-3, *Anopheles dirus* glutathione transferase Delta class homodimer of subunit 3; CDNB, 1-chloro-2,4-dinitrobenzene; DTT, dithiothreitol; FDNB, 1-fluoro-2,4-dinitrobenzene; GdmCl, guanidinium chloride; GSH, glutathione; G-site, GSH binding site; GST, glutathione transferase; PtGSTU1-1, plant Tau class GST.

[1] To whom correspondence should be addressed (email frakt@mahidol.ac.th).

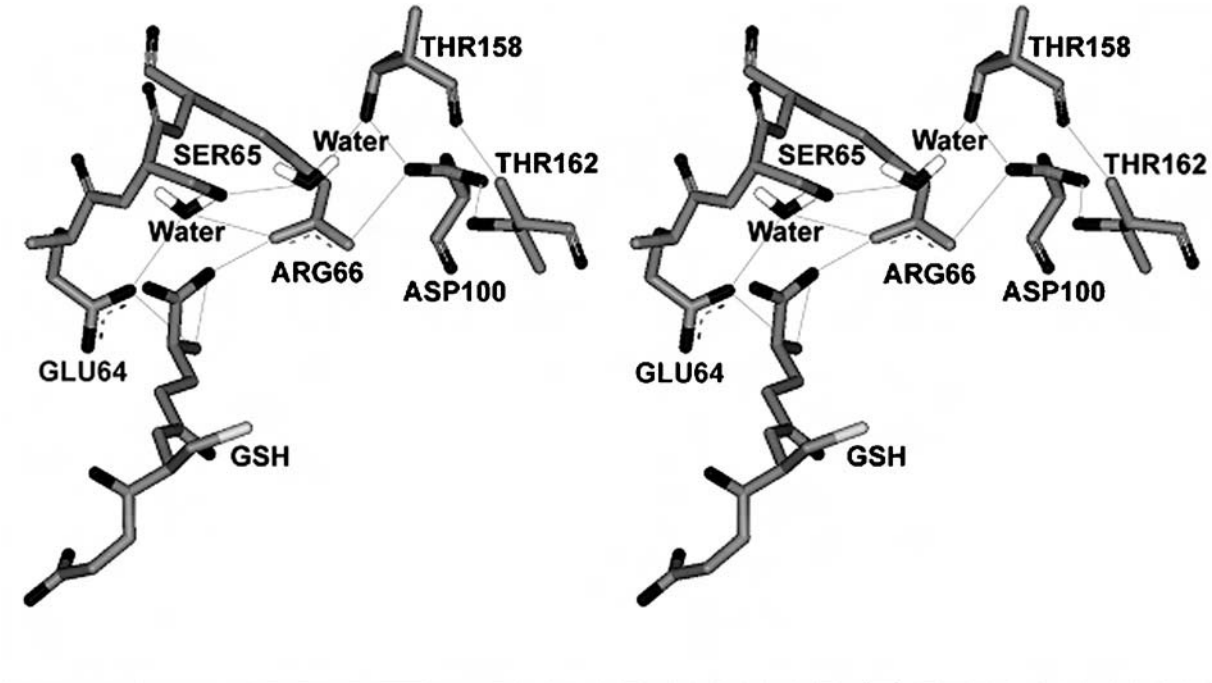

NCBI Seq ID	GST class	Source	Isoform																											
AAG38505	Delta	*A.dirus*	3	52	I	P	T	L	V	D	N	-	G	F	A	L	W	E	S	R	A	I	C	T	Y	L	A	E	K	Y	G
NP_000844.1	Theta	*H.sapiens*	1	54	V	P	A	L	K	D	G	-	D	F	T	L	T	E	S	V	A	I	L	L	Y	L	T	R	K	Y	K
AH004172.1	Omega	*H.sapiens*	1	72	V	P	V	L	E	N	S	Q	G	Q	L	I	Y	E	S	A	I	T	C	E	Y	L	D	E	A	Y	P
CAC94005.1	Tau	*T.aestivum*	1	59	V	P	V	L	I	H	N	-	G	R	P	V	C	E	S	L	L	I	L	E	Y	L	D	D	A	V	G
CAD29575.1	Phi	*T.aestivum*	1	55	I	P	A	F	Q	D	G	-	D	L	L	L	F	E	S	R	A	I	A	R	Y	V	L	R	K	Y	K
P15214	Beta	*P.mirabilis*	1	52	V	P	V	L	Q	L	D	N	G	D	I	L	T	E	G	V	A	I	V	Q	Y	L	A	D	L	K	P
NP_611323.1	Epsilon	*D.melanogaster*	1	57	V	P	M	L	D	D	N	-	G	T	F	I	W	D	S	H	A	I	A	A	Y	L	V	D	K	Y	A
A37378	Pi	*H.sapiens*	1	53	L	P	K	F	Q	D	G	-	D	L	T	L	Y	Q	S	N	T	I	L	R	H	L	G	R	T	L	G
NP_665683.1	Alpha	*H.sapiens*	1	55	V	P	M	V	E	I	D	-	G	M	K	L	V	Q	T	R	A	I	L	N	Y	I	A	S	K	Y	N
P46088	Sigma	*O.sloani*	1	51	M	P	V	L	D	I	D	-	G	T	K	M	S	Q	S	M	C	I	A	R	H	L	A	R	E	F	G
NP_000552	Mu	*H.sapiens*	1	60	L	P	Y	L	I	D	G	-	A	H	K	I	T	Q	S	N	A	I	L	C	Y	I	A	R	K	H	N
O43708	Zeta	*H.sapiens*	1	59	V	P	T	L	K	I	D	-	G	I	T	I	H	Q	S	L	A	I	I	E	Y	L	E	E	T	R	P

Figure 1 Newly identified extension of an electron-sharing network in adGSTD3-3

The electron-sharing network is an ionic interaction between negatively charged and positively charged residues stabilized by a network of hydrogen-bonds. The stereo view of corresponding three-dimensional structure of the electron-sharing network is shown in the upper panel. The lines show the putative electron movement pathway with distances between 2.5 and 3.0 Å. The lower panel shows the sequence alignment of amino acid residues in Delta, Theta, Omega, Tau, Phi, Beta, Epsilon, Pi, Alpha, Sigma, Mu and Zeta class GSTs. The newly identified functionally conserved glutamate, aspartate and glutamine in the electron-sharing network are identified by an arrow.

bridge interaction between the negatively charged glutamyl α-carboxylate of GSH, a positively charged residue and a negatively charged residue, forming a resonance motif stabilized by a network of hydrogen-bonds with surrounding residues. The network is distributed among multiple interacting amino acids that collectively provide a network function. This conserved motif's contribution to the base-assisted deprotonation is essential for the GSH ionization step of catalysis.

The functionally conserved glutamate residue, Glu^{64} in adGSTD3-3 (*Anopheles dirus* GST Delta class homodimer of subunit 3) is located in the same region as the electron-sharing network (Figure 1). Initial characterization of the electron-sharing network has provided further insight into this motif [25]. The carboxylic group of Glu^{64} interacts directly with the glutamyl α-amino group of GSH. Moreover, by observing the configuration of the GSH glutamyl α-carboxylate, the GSH glutamyl α-amino, Glu^{64} and the electron-sharing network, it is now possible to extend this conserved motif, which is maintained in all GSTs. The aim of the present paper was to ascertain the validity of Glu^{64} function in the electron-sharing network. We have observed previously [25] that alanine replacement of Glu^{64} caused the enzyme to be expressed in an insoluble form. This suggested that Glu^{64} is a critical residue involved in tertiary structure or initial folding of the enzyme. Therefore the contribution of this residue to structural maintenance and initial folding was also examined. The results of the present paper indicate that Glu^{64} is a part of the functionally conserved electron-sharing network and has roles both in catalysis as well as structural folding and maintenance.

MATERIALS AND METHODS

Site-directed mutagenesis

The plasmid pET3a-adgstD3, described previously [26], was used as the template to generate the single point mutations via PCR-based site-directed mutagenesis. The functionally conserved active-site residue Glu^{64} was replaced by an alanine, leucine, valine, lysine, glutamine, asparagine or aspartate residue by using

PCR primers based on the wild-type *adgstD3* gene sequence (Genbank accession number AF273039). Mutants were screened randomly by restriction enzyme digestion analysis. Mutant plasmids could be distinguished from the wild-type template by digestion with restriction enzymes corresponding to the restriction recognition site introduced by the mutagenic primers. The full-length GST coding sequence carrying E64A, E64L, E64V, E64K, E64Q, E64D and E64N mutations were verified by the dideoxy chain termination method.

Heterologous expression and purification

The proteins were expressed from the pET3a-adgstD3 vector in *Escherichia coli* BL21 (DE3) pLysS cells. The cells were grown to $D_{600} = 0.5$ and expression was induced by addition of 0.1 mM isopropyl β-D-thiogalactoside. Following a 3 h induction, cells were collected by centrifugation at 10000 ***g*** for 20 min at 4 °C and lysed by sonication using an Ultrasonic processor XL (Misonix) at power level 3 for 10 s, paused for 1 min and repeated three times at 4 °C. The soluble recombinant GST proteins were purified by GSTrap™ affinity chromatography (Amersham Biosciences) or *S*-hexylglutathione agarose (Sigma–Aldrich) affinity chromatography. The protein concentration was determined by the Bradford method [27] using BSA as a standard.

Steady-state kinetics

Steady-state kinetics were studied for wild-type and mutant enzymes at varying concentrations of CDNB (1-chloro-2,4-dinitrobenzene) and GSH in 0.1 M phosphate buffer pH 6.5. The reaction was monitored at 340 nm, ε 9600 $M^{-1}cm^{-1}$. Apparent kinetic constants, k_{cat}, K_m and k_{cat}/K_m were determined by fitting the collected data to a Michaelis–Menten equation by non-linear regression analysis using GraphPad Prism (GraphPad software).

pH dependence of kinetic constants

The pH dependence of k_{cat}/K_m^{CDNB} was obtained as stated above by recording the enzymatic reaction in the following buffers: 0.1 M sodium acetate buffers (from pH 5.0 to 5.5) and 0.1 M potassium phosphate buffer (from pH 6.0 to 8.5). The pH was altered in increments of 0.5, and control experiments showed no discontinuities from buffer types. pK_a values were obtained by fitting the data to eqn (1) [20]:

$$y = y_{lim}/(1 + 10^{pKa-pH}) \quad (1)$$

Fluoride/chloride leaving group replacement

The second order kinetic constants at pH 6.5 for the spontaneous reaction of GSH with CDNB and FDNB (1-fluoro-2,4-dinitrobenzene) and the catalytic-centre activities at pH 6.5 for adGSTD3-3 with CDNB and FDNB as co-substrates were obtained as described previously [28].

Viscosity effect on the kinetic parameters

The effect of viscosity on kinetic parameters was obtained by using 0.1 M potassium phosphate buffer pH 6.5 with various glycerol concentrations. Viscosity values (η) at 25 °C were calculated as described previously [29].

Structural studies

A Jasco J-714 spectropolarimeter was used for CD measurements in the far-UV region from 190–260 nm. Spectra were recorded using 0.3 mg/ml of protein in 2-mm path length cuvettes. Intrinsic fluorescence emission spectra were measured with a Jasco FP-6300 spectrofluorimeter. The excitation wavelength was 295 nm and the λ_{max} and the fluorescence intensity of emission spectra were analysed at a protein concentration of 0.2 mg/ml.

Kinetics of thermal denaturation

Heat inactivation of the wild-type and Glu[64] mutant enzymes was monitored at different temperatures. Enzymes (40 μM) were incubated in 0.1 mM potassium phosphate buffer pH 6.5, 1 mM EDTA and 5 mM DTT (dithiothreitol). The inactivation time-courses were determined by withdrawing suitable aliquots at different time points to assay the remaining activity using the first time point as 100 % native protein. An equation describing a single exponential decay with a rate constant of thermal unfolding k_u was fitted to the data according to eqn (2) [30]:

$$-\ln(\%\text{native}/100\%) = k_u t \quad (2)$$

The free-energy of activation of thermal unfolding (ΔG_u) was calculated according to Eyring theory as eqn (3) [30]:

$$\ln k_u = \ln\frac{K k_b T}{h} - \frac{\Delta G_u}{RT} \quad (3)$$

where k_b is the Boltzmann constant; T, absolute temperature Kelvin; h, Plank's constant; R, the gas constant; and K is the transmission factor, which was set to unity. The difference of free-energy of activation of the thermal denaturation between wild-type (wt) and each mutant (mut) protein ($\Delta\Delta G_u$) was calculated according to eqn (4) [30]:

$$\Delta\Delta G_u = \Delta G_u^{wt} - \Delta G_u^{mut} = -RT \times \ln\left(k_u^{wt}/k_u^{mut}\right) \quad (4)$$

Substitution of Equation 5:

$$\Delta G_u = \Delta H_u - T\Delta S_u \quad (5)$$

into eqn (3) yields eqn (6):

$$\ln\frac{k_u}{T} = \ln\frac{K \times k_b}{h} - \frac{\Delta H_u}{R} \times \frac{1}{T} + \frac{\Delta S_u}{R} \quad (6)$$

Both activation enthalpy ΔH_u and entropy ΔS_u were determined from the temperature dependence of k_u.

Temperature dependence of refolding *in vitro*

The *in vitro* refolding of the wild-type and Glu[64] mutant enzymes were monitored at different temperatures. Enzyme (20 μM) was first denatured in 4 M GdmCl (guanidinium chloride) in renaturation buffer (0.2 M potassium phosphate buffer, 1 mM EDTA and 5 mM DTT, pH 7.0) at room temperature (25 °C) for 30 min and then rapidly diluted (defining time 0) 1:40 (v/v) into renaturation buffer at 18, 25 and 33 °C. The final GdmCl concentration was 0.1 M during refolding. All refolding experiments were carried out by rapid addition of the denatured enzyme to renaturation buffer. The recovery of activity of the proteins was monitored as a function of time by withdrawal of appropriate aliquots of the renaturation mixture and immediately assaying for activity at 25 °C. Refolding rate constants were determined by nonlinear regression analysis of the experimental data by using SigmaPlot 2001 for Windows version 7.0 (SPSS). The refolding rates of all variants were independent, in the range 10 to 30 μM, of the protein concentration. At greater enzyme concentrations all

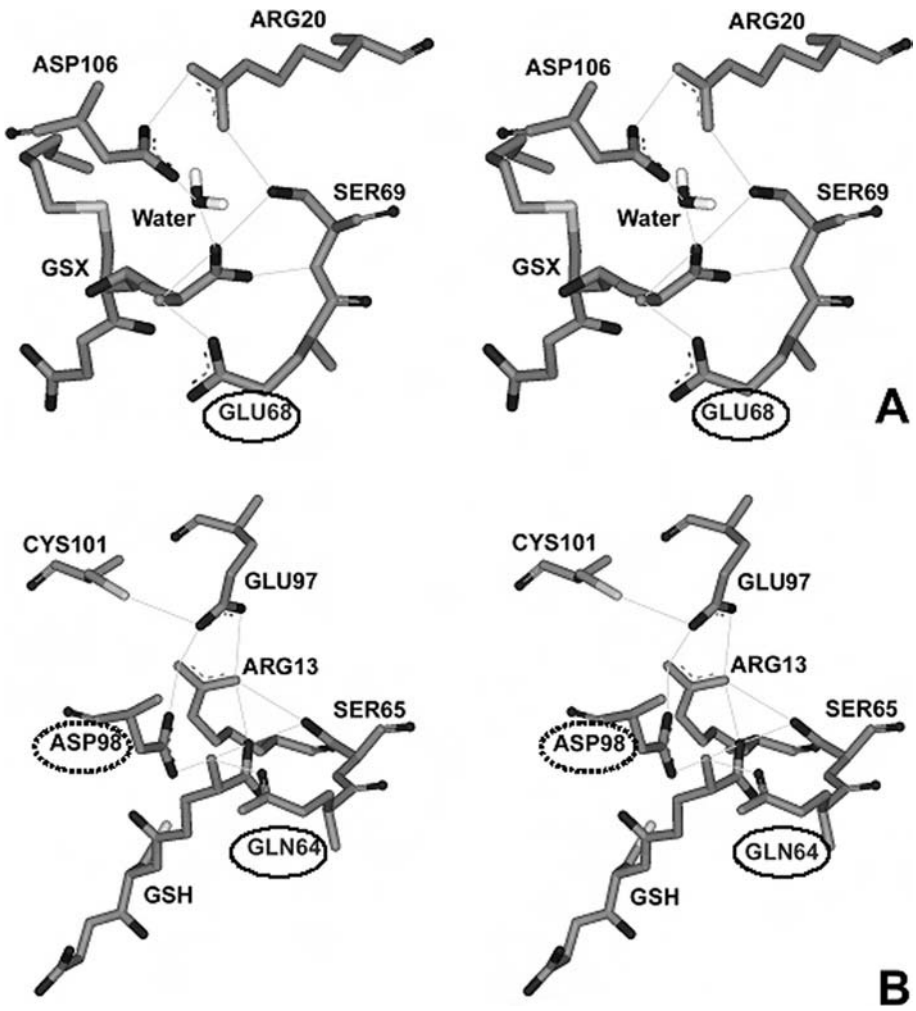

Figure 2 Stereo views of examples of electron-sharing networks for type I (A) and type II (B) of GSTs

Categorization is based on properties of the equivalent amino acid at position 64 and configuration of the electron-sharing network. (**A**) Electron-sharing network type I is composed of only one conserved acidic amino acid (circled), which forms an ionic interaction. Wheat Tau GSTI (PDB accession number 1GWC). (**B**) Electron-sharing network type II contains two strictly conserved polar and acidic residues (circled by solid and dotted lines respectively), which participate in an ionic bridge interaction. Human Pi hGSTP1-1 (PDB accession number 1PKW).

variants were characterized by reduced refolding yield. The values reported represent the means for three different experimental data sets. Under these conditions, an equation describing a single exponential reaction can be fitted to the data:

$$F(\mathrm{t}) = A[1 - \exp(-k_{\mathrm{ref}})] + B \quad (7)$$

where $F(\mathrm{t})$ is the activity at time t; A, the amplitude; k_{ref}, the rate constant; and B, the reactivation value at time 0 [31]. The effect of mutation on the energy of the transition state of folding can be calculated using transition-state theory in a similar manner to that reported by Jackson et al. [32]. The stability of the transition state of a mutant protein relative to that of the wild-type is calculated from:

$$\Delta\Delta G_{\mathrm{ref}} = -RT \times \ln\left(k_{\mathrm{ref}}{}^{\mathrm{wt}} / k_{\mathrm{ref}}{}^{\mathrm{mut}}\right) \quad (8)$$

where $\Delta\Delta G_{\mathrm{ref}}$ is the difference in energy of the transition state of folding relative to the unfolded state between wild-type (wt) and mutant (mut) proteins and k_{ref}, the rate constants of refolding [32].

RESULTS AND DISCUSSION

A functionally conserved electron-sharing network can be observed in the same region for all GSTs, but with slightly different residue positions [22]. However, a primary sequence alignment of the known GST classes suggests that Glu^{64} is one of a few residues that is functionally conserved in the GST superfamily. Observation of available crystal structures; adGSTD3-3, hGSTP1-1 (human Pi GST1), hGSTA1-1 (human Alpha GST1), rGSTM1-1 (rat Mu GST1), hGSTO1-1 (human Omega GST1), hGSTT2-2 (human Theta GST2), squid Sigma GST and wheat Tau GST, as well as consideration of the property of the equivalent residue at position 64, acidic or polar, suggests that the GST electron-sharing motif can be divided into two types (Figure 2). Electron-sharing network type I, consisting of GSTs from Delta, Theta, Omega, Pi and Tau classes, contain an acidic amino acid (glutamate or aspartate) at this position. The equivalent residue is the only amino acid in an acceptable distance range to form an ionic interaction between its own negatively charged side chain and the positively charged GSH glutamyl α-amino (Figure 2A). On the other hand, electron-sharing network type II GSTs from the Alpha, Mu, Pi and Sigma classes have a polar amino acid (glutamine) side-chain

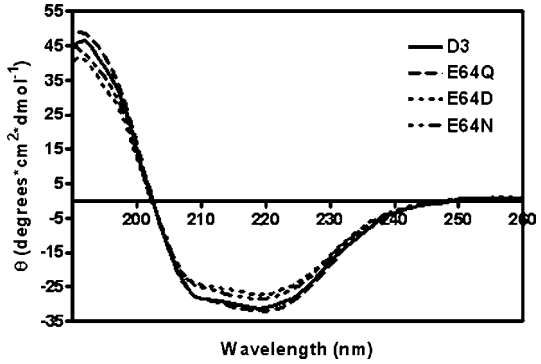

Figure 3 Far-UV CD spectra of adGSTD3-3 and mutants

CD spectra were measured in far-UV region from 190–260 nm. Spectra were recorded at a protein concentration of 0.3 mg/ml with cuvettes with a 2-μm path-length. D3, wild-type adGSTD3-3.

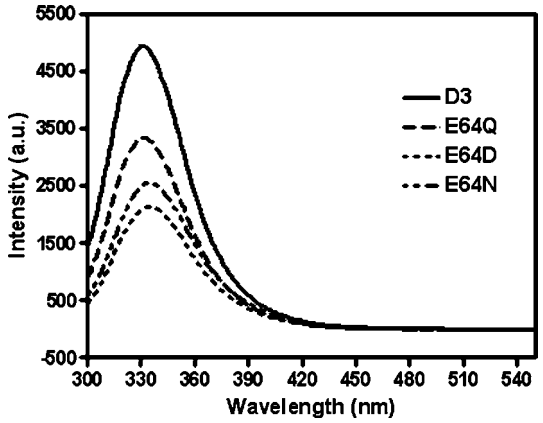

Figure 4 Intrinsic fluorescence spectra of wild-type and mutant adGSTD3-3

Intrinsic fluorescence emission spectra were measured with the excitation wavelength 295 nm. The λ_{max} and the fluorescence intensity of emission spectra were analysed at a protein concentration of 0.2 mg/ml. The λ_{max} are 331 nm for wild-type (D3), 332 nm for E64Q, 335 nm for E64D and 334 nm for E64N. The intensity is shown in arbitrary units. The results are means $\pm$ S.D. for experiments performed in triplicate.

that interacts directly with the GSH glutamyl α-amino. In addition, type II networks have a strictly conserved acidic amino acid (Asp[98] in the Pi class, Asp[101] in the Alpha class, Asp[105] in the Mu class and Asp[97] in the Sigma class) that participates in an ionic interaction (Figure 2B). In the Pi class GSTs, replacement of this acidic residue (Asp[98] with asparagine) was shown to increase the pK_a for GSH by approx. 0.5 pH unit [33]. These results suggest the importance of a negative charge involvement with the positively charged GSH glutamyl α-amino to fulfil the function of the electron-sharing network in the ionization process [33]. Dividing the electron-sharing network into two types is supported by studies of binding, activation and ionization of GSH, including the fate of the thiol proton in Pi, Alpha, Mu and Delta class GSTs [23]. It has been reported that GST classes Pi, Alpha and Mu, which are classified as electron-sharing network type II GSTs, display similarities in the multi-step mechanism for binding of the substrate and also yield a similar fate for the thiol proton. The Delta class GST, which we propose belongs to electron-sharing network type I, shows a difference in proton extrusion that implies a different activation mechanism for GSH. Moreover, the modality of proton output is also preserved in Pi, Alpha and Mu class enzymes. This mechanistic difference suggests that Delta GST is distantly related to Pi, Alpha and Mu GSTs in evolutionary terms.

To investigate the role of the functionally conserved Glu[64] residue in adGSTD3-3, this residue was replaced with seven amino acids; alanine, leucine, valine, lysine, glutamine, aspartate or asparagine. Evidence suggested that the replacements were temperature-sensitive therefore protein expression was performed at 18, 25 and 37 °C. The E64A, E64L, E64V and E64K mutants were expressed as insoluble proteins at all temperatures. Attempts at refolding these four proteins were unsuccessful. The yields of the E64Q, E64D and E64N mutants were less than wild-type and clearly decreased with increasing temperature (results not shown). This probably reflects the fact that the E64Q, E64D and E64N molecules fail to achieve the native folding at near physiological temperatures. Therefore, proteins expressed at the more permissive temperature of 18 °C were utilized in this study.

In the present study, a structural role for Glu[64] for stability and folding was examined. The similarity of the far-UV CD spectra of all the Glu[64] mutants indicated that the secondary structure content of the proteins are essentially unaffected by the mutations (Figure 3). The intrinsic fluorescence spectra show differences between the wild-type and all of the Glu[64] mutants (Figure 4). The spectra of the Glu[64] mutants were slightly red-shifted compared with the wild-type protein (λ_{max} at 331 nm) to give a λ_{max} at 332 nm for E64Q, 335 nm for E64D and 334 nm for E64N. The normalized intensities of the fluorescence of the mutants were slightly less than that of the wild-type. Changes in amino acid side-chains around Trp[63] resulted in an alteration in fluorescence intensity, and a red-shifted spectrum is observed as the protein unfolds to random coil [34]. Consequently, the differences in both λ_{max} and fluorescence intensity suggest that the mutation of Glu[64] causes the tryptophan residue to be more exposed to the solvent. Heat inactivation of wild-type and Glu[64] mutants was performed at different temperatures (Figure 5). Furthermore, the E64Q and E64N mutants were much more unstable than the wild-type or E64D mutant. It is important to note that the single Glu[64] replacement with polar residues (glutamine and asparagine) became unstable at a lower temperature than the negatively charged residues (wild-type and E64D) and their inactivation generated the formation of protein aggregates under the experimental conditions used. Thermal denaturation of all variants was irreversible, showing that inactivation kinetics could not be used to determine thermodynamic parameters at equilibrium. However, making use of the temperature dependence of the unfolding rate, the application of Eyring formalism provides the thermodynamic parameters of the activation barrier of the thermal denaturation [30]. The heat inactivation of all variants is described by straight lines in an Eyring plot. This indicates that the temperature dependence of both the unfolding activation enthalpy (ΔH) and activation entropy (ΔS) is negligible. The temperature dependence of ΔG is reflected in the slope of the linear fit, dependent on ΔH. Table 1 summarizes the kinetic and thermodynamic constants for the activation barrier of thermal denaturation for the wild-type and Glu[64] mutant enzymes. The large energy changes of Glu[64] mutants compared with the wild-type ($\Delta\Delta H$) are almost completely compensated for by an accompanying reduction in ΔS (that is, $\Delta\Delta S$). At 42 °C, this corresponds to lower values of the unfolding free-energy for all the Glu[64] mutant enzymes ($\Delta\Delta G$). The Glu[64] mutants were remarkably more destabilized than the wild-type enzyme, especially for the polar amino acids glutamine and asparagine (Table 1). This corresponds to an unfolding free-energy difference ($\Delta\Delta G$) for the polar amino acid replacements compared with the wild-type, being greater

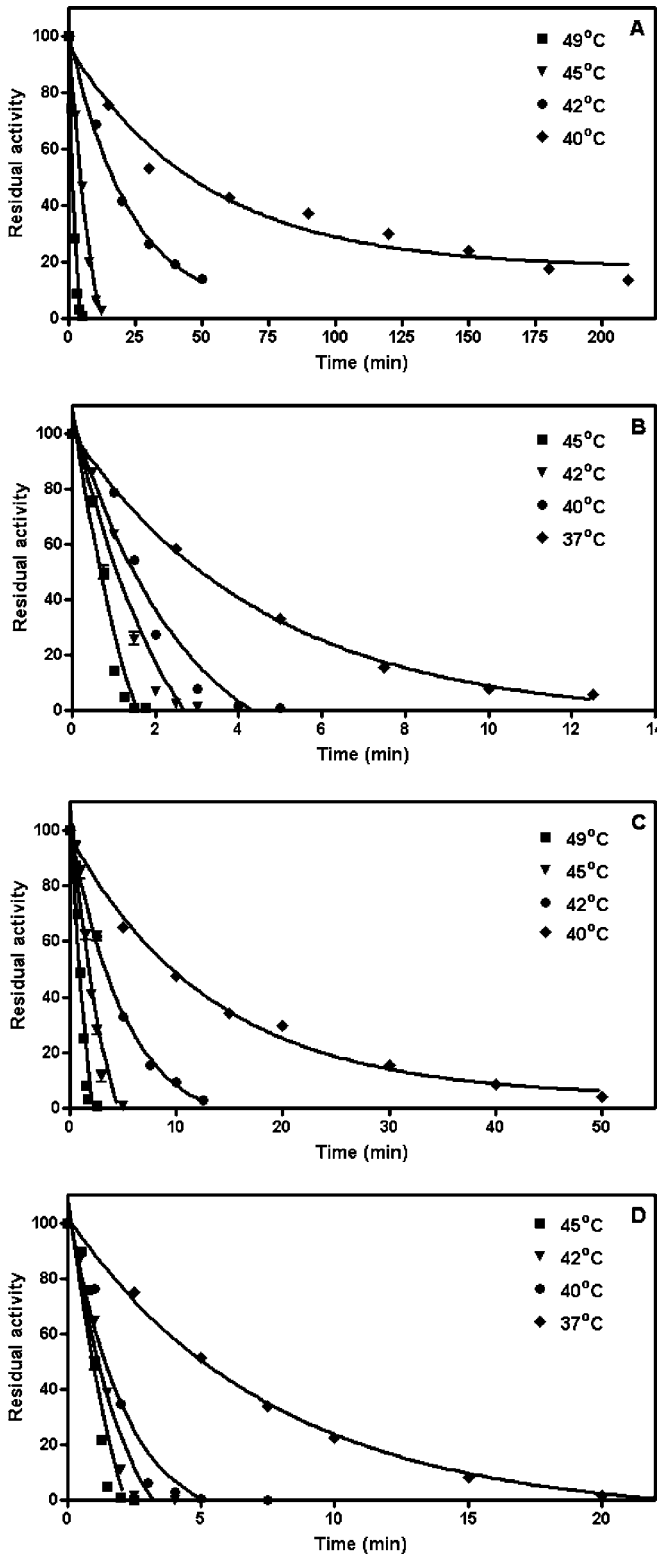

Figure 5 Thermal stability of wild-type adGSTD3-3 (A), E64Q (B), E64D (C) and E64N (D) mutants at different temperatures

Each enzyme (40 μM) was incubated at various temperatures in 0.1 M potassium phosphate buffer, pH 6.5, 1 mM EDTA and 5 mM DTT. Appropriate aliquots from an incubation mixture were assayed at 25 °C to monitor residual activity. The lines represent fits according to eqn (2), as described in the Materials and methods section.

than with the acidic residue aspartate. The Gibbs free-energy for the unfolding process of wild-type and Glu^{64} mutants were comparable, with general estimations of Gibbs free-energy for small globular proteins based on the summation of increments of the different stabilizing forces that give values in the range 42–84 kJ/mol [35]. Due to the large decrease in activation enthalpy ($\Delta\Delta H$, 131–220 kJ/mol), the destabilizing effects of the Glu^{64} mutants were clearly significant to the structural properties of the enzymes. In addition the magnitude of $T\Delta\Delta S$ at 42 °C, which is the energy difference from decreases in the entropy of the thermal unfolding pathway (198.4, 126.0 and 211.0 kJ/mol for E64Q, E64D and E64N respectively), indicates that major changes in the conformational freedom characterizes the denaturation of the wild-type protein compared with those occurring during the thermal inactivation of the Glu^{64} mutants [36]. This means that the wild-type adGSTD3-3, because it is more rigid than the Glu^{64} mutants, tolerates larger perturbations of its structure before the unfolding transition state is reached. The replacement of polar amino acids, both glutamine and asparagine, give greater values of all thermodynamic constants than for the acidic amino acids glutamate and aspartate. This data suggests that the negatively charged residue forming an ionic bridge interaction in this position plays an essential role for the overall stability of the protein. Recent studies proposed that Glu^{64} is a critical residue involved in the determination of the direction of the polypeptide chain during folding [25]. One consequence of replacing Glu^{64} with other amino acid residues results in a completely impaired folding property (for E64A, E64L, E64V and E64K) or temperature-sensitive folding (for E64Q, E64D and E64N). To test this hypothesis, reactivation yields of adGSTD3-3 and its mutants at different temperatures were determined. The denaturant 4 M GdmCl was sufficient to completely unfold 20 μM enzyme, as shown by CD spectrum (results not shown). The reactivation yields of the Glu^{64} mutants were very different from the wild-type protein at increasing temperatures of refolding (Table 2 and Figure 6). The reactivation yield of the wild-type enzyme was unaffected by temperatures from 18–33 °C, whereas the yield of the mutants, although to different extents, decreased markedly with increasing temperature. All data sets were fit to a single exponential equation for the refolding kinetics (Figure 6). At each temperature, as shown in Table 2, the temperature-dependent refolding rates show a similar tendency in the wild-type and Glu^{64} mutants that was expected, that is, the enzymes refold at higher temperature more rapidly than at lower temperature. The refolding rates of both E64Q and E64D mutants were slightly different from the wild-type at all temperatures. These differences in refolding rates reflect changes in free-energy of activation of folding for a mutation. Estimated free-energy values ($\Delta\Delta G_{ref}$) at 18 °C that were significantly different from zero indicate that interactions of the residue at position 64 toward neighbouring residues are present in the transition state of the reactivation process. The *in vitro* refolding experiments suggest that the thermal stability of the final structure of the mutants reflects differences in the conformational properties of a productive folding intermediate. Reactivation *in vitro* of all Glu^{64} mutants was thermosensitive, and so the refolding yields of the Glu^{64} mutants, although to different extents, decreased markedly with increasing temperature. The analysis of the reactivation at 18 °C indicates that amino acid replacement of Glu^{64} destabilizes the transition of folding. It should be noted that a single exponential equation could be fitted to refolding data for all adGSTD3-3 variants indicating that no significant amount of intermediate is accumulated during the reactivation of wild-type and variants, and that none of the mutations had a major change on the refolding pathway. Upon

Table 1 Kinetic and thermodynamic parameters for the activation barrier of thermal denaturation for wild-type and Glu[64] mutants of adGSTD3-3

Enzyme	k_u (min^{-1})	$k_u/k_{u,wt}$*	ΔG_u* (kJ/mol)	$\Delta\Delta G_u$ (kJ/mol)	ΔH_u† (kJ/mol)	$\Delta\Delta H_u$† (kJ/mol)	ΔS_u† (kJ/mol · K)	$\Delta\Delta S_u$† (kJ/mol · K)
Wild-type	0.040 ± 0.001	1	85.69 ± 0.09	0	439.00 ± 4.90	0	1.120 ± 0.015	0
E64Q	1.583 ± 0.028	39.58	76.08 ± 0.05	9.63	231.38 ± 13.02	207.62	0.490 ± 0.041	0.630
E64D	0.256 ± 0.008	6.40	80.85 ± 0.08	4.86	307.51 ± 1.28	131.49	0.720 ± 0.004	0.400
E64N	1.590 ± 0.045	39.75	76.07 ± 0.08	9.64	218.52 ± 10.92	220.48	0.450 ± 0.035	0.670

* From denaturation kinetics at 42 °C according to eqns 2 and 4.
† From temperature dependence of thermal unfolding (Eyring plot) according to eqn 6.

Table 2 Kinetics of the reactivation and percentage recovery of wild-type adGSTD3-3 and Glu[64] mutants during refolding at different temperatures and changes in free energy of the transition state of folding at 18 °C

Statistics performed using one-way ANOVA and Tukey–Kramer multiple comparisons test. Values significantly different from wild-type are shown by * $P < 0.001$. Nd, not determined, low enzymatic activity precluded performing this experiment.

	18 °C		25 °C		37 °C		
Enzyme	k_{ref} (min^{-1})	% recovery	k_{ref} (min^{-1})	% recovery	k_{ref} (min^{-1})	% recovery	$\Delta\Delta G_{ref}$ at 18 °C (kJ/mol)
Wild-type	0.169 ± 0.020	60.9 ± 0.4	0.518 ± 0.053	35.1 ± 3.4	0.957 ± 0.027	35.1 ± 0.6	0
E64Q	0.074 ± 0.003	63.8 ± 0.7	0.289 ± 0.004	40.0 ± 0.3	1.073 ± 0.124	10.6 ± 0.3	−1.987 ± 0.371*
E64D	0.059 ± 0.005	93.0 ± 6.5	0.242 ± 0.024	57.7 ± 1.1	0.981 ± 0.030	34.5 ± 1.3	−2.521 ± 0.129*
E64N	Nd	Nd	Nd	Nd	Nd	Nd	Nd

mutation of adGSTD3-3, rate constants decreased for all mutants (Table 2). This is because the removal of the negative charge or size decrease of the side-chain at this position destabilized the transition state and thereby increased the activation energy for folding. In particular, the $\Delta\Delta G_{ref}$ value for E64D is greater than E64Q, suggesting that the functional group size is important for the Glu[64] position, which contributes to stabilizing the transition state. Previous investigations of the equivalent residue, Glu[66], in PtGSTU1-1 (plant Tau class GST) demonstrated that alanine replacement made the enzyme unstable at 50 °C, retaining only about 15 % of its activity compared with 95 % for the wild-type enzyme [37]. In contrast, the reactivation yield of E66A was 2-fold greater than the wild-type. The effect of the mutation at this equivalent residue in PtGSTU1-1 was less than found in adGSTD3-3, an insect Delta class GST. This result might be explained by data for Glu[64] in adGSTD4-4, an alternatively spliced product derived from the same gene as adGSTD3-3. Glu[64] is not only located at the dimeric interface of the enzyme, but has also been identified as a 'lock' residue in the Delta class specific 'lock-and-key clasp' motif, which is not found in plant Tau class GST [38]. The lock-and-key motif, including the Delta class specific lock-and-key clasp motif, is located at the intersubunit interface and plays a crucial role in the structural stability of dimeric GSTs [39,40]. These data therefore confirm a critical structural role for the functionally conserved Glu[64] residue for both overall protein stability and initial folding process.

Steady-state kinetic constants were obtained with various concentrations of GSH and CDNB substrate. Michaelis–Menten kinetic analysis was performed using non-linear regression (Table 3). All of the mutations showed significantly increased K_m values for GSH. Individually, the mutants; E64Q, E64D and E64N had values 26-, 34- and 29-fold greater than wild-type. Conversely, no significant changes were found in the K_m values for CDNB substrate when compared with the wild-type enzyme. The differences in k_{cat} values with CDNB observed for E64D and E64N decreased approximately 1.5- and 25-fold respectively. The kinetic studies of soluble Glu[64] mutant enzymes demonstrated that replacement with a glutamine residue, a similar size and property functional group, preserved the catalytic activity, whereas replacement with the slightly smaller amino acids aspartate and asparagine reduced k_{cat}, especially the arparagine replacement, which nearly abolished enzyme activity. This suggests that the volume of the amino acid at this position affects packing of the active-site, which directly impacts upon enzyme catalysis. However, all the mutants showed a substantially lower affinity (greater K_m) towards GSH indicating that the Glu[64] position impacts upon the binding of GSH possibly through active-site rearrangement. Catalytic efficiency can be related to the difference in free-energy change for formation of transition states in the mutant and wild-type enzymes ($\Delta\Delta G$), as calculated from eqn (9) [41]:

$$\Delta\Delta G = -RT \times \ln\left(k_{cat}/K_m^{GSH}\right)_{mut} / \left(k_{cat}/K_m^{GSH}\right)_{wt} \quad (9)$$

These calculated values are 8.03 kJ/mol for E64Q, 9.94 kJ/mol for E64D and 16.33 kJ/mol for E64N at 25 °C, indicative of a decreased stabilization of the transition state for the Glu[64] mutations. Stabilization of the transition state may occur through a pre-organized active-site contributing to catalysis through multiple mechanisms: binding interaction with GSH, activation of GSH by thiol deprotonation or nucleophilic attack at the electrophilic centre (σ-bond formation) by the thiolate. Deficiency in the pre-organized environment (the changes that occur along the reaction pathway from reactants to the transition state) would decrease the rate of catalysis by incompletely providing a stabilization of the transition state [42]. Therefore, the effect on the rate-limiting step in the catalytic mechanism was examined. The pH dependence of k_{cat}/K_m^{CDNB} reflects a kinetically relevant ionization of the GST–GSH complex. Therefore, an apparent pK_a value of 6.36 was determined for the wild-type adGSTD3-3. To differentiate the influence of the functional group of Glu[64] on the GSH thiol ionization, the pK_a values for Glu[64] mutants were measured by this kinetic approach (Table 3). An increased pK_a for bound GSH of approx. 0.6 and 1 pH unit greater than that found for wild-type were observed for the E64Q and E64N mutants. It has been shown previously that a crucial function of the electron-sharing

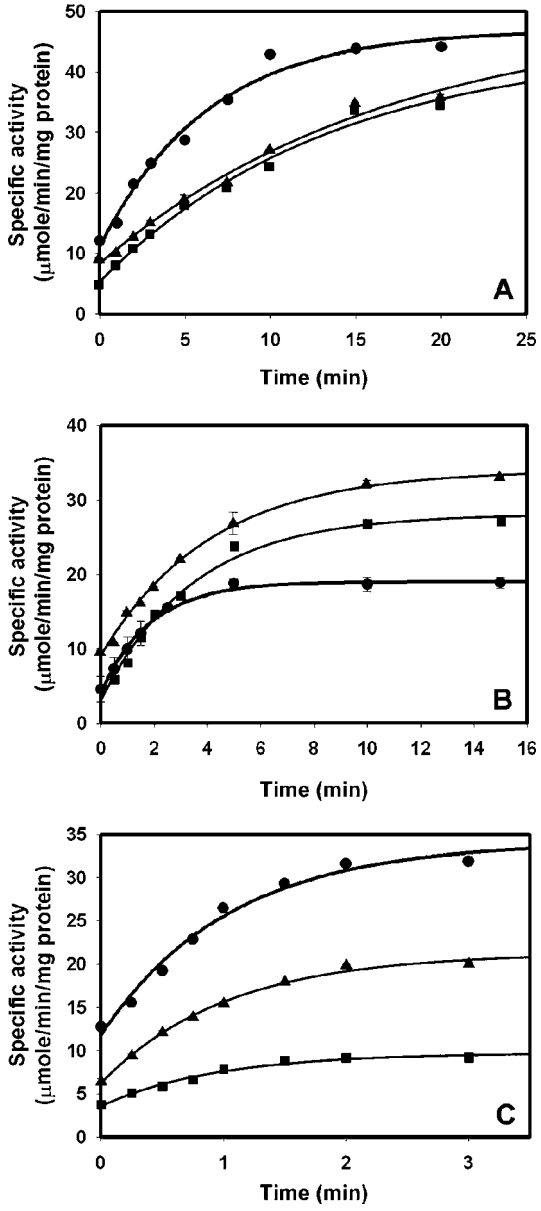

Figure 6 Kinetics of reactivation of wild-type adGSTD3-3 (●), E64Q (■) and E64D (▲) during refolding at different temperatures: 18 °C (A), 25 °C (B) and 33 °C (C)

Purified enzyme (20 μM), heterologously expressed at 18 °C, was first denatured in 4 M GdmCl for 30 min. This denaturant concentration was sufficient to completely unfold the proteins, as indicated by the loss of secondary structure shown by CD. Successive aliquots of unfolded enzyme were diluted (defining time 0) 1:40 into renaturation buffer at the different temperatures. The final GdmCl concentration was 0.1 M during the refolding. Appropriate aliquots from this incubation mixture were immediately assayed for catalytic activity at 25 °C.

network is to lower the pK_a of the thiol group of the bound GSH [22]. Our results show that Glu^{64} replacement with the polar amino acids glutamine and asparagine increased the pK_a values by about 0.5–1.0 pH unit. This consequence appears to be due to the deletion of the negative charge, resulting in loss of ionic interaction within the electron-sharing network. This is supported by the replacement of the critical glutamate residue with the negatively charged aspartate, which has no affect on the ionization process. Therefore, an acidic amino acid in this position is essential to form an ionic interaction to fulfil the function of the electron-sharing network in the ionization process. However, the formation of a σ-complex intermediate in the enzyme-catalysed reaction was affected by the replacement with glutamine and aspartate. It is well established that the bimolecular nucleophilic substitution reactions proceed through a σ-complex intermediate [43]. Thus, the rate-limiting formation of a spontaneous σ-complex intermediate can be increased by replacement of chlorine in the CDNB molecule with the more electronegative fluorine. The ratio of the catalytic rate of GSH with FDNB and CDNB was comparable to the ratio of the second-order rate constants for a spontaneous uncatalysed reaction. That is, $k_{cat}^{FDNB}/k_{cat}^{CDNB} = 40$ is similar to $k_c^{FDNB}/k_c^{CDNB} = 47$, which indicates that the σ-complex formation is the rate-limiting step. Although the $k_{cat}^{FDNB}/k_{cat}^{CDNB}$ of all Glu^{64} mutants reflected varying insensitivity to the nature of the leaving group, there were two mutants E64Q and E64D that exhibited significant differences in the catalytic efficiency (k_{cat}/K_m) (Table 4). For the E64N mutant, it appears that an alteration of the relative turn-over number is a consequence of changes in binding affinity towards different substrate leaving groups rather than a reflection of the rate of σ-complex formation. Differences in relative catalytic efficiency (k_{cat}/K_m) for the fluoride/chloride leaving group replacement may not strongly support the idea that the rate-determining step to σ-complex formation for E64Q and E64D was changed. Although it appears that transition state stability of the enzyme–intermediate complex, influenced by electron density and distribution in the σ-complex, was partially altered by these two amino acid replacements [43,44].

Table 3 Steady-state kinetic constants and pK_a values for the thiol group of GSH of wild-type and mutants of adGSTD3-3 for the CDNB conjugation reaction at pH 6.5 and 25 °C

The enzyme activities were measured at various concentrations of CDNB and GSH in 0.1 M phosphate buffer pH 6.5. The pK_a was obtained by using 0.1 M sodium acetate buffers (from pH 5.0 to 5.5) and 0.1 M potassium phosphate buffer (from pH 6.0 to 8.5).The reaction was monitored at 340 nm, ε 9600 $M^{-1}cm^{-1}$. Statistics were performed using one-way ANOVA and Tukey–Kramer multiple comparisons test. Values significantly different from wild-type are shown by * $P < 0.001$. The wild-type values have been reported previously [25].

Enzyme	k_{cat} (s^{-1})	K_m^{GSH} (mM)	K_m^{CDNB} (mM)	k_{cat}/K_m^{GSH} (s^{-1}/mM)	k_{cat}/K_m^{CDNB} (s^{-1}/mM)	pK_a
Wild-type	35.4	0.27 ± 0.05	0.14 ± 0.01	131	246	6.36 ± 0.11
E64Q	36.3	7.10 ± 0.28*	0.43 ± 0.03	5.11	83.6	6.97 ± 0.14*
E64D	21.6	9.12 ± 0.20*	0.28 ± 0.01	2.37	75.8	6.42 ± 0.12
E64N	1.4	7.89 ± 0.19*	0.33 ± 0.01	0.18	4.4	7.37 ± 0.07*

Table 4 Effect of fluoride/chloride leaving group substitution on the rate of catalysis

The ratios of kinetic constants for the conjugation reaction catalyzed by adGSTD3-3 enzymes for GSH with CDNB or FDNB as co-substrates were calculated at pH 6.5. Statistics performed using one-way ANOVA and Tukey–Kramer multiple comparisons test. Values significantly different from wild-type are shown by * $P < 0.001$. The wild-type values have been reported previously [25].

Enzyme	$k_{cat}^{FDNB}/k_{cat}^{CDNB}$	$(k_{cat}/K_m)^{FDNB}/(k_{cat}/K_m)^{CDNB}$
Wild-type	2.40 ± 0.08	6.72 ± 0.34
E64Q	6.97 ± 0.24*	14.36 ± 1.22*
E64D	8.40 ± 0.08*	10.31 ± 0.38*
E64N	5.92 ± 0.05*	6.58 ± 0.05

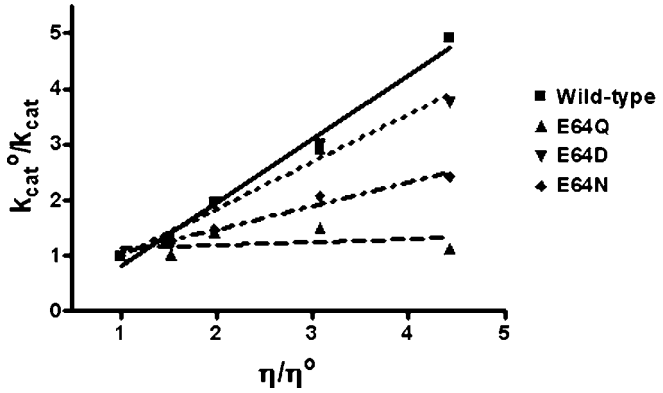

Figure 7 Viscosity effect on kinetic parameters of wild-type adGSTD3-3 and mutant enzymes

The effect of viscosity on kinetic constants was assayed by using 0.1 M potassium phosphate buffer, pH 6.5, with various glycerol concentrations. Dependence of the reciprocal of the relative turn-over number (k_{cat}^{o}/k_{cat}) on the relative viscosity (η/η^{o}) for CDNB as a co-substrate. The experiment was performed in triplicate and the lines were calculated by linear regression analysis. The slopes of the linear regression lines are 1.14 ± 0.01 for wild-type, 0.05 ± 0.01 for E64Q, 0.85 ± 0.01 for E64D and 0.42 ± 0.02 for E64N.

The effect of viscosity on kinetic parameters was examined to elucidate the rate-limiting step in the catalytic reaction. A decrease in the rate constant with increasing medium viscosity should reflect the weight of diffusion events on catalysis [45]. It would indicate that the rate-limiting step is related to diffusion-controlled motions of the protein or the dissociation of the product. A plot of the reciprocal of the relative catalytic constant (k_{cat}^{o}/k_{cat}) against the relative viscosity (η/η^{o}) should be linear. The slope should be equal to unity when the product release or structural transition is limited by a strictly diffusional barrier. If the slope approaches zero either the chemistry or another non-diffusion barrier is rate-limiting. For wild-type adGSTD3-3, a plot of the inverse relative rate constant (k_{cat}^{o}/k_{cat}) versus the relative viscosity (η/η_{o}) gives a linear dependence with a slope (1.14 ± 0.01) very close to unity (Figure 7). In contrast the E64Q mutant enzyme yields plots that are fully viscosity independent, with a slope approaching zero (0.05 ± 0.01). The other mutants, E64D and E64N, exhibited k_{cat} values with different degrees of viscosity dependence compared with the wild-type enzyme. The viscosity experiment showed that the rate-limiting step catalysed by adGSTD3-3 is a non-physical step (Figure 7). However, structural alterations in the Glu[64] mutants decreased the viscosity effects on the enzyme to intermediate values ($0 < \text{slope} < 1$), especially for the replacement with the polar residues glutamine and asparagine. This indicates that the rate-limiting step is not strictly dependent on a diffusion barrier or other viscosity-dependent motions and that conformational changes of the engineered proteins contribute to the rate-limiting step [45]. This suggests that the structural flexibility of functionally important regions of the engineered enzymes have been altered. Previously, we have observed [22] that changing the residues in the electron-sharing network can influence the topology of the active-site, which affects both the catalytic mechanism as well as the structural maintenance of the enzyme. The results of the present study demonstrate that the functionally conserved Glu[64], which is now identified as being part of the electron-sharing network, impacts upon enzyme catalysis not only through its negative charge but also through structural effects.

In conclusion, the results of the present paper, as well as the high level of functional conservation of the residue at position 64 among all classes of GSTs supports the hypothesis that Glu[64] is part of a functionally conserved electron-sharing network. The present paper now extends the network identified previously to include three critical residues that form ionic bridge interactions. These are between a negatively charged/polar active site residue (glutamate, aspartate or glutamine), a positively charged GSH glutamyl α-amino, a negatively charged GSH glutamyl α-carboxylate, a positively charged active-site residue (primarily arginine) and a negatively charged active-site residue (glutamate or aspartate) stabilized by hydrogen-bonding networks with surrounding residues (serine, threonine and/or water mediated contact). Glu[64] in the electron-sharing network contributes to the function of this motif and the base-assisted deprotonation model which are essential for the GSH ionization process in the catalytic mechanism. However, this residue also appears to affect additional steps in the enzyme catalytic strategy including binding of GSH to the enzyme active site, nucleophilic attack by thiolate at the electrophilic centre and product formation. Therefore, the Glu[64] position also appears to impact upon catalysis through roles in both initial folding and structural maintenance.

This work was supported by the Thailand Research Fund. P.W. was supported by a Royal Golden Jubilee Scholarship and a scholarship from the Senior Research Fellowship of Professor Emeritus Sakol Panyim.

REFERENCES

1 Sheehan, D., Meade, G., Foley, V. M. and Dowd, C. A. (2001) Structure, function and evolution of glutathione transferases: implications for classification of non-mammalian members of an ancient enzyme superfamily. Biochem. J. **360**, 1–16
2 Cho, S.-G., Lee, Y. H., Park, H.-S., Ryoo, K., Kang, K. W., Park, J., Eom, S.-J., Kim, M. J., Chang, T.-S., Choi, S.-Y. et al. (2001) Glutathione *S*-transferase Mu modulates the stress-activated signals by suppressing apoptosis signal-regulating kinase 1. J. Biol. Chem. **276**, 12749–12755
3 Gate, L., Majumdar, R. S., Lunk, A. and Tew, K. D. (2004) Increased myeloproliferation in glutathione *S*-transferase π deficient mice is associated with a deregulation of JNK and janus kinase/STAT. J. Biol. Chem. **279**, 8608–8616
4 Ronai, Z. (2001) Coordinated regulation of stress kinases by GSTp. Chem. Biol. Interact. **133**, 285–286
5 Hayes, J. D. and Pulford, D. J. (1995) The glutathione S-transferase supergene family: regulation of GST and the contribution of the isoenzymes to cancer chemoprotection and drug resistance. CRC Crit. Rev. Biochem. Mol. Biol. **30**, 445–600
6 Mannervik, B. and Danielson, U. H. (1988) Glutathione transferases: structure and catalytic activity. CRC Crit. Rev. Biochem. **23**, 283–337
7 Armstrong, R. N. (1997) Structure, catalytic mechanism, and evolution of the glutathione transferases. Chem. Res. Toxicol. **10**, 2–18
8 Habig, W. H., Pabst, M. J. and Jakoby, W. B. (1974) Glutathione *S*-transferases. The first enzymatic step in mercapturic acid formation. J. Biol. Chem. **249**, 7130–7139
9 Ahmad, H., Wilson, D. E., Fritz, R. R., Singh, S. V., Medh, R. D., Nagle, G. T., Awasthi, Y. C. and Kurosky, A. (1990) Primary and secondary structural analyses of glutathione S-transferase π from human placenta. Arch. Biochem. Biophys. **278**, 398–408
10 Board, P., Baker, R. T., Chelvanayagam, G. and Jermiin, L. S. (1997) Zeta, a novel class of glutathione transferases in a range of species from plants to humans. Biochem. J. **328**, 929–935
11 Mannervik, B., Ålin, P., Guthenberg, C., Jensson, H., Tahir, M. K., Warholm, M. and Jörnvall, H. (1985) Identification of three classes of cytosolic glutathione transferase common to several mammalian species: correlation between structural data and enzymatic properties. Proc. Natl. Acad. Sci. U.S.A. **82**, 7202–7206
12 Mannervik, B., Awasthi, Y. C., Board, P. G., Hayes, J. D., Di Ilio, C., Ketterer, B., Listowsky, I., Morgenstern, R., Muramatsu, M., Pearson, W. R. et al. (1992) Nomenclature for human glutathione transferases. Biochem. J. **282**, 305–306
13 Meyer, D. J., Coles, B., Pemble, S. E., Gilmore, K. S., Fraser, G. M. and Ketterer, B. (1991) Theta, a new class of glutathione transferases purified from rat and man. Biochem. J. **274**, 409–414
14 Motoyama, N. and Dauterman, W. C. (1978) Molecular weight, subunits, and multiple forms of glutathione S-transferase from the house fly. Insect Biochem. **8**, 337–348

15 Pemble, S. E. and Taylor, J. B. (1992) An evolutionary perspective on glutathione transferases inferred from class-Theta glutathione transferase cDNA sequences. Biochem. J. **287**, 957–963
16 Ding, Y., Ortelli, F., Rossiter, L. C., Hemingway, J. and Ranson, H. (2003) The *Anopheles gambiae* glutathione transferase supergene family: annotation, phylogeny and expression profiles. BMC Genomics **4**, 35–50
17 Wilce, M. C. J. and Parker, M. W. (1994) Structure and function of glutathione S-transferases. Biochim. Biophys. Acta **1205**, 1–18
18 Armstrong, R. N., Rife, C. and Wang, Z. (2001) Structure, mechanism and evolution of thiol transferases. Chem. Biol. Interact. **133**, 167–169
19 Caccuri, A. M., Ascenzi, P., Antonini, G., Parker, M. W., Oakley, A. J., Chiessi, E., Nuccetelli, M., Battistoni, A., Bellizia, A. and Ricci, G. (1996) Structural flexibility modulates the activity of human glutathione transferase P1-1. Influence of a poor co-substrate on dynamics and kinetics of human glutathione transferase. J. Biol. Chem. **271**, 16193–16198
20 Caccuri, A. M., Antonini, G., Nicotra, M., Battistoni, A., Lo Bello, M., Board, P. G., Parker, M. W. and Ricci, G. (1997) Catalytic mechanism and role of hydroxyl residues in the active site of theta class glutathione S-transferases. Investigation of Ser-9 and Tyr-113 in a glutathione S-transferase from the Australian sheep blowfly, *Lucilia cuprina*. J. Biol. Chem. **272**, 29681–29686
21 Gustafsson, A., Pettersson, P. L., Grehn, L., Jemth, P. and Mannervik, B. (2001) Role of the glutamyl α-carboxylate of the substrate glutathione in the catalytic mechanism of human glutathione transferase A1-1. Biochemistry **40**, 15835–15845
22 Winayanuwattikun, P. and Ketterman, A. J. (2005) An electron-sharing network involved in the catalytic mechanism is functionally conserved in different glutathione transferase classes. J. Biol. Chem. **280**, 31776–31782
23 Caccuri, A. M., Antonini, G., Board, P. G., Parker, M. W., Nicotra, M., Lo Bello, M., Federici, G. and Ricci, G. (1999) Proton release on binding of glutathione to Alpha, Mu and Delta class glutathione transferases. Biochem. J. **344**, 419–425
24 Tan, K.-L., Chelvanayagam, G., Parker, M. W. and Board, P. G. (1996) Mutagenesis of the active site of the human Theta-class glutathione transferase GSTT2-2: catalysis with different substrates involves different residues. Biochem. J. **319**, 315–321
25 Winayanuwattikun, P. and Ketterman, A. J. (2004) Catalytic and structural contributions for glutathione binding residues in a delta class glutathione S-transferase. Biochem. J. **382**, 751–757
26 Jirajaroenrat, K., Pongjaroenkit, S., Krittanai, C., Prapanthadara, L. and Ketterman, A. J. (2001) Heterologous expression and characterization of alternatively spliced glutathione *S*-transferases from a single *Anopheles* gene. Insect Biochem. Mol. Biol. **31**, 867–875
27 Bradford, M. M. (1976) A rapid and sensitive method for the quantitation of microgram quantities of protein utilizing the principle of protein-dye binding. Anal. Biochem. **72**, 248–254
28 Caccuri, A. M., Ascenzi, P., Lo Bello, M., Federici, G., Battistoni, A., Mazzetti, P. and Ricci, G. (1994) Are the steady state kinetics of glutathione transferase always dependent on the deprotonation of the bound glutathione? New insights in the kinetic mechanism of GST P1-1. Biochem. Biophys. Res. Commun. **200**, 1428–1434
29 Wolf, A. V., Brown, M. G. and Prentiss, P. G. (1985) Handbook of Chemistry and Physics, CRC Press, Boca Raton
30 Kong, G. K. W., Polekhina, G., McKinstry, W. J., Parker, M. W., Dragani, B., Aceto, A., Paludi, D., Principe, D. R., Mannervik, B. and Stenberg, G. (2003) Contribution of glycine 146 to a conserved folding module affecting stability and refolding of human glutathione transferase P1-1. J. Biol. Chem. **278**, 1291–1302
31 Stenberg, G., Dragani, B., Cocco, R., Principe, D. R., Mannervik, B. and Aceto, A. (2001) A conserved 'hydrophobic staple motif' plays a crucial role in the refolding of human glutathione transferase P1-P1. Chem. Biol. Interact. **133**, 49–50
32 Jackson, S. E., el Masry, N. and Fersht, A. R. (1993) Structure of the hydrophobic core in the transition state for folding of chymotrypsin inhibitor 2: a critical test of the protein engineering method of analysis. Biochemistry **32**, 11270–11278
33 Widersten, M., Kolm, R. H., Björnestedt, R. and Mannervik, B. (1992) Contribution of five amino acid residues in the glutathione binding site to the function of human glutathione transferase P1-1. Biochem. J. **285**, 377–381
34 Dirr, H. W. and Wallace, L. A. (1999) Role of the C-terminal helix 9 in the stability and ligandin function of class a glutathione transferase A1-1. Biochemistry **38**, 15631–15640
35 Jones, M. N. (1979) In Biochemical Thermodynamics (Studies in Modern Thermodynamics). (Jones, M. N., ed.), pp. 75–115, Elsevier, Oxford
36 Haynie, D. T. (2001) Statistical thermodynamics. In Biological thermodynamics, pp. 185–222, Cambridge University Press, Cambridge
37 Zeng, Q.-Y. and Wang, X.-R. (2005) Catalytic properties of glutathione-binding residues in a τ class glutathione transferase (PtGSTU1) from *Pinus tabulaeformis*. FEBS Lett. **579**, 2657–2662
38 Wongsantichon, J. and Ketterman, A. J. (2006) An intersubunit lock-and-key 'clasp' motif in the dimer interface of delta class glutathione transferase. Biochem. J. **394**, 135–144
39 Sayed, Y., Wallace, L. A. and Dirr, H. W. (2000) The hydrophobic lock-and-key intersubunit motif of glutathione transferase A1-1: implications for catalysis, ligandin function and stability. FEBS Lett. **465**, 169–172
40 Stenberg, G., Abdalla, A.-M. and Mannervik, B. (2000) Tyrosine 50 at the subunit interface of dimeric human glutathione transferase P1-1 is a structural key residue for modulating protein stability and catalytic function. Biochem. Biophys. Res. Commun. **271**, 59–63
41 Dirr, H. W., Little, T., Kuhnert, D. C. and Sayed, Y. (2005) A conserved N-capping motif contributes significantly to the stabilisation and dynamics of the C-terminal region of class alpha glutathione transferases. J. Biol. Chem. **280**, 19480–19487
42 Garcia-Viloca, M., Gao, J., Karplus, M. and Truhlar, D. G. (2004) How enzymes work: analysis by modern rate theory and computer simulations. Science **303**, 186–195
43 Chen, W.-J., Graminski, G. F. and Armstrong, R. N. (1988) Dissection of the catalytic mechanism of isozyme 4–4 of glutathione S-transferase with alternative substrates. Biochemistry **27**, 647–654
44 Graminski, G. F., Zhang, P., Sesay, M. A., Ammon, H. L. and Armstrong, R. N. (1989) Formation of the 1-(*S*-glutathionyl)-2,4,6-trinitrocyclohexadienate anion at the active site of glutathione *S*-transferase: evidence for enzymic stabilization of σ-complex intermediates in nucleophilic aromatic substitution reactions. Biochemistry **28**, 6252–6258
45 Johnson, W. W., Liu, S., Ji, X., Gilliland, G. L. and Armstrong, R. N. (1993) Tyrosine 115 participates both in chemical and physical steps of the catalytic mechanism of a glutathione S-transferase. J. Biol. Chem. **268**, 11508–11511

Received 16 August 2006/19 October 2006; accepted 14 November 2006
Published as BJ Immediate Publication 14 November 2006, doi:10.1042/BJ20061253

BJ www.biochemj.org

BJ Structure

Biochem. J. (2007) **401**, 635–644 (Printed in Great Britain) doi:10.1042/BJ20060603

Reprint 3 **635**

Differences in the subunit interface residues of alternatively spliced glutathione transferases affects catalytic and structural functions

Juthamart PIROMJITPONG, Jantana WONGSANTICHON and Albert J. KETTERMAN[1]

Institute of Molecular Biology and Genetics, Mahidol University, Salaya Campus, Nakhon Pathom 73170, Thailand

GSTs (glutathione transferases) are multifunctional widespread enzymes. Currently there are 13 identified classes within this family. Previously most structural characterization has been reported for mammalian Alpha, Mu and Pi class GSTs. In the present study we characterize two enzymes from the insect-specific Delta class, adGSTD3-3 and adGSTD4-4. These two proteins are alternatively spliced products from the same gene and have very similar tertiary structures. Several major contributions to the dimer interface area can be separated into three regions: conserved electrostatic interactions in region 1, hydrophobic interactions in region 2 and an ionic network in region 3. The four amino acid side chains studied in region 1 interact with each other as a planar rectangle. These interactions are highly conserved among the GST classes, Delta, Sigma and Theta. The hydrophobic residues in region 2 are not only subunit interface residues but also active site residues. Overall these three regions provide important contributions to stabilization and folding of the protein. In addition, decreases in yield as well as catalytic activity changes, suggest that the mutations in these regions can disrupt the active site conformation which decreases binding affinity, alters kinetic constants and alters substrate specificity. Several of these residues have only a slight effect on the initial folding of each subunit but have more influence on the dimerization process as well as impacting upon appropriate active site conformation. The results also suggest that even splicing products from the same gene may have specific features in the subunit interface area that would preclude heterodimerization.

Key words: *Anopheles dirus*, glutathione transferase (GST), hydrophobic interaction, subunit interface.

INTRODUCTION

GSTs (glutathione transferases; EC 2.5.1.18) are a supergene family of multifunctional enzymes which are widely distributed in nature and found in most aerobic eukaryotes and prokaryotes. The dimeric cytosolic GSTs catalyse reactions with a broad range of substrates and play an essential role in detoxification of endogenous and xenobiotic compounds [1,2]. The dimerization of the GSTs not only contributes to stabilization of the subunit tertiary structure, but also allows for the construction of a fully functional active site [3]. Although tertiary structures of all classes of GSTs are similar, dimerization is highly specific and is thought to occur only between subunits within the same class [4,5].

The structural features at the dimer interface of the GSTs suggest at least two major subunit interaction areas [6]. The first area is the predominantly hydrophobic interaction at the outer ends of the interface called a hydrophobic 'lock-and-key' (also referred to as a 'ball-and-socket') motif which is formed by the insertion of an aromatic residue from domain I of one subunit into a 'lock' of five residues of domain II in the other subunit [6–9]. The second major subunit interaction area is the symmetry axis interactions at the 2-fold axis of the protein which show highly conserved electrostatic interactions at one edge of the subunit interface and a variety of interactions along the interface depending on the GST class. The *Anopheles dirus* mosquito is an important malaria vector in South East Asia. From an *A. dirus* genomic library, a 7.5 kb fragment containing the adgst1AS1 gene (*A. dirus* alternatively spliced GST gene) was identified [10]. This gene contains six exons that encode four Delta class GSTs, adGSTD1-1, 2-2, 3-3 and 4-4, which possess 61–77 % amino acid identity compared among themselves. Previously these proteins had been named adGST1-1, 1-2, 1-3 and 1-4, according to insect GST nomenclature in use (that is, insect class 1-protein 1, 2, 3 and 4 respectively). However, to be in alignment with a proposed universal GST nomenclature, the proteins were renamed adGSTD1-1, adGSTD2-2, adGSTD3-3 and adGSTD4-4 respectively [11,12]. The subunit number remains the same, since subunits were enumerated as they were initially discovered, 'D' refers to GST Delta class and '4-4' refers to the homodimeric isoenzyme. These four GSTs share an untranslated exon 1 and a translated exon 2 coding for 45 amino acids at the N-terminus but vary between four different exon 3 sequences (exons 3A–3D). The arrangement of each exon is similar to the aggst1α gene from *A. gambiae,* the major malaria vector in Africa, with approx. 79 % nucleotide identity for the two genes [13]. In *A. dirus*, although four splice products are encoded from the same gene, the enzymes possess distinct enzyme kinetic properties for substrates, inhibitors, including insecticides, as well as physical properties such as stability [14,15]. Although two splice products, adgstD3-3 (PDB accession number: 1JLV) and adgstD4-4 (PDB accession number: 1JLW), have very similar tertiary structures when aligned, the amino acid identity is only 68 % [16].

When compared with human Alpha, Mu and Pi classes, the dimer interfaces of both Delta class isoenzymes are more extensively hydrophilic. Although lacking the previously identified hydrophobic 'lock-and-key' motif (a conserved motif in human Alpha, Mu and Pi classes), the Delta class does possess a 'Clasp' motif with a similar function [17]. In addition to this motif, there are nine amino acids making major contributions to the interactions within this interface area, which can be separated into three regions: conserved electrostatic interactions in region

Abbreviations used: ANS, 8-anilino-1-naphthalene sulfonate; CDNB, 1-chloro-2,4-dinitrobenzene; DCNB, 1,2-dichloro-4-nitrobenzene; EA, ethacrynic acid; GST, glutathione transferase; PNBC, p-nitrobenzyl chloride; PNPB, p-nitrophenethyl bromide.

[1] To whom correspondence should be addressed (email albertketterman@yahoo.com).

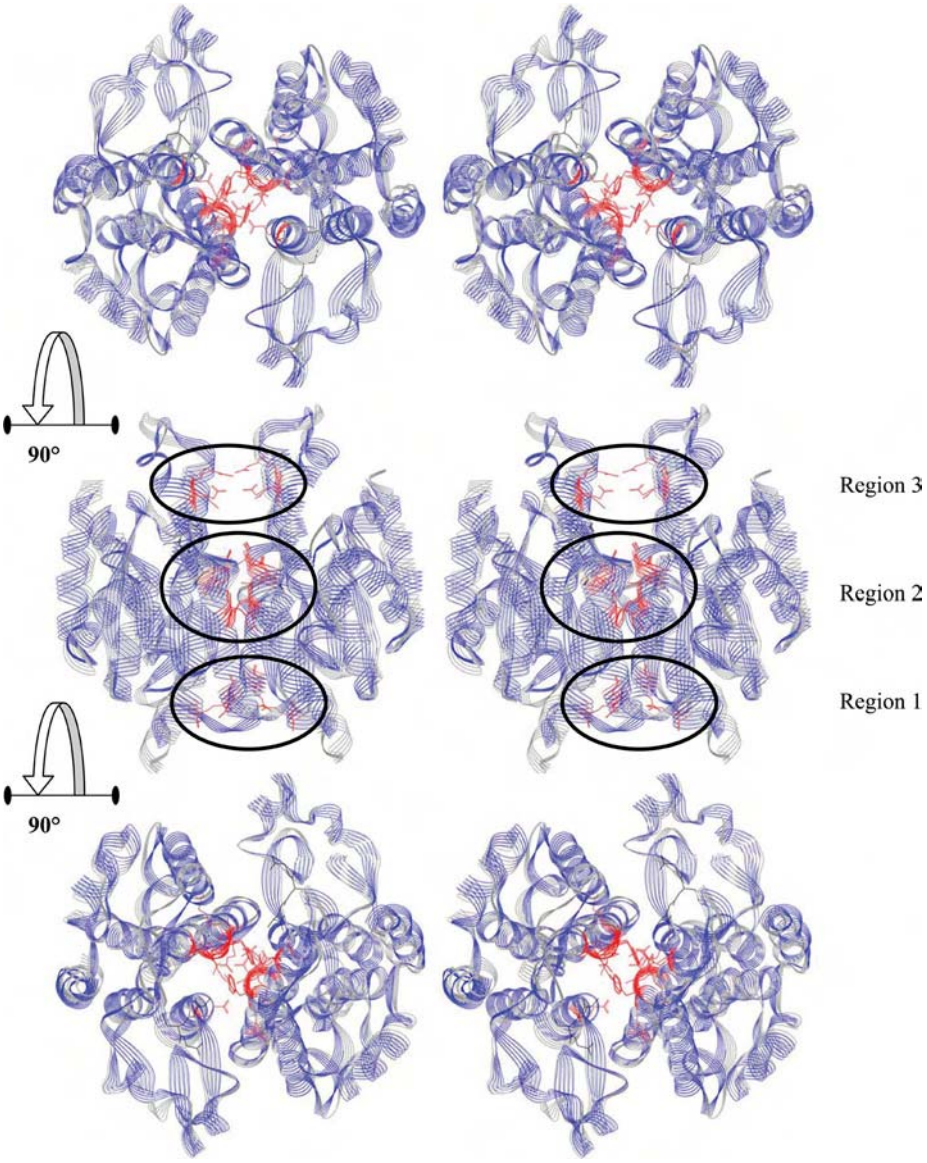

Figure 1 The three regions of the interface characterized in the present study

The two GST proteins are carbon backbone aligned with the adGSTD3-3 secondary structure wire ribbon shown in blue and the adGSTD4-4 secondary structure ribbon shown in grey. The GSH in the two active sites is shown as a black stick; the residues engineered in the present study are shown in red. The top panel is a stereo view looking at the 2-fold axis from the side opposite to the active sites. The middle panel shows the proteins rotated 90°, to show the position of the studied interface residues down the length of α-helices 3 and 4. The bottom panel shows the proteins rotated a further 90° and looking down upon the 2-fold axis on to the active sites. The Figure was created using Accelrys DS ViewerPro 5.0.

1, hydrophobic interactions in region 2 and an ionic network in region 3 (Figure 1).

The conserved electrostatic interactions in region 1 of the subunit interface are formed by two amino acid residues from one subunit (a glutamate residue in α-helix 3 and an arginine residue in α-helix 4) interacting with the same two amino acids from the other subunit. These interactions are of interest because the four amino acid side chains interact with each other as a planar rectangle with distances of 3.83–4.26 Å (1Å = 0.1 nm). These interactions are highly conserved among the GST classes, Delta, Sigma and Theta, however at present there are no reports of these interactions for any of the three GST classes. In adGSTD4-4, each arginine residue not only interacts with both of the negatively charged Glu^{75} residues in both subunits, but also forms cation–π interactions with the aromatic ring of Tyr^{89} and an ionic interaction with the carboxy group of Pro^{90}. In adGSTD3-3, the equivalent residues to Glu^{75} and Arg^{96} of adGSTD4-4 are Glu^{74} and Arg^{90}. These residues also form the same planar rectangle arrangement within adGSTD3-3 and are stabilized in a similar manner by interactions with Tyr^{83} and Pro^{84} (Tyr^{89} and Pro^{90} in adGSTD4-4). Therefore as the motif appears to be highly conserved in both proteins it was only studied in adGSTD4-4. In addition, these interactions appear to be highly conserved among the insect GST classes. Therefore the aim of the present study was to determine whether the inter- and intra-subunit electrostatic interactions of these residues are important contributions that help to maintain tertiary and quaternary structures.

Region 2 at the subunit interface shows the most variation in amino acid residues at equivalent positions between the two isoenzymes, Tyr^{98}, Met^{101} and Gly^{102} of adGSTD3-3 and Phe^{104},

Val[107] and Ala[108] of adGSTD4-4 respectively. These residues are of interest because they are not only subunit interface residues but also active site residues with several of them involved in both active sites of the dimeric enzyme. Therefore the amino acids at the equivalent positions of the two isoenzymes were studied by switching the amino acids of the two proteins; Y98F, M101V, G102A and Y98F/M101V/G102A of adGSTD3-3 and F104Y, V107M, A108G and F104Y/V107M/A108G of adGSTD4-4.

The last region is the hydrophilic area in region 3 of the subunit interface, Asp[110] of adGSTD3-3 and Glu[116] of adGSTD4-4. Not only are these subunit interface residues, but these two equivalent positions also are involved in the active site as part of the H-site (hydrophobic substrate-binding site). For adGSTD4-4, Glu[116] forms hydrogen bonds with Arg[134] in both inter- and intra-subunit interactions; however, these interactions do not appear in adGSTD3-3. For adGSTD3-3, there are hydrogen bonds only in the same subunit between Asp[110] and the highly conserved residue Glu[106]. To study the influence of the ionic network in region 3 of the subunit interface and whether it impacts upon the catalytic activity and stability of the enzymes, mutations at the equivalent positions of these two isoenzymes were generated, that is, D110A of adGSTD3-3 and E116A of adGSTD4-4.

MATERIALS AND METHODS

Site-directed mutagenesis and protein purification

The adGSTD3-3 and adGSTD4-4 plasmid DNA templates were prepared from previous constructs [14]. The construction of the mutants was based on the Stratagene QuikChange® site-directed mutagenesis kit using *pfu* DNA polymerase. The expression constructs of recombinant plasmid that were obtained were sequenced at least twice and transformed into *Escherichia coli* BL21DE3plysS. The soluble recombinant GSTs were purified by GSTrap affinity chromatography (Amersham Phamacia) as previously described [14]. After purification, proteins were homogeneous as judged by SDS/PAGE, and the protein concentration was determined using the Bradford protein reagent with bovine serum albumin as a standard [18].

Catalytic activity and kinetic studies

Steady-state kinetics were studied at various concentrations of CDNB (1-chloro-2,4-dinitrobenzene) and GSH in 0.1 M phosphate buffer (pH 6.5). The reaction was monitored at 340 nm, $\varepsilon = 9600\ M^{-1} \cdot cm^{-1}$. Apparent kinetic parameters, k_{cat}, K_m and k_{cat}/K_m were determined by fitting the collected data to a Michaelis–Menten equation by non-linear regression analysis using GraphPad Prism version 4 (GraphPad software; www.graphpad.com) [19,20]. Specific activities of the enzymes were determined with five different substrates; CDNB, DCNB (1,2-dichloro-4-nitrobenzene), EA (ethacrynic acid), PNPB (p-nitrophenethyl bromide) and PNBC (p-nitrobenzyl chloride) as previously described [21]. Specific activities reported are the means ± S.D. from at least three independent experiments. One-way ANOVA with Dunnett's post test was performed using GraphPad InStat version 3.06 for Windows (GraphPad software; www.graphpad.com).

Structural studies

Enzymes at 0.1 mg/ml final concentration were incubated at 45 °C. Inactivation time courses were determined by withdrawing suitable aliquots at different time points for an assay of remaining activity to calculate the half-life of the enzyme [22]. Data are the means ± S.D. from at least three independent experiments.

Spectroscopic properties of wild-type and mutant proteins were measured for evidence of conformational changes. Intrinsic fluorescence emission spectra were measured at an excitation wavelength of 295 nm and λ_{max} and fluorescence intensity of emission spectra were analysed at a protein concentration of 0.2 mg/ml [23].

A refolding experiment was performed with enzymes first being denatured in 4 M guanidinium chloride in renaturation buffer [0.2 M phosphate, 1 mM EDTA and 5 mM dithiothreitol (pH 7.0)] at room temperature (25 °C) for 1 h and then rapidly diluted (defining time zero) 1:40 into renaturation buffer. Therefore the final guanidinium chloride concentration was 0.1 M during refolding. Recovered activity was monitored as a function of time by withdrawal of appropriate aliquots of renaturation mixture and immediately assaying for activity. Refolding rate constants were determined by non-linear regression analysis using a single exponential equation [23].

The ANS (8-anilino-1-naphthalenesulfonate) binding assay was monitored using a PerkinElmer Luminescence spectrometer LS50B. ANS [200 μM in 0.1 M sodium phosphate buffer (pH 6.5)] was added to a final concentration of 2 μM enzyme in a 400 μl reaction mixture [24]. The spectrum of ANS in phosphate buffer (pH 6.5) was subtracted from the spectrum of protein-binding ANS. A total of three scans each for blank and sample were recorded and averaged for each enzyme. Reported spectra are the means from at least three independent experiments. Enzyme activity measurements in the presence of ANS were assessed immediately after adding ANS by using the standard reaction assay.

RESULTS AND DISCUSSION

The investigations of GST dimerization performed in mammalian GSTs indicated that the subunit interactions are a significant source of stabilization not only for the association of subunits but also for tertiary structures of the individual subunits [9,25,26]. In the present study, most mutations gave similar purification yields as the wild-type with the exception of the E75A and R96A mutants of adGSTD4-4, which had yields approx. 2 and 0.4 % of the wild-type respectively. As the proteins were expressed in similar amounts, it appears that the alteration of these residues disrupts the intra-subunit interaction between helix 3 and helix 4 which impacts upon the active site architecture thereby affecting binding to the affinity matrix.

Both adGSTD3-3 and adGSTD4-4 have two tryptophan residues in each subunit that are located in β-sheet 4 in domain I and α-helix 7 in domain II. The tryptophan residue located in β-sheet 4 in domain I (Trp[63]) is in close proximity to the active site, with an involvement in sequestering the substrate glutathione, as well as being in the subunit interface. This makes it a sensitive fluorescence probe to monitor conformational changes at/near the active site. The normalized fluorescence spectra of adGSTD3-3 and adGSTD4-4 wild-type compared with the mutants were obtained to study the effect of mutations on the enzyme tertiary structure (Figure 2). The results showed that although every mutant had the same λ_{max} as the wild-type, several mutants presented differences in the normalized intensities of fluorescence, implying that the mutations caused significant conformational changes in the environment of the tryptophan residues located near the subunit interface and the mutation site. The mutants also had different intensities from their wild-type especially R96A, with the intensity of fluorescence decreased by approx. 66 %. This finding suggests that there are significant conformational changes in the tryptophan residue neighbourhood that distinguish the final structure of the mutant from that of the wild-type. This decrease

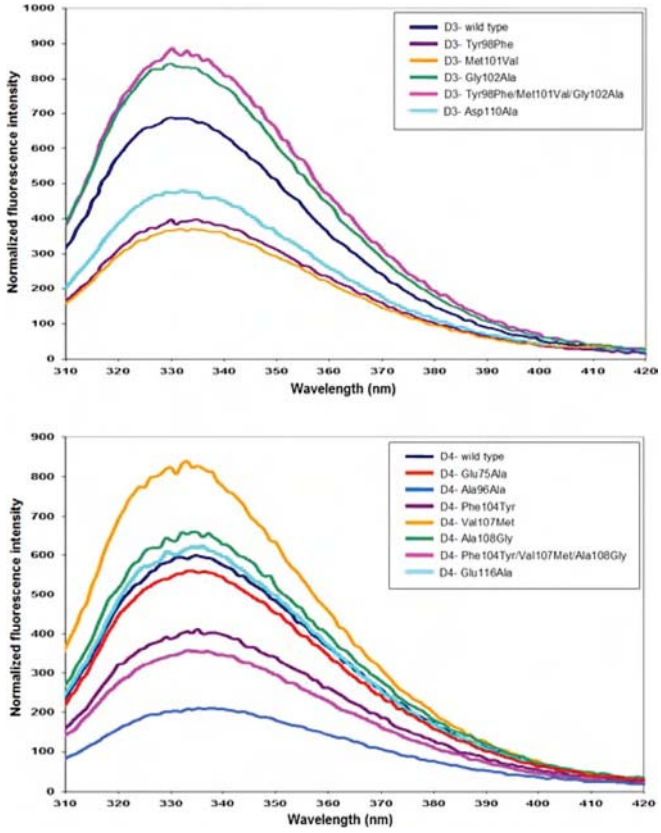

Figure 2 Normalized intrinsic tryptophan residue fluorescence spectra of the adGSTD3-3 and adGSTD4-4 (wild-type) and the recombinant mutant GSTs

The same colour represents the equivalent position. The data are means of three independent experiments.

demonstrates that movements have occurred in the tryptophan residues or in the surrounding fluorescence quenching groups.

The half-life of the enzymes corresponds to the time of incubation when there is 50 % remaining activity (Table 1). The conserved cation–π interaction residue, Arg[96], and the conserved electrostatic interaction residue, Glu[75], have important roles in stabilizing enzyme structure as shown by a much decreased stability for R96A and E75A of approx. 15- and 7.4-fold respectively. For region 2, several mutants possessed similar stability as the wild-type enzymes. However, there were three mutants which had very different thermal stabilities. Two of the mutations were at an equivalent position, adGSTD3-3 Gly[102] and adGSTD4-4 Ala[108]. Replacement of a glycine residue by an alanine residue in adGSTD3-3 at this position caused decreases of about 8-fold in half-life, whereas a glycine residue substitution of adGSTD4-4 showed an increase in half-life of about 4.7-fold. The other mutant that showed stability changes was the V104M protein which decreased the half-life by approx. 3-fold. For region 3, the half-life of D110A of adGSTD3-3 was similar to the wild-type. However, the equivalent adGSTD4-4 mutation E116A disrupted the charge–charge network and showed a 64 % decreased stability for the enzyme. The results showed that the positively charged residue at the edge of the subunit interface of adGSTD4-4 participates in stabilizing the enzyme structure while the equivalent residue of adGSTD3-3 appeared to have only a minor contribution.

Three mutations in adGSTD4-4, E75A, R96A and V107M, did not recover activity after being unfolded by 4 M guanidinium chloride (Table 1). This implies that these residues play a critical role in the folding process of the enzymes. For the remaining mutants, the refolding rate constants were similar. The activity recovered illustrates the ability of the enzymes to recover their appropriate active site conformation for catalytic activity. After unfolding, the enzymes were able to recover activity ranging from 19 % to 94 %. To study the influence of mutations on protein folding and to assess whether the changes affected tertiary folding of each subunit or dimerization of the two subunits, intrinsic tryptophan residue fluorescence spectroscopy was performed. The fluorescence spectra of native, unfolded and refolded enzymes were monitored to compare the tertiary structure of the proteins in each state (Figures 3 and 4). The λ_{max} values of the native (335 nm) and the unfolded form (355 nm) of the protein were observed for every enzyme. The data showed that the enzymes were refolded in a similar manner as the native form, as shown by similar λ_{max} values, including the E75A, R96A and V107M mutants, although

Table 1 Half-life, refolding rate constants, activity recovered (%) and the effect of ANS on CDNB specific activity of the adGSTD3-3 and adGSTD4-4 (wild-type) and the recombinant engineered GSTs

The data are means ± S.D. for at least three independent experiments. One-way ANOVA with Dunnett's post test was performed to show statistical significance with $*P < 0.05$ and $\dagger P < 0.01$. D3 and D4 indicate adGSTD3-3 and adGSTD4-4 respectively. Inside parentheses the numbers indicate the subunit interface region: 1 is region 1, 2 is region 2 and 3 is region 3; and the same lowercase letter indicates an equivalent residue position for the two GST isoenzymes. nd, not detectable.

Enzymes	Half-life (min)	Refolding rate constant (min^{-1})	Activity recovered (%)	Inhibition by ANS (%)
D3-wild-type	2.71 ± 0.35	0.87 ± 0.09	56.9 ± 0.23	24.6 ± 1.41
D3-Y98F (2/a)	3.12 ± 0.33	0.58 ± 0.05†	66.1 ± 2.83*	13.1 ± 0.54†
D3-M101V (2/b)	2.77 ± 0.43	0.42 ± 0.05†	40.5 ± 1.93†	11.9 ± 0.80†
D3-G102A (2/c)	0.34 ± 0.03†	0.38 ± 0.07†	94.4 ± 5.77†	13.7 ± 2.66†
D3-Y98F/M101V/G102A (2/d)	1.88 ± 0.01*	0.31 ± 0.03†	85.8 ± 4.39†	18.4 ± 0.65†
D3-D110A (3/e)	2.21 ± 0.24	0.58 ± 0.11†	80.5 ± 3.48†	23.4 ± 1.83
D4-wild-type	14.0 ± 1.70	0.59 ± 0.03	19.7 ± 0.70	18.4 ± 1.20
D4-G75A(1)	1.89 ± 0.13†	nd	0.00	22.5 ± 0.82
D4-R96A(1)	0.91 ± 0.07†	nd	0.00	18.8 ± 3.89
D4-F104Y (2/a)	17.1 ± 1.76*	0.28 ± 0.02†	23.5 ± 0.51	31.9 ± 1.96†
D4-V107M (2/b)	4.76 ± 0.15†	nd	0.00	25.4 ± 1.41†
D4-A108G (2/c)	65.4 ± 1.45†	0.32 ± 0.04†	69.6 ± 7.55†	32.8 ± 1.03†
D4-F104Y/V107M/A108G (2/d)	16.7 ± 1.23	0.60 ± 0.10	25.0 ± 0.18	21.1 ± 1.83
D4-E116A (3/e)	5.16 ± 0.93†	0.68 ± 0.11	9.93 ± 0.68*	17.3 ± 2.05

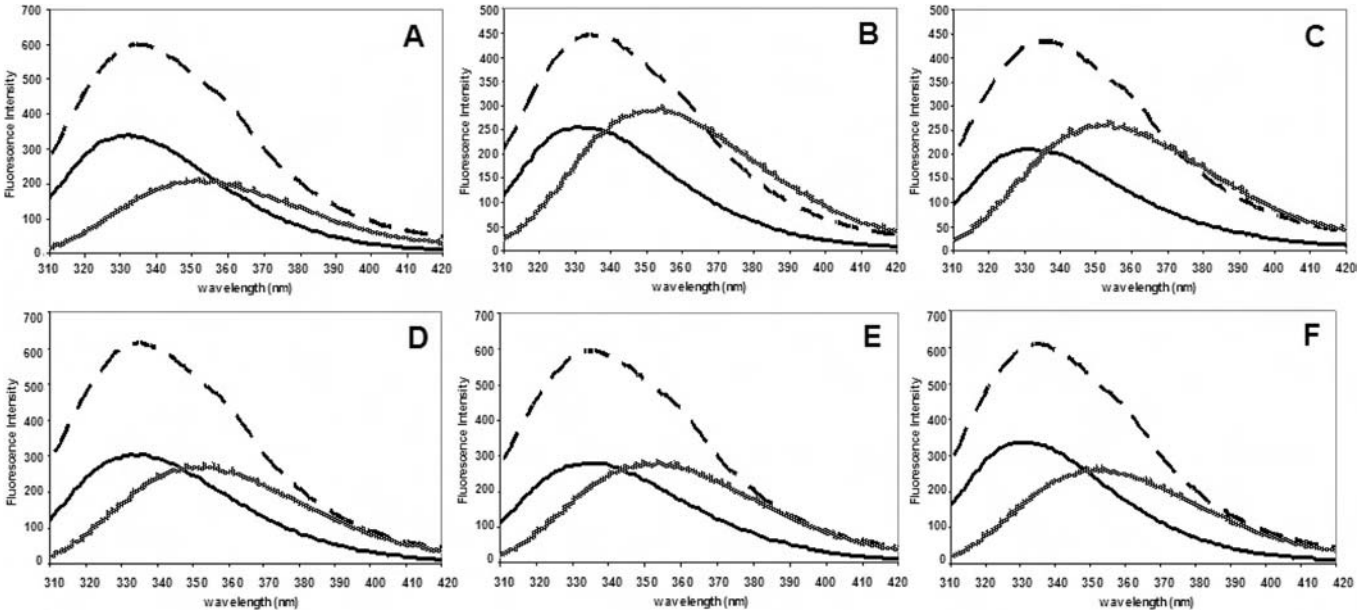

Figure 3 Normalized intrinsic tryptophan residue fluorescence spectra compared with the native, refolded and unfolded forms of the adGSTD3-3 (wild-type) and the recombinant mutant GSTs

(**A**) Wild-type, (**B**) Y98F, (**C**) M101V, (**D**) G102A, (**E**) Y98F/M101V/G102A and (**F**) D110A. The data are means for at least three independent experiments. Solid line, native form; dashed line, refolded form; and hashed line, unfolded form of the enzyme.

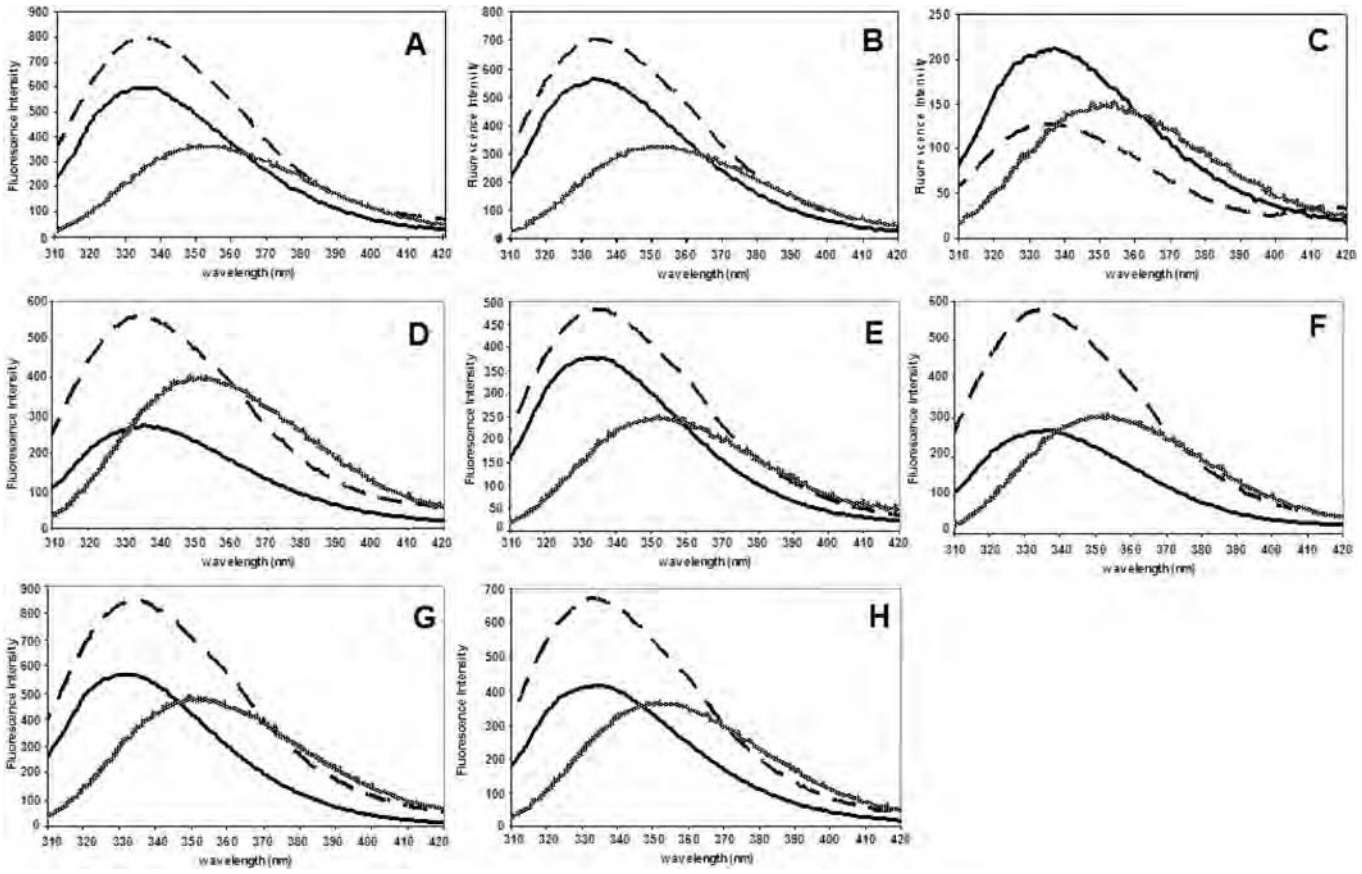

Figure 4 Normalized intrinsic tryptophan residue fluorescence spectra compared with the native, refolded and unfolded forms of the adGSTD4-4 (wild-type) and the recombinant mutant GSTs

(**A**) Wild-type, (**B**) G75A, (**C**) R96A, (**D**) F104Y, (**E**) V107M, (**F**) A108G, (**G**) F104Y/V107M/A108G and (**H**) E116A. The data are means for at least three independent experiments. Solid line, native form; dashed line, refolded form; and hashed line, unfolded form of the enzyme.

these enzymes could not recover catalytic activity. As shown by the similar patterns of the adGSTD3-3 mutant spectra, the mutations did not affect the tertiary folding of each subunit but influenced the dimerization process, which is necessary to achieve an appropriate active site conformation. Therefore both catalytic and structural data suggest that the single mutation of Gly^{102} and the triple mutation had significant effects on the dimerization of the enzymes by increasing the activity recovered from 56.9 % for wild-type to approx. 94.4 % and 85.8 % for the two proteins respectively (Table 1). In both catalytic and structural experiments, the refolding data showed that loss of the conserved electrostatic interactions, E75A and R96A, and the hydrophobic residue, V107M, had a dramatic effect on the dimerization process, which is critical to formation of the complete active site pocket. The results for the Arg^{96} position indicated that not only does this residue have a critical role in the dimerization process, but it is also important for the protein folding pathway of each monomeric subunit.

The anionic dye ANS has been shown to bind in the solvent-exposed cleft in the subunit interface of class Alpha and Pi enzymes [27–29]. Therefore ANS was utilized as a probe to monitor the appearance/disappearance of hydrophobic patches or surfaces on the proteins that were undergoing structural changes. When ANS was bound to the proteins the fluorescence was enhanced, accompanied by a blue shift in its emission maximum from 514 nm (free ANS in buffer) to 498 nm for adGSTD3-3 and 482 nm for wild-type adGSTD4-4, indicating that the polarity of the binding site had become more hydrophobic, with decreasing polarity the greater the blue shift.

When compared with the wild-type proteins, there was no change in the emission maximum wavelength of ANS bound to all mutants (Figure 5). For the ANS fluorescence intensity, which reflects the degree of solvent quenching of ANS bound to the protein, the adGSTD4-4 mutants showed variations in the amount of ANS bound, except E75A, which showed a similar intensity to the wild-type. However, there was no relative intensity change for the adGSTD3-3 mutants. The results showed that the residue substitutions of adGSTD4-4 with the adGSTD3-3 amino acids had a dramatic effect at the subunit interface, much more than for adGSTD3-3.

To study the impact of ANS on the enzyme conformation, the enzyme activity in the presence and absence of ANS was measured using the standard reaction assay. The results showed that for the mutants, ANS molecules can bind and alter the active site architecture in a manner similar to the wild-type (Table 1). It implied that differences in ANS spectra intensities in Figure 5 occurred only from an alteration of a hydrophobic patch at the subunit-binding site.

In general, the engineered enzyme reactions followed Michaelis–Menten kinetics as did the wild-type except for E75A, F104Y and E116A of adGSTD4-4 which showed positive co-operativity upon substrate binding. Positive co-operativity is shown by a sigmoidal velocity curve which reflects the substrate binding in the first active site, that then facilitates a second substrate molecule binding in the second active site by increasing the binding affinity of the vacant binding site [30]. For CDNB, two of the enzymes had significantly different Hill coefficients (shown by one-way ANOVA with Dunnett's post test) compared with wild-type enzyme [Hill coefficients for wild-type 1.08 ± 0.08 versus E75A 1.79 ± 0.03 ($P < 0.01$) and E116A 1.40 ± 0.20 ($P < 0.05$)]. For GSH only F104Y had a significantly different Hill coefficient (shown by one-way ANOVA with Dunnett's post test) compared with wild-type enzyme [Hill coefficients for wild-type 1.06 ± 0.14 versus F104Y 2.01 ± 0.09 ($P < 0.01$)]. These data show that two of the mutant enzymes, E75A and F104Y, had very strong positive co-operativity, with the Hill coefficients approaching the number of substrate-binding sites. In addition, comparison of the kinetic constants of the mutants with the wild-type values showed that the residue changes affected additional enzymatic properties (Table 2). These effects on the active site were also reflected in changes in substrate specificity with changes in the equivalent residue position showing different effects on the two isoforms (Table 3). For example, D110A activity was significantly decreased with CDNB and DCNB in adGSTD3-3 but E116A activity was significantly increased with CDNB and showed no significant activity with DCNB in adGSTD4-4. For another position, M101V in adGSTD3-3 equivalent to V107M in adGSTD4-4, both enzymes showed significant decreases in activity with CDNB. However, the adGSTD4-4 enzyme showed significant increases in activity with DCNB and EA, whereas the adGSTD3-3 enzyme showed a significant decrease with DCNB and no significant change with EA.

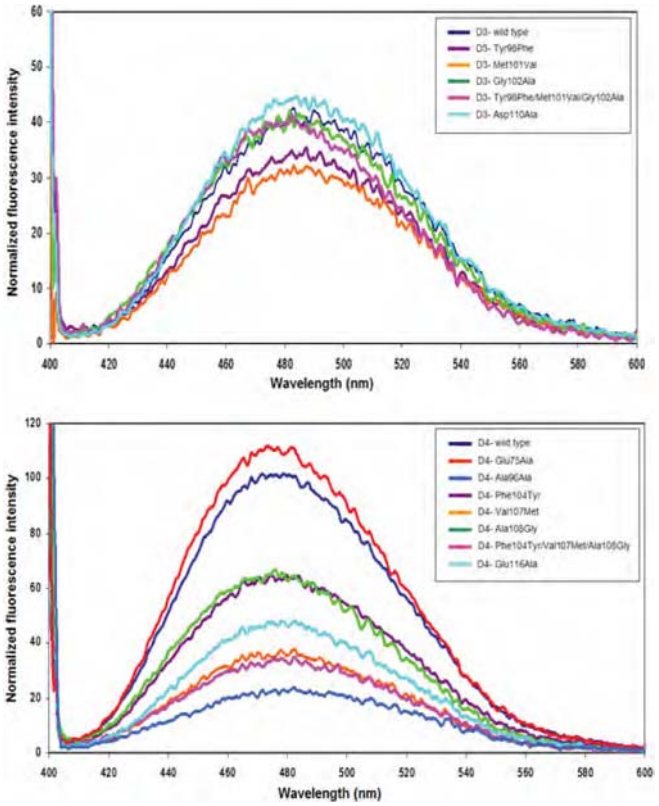

Figure 5 ANS binding spectra of the adGSTD3-3 and adGSTD4-4 (wild-type) and the recombinant mutant GSTs

The same colour represents the equivalent position. The spectra were measured immediately after addition of ANS. As ANS fluorescence is quenched by water, alteration of the fluorescence intensity of protein-bound ANS is highly dependent upon its accessibility to water. The data are means for at least three independent experiments.

The insect GST class Delta has a conserved planar rectangular electrostatic motif formed by four amino acid residues from different helices of both subunits (Glu^{75} in α-helix 3 and Arg^{96} in α-helix 4) (Figure 6). These interactions are highly conserved among GST classes Delta, Sigma and Theta. This is the first report of these interactions for any of these three classes. To study the function of this motif two mutants were generated, E75A and R96A, which break the conserved electrostatic interactions and ionic network at the dimer interface of adGSTD4-4. The results showed that the motif provides an important contribution

Table 2 Yield of purification and kinetic parameters of the adGSTD3-3 and adGSTD4-4 (wild-type) and the recombinant engineered GSTs

The data are means ± S.D. for at least three independent experiments. One-way ANOVA with Dunnett's post test was performed to show statistical significance with $*P < 0.05$ and $\dagger P < 0.01$. D3 and D4 indicate adGSTD3-3 and adGSTD4-4 respectively. Inside parentheses the numbers indicate the subunit interface region: 1 is region 1, 2 is region 2 and 3 is region 3; and the same lowercase letter indicates an equivalent residue position for the two GST isoenzymes.

Enzymes	CDNB k_{cat} (s^{-1})	CDNB K_m (mM)	CDNB k_{cat}/K_m ($mM^{-1}•s^{-1}$)	GSH K_m (mM)	GSH k_{cat}/K_m ($mM^{-1}•s^{-1}$)	Purification yield (%)
D3-wild-type	39.2	0.15 ± 0.01	258	0.29 ± 0.04	114	53.7
D3-Y98F (2/a)	24.9†	0.12 ± 0.01	213	0.47 ± 0.05	53.1	49.2
D3-M101V (2/b)	26.0†	0.72 ± 0.06†	36.3	1.04 ± 0.06†	25.0	60.0
D3-G102A (2/c)	23.5†	0.37 ± 0.02†	63.3	2.94 ± 0.38†	7.99	47.6
D3-Y98F/M101V/G102A (2/d)	40.7	0.28 ± 0.03†	147	1.12 ± 0.07†	36.7	58.3
D3-D110A (3/e)	51.7†	0.49 ± 0.07†	106	0.54 ± 0.04	95.8	34.3
D4-wild-type	22.5	0.63 ± 0.09	35.7	0.67 ± 0.05	33.6	61.3
D4-G75A (1)	23.3	8.26 ± 2.63†	2.82	0.54 ± 0.06	43	5.5
D4-R96A (1)	16.2†	0.80 ± 0.06	22.0	1.08 ± 0.02	15.0	1.4
D4-F104Y (2/a)	15.5†	0.52 ± 0.03	29.8	24.01 ± 2.94†	0.65	42.2
D4-V107M (2/b)	13.7†	1.6 ± 0.08	8.56	0.76 ± 0.11	18.0	60.0
D4-A108G (2/c)	26.8	0.87 ± 0.07	26.8	0.73 ± 0.12	36.7	59.2
D4-F104Y/V107M/A108G (2/d)	32.5†	0.72 ± 0.04	45.2	0.25 ± 0.02	130	59.2
D4- E116A (3/e)	46.1†	1.55 ± 0.01	29.7	1.24 ± 0.06	37.1	37.1

Table 3 Specific activities of the adGSTD3-3 and adGSTD4-4 (wild-type) and the recombinant engineered GSTs

The data are means ± S.D. for at least three independent experiments. One-way ANOVA with Dunnett's post test was performed to show statistical significance with $*P < 0.05$ and $\dagger P < 0.01$. The substrate concentrations used were 1 mM CDNB for adGSTD3 and 3 mM CDNB for adGSTD4, 1 mM DCNB, 0.1 mM PNBC, 0.1 mM PNPB and 0.2 mM EA. D3 and D4 indicate adGSTD3-3 and adGSTD4-4 respectively. Inside parentheses the numbers indicate the subunit interface region: 1 is region 1, 2 is region 2 and 3 is region 3; and the same lowercase letter indicates an equivalent residue position for the two GST isoenzymes. nd is not detectable.

Enzymes	Specific Activity (μmol/min/mg) CDNB	DCNB	EA	PNPB	PNBC
D3-wild-type	85.3 ± 3.23	0.25 ± 0.01	0.10 ± 0.05	nd	0.13 ± 0.01
D3-Y98F (2/a)	46.9 ± 6.38†	0.23 ± 0.03	0.03 ± 0.01*	nd	0.05 ± 0.00†
D3-M101V (2/b)	41.1 ± 0.81†	0.05 ± 0.01†	0.08 ± 0.02	nd	0.09 ± 0.00†
D3-G102A (2/c)	46.8 ± 0.25†	0.08 ± 0.01†	nd	nd	0.05 ± 0.00†
D3-Y98F/M101V/G102A (2/d)	84.8 ± 5.47	0.21 ± 0.01*	0.15 ± 0.01	nd	0.08 ± 0.00†
D3-D110A (3/e)	71.6 ± 2.69†	0.16 ± 0.01†	0.01 ± 0.01†	0.03 ± 0.01	0.07 ± 0.01†
D4-wild-type	48.0 ± 1.98	0.03 ± 0.00	0.27 ± 0.00	0.06 ± 0.01	0.03 ± 0.01
D4-E75A (1)	36.6 ± 5.03†	0.06 ± 0.01	0.12 ± 0.01	0.02 ± 0.01	0.06 ± 0.00
D4-R96A (1)	26.0 ± 0.13†	0.27 ± 0.04†	0.18 ± 0.01	0.23 ± 0.02	nd
D4-F104Y (2/a)	28.5 ± 2.24†	0.06 ± 0.01	0.14 ± 0.01	0.05 ± 0.01	0.11 ± 0.05
D4-V107M (2/b)	22.0 ± 2.29†	0.08 ± 0.004*	2.06 ± 0.29†	0.31 ± 0.08	nd
D4-A108G (2/c)	55.3 ± 2.07	0.06 ± 0.02	0.32 ± 0.01	nd	0.08 ± 0.02
D4-F104Y/V107M/A108G (2/d)	53.8 ± 1.43	0.05 ± 0.01	0.02 ± 0.00*	nd	0.04 ± 0.01
D4- E116A (3/e)	56.3 ± 6.83*	0.06 ± 0.01	0.01 ± 0.01*	0.04 ± 0.01	0.04 ± 0.01

to the stabilization and folding of the protein. The mutants were expressed in both inclusion and soluble forms, with the R96A mutant mostly being expressed as an inclusion body. This evidence and the results from the refolding assay (Table 1; Figures 3 and 4) indicated that the folding process was altered by the mutations. In addition, decreases in yield as well as catalytic activity changes (Table 2), suggest that the mutations disrupt the active site conformation which decreases binding affinity, alters kinetic constants and substrate specificities.

Although both Glu^{75} and Arg^{96} are located in the same area, in the present study region 1 of the subunit interface, there is a conserved amino acid sequence around Arg^{96} which forms a pocket around the arginine residue. Arg^{96} is stabilized by several highly conserved residues in a cation–π interaction with Tyr^{89} and Pro^{90}, whereas Glu^{75} does not have amino acids surrounding it, except Arg^{96}, as it is located within a hole in the subunit interface edge (Figure 6). Therefore substitution of an alanine residue for Arg^{96} appears to have more impact on the tertiary and quaternary structure of the protein compared with Glu^{75}, as shown by decreases in the fluorescence intensities of both intrinsic tryptophan spectroscopy (Figure 2) and the ANS binding assay (Figure 5). This also suggests that there are significant conformational changes in amino acid side chains near the subunit interface and the mutation site. However, disappearance of the salt bridges with the loss of either Glu^{75} or Arg^{96} affected both initial protein folding, as shown in the refolding experiment, and the protein stability as shown by decreased half-life. Although Arg^{96} is not located in the active site pocket, structural changes that occurred due to this mutation also affected the active site conformation, probably through packing effects (Tables 2 and 3).

Region 2 of the subunit interface, which shows the most variation in amino acid residues at the equivalent positions between adGSTD3-3 and adGSTD4-4, is of interest because the residues are not only in the interface but also in the active site,

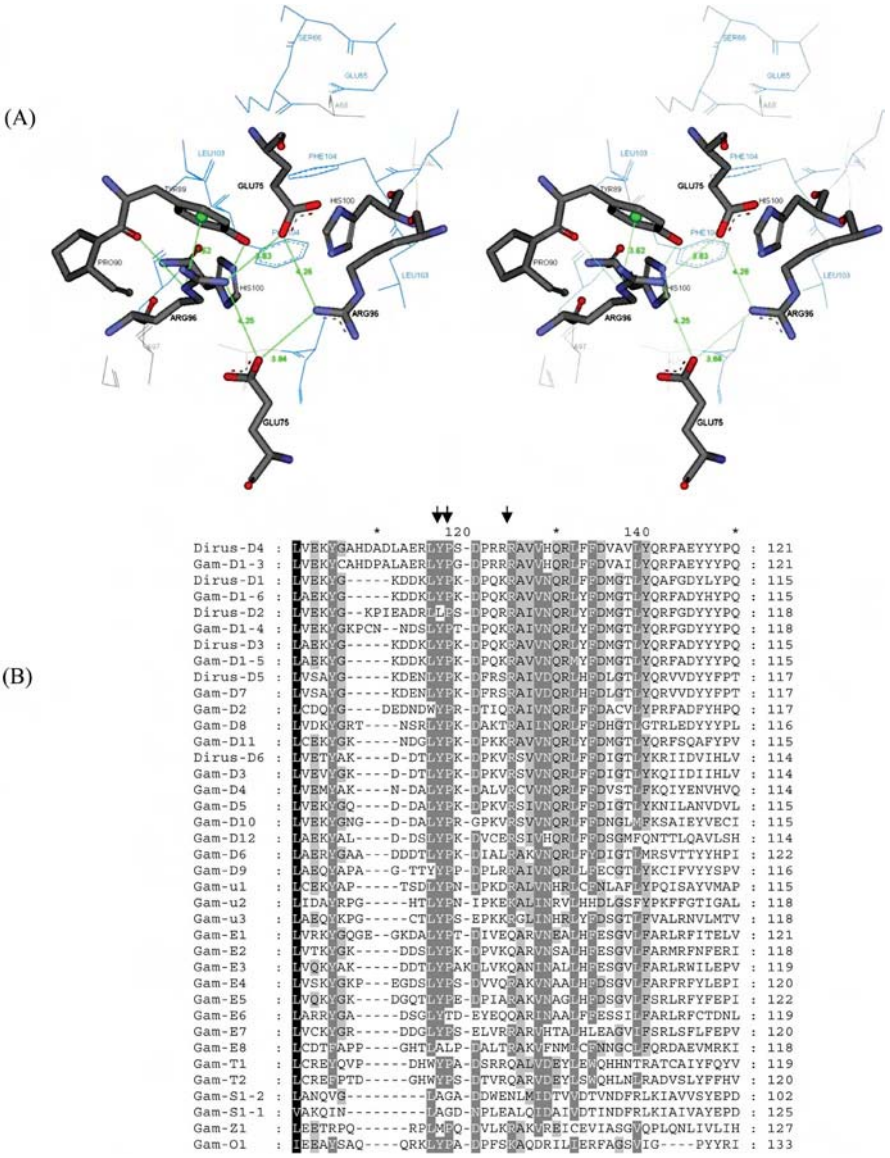

Figure 6 Conserved electrostatic interaction in region 1 of the subunit interface

(**A**) The planar rectangle electrostatic interaction of Glu^{75} and Arg^{96} from both subunits. Distances between the charged atoms are shown in Å. Also shown are the conserved anion–cation–π interactions between Tyr^{89}, Pro^{90} and Arg^{96}. (**B**) Amino acid alignment of insect GST classes. Dirus is *A. dirus* and Gam is *A. gambiae*. The arrows point to the highly conserved tyrosine, proline and arginine residues. D is Delta, u is unclassified, E is Epsilon, T is Theta, S is Sigma, Z is Zeta and O is Omega GST class. GenBank® accession numbers: adGSTD1 (AF273041), adGSTD2 (AF273038), adGSTD3 (AF273039), adGSTD4 (AF273040), adGSTD5 (AF251478), adGSTD6 (AY014406), agGSTD1-3 (Protein ID AAC79992), agGSTD1-4 (Protein ID AAC79994), agGSTD1-5 (Protein ID AAC79993), agGSTD1-6 (Protein ID AAC79995), agGSTD2 (Z71480), agGSTD3 (AF513638), agGSTD4 (AF513635), agGSTD5 (AF513634), agGSTD6 (AF513636), agGSTD7 (AF071161), agGSTD8 (AF316637), agGSTD9 (AY255857), agGSTD10 (AF515527), agGSTD11 (AF513637), agGSTD12 (AF316638), agGSTu1 (AF515521), agGSTu2 (AF515523), agGSTu3 (AF515524), agGSTE1 (AF316635), agGSTE2 (AF316636), agGSTE3 (AY070234), agGSTE4 (AY070254), agGSTE5 (AY070255), agGSTE6 (AY070256), agGSTE7 (AF491816), agGSTE8 (AY070257), agGSTT1 (AF515526), agGSTT2 (AF515525), agGSTS1-1 (L07880), agGSTS1-2 (AF513639), agGSTZ1 (AF515522), agGSTO1 (AY255856). agGSTD6 and agGSTD9 were suggested to be pseudogenes [33]. The Figure in (**A**) was created using Accelrys DS ViewerPro 5.0.

with several residues involved in both active sites of the dimer. The effects of the different hydrophobic amino acids at the equivalent positions of the two isoenzymes were studied by switching the equivalent amino acids with the amino acid from the other protein; that is, Y98F, M101V, G102A and Y98F/M101V/G102A for adGSTD3-3 and F104Y, V107M, A108G and F104Y/V107M/A108G for adGSTD4-4. The refolding experiments demonstrated that every enzyme could be refolded, although the activity recovered varied (Table 1). This indicates that the mutations have only a slight effect on the initial folding of each subunit but have more influence on the dimerization process through subunit interface conformation, as well as other structural aspects which impact upon appropriate active site conformation. When comparing the two isoforms adGSTD3-3 and adGSTD4-4, in terms of changes in catalytic activity, the mutations affected the proteins in different ways for the equivalent residues, as shown in Table 2. The crystal structures show that all selected equivalent positions are located in the active site pocket suggesting that the whole electrostatic field in the active site pocket was disturbed by the mutations, which thereby altered catalytic parameters of the enzymes. Moreover, these residues are also located at the interface of the two active

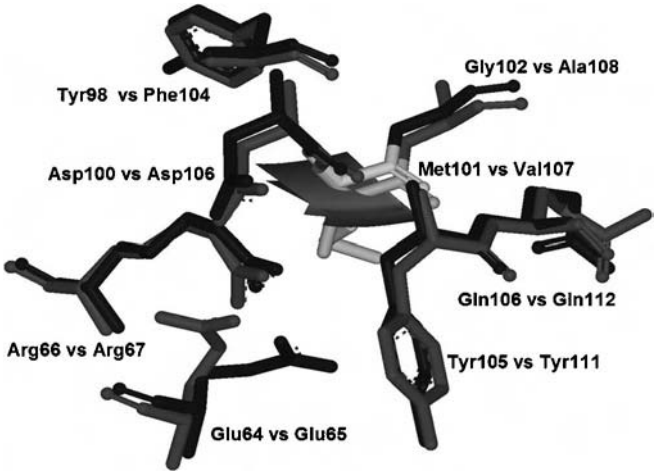

Figure 7 In region 2 the amino acid milieu of adGSTD3-Met[101] and adGSTD4-Val[107]

The dark grey represents adGSTD3-3 and medium grey is adGSTD4-4. The Figure was created using Accelrys DS ViewerPro 5.0.

site areas which provide different substrate-binding sites for GSH and the hydrophobic substrate. Therefore these positions would allow the residues to influence binding of both substrates as shown by the K_m values.

The first sphere milieu of the equivalent positions, Met[101] of adGSTD3-3 and Val[107] of adGSTD4-4, consists of seven amino acids of which only two residues are different between the two isoforms, adGSTD3-3 Tyr[98] compared with adGSTD4-4 Phe[104] and adGSTD3-3 Gly[102] compared with adGSTD4-4 Ala[108] (Figure 7). However, the triple mutations which changed all three amino acids at these equivalent positions to the amino acid of the other isoform, showed that they had only a slight effect on the half-life. Steric interactions and van der Waals forces are important interactions for the stability of proteins [31,32]. The side chain size of the three amino acids at these equivalent positions had a major impact on subunit interface packing, with differences between the two splice forms, especially Met[101] and Gly[102] of adGSTD3-3 and Val[107] and Ala[108] of adGSTD4-4. Although the amino acids possess similar properties, the packing effects were great enough to alter the protein and enzyme properties.

From the conserved electrostatic interactions in region 1 to the hydrophobic area in region 2 of the subunit interface, every residue appears to contribute to either maintaining structure or subunit binding. The last area to be examined was the hydrophilic area in region 3 of the subunit interface, Asp[110] of adGSTD3-3 and Glu[116] of adGSTD4-4. Both mutations, D110A of adGSTD3-3 and G116A of adGSTD4-4, affected catalysis as shown by changes in both specific activity and kinetic constants. The equivalent residue in the human Alpha class A1-1 is Glu[104] whereas in the human Pi class GST it is a polar Ser[105]. In insects, the acidic residue appears to be conserved within the Delta class, however in the Epsilon class it is generally an aromatic amino acid and in the other insect classes, such as Sigma, Theta and Zeta, the residue is hydrophobic. This residue therefore appears to be conserved within a class and would contribute to class specific dimerization motifs. Additionally, in adGSTD4-4 the Glu[116] interacts with Arg[134] in a similar fashion to Glu[75] and Arg[96] in region 1 (Figure 8). That is, electrostatic interactions occur between the two residues within the same subunit as well as with the identical residues from the other subunit. So in adGSTD4-4 but not in adGSTD3-3 similar intra- and inter-subunit electrostatic interactions occur in both regions 1 and 3 of the subunit interface. In adGSTD3-3 the equivalent residue to Arg[134] is Asn[126] and so, because of the shorter side chains of the Asp[110] and the Asn[126], the distances preclude electrostatic interaction across the subunits.

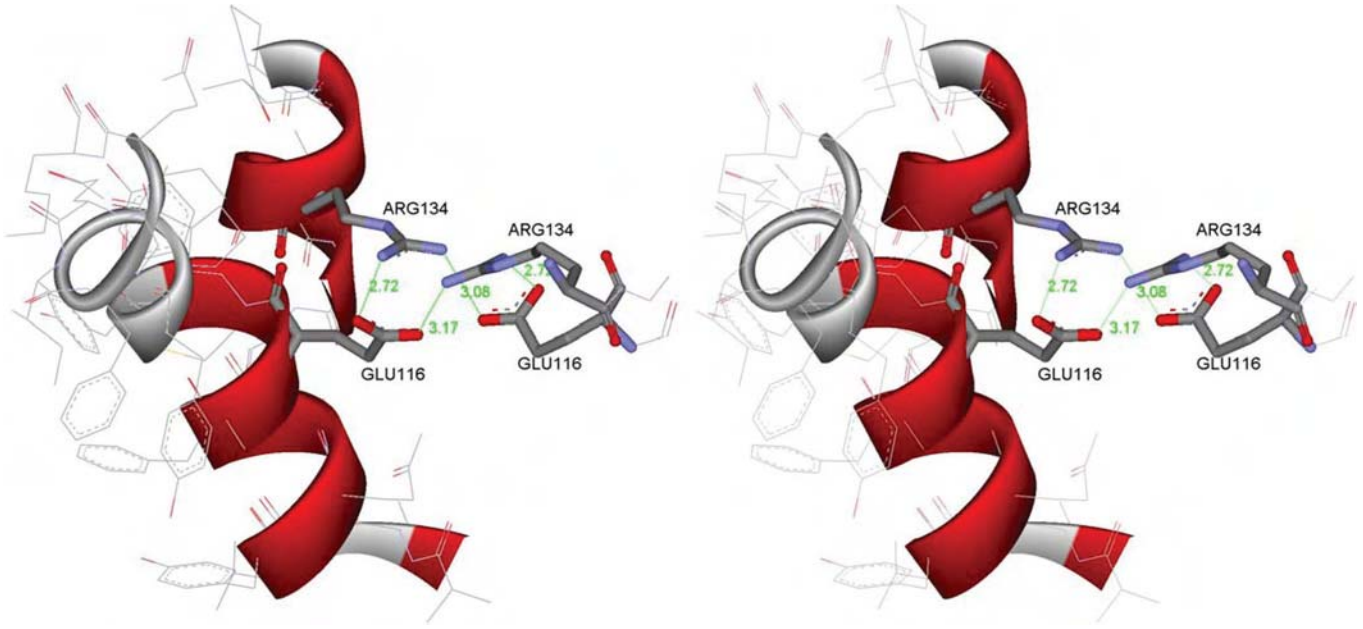

Figure 8 The electrostatic interaction in region 3 of Glu[116] and Arg[134] in adGSTD4-4

The two residues from each subunit are in proximity to interact electrostatically with each other as well as with the same residues from the other subunit. For the first subunit parts of α-helices 4 and 5, containing Glu[116] and Arg[134] respectively, are shown. For clarity only Glu[116] and Arg[134] from the second subunit are shown. Distances between the charged atoms are shown in Å. The Figure was created using Accelrys DS ViewerPro 5.0.

In conclusion, the conserved electrostatic interactions between the charged residues from α-helix 3 and α-helix 4 show important roles for protein folding, stabilization and dimerization of the alternatively spliced enzymes. However, the subunit interface region with the most variation in amino acid residues at equivalent positions between adGSTD3-3 and adGSTD4-4 showed that although the mutations did not alter the overall protein folding, the enzyme properties were changed, especially the catalytic activity, thermal stability and subunit interface. Even highly conservative amino acid replacements changed the protein properties. The results suggest that even splicing products from the same gene may have specific features in the subunit interface area that would preclude heterodimerization.

This work was funded by the TRF (Thailand Research Fund). J. P. held a DPST (Development and Promotion of Science and Technology Talent) scholarship. J. W. was supported by a Royal Golden Jubilee scholarship.

REFERENCES

1 Ketterer, B. (2001) A bird's eye view of the glutathione transferase field. Chem.-Biol. Interact. **138**, 27–42
2 Hayes, J. D., Flanagan, J. U. and Jowsey, I. R. (2005) Glutathione transferases. Annu. Rev. Pharmacol. Toxicol. **45**, 51–88
3 Luo, J.-K., Hornby, J. A. T., Wallace, L. A., Chen, J., Armstrong, R. N. and Dirr, H. W. (2002) Impact of domain interchange on conformational stability and equilibrium folding of chimeric class μ glutathione transferases. Protein Sci. **11**, 2208–2217
4 Hornby, J. A. T., Luo, J.-K., Stevens, J. M., Wallace, L. A., Kaplan, W., Armstrong, R. N. and Dirr, H. W. (2000) Equilibrium folding of dimeric class μ glutathione transferases involves a stable monomeric intermediate. Biochemistry **39**, 12336–12344
5 Luo, J.-K., Hornby, J. A. T., Armstrong, R. N. and Dirr, H. W. (2001) Equilibrium unfolding and enzyme kinetics of chimeric Mu class glutathione transferases. Chem.-Biol. Interact. **133**, 58–59
6 Sinning, I., Kleywegt, G. J., Cowan, S. W., Reinemer, P., Dirr, H. W., Huber, R., Gilliland, G. L., Armstrong, R. N., Ji, X., Board, P. G. et al. (1993) Structure determination and refinement of human Alpha class glutathione transferase A1-1, and a comparison with the Mu and Pi class enzymes. J. Mol. Biol. **232**, 192–212
7 Ji, X., Zhang, P., Armstrong, R. N. and Gilliland, G. L. (1992) The three-dimensional structure of a glutathione S-transferase from the Mu gene class: structural analysis of the binary complex of isoenzyme 3-3 and glutathione at 2.2 Å resolution. Biochemistry **31**, 10169–10184
8 Reinemer, P., Dirr, H. W., Ladenstein, R., Huber, R., Lo Bello, M., Federici, G. and Parker, M. W. (1992) Three-dimensional structure of class π glutathione S-transferase from human placenta in complex with S-hexylglutathione at 2.8 Å resolution. J. Mol. Biol. **227**, 214–226
9 Hornby, J. A. T., Codreanu, S. G., Armstrong, R. N. and Dirr, H. W. (2002) Molecular recognition at the dimer interface of a class Mu glutathione transferase: role of a hydrophobic interaction motif in dimer stability and protein function. Biochemistry **41**, 14238–14247
10 Pongjaroenkit, S., Jirajaroenrat, K., Boonchauy, C., Chanama, U., Leetachewa, S., Prapanthadara, L. and Ketterman, A. J. (2001) Genomic organization and putative promotors of highly conserved glutathione S-transferases originating by alternative splicing in *Anopheles dirus*. Insect Biochem. Mol. Biol. **31**, 75–85
11 Chelvanayagam, G., Parker, M. W. and Board, P. G. (2001) Fly fishing for GSTs: a unified nomenclature for mammalian and insect glutathione transferases. Chem.-Biol. Interact. **133**, 256–260
12 Wongsantichon, J., Harnnoi, T. and Ketterman, A. J. (2003) A sensitive core region in the structure of glutathione S-transferases. Biochem. J. **373**, 759–765
13 Ranson, H., Collins, F. and Hemingway, J. (1998) The role of alternative mRNA splicing in generating heterogeneity within the *Anopheles gambiae* class I glutathione S-transferase family. Proc. Natl. Acad. Sci. U.S.A. **95**, 14284–14289
14 Jirajaroenrat, K., Pongjaroenkit, S., Krittanai, C., Prapanthadara, L. and Ketterman, A. J. (2001) Heterologous expression and characterization of alternatively spliced glutathione S-transferases from a single *Anopheles* gene. Insect Biochem. Mol. Biol. **31**, 867–875
15 Ketterman, A. J., Prommeenate, P., Boonchauy, C., Chanama, U., Leetachewa, S., Promtet, N. and Prapanthadara, L. (2001) Single amino acid changes outside the active site significantly affect activity of glutathione S-transferases. Insect Biochem. Mol. Biol. **31**, 65–74
16 Oakley, A. J., Harnnoi, T., Udomsinprasert, R., Jirajaroenrat, K., Ketterman, A. J. and Wilce, M. C. J. (2001) The crystal structures of glutathione S-transferases isozymes 1-3 and 1-4 from *Anopheles dirus* species B. Protein Sci. **10**, 2176–2185
17 Wongsantichon, J. and Ketterman, A. J. (2006) An intersubunit lock-and-key 'Clasp' motif in the dimer interface of Delta class glutathione transferase. Biochem. J. **394**, 135–144
18 Bradford, M. M. (1976) A rapid and sensitive method for the quantitation of microgram quantities of protein utilizing the principle of protein–dye binding. Anal. Biochem. **72**, 248–254
19 Prapanthadara, L., Koottathep, S., Promtet, N., Hemingway, J. and Ketterman, A. J. (1996) Purification and characterization of a major glutathione S-transferase from the mosquito *Anopheles dirus* (species B). Insect Biochem. Mol. Biol. **26**, 277–285
20 Udomsinprasert, R. and Ketterman, A. J. (2002) Expression and characterization of a novel class of glutathione S-transferase from *Anopheles dirus*. Insect Biochem. Mol. Biol. **32**, 425–433
21 Habig, W. H., Pabst, M. J. and Jakoby, W. B. (1974) Glutathione S-transferases: the first enzymatic step in mercapturic acid formation. J. Biol. Chem. **249**, 7130–7139
22 Vararattanavech, A. and Ketterman, A. (2003) Multiple roles of glutathione binding-site residues of glutathione S-transferase. Protein Pept. Lett. **10**, 441–448
23 Stenberg, G., Dragani, B., Cocco, R., Mannervik, B. and Aceto, A. (2000) A conserved 'hydrophobic staple motif' plays a crucial role in the refolding of human glutathione transferase P1-1. J. Biol. Chem. **275**, 10421–10428
24 Stevens, J. M., Hornby, J. A. T., Armstrong, R. N. and Dirr, H. W. (1998) Class Sigma glutathione transferase unfolds via a dimeric and a monomeric intermediate: impact of subunit interface on conformational stability in the superfamily. Biochemistry **37**, 15534–15541
25 Dirr, H. (2001) Folding and assembly of glutathione transferases. Chem.-Biol. Interact. **133**, 19–23
26 Sayed, Y., Wallace, L. A. and Dirr, H. W. (2000) The hydrophobic lock-and-key intersubunit motif of glutathione transferase A1-1: implications for catalysis, ligandin function and stability. FEBS Lett. **465**, 169–172
27 Sluis-Cremer, N., Naidoo, N. and Dirr, H. (1996) Class-Pi glutathione S-transferase is unable to regain its native conformation after oxidative inactivation by hydrogen peroxide. Eur. J. Biochem. **242**, 301–307
28 Sayed, Y., Hornby, J. A. T., Lopez, M. and Dirr, H. (2002) Thermodynamics of the ligandin function of human class Alpha glutathione transferase A1-1: energetics of organic anion ligand binding. Biochem. J. **363**, 341–346
29 Sluis-Cremer, N., Naidoo, N. N., Kaplan, K. H., Manoharan, T. H., Fahl, W. E. and Dirr, H. W. (1996) Determination of a binding site for a nonsubstrate ligand in mammalian cytosolic glutathione S-transferases by means of fluorescence-resonance energy transfer. Eur. J. Biochem. **241**, 484–488
30 Segel, I. H. (1993) Enzyme kinetics, Behavior and Analysis of Rapid Equilibrium and Steady State Enzyme Systems. John Wiley & Sons, New York
31 Otzen, D. E., Rheinnecker, M. and Fersht, A. R. (1995) Structural factors contributing to the hydrophobic effect: the partly exposed hydrophobic minicore in chymotrypsin inhibitor 2. Biochemistry **34**, 13051–13058
32 Xu, J., Baase, W. A., Baldwin, E. and Matthews, B. W. (1998) The response of T4 lysozyme to large-to-small substitutions within the core and its relation to the hydrophobic effect. Protein Sci. **7**, 158–177
33 Ding, Y., Ortelli, F., Rossiter, L. C., Hemingway, J. and Ranson, H. (2003) The *Anopheles gambiae* glutathione transferase supergene family: annotation, phylogeny and expression profiles. BMC Genomics **4**, 35–50

Received 24 April 2006/21 August 2006; accepted 29 August 2006
Published as BJ Immediate Publication 29 August 2006, doi:10.1042/BJ20060603

crystallization communications

Acta Crystallographica Section F
Structural Biology and Crystallization Communications
ISSN 1744-3091

Crystallization and preliminary X-ray crystallographic analysis of a highly stable mutant V107A of glutathione transferase from *Anopheles dirus* in complex with glutathione

Jantana Wongsantichon,[a] Jirundon Yuvaniyama[b] and Albert J. Ketterman[a]*

[a]Institute of Molecular Biology and Genetics, Mahidol University, Salaya Campus, Nakorn Pathom 73170, Thailand, and [b]Department of Biochemistry and Center for Excellence in Protein Structure and Function, Faculty of Science, Mahidol University, Rama 6 Road, Phayathai, Bangkok 10400, Thailand

Correspondence e-mail: frakt@mahidol.ac.th

Received 26 October 2005
Accepted 22 February 2006

An engineered mutant V107A of the dimeric glutathione transferase enzyme from *Anopheles dirus* (adgstD4-4) was cocrystallized with glutathione substrate using the hanging-drop vapour-diffusion method. The crystal diffracted to 2.47 Å resolution in space group $P3_221$ (unit-cell parameters $a = b = 49.4$, $c = 272.4$ Å). Although the crystal morphology differed from that previously obtained for the wild-type enzyme, the crystal packing was the same. At 318 K, the engineered mutant showed an enzyme stability that was increased by about 32-fold, while possessing a similar catalytic function to the wild type. Structural determination will provide valuable understanding of the role of Val107. This residue is in the dimeric interface and appears to contribute towards enhancing the physical properties of the entire protein.

1. Introduction

Glutathione transferases (GSTs; EC 2.5.1.18) are dimeric enzymes involved in phase II detoxication processes by conjugation of a thiol group from reduced glutathione (γ-glutamyl-cysteinyl-glyine; GSH) to an electrophilic centre of diverse xenobiotic compounds, producing less reactive and more polar substances in order to facilitate elimination from cells (Armstrong, 1991; Mannervik & Danielson, 1988). Cytosolic GSTs are generally found as multiple isoenzymes within organisms and with varying substrate selectivity (Hayes *et al.*, 2005; Hayes & Pulford, 1995). In the various GST dimeric structures, subunits are assembled by twofold symmetry, with subunit interactions that vary between the GST classes but generate a buried interface area of about 2700–3400 Å^2 (Dixon *et al.*, 2002). Therefore, homodimeric or heterodimeric GSTs are only formed by subunits from the same gene class and with comparable molecular recognition at the subunit interface.

The structural model of the wild-type GST adgstD4-4 from *Anopheles dirus* shows that Val107 is located in the subunit-interface region of the dimeric GST, forming part of an intersubunit lock-and-key 'clasp' motif (Oakley, Harnnoi *et al.*, 2001; Wongsantichon & Ketterman, 2006). The 'key' residue not only inserts into a hydrophobic pocket of the neighbouring subunit, but also itself acts as part of the 'lock' for the other subunit 'key'. In addition, the 'key' residues from both subunits hook around each other in an aromatic π–π interaction through slightly offset aromatic ring stacking, generating a 'clasp' in the middle of the subunit interface. A special characteristic of the motif is to stabilize the GST dimeric structure in the middle region of the twofold axis. The motif was found to be highly conserved in many classes of insect GSTs, as shown by primary sequence alignments (Wongsantichon & Ketterman, 2006). The available crystal structures of insect-specific δ-class GSTs such as *Lucilia* GST (Wilce *et al.*, 1994, 1995), adgstD3-3 (PDB code 1jlv; Oakley, Harnnoi *et al.*, 2001), adgstD4-4 (PDB code 1jlw; Oakley, Harnnoi *et al.*, 2001), adgstD5-5 (PDB code 1r5a; Udomsinprasert *et al.*, 2005), adgstD6-6 (PDB code 1v2a; Udomsinprasert *et al.*, 2005) and aggstD1-6 (PDB code 1pn9; Chen *et al.*, 2003) also reveal the highly conserved clasp-like motif (Wongsantichon & Ketterman, 2006). In the apo structure of adgstD4-4, the residue Val107 is also part of the wall of the active site. This residue's surface area is about 100–130 Å^2 and is only exposed to solvent in the active-site pocket. However, the residue is also part of the first-sphere interaction of

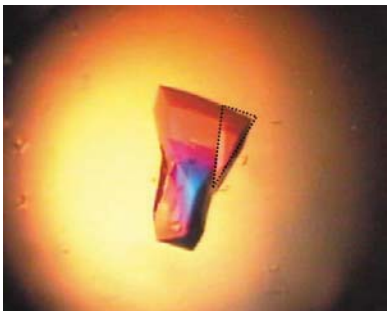

Leu103, which generates a small hydrophobic core interior to the active site and subunit interface (Wongsantichon *et al.*, 2003). In addition to this spatial motif, adgstD4-4 also possesses several other intersubunit interactions which contribute to interface formation, as previously discussed in Wongsantichon & Ketterman (2005). The Val107 residue has been studied by substitution with six different amino acids of various sizes and properties in order to elucidate its role in the dimeric enzyme (Wongsantichon & Ketterman, 2006). All engineered mutants were found to be catalytically active, demonstrating the presence of dimeric active forms, which suggests that the residue position is not critical for dimerization. Steady-state kinetics studies using GSH and CDNB as co-substrates show that substitutions by hydrophobic and uncharged residues at the Val107 position have no effect on the catalytic properties, whereas positively and negatively charged residues diminish the enzyme catalytic rate (k_{cat}) and weaken the binding affinity towards GSH substrate (K_m), with positive cooperativity observed upon binding. In this regard, charged residue replacements were considered to be unfavourable in the region. However, all engineered mutants appeared to enhance thermal stability as demonstrated by a heat-inactivation assay at 318 K, suggesting that the residue also plays a role in structural stabilization. Of the mutants, adgstD4-4 V107A shows the greatest half-life (390.2 $\pm$ 22.4 min), which is about 32 times that of the wild type (12.3 $\pm$ 0.9 min). There is no marked alteration in the secondary or tertiary structure of V107A as shown by far-UV circular dichroism and tryptophan intrinsic fluorescence, respectively. Nevertheless, conformational rearrangement at the quaternary structural level or subunit dimerization of the engineered enzyme was observed by fluorescence dye binding using 1-anilinonaphthalene-8-sulfonic acid (ANS), which is reported to bind in the hydrophobic cleft along the dimeric interface in GST class α (Sayed *et al.*, 2002). As shown by the above data, substitution of valine by alanine at position 107 in adgstD4-4 appears to be structurally important and alters the enzyme stability and subunit dimerization, while maintaining similar catalytic properties to the wild type. Therefore, structural determination of the mutant is of interest and would be useful in understanding the protein structure–function correlation, particularly for enzyme stability.

2. Material and methods

2.1. Construction and purification of V107A

A single point mutation of *A. dirus* glutathione transferase isoform 4 (adgstD4-4) was obtained by PCR-based site-directed mutagenesis, replacing valine with alanine at position 107 using the Stratagene Quick Change site-directed mutagenesis kit (Stratagene). The engineered enzyme was overexpressed by 0.1 m*M* IPTG (isopropyl 1-thio-β-D-galactopyranoside) induction at 298 K in *Escherichia coli* BL21(DE3) pLysS as soluble protein and was purified using GSTrap FF affinity chromatography (Amersham Pharmacia) as previously described (Wongtrakul *et al.*, 2003).

2.2. Crystallization and X-ray data collection

The purified protein was concentrated using an Amicon Ultra-15 centrifugal filter device (Millipore) with 10 kDa cutoff and filtered through an Ultrafree-MC 0.22 µm centrifugal filter unit (Millipore). Prior to crystallization, the protein concentration was adjusted to 9 mg ml^{-1} in 50 m*M* Tris–HCl pH 7.5, 10 m*M* DTT in the presence of 10 m*M* GSH substrate. The hanging-drop vapour-diffusion method was used with a crystallization droplet comprising of 2 µl protein solution and 2 µl reservoir solution consisting of 0.1 *M* imidazole pH 7.0, 0.35 *M* ammonium acetate and 30%(*w*/*v*) polyethylene glycol (PEG) 4000. The volume of solution in the reservoir was 0.5 ml. Crystals appeared within one week at 295 K. A single prismatic crystal with dimensions 0.46 × 0.30 × 0.18 mm was obtained; it was dissected into a smaller piece of dimensions 0.28 × 0.08 × 0.07 mm and briefly soaked in a cryosolution consisting of 0.1 *M* imidazole pH 7.0, 0.368 *M* ammonium acetate, 32%(*w*/*v*) PEG 4000 and 10%(*v*/*v*) glycerol before being flash-frozen in a liquid-nitrogen stream at 110 K.

X-ray diffraction data were collected at the Center for Excellence in Protein Structure and Function, Faculty of Science, Mahidol University, Thailand. X-ray diffraction patterns were recorded on an R-AXIS IV^{++} image-plate system (Rigaku/MSC) using Cu $K\alpha$ radiation from a Rigaku RU-H3R rotating-anode X-ray generator operating at 50 kV and 100 mA equipped with Osmic Confocal Maxflux multi-layer optics and a 0.3 mm collimator. The crystal was flash-frozen using an X-Stream 2000 low-temperature system (Rigaku/MSC). Data were processed and scaled using the *CrystalClear*/*d***TREK* program suite (Pflugrath, 1999).

3. Results and discussion

After initial screening, the crystallization conditions were optimized by varying the pH of the buffer from 4.6 to 7.5 and the concentration of ammonium acetate from 0.25 to 0.40 *M*. Two different crystal morphologies, fine rod-shaped and prism-shaped, were obtained from the screening in 0.1 *M* imidazole pH 7.0 within a week. A single prism-shaped crystal chosen for X-ray diffraction was obtained from conditions consisting of 32%(*w*/*v*) PEG 4000, 0.35 *M* ammonium acetate, 0.1 *M* imidazole pH 7.0 in the presence of 10 m*M* GSH. However, owing to its large dimensions of 0.46 × 0.30 × 0.18 mm, as shown in Fig. 1, a glass fibre was used to dissect the crystal to a smaller volume to facilitate freezing on a cryoloop. The crystal slice was briefly soaked in a cryosolution consisting of reservoir solution containing 10%(*v*/*v*) glycerol and approximately 5% higher concentrations of PEG 4000 and ammonium acetate. The crystal slice was flash-frozen in a liquid-nitrogen stream. Diffraction data were collected to an effective resolution of 2.47 Å using a 240 mm crystal-to-detector distance with an exposure time of 150 s and covering 0.25° oscillation per image (Fig. 2).

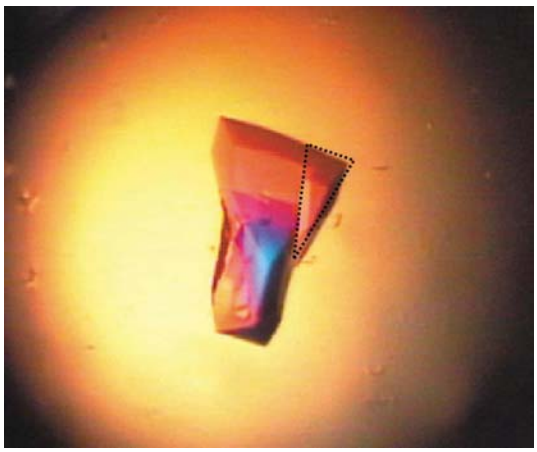

Figure 1
A prism-shaped crystal of adgstD4-V107A photographed under polarized light. The crystal size is 0.46 × 0.30 × 0.18 mm for the largest dimensions. The dotted triangle represents the crystal slice that was used for X-ray diffraction.

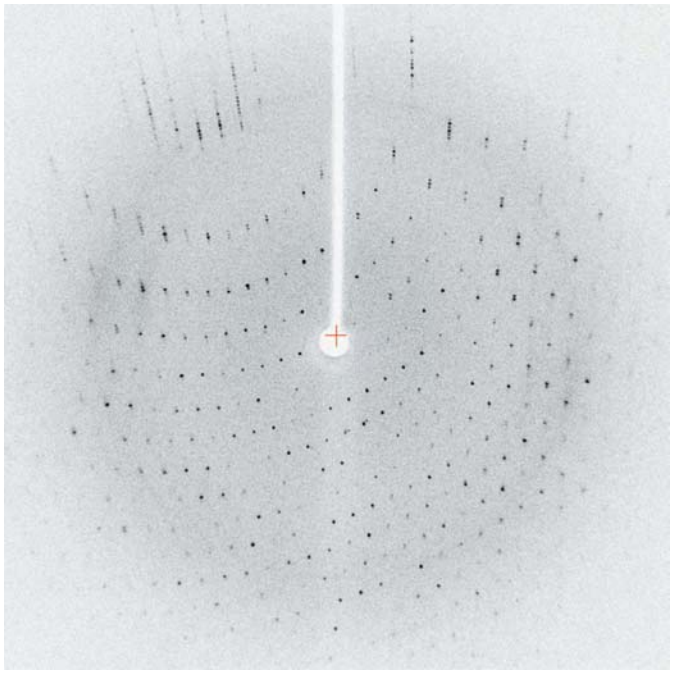

Figure 2
A 0.25° rotation photograph showing the X-ray diffraction pattern from the crystal slice.

The engineered mutant in this study can also be crystallized using the conditions previously reported for the wild-type enzyme (Oakley, Jirajaroenrat *et al.*, 2001), consisting of 30%(*w*/*v*) PEG 8000, 0.2 *M* sodium acetate and 0.1 *M* sodium cacodylate pH 6.5, generating fine rod-shaped crystals. In this regard, the present study demonstrates that different crystal morphologies can be derived from different crystallization conditions. However, preliminary X-ray crystallographic analysis shows that the diffraction patterns of a prism-shaped crystal from the engineered mutant and of a rod-shaped $P3_221$ crystal of the wild type (PDB code 1jlw) are isomorphous (Oakley, Jirajaroenrat *et al.*, 2001). Diffraction spots of the mutant were initially scaled and merged in space group *P*321 (as summarized in Table 1) even though they showed absences that could be characteristic of either of the trigonal space groups $P3_121$ or $P3_221$. This was to preserve all the data for subsequent verification of the correct space group by molecular-replacement calculations. The initial phases of the adgstD4-4 V107A structure were determined with *AMoRe* from the *CCP*4 program suite (Collaborative Computational Project, Number 4, 1994; Navaza, 1994) using chain *A* of the wild-type structure as a search model. Translation searches in the three space groups *P*321, $P3_121$ and $P3_221$ showed a good result for calculation in space group $P3_221$, which gave an amplitude correlation coefficient (CC) of 43.1% and an *R* factor of 48.1% for the best solution, compared with CC = 20.7%, *R* = 56.6% and CC = 23.1%, *R* = 55.0% for the other two space groups. Addition of the second molecule resulted in a CC of 72.3% on amplitude and 76.4% on intensity with an *R* factor of 35.8% after the fitting calculation. Examination of the best solution revealed good crystal packing and no clashes between symmetry-related molecules. This shows that the molecular packing is preserved, suggesting that the V107A mutation and the presence of GSH do not cause large structural deviation from the non-ligand-bound wild-type structure. This preliminary model of the engineered mutant is currently being refined and will be further studied to investigate the marked increase in structural stability.

Table 1
Data-collection statistics for adgstD4-4 V107A crystals in complex with GSH.

Values in parentheses correspond to the highest resolution shell.

Space group	$P3_221$
Unit-cell parameters	
a, *b* (Å)	49.4
c (Å)	272.4
α, β (°)	90
γ (°)	120
Unit-cell volume (Å^3)	575799
Resolution limits (Å)	42.78–2.47 (2.56–2.47)
No. of observed reflections	65482
No. of unique reflections	14436
Completeness (%)	95.3 (80.0)
Multiplicity	2.55 (1.5)
$R_{\rm merge}$† (%)	10.2 (16.8)
$\langle I/\sigma(I)\rangle$	4.9 (2.2)
$V_{\rm M}$ (Å^3 Da^{-1})	1.9
Solvent content (%)	35.4
No. of molecules per ASU	2

† $R_{\rm merge} = \sum_{hkl}\sum_i |I_i(hkl) - \langle I(hkl)\rangle| / \sum_{hkl}\sum_i I_i(hkl)$, where I_i is the intensity of the *i*th measurement of an equivalent reflection with indices *hkl*.

This work was supported by a grant from the Thailand Research Fund to AJK and a Royal Golden Jubilee scholarship to JW.

References

Armstrong, R. N. (1991). *Chem. Res. Toxicol.* **4**, 131–140.
Chen, L., Hall, P. R., Zhou, X. E., Ranson, H., Hemingway, J. & Meehan, E. J. (2003). *Acta Cryst.* D**59**, 2211–2217.
Collaborative Computational Project, Number 4 (1994). *Acta Cryst.* D**50**, 760–763.
Dixon, D. P., Lapthorn, A. & Edwards, R. (2002). *Genome Biol.* **3**, 1–10.
Hayes, J. D., Flanagan, J. U. & Jowsey, I. R. (2005). *Annu. Rev. Pharmacol. Toxicol.* **45**, 51–88.
Hayes, J. D. & Pulford, D. J. (1995). *CRC Crit. Rev. Biochem. Mol. Biol.* **30**, 445–600.
Mannervik, B. & Danielson, U. H. (1988). *CRC Crit. Rev. Biochem.* **23**, 283–337.
Navaza, J. (1994). *Acta Cryst.* A**50**, 157–163.
Oakley, A. J., Harnnoi, T., Udomsinprasert, R., Jirajaroenrat, K., Ketterman, A. J. & Wilce, M. C. J. (2001). *Protein Sci.* **10**, 2176–2185.
Oakley, A. J., Jirajaroenrat, K., Harnnoi, T., Ketterman, A. J. & Wilce, M. C. J. (2001). *Acta Cryst.* D**57**, 870–872.
Pflugrath, J. W. (1999). *Acta Cryst.* D**55**, 1718–1725.
Sayed, Y., Hornby, J. A. T., Lopez, M. & Dirr, H. (2002). *Biochem. J.* **363**, 341–346.
Udomsinprasert, R., Pongjaroenkit, S., Wongsantichon, J., Oakley, A. J., Prapanthadara, L., Wilce, M. C. J. & Ketterman, A. J. (2005). *Biochem. J.* **388**, 763–771.
Wilce, M. C. J., Board, P. G., Feil, S. C. & Parker, M. W. (1995). *EMBO J.* **14**, 2133–2143.
Wilce, M. C. J., Feil, S. C., Board, P. G. & Parker, M. W. (1994). *J. Mol. Biol.* **236**, 1407–1409.
Wongsantichon, J., Harnnoi, T. & Ketterman, A. J. (2003). *Biochem. J.* **373**, 759–765.
Wongsantichon, J. & Ketterman, A. (2005). *Methods Enzymol.* **401**, 100–116.
Wongsantichon, J. & Ketterman, A. J. (2006). *Biochem. J.* **394**, 135–144.
Wongtrakul, J., Udomsinprasert, R. & Ketterman, A. (2003). *Insect Biochem. Mol. Biol.* **33**, 971–979.

Available online at www.sciencedirect.com
SCIENCE DIRECT
Food and Chemical Toxicology 44 (2006) 1348–1354
Reprint 5
Food and Chemical Toxicology
www.elsevier.com/locate/foodchemtox

Effect of different Thai traditional processing of various hot chili peppers on urethane-induced somatic mutation and recombination in *Drosophila melanogaster*: Assessment of the role of glutathione transferase activity

P. Laohavechvanich [a,*], K. Kangsadalampai [a], N. Tirawanchai [b], A.J. Ketterman [c]

[a] *Institute of Nutrition, Mahidol University, Salaya, Phutthamonthon 4, Nakhon Pathom 73170, Thailand*
[b] *Department of Biochemistry, Medicine Faculty, Siriraj Hospital, Bangkok 10700, Thailand*
[c] *Institute of Molecular Biology and Genetics, Mahidol University, Nakhon Pathom 73170, Thailand*

Received 14 June 2005; accepted 23 February 2006

Abstract

Four different Thai traditional chili peppers, namely bird pepper (*Capsicum frutescens*), red chili spur peppers (*Capsicum annuum*), green bell peppers and sweet pepper (*C. annuum*) were investigated for their antimutagenic properties. Each chili was prepared in three formulations commonly used for chili food processing; raw paste (chili ground in water), pickled in vinegar or stir-fried in palm oil. Each sample was tested for its antimutagenic effect against urethane by using the somatic mutation and recombination of wing hair of *Drosophila melanogaster* as an indicator. Three-day-old larvae, *trans*-heterozygous for two genetic markers, multiple wing hairs *mwh* and orrigon (ORR; flr^3), were exposed to urethane alone or in combination with each chili formulation. The various processing methods for chilies differentially extracted the antimutagenic chili components. The specific chili as well as the method of processing influenced the observed antimutagenic properties against urethane. This suggested each chili contains a unique complex mixture of many antimutagens. Co-treatment and pre-treatment experiments showed that both direct and indirect protective mechanisms are involved in an 'activation' process to give antimutagenesis effects. An association between antigenotoxicity and glutathione transferase activity could not be established.

Keywords: Chili; Urethane; SMART; Glutathione transferase; Antimutagens

1. Introduction

Hot chili pepper is a common spice in Thai cuisine and it is widely consumed as a food additive throughout the world, particularly in South East Asia and Latin-American countries. The consumption of pepper (*Capsicum annuum*) has been traditional for thousands of years in some parts of the world with estimates of per capita dietary intake to be about 40 g/day (Gonzalez de Mejia et al., 1998). Peppers are an important source of β-carotene, which have antimutagenic and/or anticarcinogenic properties (Monsereenusorn et al., 1982). Initial work showed that rats fed diets containing 10% chili pepper developed liver tumors (Hoch-Ligeti, 1952). Contrastingly, extracts of certain spices or their isolated constituents could block the processes of experimental carcinogenesis and mutagenesis (Unnikrishnan and Kuttan, 1990). A recent study reported that green pepper juice had antimutagenic effects on the nitrosation process of methyl urea and sodium nitrite in a Drosophila spot test (Ramirez-Victoria et al., 2001). Although it is not clear whether the green pepper juice

Abbreviations: CYP, cytochrome; SMART, somatic mutation and recombination test.

* Corresponding author. Tel.: +66 2 800 2380x116; fax: +66 2 441 9344.
E-mail address: nuplh@mahidol.ac.th (P. Laohavechvanich).

0278-6915/$ - see front matter © 2006 Elsevier Ltd. All rights reserved.
doi:10.1016/j.fct.2006.02.013

had an inhibitory effect on the nitrosation process, or had an inhibitory effect on the mutagenic activity of the nitrosation product. Furthermore, El Hamss showed that bell peppers and black peppers possessed antimutagenic activity shown by somatic mutation and recombination assay using *Drosophila* at concentrations of bell pepper of 5% and 10% (w/v) and black peppers of 1% and 2% (w/v) (El Hamss et al., 2003).

In Asian cuisine, chilies are consumed in several different ways such as fresh chili, chili in vinegar or stir fried chili. These different methods of processing chili have never been tested to determine antimutagenicity effects. Four different Thai traditional chili peppers, namely bird pepper, red chili spur pepper, green bell pepper and sweet pepper were investigated for their antimutagenicity. Each chili was prepared to be a raw paste (chili ground in water), pickled in vinegar or stir-fried in palm oil. The solid and liquid extract (chili extract) of each sample were tested for their effect on the mutagenic activity of urethane using the somatic mutation and recombination test (SMART) of wing hair of *Drosophila melanogaster* as an indicator. The SMART assay is based on induced loss of heterozygosity, which may occur through various mechanisms, such as point mutation, deletions, certain types of chromosome aberrations as well as mitotic recombination and gene conversion (Graf et al., 1984). It is also well suited to determine the antimutagenic properties of single compounds or complex mixtures (Negishi et al., 1989; Graf et al., 1998). The high bioactivation (HB) strain of *D. melanogaster* used in this study is characterized by an increased cytochrome P450-dependent bioactivation capacity for promutagens and procarcinogens. We also examined whether the activity of the detoxication enzyme, glutathione transferase, changed with exposure to the chili samples in the presence and absence of urethane.

2. Material and methods

2.1. Chemical compounds and media

Ethyl carbamate (Urethane; CAS no. 51-79-6) purchased from Sigma, was dissolved in distilled water and mixed into the yeast–glucose–agar Drosophila medium which was slightly modified from the formula of (Robert, 1986). Reduced glutathione (GSH; CAS no.70-18-8), 1-chloro-2,4-dinitrobenzene (CAS no. 97-00-7) were purchased from Sigma Company. Bradford reagent (CAS no. 500-0006) was obtained from Bio-Rad Laboratories.

2.2. Chili preparation

This study used four types of chili. Three types of chilies were *C. annuum* L.; red chili spur pepper (hot pepper), green bell pepper and sweet pepper (non-hot chili). The fourth type was *Capsicum frutescens*, that is, bird chili pepper (hot pepper).

Chilies were purchased from the local market. Pedicles were removed and the chilies cleaned with tap water several times and soaked in sodium lauryl ether sulfate 7% (w/w) 20 min to remove adhering contaminants. Each chili was chopped into pieces and ground in an electrical blender and freeze dried. After freeze dry processing the chili were ground again in a blender.

Ground chili (0.5 g) was mixed with 4.5 ml water (1:9 w/w) or 5% distilled vinegar , and then added to the medium (corn flour 0.562, sugar 0.45 g, yeast 0.225 g, agar 0 .063 g). For the stir-fried chili in palm oil sample, ground chili (0.5 g) was stir-fried with palm oil 1.5 g (1:3 w/w) and mixed with medium.

Ground chili was suspended in water or vinegar (1:9 w/w) and then was further processed using a polytron homogenizer. The homogenate was filtered through Whatman paper No. 54 to obtain soluble fraction and residual fiber. The stir-fried chili in palm oil (1:3 w/w), after grinding, was extracted with 2 ml hexane and then filtered through cotton mesh and Whatman paper and dried under nitrogen gas. Chili extract (water extract, vinegar extract and oil extract) was diluted by adding the equivalent weight of chili extract to water (or vinegar) (1:1) and then mixed with medium.

2.3. D. melanogaster strains and crosses

Two strains of *D. melanogaster* were used. Virgin Females of *ORR/ORR;flr*^{3}*/In (3LR) TM3, ri p*^{p} *sep l (3) 89Aa bx*^{34e} *e Bd*^{s}, *Ser* were crossed with males of *mwh/mwh*. Both strains were obtained from the Institute of Toxicology, Swiss Federal Institute of Technology and University of Zurich.

2.4. Somatic mutation and recombination test (SMART assay)

The Virgin *ORR;flr3* females and *mwh* males were mated on the standard medium. Six days after mating, the 3-day-old larvae were transferred in equal batches to experimental medium (chili control), the experimental medium containing 20 mM urethane (test model), standard medium (negative control) and standard medium containing 20 mM urethane (positive control). The surviving adult flies were collected on days 7–10 after pupation. Only the insects bearing the marker *trans*-heterozygous (*mwh+/+flr*^{3}) indicated by round wings were stored in 70% ethanol. Subsequently, the wings were removed, mounted and scored by using a compound microscope for observation of the wing spots (Graf et al., 1984; Graf et al., 1989; Graf et al., 1994).

2.5. Co-treatment

Three day old larvae were transferred to a tube with *Drosophila* medium that contained one of the 3 different processed forms of each chili. Three different processed forms of each chili, urethane and each processed chili with urethane were used for chronic larval feeding. For negative controls, the larvae were transferred into medium prepared with distilled water, or 5% distilled vinegar, or palm oil.

2.6. Pre-treatment

The flies were mated on the experimental medium. Six days after mating, the 3-day-old larvae were transferred in equal batches to either experimental medium containing 20 mM urethane or the experimental medium without urethane as sample control. Negative and positive controls were conducted similarly to those in co-administration study. The surviving adult flies were collected on days 10–12 after pupation.

2.7. Data evaluation and statistical analysis

To obtain a statistical assessment of antimutagenicity, the frequencies of total spots per wing were compared in pairs (that is, urethane alone versus urethane plus each chili; urethane plus each chili versus urethane plus each chili) using the non-parametric Mann–Whitney *U*-test (Frei and Wurgler, 1995). Level of significance was set for $p < 0.05$. To allow a quantitative comparison, the percentage of inhibition was determined for each category of spot. The percentage of inhibition was also calculated as following $100(a - b)/a$ where a is the frequency of spots induced by urethane alone and b the frequency of spots induced by urethane in the presence of chili (Abraham, 1994).

2.8. Assay of glutathione transferase activity

All subsequent preparation procedures were carried out below 4 °C. Larvae were ground in 0.2 M phosphate buffer, pH 6.5 at the ratio of 0.5 g per 0.5 ml buffer with a glass rod. The homogenate was centrifuged at 15,000 g. for 10 min. The supernatant was diluted immediately (1:5) with 0.1 M phosphate buffer before assaying glutathione transferase activity. This assay is based on the reaction between 1 mM 1-chloro-2,4-dinitrobenzene and 10 mM glutathione in 0.1 M sodium phosphate buffer, pH 6.5 (Habig et al., 1974). Protein concentration was determined by the Bradford method (Bradford, 1976) using the Bio-Rad Laboratories (Hercules, CA, USA) protein reagent with bovine serum albumin as standard protein.

3. Result

The ground chili pastes (ground chili in water, in vinegar and in oil) as well as each chili extract were not toxic in 48 h larval feeding. The frequency of total spots per wing recorded in these sample controls was 0.00–0.15 (data not shown). In the negative control series (water, vinegar and oil) the frequency of spots was within the range of 0.12– 0.35 (Tables 1–6). The data given in Tables 1–6 demonstrate that the different processing were not equally effective in significantly reducing the mutagenicity of urethane. In the pre-treatment experiments, each of the chili showed a broad but differing range of effectiveness with bird pepper (3–95%), red chili spur pepper (17–82%), green bell pepper (8–31%) and sweet pepper (24–54%). In general the different processing, when effective, significantly reduced not only the total spot frequency but also the twin spot frequency. Single spots are produced either by mitotic recombination or by somatic mutation, deletion or other changes. Twin spots are produced exclusively by mitotic recombination occurring between the proximal marker *flr* and the centromere.

Hot chili pepper (bird pepper; *C. frutescens*) in oil extract reduced mutagenicity more than green bell pepper or sweet pepper (*C. annuum*) in both pre-treatment and co-treatment (Fig. 1). However, sweet pepper gave greater

Table 1
Inhibitory effect of ground chili in water on 20 mM urethane induced mutagenicity in pre-treatment

Pre-treatment study of ground chili in water	Frequency of spots per wing (number of spots from 40 wings)*								% Inhibition
	Small single spots (1–2 cells)		Large single spots (>2 cells)		Twin spots		Total spots		
Water control	0.33	(13)	0.03	(1)	0.00	(0)	0.35	(14)	
Urethane (URE)	5.58	(223)^{a}	1.85	(74)^{a}	1.35	(54)^{a}	8.78	(351)^{a}	
Bird pepper + URE	3.73	(149)^{b}	1.43	(57)^{a}	1.15	(46)^{ab}	6.30	(252)^{c}	28
Red chili spur pepper + URE	3.98	(159)^{b}	1.83	(73)^{a}	1.33	(53)^{a}	7.13	(285)^{b}	19
Green bell pepper + URE	3.90	(156)^{b}	1.55	(62)^{a}	1.20	(48)^{a}	6.65	(266)^{bc}	24
Sweet pepper + URE	4.08	(163)^{b}	1.63	(65)^{a}	0.95	(38)^{b}	6.65	(266)^{bc}	24

* Within a column different superscripts are significantly different at $p < 0.05$.

Table 2
Inhibitory effect of ground chili in vinegar on 20 mM urethane induced mutagenicity in pre-treatment

Pre-treatment study of ground chili in vinegar	Frequency of spots per wing (number of spots from 40 wings)*								% Inhibition
	Small single spots (1–2 cells)		Large single spots (>2 cells)		Twin spots		Total spots		
Vinegar control	0.18	(7)	0.00	(0)	0.00	(0)	0.18	(7)	
Urethane (URE)	5.00	(200)^{a}	1.53	(61)^{a}	1.13	(45)^{a}	7.65	(306)^{a}	
Bird pepper + URE	3.15	(126)^{bc}	1.05	(42)^{b}	0.50	(20)^{bc}	4.70	(188)^{c}	39
Red chili spur pepper + URE	3.00	(120)^{c}	1.00	(40)^{b}	0.50	(20)^{bc}	4.50	(180)^{c}	41
Green bell pepper + URE	3.48	(139)^{b}	1.15	(46)^{b}	0.63	(25)^{b}	5.25	(210)^{b}	31
Sweet pepper + URE	2.83	(113)^{c}	0.63	(25)^{c}	0.28	(11)^{c}	3.73	(149)^{d}	51

* Within a column different superscripts are significantly different at $p < 0.05$.

Table 3
Inhibitory effect of ground chili in oil on 20 mM urethane induced mutagenicity in pre-treatment

Pre-treatment study of ground chili in oil	Frequency of spots per wing (number of spots from 40 wings)*								% Inhibition
	Small single spots (1–2 cells)		Large single spots (>2cells)		Twin spots		Total spots		
Oil control	0.10	(4)	0.02	(1)	0.00	(0)	0.12	(5)	
Urethane (URE)	4.88	(195)^{a}	1.65	(66)^{a}	1.18	(47)^{a}	7.70	(308)^{a}	
Bird pepper + URE	0.90	(36)^{d}	0.23	(9)^{d}	0.10	(4)^{c}	1.23	(49)^{e}	84
Red chili spur pepper + URE	2.98	(119)^{c}	0.80	(32)^{b}	0.43	(17)^{b}	4.20	(168)^{c}	45
Green bell pepper + URE	3.68	(147)^{b}	1.60	(64)^{a}	1.10	(44)^{a}	6.38	(255)^{b}	17
Sweet pepper + URE	2.68	(107)^{c}	0.55	(22)^{b}	0.33	(13)^{b}	3.55	(142)^{d}	54

* Within a column different superscripts are significantly different at $p < 0.05$.

Table 4
Inhibitory effect of water extract on 20 mM urethane induced mutagenicity in pre-treatment

Pre-treatment study of water extract of each chili	Frequency of spots per wing (number of spots from 40 wings)*								% Inhibition
	Small single spots (1–2 cells)		Large single spots (>2 cells)		Twin spots		Total spots		
Water control	0.22	(9)	0.02	(1)	0.00	(0)	0.25	(10)	
Urethane (URE)	5.50	(220)^{a}	2.13	(85)^{a}	1.55	(62)^{a}	9.18	(367)^{a}	
Bird pepper + URE	2.55	(102)^{d}	0.90	(36)^{d}	0.78	(31)^{b}	4.23	(169)^{d}	54
Red chili spur pepper + URE	3.08	(123)^{c}	1.28	(51)^{c}	0.85	(34)^{b}	5.20	(208)^{c}	43
Green bell pepper + URE	4.48	(179)^{b}	1.55	(62)^{b}	0.93	(37)^{b}	6.95	(278)^{b}	24
Sweet pepper + URE	4.43	(177)^{b}	1.50	(60)^{bc}	1.03	(41)^{b}	6.95	(278)^{b}	24

* Within a column different superscripts are significantly different at $p < 0.05$.

Table 5
Inhibitory effect of vinegar extract on 20 mM urethane induced mutagenicity in pre-treatment

Pre-treatment study of vinegar extract of each chili	Frequency of spots per wing (number of spots from 40 wings)*								% Inhibition
	Small single spots (1–2 cells)		Large single spots (>2 cells)		Twin spots		Total spots		
Vinegar control	0.22	(9)	0.00	(0)	0.00	(0)	0.22	(9)	
Urethane (URE)	6.15	(246)^{a}	2.15	(86)^{a}	1.35	(54)^{a}	9.65	(386)^{a}	
Bird pepper + URE	5.90	(236)^{a}	2.10	(84)^{ab}	1.35	(54)^{a}	9.35	(374)^{ab}	3
Red chili spur pepper + URE	4.78	(191)^{b}	2.15	(86)^{ab}	1.08	(43)^{ab}	8.00	(320)^{c}	17
Green bell pepper + URE	5.63	(225)^{a}	1.98	(79)^{ab}	1.28	(51)^{a}	8.88	(355)^{b}	8
Sweet pepper + URE	3.53	(141)^{c}	1.73	(69)^{b}	1.03	(41)^{b}	6.28	(251)^{d}	35

* Within a column different superscripts are significantly different at $p < 0.05$.

Table 6
Inhibitory effect of oil extract on 20 mM urethane induced mutagenicity in pre-treatment

Pre-treatment study of oil extract of each chili	Frequency of spots per wing (number of spots from 40 wings)*								% Inhibition
	Small single spots (1–2 cells)		Large single spots (>2 cells)		Twin spots		Total spots		
Oil control	0.10	(4)	0.05	(2)	0.00	(0)	0.15	(6)	
Urethane (URE)	4.38	(175)^{a}	1.68	(67)^{a}	1.13	(45)^{a}	7.18	(287)^{a}	
Bird pepper + URE	0.30	(12)^{e}	0.08	(3)^{d}	0.00	(0)^{d}	0.38	(15)^{e}	95
Red chili spur pepper + URE	0.90	(36)^{d}	0.28	(11)^{c}	0.10	(4)^{c}	1.28	(51)^{d}	82
Green bell pepper + URE	3.58	(143)^{b}	1.43	(57)^{a}	0.75	(30)^{b}	5.75	(230)^{b}	20
Sweet pepper + URE	2.55	(102)^{c}	0.68	(27)^{b}	0.45	(18)^{b}	3.68	(147)^{c}	49

* Within a column different superscripts are significantly different at $p < 0.05$.

inhibition of mutagenicity than green bell pepper in all processing (Fig. 1c and d). In general, oil extracts of the chili showed greater antimutagenicity than the vinegar or water extracts in the co-treatment study (Fig. 1).

To determine whether glutathione transferase is involved in antimutagenicity of the chili two chili treatment groups showing the greatest effects were selected to assay glutathione transferase activity. No significant change in glutathione transferase activity was observed. This suggests that glutathione transferase is not involved in the antimutagenicity.

4. Discussion

This project was to compare the antimutagenic properties of various chili processed in several ways. The processing methods employed were chosen to mimic the processing used for chili in human diet. The antimutagenic properties were evaluated in the *Drosophila* wing spot test (SMART); using chili as a protective agent against genotoxic effects induced by urethane, which is a promutagen requiring metabolic activation. The results show the specific chili as well as the method of processing influence the observed antimutagenic properties against urethane. The genotoxicity of urethane and the reactive metabolites have been investigated in a variety of test systems or organisms, such as bacteria, yeast, mammalian cells, *Drosophila*, and rodents (Mirvish, 1996; Mirvish, 1968; Zimmerli and Schlatter, 1991; Giri, 1995; Ballering et al., 1996). The high bioactivation (HB) *D. melanogaster* strain used in the present study is highly sensitive to the genotoxic effects of urethane because of its high constitutive level of cytochrome P-450 activity (Frolich and Wurgler, 1990; Graf and van Schaik, 1992). Hence, it represents an extreme state of genetic

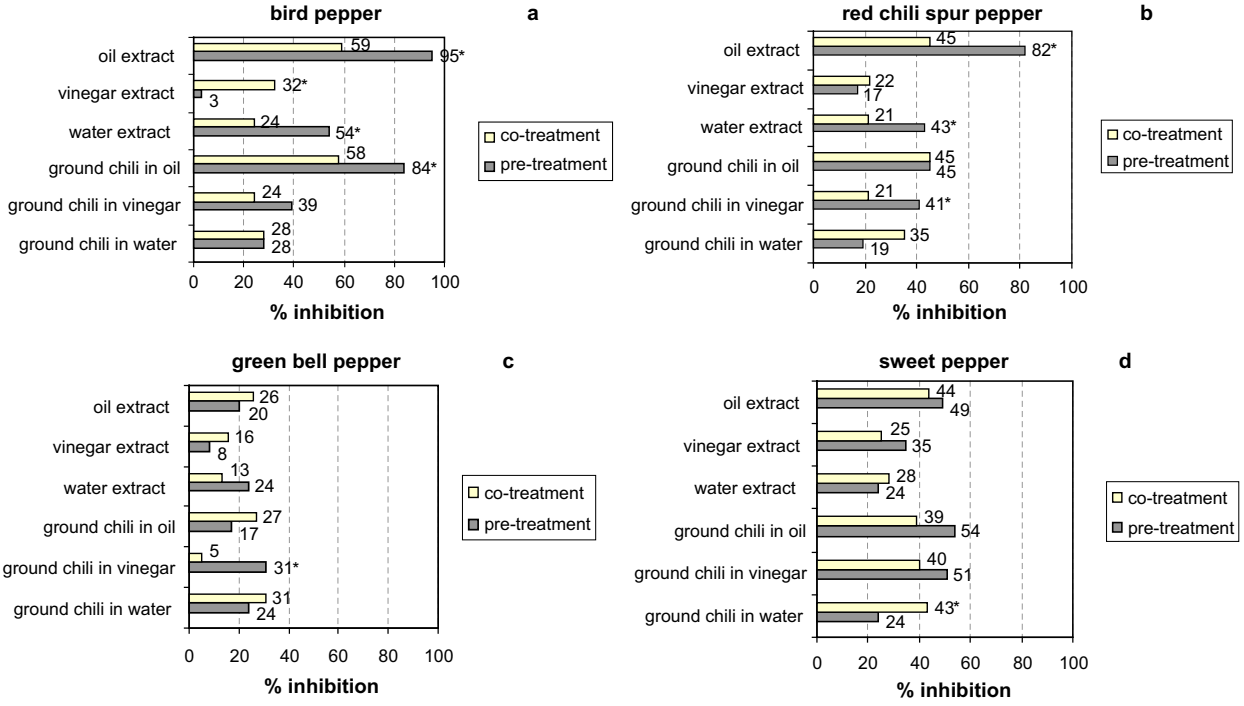

Fig. 1. Co-treatment and pre-treatment effects with four kinds of chili (bird pepper, red chili spur pepper, green bell pepper, and sweet pepper) on the mutagenicity of urethane in *D. melanogaster*. The experimental medium consisted of ground chili mixed with (1:9 w/w) water or 5% distilled vinegar and then added to the medium. For the stir-fried chili in palm oil sample, ground chili was stir-fried with palm oil (1:3 w/w) and mixed with medium. Chili extract (water, vinegar, oil) was the soluble fraction from extraction of the ground chili in water, in vinegar and in oil samples. Larvae of 72 h were exposed to experimental medium containing 20 mM urethane (co-treatment). For pre-treatment, the tester strain flies were mated on the experimental medium and then transferred in the experimental medium containing 20 mM urethane. The values beside the bars in the plots are percent inhibition of urethane mutagenicity. The significantly different ($p < 0.05$) values are indicated with an ∗. The inhibition of urethane mutagenicity by experimental medium which was calculated as follows: (genotoxin alone-genotoxin plus chili treatment/genotoxin alone) × 100.

susceptibility to urethane. The pathway of activation of urethane is thought to involve two steps, both catalyzed by the cytochrome P-450 CYP 2E1; these steps are desaturation or urethane to vinyl carbamate, followed by oxidation to vinyl carbamate epoxide (Guengerich et al., 1991). The metabolic activation of urethane to DNA binding metabolites also involves cytochrome P-450 dependent enzyme activities in *D. melanogaster*. Urethane is found in very small quantities in several fermented foods and beverages such as stone-fruit brandies, sherries and table wines (Schlatter and Lutz, 1990; Stoewsand et al., 1991). This has evoked interest in carrying out investigations to identify chili pepper that can inhibit the carcinogenic effects of urethane.

Although to different extents, the chilies studied reduced all types of mutations induced by urethane. The differences in antimutagenic effect suggest that the mixture of anti- mutagenic compounds varied among the tested chilies. Moreover, the extraction of the available antimutagenic compounds occurred with different efficiencies depending on the chili processing method employed. In addition the treatment condition, co- or pre-treatment, also impacted upon the chili antimutagenic affects. This suggests that some of the components either must undergo some sort of 'activation' or must induce or activate a biological pathway in vivo. This of course does not exclude the concept that some of these components may also react directly with the electrophilic mutagens. Thus the reduction in mutated cells produced by co-treatment and pre-treatment suggest that both direct and indirect protective mechanisms are involved in countering urethane-induced mutagenesis.

One of the possible antimutagenic components found in peppers are carotenoids. These compounds isolated from the fruits of red paprika (*C. annuum* L.) exhibit potent antitumor-promoting activity in vivo and in vitro (Maoka et al., 2001). Peppers are also important sources of carotenoids, mainly β-carotene followed by α-carotene and β-cryptoxanthin (Mejia et al., 1988). Extracts from bell pepper were found to give 87%, 79% and 73% inhibition on 1-nitropyrene; 1,6-dinitropyrene and 1,8-dinitropyrene mutagenicity, respectively (Gonzalez de Mejia et al., 1998). Antioxidants such as α- or β-carotene, xanthophylls and retinoid have been reported to inhibit some types of cancers (Hayatsu et al., 1988; Gross, 1991). These constituents also appear to inhibit a large number of mutagens in different test systems (Edenharder et al., 1998; Bianchi et al., 1996; Arriaga-Alba et al., 2000).

Capsaicin is the most pungent of the group of compounds called capsaicinoids that can be isolated from chili

peppers and also are sparingly soluble in water, but very soluble in fats. Hydrophobic compounds like capsaicin, analogs of capsaicin, and β-carotene would be found in chili extracts at higher concentrations in oil compared to a water extract. Green bell pepper showed the least inhibition of genotoxicity for all processed chili in both co-treatment and pre-treatment experiments. The hot chili peppers (bird pepper, red chili spur pepper) showed greater inhibition of genotoxicity. The capsaicin content is greater in the Thai peppers (50,000–100,000 Scoville unit) than the bell peppers (zero Scoville units) (Prapanoppasin and Sukprakan, personal communication). Capsaicin has been shown to inhibit the mutagenicity and/or tumorigenicity of vinyl carbamate, a metabolite of urethane activated by cytochrome P450 2E1 (Surh et al., 1995). This result agreed with previous reports that capsaicin inhibited rodent CYP2E1 activity in vitro (Surh et al., 1995) and dihydrocapsaicin, the saturated analogue of capsaicin, is a suicide or mechanism-based inhibitor of cytochrome P4502E1(CYP2E1) (Gannett et al., 1990).

In this study, we investigated the possible role of glutathione transferase in detoxication of urethane. The results suggested that glutathione transferase is not involved in antimutagenicity of chili. A similar effect was observed in male Swiss albino mice with aqueous extracts of spices (cinnamon, pepper, cumin, clove and cardamom) against the mutagenicity of urethane (Abraham et al., 1998). These extracts did not exert any significant effect on glutathione transferase activity. The chili may exert their antigenotoxic effect on urethane through inhibition of the cytochrome P-450 enzymes responsible for bio-activation of urethane. This has been reported previously where capsaicin pre-treatment gave a small but statistically significant inhibition of CYP1A2 activity which correlated with its antimutagenic activity against selected heterocyclic amine (Teel et al., 1997).

5. Conclusion

In conclusion, our study has shown that four types of chili, ground into a paste (with water, vinegar or oil) or equivalent extracts of each chili inhibit the genotoxic effects of urethane. Several commonly used food processing methods for chilies differentially extracted the antimutagenic chili components. This suggests each chili contains a unique complex mixture of many antimutagens. Co-treatment and pre-treatment experiments showed that both direct and indirect protective mechanisms are involved in an 'activation' process to give antimutagenesis effects. An association between antigenotoxicity and glutathione transferase activity could not be established.

Acknowledgements

We are grateful to Jantana Wongsantichon for her technical support in the determination of glutathione transferase activity. This thesis was supported by the Faculty of Graduate Studies, Mahidol University in the academic year of 2005.

References

Abraham, S.K., 1994. Antigenotoxicity of coffee in the Drosophila assay for somatic mutation and recombination. Mutagenesis 9, 383–386.

Abraham, S.K., Singh, S.P., Kesavan, P.C., 1998. In vivo antigenotoxic effects of dietary agents and beverages co-administered with urethane: assessment of the role of glutathione *S*-transferase activity. Mutat. Res. 413, 103–110.

Arriaga-Alba, M., Rivera-Sanchez, R., Parra-Cervantes, G., Barro-Moreno, F., Flores-Paz, R., Garcia-Jimenez, E., 2000. Antimutagenesis of beta-carotene to mutations induced by quinolone on *Salmonella typhimurium*. Arch. Med. Res. 31, 156–161.

Ballering, L.A., Nivard, M.J., Vogel, E.W., 1996. Characterization by two-endpoint comparisons of the genetic toxicity profiles of vinyl chloride and related etheno-adduct forming carcinogens in Drosophila. Carcinogenesis 17, 1083–1092.

Bianchi, L., Melli, R., Pizzala, R., Stivala, L.A., Rehak, L., Quarta, S., Vannini, V., 1996. Effects of beta-carotene and alpha-tocopherol on photogenotoxicity induced by 8-methoxypsoralen: the role of oxygen. Mutat. Res. 369, 183–194.

Bradford, M.M., 1976. A rapid and sensitive method for the quantitation of microgram quantities of protein utilizing the principle of protein-dye binding. Anal. Biochem. 72, 248–254.

Edenharder, R., Kerkhoff, G., Dunkelberg, H., 1998. Effects of beta-carotene, retinal, riboflavin, alpha-tocopherol and vitamins C and K1 on sister-chromatid exchanges induced by 3-amino-1-methyl-5H-pyrido[4,3-*b*]indole (Trp-P-2) and cyclophosphamide in human lymphocyte cultures. Food Chem. Toxicol. 36, 897–906.

El Hamss, R., Idaomar, M., Alonso-Moraga, A., Munoz Serrano, A., 2003. Antimutagenic properties of bell and black peppers. Food Chem. Toxicol. 41, 41–47.

Frei, H., Wurgler, F.E., 1995. Optimal experimental design and sample size for the statistical evaluation of ethyl carbamate (urethane) in mice. Food Chem. Toxicol. 29, 291–295.

Frolich, A., Wurgler, F.E., 1990. Genotoxicity of ethyl carbamate in the *Drosophila* wing-spot test: dependence on genotype-controlled metabolic capacity. Mutat. Res. 244, 201–208.

Gannett, P., Iversen, P., Iawson, T., 1990. The mechanism of inhibition of cytochrome P450IIE1 by dihydrocapsaicin. Bioorg. Chem. 18, 185–198.

Giri, A.K., 1995. Genetic toxicology of vinyl chloride—a review. Mutat. Res. 339, 1–14.

Gonzalez de Mejia, E., Quintanar-Hernandez, A., Loarca-Pina, G., 1998. Antimutagenic activity of carotenoids in green peppers against some nitroarenes. Mutat. Res. 416, 11–19.

Graf, U., Abraham, S.K., Judith, G., Wurgler, F.E., 1998. Antigenotoxicity studies in *Drosophila melanogaster*. Mutat. Res. 1998, 203–209.

Graf, U., Frei, H., Kagi, A., Katz, A.J., Wurgler, F.E., 1989. Thirty compounds tested in the Drosophila wing spot test. Mutat. Res. 222, 359–373.

Graf, U., Moraga, A.A., Castro, R., Diaz Carrillo, E., 1994. Genotoxicity testing of different types of beverages in the Drosophila wing somatic mutation and recombination test. Food Chem. Toxicol. 32, 423–430.

Graf, U., van Schaik, N., 1992. Improved high bioactivation cross for the wing somatic mutation and recombination test in *Drosophila melanogaster*. Mutat. Res. 271, 59–67.

Graf, U., Wurgler, F.E., Katz, A.J., Frei, H., Juon, H., Hall, C.B., Kale, P.G., 1984. Somatic mutation and recombination test in *Drosophila melanogaster*. Environ. Mutagen. 6, 153–188.

Gross, J., 1991. In: Gross, J. (Ed.), Pigments in Vegetables, Chlorophylls and Carotenoids, New York, pp. 75–79.

Guengerich, F., Kim, D., Iwasaki, M., 1991. Role of human P-450IIE1 in the oxidation of many low molecular weight cancer suspects. Chem. Res. Toxicol. 4, 168–179.

Habig, W.H., Pabst, M.J., Jakoby, W.B., 1974. Glutathione *S*-transferase. J. Biol. Chem. 249, 7130–7139.

Hayatsu, H., Arimoto, S., Negishi, T., 1988. Dietary inhibitors of mutagenesis and carcinogenesis. Mutat. Res. 202, 429–446.

Hoch-Ligeti, C., 1952. Naturally occurring dietary agents and their role in production of tumors. Tex. Rep. Biol. Med. 10, 996–1005.

Maoka, T., Mochida, K., Kozuka, M., Ito, Y., Fujiwara, Y., Hashimoto, K., Enjo, F., Ogata, M., Nobukuni, Y., Tokuda, H., Nishino, H., 2001. Cancer chemopreventive activity of carotenoids in the fruits of red paprika *Capsicum annuum* L. Cancer Lett. 172, 103–109.

Mejia, L., Hudson, E., Gonzalez de Mejia, E., Vazquez, F., 1988. Carotenoid content and vitamin A activity of some common cultivars of Mexican peppers (*Capsicum annuum*) as determined by HPLC. J. Food Sci. 53, 1448–1451.

Mirvish, S.S., 1968. The carcinogenic action and metabolism of urethane and *N*-hydroxyurethan. Adv. Cancer Res. 11, 1–42.

Mirvish, S.S., 1996. Inhibition by vitamins C and E of in vivo nitrosation and vitamin C occurrence in the stomach. Eur. J. Cancer Prev. 5 (Suppl. 1), 131–136.

Monsereenusorn, Y., Kongsamut, S., Pezalla, P.D., 1982. Capsaicin in: literature survey. CRC Crit. Rev. Toxicol. 10, 321–339.

Negishi, T., Arimoto, S., Nishizaki, C., Hayatsu, H., 1989. Inhibitory effect of chlorophyll on the genotoxicity of 3 amino-1-methyl-5*H*-pyrido[4,3-*b*] indole (Try-p-2). Carcinogenesis 10, 145–149.

Ramirez-Victoria, P., Guzman-Rincon, J., Espinosa-Aguirre, J.J., Murillo-Romero, S., 2001. Antimutagenic effect of one variety of green pepper (*Capsicum* spp.) and its possible interference with the nitrosation process. Mutat. Res. 496, 39–45.

Robert, D.B., 1986. Basic *Drosophila* care and techniques. In: Robert, D.B. (Ed.), Drosophila: A Practical Approach. IRL Press, Oxford, pp. 1–38.

Schlatter, J., Lutz, W.K., 1990. The carcinogenic potential of ethyl carbamate (urethane): risk assessment at human dietary exposure levels. Food Chem. Toxicol. 28, 205–211.

Stoewsand, G.S., Anderson, J.L., Munson, L., 1991. Inhibition by wine of tumorigenesis induced by ethyl carbamate (urethane) in mice. Food Chem. Toxicol. 29, 291–295.

Surh, Y.J., Lee, R.C., Park, K.K., Mayne, S.T., Liem, A., Miller, J.A., 1995. Chemoprotective effects of capsaicin and diallyl sulfide against mutagenesis or tumorigenesis by vinyl carbamate and *N*-nitrosodimethylamine. Carcinogenesis 16, 2467–2471.

Teel, R., Zhang, Z., Huynh, S., Hamilton, S., 1997. Effects of capsaicin on the metabolic activation of heterocyclic amines and on cytochrome P450 1A2 activity in hamster liver microsomes. Proc. Am. Assoc. Cancer Res. 38, 363.

Unnikrishnan, M., Kuttan, R., 1990. Tumor reducing and anticarcinogenic activity of selected spices. Cancer Lett. 51, 85–89.

Zimmerli, B., Schlatter, J., 1991. Ethyl carbamate: analytical methodology, occurrence, formation, biological activity and risk assessment. Mutat. Res. 259, 325–350.

RESEARCH ARTICLE
doi: 10.2306/scienceasia1513-1874.2006.32.159

ScienceAsia 32 (2006): 159-165

Reprint 6

Characterization of *Anopheles dirus* Glutathione Transferase Epsilon 4

Gulsiri Charoensilp[a], Ardcharaporn Vararattanavech[a], Posri Leelapat[b], La-aied Prapanthadara[b] and Albert J. Ketterman[a*]

[a] Institute of Molecular Biology and Genetics, Mahidol University, Salaya Campus, Nakhon Pathom 73170, Thailand.
[b] Research Institute for Health Sciences, Chiang Mai University, P.O. Box 80, Chiang Mai 50202, Thailand.

* Corresponding author, E-mail: frakt@mahidol.ac.th

Received 4 Nov 2005
Accepted 8 Feb 2006

ABSTRACT: The coding sequences of a wild type glutathione transferase (GST) Epsilon 4 and three isoenzymes were obtained by RT-PCR from a Thai malaria mosquito, *Anopheles dirus*. After confirmation by sequencing, the RT-PCR products were subcloned into an expression vector and proteins were expressed, purified, and biochemically characterized to study the function of these enzymes and for comparison with two orthologs from *An. gambiae* (agGSTE4-4) and *Aedes aegypti* (aaGSTE4-4). The results showed that *An. dirus* GST Epsilon 4 (adGSTE4-4) shares more than 85% amino acid sequence similarity with agGSTE4-4 and aaGSTE4-4. However, adGSTE4-4 possesses a greater catalytic efficiency (k_{cat}/K_m) for 1-chloro-2,4-dinitrobenzene as well as greater activities for several other substrates compared with agGSTE4-4 and aaGSTE4-4. Moreover, adGSTE4-4 enzyme possesses peroxidase and DDT dehydrochlorinase activities while these activities were not observed for agGSTE4-4. In addition, adGSTE4-4 binds two pyrethroid insecticides (permethrin and l–cyhalothrin) with a relatively high affinity. We conclude that adGSTE4-4, unlike agGSTE4-4, can contribute to DDT resistance by DDT dehydrochlorinase activity as well as to pyrethroid resistance by sequestration and protection against oxidation from secondary pyrethroid metabolites via its peroxidase activity.

KEYWORDS: Glutathione transferase; Epsilon class; *Anopheles dirus*; DDT dehydrochlorinase; pyrethroid insecticide.

INTRODUCTION

Glutathione transferases (GSTs: E.C. 2.5.1.18) are a diverse family of multifunctional enzymes that play roles in metabolism, transportation, xenobiotic compound detoxification, and cell mediation against oxidative stress[1]. They are found in almost all living organisms and catalyze a conjugation reaction by transferring the thiol group of reduced glutathione (GSH) to an electrophilic substrate, making the resultant products more water soluble and excretable. GSTs are composed of two subunits and each subunit consists of two domains containing a highly conserved glutathione binding site (or G site) and a hydrophobic substrate binding site (or H site). Currently, more than 40 GST genes have been detected and grouped into at least 13 different classes[1,2]. Generally, the intra-class GSTs have greater than 40% amino acid sequence identity whereas the inter-class GSTs have amino acid sequence identity less than 30%[3]. The insect GSTs are of particular interest because they have the potential to confer resistance to all major groups of insecticides. GST-based resistance has been detected by elevated levels of GST activity in strains of insects resistant to organophosphates[4], organochlorines[5], and pyrethroids[6]. The mechanisms that GSTs use to detoxify insecticides are direct metabolism of insecticides or the secondary products, prevention of the oxidative damage induced by insecticide and sequestration[7]. Recently, the complete genome of *Anopheles gambiae* (an African malaria mosquito) was obtained and GST genes in this species have been annotated into at least six different classes (namely Theta, Sigma, Zeta, Omega, Delta, and Epsilon). Two insect specific classes, Delta and Epsilon, encode two-thirds of the *An. gambiae* cytosolic GSTs[2]. Moreover, a cluster of eight insect-specific epsilon class GSTs (*gste1 - gste8*) have been identified and co-localized with a DDT resistance locus, *rtd1*, on polytene chromosome arm 3R division 33B[8]. In addition, a quantitative PCR assay showed five of the eight epsilon GSTs (namely *gste1, gste2, gste3, gste4*, and *gste7*) are expressed at significantly greater levels in the DDT resistant strain[2]. Earlier studies had shown that GSTE2-2 was very efficient at metabolizing DDT, GSTE1-1 possessed peroxidase activity whereas GSTE4-4 and GSTE8-8 had no detectable DDT dehydrochlorinase or peroxidase activities[9]. In our laboratory, we are interested in Epsilon class GSTs in

the malaria mosquito, *Anopheles dirus*. Malaria is a major public health problem in Thailand, resulting in 325 reported deaths and 37,335 cases in 2003[10]. Furthermore, a comparison between the genomes of *An. dirus* and *An. gambiae* showed that the two Anopheline species possess a similar pattern of GST isoenzymes, although the individual enzymes differ significantly at the functional level[11]. For example, when comparing the equivalent alternatively spliced GSTs from *An. dirus GST1AS1* and *An. gambiae GST1a*, the amino acid sequence identities for adGSTD1-1 versus agGSTD1-6, and adGSTD3-3 versus agGSTD1-5 are 93% and 92%, respectively[12], but the catalytic efficiencies toward 1-chloro-2,4-dinitrobenzene (CDNB) are 16.5-fold and 1.5-fold different, respectively[13,14]. Despite the high level of sequence identity between GST enzymes from *An. dirus* and *An. gambiae*, the enzymes display different kinetic properties and substrate specificities that may lead to differences at the functional level. The aim of this study was to obtain and characterize Epsilon GSTs from the Thai malaria vector, *An. dirus*. To be in alignment with a proposed universal GST nomenclature the enzyme reported here was named adGSTE4-4 (in insect GST nomenclature, "E" refers to the Epsilon class and "4-4" refers to the homodimeric isoenzyme[15,3]). Here we report the amino acid sequences of GST Epsilon 4 (adGSTE4-4) enzyme and three variant isoenzymes from *An. dirus,* and compare with the orthologous enzymes from *An. gambiae* and *Aedes aegypti*.

Materials and Methods

Mosquito Strain

An *Anopheles dirus* B colony established at the Department of Parasitology, Faculty of Medicine, Chiang Mai University, was used in this study. The colony was identified on the basis of its morphological and chromosomal characteristics[16].

RT-PCR and cDNA Sequencing of *An. dirus gste4*

Total RNA was extracted from 0.1 g of fourth instar larvae of *An. dirus* using TRI reagent (SIGMA, USA), according to the manufacturer's instructions. Then mRNA was reverse transcribed into cDNA using ImProm-II™ Reverse Transcriptase (Promega, USA) and oligo(dT) primer (5'-CGGTCGACATATG$(dT)_{18}$-3') following the instructions from Promega. PCR used cDNA as a template, a 5' primer started at ATG codon based on *An. gambiae gste4* sequence (5'-ATGCCGA ACATCAAGCTGTAC-3'), a 3' oligo(dT) primer, and *Taq* DNA Polymerase (Promega, USA). PCR (consisted of 35 cycles of 94°C for 10 s, 55°C for 30 s, 72°C for 1 min) was performed in a Perkin–Elmer thermocycler (USA). Then RT-PCR product was directly sequenced in both directions using a Bigdye™ terminator cycle sequencing kit (Perkin Elmer, USA). Multiple alignments of nucleotide sequences and translated amino acid sequences were analyzed using the ClustalX program.

5'Rapid Amplification of cDNA Ends (RACE) of *An. dirus gste4*

To determine 5' amino acid sequence identity of *An. dirus gste*, 5' RACE was performed according to the 5' RACE System for Rapid Amplification of cDNA Ends, Version 2.0 instruction manual (GIBCO BRL, USA). Total RNA was extracted and reverse transcribed into cDNA as previously described using *adgste4* gene specific primer 1 (5'-ATTCGT CGCCGCATAGTAGGG-3') to obtain full-length *An. dirus gste4* coding sequence.

Cloning, Expression and Purification of *An. dirus gste4*

Full-length coding region of *An. dirus gste4* was amplified by RT-PCR as described above using *Taq* DNA Polymerase, 3' primer containing *Bam*HI site (5'-GC**GGATCC**TCACTTTGCTTTAGCACGGTTC-3'), and two different 5' primers containing *Bam*HI site (5'-AAAC**CCATGG**ATCCATGCCGAA CATCAAGCTG-3') or *Nde*I site (5'-CG**CATATG**CCAAACATTAAGCTGTA CACGG-3'). These two RT-PCR products were subcloned into two different sites (*Bam*HI site or *Nde*I–*Bam*HI site) of the pET3a expression vector (Novagen, USA) to generate adGSTE4-4 enzymes with or without a T7tag on the N-terminus, respectively. Then recombinant plasmids were analyzed by restriction digestion, sequenced and transformed into *E. coli* BL21(DE3)pLysS. Proteins were expressed as previously described[17] and soluble target proteins were purified using cation exchange chromatography using a SP-XL column, followed by hydrophobic interaction chromatography using a HiTrap Phenyl Sepharose column (Amersham Biosciences, USA). The SP-XL column was equilibrated with 50 mM phosphate buffer pH 7 and lysate was applied to the column. The adGSTE4-4 enzymes did not bind to the SP-XL column, so flow-through was collected and NaCl added to a final concentration of 3 M before loading to a HiTrap Phenyl Sepharose column pre-equilibrated with 50 mM phosphate buffer, pH 7, containing 3 M NaCl. Protein was eluted with a linear gradient from 2 - 0.75 M NaCl in 50 mM phosphate buffer, pH 7, containing 10 mM dithiothreitol (DTT). The major activity of adGSTE4-4 enzymes were eluted in 50 mM phosphate buffer, pH 7, containing 1 or 0.75 M NaCl. Purified enzymes were concentrated and desalted by Hitrap desalting columns (Amersham Biosciences, USA) as previously described[18]. GSTs were observed to be homogenous by SDS-PAGE. The enzymes were stored in 50 mM phosphate buffer, pH 6.5, 10 mM DTT, 50% (v/v)

glycerol at -20°C. Protein concentrations were determined by Bio-Rad protein reagent (Bio-Rad) with bovine serum albumin as standard protein[19].

Enzyme Characterization

Steady-state kinetics were performed by varying concentrations of 1-chloro-2,4-dinitrobenzene (CDNB) and glutathione (GSH) in 0.1 M phosphate buffer, pH 6.5, as previously described to obtain kinetic parameters, k_{cat}, K_m and k_{cat}/K_m, of wild type adGSTE4-4 and variant enzymes [17]. Substrate specificity of the enzymes were determined as previously described with five different substrates; CDNB, 1,2-dichloro-4-nitrobenzene (DCNB), ethacrynic acid (EA), *p*-nitrophenethyl bromide (PNPB) and *p*-nitrobenzyl chloride (PNBC)[17]. A thermal stability assay was performed to determine half life of wild type and variant enzymes by incubating enzymes (1 mg/ml in 0.1 M potassium phosphate, pH 6.5, containing 5 mM DTT and 1 mM EDTA) at 45°C and enzyme aliquots were assayed for activity at different time-points as previously described[17]. Insecticide K_i experiments for permethrin and λ-cyhalothrin (SUPELCO, USA) were performed by varying CDNB concentrations with 30 mM GSH in the presence and absence of the pyrethroid insecticides. The initial rate of reaction was used to construct a double reciprocal plot, 1/*V* versus 1/*S*, and the inhibition constant (K_i) was determined as previously described[20,13]. Peroxidase activities of wild type and variant enzymes were determined at 340 nm by coupling the reduction of cumene hydroperoxide (CHP) to the oxidation of NADPH by oxidized GSH with glutathione reductase as previously described[21]. DDT dehydrochlorinase activity was determined by conversion of DDT to 1,1-dichloro-2,2-bis-(*p*-chlorophenyl)ethane (DDE) detected by high-

```
                      *        20         *        40         *        60         *        80
adGSTE4-4 WT       : MPNIKLYTAKLSPPGRAVELTGKALGLEFDISPINLIAGDHLREEFRKLNPQHTIPLIDD-AGTIVYESHAIIVYLVTKY
:  79
adGSTE4-4 Pro14Leu : .............L.............................................-...................
:  79
adGSTE4-4 Glu44Lys : ..........................................K.................-...................
:  79
adGSTE4-4 Ile131Thr: ..........................................................-...................
:  79
agGSTE4-4          : ................S....A......L..V......QE..T.A................-N.....D....N.......
:  79
aaGSTE4-4          : .GK.Q.................A.....DL..H...........P..V...........V.ED.....D............
:  80
adGSTD3-3          : ---.DF.YLPG.A.C......AA.....L..KLT.....E...P..L......C..T.V.-N.FA....R..CT..AE..
:  76


                             *       100         *       120         *       140         *       160
adGSTE4-4 WT       : G--ADDSLYPSDAVTRSKVNAALHFDSGVLFARLRFYLEPILYYGSTETPQEKIDNLYRAYELLNATLVD--DYIVGSRL
: 155
adGSTE4-4 Pro14Leu : .--.....................................................................--........
: 155
adGSTE4-4 Glu44Lys : .--.....................................................................--........
: 155
adGSTE4-4 Ile131Thr: .--.....................................................T................--........
: 155
agGSTE4-4          : .KPEG.......V.Q.A.................F...........A...................D....--E....NE.
: 157
aaGSTE4-4          : A--K......K.IA..A.............................PD...D...YAC.......D....--E....N..
: 156
adGSTD3-3          : .--K..K...K.PQK.AV..QR.Y..M.T..Q.FAD.YY.Q..AKQPAN-A.NEKK.KD.VDF..-.F..GHK..A.DS.
: 152


                             *       180         *       200         *       220
adGSTE4-4 WT       : TLADLSCVASIASMHAIFPIDAGKYPKLLAWVERIAKLPYYAATNQAGAEELAQLYHAKLAENRAKAK : 223
adGSTE4-4 Pro14Leu : ..................................................................... : 223
adGSTE4-4 Glu44Lys : ..................................................................... : 223
adGSTE4-4 Ile131Thr: ..................................................................... : 223
agGSTE4-4          : ............................AG..K........E...R..........R...E...TN.. : 225
aaGSTE4-4          : ..............Y........A.....A......E.....KG...E......A..RD.......GK. : 224
adGSTD3-3          : ......V....S.YDVAG-FELA...H.A..Y..TR.EAPG..I....I..FRKY.EK---------- : 209
```

Fig 1. Amino acid sequence alignment of *An. dirus* GSTE4-4 wild type (adGSTE4-4 WT) and variants (Pro14Leu, Glu44Lys, and Ile131Thr), *An. gambiae* GSTE4-4 (agGSTE4-4), *Aedes aegypti* GSTE4-4 (aaGSTE4-4), and *An. dirus* GSTD3-3 (adGSTD3-3). Gaps introduced to maximize sequence similarity are shown by a horizontal dash while a dot represents the same amino acid. GenBank accession numbers for the sequences are: adGSTE4-4, DQ168030; agGSTE4-4, AY070254; aaGSTE4-4, AY819709; adGSTD3-3, AF273039.

Table 1. Substrate specificities, kinetic parameters, and half life of *Anopheles dirus* and *Anopheles gambiae* GSTE4-4 enzymes.

	adGSTE4-4 WT	adGSTE4-4 T7WT	adGSTE4-4 Pro14Leu	adGSTE4-4 Glu44Lys	adGSTE4-4 Ile131Thr	agGSTE4-4
Substrate specificity						
CDNB (μmol/min/mg)	79.95 ± 0.81	77.03 ± 1.11	1.43 ± 0.08	71.21 ± 3.72	53.56 ± 2.71	16.50 ± 1.02
DCNB (μmol/min/mg)	0.324 ± 0.011	0.462 ± 0.011	0.002 ± 0.000	0.381 ± 0.016	0.276 ± 0.021	0.070 ± 0.010
PNPB (μmol/min/mg)	0.113 ± 0.009	0.123 ± 0.011	not detected	0.099 ± 0.005	0.128 ± 0.007	-
PNBC (μmol/min/mg)	0.140 ± 0.006	0.133 ± 0.008	not detected	0.124 ± 0.004	0.134 ± 0.001	-
EA (μmol/min/mg)	0.034 ± 0.006	0.095 ± 0.007	0.007 ± 0.002	0.029 ± 0.005	0.007 ± 0.004	-
CHP (nmol/min/mg)	118.02 ± 6.19	-	not detected	74.90 ± 6.46	not detected	not detected
DDTase activity (nmol of DDE/mg)	2.56 ± 0.32	-	-	-	-	not detected
Kinetic parameters						
V_{max} (μmol/min/mg)	94.83 ± 5.06	87.55 ± 1.73	1.65 ± 0.04	83.17 ± 0.83	69.20 ± 1.05	16.30 ± 1.59
k_{cat} (S^{-1})	39.28	36.26	0.69	34.45	28.66	13.74
K_m for GSH (mM)	4.53 ± 1.04	7.15 ± 0.18	11.26 ± 1.30	3.81 ± 0.15	5.12 ± 0.21	5.38 ± 0.79
k_{cat}/K_m for GSH ($S^{-1}.mM^{-1}$)	8.7	5.1	0.06	9	5.6	2.5
K_m for CDNB (mM)	0.076 ± 0.010	0.060 ± 0.006	0.144 ± 0.017	0.070 ± 0.010	0.040 ± 0.004	0.131 ± 0.026
k_{cat}/K_m for CDNB ($S^{-1}.mM^{-1}$)	517	604	4.8	492	717	105
K_i for permethrin (μM)	66.27 ± 2.75	-	not inhibited	53.28 ± 3.42	669.28 ± 27.42	-
K_i for λ-cyhalothrin (μM)	115.43 ± 15.16	-	not inhibited	72.20 ± 1.66	433.79 ± 11.63	-
Half life at 45°C (min)	21.48 ± 0.40	18.93 ± 1.78	32.16 ± 2.53	13.93 ± 0.61	6.97 ± 0.85	-

The data are means ± standard deviation for at least three separate experiments. adGSTE4-4 T7WT indicates wild type GSTE4 containing the T7 tag on the N-terminus.
A dash indicates data not determined.
For substrate specificity, the concentrations used were: 1 mM CDNB (1-chloro-2,4-dinitrobenzene); 1 mM DCNB (1,2-dichloro-4-nitrobenzene); 0.1 mM PNPB (*p*-nitrophenethyl bromide); 0.1 mM PNBC (*p*-nitrobenzyl chloride); 0.2 mM EA (ethacrynic acid); and 1 mM CHP (cumene hydroperoxide). *An. gambiae* data are given for comparison[9].

performance liquid chromatography as described previously[13].

Results

Cloning, Expression and Purification of adGSTE4-4 Enzymes

The full-length coding sequence of *An. dirus gste4* contains 672 bp translated to give a polypeptide of 223 amino acids which is the same length as *Aedes aegypti gste4*[22] but two amino acids less than *An. gambiae gste4*[2]. A comparison of *An. dirus gste4* with *An. gambiae* and *Ae. aegypti* enzymes shows amino acid sequence identity/similarity for the enzymes of 81%/90% and 74%/85%, respectively (Fig. 1). In the 52 region *An. dirus gste4* had only two nucleotides differ from *An. gambiae gste4* although the same amino acids were still encoded. However, from 12 full-length sequenced clones of *An. dirus gste4*, three clones showed variations in amino acid sequences; the first (adGSTE4-4 Pro14Leu) had Pro14 changed to Leu, the second (adGSTE4-4 Glu44Lys) had Glu44 changed to Lys, and the third (adGSTE4-4 Ile131Thr) had Ile131 changed to Thr (Fig. 1). These variants and wild type *adgste4* were subcloned into the *Nde*I-*Bam*HI site of pET3a expression vector to generate enzymes without a fusion tag. Additionally a wild type *adgste4* sequence was subcloned into the *Bam*HI site of pET3a to generate adGSTE4-4 enzyme with a T7 tag on the N-terminus. This was to observe the effect of the T7 tag on enzyme properties and for comparison with *An. gambiae* GSTE4-4 enzyme which possessed a T7 tag[9]. Five adGSTE4-4 enzymes, wild type with or without T7 tag and three variants without T7 tag, were expressed as soluble proteins at high levels. These enzymes were purified by using cation exchange chromatography followed by hydrophobic interaction chromatography, which gave a 3-fold greater yield for wild type adGSTE4-4 enzyme without T7 tag when compared with purification by S-hexylglutathione affinity chromatography (data not shown).

Substrate Specificity, Kinetic Properties, and Half Life Stability of adGSTE4-4 Enzymes

Six GST substrates were used to determine substrate specificity (Table 1). *An. dirus* adGSTE4-4 had 5-fold greater activities for CDNB and DCNB than the *An. gambiae* enzyme. Moreover, wild type adGSTE4-4 exhibited peroxidase and DDT dehydrochlorinase activities whereas these activities for *An. gambiae* agGSTE4-4 were undetectable. These results showed variation in substrate specificities among wild type adGSTE4-4 with or without T7tag, adGSTE4-4 variants, and the orthologous enzyme from *An. gambiae*. The kinetic property differences between these two enzymes may originate from either the 14 N-terminus amino acids (T7tag) of agGSTE4-4 or the 41 amino acids that are different between agGSTE4-4 and wild

type adGSTE4-4. However, the kinetic properties between wild type adGSTE4-4 with and without T7 tag were similar, which suggests the T7 tag had little effect on adGSTE4-4 kinetic properties, supporting the idea that the enzyme differences originate with the sequence differences.

When comparing wild type adGSTE4-4 with the variant enzymes, we observed that adGSTE4-4 Pro14Leu exhibited the lowest enzyme activities for all substrates tested including a dramatically decreased catalytic efficiency toward CDNB (107-fold). Thus Pro14 appeared to have a major impact on enzyme catalysis. In contrast, adGSTE4-4 Glu44Lys had similar kinetic properties to the wild type enzyme. Whereas adGSTE4-4 Ile131Thr had no detectable peroxidase activity and showed 5-fold lower activity for EA than the wild type.

The insecticide inhibition kinetics of permethrin and λ-cyhalothrin were shown to be a non-competitive inhibitor for two variants (adGSTE4-4 Glu44Lys, and adGSTE4-4 Ile131Thr). However, for wild type adGSTE4-4 permethrin and λ-cyhalothrin were found to be a non-competitive inhibitor and mixed inhibitor, respectively. A comparison of K_i values for permethrin and λ-cyhalothrin illustrates differences between various *An. dirus* enzymes (Table 1), the most notable one being adGSTE4-4 Pro14Leu which showed no inhibition with either permethrin or λ-cyhalothrin.

The half lives of wild type adGSTE4-4 with and without T7 tag at 45°C were similar (Table 1). The half-life of adGSTE4-4 Pro14Leu increased 1.5-fold whereas those of adGSTE4-4 Glu44Lys and adGSTE4-4 Ile131Thr decreased 1.5- and 3-fold, respectively, when compared with the wild type enzyme. These residue changes therefore showed only small affects on the structural stability of the enzyme.

Discussion

Despite the high degree of sequence identity between the two orthologous GSTE4-4 enzymes from *An. dirus* and *An. gambiae*, they displayed differences in kinetic properties and substrate specificity, especially for peroxidase and DDT dehydrochlorinase activities which were only observed for the *An. dirus* enzyme. In contrast to *An. gambiae* agGSTE2-2, agGSTE4-4 and agGSTE8-8 enzymes, which have undetectable peroxidase activities, *An. dirus* adGSTE4-4 possesses peroxidase activity comparable to the *Ae. aegypti* aaGSTE2-2 (0.11 mmol/min/mg), but 88.7-fold greater activity than agGSTE1-1 from the DDT resistant strain of *An. gambiae* (1.33 nmol/min/mg)[9,22]. This peroxidase activity has been shown to be protective against the damage caused by lipid peroxidation products induced by exposure to pyrethroid insecticides[23]. In contrast, several GSTs from the DDT resistant strain of *An. gambiae*, agGSTE1-1, agGSTE4-4, and agGSTE8-8, showed no detectable DDT dehydrochlorinase activity whereas, *An. dirus* adGSTE4-4 possessed DDT dehydrochlorinase activity (2.56 nmole of DDE/mg). However, this enzyme has 1000-fold lower DDT dehydrochlorinase activity than those of agGSTE2-2 and aaGSTE2-2 from the DDT resistant strains of *An. gambiae* (2.77 nmole of DDE/μg) and *Ae. aegypti* (4.16 nmole DDE/μg), respectively[9,22]. Previously it has been reported that GST enzymes protect against pyrethroid toxicity in insects by sequestering the insecticide[6]. In the pyrethroid inhibition study, *An. dirus* GSTE4-4 enzyme was affected by a non-competitive and mixed type inhibition by permethrin and λ-cyhalothrin, respectively, which demonstrates that both pyrethroids interacted with the enzyme although not in the active site. The K_i value of adGSTE4-4 for permethrin indicates that it has similar permethrin binding affinity to *An. dirus* Delta class GSTs for which the K_i values range from 9 – 53 mM[13].

Three variants of adGSTE4-4 enzymes (Pro14Leu, Glu44Lys, and Ile131Thr) were also obtained by RT-PCR. As no Epsilon GST structure is currently available we used the structure of adGSTD3-3[24] to model the variant residue positions (Fig. 2). Pro14Leu is near the critical active site serine residue involved in thiol deprotonation of GSH. The Pro14 residue is a highly conserved active-site residue in Delta, Epsilon, Theta, and several unclassified GSTs in insects[2,22,25], suggesting its importance for backbone orientation. As proline causes a kink in the peptide backbone, when changed to leucine it would therefore change the conformation of the active site pocket, impacting on substrate specificity as well as catalysis. In addition, the Pro14Leu variant enzyme was not inhibited by permethrin or λ-cyhalothrin. It appears that the Pro14Leu variant enzyme lost the pyrethroid binding site due to a change in the enzyme topology. The second variant enzyme, containing a Glu44Lys change had the same kinetic properties and permethrin binding affinity as wild type, but surprisingly had peroxidase activity slightly lower than the *An. dirus* wild type enzyme, which was similar to *Ae. aegypti* GSTE2-2. Glu44Lys had a 56.3-fold greater peroxidase activity than agGSTE1-1 from a resistant strain of *An. gambiae*[9,22]. Moreover, Glu44Lys variant enzyme had a 1.6-fold greater λ-cyhalothrin binding affinity when compared to the wild type adGSTE4-4. The Glu44 residue is a conserved negative charge residue in the Epsilon class GSTs[2]. It is difficult to interpret the contribution of the Glu44 residue to peroxidase activity and specificity as no Epsilon structure is currently available. However the model suggests Glu44 is in α helix 2 which is known to be involved in the active site through GSH binding but also influencing specificity

of the hydrophobic substrate as well[26]. In contrast, the third variant enzyme, Ile131Thr in α helix five, showed no peroxidase activity and had 10- and 3.7-fold lower binding affinities to permethrin and λ-cyhalothrin, respectively. The above data suggests one putative surface site of interaction for the pyrethroids is a hydrophobic groove consisting of four motifs from both domains 1 and 2. These four motifs include 1) residues 32-41 in the loop between β2 sheet and α helix, 2) the C-terminus of α4 and loop residues between and including the N-terminus of α5, 3) the C-terminus of α6 and 4) the C-terminus of α8. This area would be affected through structural adjustments brought about by the residue changes observed in this study.

In conclusion, the Epsilon 4 GST of *An. dirus* shares more than 85% amino acid sequence similarity with the two orthologs from *An. gambiae* and *Ae. aegypti*. However, adGSTE4-4 possesses greater catalytic efficiency (k_{cat}/K_m) for CDNB as well as greater activity for several other substrates. In contrast, the *An. dirus* adGSTE4-4 enzyme possesses peroxidase and DDT dehydrochlorinase activities while these activities were not observed for the *An. gambiae* enzyme. In addition, we have shown the *An. dirus* enzyme binds two pyrethroid insecticides (permethrin and λ–cyhalothrin) with relatively high affinity. From these results, we conclude that *An. dirus* GST Epsilon 4 enzyme can contribute to DDT resistance by DDT dehydrochlorinase activity and to pyrethroid insecticide resistance by sequestration as well as protect against oxidation from the secondary pyrethroid metabolites via its peroxidase activity.

Acknowledgements

This project was funded by the Thailand Research Fund. G.C. and A.V. were funded by Royal Golden Jubilee Ph.D. scholarships.

References

1. Hayes JD, Flanagan JU and Jowsey IR (2005) Glutathione transferases. *Annu Rev Pharmacol Toxicol* **45**, 51-88.
2. Ding Y, Ortelli F, Rossiter LC, Hemingway J and Ranson H (2003) The *Anopheles gambiae* glutathione transferase supergene family: annotation, phylogeny and expression profiles. *BMC Genomics* **4**, 35-50.
3. Chelvanayagam G, Parker MW and Board PG (2001) Fly fishing for GSTs: a unified nomenclature for mammalian and insect glutathione transferases. *Chem Biol Interact* **133**, 256-60.

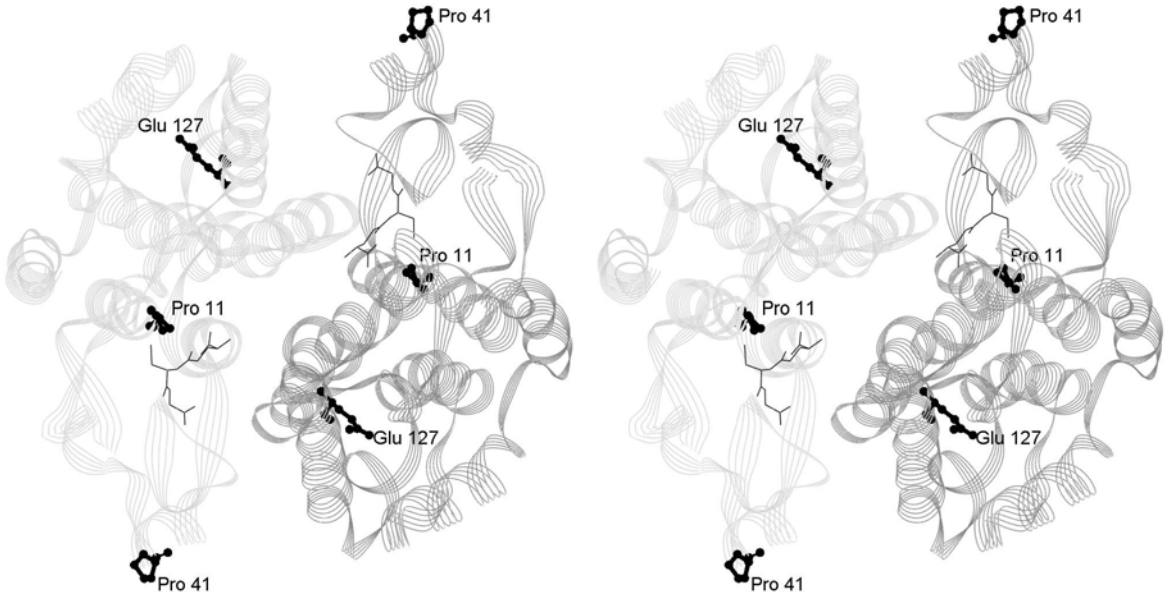

Fig 2. Stereo view of three amino acid residues in adGSTD3-3[24]. These three amino acids (Pro11, Pro41, and Glu127) are equivalent, as shown by amino acid alignment (Fig. 1), to the variant amino acid residues in adGSTE4-4: Pro14Leu, Glu44Lys, and Ile131Thr, respectively. This stereo view is looking at the two-fold axis on to the active sites. The three residues are shown as black ball-and-stick. GSH is shown in black stick in the active sites. The two subunits are shown in light gray and dark gray. The figure was generated using the program DS Viewer Pro.

4. Fournier D, Bride J-M, Poirié M, Bergé J-B and Plapp FW (1992) Insect glutathione S-transferases. Biochemical characteristics of the major forms from houseflies susceptible and resistant to insecticides. *J Biol Chem* **267**, 1840-5.
5. Grant DF and Hammock BD (1992) Genetic and molecular evidence for a *trans*-acting regulatory locus controlling glutathione S-transferase-2 expression in *Aedes aegypti*. *Mol Gen Genet* **234**, 169-76.
6. Kostaropoulos I, Papadopoulos AI, Metaxakis A, Boukouvala E and Papadopoulou-Mourkidou E (2001) Glutathione S-transferase in the defence against pyrethroids in insects. *Insect Biochem Molec Biol* **31**, 313-9.
7. Hemingway J, Hawkes NJ, McCarroll L and Ranson H (2004) The molecular basis of insecticide resistance in mosquitoes. *Insect Biochem Molec Biol* **34**, 653-65.
8. Ranson H, Jensen B, Wang X, Prapanthadara L, Hemingway J and Collins FH (2000) Genetic mapping of two loci affecting DDT resistance in the malaria vector *Anopheles gambiae*. *Insect Molecular Biology* **9**, 499-507.
9. Ortelli F, Rossiter LC, Vontas J, Ranson H and Hemingway J (2003) Heterologous expression of four glutathione transferase genes genetically linked to a major insecticide-resistance locus from the malaria vector *Anopheles gambiae*. *Biochem J* **373**, 957-63.
10. (2005) *http://w3.whosea.org/EN/Section10/Section21/Section340_4027 htm*
11. Prapanthadara L, Promtet N, Koottathep S, Somboon P and Ketterman AJ (2000) Isoenzymes of glutathione S-transferase from the mosquito Anopheles dirus species B: the purification, partial characterization and interaction with various insecticides. *Insect Biochem Molec Biol* **30**, 395-403.
12. Pongjaroenkit S, Jirajaroenrat K, Boonchauy C, Chanama U, Leetachewa S, Prapanthadara L and Ketterman AJ (2001) Genomic organization and putative promotors of highly conserved glutathione S-transferases originating by alternative splicing in *Anopheles dirus*. *Insect Biochem Molec Biol* **31**, 75-85.
13. Jirajaroenrat K, Pongjaroenkit S, Krittanai C, Prapanthadara L and Ketterman AJ (2001) Heterologous expression and characterization of alternatively spliced glutathione *S*-transferases from a single *Anopheles* gene. *Insect Biochem Molec Biol* **31**, 867-75.
14. Ranson H, Prapanthadara L and Hemingway J (1997) Cloning and characterization of two glutathione S-transferases from a DDT-resistant strain of *Anopheles gambiae*. *Biochem J* **324**, 97-102.
15. Mannervik B, Awasthi YC, Board PG, Hayes JD, Di Ilio C, Ketterer B, Listowsky I et al. (1992) Nomenclature for human glutathione transferases. *Biochem J* **282**, 305-6.
16. Baimai V (1989) Speciation and species complexes of the anopheles malaria vectors in Thailand.*The third conference on malaria research, Thailand*, 146-52.
17. Vararattanavech A and Ketterman A (2003) Multiple roles of glutathione binding-site residues of glutathione S-transferase. *Protein and Peptide Letters* **10**, 441-8.
18. Udomsinprasert R and Ketterman AJ (2002) Expression and characterization of a novel class of glutathione S-transferase from *Anopheles dirus*. *Insect Biochem Molec Biol* **32**, 425-433.
19. Bradford MM (1976) A rapid and sensitive method for the quantitation of microgram quantities of protein utilizing the principle of protein-dye binding. *Anal Biochem* **72**, 248-54.
20. Dixon M and Webb EC (1979) Enzyme inhibition and activation.**3**, 332-467.
21. Wendel A (1981) Glutathione peroxidase. *Methods Enzymol* **77**, 325-33.
22. Lumjuan N, McCarroll L, Prapanthadara L, Hemingway J and Ranson H (2005) Elevated activity of an epsilon class glutathione transferase confers DDT resistance in the dengue vector, *Aedes aegypti*. *Insect Biochem Molec Biol* **35**, 861-71.
23. Singh SP, Coronella JA, Beneš H, Cochrane BJ and Zimniak P (2001) Catalytic function of *Drosophila melanogaster* glutathione S-transferase DmGSTS1-1 (GST-2) in conjugation of lipid peroxidation end products. *Eur J Biochem* **268**, 2912-23.
24. Oakley AJ, Harnnoi T, Udomsinprasert R, Jirajaroenrat K, Ketterman AJ and Wilce MCJ (2001) The crystal structures of glutathione S-transferases isozymes 1–3 and 1–4 from *Anopheles dirus* species B. *Protein Science* **10**, 2176-85.
25. Sawicki R, Singh SP, Mondal AK, Beneš H and Zimniak P (2003) Cloning, expression and biochemical characterization of one Epsilon-class (GST-3) and ten Delta-class (GST-1) glutathione S-transferases from *Drosophila melanogaster*, and identification of additional nine members of the Epsilon class. *Biochem J* **370**, 661-9.
26. Ricci G, Caccuri AM, Lo Bello M, Rosato N, Mei G, Nicotra M, Chiessi E et al. (1996) Structural flexibility modulates the activity of human glutathione transferase P1-1. Role of helix 2 flexibility in the catalytic mechanism. *J Biol Chem* **271**, 16187-92.

Biochem. J. (2006) **394**, 135–144 (Printed in Great Britain) doi:10.1042/BJ20050915

An intersubunit lock-and-key 'Clasp' motif in the dimer interface of Delta class glutathione transferase

Jantana WONGSANTICHON and Albert J. KETTERMAN[1]

Institute of Molecular Biology and Genetics, Mahidol University, Salaya Campus, 25/25 Phutthamonthol Road 4, Salaya, Nakhon Pathom 73170, Thailand

Structural investigations of a GST (glutathione transferase), adGSTD4-4, from the malaria vector *Anopheles dirus* show a novel lock-and-key 'Clasp' motif in the dimer interface of the Delta class enzyme. This motif also appears to be highly conserved across several insect GST classes, but differs from a previously reported mammalian lock-and-key motif. The aromatic 'key' residue not only inserts into a hydrophobic pocket, the 'lock', of the neighbouring subunit, but also acts as part of the 'lock' for the other subunit 'key'. The 'key' residues from both subunits show aromatic ring stacking with each other in a pi–pi interaction, generating a 'Clasp' in the middle of the subunit interface. Enzyme catalytic and structural characterizations revealed that single amino acid replacements in this 'Clasp' motif impacted on catalytic efficiencies, substrate selectivity and stability. Substitutions to the 'key' residue create strong positive co-operativity for glutathione binding, with a Hill coefficient approaching 2. The lock-and-key motif in general and especially the 'Clasp' motif with the pi–pi interaction appear to play a pivotal role in subunit communication between active sites, as well as in stabilizing the quaternary structure. Evidence of allosteric effects suggests an important role for this particular intersubunit architecture in regulating catalytic activity through conformational transitions of subunits. The observation of co-operativity in the mutants also implies that glutathione ligand binding and dimerization are linked. Quaternary structural changes of all mutants suggest that subunit assembly or dimerization basically manipulates subunit communication.

Key words: *Anopheles dirus*, aromatic ring stacking, glutathione transferase, lock-and-key, pi–pi interaction, subunit interface.

INTRODUCTION

Glutathione transferases (GST; EC 2.5.1.18) are dimeric enzymes playing a major role in detoxication mechanisms by nucleophilic addition of GSH (γ-glutamyl-L-cysteinyl-glycine) to the electrophilic centre of diverse non-polar endogenous and xenobiotic compounds, rendering them less reactive and more water-soluble substances [1–4]. Cytosolic GSTs are ubiquitous enzymes found in all organisms to date. The nomenclature of this enzyme has now been categorized to contain at least 13 classes, including seven mammalian classes (Alpha, Mu, Pi, Sigma, Theta, Omega and Zeta) and six non-mammalian classes (Beta, Delta, Epsilon, Lambda, Phi and Tau) [4,5]. In addition, members in this enzyme superfamily are increasing due to the massive growth of genomic information, which also yields a number of novel unclassified GSTs [6], a so-called 'U' class.

In general, all GSTs adopt the same highly conserved tertiary structure [2]. A dimeric quaternary structure is thought to be essential for a fully functional active site, since the active site is formed by amino acid residues from both subunits. The dimeric structure also has been shown to be involved in stabilization of tertiary structures of individual subunits [7], as well as to provide a non-substrate ligand-binding site at the dimer interface [8,9]. Studies of equilibrium folding revealed that dimeric formation of GSTs such as Alpha [10], Pi [11] and Sj26GST [12] has significant impact on stabilization of subunit tertiary structure, whereas the dimerization of GSTs such as Sigma [13] and Mu [14] has less influence on subunit stability, due to the presence of stable monomeric intermediates in an unfolding/refolding pathway [15]. Therefore, although the overall tertiary structure is conserved, structural variations occur that generate diversity between the GST classes.

Structural observations of GSTs demonstrate two distinct types of intersubunit interactions [3]. The first is a 'ball-and-socket' or so-called 'lock-and-key' hydrophobic interaction, involving an aromatic 'key' residue from domain I of one subunit that inserts into several hydrophobic 'lock' residues of domain II in the other subunit. This interaction was reported to be specific to mammalian Alpha/Mu/Pi classes [16–19]. The second type of intersubunit interaction is more hydrophilic and lacks the 'lock-and-key' motif, as in Theta/Sigma classes [20,21]. The class-specific intersubunit interactions result in different interface topologies and contribute to interface specificity. Accordingly, only subunits with the same interfacing type appear to be compatible for dimerization.

In the present study, an available refined crystal structure of adGSTD4-4, an insect Delta class GST from the mosquito malaria vector *Anopheles dirus* [22], was investigated for intersubunit interactions along the dimer interface. The enzyme was previously reported as adGST1-4 and later renamed to be in concord with a universal GST nomenclature [23]. This Delta GST was also observed to possess a lock-and-key motif. However, this lock-and-key 'Clasp' motif is found in the centre of a 2-fold axis. Therefore the motif appears to be different from those reported in mammalian Alpha/Mu/Pi classes. A striking characteristic of this motif involving the 'key' residue is that it not only inserts into a hydrophobic pocket of the neighbouring subunit, but also itself acts as part of the 'lock' for the other subunit 'key'. In addition, the 'key' residues from both subunits 'hook around' each other in an aromatic pi–pi interaction, through slightly offset

Abbreviations used: ANS, 8-anilinonaphthalene-l-sulphonic acid; CDNB, 1-chloro-2,4-dinitrobenzene; CPK, Corey–Pauling–Koltun; DCNB, 1,2-dichloro-4-nitrobenzene; EA, ethacrynic acid; GST, glutathione transferase; PNBC, *p*-nitrobenzyl chloride; PNPB, *p*-nitrophenethyl bromide; TIM, triosephosphate isomerase.

[1] To whom correspondence should be addressed (email frakt@mahidol.ac.th).

aromatic ring stacking, generating a 'clasp' in the middle of the subunit interface. To examine the contribution of the lock-and-key 'Clasp' motif to Delta class structure and function, site-directed mutagenesis was performed to Phe-104 (the 'key' residue) and Val-107 (one of the 'lock' residues). Mutant recombinant enzymes were characterized for both enzymatic and structural properties by enzyme steady-state kinetics, substrate specificity, thermal stability, far-UV CD, tryptophan intrinsic fluorescence and fluorescent dye binding.

EXPERIMENTAL

Construction of mutants

A pET3a plasmid containing the full coding sequence of the *A. dirus* Delta class GST isoform 4, adGSTD4-4 (GenBank® accession number AF273040), was derived from a previous study [24]. PCR-based site-directed mutagenesis following the method of Stratagene Quik Change™ Site-Directed Mutagenesis kit (Stratagene, La Jolla, CA, U.S.A.) was used to introduce point mutations to the amino acid 104 or 107 of the wild-type enzyme. A clone with double mutations at both positions was also generated. The entire full-length regions encoding all mutant adGSTD4-4 were verified, using BigDye™ terminator cycle sequencing ready reaction kit version 3.1, at least twice to confirm the absence of undesirable mutations elsewhere. V107M mutagenic plasmid was kindly provided by J. Piromjitpong (Institute of Molecular Biology and Genetics, Mahidol University).

Protein expression and purification

Wild-type adGSTD4-4 and mutants were expressed in *Escherichia coli* BL21(DE3)pLysS as previously described [24]. The temperature of 25 °C was used during protein expression under 0.1 mM isopropyl β-D-thiogalactoside induction. Cells were harvested by centrifugation at 5000 ***g*** for 10 min. The cell pellet was treated with lysozyme to a final concentration of 0.4 mg/ml and then incubated on ice for 20 min. Cell lysate was additionally disrupted by sonication, followed by cell debris separation by centrifugation at 10000 ***g*** for 20 min at 4 °C. The soluble recombinant GST proteins were purified from the supernatant by using GSTrap™ FF affinity chromatography (Amersham Biosciences), except for those incapable of binding to the GSH matrix. In these cases, cation-exchange chromatography by HiTrap™ SP XL (Amersham Biosciences) and hydrophobic-interaction chromatography by HiTrap™ phenyl-Sepharose HP (Amersham Biosciences) were employed. The details of cationic and hydrophobic chromatography have been previously reported [25]. Purified recombinant proteins were homogeneous as judged by SDS/PAGE.

Enzyme characterization and protein assay

Enzyme activity conjugating GSH to the CDNB (1-chloro-2,4-dinitrobenzene) substrate was determined by monitoring the increase in absorbance (A) at 340 nm over time using a SpectraMax® 250 spectrophotometer following a previously described method [26]. The dependence of the initial rate on the substrate concentration was analysed according to the Michaelis–Menten equation (eqn 1), where V is the initial rate of the reaction, V_{max} is the maximum velocity, [S] is the concentration of substrate and K_m is the substrate concentration that gives the rate of the reaction equal to one-half of V_{max}:

$$V/V_{max} = [S]/(K_m + [S]) \quad (1)$$

The values for the kinetic parameters (K_m and V_{max}) were calculated by using GraphPad Prism® 4 software, version 4.01. The steady-state kinetics and substrate-specificity studies were performed as described previously [24]. Five different hydrophobic electrophilic compounds were used in a substrate-specificity study. The results shown are means ± S.D. for at least three independent experiments. Protein concentration was determined by the Bradford method [27] using the Bio-Rad Laboratories (Hercules, CA, U.S.A.) protein reagent with BSA as the standard protein.

With evidence of co-operativity upon GSH binding, demonstrated by a sigmoidal curve instead of a hyperbolic curve on a Michaelis–Menten plot, a Hill equation (eqn 2) was used to fit the experimental kinetic data on the plot. $K_{0.5}$ is the substrate concentration that gives the rate of reaction at one-half of V_{max}, similar to the K_m value for non-co-operative binding ($h = 1$):

$$Y = V/V_{max} = [S]^h/(K_{0.5} + [S]^h) \quad (2)$$

$$\log[Y/(1-Y)] = h\log[S] - \log K_{0.5} \quad (3)$$

A sigmoidal Hill equation was transformed into a linear rate equation (eqn 3), where Y is the fractional saturation, h is the Hill coefficient and $K_{0.5}$ is an averaged binding constant at $Y = 0.5$. A Hill plot, a plot between $\log[Y/(1-Y)]$ and $\log[S]$, was employed to determine the degree of co-operativity by the slope of the plot which yields the Hill coefficient (h) [28].

Thermal stability assay

Enzymes derived from the different engineered clones [each at a concentration of 0.1 and 1 mg/ml in 0.1 M phosphate buffer (pH 6.5) containing 5 mM dithiothreitol and 1 mM EDTA] were incubated at 45 °C. Enzymatic activity was measured as a function of time. An appropriate amount of incubated mixture (adjusted for the specific activity of each engineered enzyme) was taken to assay for residual GST activity at various time points ranging from 0 to 420 min. The log percentage of original activity was plotted versus preincubation time. Slopes from linear regression analysis using GraphPad Prism® 4 software were used for the half-life calculation [28], $t_{1/2} = -(0.693/2.3)/\text{Slope}$.

CD

Far-UV CD measurements were carried out on a Jasco J715 spectropolarimeter. CD spectra of proteins at a concentration of 0.4 mg/ml in 0.1 M phosphate buffer (pH 6.5) with no additives were measured in a 0.2 cm path length quartz cell at room temperature (25 °C). Spectra were recorded from 190 to 260 nm with 1 nm steps, averaged over three scans at a scan rate of 50 nm/min and corrected by subtraction of solvent spectra under identical conditions.

Fluorescence measurements

Both intrinsic and ANS (8-anilinonaphthalene-l-sulphonic acid) fluorescence emission spectra were carried out on a Jasco model FP-6300 spectrofluorimeter in a 0.5 cm path length quartz cell. Excitation and emission bandwidths were kept at 2.5 nm. Fluorescence spectra of 2 μM enzyme in 0.1 M phosphate buffer (pH 6.5) with no additives were recorded at room temperature. All measurements were averaged over three scans at a scanning speed of 500 nm/min and corrected by subtraction of the solvent spectra under identical conditions.

Intrinsic fluorescence measurements were performed at an excitation wavelength of 295 nm and the emission spectra were recorded from 300 to 500 nm, whereas ANS fluorescence

Table 1 Steady-state kinetic constants of engineered GSTs compared with adGSTD4-4 (wild-type)

The results shown are the means ± S.D. for at least three independent experiments.

Enzyme	V_{max} (μmol · min^{-1} · mg^{-1})	k_{cat} (s^{-1})	K_m (mM)		k_{cat}/K_m (mM^{-1} · s^{-1})	
			GSH	CDNB	GSH	CDNB
Wild-type	44.7 ± 2.3	18.60	0.59 ± 0.06	0.73 ± 0.07	31.53	25.49
F104A	23.3 ± 1.7	9.67	11.99 ± 0.20	2.27 ± 0.31	0.85	4.26
F104L	49.3 ± 1.8	20.59	3.55 ± 0.40	0.69 ± 0.15	6.32	29.85
F104M	42.1 ± 1.9	17.51	2.21 ± 0.11	0.82 ± 0.06	10.81	21.36
F104Y	42.7 ± 1.2	17.86	6.96 ± 0.31	0.57 ± 0.05	2.76	31.34
F104W	3.9 ± 0.3	1.63	15.26 ± 0.54	1.49 ± 0.12	0.13	1.09
F104H	1.8 ± 0.1	0.74	16.97 ± 1.54	0.79 ± 0.05	0.04	0.94
F104Q	9.5 ± 0.4	3.97	15.35 ± 1.21	1.32 ± 0.11	0.29	3.00
F104E	4.6 ± 0.3	1.91	16.54 ± 1.34	1.86 ± 0.14	0.12	1.03
F104K	0.17 ± 0.01	0.07	6.62 ± 0.14	0.85 ± 0.13	0.01	0.08
F104A/V107A	15.3 ± 0.6	6.34	10.06 ± 0.58	2.07 ± 0.18	0.63	3.06
V107A	50.6 ± 1.5	21.04	0.73 ± 0.13	0.56 ± 0.02	28.82	37.57
V107L	46.9 ± 1.7	19.53	0.40 ± 0.03	0.47 ± 0.05	48.83	41.56
V107M	49.9 ± 0.8	20.89	0.64 ± 0.10	0.79 ± 0.04	32.64	26.44
V107N	37.2 ± 2.2	15.49	0.45 ± 0.09	0.68 ± 0.09	34.43	22.78
V107D	13.5 ± 0.4	5.62	1.23 ± 0.16	0.51 ± 0.03	6.32	11.02
V107K	0.29 ± 0.01	0.12	8.88 ± 0.19	0.71 ± 0.05	0.02	0.17

measurements were at an excitation wavelength of 395 nm and the emission spectra were recorded from 400 to 600 nm. The final concentration of 200 μM ANS was homogeneously mixed with enzyme solutions prior to the measurements.

RESULTS

Protein expression and purification

All recombinant proteins were effectively expressed at comparable levels in *E. coli* as soluble protein with a size of approx. 25 kDa. Generally, adGSTD4-4 was easily purified in a single chromatographic step using an immobilized GSH affinity chromatography column. It was found that the affinity for this matrix was strongly reduced for many mutants. Therefore an alternative method of cation-exchange and hydrophobic-interaction chromatography was employed. Protein purities from both techniques proved to be equivalent. All mutants were successfully purified and subjected to both enzymatic and structural characterizations.

Enzymatic properties

Enzyme kinetics

Steady-state kinetics was performed using CDNB as a co-substrate for GSH conjugation. Mutant recombinant enzymes with an amino acid substitution at Phe-104 possessed altered catalytic rates (k_{cat}) ranging from approximately wild-type to 266-fold less than wild-type activity (Table 1). Substitutions with bulky (F104W) or polar/charged residues (F104H, F104Q, F104E and F104K) are catalytically unfavourable at position 104, as shown by a decrease of 5- to 266-fold in k_{cat}. The binding affinity towards GSH (K_m^{GSH}) for all Phe-104 mutants was dramatically affected in the range of 4–29-fold less than the wild-type. These decreases in binding affinity were also accompanied by a change to positive co-operativity for GSH binding. For positive co-operativity, a sigmoidal curve was obtained from Michaelis–Menten plots instead of a hyperbolic curve. The degree of co-operativity as shown by the Hill coefficients illustrates that communication occurs between the active sites (Table 2). The sigmoidal-shaped curve for GSH binding signifies that the binding of one molecule of GSH in one active site increases the affinity of the protein for that substrate in the neighbouring active site of the other subunit, reflecting the role of the residue in communication between subunits to stabilize the GSH binding. In addition, the binding affinity towards CDNB substrate (K_m^{CDNB}) of the Phe-104 mutants varied slightly as well in the range of 1–3-fold, which most probably results from structural perturbation within the active-site pocket.

Table 2 Hill coefficients (*h*) for the binding of GSH substrate

The results shown are the means ± S.D. for at least three independent experiments. ANOVA with Dunnett multiple comparisons test was applied with wild-type enzyme as control.

Enzyme	*h*
Wild-type	1.02 ± 0.14
F104A	1.67 ± 0.09*
F104L	1.44 ± 0.12*
F104M	1.23 ± 0.08
F104Y	1.73 ± 0.08*
F104W	1.33 ± 0.15*
F104H	2.10 ± 0.05*
F104Q	1.64 ± 0.11*
F104E	1.99 ± 0.15*
F104K	1.58 ± 0.05*
F104A/V107A	0.99 ± 0.09
V107A	0.96 ± 0.07
V107L	0.99 ± 0.14
V107M	0.93 ± 0.09
V107N	0.99 ± 0.11
V107D	1.34 ± 0.13*
V107K	1.44 ± 0.11*

* Significantly different ($P < 0.01$).

Amino acid replacements at the position Val-107 demonstrated that a charged residue substitution would impact upon the catalytic efficiency of the enzyme by reducing k_{cat} and increasing K_m^{GSH}, in addition to inducing positive co-operativity for GSH binding. In contrast, substitutions with polar, uncharged or non-polar amino acid residues with various sized side chains show little impact on catalytic properties. Kinetic constants of the double mutant F104A/V107A also demonstrated that the disruption at the Phe-104 position has a major influence on catalysis, as

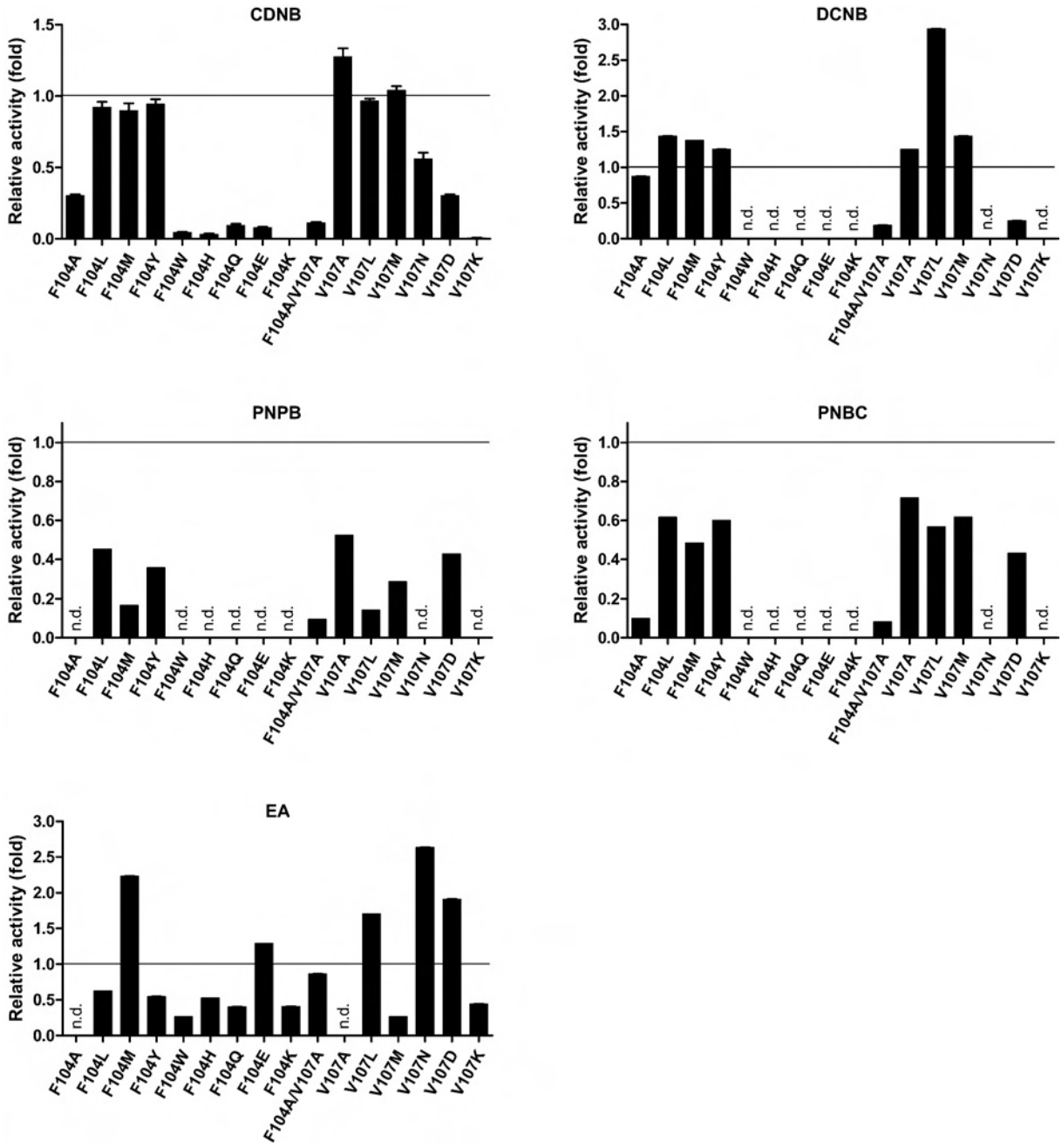

Figure 1 Plots of the changes in substrate specificity for engineered GSTs relative to the wild-type enzyme

The change in specific activity of each enzyme for each substrate is shown as fold change relative to the wild-type enzyme. The experiment was performed in triplicate and the results shown are means ± S.D.; n.d., no detectable activity.

shown by the kinetic properties of the single alanine mutations to either Phe-104 or Val-107. However, this double-mutation enzyme displayed a different characteristic from F104A by possessing non-co-operative binding for GSH substrate (Table 2). This demonstrates that the alanine substitution at Val-107 confers a different structural arrangement that affects the communication between subunits.

Substrate specificity

Five different hydrophobic substrates were used to investigate the changes in substrate specificities of the mutant recombinant enzymes (Figure 1). Each engineered GST displayed a different pattern of substrate specificity. The engineered GSTs with low affinity towards GSH (high K_m^{GSH}) also appeared to possess low activity towards most hydrophobic substrates tested, including CDNB. In this regard, the decrease in activity appears to result from a major disturbance to the G-site (GSH-binding site). This disturbance produces active-site atom movements as well as electrostatic field rearrangement, causing substrate orientation to be in less suitable configurations resulting in catalytic changes. Interestingly, F104L, F104M and F104Y possess comparable activity and specificity with the wild-type enzyme towards CDNB, as shown by k_{cat} and $(k_{cat}/K_m)^{CDNB}$. However, these

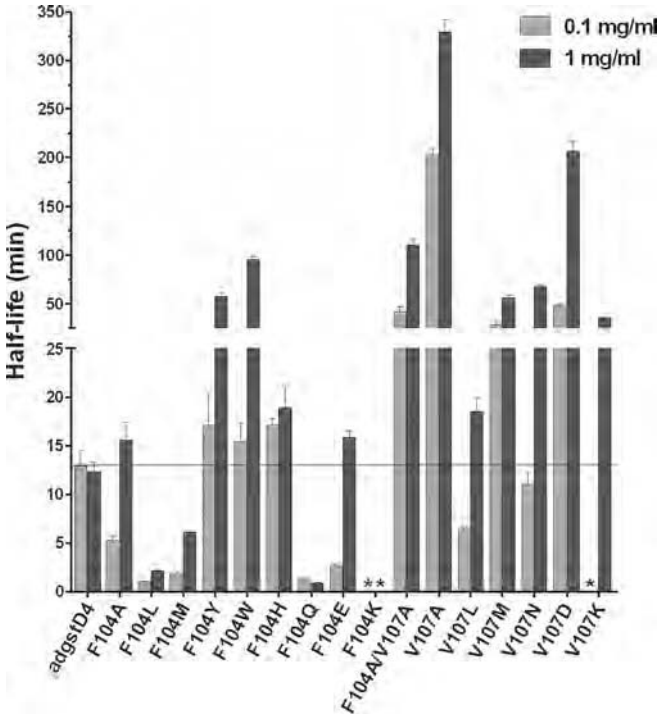

Figure 2 Thermal stability of engineered GSTs compared with the wild-type adGSTD4-4

Half-life determinations were from at least three independent experiments at 45 °C. Enzyme concentrations for heat inactivation are 0.1 and 1 mg/ml respectively. The bar graph represents mean ± S.D. (An asterisk indicates that enzyme activity was undetectable upon heat inactivation, which precluded half-life determination.)

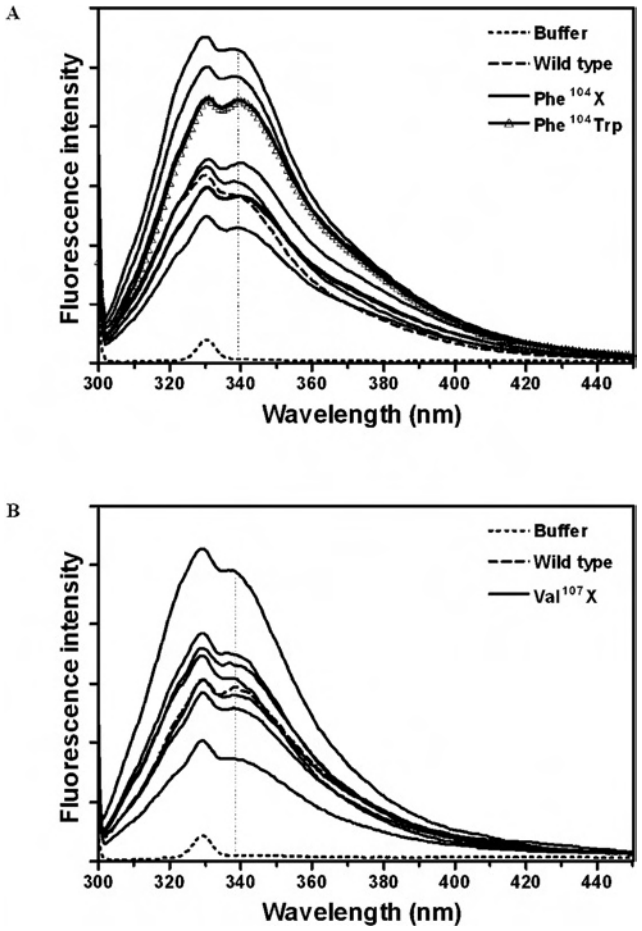

Figure 3 Intrinsic fluorescence of engineered GSTs compared with wild-type adGSTD4-4

F104X, F104W and V107X represent spectra of replacements of (**A**) Phe-104 with one of the amino acids in the present study, replacement of Phe-104 with Trp, and (**B**) replacements of Val-107 with one of the amino acids in the present study respectively. Fluorescence intensity was measured in arbitrary units. Additional lines illustrate variation between all the engineered GSTs.

enzymes displayed higher specific activity with DCNB (1,2-dichloro-4-nitrobenzene), lower specific activity with PNPB (*p*-nitrophenethyl bromide) and PNBC (*p*-nitrobenzyl chloride), but a variable activity with EA (ethacrynic acid) as the substrate. This evidence suggests that the replacement residues in the G-site Phe-104 position have significant consequences on the H-site (hydrophobic substrate-binding site) of the enzyme. Therefore diverse effects on the enzyme activities towards various substrates demonstrate that the different enzyme–substrate interactions that occur are affected in distinctly different ways.

The positively charged replacement V107K performed poorly with all hydrophobic substrates tested, whereas the other mutants showed variable activity towards the different substrates. The double mutant F104A/V107A had low specificity for most of the hydrophobic substrates tested. However, the enzyme demonstrated EA activity comparable with the wild-type, although no detectable EA activity was shown by either of the alanine single-mutation enzymes. Accordingly, the properties of F104A/V107A are not additive influences of F104A and V107A, but result from a particular rearrangement of the enzyme active site that occurs upon packing changes induced by the double mutation.

Structural properties

Enzyme stability

Thermal stability was monitored to demonstrate that amino acid substitutions at either Phe-104 or Val-107, residues involved in the lock-and-key 'Clasp' motif, have a role in structural stability of adGSTD4-4 (Figure 2). Most of the mutants showed a concentration-dependent thermal stability in which increasing concentration showed greater stability. The engineered enzymes appeared to undergo structural changes more rapidly at low concentrations compared with the wild-type, which displayed similar stability at both concentrations used. The results suggest that residue 104 is involved in regulating structural integrity of the enzyme, while substitutions to residue 107 appeared to enhance structural maintenance as shown by an increase in half-life.

CD

CD was used to monitor for protein secondary-structure disruption. The ellipticity spectra measured for the Phe-104 mutants were similar to the spectrum of the wild-type enzyme, with ellipticity minima at 208 and 222 nm. This is characteristic of an α-helix predominant structure and suggests no overall secondary-structure change (results not shown).

Intrinsic fluorescence

Tryptophan intrinsic fluorescence (excitation at 295 nm) was used as a tertiary-structure probe. Each adGSTD4-4 subunit possesses two tryptophan residues located at positions 64 and 191. All mutants showed roughly the same emission maximum of 339 ± 2 nm (Figure 3). As expected, the F104W enzyme, with one additional tryptophan residue, also showed the same emission

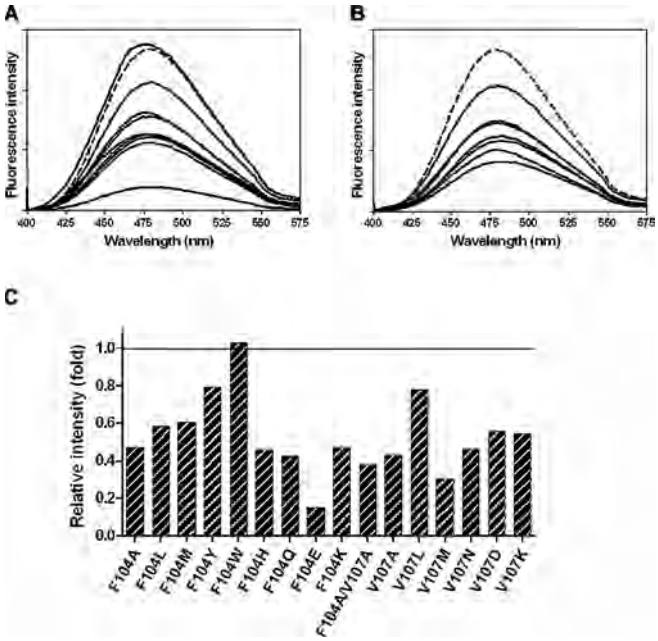

Figure 4 Fluorescence spectrophotometry of ANS binding

(**A**) Fluorescence spectra of Phe-104 mutants. (**B**) Fluorescence spectra of Val-107 mutants. (**C**) A bar graph representation of relative fluorescence intensity compared with the wild-type enzyme. Fluorescence intensity was measured in arbitrary units. Additional lines illustrate variation between all the engineered GSTs.

maximum (Figure 3A), demonstrating that residue 104 is buried in the interior core of the GST dimer interface. Although all substitutions in the present study had no impact on solvent exposure of the tryptophan residues, the variable fluorescent intensities from the different mutants indicate that differences occur in local quenching by the surrounding amino acids such as cysteine, histidine, glutamine and asparagine [29].

Fluorescent dye binding

ANS (extrinsic fluorophore) binding was used as a quaternary structure probe. Upon binding, ANS fluorescence was significantly enhanced and its emission maximum wavelength shifted from 515 nm to approx. 479 nm. Most Phe-104 and Val-107 mutants showed a reduction of fluorescence intensity compared with wild-type (Figure 4). Only F104W slightly increased the fluorescent signal (Figure 4C). Both quenching and enhancement of the fluorescent signals demonstrate conformational changes in the non-substrate ligand-binding site for ANS.

DISCUSSION

The lock-and-key 'Clasp' motif shows some similar characteristics to previously investigated lock-and-key motifs in the GST classes Alpha [30], Mu [31] and Pi [32], for example, stabilization of the dimeric structure through intersubunit interactions. However, the 'Clasp' motif is situated in a different location along the dimer interface and possesses a unique feature (Figure 5). Using the completed *Anopheles gambiae* genome project, an African mosquito malarial vector, members of the GST supergene family have been identified as insecticide-resistant-associated enzymes to enable the monitoring of resistance status of mosquitoes [33]. Putative GST genes were confirmed at the transcriptional level and 12 out of 28 putative genes were classified as insect-specific Delta class [6]. Primary sequences of *A. gambiae* GSTs were aligned with available *A. dirus* Delta class GSTs. Equivalent amino acid residues involved in the 'Clasp' motif of Anopheline GSTs are shown in Table 3, as well as residues of the Australian sheep blowfly (*Lucilia cuprina*) GST. The amino acid residues involved in the motif are shown to be highly conserved across several insect GST classes (Table 3). Available X-ray crystal structures of six Delta class GSTs show their structural conservation in the quaternary structure. Three-dimensional superimposition of equivalent residues in each of the Delta class enzymes shows conserved residues in similar environments (Figure 6). Several of the lock residues have been previously studied by alanine scanning in adGSTD3-3, which is an alternatively spliced product derived from the same gene as adGSTD4-4 [34]. The corresponding residue to adGSTD4-4 Glu-65 (Glu-64 in adGSTD3-3) was suggested to be involved in an initial folding step of the enzyme and this residue is highly conserved among GST classes. The corresponding residue to adGSTD4-4 Arg-67 (Arg-66 in adGSTD3-3) revealed a significant impact on the ionization process of GSH, as well as structural stabilization. However, the corresponding residue to adGSTD4-4 Val-107 (Met-101 in adGSTD3-3) showed no significant functional or structural effects. Leu-103 has previously been characterized in adGSTD4-4 and shown to be important for GSH binding, with evidence for positive co-operativity in some mutants, as well as being involved in structural

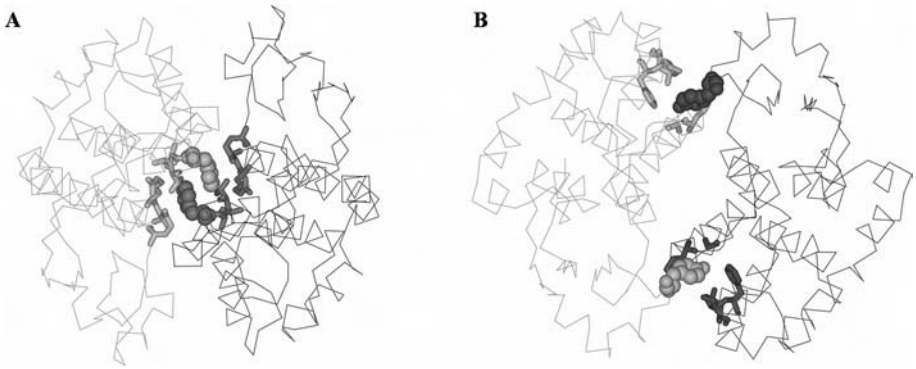

Figure 5 Two types of intersubunit lock-and-key motifs found in different GST classes

(**A**) Lock-and-key 'Clasp' motif in adGSTD4-4 (PDB id: 1JLW). (**B**) Lock-and-key motif in human GST class Pi, GSTP1-1 (PDB id: 1GSS). Subunits are distinguished by colouring in grey and dark grey, amino acid residues involved in the 'lock' are shown by stick representation, whereas the 'key' residues, Phe-104 in adGSTD4-4 or Tyr-50 in human GSTP1-1, are shown in CPK (Corey–Pauling–Koltun) space-filling mode.

Table 3 Lock-and-key 'Clasp' residues in insect GST classes

Numbering of residues is based on adGSTD4 sequence. * adGST, agGST and LcGST represent GSTs from *A. dirus*, *A. gambiae* and *L. cuprina* respectively. D is Delta, u is unclassified, E is Epsilon, T is Theta, S is Sigma, Z is Zeta and O is Omega GST class. GenBank® accession numbers: adGSTD1 (AF273041), adGSTD2 (AF273038), adGSTD3 (AF273039), adGSTD4 (AF273040), adGSTD5 (AF251478), adGSTD6 (AY014406), agGSTD1-3 (Protein ID AAC79992), agGSTD1-4 (Protein ID AAC79994), agGSTD1-5 (Protein ID AAC79993), agGSTD1-6 (Protein ID AAC79995), agGSTD2 (Z71480), agGSTD3 (AF513638), agGSTD4 (AF513635), agGSTD5 (AF513634), agGSTD6 (AF513636), agGSTD7 (AF071161), agGSTD8 (AF316637), agGSTD9 (AY255857), agGSTD10 (AF515527), agGSTD11 (AF513637), agGSTD12 (AF316638), agGSTu1 (AF515521), agGSTu2 (AF515523), agGSTu3 (AF515524), agGSTE1 (AF316635), agGSTE2 (AF316636), agGSTE3 (AY070234), agGSTE4 (AY070254), agGSTE5 (AY070255), agGSTE6 (AY070256), agGSTE7 (AF491816), agGSTE8 (AY070257), agGSTT1 (AF515526), agGSTT2 (AF515525), agGSTS1-1 (L07880), agGSTS1-2 (AF513639), agGSTZ1 (AF515522), agGSTO1 (AY255856) and LcGST (P42860). † 104a and 104b indicate that the residue at this position is from different subunits. ‡ agGSTD6 and agGSTD9 were suggested to be pseudogenes [6].

	Key residue			Lock residue			
Enzyme*	104a†	65	67	68	103	104b†	107
adGSTD4	F	E	R	A	L	F	V
adGSTD1	F	E	R	A	L	F	M
adGSTD2	Y	E	R	A	L	Y	M
adGSTD3	Y	E	R	A	L	Y	M
adGSTD5	H	E	R	V	L	H	L
adGSTD6	F	E	Y	A	L	F	I
agGSTD1-3	F	E	R	A	L	F	V
agGSTD1-4	Y	E	R	A	L	Y	M
agGSTD1-5	Y	E	R	A	M	Y	M
agGSTD1-6	Y	E	R	A	L	Y	M
agGSTD2	F	E	R	A	L	F	A
agGSTD3	F	E	Y	A	L	F	I
agGSTD4	F	E	C	A	L	F	V
agGSTD5	F	E	Y	A	L	F	I
agGSTD6‡	F	E	S	A	L	F	I
agGSTD7	H	E	R	V	L	H	L
agGSTD8	F	E	R	A	L	F	H
agGSTD9‡	L	E	G	A	L	L	C
agGSTD10	F	E	Y	A	L	F	N
agGSTD11	Y	E	R	A	L	Y	M
agGSTD12	F	E	Y	A	L	F	S
agGSTu1	C	E	N	A	L	C	L
agGSTu2	H	E	R	A	L	H	L
agGSTu3	Y	E	K	A	L	Y	S
agGSTE1	H	E	H	A	L	H	S
agGSTE2	H	E	H	A	L	H	S
agGSTE3	H	D	H	A	L	H	S
agGSTE4	H	D	H	A	L	H	S
agGSTE5	H	D	H	A	L	H	S
agGSTE7	H	A	H	A	L	H	A
agGSTE6	F	D	H	A	L	F	S
agGSTE8	C	D	H	A	L	C	N
agGSTT1	E	E	V	A	L	E	H
agGSTT2	S	E	V	A	L	S	H
agGSTS1-1	D	Q	L	A	V	D	N
agGSTS1-2	D	Q	V	A	V	D	N
agGSTZ1	E	E	V	S	C	E	A
agGSTO1	E	E	L	V	I	E	A
LcGST	Y	E	R	A	L	Y	M

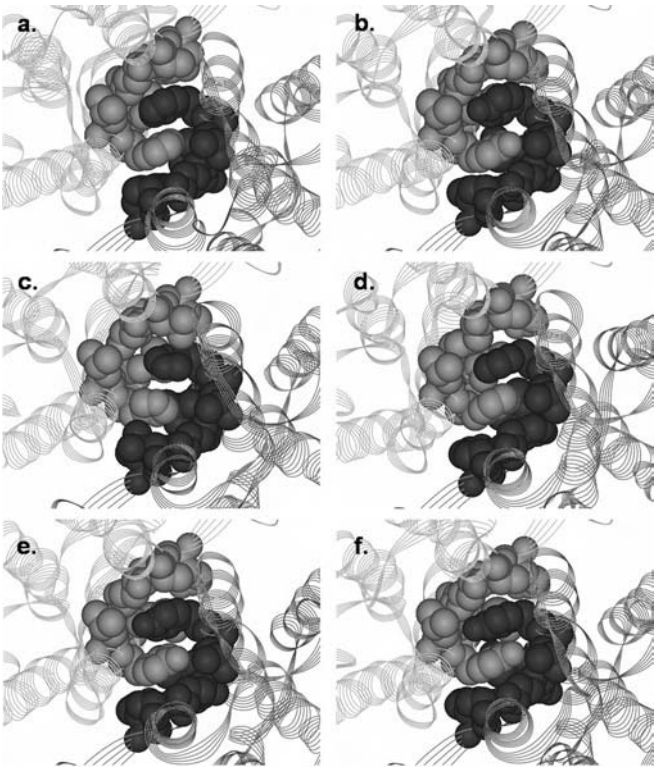

Figure 6 Structural representations of highly conserved lock-and-key 'Clasp' motifs in various Delta class GSTs

(**a**) *A. dirus* adGSTD4; (**b**) *A. dirus* adGSTD3; (**c**) *A. dirus* adGSTD5; (**d**) *A. dirus* adGSTD6; (**e**) *L. cuprina* LcGST; and (**f**) *A. gambiae* agGSTD1-6. Subunits are differentiated by grey and dark grey colours. Lock-and-key 'Clasp' residues are shown in CPK.

stabilization [35]. In an attempt to characterize the contribution of the lock-and-key 'Clasp' motif, the 'key' residue Phe-104 and the 'lock' residue Val-107 of adGSTD4-4 were investigated.

Enzymatic properties of the Phe-104 mutants demonstrated a major impact for this particular position on GSH binding affinity, as shown by increased K_m^{GSH} values for all of the Phe-104 mutants. The altered side chains at position 104 in both subunits would impact on their interface interaction as well as causing a G-site topology change through rearrangement of 'lock' residues, several of which are in the G-site. Replacements with hydrophobic amino acids generated enzymes with varying catalytic rates. Reduced catalytic rates were observed for both F104A and F104W, indicating that not only hydrophobic packing in the region but also the size of the replaced residue is important for efficient subunit dimerization. Structural investigation reveals that the 'Clasp' motif resides within the interior core of the dimer interface that connects the G-site of one subunit to the other (Figure 7A). The communication between subunits through this Clasp motif was illustrated by catalytic co-operativity for GSH binding in all Phe-104 mutants, as shown by Hill coefficients (Table 2). In this regard, the h value of 2.10 ± 0.05 upon GSH binding for F104H is likely to be statistically similar (95% confidence interval) to the maximum number of interacting sites of 2, which demonstrates extremely strong positive co-operativity or complete co-operativity between subunits. Therefore it is reasonable to state that the 'key' residue Phe-104 plays a pivotal role in the dimeric structure of adGSTD4-4 in modulation of GSH binding for both subunits.

The co-operativity event upon GSH binding has been previously reported for several GST studies. Interestingly, co-operativity from point mutations of a human GSTP1-1 at position Gly-41 [36], Cys-47 [37] and Lys-54 [38] was suggested to be a consequence of structural perturbation of helix $\alpha 2$, which in turn was transmitted to Tyr-50 and passed to the neighbouring subunit through the intersubunit lock-and-key motif, where Tyr-50 is the 'key' residue. Likewise, a single point mutation at His-38 located in helix $\alpha 2$ of adGSTD4-4 also revealed positive co-operativity for GSH binding [25]. In this case, three-dimensional

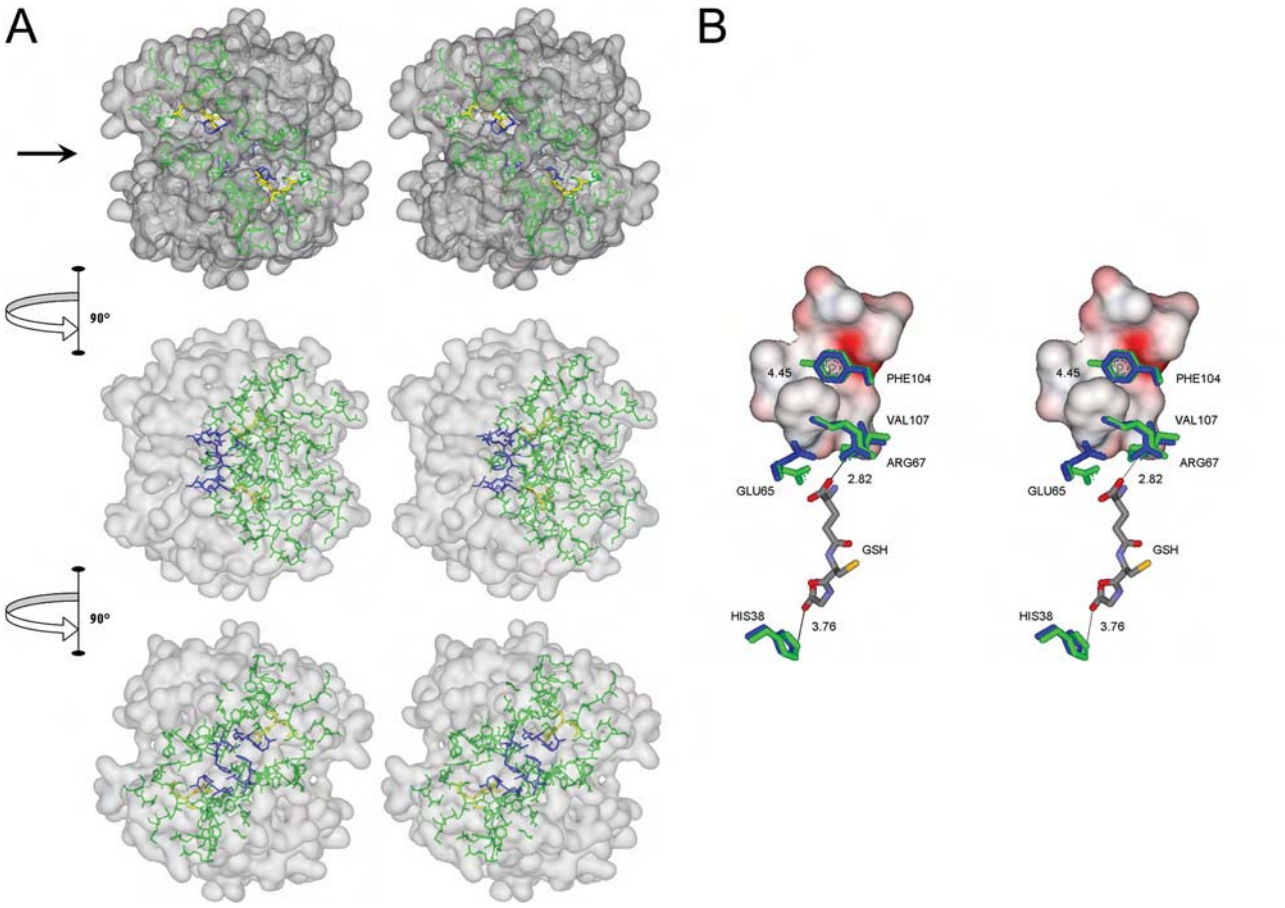

Figure 7 Interactions of amino acids in the lock-and-key 'Clasp' motif of adGSTD4-4

(**A**) Stereo view of the lock-and-key 'Clasp' motif connecting two active site pockets of adGSTD4-4. The surface of the dimeric enzyme is shown in grey, GSH in each active site in yellow, the active-site amino acids in green and the Clasp residues in blue. Five of the six Clasp amino acids are also active-site residues. The top panel is looking down on to the 2-fold axis at the two active sites, which are diagonal to each other. The arrow in the top panel points to the interface groove that runs across the protein. The middle panel shows the GST rotated 90° in the direction indicated and the bottom panel shows the GST rotated a further 90° in the same direction. (**B**) Stereo view showing communication of GSH binding from one active site to the other through residues involved in the Clasp motif. Crystal structure of adGSTD4-4 (PDB id: 1JLW) is superimposed on adGSTD3-3 (PDB id: 1JLV) by fitting 1616 backbone atoms, with an R.M.S.D. (root mean square deviation) of 0.82 Å (1 Å = 0.1 nm). Distances between centroids of aromatic 'key' residues are monitored from adGSTD4-4, whereas distances of GSH-interacting residues are monitored from the adGSTD3-3 enzyme complex. Amino acid labelling is for adGSTD4-4. Amino acid residues of adGSTD4-4 and adGSTD3-3 are coloured in blue and green respectively. The surface representation is of 'lock' residues from the subunit partner.

structure suggests that His-38 is a G-site residue in close contact with the glycine moiety of GSH. Therefore an alteration at His-38 may be transmitted to the lock-and-key 'Clasp' motif by the glutamyl moiety of GSH (Figure 7B). For subunit interface residues, co-operativity for GSH binding was evident in studies of Tyr-50 of human GSTP1-1 [32] as well as co-operativity for GSH conjugation of 4-hydroxynonenal through Arg-69 of murine GSTA4-4 [39] and Asp-101 of human GSTA1-1 [40]. As a whole, although the co-operativity mechanism upon substrate binding is unclear, the subunit communication is apparently triggered from one substrate binding site to the other neighbouring subunit through an existing subunit interface interaction that varies among the GST classes, and the Clasp motif seems to possess a major role in Delta class GSTs.

The Val-107 position exhibited the greatest influence on enzymatic properties when substituted with charged residues. This suggests that a hydrophobic amino acid is not necessary at this position, as shown by V107N. However, decreases in catalytic rates and affinity towards GSH with co-operativity on GSH binding of V107D and V107K suggest that these replacements might create additional electrostatic interactions to residues in close proximity, such as Glu-65 or Arg-67, that subsequently cause structural perturbation to the G-site. Particularly, the Val-107 position is of interest because almost all substitutions seemed to enhance structural stability of the enzyme, especially V107A. It is very unusual for mutants to be significantly more stable than the wild-type. The Clasp motif is composed of hydrophobic residues that can stabilize the structure through hydrophobic force as well as polar/charged residues that would maintain structural integrity by ionic interactions. The changes at the Val-107 position appear to contribute stabilizing forces between subunits and weaken conformational strain of the dimerization. V107A displayed appreciably improved stability while maintaining functionality.

There was no secondary or tertiary structural changes detected by CD or intrinsic fluorescence measurements of tryptophan. However, intensity differences of ANS binding indicate conformational alterations at the quaternary level. Blue shift of the fluorescence emission maximum of bound ANS indicates that the ANS-binding site in adGSTD4-4 is similar to hGSTA1-1 [30] and pGSTP1-1 [41] with an emission maximum of approx. 480 nm, but more hydrophobic than in squid GSTS1-1 [13], hGSTM1-1 [14] and rGSTM1-1 [31] which have emission

maxima in the range 490–500 nm. In hGSTA1-1, ANS binding was suggested to be at the cleft in the dimer interface binding one molecule per subunit in a native protein [42]. Assuming that ANS binding of adGSTD4-4 is also located along the subunit interface, the present study shows that the Clasp motif influenced ANS binding. Since ANS fluorescence is quenched by water, the reduction of fluorescence intensity of protein-bound ANS in mutants illustrates greater exposure of ANS to solvent. This suggests that amino acid substitution to either Phe-104 or Val-107 alters the binding-site topology/solvent exposure for ANS.

The aromatic stacking of the 'key' residues suggests aromatic residues to be important for enzyme stability, as shown by half-life data for F104Y, F104W and F104H, although these replacements are not always favourable for catalytic function. The presence of aromatic residues protruding from one subunit to the other was suggested to be advantageous for increasing interface affinity, hence gluing protein subunits together [43]. However, different aromatic residues employed in diverse Delta class GSTs would generate isoform-specific subunit interfaces. Therefore substitutions with 'key' residues from other Delta class GSTs such as in F104Y and F104H appear to induce conformation changes that impact upon catalytic function.

Phenylalanine residues interacting across a 2-fold axis also were shown at the dimer interface of the TIM (triosephosphate isomerase) enzyme family. The interface between TIM subunits is mainly composed of loops 1–3 from both monomers. At the tip of loop 2 in trypanosomal TIM, a phenylalanine residue (Phe-45) forms a hydrophobic contact across the dimer interface to the equivalent residue on the other subunit. In *Escherichia coli* TIM, the residue was replaced by a glutamate residue (Glu-46) [44]. The Glu-46 also interacts with its corresponding residue on the neighbouring subunit contributing extensive van der Waals contacts with its local environment, as a result inducing conformational changes to the remaining intersubunit contacts which are different from that observed in other TIMs [44]. This implies that intersubunit residue interactions of oligomeric enzymes are to stabilize quaternary structure or dimerization. With similar features to GSTs, all TIMs are active only in the dimeric form, although each monomer has its own active site [45]. In view of an important glycolytic function, TIMs are of major interest in recent years as a potential target for therapeutic drug design, principally by disturbing some of the intersubunit contacts of the protein. For example, disruption of subunit assembly through effects on pi–pi interactions of two aromatic clusters in the interface of trypanosomal TIM [46,47] and *Plasmodium falciparum* TIM [48,49] was investigated for anti-trypanosomal agents and antimalarial drug design.

We have shown that an intersubunit lock-and-key 'Clasp' motif of adGSTD4-4 demonstrates functional and structural significance of the amino acids that interact across the dimer interface. Although residues of this motif do not provide the only interaction between subunits of adGSTD4-4, it is noteworthy that the unique characteristic of aromatic stacking in the middle of the dimer interface in fact connects the two active sites, enabling them to work in a co-operative manner. Evidence of allosteric effects suggests an important role for this particular intersubunit architecture in regulating catalytic activity through conformational transitions of subunits. Quaternary structural changes of all mutants detected by ANS dye binding suggest that subunit assembly or dimerization basically manipulates subunit communication. The observation of co-operativity in the mutants also implies that GSH ligand binding and dimerization are linked, consistent with the ANS-indicated quaternary structural changes; consequently, GSTs are catalytically active only in their dimeric forms. Correlations between oligomerization and ligand binding have also been shown for many other enzymes, such as dimerization of pyrophosphatase subunits improving its ligand binding, and vice versa with active-site adjustments upon metal cofactor or substrate binding increasing the stability of the dimer [50].

In conclusion, for GSTs, the lock-and-key motif in general, and especially the 'Clasp' motif with the pi–pi interaction, appear to play a pivotal role in subunit communication between active sites as well as in stabilizing the quaternary structure. Continued elucidation of the mechanism of positive co-operativity between subunits of oligomeric proteins would provide useful information for protein engineering.

This work was funded by the Thailand Research Fund. J.W. was supported by a Royal Golden Jubilee scholarship.

REFERENCES

1 Armstrong, R. N. (1991) Glutathione S-transferases: reaction mechanism, structure, and function. Chem. Res. Toxicol. **4**, 131–140
2 Wilce, M. C. J. and Parker, M. W. (1994) Structure and function of glutathione S-transferases. Biochim. Biophys. Acta **1205**, 1–18
3 Armstrong, R. N. (1997) Structure, catalytic mechanism, and evolution of the glutathione transferases. Chem. Res. Toxicol. **10**, 2–18
4 Hayes, J. D., Flanagan, J. U. and Jowsey, I. R. (2005) Glutathione transferases. Annu. Rev. Pharmacol. Toxicol. **45**, 51–88
5 Sheehan, D., Meade, G., Foley, V. M. and Dowd, C. A. (2001) Structure, function and evolution of glutathione transferases: implications for classification of non-mammalian members of an ancient enzyme superfamily. Biochem. J. **360**, 1–16
6 Ding, Y., Ortelli, F., Rossiter, L. C., Hemingway, J. and Ranson, H. (2003) The *Anopheles gambiae* glutathione transferase supergene family: annotation, phylogeny and expression profiles. BMC Genomics **4**, 35–50
7 Erhardt, J. and Dirr, H. (1995) Native dimer stabilizes the subunit tertiary structure of porcine class pi glutathione *S*-transferase. Eur. J. Biochem. **230**, 614–620
8 Le Trong, I., Strenkamp, R. E., Ibarra, C., Atkins, W. M. and Adman, E. T. (2002) 1.3-Å resolution structure of human glutathione S-transferase with S-hexyl glutathione bound reveals possible extended ligandin binding site. Proteins Struct. Funct. Genet. **48**, 618–627
9 Yassin, Z., Ortiz-Salmerón, E., García-Maroto, F., Barón, C. and García-Fuentes, L. (2004) Implications of the ligandin binding site on the binding of non-substrate ligands to *Schistosoma japonicum*-glutathione transferase. Biochim. Biophys. Acta **1698**, 227–237
10 Wallace, L. A., Sluis-Cremer, N. and Dirr, H. W. (1998) Equilibrium and kinetic unfolding properties of dimeric human glutathione transferase A1-1. Biochemistry **37**, 5320–5328
11 Dirr, H. W. and Reinemer, P. (1991) Equilibrium unfolding of class Pi glutathione *S*-transferase. Biochem. Biophys. Res. Commun. **180**, 294–300
12 Andújar-Sánchez, M., Clemente-Jiménez, J. M., Rodríguez-Vico, F., Las Heras-Vazquez, F. J., Jara-Pérez, V. and Cámara-Artigas, A. (2004) A monomer form of the glutathione S-transferase Y7F mutant from *Schistosoma japonicum* at acidic pH. Biochem. Biophys. Res. Commun. **314**, 6–10
13 Stevens, J. M., Hornby, J. A. T., Armstrong, R. N. and Dirr, H. W. (1998) Class sigma glutathione transferase unfolds via a dimeric and a monomeric intermediate: impact of subunit interface on conformational stability in the superfamily. Biochemistry **37**, 15534–15541
14 Hornby, J. A. T., Luo, J.-K., Stevens, J. M., Wallace, L. A., Kaplan, W., Armstrong, R. N. and Dirr, H. W. (2000) Equilibrium folding of dimeric class Mu glutathione transferases involves a stable monomeric intermediate. Biochemistry **39**, 12336–12344
15 Dirr, H. (2001) Folding and assembly of glutathione transferases. Chem. Biol. Interact. **133**, 19–23
16 Reinemer, P., Dirr, H. W., Ladenstein, R., Schäffer, J., Gallay, O. and Huber, R. (1991) The three-dimensional structure of class Pi glutathione S-transferase in complex with glutathione sulfonate at 2.3 Å resolution. EMBO J. **10**, 1997–2005
17 Ji, X., Zhang, P., Armstrong, R. N. and Gilliland, G. L. (1992) The three-dimensional structure of a glutathione S-transferase from the Mu gene class. Structural analysis of the binary complex of isoenzyme 3-3 and glutathione at 2.2-Å resolution. Biochemistry **31**, 10169–10184
18 Reinemer, P., Dirr, H. W., Ladenstein, R., Huber, R., Lo Bello, M., Federici, G. and Parker, M. W. (1992) Three-dimensional structure of class Pi glutathione S-transferase from human placenta in complex with S-hexylglutathione at 2.8 Å resolution. J. Mol. Biol. **227**, 214–226

19 Sinning, I., Kleywegt, G. J., Cowan, S. W., Reinemer, P., Dirr, H. W., Huber, R., Gilliland, G. L., Armstrong, R. N., Ji, X., Board, P. G. et al. (1993) Structure determination and refinement of human Alpha class glutathione transferase A1-1, and a comparison with the Mu and Pi class enzymes. J. Mol. Biol. **232**, 192–212
20 Ji, X., Von Rosenvinge, E. C., Johnson, W. W., Tomarev, S. I., Paitigorsky, J., Armstrong, R. N. and Gilliland, G. L. (1995) Three-dimensional structure, catalytic properties, and evolution of a sigma class glutathione transferase from squid, a progenitor of the lens S-crystallins of cephalopods. Biochemistry **34**, 5317–5328
21 Rossjohn, J., McKinstry, W. J., Oakley, A. J., Verger, D., Flanagan, J., Chelvanayagam, G., Tan, K.-L., Board, P. G. and Parker, M. W. (1998) Human theta class glutathione transferase: the crystal structure reveals a sulfate-binding pocket within a buried active site. Structure **6**, 309–322
22 Oakley, A. J., Harnnoi, T., Udomsinprasert, R., Jirajaroenrat, K., Ketterman, A. J. and Wilce, M. C. J. (2001) The crystal structures of glutathione S-transferases isozymes 1-3 and 1-4 from *Anopheles dirus* species B. Protein Sci. **10**, 2176–2185
23 Chelvanayagam, G., Parker, M. W. and Board, P. G. (2001) Fly fishing for GSTs: a unified nomenclature for mammalian and insect glutathione transferases. Chem. Biol. Interact. **133**, 256–260
24 Jirajaroenrat, K., Pongjaroenkit, S., Krittanai, C., Prapanthadara, L. and Ketterman, A. J. (2001) Heterologous expression and characterization of alternatively spliced glutathione S-transferases from a single *Anopheles* gene. Insect Biochem. Mol. Biol. **31**, 867–875
25 Vararattanavech, A. and Ketterman, A. (2003) Multiple roles of glutathione binding-site residues of glutathione S-transferase. Protein Pept. Lett. **10**, 441–448
26 Habig, W. H., Pabst, M. J. and Jakoby, W. B. (1974) Glutathione S-transferases. The first enzymatic step in mercapturic acid formation. J. Biol. Chem. **249**, 7130–7139
27 Bradford, M. M. (1976) A rapid and sensitive method for the quantitation of microgram quantities of protein utilizing the principle of protein-dye binding. Anal. Biochem. **72**, 248–254
28 Segel, I. H. (1993) Enzyme Kinetics. Behavior and Analysis of Rapid Equilibrium and Steady-State Enzyme Systems, John Wiley & Sons, New York
29 Gore, M. G. (2000) Spectrophotometry and Spectrofluorimetry, Oxford University Press, Oxford
30 Sayed, Y., Wallace, L. A. and Dirr, H. W. (2000) The hydrophobic lock-and-key intersubunit motif of glutathione transferase A1-1: implications for catalysis, ligandin function and stability. FEBS Lett. **465**, 169–172
31 Hornby, J. A. T., Codreanu, S. G., Armstrong, R. N. and Dirr, H. W. (2002) Molecular recognition at the dimer interface of a class Mu glutathione transferase: role of a hydrophobic interaction motif in dimer stability and protein function. Biochemistry **41**, 14238–14247
32 Stenberg, G., Abdalla, A.-M. and Mannervik, B. (2000) Tyrosine 50 at the subunit interface of dimeric human glutathione transferase P1-1 is a structural key residue for modulating protein stability and catalytic function. Biochem. Biophys. Res. Commun. **271**, 59–63
33 Ranson, H., Claudianos, C., Ortelli, F., Abgrall, C., Hemingway, J., Sharakhova, M. V., Unger, M., Collins, F. H. and Feyereisen, R. (2002) Evolution of supergene families associated with insecticide resistance. Science **298**, 179–181
34 Winayanuwattikun, P. and Ketterman, A. J. (2004) Catalytic and structural contributions for glutathione binding residues in a delta class glutathione S-transferase. Biochem. J. **382**, 751–757
35 Wongsantichon, J., Harnnoi, T. and Ketterman, A. J. (2003) A sensitive core region in the structure of glutathione S-transferases. Biochem. J. **373**, 759–765
36 Lo Bello, M., Nuccetelli, M., Chiessi, E., Lahm, A., Mazzetti, A. P., Parker, M. W., Tramontano, A., Federici, G. and Ricci, G. (1998) Mutations of Gly to Ala in human glutathione transferase P1-1 affect helix 2 (G-Site) and induce positive cooperativity in the binding of glutathione. J. Mol. Biol. **284**, 1717–1725
37 Ricci, G., Lo Bello, M., Caccuri, A. M., Pastore, A., Nuccetelli, M., Parker, M. W. and Federici, G. (1995) Site-directed mutagenesis of human glutathione transferase P1-1. Mutation of Cys-47 induces a positive cooperativity in glutathione transferase P1-1. J. Biol. Chem. **270**, 1243–1248
38 Lo Bello, M., Battistoni, A., Mazzetti, A. P., Board, P. G., Muramatsu, M., Federici, G. and Ricci, G. (1995) Site-directed mutatgenesis of human glutathione transferase P1-1: spectral, kinetic, and structural properties of Cys-47 and Lys-54 mutants. J. Biol. Chem. **270**, 1249–1253
39 Xiao, B., Singh, S. P., Nanduri, B., Awasthi, Y. C., Zimniak, P. and Ji, X. (1999) Crystal structure of a murine glutathione S-transferase in complex with a glutathione conjugate of 4-hydroxynon-2-enal in one subunit and glutathione in the other: evidence of signaling across the dimer interface. Biochemistry **38**, 11887–11894
40 Lien, S., Gustafsson, A., Andersson, A.-K. and Mannervik, B. (2001) Human glutathione transferase A1-1 demonstrates both half-of-the-sites and all-of-the-sites reactivity. J. Biol. Chem. **276**, 35599–35605
41 Bico, P., Erhardt, J., Kaplan, W. and Dirr, H. (1995) Porcine class Pi glutathione S-transferase: anionic ligand binding and conformational analysis. Biochim. Biophys. Acta **1247**, 225–230
42 Sayed, Y., Hornby, J. A. T., Lopez, M. and Dirr, H. (2002) Thermodynamics of the ligandin function of human class Alpha glutathione transferase A1-1: energetics of organic anion ligand binding. Biochem. J. **363**, 341–346
43 Jones, S. and Thornton, J. M. (1995) Protein-protein interactions: a review of protein dimer structure. Prog. Biophys. Mol. Biol. **63**, 31–65
44 Noble, M. E. M., Zeelen, J. Ph., Wierenga, R. K., Mainfroid, V., Goraj, K., Gohimont, A.-C. and Martial, J. A. (1993) Structure of triosephosphate isomerase from *Escherichia coli* determined at 2.6 Å resolution. Acta Crystallogr. Sect. D Biol. Crystallogr. **49**, 403–417
45 Waley, S. G. (1973) Refolding of triosephosphate isomerase. Biochem. J. **135**, 165–172
46 Téllez-Valencia, A., Olivares-Illana, V., Hernández-Santoyo, A., Pérez-Montfort, R., Costas, M., Rodríguez-Romero, A., López-Calahorra, F., de Gómez-Puyou, M. T. and Gómez-Puyou, A. (2004) Inactivation of triosephosphate isomerase from *Trypanosoma cruzi* by an agent that perturbs its dimer interface. J. Mol. Biol. **341**, 1355–1365
47 Espinoza-Fonseca, L. M. and Trujillo-Ferrara, J. G. (2005) Structural considerations for the rational design of selective anti-trypanosomal agents: the role of the aromatic clusters at the interface of triosephosphate isomerase dimer. Biochem. Biophys. Res. Commun. **328**, 922–928
48 Singh, S. K., Maithal, K., Balaram, H. and Balaram, P. (2001) Synthetic peptides as inactivators of multimeric enzymes: inhibition of *Plasmodium falciparum* triosephosphate isomerase by interface peptides. FEBS Lett. **501**, 19–23
49 Maithal, K., Ravindra, G., Nagaraj, G., Singh, S. K., Balaram, H. and Balaram, P. (2002) Subunit interface mutation disrupting an aromatic cluster in *Plasmodium falciparum* triosephosphate isomerase: effect on dimer stability. Protein Eng. **15**, 575–584
50 Salminen, A., Parfenyev, A. N., Salli, K., Efimova, I. S., Magretova, N. N., Goldman, A., Baykov, A. A. and Lahti, R. (2002) Modulation of dimer stability in yeast pyrophosphatase by mutations at the subunit interface and ligand binding to the active site. J. Biol. Chem. **277**, 15465–15471

Received 8 June 2005/7 September 2005; accepted 14 October 2005
Published as BJ Immediate Publication 14 October 2005, doi:10.1042/BJ20050915

Biochem. J. (2006) **393**, 89–95 (Printed in Great Britain) doi:10.1042/BJ20050555

The structural roles of a conserved small hydrophobic core in the active site and an ionic bridge in domain I of Delta class glutathione S-transferase

Ardcharaporn VARARATTANAVECH*, Peerada PROMMEENATE† and Albert J. KETTERMAN*[1]

*Institute of Molecular Biology and Genetics, Mahidol University, Salaya campus, 25/25 Putthamonthol Road 4, Salaya, Nakhon Pathom, 73170 Thailand, and †BEC Unit, National Center for Genetic Engineering and Biotechnology, 83 Moo 8, Thakham, Bangkhuntien, Bangkok 10150, Thailand

GSTs (glutathione S-transferases; E.C.2.5.1.18) are a supergene family of dimeric multifunctional enzymes that have a major role in detoxification pathways. Using a GST from the mosquito *Anopheles dirus* (adGSTD4-4), we have characterized the enzymatic and physical properties of Leu-6, Thr-31, Leu-33, Ala-35, Glu-37, Lys-40 and Glu-42. These residues generate two motifs located in the N-terminal domain (domain I) that are functionally conserved across GST classes. The aim of this study was to understand the function of these two motifs. The first motif is a small hydrophobic core in the G-site (glutathione-binding site) wall, and the second motif contains an ionic bridge at the N-terminus of the α2 helix and is also part of the G-site. The mutations in the small hydrophobic core appear to have structural effects, as shown by the thermal stability, refolding rate and intrinsic fluorescence differences. In the Delta class GST, interactions form an ionic bridge motif located at the beginning of the α2 helix. The data suggest that electrostatic interactions in the α2 helix are involved in α-helix stabilization, and disruption of this ionic bridge interaction changes the movement of the α2-helix region, thereby modulating the interaction of the enzyme with substrates. These results show that the small hydrophobic core and ionic bridge have a major impact on structural stabilization, as well as being required to maintain structural conformation of the enzyme. These structural effects are also transmitted to the active site to influence substrate binding and specificity. Therefore changes in the conformation of the G-site wall in the active site appear to be capable of exerting influences on the tertiary structural organization of the whole GST protein.

Key words: *Anopheles dirus*, Delta class glutathione S-transferase, mosquito, site-directed mutagenesis.

INTRODUCTION

Cytosolic GSTs (glutathione transferases; E.C. 2.5.1.18) are a family of dimeric isoenzymes that catalyse the conjugation of glutathione (GSH) to a variety of organic compounds containing an electrophilic centre [1,2], many with carcinogenic and toxic properties [3–7]. This reaction plays an important part in cellular metabolism, transport and subsequent excretion of toxic organic compounds. Other functions of GSTs have been reported, including binding of bilirubin and carcinogens [8,9], isomerization of maleyl acetoacetate [10–12], regulation of the stress kinases [13] and modulation of the ryanodine receptor (a calcium ion channel; [14,15]). A membrane-bound microsomal GST has been well characterized, and seems to be structurally and genetically distinct from the cytosolic enzymes [16]. Despite low sequence homology among GST classes, all of these isoenzymes have very similar tertiary structures, topography of the active site and GSH-binding site [17–19].

The *Anopheles dirus* mosquito is an important malaria vector in South-East Asia. AdGSTD4-4 is one of four alternatively spliced products from 7.5 kb of the *adgst1*AS1 gene (*An. dirus* alternatively spliced GST gene), which has been identified from an *An. dirus* genomic library [20]. All four spliced products have 45 identical amino acids at the N-terminus, and were named adGST1-1, adGST1-2, adGST1-3 and adGST1-4, according to insect GST nomenclature that is in use [that is, GST-(insect class 1)-(protein 1, 2, 3 and 4) respectively]. However, to be in alignment with a proposed universal GST nomenclature, these were renamed adGSTD1-1, adGSTD2-2, adGSTD3-3 and adGSTD4-4 [21,22]. The subunit number remains the same, since subunits were enumerated as they were initially discovered; 'D' refers to GST Delta class and '4-4' refers to the homodimeric isoenzyme. Two available tertiary structures, for adGSTD3-3 and adGSTD4-4, have assisted studies on these proteins [23]. Moreover, GSTs are highly conserved across the insect GST Delta class at the N-terminus (e.g. in *An. dirus*, *An. gambiae*, *Lucilia cuprina*, *Musca domestica* and *Drosophila melanogaster*). Therefore, in the present study, characterization of the N-terminal residues in adGSTD4-4 can be used to understand their functions for all insect Delta class GSTs [21,24].

Many hydrophobic residues are found inside a folded protein contributing to tertiary structure as a hydrophobic core. In the G-site (GSH-binding site), there are several such residues (Leu-6, Leu-33 and Ile-52) surrounding the glycine moiety of GSH. In previous studies [25,26], Leu-33 and Ile-52 were shown to impact on structural aspects of the protein, such as folding and stability. In the present paper, we extend our previous studies on the small hydrophobic core in the G-site wall containing Leu-6, Thr-31, Leu-33 and Ile-52.

An induced-fit mechanism apparently conserved across all GST classes occurs through movement of the α2 helix and its flanking regions to modulate G-site affinity for GSH; however, the relative contributions of residues to the flexibility in the α2 helix have not been determined [27–30]. At the N-terminus of the α2 helix, there is an ionic bridge interaction formed by Glu-37, Lys-40 and Glu-42. These residues are on the outside of the protein surface exposed to solvent. This ionic bridge interaction should impact upon movement of part of the active site, in addition to involvement in structural stabilization of the enzyme. Therefore the residues Glu-37, Lys-40 and Glu-42 were studied;

Abbreviations used: CDNB, 1-chloro-2,4-dinitrobenzene; DCNB, 1,2-dichloro-4-nitrobenzene; DTT, dithiothreitol; EA, ethacrynic acid; G-site, glutathione-binding site; GST, glutathione S-transferase; PNBC, *p*-nitrobenzyl chloride; PNPBr, *p*-nitrophenethyl bromide.

[1] To whom correspondence should be addressed (email frakt@mahidol.ac.th).

furthermore, Ala-35 was changed to arginine in an attempt to increase the ionic bridge interaction in the α2-helix region.

MATERIALS AND METHODS

Site-directed mutagenesis

The mutants were generated using the QuikChange® site-directed mutagenesis protocol (Stratagene). The mutagenic primers used in these experiments were designed based on the sequence of the adGSTD4-4 wild-type gene (GenBank® accession number AF273040). The oligonucleotide primers, each complementary to opposite strands of the vector, were extended during temperature cycling by means of *Pfu* DNA polymerase, which replicates both plasmid strands with high fidelity. Each mutant was randomly screened by restriction digestion analysis. Mutant plasmids could be distinguished from template by digestion with restriction enzyme corresponding to the restriction recognition site introduced by the mutagenic primers. Then, full-length DNA sequencing in both directions was performed to confirm the engineered clone sequence.

Protein expression and purification

After transformation of the mutant plasmids into *Escherichia coli* BL21(DE3)pLysS, protein expression was performed. All of the adGSTD4-4 clones were expressed in LB (Luria–Bertani) broth (containing 100 μg/ml ampicillin and 34 μg/ml chloramphenicol) and induced with 0.1 mM IPTG (isopropyl β-thiogalactoside) for 3 h at 37 °C. The pellets were collected and kept at − 20 °C until used. The expression levels of the protein were determined by SDS/PAGE. The cell pellets from 50 ml of culture were suspended by mixing with 4.8 ml of 50 mM Tris/HCl, pH 7.4, containing 1 mM EDTA, 200 μl of 100 mg/ml lysozyme and 3.6 μl of 1.4 M 2-mercaptoethanol. The suspension was incubated on ice for 20 min, then 50 μl of 1 M DTT (dithiothreitol) was added and the suspension was lysed at 900 lbf/in^2 (1 lbf/in^2 $\approx$ 6.9 kPa) in a French Press cell. The lysate was then centrifuged at 10000 ***g*** at 4 °C for 20 min. The supernatant containing the soluble form of the recombinant enzyme was separated from the pellet. The recombinant adGSTD4-4 mutants and the wild-type protein were purified by using either GSH-affinity chromatography or cation exchange followed by hydrophobic interaction chromatography, as described previously [25]. GSH-affinity chromatography was used according to manufacturer's instructions (Amersham Biosciences). A cation-exchange column (SP-XL) followed by hydrophobic interaction chromatography (phenyl-Sepharose column) was used for mutants that could not be purified on the GSH-affinity chromatography column. Briefly, cation-exchange chromatography employed an SP-XL column that was equilibrated with buffer A (20 mM phosphate buffer, pH 7.0, containing 10 mM DTT). After the lysate was applied to the column, the column was washed with buffer A. Then protein was eluted with a linear gradient from 80–500 mM NaCl in buffer A. The major amount of GST enzyme eluted in buffer A containing approx. 250 mM NaCl. The eluted GST fractions were pooled and loaded on to a phenyl-Sepharose column that was equilibrated with buffer A containing 2 M NaCl. Washing steps were performed by using stepwise decreases in salt concentration in buffer A. The GST enzyme was eluted from the phenyl-Sepharose column by using 20 % (v/v) ethylene glycol containing 10 mM DTT. The purified enzymes (in 50 mM potassium phosphate, pH 6.5) were stored in 50 % (v/v) glycerol at − 20 °C until used. Concentrations of the proteins were determined by Bio-Rad protein reagent (Bio-Rad) using BSA as the standard protein, and purity of the proteins was analysed by SDS/PAGE.

Enzymatic characterization

The standard GST assay was performed in 0.1 M potassium phosphate buffer, pH 6.5, in the presence of 3 mM CDNB (1-chloro-2,4-dinitrobenzene) and 10 mM GSH [31]. The rate of conjugation between GSH and CDNB was monitored by measuring continuously the increase in absorbance at 340 nm for 1 min using a SpectraMax 250 apparatus at 25–27 °C. The molar absorption coefficient of 9.6 $mM^{-1} \cdot cm^{-1}$ was used to convert absorbance into moles [32].

The kinetic experiments were performed as described previously [31]. In brief, CDNB was chosen as the electrophilic substrate for determination of V_{max}, K_m, k_{cat} and k_{cat}/K_m values. The kinetic parameters were determined by varying the CDNB concentration (0.031–3.0 mM) while GSH was held constant at a saturating concentration, and by varying GSH concentrations (0.25–20 mM) at a saturating concentration of CDNB. The initial rate of the enzymatic reaction was measured spectrophotometrically as described for the GST activity assay determination. The steady-state kinetics followed Michaelis–Menten kinetics, except where stated. The maximal velocity (V_{max}) and the Michaelis constant (K_m) were determined by non-linear regression software analysis (GraphPad Prism 4). The turnover number (or catalytic-centre activity; k_{cat}) and catalytic efficiency (k_{cat}/K_m) were calculated on an active-site basis using the subunit molecular mass of each enzyme. The kinetic parameters are the means $\pm$ S.D. for at least three independent experiments.

The specific activities towards several GST substrates were determined as described previously [31]. All measurements were performed at 25–27 °C in 0.1 M potassium phosphate buffer at either pH 6.5 or 7.5. The GST activities were measured with GSH and five hydrophobic substrates: CDNB, DCNB (1,2-dichloro-4-nitrobenzene), EA (ethacrynic acid), PNPBr (*p*-nitrophenethyl bromide) and PNBC (*p*-nitrobenzyl chloride). Specific activities were calculated using the molar absorption coefficient for each substrate [32].

Physical characterization

The enzymes at 0.1 mg/ml in 0.1 M phosphate buffer, pH 6.5, containing 1 mM EDTA and 5 mM DTT were incubated at 45 °C for various times, and the remaining activity was measured in the standard GST assay. Data were plotted as logarithms of the percentage of remaining activity against pre-incubation time. The half-life of the enzyme at 45 °C was calculated from the slope of the plot using the equation: slope $= k/2.3$, where $k = 0.693/t_{1/2}$.

Enzymes were completely unfolded by incubating 0.5 mg/ml enzymes in unfolding buffer [0.2 M phosphate buffer (pH 7.0)/1 mM EDTA/5 mM dithiothreitol] containing 4 M guanidinium chloride at room temperature ($\approx$25 °C) for 10 min. Unfolded enzymes were allowed to begin refolding by diluting 40-fold in 0.1 M phosphate buffer, pH 6.5, to a final guanidinium chloride concentration of 0.1 M. Appropriate aliquots from this incubation mixture were measured for reactivation by measuring GST activity as a function of time after dilution. GST activity versus time of refolding followed a non-linear regression single-exponential equation [33].

Intrinsic fluorescence of adGSTD4-4 was measured in a single-photon-counting spectrofluorimeter. Excitation was at 295 nm, and emission was scanned from 300–450 nm. Samples contained 0.1 mg/ml GST in 0.1 M potassium phosphate buffer, pH 6.5, and were prepared similarly for wild-type and mutant enzymes. The wavelength that gives the maximum fluorescence intensity (λ_{max}) and the fluorescence intensity at λ_{max} were observed. The experimental data were corrected for both dilution and inner-filter effects, and normalized after background subtraction.

Table 1 Steady-state kinetic constants using GSH and CDNB as GST substrates

The rate of conjugation was monitored continuously by measuring the increase in absorbance at 340 nm for 1 min. The units of V_{max}, k_{cat}, K_m and k_{cat}/K_m are μmol · min^{-1} · mg protein^{-1}, S^{-1}, mM and S^{-1} · mM^{-1} respectively.

			CDNB		GSH	
Enzyme	V_{max}	k_{cat}	K_m	k_{cat}/K_m	K_m	k_{cat}/K_m
Wild-type	62.5 ± 1.24	26.1	0.50 ± 0.02	51.8	0.50 ± 0.10	52.1
L33A	23.5 ± 0.5†	9.70	1.17 ± 0.05†	8.30	8.20 ± 0.43†	1.20
L33Y	0.32 ± 0.01†	0.14	0.81 ± 0.12†	0.17	1.10 ± 0.12§	0.13
L33F	1.55 ± 0.03†	0.65	1.30 ± 0.06†	0.50	2.42 ± 0.22†	0.27
L33I	53.0 ± 1.71†	22.2	0.73 ± 0.05§	30.3	0.42 ± 0.01	52.8
L6A	42.3 ± 1.64†	17.7	1.49 ± 0.15†	11.9	0.31 ± 0.01	57.1
T31A	23.3 ± 0.35†	9.73	0.77 ± 0.05‡	12.6	11.4 ± 0.53*†	0.85
I52A	0.630 ± 0.006†	0.26	0.32 ± 0.02	0.81	7.04 ± 0.05*†	0.04
I52L	43.8 ± 1.24†	18.3	0.74 ± 0.02‡	24.8	0.30 ± 0.04	61.1
E37A	48.5 ± 1.45†	20.4	0.54 ± 0.03	37.7	1.85 ± 0.09†	11.0
E37Q	62.8 ± 0.92	26.3	0.58 ± 0.05	45.3	2.26 ± 0.04†	11.6
K40A	51.3 ± 1.24†	21.5	0.62 ± 0.04	34.6	1.14 ± 0.08§	18.8
E42A	63.4 ± 1.95	26.5	0.57 ± 0.05	46.4	0.63 ± 0.04	42.0
A35R	53.6 ± 1.18†	22.4	0.52 ± 0.06	42.7	0.73 ± 0.05	30.7

* The mutants T31A and I52A showed positive co-operativity upon GSH binding, with Hill coefficients of 1.62 ± 0.09 and 1.49 ± 0.03 respectively.

ANOVA analysis revealed significant differences compared with the wild-type, where indicated: †$P < 0.001$; ‡$P < 0.01$; and §$P < 0.05$. The absence of a symbol indicates no significant difference compared with wild-type.

CD measurements in the far-UV region from 200–250 nm were performed with a spectropolarimeter. The enzymes at 0.2 mg/ml in 0.1 M phosphate buffer, pH 6.5, were measured at 25 °C. A cell of 1 cm path length and a 1 nm bandwidth were used. Spectra are the averages of ten scans after subtraction of the average of ten baseline scans.

RESULTS AND DISCUSSION

Protein expression and purification

In the present study we have characterized Leu-6, Thr-31, Leu-33, Ile-52, Ala-35, Glu-37, Lys-40 and Glu-42, located in domain I in the highly flexible loop region between the β2–α2 or α2–β3 loops. These residues were hypothesized to be involved in structural maintenance or stabilization of the proteins. The mutagenesis study was performed by individually changing each residue chosen to alanine and/or a conservative or non-conservative amino acid. In the present study, Leu-33 mutations generated for a previous report were included to extend that study with further experiments. An additional conservative amino acid replacement, L33I, was generated to confirm the function of Leu-33 in packing of the active site. In addition, Ala-35 was mutated to an arginine in an attempt to increase the ionic bridge interaction in the α2-helix region. All 13 engineered enzymes could be expressed in soluble form at 37 °C in *E. coli* lysates. Two procedures were utilized for protein purifications: an affinity chromatography on immobilized GSH or sequential purification by ion-exchange chromatography (SP-XL) followed by phenyl-Sepharose chromatography. The latter procedure was used for the engineered enzymes that could not be purified by GSH-affinity chromatography, including L33A, L33F, L33Y and T31A. Purified enzymes gave a single band on SDS/PAGE, with a size of approx. 25 kDa, corresponding to the calculated molecular mass of the GST subunits.

Enzymatic characterization

The kinetic constants for CDNB and GSH show that most of the residue positions only slightly affected enzyme catalysis (Table 1). All of these residues are located in the GSH-binding site, so it is interesting to note that Leu-6 changed the active-site conformation enough to significantly increase K_m for the hydrophobic substrate CDNB (3-fold; ANOVA, $P < 0.001$) and decrease the K_m for GSH (1.7-fold; ANOVA, $P < 0.05$). GSH steady-state kinetics of the T31A enzyme showed positive co-operativity, with a Hill coefficient of 1.62 ± 0.09 (the Hill coefficient for wild-type enzyme is 0.91 ± 0.02). Positive co-operativity indicates GSH binding in the first active site, then facilitates another GSH binding in the second active site by increasing binding affinity of the vacant binding site [34]. Thr-31 is located in the loop before the α2 helix, and its side chain faces into the G-site in addition to being close to His-38, which interacts directly with GSH. The alanine mutation at Thr-31 must cause a packing rearrangement of the G-site, which increases the K_m for GSH 23-fold, as well as generating intersubunit communication between the two active sites. One explanation is that the rearrangement would disturb His-38, which directly interacts with GSH. Mutations of His-38 were shown to have large effects on GSH binding affinity, as well as generating positive co-operativity [25]. The mutation of Ile-52 to alanine caused very large effects on catalysis, as exhibited by a decrease in k_{cat} (1 % of wild-type activity) and affinity (14-fold increase in K_m), as well as positive co-operativity. The conservative change of Ile-52 to leucine showed smaller effects, including a slight increase in GSH affinity. Mutations of ionic-bridge residues showed only small effects on catalysis, although the GSH binding affinity was affected to a greater extent. Both Glu-37 and Lys-40, located in the middle of the β2–α2 loop, appeared to impact more, suggesting a greater influence on α2-helix movement during induced-fit conformational changes.

Although the residues studied are in or behind G-site residues, the substrate-specificity results show that these mutations yielded various changes in specificity for several hydrophobic substrates compared with wild-type GST (Table 2). As shown by the kinetic constants, these residues are not critical for enzyme catalysis or substrate binding; however, the mutations influence the enzymes' hydrophobic substrate interaction and catalysis. Compared with wild-type, the mutations at Leu-6, Thr-31 and Ile-52 resulted in decreases in specificity towards several substrates, especially

Table 2 Substrate specificity changes of the engineered enzymes relative to the wild-type adGSTD4-4

The substrates were used at the following concentrations: CDNB, 3 mM; DCNB, 1 mM; PNPBr, 0.1 mM; PNBC, 0.1 mM; and EA, 0.2 mM. The reactions were performed at a constant GSH concentration.

		Substrate specificity (μmol · min^{-1} · mg protein^{-1})				
Enzyme	Substrate . . .	CDNB	DCNB	EA	PNPBr	PNBC
Wild-type		52.5 ± 0.52	0.035 ± 0.006	0.286 ± 0.062	0.074 ± 0.012	0.064 ± 0.002*
L33A		18.3 ± 0.3*	0.031 ± 0.015	0.332 ± 0.061	0.019 ± 0.004*	0.024 ± 0.004*
L33Y		0.253 ± 0.001*	< 0.0016*	0.092 ± 0.006*	< 0.006*	< 0.007*
L33F		1.023 ± 0.018*	< 0.0016*	0.059 ± 0.007*	< 0.006*	< 0.007*
L33I		45.4 ± 0.37*	0.047 ± 0.002‡	0.247 ± 0.006	0.007 ± 0.001*	0.044 ± 0.002*
L6A		28.0 ± 0.53*	0.0053 ± 0.0003*	0.380 ± 0.004	0.017 ± 0.002*	0.031 ± 0.002*
T31A		17.5 ± 0.33*	0.0059 ± 0.0006*	0.186 ± 0.008†	< 0.002*	0.039 ± 0.004*
I52A		0.511 ± 0.010*	< 0.001*	0.307 ± 0.023	< 0.004*	0.011 ± 0.001*
I52L		35.4 ± 0.36*	0.025 ± 0.001	0.373 ± 0.005	0.018 ± 0.001*	0.036 ± 0.003*
E37A		39.1 ± 0.74*	0.055 ± 0.005†	0.135 ± 0.010*	< 0.008*	0.122 ± 0.006*
E37Q		47.8 ± 0.22*	0.053 ± 0.001†	0.431 ± 0.026*	0.033 ± 0.004*	0.062 ± 0.002
K40A		37.7 ± 0.16*	0.037 ± 0.001	0.110 ± 0.004*	0.038 ± 0.003*	0.080 ± 0.002*
E42A		55.1 ± 0.40‡	0.059 ± 0.001*	0.24 ± 0.02	0.016 ± 0.001*	0.045 ± 0.002*
A35R		44.9 ± 0.56*	0.056 ± 0.003*	0.37 ± 0.04	0.020 ± 0.001*	0.041 ± 0.002*

ANOVA analysis revealed significant differences compared with the wild-type, where indicated: *$P < 0.001$; †$P < 0.01$; and ‡$P < 0.05$. The absence of a symbol indicates no significant difference compared with wild-type.

DCNB and PNPBr. The remaining mutations displayed major effects with regard to PNPBr, but specificities were comparable with that of wild-type for CDNB. However, changes in specificity for EA and PNBC as substrates were varied.

Both GSH- and hydrophobic-substrate-binding sites are located in different parts of the same active-site pocket. Therefore differences in the mutant enzymes appear to occur from changes in active-site conformation that disturb orientation of the substrates, as found in the wild-type enzyme. In addition, binding modes and orientations of the various substrates in the active site appear to be unique, as shown by dissimilar effects on specificity of the mutant enzymes.

Physical characterization

The half-life at 45 °C of the mutant enzymes compared with adGSTD4-4 wild-type showed that the mutants decreased in stability, except for T31A, which displayed a slight increase (Table 3). L6A decreased enzyme stability approx. 9-fold, showing a major impact on structural maintenance. The mutation of ionic-bridge residues (Glu-37, Lys-40 and Glu-42) to alanine and the mutation of Ala-35 to arginine also resulted in decreases in enzyme stability, suggesting that the mutations cause a rearrangement of the α2-helix, owing to disruption of the ionic bridge interaction. The replacement of positively charged Glu-37 with a similarly sized, polar glutamine residue decreased enzyme stability 2.3-fold, supporting the idea of charge distribution involvement in structural stabilization of the enzyme. However, the attempt to increase charge distribution with the A35R mutation decreased the half-life of the enzyme 1.7-fold. This suggests that residues in the β2–α2-helix loop appear to affect helix dipole moment, which impacts upon structural stabilization of the enzyme.

AdGSTD4-4 became completely unfolded after incubation for 10 min in 4 M guanidinium chloride, as monitored by intrinsic fluorescence and CD spectroscopy. Refolding rates and percentages of recovered activities of wild-type and mutant enzymes were determined (Table 4). L6A showed a decreased refolding rate (2.5-fold compared with wild-type), suggesting the initial folding process was disturbed, which also slightly reduced the activity recovered as well as decreasing the enzyme stability, as described above. L33A showed an increased refolding rate of 1.6-fold and

Table 3 Thermal stability of wild-type and engineered adGSTD4-4 mutants at 45 °C

The remaining GST activity was measured after incubating the enzyme at various time points at 45 °C.

Enzyme	Half-life ($t_{1/2}$) at 45 °C (min)
Wild-type	15.3 ± 0.31
L33A	45.3 ± 1.56*
L33Y	71.7 ± 1.71*
L33F	212 ± 17.9*
L33I	30.4 ± 1.5*
L6A	1.73 ± 0.01*
T31A	22.7 ± 1.77*
I52A	9.58 ± 0.65*
I52L	18.1 ± 1.33
E37A	1.73 ± 0.04*
E37Q	6.54 ± 0.54*
K40A	3.94 ± 0.20*
E42A	8.44 ± 0.48*
A35R	9.01 ± 0.54*

ANOVA analysis revealed a significant difference compared with the wild-type enzyme, where indicated (*$P < 0.001$); the absence of an asterisk indicates no significant difference compared with wild-type (in these experiments, exclusively the I52L mutant).

3-fold greater stability than the wild-type enzyme, demonstrating that its final conformation is more stable. However, the mutants L33I and I52L showed only small effects on the refolding process. The ionic bridge mutations (Glu-37, Lys-40, Glu-42 and Ala-35) all decreased enzyme stability in the range 1.8- to 8.9-fold, although the refolding rates were altered differently. These data suggest that the changes in the refolding rates occur from differential 'flexing' of the engineered enzyme. An interesting observation for the E37A enzyme was that it possessed a slightly increased refolding rate of 1.3-fold, as well as a 1.8-fold increase in recovered activity, even though the enzyme had an 8.9-fold decreased stability (Table 3). This suggests that this residue position contributes to structural maintenance, but not to initial folding events. Therefore the ionic bridge motif appears to have a function in structural maintenance and modulation of α2-helix movement, as well as a minor effect on folding.

Table 4 Refolding rate constants and percentages of recovered activity from the reversible refolding experiment for the wild-type adGSTD4-4 enzyme and its engineered mutants

The proteins were denatured initially with 4 M guanidinium chloride at room temperature for 10 min. Refolding rate constants (k_{ref}) were determined by non-linear regression analysis using a single-exponential equation (GraphPad Prism 4).

	Refolding experiment	
Enzyme	Refolding rate constant (min^{-1})	% recovery
Wild-type	0.54 ± 0.02	20.7 ± 0.67
L33A	0.85 ± 0.05*	18.6 ± 0.55
L33Y	nd	nd
L33F	nd	nd
L33I	0.53 ± 0.01	14.7 ± 0.76*
L6A	0.22 ± 0.02*	14.9 ± 0.77*
T31A	0.41 ± 0.02*	10.1 ± 0.41*
I52A	nd	nd
I52L	0.67 ± 0.02*	20.1 ± 0.61
E37A	0.69 ± 0.05*	37.7 ± 1.49*
E37Q	0.74 ± 0.03*	14.0 ± 0.32*
K40A	0.26 ± 0.02*	14.2 ± 0.95*
E42A	0.32 ± 0.02*	31.5 ± 1.44*
A35R	0.40 ± 0.01‡	29.6 ± 0.64†

ANOVA analysis revealed significant differences compared with the wild-type, where indicated: *$P < 0.001$; †$P < 0.01$; and ‡$P < 0.05$. The absence of a symbol indicates no significant difference compared with the wild-type. nd, not determined (low activity precluded measurement).

Table 5 The maximum emission wavelength (λ_{max}) and intrinsic fluorescence intensity at λ_{max} of tryptophan fluorescence of adGSTD4-4 and the engineered enzymes

The excitation wavelength (λ_{ex}) was set at 295 nm, and emission was scanned from 300–450 nm. Samples ($n = 3$) contained 0.1 mg/ml protein in 0.1 M potassium phosphate buffer, pH 6.5. The percentage intensities compared with wild-type enzyme were measured at fluorescence λ_{max} averaged over three scans, corrected for dilution and inner-filter effects.

	Intrinsic fluorescence (λ_{ex} 295 nm)	
Enzyme	λ_{max} (nm)	% intensity
Wild-type	333 ± 0	100
L33A	334 ± 0	60.8*
L33Y	334 ± 0	51.6*
L33F	334 ± 0	47.9*
L33I	333 ± 0	109.1
L6A	334 ± 0	138.6*
T31A	334 ± 0	99.1
I52A	339 ± 0	98.8
I52L	333 ± 0	115.5*
E37A	333 ± 0	66.8*
E37Q	334 ± 0	107.7
K40A	334 ± 0	68.4*
E42A	333 ± 0	75.5*
A35R	334 ± 0	102.1

ANOVA analysis revealed a significant difference compared with the wild-type enzyme, where indicated (*$P < 0.001$); the absence of an asterisk indicates no significant difference compared with the wild-type.

The intrinsic fluorescence property of tryptophan in proteins is modulated by various interactions in the environment around the tryptophan residue. Therefore changes in λ_{max} and the fluorescence intensity of the intrinsic fluorescence spectrum can suggest that changes have occurred in the local tertiary structure of the protein. There are two tryptophan residues present in adGSTD4-4 (Trp-64 and Trp-191). Trp-64 has the side chain exposed to solvent, located in the subunit interface at the base of the GSH-binding site, whereas Trp-191 is buried in the interior of domain II. Therefore this technique can be used to monitor active-site conformation indirectly. The same protein concentration of wild-type and mutant enzymes was used for comparison of the maximum emission wavelengths (λ_{max}) and fluorescence intensities (Table 5). The λ_{max} of intrinsic tryptophan fluorescence for the mutants was approximately the same as that for the wild-type (333 ± 1 nm), except for I52A, which displayed a red-shifted spectrum with a λ_{max} at 339 nm. Therefore I52A affected tertiary structure at the active site, causing a change in polarity in the tryptophan environment. In addition, there were differences in intensity of fluorescence between wild-type and several mutant proteins, indicating a limited conformational alteration in the active site of the final structure. The charged residue mutations (Glu-37, Lys-40 and Glu-42) displayed decreased fluorescence intensity. Located at the C-terminal end of the β4-sheet, Trp-64 is in proximity with the α2-helix from which the ND2 side-chain nitrogen of Asn-47 extends 3.07 Å (1 Å = 0.1 nm) to have a cation–π interaction with the aromatic ring of Trp-64. Disruption of the ionic bridge interaction would most likely increase flexibility of the α2 helix, thereby disrupting this interaction and increasing solvent exposure of Trp-64, with a concomitant decrease in fluorescence. In addition, a rearrangement of the active-site topology appears to occur for the G-site-residue mutations Leu-6, Thr-31, Leu-33 and Ile-52, which affects orientation of Trp-64, as well as of its neighbouring residues, which also may contribute to changes in fluorescence.

CD spectroscopy was performed to determine whether secondary structure content of the proteins had changed. CD spectroscopy showed two 'troughs' at 210 and 222 nm, owing to the high helical content of the proteins. All the proteins had a similar far-UV CD spectrum (results not shown). This shows that, although some mutations affect active-site conformation, the overall secondary structure content of the enzymes has not been altered.

In the present paper, we have sought to understand the function of two features in domain I of adGSTD4-4 that have been found in all insect Delta class GSTs: a small hydrophobic core in the G-site and an ionic bridge at the N-terminus of the α2-helix. The available structure of adGSTD4-4 shows that Leu-6, Thr-31, Leu-33 and Ile-52 form part of the wall in the GSH-binding site (Figure 1A). The mutation of Leu-6 leads to a structural perturbation in the G-site, resulting in altered substrate specificity, decreased stability, as well as modulation of the refolding of the enzyme. From a previous study [25], increasing hydrophobicity of the residue in the Leu-33 position increased enzyme stability 3- to 14-fold, although the mutants lost enzyme activity (0.9–62 % compared with wild type). In the present study, Leu-33 mutations altered intrinsic fluorescence intensity when compared with wild-type enzyme, suggesting changes in topology of the active site. The change in structural conformation and active-site topology of the Leu-33 mutations was confirmed by a trypsin proteolytic experiment: the mutation of Leu-33 to alanine increased the proteolytic rate almost 2-fold compared with the wild-type (results not shown).The conservative mutation of Leu-33 to isoleucine resulted in small effects on specificity and catalysis, the most notable of which was a 10-fold decrease for PNBr. L33I displayed only a 2-fold increase in half-life, with all other physical properties being similar to those of the wild-type. These data support the idea that the role of Leu-33 is to contribute to the small hydrophobic core for structural maintenance. Previously, Ile-52 had been characterized in adGSTD3-3 [26]. In the tertiary structures of adGSTD3-3 (PDB identification no. 1JLV) and adGSTD4-4 (PDB identification no. 1JLW), the location of Ile-52 is identical in both structures. A mutation of Ile-52 to alanine showed a decrease in enzyme stability of approx. 5.5-fold, a 24-fold increase

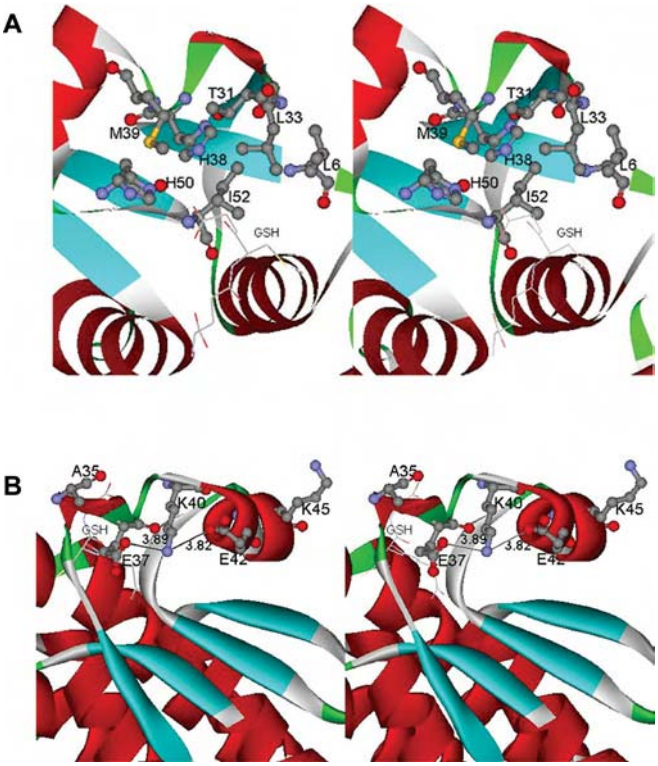

Figure 1 Stereo views of domain I region characterized in this study

(**A**) Stereo view of the active-site pocket of adGSTD4-4. Leu-6, Leu-33, Thr-31 and Ile-52 form part of the G-site wall. The hydrophobic residues Leu-6, Leu-33 and Ile-52 form a small hydrophobic cluster in the G-site. GSH in the active site is shown in stick form. (**B**) Stereo view of the charged residues located near the α2 helix of adGSTD4-4. The ionic bridge motif formed by the charged residues (Glu-37, Lys-40 and Glu-42) is exposed to the solvent, located at the N-terminus of the α2 helix. GSH in the active site is shown in stick form. Both parts of the Figure were created with Accelrys DS ViewerPro 5.0.

in the K_m for GSH and a 2-fold decrease in k_{cat} [26]. For adGSTD4-4, the I52A mutant showed different effects, with a 1.6-fold decrease in stability, a 14-fold increase in the K_m for GSH and a 100-fold decrease in k_{cat}. The conservative replacement of Ile-52 with leucine showed smaller effects in enzyme properties, and the I52L mutant was very similar to the wild-type enzyme in terms of its physical properties. These data show that Ile-52 has roles in structural integrity and maintenance, as well as in the initial folding of the protein. Therefore it may be surmised that the small hydrophobic core formed by Leu-6, Leu-33 and Ile-52 at the G-site wall plays a critical role in packing and stabilization of the active site into an appropriate conformation, and this packing also impacts upon tertiary structure of the whole protein. A study of available crystal structures of other GST classes shows several hydrophobic residues clustered in the G-site wall in a similar fashion. For example, in the human GST isoenzyme hGSTP1-1 (PDB identification no. 11GS), these residues are Phe-8, Trp-38 and Leu-52, whereas in maize GST-I (PDB identification no. 1AXD) they are Phe-35, Ile-33 and Val-54. These residues are located in the G-site wall, and therefore are probably involved in packing of the active-site conformation as well.

Several studies show α2 helices of Delta, Theta, Sigma and Pi GSTs to have high conformational flexibility and to display the highest temperature factors of the whole protein [29,35,36]. In insect Delta class GSTs, there is a unique ionic bridge motif exposed to solvent on the α2 helix consisting of three charged residues: Glu-37, Lys-40 and Glu-42 (Figure 1B). The data suggest that this feature influences the flexibility of the α2 helix and its flanking region in Delta class GSTs. In the present study, the alanine mutations of Glu-37, Lys-40 and Glu-42 in adGSTD4-4 showed structural effects in the domain I region, as shown by decreased thermal stability and changes in refolding rates and intrinsic fluorescence intensities. The apparent changes in α2-helix movements resulting from mutations of the charged residues also appear to modulate interaction of the enzymes with substrates, as shown by changes in substrate specificity. The charged residues and ionic bridge motif in this region appear to play a role in maintenance of a stable conformation, as well as in influencing refolding of the enzymes. The attempt to increase the ionic-bridge interaction by constructing the A35R mutant did not result in any improvement in kinetic properties or enzyme stability, although it did appear to have some effects on substrate specificity. This may be because the side chain of arginine in A35R is not in the correct orientation for interacting with the other residues. In hGSTP1-1, there is an ion pair formed by Cys-47 and Lys-54 at the end of the α2 helix. The disruption of the electrostatic interaction between Cys-47 and Lys-54 causes an increased mobility of the α2 helix, local structural changes, lowered GSH-binding affinity and strong positive co-operativity towards GSH [37,38]. Therefore electrostatic interactions in the α2 helix appear to be involved in α-helix stabilization for GSTs in general. In cephalopod Sigma class GSTS1-1, charged residues at each end of the α2 helix (Asp-37 and Lys-42 at the N- and C-termini of the α2 helix respectively) have been described to interact with the helix dipole, and thereby stabilize the helix [39]. This feature is also found in adGSTD4-4 (residues Glu-37 and Lys-45), as well as in the blood fluke (*Schistosoma japonicum*) GST, Sj26GST, a GST of 26 kDa (PDB identification no. 1M9A; residues Glu-37 and Lys-44). These charged residues would appear therefore to interact with the helix dipole, and contribute to stabilizing the α2 helix.

In the present study of adGSTD4-4, we examined the roles of conserved residues in the N-terminal domain (domain I) that are involved in a small hydrophobic core in the G-site wall and an ionic bridge motif in the N-terminus of the α2 helix. The results have shown that both the small hydrophobic core and the ionic bridge motif can have a major impact on structural stabilization, as well as being required to maintain the structural conformation of the enzyme. The packing of the small hydrophobic core is important for structural integrity and, as part of the G-site wall, directly affects GSH binding. These packing effects in the active site appear not only to affect the G-site, but are transmitted through rearrangement of the active-site residues to the adjacent H-site, thereby impacting on specificity as well as catalysis.

This work was funded by the TRF (Thailand Research Fund). A.V. was supported by a Royal Golden Jubilee Ph.D. Research Scholarship.

REFERENCES

1 Jakoby, W. B. and Habig, W. H. (1980) Glutathione transferases. In Enzymatic Basis of Detoxication, vol. 2 (Jakoby, W. B., ed.), pp. 63–94, Academic Press, New York
2 Hayes, J. D., Flanagan, J. U. and Jowsey, I. R. (2005) Glutathione transferases. Annu. Rev. Pharmacol. Toxicol. **45**, 51–88
3 Armstrong, R. N. (1997) Structure, catalytic mechanism, and evolution of the glutathione transferases. Chem. Res. Toxicol. **10**, 2–18
4 Mannervik, B., Funk, M., Frank, H. and Seidel, A. (1996) Glutathione S-transferase A1-1-catalysed conjugation of bay and fjord region diol epoxides of polycyclic aromatic hydrocarbons with glutathione. Carcinogenesis **17**, 1491–1498
5 Mannervik, B. and Danielson, U. H. (1988) Glutathione transferases – structure and catalytic activity. CRC Crit. Rev. Biochem. **23**, 283–337
6 Wilce, M. C. J. and Parker, M. W. (1994) Structure and function of glutathione S-transferases. Biochim. Biophys. Acta **1205**, 1–18

7 Ketterer, B. (2001) A bird's eye view of the glutathione transferase field. Chem. Biol. Interact. **138**, 27–42
8 Litwack, G., Ketterer, B. and Arias, I. M. (1971) Ligandin: a hepatic protein which binds steroids, bilirubin, carcinogens and a number of exogenous organic anions. Nature (London) **234**, 466–467
9 Hayes, J. D. and Pulford, D. J. (1995) The glutathione S-transferase supergene family: regulation of GST and the contribution of the isoenzymes to cancer chemoprotection and drug resistance. CRC Crit. Rev. Biochem. Mol. Biol. **30**, 445–600
10 Board, P., Baker, R. T., Chelvanayagam, G. and Jermiin, L. S. (1997) Zeta, a novel class of glutathione transferases in a range of species from plants to humans. Biochem. J. **328**, 929–935
11 Polekhina, G., Board, P. G., Blackburn, A. C. and Parker, M. W. (2001) Crystal structure of maleylacetoacetate isomerase/glutathione transferase zeta reveals the molecular basis for its remarkable catalytic promiscuity. Biochemistry **40**, 1567–1576
12 Board, P. G., Taylor, M. C., Coggan, M., Parker, M. W., Lantum, H. B. and Anders, M. W. (2003) Clarification of the role of key active site residues of glutathione transferase Zeta/maleylacetoacetate isomerase by a new spectrophotometric technique. Biochem. J. **374**, 731–737
13 Adler, V., Yin, Z., Fuchs, S. Y., Benezra, M., Rosario, L., Tew, K. D., Pincus, M. R., Sardana, M., Henderson, C. J., Wolf, C. R. et al. (1999) Regulation of JNK signaling by GSTp. EMBO J. **18**, 1321–1334
14 Dulhunty, A., Gage, P., Curtis, S., Chelvanayagam, G. and Board, P. (2001) The glutathione transferase structural family includes a nuclear chloride channel and a ryanodine receptor calcium release channel modulator. J. Biol. Chem. **276**, 3319–3323
15 Board, P. G., Coggan, M., Chelvanayagam, G., Easteal, S., Jermiin, L. S., Schulte, G. K., Danley, D. E., Hoth, L. R., Griffor, M. C., Kamath, A. V. et al. (2000) Identification, characterization, and crystal structure of the omega class glutathione transferases. J. Biol. Chem. **275**, 24798–24806
16 Jakobsson, P.-J., Morgenstern, R., Mancini, J., Ford-Hutchinson, A. and Persson, B. (1999) Common structural features of MAPEG – a widespread superfamily of membrane associated proteins with highly divergent functions in eicosanoid and glutathione metabolism. Protein Sci. **8**, 689–692
17 Dirr, H., Reinemer, P. and Huber, R. (1994) X-ray crystal structures of cytosolic glutathione S-transferases. Implications for protein architecture, substrate recognition and catalytic function. Eur. J. Biochem. **220**, 645–661
18 Wilce, M. C. J., Board, P. G., Feil, S. C. and Parker, M. W. (1995) Crystal structure of a theta-class glutathione transferase. EMBO J. **14**, 2133–2143
19 Rossjohn, J., McKinstry, W. J., Oakley, A. J., Verger, D., Flanagan, J., Chelvanayagam, G., Tan, K.-L., Board, P. G. and Parker, M. W. (1998) Human theta class glutathione transferase: the crystal structure reveals a sulfate-binding pocket within a buried active site. Structure **6**, 309–322
20 Pongjaroenkit, S., Jirajaroenrat, K., Boonchauy, C., Chanama, U., Leetachewa, S., Prapanthadara, L. and Ketterman, A. J. (2001) Genomic organization and putative promoters of highly conserved glutathione S-transferases originating by alternative splicing in *Anopheles dirus*. Insect Biochem. Mol. Biol. **31**, 75–85
21 Chelvanayagam, G., Parker, M. W. and Board, P. G. (2001) Fly fishing for GSTs: a unified nomenclature for mammalian and insect glutathione transferases. Chem. Biol. Interact. **133**, 256–260
22 Wongsantichon, J., Harnnoi, T. and Ketterman, A. J. (2003) A sensitive core region in the structure of glutathione S-transferases. Biochem. J. **373**, 759–765
23 Oakley, A. J., Harnnoi, T., Udomsinprasert, R., Jirajaroenrat, K., Ketterman, A. J. and Wilce, M. C. J. (2001) The crystal structures of glutathione S-transferases isozymes 1-3 and 1-4 from *Anopheles dirus* species B. Protein Sci. **10**, 2176–2185
24 Mannervik, B., Awasthi, Y. C., Board, P. G., Hayes, J. D., Di Ilio, C., Ketterer, B., Listowsky, I., Morgenstern, R., Muramatsu, M., Pearson, W. R. et al. (1992) Nomenclature for human glutathione transferases. Biochem. J. **282**, 305–306
25 Vararattanavech, A. and Ketterman, A. (2003) Multiple roles of glutathione binding-site residues of glutathione S-transferase. Protein Pept. Lett. **10**, 441–448
26 Winayanuwattikun, P. and Ketterman, A. J. (2004) Catalytic and structural contributions for glutathione binding residues in a delta class glutathione S-transferase. Biochem. J. **382**, 751–757
27 Ricci, G., Caccuri, A. M., Lo Bello, M., Rosato, N., Mei, G., Nicotra, M., Chiessi, E., Mazzetti, A. P. and Federici, G. (1996) Structural flexibility modulates the activity of human glutathione transferase P1-1. Role of helix 2 flexibility in the catalytic mechanism. J. Biol. Chem. **271**, 16187–16192
28 Stella, L., Caccuri, A. M., Rosato, N., Nicotra, M., Lo Bello, M., De Matteis, F., Mazzetti, A. P., Federici, G. and Ricci, G. (1998) Flexibility of helix 2 in the human glutathione transferase P1-1. Time-resolved fluorescence spectroscopy. J. Biol. Chem. **273**, 23267–23273
29 Stella, L., Nicotra, M., Ricci, G., Rosato, N. and Di Iorio, E. E. (1999) Molecular dynamics simulations of human glutathione transferase P1-1: analysis of the induced-fit mechanism by GSH binding. Proteins **37**, 1–9
30 Labrou, N. E., Mello, L. V. and Clonis, Y. D. (2001) Functional and structural roles of the glutathione-binding residues in maize (*Zea mays*) glutathione S-transferase I. Biochem. J. **358**, 101–110
31 Jirajaroenrat, K., Pongjaroenkit, S., Krittanai, C., Prapanthadara, L. and Ketterman, A. J. (2001) Heterologous expression and characterization of alternatively spliced glutathione S-transferases from a single *Anopheles* gene. Insect Biochem. Mol. Biol. **31**, 867–875
32 Habig, W. H., Pabst, M. J. and Jakoby, W. B. (1974) Glutathione S-transferases. The first enzymatic step in mercapturic acid formation. J. Biol. Chem. **249**, 7130–7139
33 Stenberg, G., Dragani, B., Cocco, R., Mannervik, B. and Aceto, A. (2000) A conserved "hydrophobic staple motif" plays a crucial role in the refolding of human glutathione transferase P1-1. J. Biol. Chem. **275**, 10421–10428
34 Segel, I. H. (1993) Enzyme kinetics. Behavior and analysis of rapid equilibrium and steady-state enzyme systems, John Wiley & Sons, Inc., New York.
35 Ji, X., Von Rosenvinge, E. C., Johnson, W. W., Tomarev, S. I., Paitigorsky, J., Armstrong, R. N. and Gilliland, G. L. (1995) Three-dimensional structure, catalytic properties, and evolution of a sigma class glutathione transferase from squid, a progenitor of the lens S-crystallins of cephalopods. Biochemistry **34**, 5317–5328
36 Oakley, A. J., Lo Bello, M., Ricci, G., Federici, G. and Parker, M. W. (1998) Evidence for an induced-fit mechanism operating in Pi class glutathione transferases. Biochemistry **37**, 9912–9917
37 Ricci, G., Lo Bello, M., Caccuri, A. M., Pastore, A., Nuccetelli, M., Parker, M. W. and Federici, G. (1995) Site-directed mutagenesis of human glutathione transferase P1-1. Mutation of Cys-47 induces a positive cooperativity in glutathione transferase P1–1. J. Biol. Chem. **270**, 1243–1248
38 Lo Bello, M., Battistoni, A., Mazzetti, A. P., Board, P. G., Muramatsu, M., Federici, G. and Ricci, G. (1995) Site-directed mutagenesis of human glutathione transferase P1-1. Spectral, kinetic, and structural properties of Cys-47 and Lys-54 mutants. J. Biol. Chem. **270**, 1249–1253
39 Stevens, J. M., Armstrong, R. N. and Dirr, H. W. (2000) Electrostatic interactions affecting the active site of class Sigma glutathione S-transferase. Biochem. J. **347**, 193–197

Received 5 April 2005/30 August 2005; accepted 12 September 2005
Published as BJ Immediate Publication 12 September 2005, doi:10.1042/BJ20050555

Available online at www.sciencedirect.com
SCIENCE DIRECT
Biochimica et Biophysica Acta 1754 (2005) 79 – 99
Reprint 9
BIOCHIMICA ET BIOPHYSICA ACTA
BBA
http://www.elsevier.com/locate/bba

Review

Peptide inhibitors of protein kinases—discovery, characterisation and use

Marie A. Bogoyevitch [a,*], Renae K. Barr [a], Albert J. Ketterman [b]

[a] *Cell Signalling Laboratory, Biochemistry and Molecular Biology (M310), School of Biomedical, Biomolecular and Chemical Sciences, University of Western Australia, 35 Stirling Highway, Crawley, Western Australia 6009, Australia*
[b] *Institute of Molecular Biology and Genetics, Mahidol University, Salaya Campus, Nakorn Pathom 73170, Thailand*

Received 19 July 2005; received in revised form 26 July 2005; accepted 28 July 2005
Available online 8 September 2005

Abstract

Protein kinases are now the second largest group of drug targets, and most protein kinase inhibitors in clinical development are directed towards the ATP-binding site. However, these inhibitors must compete with high intracellular ATP concentrations and they must discriminate between the ATP-binding sites of all protein kinases as well the other proteins that also utilise ATP. It would therefore be beneficial to target sites on protein kinases other than the ATP-binding site. This review describes the discovery, characterisation and use of peptide inhibitors of protein kinases. In many cases, the development of these peptides has resulted from an understanding of the specific protein-binding partners for a particular protein kinase. In addition, novel peptide sequences have been discovered in library screening approaches and have provided new leads in the discovery and/or design of peptide inhibitors of protein kinases. These approaches are therefore providing exciting new opportunities in the development of ATP non-competitive inhibitors of protein kinases.

Keywords: Peptide inhibitor; Endogenous inhibitor; Pseudosubstrate; Library screening; Peptide design; Small molecule ATP non-competitive inhibitor

1. Introduction

Protein kinases comprise a large family of enzymes that catalyse the transfer of the terminal phosphoryl group of ATP to their specific protein substrates. When the sequences of protein kinases have been aligned, multiple conserved motifs have been identified [1]. This information has lead to the development of a standard nomenclature that defines critical subdomains or motifs within the protein kinase fold. These motifs have provided a powerful predictive tool in the identification of new protein kinases, and have revealed the presence of ~500 protein kinases within the human or mouse genomes [2,3].

It has been recognised for more than 50 years that protein phosphorylation regulates many aspects of cellular function such as metabolism, division, movement, survival and death. Thus, any disruption of normal phosphorylation can alter cell function and cause disease [4]. Protein kinases are now the second largest group of drug targets, coming after only the G-protein-coupled receptors [4]. To date, most protein kinase inhibitors in clinical development have been directed towards the ATP-binding site. However, one drawback with this current strategy is that these inhibitors must compete with high intracellular ATP concentrations. Furthermore, if they are to be specific, these inhibitors must discriminate between the ATP-binding sites of all protein kinases as well as >200 other human proteins that also utilise ATP (see review [5]).

For these reasons, it would be beneficial to target sites on protein kinases other than the ATP-binding site. However, protein–protein interaction interfaces have generally been considered as difficult targets for small molecule drug discovery. This is largely because the interactions appear to involve larger and frequently less well-defined contact areas when compared with classical drug targets such as enzyme active sites and ligand-binding sites on receptors. There have been some notable successes. For example, small molecule

Abbreviations: AKAP, A-Kinase Anchoring Protein; EGF-R, Epidermal Growth Factor-Receptor; GSK, Glycogen Synthase Kinase; IC_{50}, concentration of compound to achieve 50% inhibition; JIP, JNK Interacting Protein; JNK, c-Jun N-terminal Kinase; K_i, inhibition constant; MLCK, Myosin Light Chain Kinase; PKC, Protein Kinase C; PKI, Protein Kinase A Inhibitor; RACK, Receptor for Activated C-Kinase; SOCS, Suppressor of Cytokine Signalling; TI-JIP, truncated inhibitory region of JIP

* Corresponding author. Tel.: +61 8 6488 1348; fax: +61 8 6488 1148.
E-mail address: marieb@cyllene.uwa.edu.au (M.A. Bogoyevitch).

1570-9639/$ - see front matter © 2005 Elsevier B.V. All rights reserved.
doi:10.1016/j.bbapap.2005.07.025

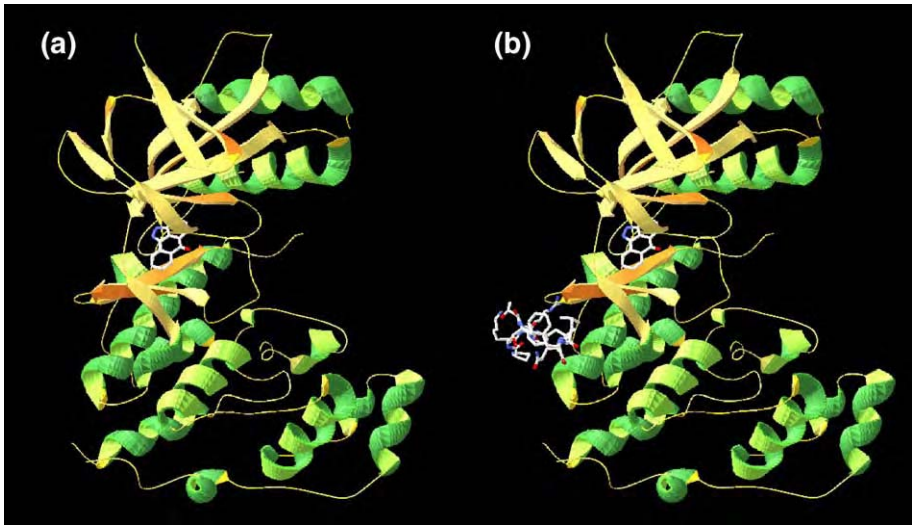

Fig. 1. Protein Kinase Interactions with ATP-competitive and ATP-noncompetitive inhibitors: c-Jun N-terminal Kinase. (a) In a recent example, structural analysis has shown that the ATP-binding site of the protein kinase c-Jun N-terminal Kinase (JNK) is occupied by an ATP-competitive inhibitor of JNKs, SP600125 [9]. (b) In this same study, the structure of the complex between JNK1 and the peptide inhibitor derived from the JNK pathway scaffold protein, JIP1, was solved. This shows the interaction of the JNK1 protein with the peptide inhibitor at a site remote from the ATP-binding pocket.

inhibitors of the interaction of p53 with its suppressor protein HDM2 have been designed, synthesised, tested in vitro and shown to have in vivo efficacy (see review [6]).

In this review, the discovery, characterisation and use of peptide inhibitors of protein kinases are considered. As will be shown, the development of many of these peptides has resulted from an understanding of the specific protein-binding partners for a particular protein kinase. In addition, novel peptide sequences as discovered in library screening approaches have provided new leads in the discovery and/or design of peptide inhibitors of protein kinases. Lastly, how information on peptide inhibitors can aid the development of new non-peptide small molecule inhibitors is considered alongside a number of examples of small molecule ATP-noncompetitive inhibitors of protein kinases. In combination, these approaches provide exciting new opportunities in the development of ATP non-competitive inhibitors of protein kinases.

2. Protein kinase inhibitors derived from biologically-relevant protein partners

The crystal structure of cAMP-dependent protein kinase [7] has provided insights into the organization of the catalytic core of serine/threonine kinases. Striking similarities have been

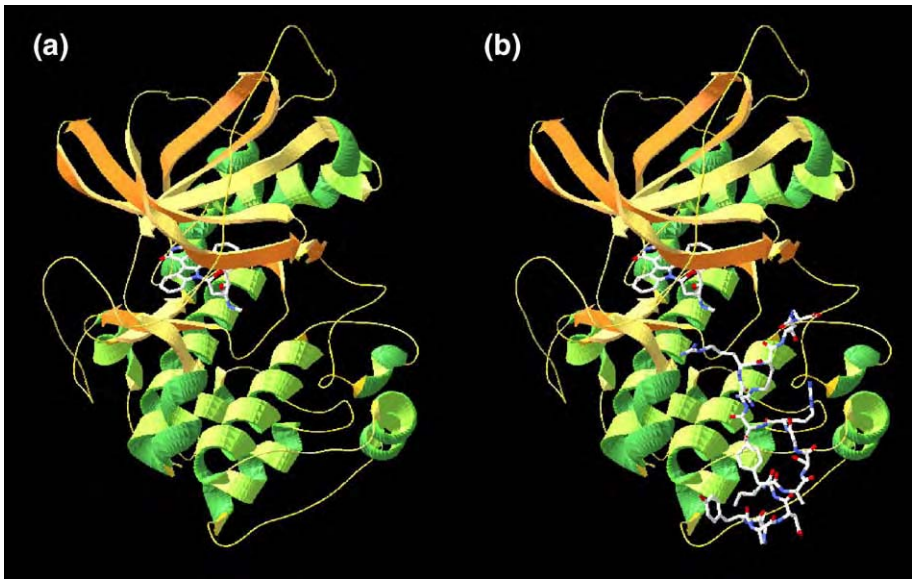

Fig. 2. Protein Kinase Interactions with ATP-competitive and ATP-noncompetitive inhibitors: cAMP-dependent Protein Kinase. (a) Structural analysis has shown that the ATP-binding site of cAMP-dependent protein kinase is occupied by an ATP-competitive inhibitor of protein kinases, staurosporine. (b) The structure of the complex between cAMP-dependent protein kinase and the peptide inhibitor derived from the Protein Kinase Inhibitor (PKI) protein. Again, this shows the interaction of cAMP-dependent protein kinase with the peptide inhibitor at a site remote from the ATP-binding pocket.

subsequently seen in other protein kinases, including tyrosine kinases, with at least 46 unique protein kinase structures now available [8]. From these structures, it is clear that a relatively small pocket of the protein kinase constitutes the ATP-binding region. This is highlighted in Fig. 1(a), where a recent example shows the ATP-binding site of the protein kinase c-Jun N-terminal Kinase (JNK) occupied by an ATP-competitive JNK inhibitor, SP600125 [9]. Similarly, a complex of cAMP-dependent protein kinase with the ATP-competitive inhibitor staurosporine is shown in Fig. 2(a). Thus there are extensive regions outside the ATP-binding site, but the question remains which, if any, of these regions act to regulate protein kinase activity? Furthermore, it is not obvious which regions might also be regulated by the binding of small peptides or other small molecules. In Figs. 1(b) and 2(b), peptide inhibitors of JNK and cAMP-dependent protein kinase are also shown. These structures highlight that the sites of interaction of these peptides can be remote from the ATP-binding site and that the sites of peptide inhibitor interaction may differ between protein kinases. In the following subsections, the development of peptide inhibitors using information derived from biologically-relevant protein partners for a number of kinases is presented.

2.1. Peptide kinase inhibitors derived from endogenous inhibitory proteins

2.1.1. Inhibitors of cAMP-dependent protein kinase derived from the specific inhibitory protein, Protein Kinase A Inhibitor (PKI)

Studies published in the early 1970s characterising thermostable protein inhibitors of the cAMP-dependent protein kinase purified from crude tissue extracts [10–12] provided some of the first leads in the development of peptides as ATP non-competitive inhibitors of protein kinases. An 11-kDa inhibitory protein, known simply as Protein Kinase Inhibitor or PKI, was shown to interact specifically with the catalytic subunit of cAMP-dependent protein kinase, thus potently inhibiting kinase activity with an inhibition constant (K_i) of 2 nM [13]. Proteolytic digestion of PKI revealed a 20 amino acid inhibitory peptide corresponding to amino acids 11–30 [14,15]. This sequence is shown in Table 1, along with many other reported peptide inhibitor sequences that are discussed in this review. Interestingly, within this PKI-derived peptide, a short amino acid sequence resembled the optimal sequence phosphorylated by cAMP-dependent protein kinase. Thus, the peptide contained a pseudosubstrate sequence (R–R–X–S*, where S* represents the phosphoacceptor residue in the substrate that is a non-phosphorylated amino acid in the pseudosubstrate) [14]. Additional pseudosubstrate inhibitors are considered in Section 2.3 as this type of inhibition has now been observed for a number of other protein kinases.

The chemical synthesis of PKI-derived peptides has allowed further characterisation of inhibitory actions [14,15]. This revealed potent inhibition and high specificity towards cAMP-dependent protein kinase without inhibition of other protein kinases tested (phosphorylase kinase, skeletal muscle myosin light chain kinase, protein kinase C (PKC), casein kinase II or cGMP-dependent protein kinase) even when these peptides were included at millimolar concentrations in in vitro assays [14]. Further biochemical analyses of peptide sequences derived from PKI revealed the primary structural requirements for inhibition of cAMP-dependent protein kinase [16]. For example, residues 25–30 within PKI(11–30) were not essential for inhibition. Indeed, PKI(1–24) with a K_i of 4.8 nM was ~150-fold more potent than PKI(11–30). Thus, the inhibitory effects of PKI(1–24) were comparable with the PKI protein [16], and showed that the inclusion of greater numbers of amino acids did not always maintain highest inhibitory activity. Furthermore, the critical nature of the two arginine residues within the pseudosubstrate site was confirmed when their individual substitution by glycine decreased inhibitory potency of the peptides by up to 500-fold [16]. Thus, a single amino acid change in this inhibitory peptide greatly reduced inhibition.

A 20mer peptide corresponding to PKI(5–24) (Table 1) has also been shown to inhibit cAMP-dependent protein kinase with potency comparable to full-length PKI and a K_i of 2.3 nM [17]. Structural studies of PKI(5–22) revealed the secondary structure within this short sequence required for its high biological potency [18]. Amino acid substitutions further defined primary structural determinants essential for the inhibitory actions of the PKI-derived peptides [19] even prior to structural information on the peptide–protein kinase complex being available. Now that the structure of this complex has been solved [20], the amino acids making contact with the peptide have been identified and models developed on the mechanism of substrate binding and the phosphotransferase reaction. Fig. 2(b) shows the complex of cAMP-dependent protein kinase and PKI(12–24) together with the ATP-competitive inhibitor staurosporine and this highlights the spatial separation between the binding sites of the two different inhibitors. In summarising a range of studies, Walsh and Glass concluded that these PKI-based peptide inhibitors showed K_i values in the range of 4 nM to 150 μM. Table 1 shows the sequence of the most potent 9mer inhibitor, PKI(14–22), with a K_i of 36 nM [21]. This 9mer demonstrated that a minimal sequence could retain considerable affinity for inhibition of the cAMP-dependent protein kinase.

The studies on PKI or the PKI-derived peptides described thus far have emphasised the biochemical evaluation of structure–activity relationships in vitro. Studies addressing the intracellular roles of cAMP-dependent protein kinase have used various techniques for expression or delivery of PKI. An early study used a plasmid encoding PKI(1–31) to characterise the role of cAMP-dependent protein kinase in the transcriptional regulation of genes encoding collagenase, the chorionic gonadotrophin-alpha subunit, or enkephalin [22]. This plasmid-driven expression allowed continued production of the peptide intracellularly, chronic inhibition of cAMP-dependent protein kinase, and clear biological effects. Therefore, these results have demonstrated the value of this approach.

In contrast, the sensitivity of small peptides to proteolytic degradation could hamper their study in cells, particularly if longer-term inhibition is required. Thus, PKI(6–24) has been

Table 1
Peptide inhibitors of protein kinases

Peptide name	Peptide sequence	Protein kinase inhibited	Source of inhibitor	References
PKI(11–30)	I–A–S–G–R–T–G–R–R–N–A–I–H–D–I–L–V–S–S–A	cAMP-dependent protein kinase	Inhibitory Protein-PKI	[14,15]
PKI(1–24)	T–D–V–E–T–T–Y–A–D–F–I–A–S–G–R–T–G–R–R–N–A–I–H–D–I–L–V–S–S–A		Inhibitory Protein-PKI	[16]
PKI(5–24)	T–T–Y–A–D–F–I–A–S–G–R–T–G–R–R–N–A–I–H–D		Inhibitory Protein-PKI	[17]
PKI(14–22)	G–R–T–G–R–R–N–A–I		Inhibitory Protein-PKI	[21]
[Ala-5]Kemptide	L–R–R–A–A–L–G		Synthetic substrate-Kemptide	[34,35]
Ht31 peptide	V–Q–G–N–T–D–E–A–Q–E–E–L–A–W–K–I–A–K–M–I–V–S–D–V–M–Q–Q		Anchoring protein-AKAP	[120,123]
AKAP-*IS*	Q–I–E–Y–L–A–K–Q–I–V–D–N–A–I–Q–Q–A		Anchoring protein-AKAP	[134]
AKB(RI), RI specific	F–E–E–L–A–W–K–I–A–K–M–I–W–S–D–V–F–Q–Q		Anchoring protein-AKAP	[135]
n.d.[a]	Myr-R–K–R–T–L–R–R–L[b]	Protein Kinase C (PKC)	Synthetic peptide substrate modified by myristoylation	[40]
n.d.[a]	Myr- R–K–R–C–L–R–R–L[b]		Synthetic peptide substrate modified by myristoylation and Cys substitution	[42]
n.d.[a]	R–F–A–R–K–G–A–L–R–Q–K–N–V–H–E–V–K–N	PKC-α/β/γ	PKC-α/β pseudosubstrate sequence (19–36)	[65]
n.d.[a]	R–F–A–R–K–G–A–L–R–Q–K–N–V	PKC-α/β/γ	PKC-α/β pseudosubstrate sequence (19–31)	[66]
myr-ψPKC	Myr-F–A–R–K–G–A–L–R–Q[b]	PKC-α/β/γ	PKC-α/β pseudosubstrate sequence (20–28)	[76]
myr-ψPKCζ	Myr-R–R–G–A–R–R–W–R–K[b]	PKC-ζ	PKC-ζ pseudosubstrate sequence (116–124)	[82]
βC2–4	S–L–N–P–E–W–N–E–T	PKC-α/β/γ	PKC-β sequence (218–226)	[99]
δV1–1	S–F–N–S–Y–E–L–G–S–L	PKC-δ	PKC-δ sequence (8–17)	[106]
"peptide 1"	K–G–D–Y–E–K–I–L–V–A–L–C–G–G–N	PKC	Annexin-1 (332–346)	[171]
MLC(11–19)	K–K–R–A–A–R–A–T–S	Myosin light chain kinase (MLCK)	C-terminal truncation of MLC phosphorylation site	[49]
n.d.[a]	A–K–K–L–S–K–D–R–M–K–K–Y–M–A–R–R–K–W–Q–K–T–G		Myosin light chain kinase pseudosubstrate site (480–501)	[91]
n.d.[a]	K–R–R–F–K–K		Variant on pseudosubstrate site that minimizes calmodulin inhibition	[91]
CaMKII(290–302)	L–K–K–F–N–A–R–R–K–L–K–G–A	Calmodulin-dependent protein kinase	Calmodulin-dependent protein kinase II pseudo-substrate/ Calmodulin-binding (290–309)	[95]
CaM peptide 1	W–D–T–V–R–I–S–F		Random Peptide Library Screening with Calmodulin	
CaM peptide 2	W–P–S–L–Q–A–I–R			[154]
"Peptide 2"	V–E–L–D–P–E–F–E–P–R–A–R–E–R–T–Y–A–F–G–H	Akt1	Substrate based	[45]
"Peptide 4"	V–E–L–D–P–E–F–E–P–R–A–R–E–R–A–Y–A–F–G–H		Substrate based	[45]
Akt-in	A–V–T–D–H–P–D–R–L–W–A–W–E–K–F		Peptide from Activator-TCL1	[143]
KRX-014.H151	Myr-G–G–Y–N–Q–N–H–Q–K–L–F–Q–L-amide[b]		KinAce	[115]
n.d.[a]	R–K–Q–I–T–V–R	Phosphorylase kinase	Based on peptide substrate	[47]
"Peptide 3"	Y-c[Pen-Y–G–S–F–C]–K–K-amide[c]	c-Src	Substrate based	[51]
"Peptide 29"	Y-c[D-Pen-(3-Iodo-Y)–G–S–F–C]–K–R-amide[c]		Substrate based	[51]
"Peptide 30"	Y-c[D-Pen-(3,5-diIodo-Y)–G–S–F–C]–K–R-amide[c]		Substrate based	[51]
n.d.[a]	Myr-E–F–L–Y–G–V–F–F[b]		Substrate and myristoylation	[53]
n.d.[a]	Myr-E–F–L–amide[b]		Substrate and myristoylation	[53]
n.d.[a]	F–V–G–F–L–G–F–L–G		Random Peptide Library Screening with kinase	[147]
C4	T–Y–T–K–K–Q–V–L–R–M–A–H–L–V–L–K–V–L–T–F–D–L	Cyclin-dependent kinase 2	Cyclin–cyclin-dependent kinase interface	[145]
"peptide 4"	K–L–I–L–F–L–L–L–L	ZAP70	Oriented peptide library screen	[153]
TI-JIP	R–P–K–R–P–T–T–L–N–L–F	JNK	Based on JIP scaffold protein	[137]

Table 1 (*continued*)

Peptide name	Peptide sequence	Protein kinase inhibited	Source of inhibitor	References
KRX-147.D103	Myr-G–N–L–L–N–F–L–R–R–K-amide[b]	c-Kit	KinAce	[115]
KRX-702.H105	Myr-G–G–R–A–G–N–Q–Y–L-amide[b]	PDK1	KinAce	[115]
KRX123.101	Myr-G–I–V–T–Y–G–K–I-amide[b]	Lyn	KinAce	[114]
KRX-123.302	Myr-G–L–V–T–(3,5-diIodo-Y)–k–K–I–K&-amide [b,d]		KinAce	[114]
KRX-055.G106	Myr-G–R–T–N–A–V–Nle-amide[b,f]		KinAce	[115]
P1	c[C–R–N–C–T–V–I–Q–F–S–C][e]	Casein Kinase 2	Random Peptide Library	[155]
P15	c[C–W–M–S–P–R–H–L–G–T–C][e]		Screening with Substrate Peptide	
Tkip	W–L–V–F–F–V–I–F–Y–F–F–R	JAK2, EGF-R	Designed peptide	[33]

A range of approaches has been used in the discovery and development of peptide inhibitors of protein kinases. This table summarises peptide sequences and their sources as described in this review. Further details on the characterisation of these peptide inhibitors including estimates of the affinities (K_i or IC_{50} values for inhibition) and their use in cellular studies is described in the text.

[a] n.d.=not defined. No name was specifically given to these peptides.

[b] In this sequence, myr=N-terminal myristoylation.

[c] In this sequence, the sequence contained within the designation c[ ] is cyclized by the formation of a disulphide bond between the side chain of the amino acid Penicillamine (Pen) and the side chain of Cysteine (C).

[d] In this sequence, k=D-stereoisomer of K, and K&=K-ε amino benzoyl.

[e] In this sequence, the sequence contained within the designation c[ ] is cyclized by the formation of a disulphide bond between the side chains of the of the 2 Cysteine (C) residues.

[f] In this sequence, Nle—norleucine.

modified to address this concern [23]. PKI(6–24), modified in two ways by the substitution of arginine in position 18 with its D-stereoisomeric form and blocking the side chain of the C-terminal aspartate with a cyclohexyl ester group, was active intracellularly for 4 to 6 h following its microinjection. This peptide prevented the changes in cell morphology and cytoskeleton following cAMP-dependent protein kinase activation [23]. Under the same conditions, the microinjection of non-modified PKI(6–24) was without effect [23]. Others have used microinjection of PKI-derived peptides in a wide range of studies. Examples include the evaluation of the role for cAMP-dependent protein kinase in mitosis and nuclear envelope breakdown [24], and more recently in the evaluation of cell cycle progression of one-cell stage mouse fertilised eggs [25]. PKI-derived peptides have also been added to permeabilised cells to evaluate cAMP-dependent protein kinase actions in renal tubule cells [26], β_2-adrenergic receptor desensitisation [27] and the IP_3-dependent release of Ca^{2+} and relaxation of smooth muscle [28].

Intracerebroventricular injection of either PKI(6–22) or an N-terminal myristoylated form of PKI(14–22) has also significantly reversed the antinociception tolerance that followed low level morphine exposure [29]. In this example, the myristoylated PKI(14–22) was most effective, this being attributed to the lipophilic myristoyl moiety and smaller peptide size enhancing cellular permeability [29]. Similarly, the use of myristoylated PKI(14–22) has implicated cAMP-dependent protein kinase in insulin secretion by pancreatic beta-cells [30], as a mediator of ischemic preconditioning and isoprenaline-induced protection in the heart [31], and in the regulation of adenylyl cyclase and phosphodiesterase activity in smooth muscle [32]. Therefore, simple chemical modifications of the PKI-derived peptides have allowed a range of studies evaluating the biological functions of cAMP-dependent protein kinase.

2.1.2. Endogenous inhibitory proteins as new leads in the development of protein kinase inhibitors

Following the success of the approach to develop cAMP-dependent kinase inhibitors based on the endogenous inhibitory protein PKI, other protein kinase inhibitors could be developed using similar principles. To date, there are few reports of this approach to discover peptide inhibitors of protein kinases. However, as described in subsequent sections of this review, other proteins such as substrates, scaffolds or the protein kinases themselves have provided numerous leads in the development of peptide inhibitors of protein kinases. It is of interest that a peptide considered to mimic some of the actions of the Suppressors Of Cytokine Signalling (SOCS) protein family as inhibitors of Epidermal Growth Factor-Receptor (EGF-R) or JAK2 has been recently described [33]. However, a short 12mer peptide mimetic of SOCS-1, called Tkip (see Table 1), was designed to bind JAK2 and not found within the SOCS-1 sequence. Tkip is therefore considered further in Section 3.2 where approaches to the discovery of novel inhibitory peptide sequences are described in more detail.

2.2. Peptide inhibitors of protein kinases derived from substrates

2.2.1. Substrate-based inhibitors of cAMP-dependent protein kinase

As described in Section 2.1.1, the inhibitory sequence within PKI has been attributed to a sequence resembling its substrate, i.e., a pseudosubstrate sequence. This relationship between substrate and inhibitor is further emphasised by the observation that the appropriate substitution of a single amino acid in PKI-derived peptides has produced effective substrates for cAMP-dependent protein kinase. Thus, the substitution of alanine at position 21 in PKI(4–22), with the phosphorylatable serine residue (sequence: E–T–T–Y–A–D–F–I–A–S–G–

R–T–G–R–R–N–S–I), has produced a kinase substrate more effective than the standard peptide substrate Kemptide (where the Kemptide sequence is L–R–R–A–S–L–G) [19]. In both sequences, the phosphorylated serine is denoted by the underline (i.e., S). It is therefore not surprising that some of the earliest attempts to develop inhibitors of cAMP-dependent protein kinase performed the reverse modifications. Thus, substituting the phosphorylatable serine in Kemptide with alanine produced an inhibitor, [Ala-5]-Kemptide (see Table 1) [34,35]. In addition, the irreversible inactivation of cAMP-dependent protein kinase has been achieved with peptide substrate analogs, some of which bind a highly reactive active site Cys residue [36,37] as well as other residues in the cAMP-dependent protein kinase active site [38].

2.2.2. Substrate-based peptide inhibitors of protein kinase C (PKC)

Other modifications of substrate peptides of protein kinases have also produced novel inhibitors. For example, as shown in Table 1, the major PKC phosphorylation site (Thr-654) of the EGF-R (i.e., T within the sequence context R–K–R–T–L–R–R–L) when added to an N-terminal myristoyl moiety produced an 8mer PKC inhibitory peptide rather than a substrate [39,40]. This myristoylated peptide entered cells more readily and inhibited PKC-mediated interleukin-2 and interleukin-2 receptor expression in Jurkat T cells [41]. When various substitutions of this peptide were then tested for their potency in PKC inhibition, myr-R–K–R–C–L–R–R–L was the most potent of the peptides evaluated [40]. However, its potency was decreased 10-fold in the presence of the reducing reagent dithiothreitol [40]. This sensitivity to dithiothreitol suggested a covalent interaction with a conserved active site Cys in PKC. Further studies confirmed an irreversible mechanism of inhibition following S-thiolation of PKC [42]. In addition, many studies as considered in Section 2.3 have evaluated the use of pseudosubstrate sequences as inhibitors of PKC.

Lee and colleagues have further generated peptide inhibitors specific for the α-PKC isoform based on the PKC-α consensus substrate sequence (sequence: R–R–K–G–*S*–Hyd–R, where Hyd = a hydrophobic amino acid, and the phosphorylated serine is underlined) [43]. Again, the phosphorylatable serine at position 5 in this sequence was replaced with an alanine, the residues considered essential (i.e., the two arginine residues and the hydrophobic residues), were retained whereas the other 3 positions were changed through the inclusion of each one of 720 carboxylic acid moieties within an (L)-2,3-diaminopropionic acid substitution. This resulted in a number of high affinity modified peptide inhibitors of PKC-α most notably with one inhibitor showing a K_i of 0.8 nM. Interestingly this peptide also showed >350-fold preference for PKC-α over the closely-related conventional PKC isoforms, PKC-β and PKC-γ and even higher selectivity over the more distantly related PKCs (600-fold to 2730-fold). Thus, the substitutions in the original peptide sequence would appear to access a structurally distinct subsite unique to PKC-α. Further structural analysis of this complex will be of interest in the application of similar approaches to this family of kinases as well as the general approach to inhibitor design.

2.2.3. Substrate-based peptide inhibitors of Akt

Like cAMP-dependent kinase and PKC, the Akt family of kinases are serine/threonine kinases within the AGC group [2]. An optimal peptide substrate sequence (A–R–K–R–E–R–T–Y–S–F–G–H–H–A) discovered in an oriented peptide library screening approach has been shown to bind and inhibit Akt1 with a K_i of 12 μM [44]. This has more recently been used in the development of small peptide inhibitors of Akt [45]. The most effective inhibitors showed K_i values in the range of 0.1 μM. The sequence of one of these peptides is shown in Table 1, and this 100-fold improved inhibition was attributed to the addition of 9 amino acids from the FOXO3 transcription factor to the N-terminus of the original peptide and the substitution of threonine and serine residues by alanine [45]. When evaluating specificity by testing 8 other protein kinases, only Serum/Glucocorticoid-regulated Kinase SGK, which shares similar substrate preferences, was also inhibited [45].

Two approaches have been initially taken to deliver these Akt inhibitors to cells [45]. First, these peptide inhibitors were delivered to HeLa cells using the BioPORTER protein transfection reagent. This provided transient exposure to the peptide, and Glycogen Synthase Kinase (GSK)-3 phosphorylation was inhibited [45]. However, no phenotypic change in these cells was observed [45]. Thus, in a second approach, the peptide was synthesised as a fusion with a poly-arginine membrane-permeable sequence. Continuous incubation with this peptide provided a mechanism for sustained delivery. Significant inhibition of GSK3 phosphorylation was demonstrated, and growth of both HeLa and MiaPaCa cells was reduced as expected if growth inhibition required persistent Akt inhibition [45]. This has therefore demonstrated the importance of appropriate delivery mechanisms when determining the cellular efficacy of these peptide inhibitors.

2.2.4. Substrate-based peptide inhibitors of other serine/threonine kinases

In addition to the identification of peptide inhibitors of serine/threonine protein kinases based on their specific substrates as described in the preceding subsections, others have shown the ability of substrate-based peptides to inhibit protein kinase activities in vitro. Here, two additional inhibitors are considered, a minimal peptide inhibitor of phosphorylase kinase and a peptide inhibitor of smooth muscle myosin light chain kinase (MLCK).

Phosphorylase kinase is one of the key enzymes involved in glycogenolysis, catalysing the phosphorylation of phosphorylase *b* to its active form, phosphorylase *a*. Its reaction mechanism has been extensively studied, and specifically it has been of interest that other protein kinases cannot perform the function of phosphorylase kinase (see review [46]). In studying its catalytic mechanism, small peptide substrates have been identified and those poorly phosphorylated have been screened as potential competitive inhibitors [47]. Of those peptides screened, a threonine containing 7mer was studied

further in vitro [47]. This sequence is shown in Table 1. Other sequence variants have been reported as competitive inhibitors of phosphorylase kinase with K_i values ranging from 6 to 800 μM [46]. Again, the various amino acid substitutions highlighted critical amino acids within the inhibitory peptide sequence.

MLCK plays an important role in smooth muscle contraction (see review [48]). Substrate-based peptide inhibitors of MLCK have also been described based on the myosin light chain sequence and inhibition was achieved by a peptide sequence shortened by the removal of amino acids carboxy-terminal to the phosphorylated serine residue [49]. The peptide corresponding to residues 11–19 of the myosin light chain sequence is shown in Table 1. The estimated K_i of this peptide inhibitor was 10 μM [49]. Higher potency inhibitory peptides for MLCK based on pseudosubstrate sequences have been subsequently characterised and are described in greater detail in Section 2.3.2.

2.2.5. Substrate-based peptide inhibitors of Src family kinases

Inhibitors of tyrosine kinases such as the Src family kinases have also been based on protein substrate motifs. Lam and colleagues screened a 7mer peptide library in vitro for a suitable lead for c-Src substrates [50]. The resulting sequence, Y–I–Y–G–S–F–K, was characterised with a K_m value of 55 μM [50]. Over 70 analogues of this lead were subsequently tested, and the structure–activity relationships developed were used in the design of small peptide inhibitors of c-Src [51]. Because the presence of glycine in position 4 of this peptide might indicate the requirement for a β-turn to stabilise the secondary structure, a series of peptides conformationally constrained by cyclisation was tested and shown to have increased inhibitory potency [51]. "Peptide 3" as shown in Table 1 inhibited c-Src activity with an IC_{50} of approximately 3 μM and was chosen as the new lead for further development of inhibitory peptides [51].

Further testing included an evaluation of the nature of the N-terminus and the basic core, a stereochemical scan at positions 2 and 7, and a rotamer scan at position 3. These studies established two peptide sequences, "Peptide 29" and "Peptide 30" as shown in Table 1 with IC_{50} values of 0.13 and 0.54 μM, respectively [51]. These peptides showed higher affinity for c-Src when compared to the original parent peptide, and notably they both contained nonphosphorylatable tyrosine mimetics, 3-iodotyrosine and 3,5-diiodotyrosine. Whilst these peptides also showed selectivity for inhibition of c-Src when compared to the closely related family member Lyn, they were also inhibitors of another family member Lck [51]. This indicated the difficulty in designing peptides to selectively inhibit one Src kinase family member. This problem to discriminate between closely-related protein kinase family members remains as a potential obstacle in the design of all classes of protein kinase inhibitors.

A 7mer peptide M–I–Y–K–Y–Y–F has also been discovered in approaches to identify substrates for Src and has been more recently used as a template for the development of Src-specific peptide inhibitors [52]. Truncations and substitutions have been tested, and the 7mer C–I–Y–K–Y–Y–F and 6mer C–I–Y–K–Y–Y were found to have IC_{50} values of ~0.5 μM. Neither peptide inhibited Lck or Lyn when tested at concentrations up to 200 μM. Disappointingly, despite its high potency, the C–I–Y–K–Y–Y–F peptide did not significantly affect v-src transfected 3T3 cells [52]. However, the approaches taken in cell delivery were not clear, and the inability of an unmodified peptide to cross the cell membrane might provide a simple explanation for its apparent lack of effect. Perhaps more encouraging, the identification of a 4mer peptide CI(β-F)K with an IC_{50} of 11.8 μM provided a possible lead in the development of peptidomimetics and small molecule inhibitors of c-Src [52], and it will be interesting to see the future results of such studies.

Similarly, a peptide substrate for Src following its myristoylation was a slow but reversible inhibitor (Table 1) [53]. A requirement for preincubation suggested several important binding determinants must be correctly aligned for optimal binding. Interestingly, this myristoylated peptide showed competitive inhibition against both ATP and protein substrate for Src as typical for a bisubstrate inhibitor of Src [53]. This would suggest that the inhibitor bound to the peptide substrate-binding site of Src and that the acyl chain interacted with the hydrophobic pocket within the ATP-binding site [53]. The minimal inhibitory region was shown to only require a myrisotylated 3mer sequence (Table 1). Because bisubstrate inhibitors may potentially offer greater specificity of inhibition, their rational design is further considered in Section 2.2.6.

2.2.6. ATP-Peptide conjugates as bisubstrate protein kinase inhibitors

It remains possible that the selectivity of substrate-competitive inhibition of protein kinases can be improved if inhibitors were designed to interact with both protein substrate and ATP-binding sites of protein kinases. However, due to their competition with ATP, these bisubstrate inhibitors may also suffer from the potential problems facing the conventional ATP-competitive protein kinase inhibitors as described in Section 1. In particular, these bisubstrate inhibitors would need to compete with high intracellular ATP concentrations, and therefore it would be most appropriate to assess the actions of these inhibitors in assays in vitro with ATP concentrations comparable to those in vivo. Parang and Cole have extensively reviewed ovalently-linked bisubstrate analogues as protein kinase inhibitors [54]. Here, the development of bisubstrate inhibitors of cAMP-dependent protein kinase and the insulin receptor tyrosine kinase is briefly considered.

One of the first bisubstrate inhibitors was achieved when an ATP mimic, isoquinoline-5-sulfonamide, was linked to the 7mer peptide S-R_6 [55]. This inhibited cAMP-dependent kinase with a K_i of 0.004 μM, or PKC with a K_i of 0.1 μM [55]. Similarly, bisubstrate inhibitors of cAMP-dependent kinase have been based on the Kemptide peptide (L–R–R–A–S–L–G) being directly linked through the hydroxyl group of the Serine-5 residue to the γ-phosphate of ATP [56]. This generated a weak inhibitor (IC_{50} of 226 μM) that was competitive with respect to ATP-binding, but non-competitive with respect to protein substrate binding. The addition of an

acetyl spacer improved inhibition of cAMP-dependent protein kinase, retained selectivity of the inhibitor towards this kinase, but again showed ATP-competitive inhibition but non-competitive inhibition with respect to protein substrate [57]. Whilst this latter observation may not appear consistent with the expected features of a bisubstrate inhibitor, this inhibition has been explained by the ordered binding of ATP then protein substrate to the kinase [57]. Others have also explored a nucleoside-peptide conjugate, Adeonosine-5′-carboxylic acid-6-aminohexanoic acid-R_6, however, again this inhibitor was not fully competitive against both substrates [58]. Further structure–function analyses, in which different peptide fragments and different linker groups are included, should improve the understanding of these inhibitors and permit the design of improved bisubstrate inhibitors of cAMP-dependent protein kinase.

Bisubstrate analogs for the tyrosine kinase domain of the insulin-receptor have also been synthesised by linking ATPγS to a peptide substrate [59]. Specifically, a 17mer peptide based on the sequence surrounding Y727 of IRS1 [60,61] was used as the basis for this peptide. The resulting compound showed competitive inhibition for both ATP and the protein substrate with a calculated K_i of 370 nM, being 200- to 800-fold lower than the K_m values for the substrates [59]. Whilst specificity of this inhibitor was not widely evaluated, the tyrosine kinase Csk was inhibited with a significantly higher K_i of 195 μM. Furthermore, additional analyses of derivatised ATP analogues but lacking the peptide portion show these were very weak inhibitors (e.g., K_i of ~114 μM), highlighting that the peptide moiety was essential for the effective inhibition of the insulin receptor kinase activity [59]. When the crystal structure of the complex was evaluated, it confirmed features used in the inhibitor design and revealed an additional role of the linker co-ordinated to Mg^{2+} in the active site [59]. It will be of interest to see how this structural information can be used to further improve this inhibitor and whether this information can be extrapolated to the rational design of other bisubstrate protein kinase inhibitors.

2.3. Peptide inhibitors of protein kinases derived from protein kinase sequences

In this section, the use of pseudosubstrate-derived peptides as inhibitors of PKC, myosin light-chain kinase and calmodulin-dependent protein kinase are considered. The term “pseudosubstrate” as mentioned briefly in Sections 2.1.1 and 2.2.1 describes the autoinhibitory sequences that mimic features of the protein substrate phosphorylation site [62]. These inhibitors, by competing with substrates, directly disrupt the phosphorylation reaction. In addition, if other regulatory sites in the kinase can be disrupted, then this can potentially lead to inhibition of kinase activity. This approach has proven successful for the inhibition of actions of specific isoforms of PKC through the specific disruption of each isoform with its intracellular-binding protein, the so-called *R*eceptors for *a*ctivated *C k*inase or RACKs [63,64]. These inhibitors of PKC are also considered briefly in this Section. Lastly, the recent report of a peptide inhibitor based on the substrate interaction loop of the Src family kinase, Lyn, is described, with this opening the possibility for the design of other protein kinase inhibitors based on similar strategies.

2.3.1. Pseudosubstrate Inhibitors of PKC

In 1987, House and Kemp described a pseudosubstrate sequence in the N-terminal regulatory domain of PKC. The synthetic peptide corresponding to residues 19 to 36 (see Table 1) inhibited PKC with a K_i of 150 nM [65]. As this sequence is identical in PKC-α and PKC-β and differs in PKC-γ by only 1 amino acid, PKC(19–36) has been considered to equally inhibit these three conventional Ca^{2+} -dependent/phorbol ester-sensitive PKC family members. Arginine at position 22 was the most important determinant for inhibition, so that an inactive form [Ala-22]PKC(19–31) provided a valuable control for studies using pseudosubstrate peptides to explore PKC actions [66]. Again, this emphasised the importance of a single amino acid in determining binding and inhibition. The stability of this peptide towards proteolytic enzymes was improved through its retro-inverso synthesis, i.e., its synthesis in the reverse order and using D-amino acids [67]. Perhaps surprisingly, the substitution of the D-alanine at position 25 with D-serine further improved the inhibitory properties of this peptide resulting in an estimated K_i of 2 μM [67].

PKC pseudosubstrate inhibitors have been delivered to permeabilised cells to inhibit the phosphorylation of CD3 in T thymocytes [68,69] or the phosphorylation of the MARCKS (myristoylated alanine-rich C kinase substrate) protein in fibroblasts [70]. The peptide has been microinjected into sea urchin eggs [71], injected intradermally to evaluate the contribution of PKC to hyperalgesia in a model of diabetic neuropathy [72], or included in the impaling electrode when studying effects in neurons or hippocampal slices [73–75]. These studies illustrate the diversity of cell functions explored using this PKC pseudosubstrate peptide.

Eichholtz and colleagues have also delivered an N-myristoylated PKC-α/β/γ pseudosubstrate peptide inhibitor, myr-ψPKC (Table 1), to human foreskin fibroblasts and the human carcinoma KB cell line [76]. In these studies, the non-myristoylated peptide was 100-fold less effective in inhibiting MARCKs protein phosphorylation [76]. Similarly, bradykinin-stimulated phospholipase D activation in human foreskin fibroblasts was inhibited by myr-ψPKC but not the unmyristoylated peptide [76]. Others have used myr-ψPKC to evaluate the role of PKC in activation of NADPH oxidase [77], or in the insulin secretory response of pancreatic islets [78]. Importantly, the myristoylated peptide was taken up equivalently by both drug-sensitive and multidrug-resistant cancer cells, suggesting that its possible usefulness in treating PKC-α-mediated drug resistance [79]. Others have also delivered the pseudosubstrate peptides through direct linkage to cell-permeable vector sequences derived from the *Drosophila* Antennapedia protein [80]. These cell-permeable peptides have been recently reviewed [81]. This delivery of the ψPKC-peptide has shown a role for PKC in growth cone morphology [80]. Importantly, the biotinylated peptide could be detected in

all compartments of primary cultures of neuronal cells after only 1 h of incubation with the peptide [80]. This has shown that the appropriate approaches to increase cellular uptake of these peptide inhibitors can extend their utility.

A similar strategy has targeted the ζ-isoform of PKC. Because the pseudosubstrate region of PKC-ζ differs from that in PKC-α, -β and -γ, targeting this region has provided a means to discriminate between the actions of these different isoforms [82]. Thus, injection of the peptide directed against PKC-ζ has implicated this isoform in the mitogenic signalling activated downstream of insulin, whereas a role for PKC-α, -β or -γ was dismissed [82]. The specificity of these peptides in vitro was also confirmed alongside experiments in cells using PKC-ζ antisense to down regulate PKC-ζ [82]. Thus, two independent approaches yielded comparable results. It is increasingly likely that the parallel use of chemical or peptide inhibitors alongside antisense or siRNA approaches to decrease protein kinase expression will provide evidence to support the specificity of each inhibitor.

The PKC-ζ directed peptide has since been used in a number of different cell systems. It has inhibited NF-κB activation and transactivation of the HIV enhancer [83], as well as implicating PKC-ζ in human parainfluenza virus replication [84], insulin-stimulated glucose transport in myotubes [85], carbachol-stimulated insulin release [86], angiotensin II actions to increase expression of c-Fos [87], taurocholate transport in hepatocytes [88] and the late phase of long-term potentiation in synaptic transmission [89]. Its intracellular delivery has relied on the ability of lipid-modified peptides to cross the cell membrane. Whilst this approach offers many exciting new possibilities due to the apparent simplicity of the system, it has also been stressed that the large-scale synthesis of many lipid-modified peptides is not trivial due to the low water-solubility of the reactants and products. Bonnet and colleagues have solved this problem and developed a modular approach to the production of lipopeptides through the use of a shuttle system, G–R–G–R–K(Palmitoyl chain)–NH_2 that introduces the lipid palmitate, with optimal results in terms of specific activity and low basal cytotoxicity obtained when using a thiazolidine ligation reaction with the PKC-ζ peptide [90]. This approach has opened opportunities for the modification of other protein kinase inhibitory peptides in a manner that allows their lipid modification and ready delivery to cells.

2.3.2. Other pseudosubstrate inhibitors—inhibitors of the calmodulin-dependent myosin light-chain kinase (MLCK)

As mentioned previously in Section 2.2.4, MLCK plays an important role in smooth muscle contraction. MLCK is a calmodulin-dependent protein kinase and this has implications for inhibitor development. A short synthetic peptide based on a 22mer basic stretch of the MLCK sequence corresponding to amino acids 480–501 (Table 1) was shown to inhibit MLCK activity with a K_i of 46 nM [91]. However, because the MLCK pseudosubstrate analog overlaps the calmodulin-binding region in this sequence, the peptide inhibitor acted both as a calmodulin and substrate antagonist [91]. Again, structure–function studies have identified inhibitors with lesser effects on calmodulin-binding but with maintained substrate antagonist potency [91]. The sequence of a 6mer peptide with these characteristics is shown in Table 1. Interestingly, a calmodulin-independent tryptic fragment of MLCK was also inhibited by the MLCK(480–501) peptide with a K_i of 33 nM. Thus, this inhibitory peptide did not require interference with the calmodulin-binding site to explain its actions and true pseudosubstrate inhibition was effective [92].

The MLCK inhibitory peptide has been subsequently microinjected into individual smooth muscle cells [93]. This blocked contraction in response to K^+ depolarisation, despite increased Ca^{2+} concentrations [93]. This result together with the observation that a constitutively active MLCK could cause contraction in the absence of changes in Ca^{2+} concentrations supported the involvement of MLCK in contraction with it being both necessary and sufficient to trigger contraction in single smooth muscle cells. More recently, a strategy to identify MLCK inhibitors has again been based on autoinhibitory sequences of MLCK that also lack calmodulin recognition [94]. Libraries of related peptide sequences were created, and "Peptide 18" as shown in Table 1, was one of the inhibitors discovered, with an IC_{50} of 50 nM and only inhibiting calmodulin-dependent protein kinase at 4000-fold higher concentrations [94].

Care must be taken when further considering other inhibitors of calmodulin-dependent protein kinases such as calmodulin kinase II. Its regulation by calmodulin is critical and some peptide inhibitors have been shown to require interaction with calmodulin rather than a direct effect on the kinase [95]. These inhibitory peptides also inhibited calmodulin-dependent enzymes as exemplified by calmodulin-dependent phosphodiesterase [95]. However, two overlapping peptide sequences were revealed that were not calmodulin-antagonists but that were direct inhibitors of the autophosphorylated active protein kinase [95]. Of these, Peptide 290–302 as listed in Table 1 showed the greatest inhibition with an IC_{50} value of 54 μM [95]. Further N-terminal extension of this peptide sequence to give Peptide 281–309 improved inhibition 20-fold, but kinetic analysis has suggested actions that were non-competitive towards protein substrate but competitive with respect to ATP [96]. These studies have revealed additional mechanisms of protein kinase regulation, with autoinhibition of calmodulin-dependent kinase II not strictly following the simple models of pseudosubstrate inhibition [96].

2.3.3. PKC inhibitors that act via the disruption of PKC–RACK interactions

In addition to the pseudosubstrate inhibitors described in Section 2.3.1, isoform-specific PKC inhibitors have been designed using other peptide sequences in the PKC isoforms. It should be noted that the translocation of active PKC isoforms was initially thought to involve direct interaction with lipid components of the membrane. However, protease pre-treatment of membrane fractions was shown to abolish phorbol ester-induced membrane association of PKC [97]. Additional evidence such as PKC isoforms localising with cytoskeletal structures rather than membranes suggested protein–protein

interactions as the basis for PKC translocation [98]. Subsequent studies have identified several proteins in cells that bind PKC, and these are now grouped together as the RACKs. In the following paragraphs, inhibitors of PKC derived from RACK-interacting sequences in different PKC isoforms is considered. This area has been the subject of a number of excellent reviews [63,64].

Mochly-Rosen and colleagues first described the RACK1-binding site on PKC and suggested that peptides mimicking this binding site could serve as specific inhibitors of PKC translocation and function [99]. As a part of the second conserved (C2) region of PKC was implicated in the RACK1 interaction, PKC C2-derived peptide sequences were synthesised and shown to specifically inhibit hormone-induced translocation and function of the C2 domain containing isoform PKC-β in *Xenopus* oocytes [99]. The sequence of a 9mer C2-derived peptide, βC2-4, is shown in Table 1. When used in studies of oocyte maturation, the microinjection of high concentrations of the peptides (5–500 μM) was required and this was attributed to the likely proteolytic sensitivity of the peptides, particularly during the prolonged time course (hours) of the experiment [99]. Peptides such as βC2-4 have also been included in patch clamp pipettes allowing testing alongside PKC pseudosubstrate peptides. This has shown a role for PKC-β in the phorbol ester-induced inhibition of cardiac calcium channel activity [100], the strength of such studies lying in the use of two different peptide sequences yielding the same cellular effect.

The power of the use of these peptide inhibitors is further demonstrated in studies in which specific functions of the different PKC isoforms have been evaluated by comparing the results obtained with different peptide inhibitors. Thus, the 8mer peptide, εV1-2, has been derived as a novel antagonist of PKC-ε. This peptide was based on the first unique or variable region (V1) of PKC-ε following the hypothesis that this peptide would bind to the εPKC-specific RACK and prevent its interaction with PKC-ε [101]. When introduced into cardiac myocytes, εV1-2 inhibited PKC-ε translocation in response to phorbol esters and the negative chronotropy [101] as well as preconditioning induced PKC-ε translocation and protection of cardiac myocytes from hypoxic injury in vitro [102]. The use of βC2–4 and εV1–2 peptides has implicated both PKC-α and PKC-ε in the insulin response of beta-pancreatic cells to glucose [103]. Conversely, PKC-ε but not PKC-β was specifically implicated in protective effect of phorbol esters on tumour necrosis factor or calphostin C-induced apoptotic cell death of U937 histiocytic lymphoma cells [104] and PKC-ε but not PKC-β was implicated in the regulation of Na^+ channels in hippocampal neurons [105].

A PKC-δ inhibitor, δV1-1 (see Table 1), has also been synthesised based on the variable region V1 of PKC-δ [106]. Using εV1-2 and δV1-1 peptides, PKC-ε and PKC-δ have been shown to have opposing actions in cardiac damage and yet parallel effects in promoting cardiac hypertrophy [106]. The cardiac protection exerted by inhibition of PKC-δ by δV1-1 was further demonstrated in models of reperfusion damage. Specifically, the delivery of a PKC-δ specific inhibitory peptide δV1-1 during the onset of reperfusion in vivo or ex vivo was cardioprotective [107–109]. The proapoptotic events prevented by δV1-1 included caspase 3 activation, PARP inactivation and DNA laddering, as well as changes in Bad levels and Akt phosphorylation [109]. Similarly, the inhibition of PKC-δ by δV1-1 improved the survival of rat hippocampal slices subjected to oxygen-glucose deprivation in vitro as well as showing efficacy in vivo when delivered 1 to 6 h after transient middle cerebral artery occlusion as a model of stroke [110]. Interestingly, in the study of ex vivo reperfusion injury, additive effects were noted when the inhibition of PKC-δ by δV1-1 was combined with treatment to activate PKC-ε [107]. A similar observation was made with this combination of PKC modulators when evaluating ischemic injury in cardiac allografts, the function of these allografts and graft coronary artery disease [111,112]. Furthermore, the use of δV1-1 alongside the PKC-ζ pseudosubstrate peptide has suggested opposing actions of these isoforms with PKC-δ inhibiting proliferation and PKC-ζ stimulating proliferation of neonatal rat cardiac fibroblasts [113]. Therefore, the use of various combinations of peptides directed towards the different PKC isoforms has revealed the complexity of actions of the various members of this protein kinase family.

2.3.4. A peptide inhibitor of the Src family member, Lyn, based on its substrate-binding loop

The substrate-binding loop of the tyrosine kinase Src family member Lyn has been recently used as the starting point in the development of a peptide inhibitor of Lyn [114]. The rationale here was that preventing a protein kinase binding to its substrates by developing an inhibitor that binds the substrates would be an effective developmental strategy. As described by Goldenberg-Furmanov and colleagues, this approach was based on detailed structure analysis of nuclear magnetic resonance data and high resolution modelling and strongly supported by previous biochemical analyses of substrate interaction and specificity determination. This suggested that the loop between the two α-helices, specifically the "HJ loop" lying between subdomains IX and X of Lyn was fully exposed, available for interactions and that this formed the substrate-binding loop. Furthermore, analysis of the HJ loop sequence showed amino acid sequences unique to the subfamily. A series of 8mer peptides derived from the HJ loop of Lyn were therefore synthesised and tested in vitro for inhibition of Lyn alongside two other Src family members, Lck and Fyn [114]. The sequences of two examples of these peptides, KRX123.101 and KRX-123.302 are shown in Table 1. This highlights the modifications of the parental KRX-123.101 peptide to generate KRX-123.302, including the use of the tyrosine analogue, diiodotyrosine, as well as the inclusion of the D-amino acid form of lysine in position six in place of the parental sequence glycine and modifications to the C-terminal lysine to include an aminobenzoyl moiety in the ε-position. This resulting peptide did not inhibit Fyn or Lck autophosphorylation, even at concentrations up to 20 μM, but inhibited Lyn autophosphorylation when included at concentrations of 0.2 μM or higher. Further analysis showed inhibition of Lyn activity towards Syk,

a physiological substrate for Lyn, with an IC_{50} value of 0.30 μM [114].

The addition of an N-terminal myristoyl group allowed direct testing of this peptide in cellular systems. First, effects in B-lymphocytes were evaluated as the role for Lyn in signalling events downstream of B-cell antigen receptor activation has been well studied. KRX123.302 included at a concentration of 10 μM suppressed CD19 phosphorylation and Lyn trans-autophosphorylation in antibody activated splenic B-cells or Syk phosphorylation following B cell receptor activation in the B-lymphoma cell line WEHI-231 as well as enhancing ERK MAPK activation in the latter cell line [114]. These observations were all consistent with the ability of KRX123.302 to inhibit Lyn in intact cells albeit requiring higher concentrations than needed for direct inhibition of the kinase in in vitro enzyme assays [114]. Importantly, this peptide series was also used to evaluate the possibility that Lyn inhibition might inhibit the proliferation of prostate cancer cells both in vitro and in vivo. Specifically, the changes made to KRX123.101 to generate KRX123.302 increased inhibition of proliferation of both prostate cancer cell lines tested, namely DU145 and PC3. Thus, when used at a concentration of 10 μM, KRX123.101 inhibited proliferation of DU145 and PC3 cells by 73% and 52%, respectively, whereas KRX123.302 inhibited proliferation by 95% and 88%, respectively. Interestingly, KRX123.302 did not significantly affect a human colon cancer cell line HT29 that barely expressed Lyn, suggesting the specificity of actions towards Lyn within the Src family of kinases [114]. In vivo administration of KRX123.302 in a DU145 xenograft model in nude mice once the tumours had reached volumes of approximately 100 mm^3 was also performed. The treatment regime of 10 mg/kg intravenously once weekly for 5 weeks resulted in significant tumour regression whereas vehicle-treated control animals continued to show tumour growth with more than doubling of tumour volume during the time of study [114]. Morphological analysis of tumour sections showed more apoptotic cells, increasing from 1.5% in the vehicle-treated animals to 8.4% in the peptide inhibitor treated group. Thus, this new peptide appears to offer an important advance not only in kinase inhibitor design but also in the treatment of prostate cancer.

2.3.5. Additional kinase sequence based inhibitors—the KinAce approach

The principles applied to the discovery of a potent Lyn inhibitory peptide based on the substrate-binding region of that protein kinase have also been explored more generally. This strategy has been termed “KinAce” by Niv and colleagues at Keryx Biopharmaceuticals [115]. This resulted in the testing of 15 to 30 peptides from the tyrosine kinases c-Kit and Lyn and the serine/threonine kinases PDK1 and Akt. Approximately one third of these peptides were found to be active against their respective kinases. Some of these sequences are shown in Table 1. Here, we consider briefly the characterisation of one of each of these effective inhibitory sequences.

To test the KRX-147.D103 peptide as an inhibitor of c-Kit, small lung cell cancer cells with high c-Kit expression NCI-H526 were incubated with this peptide alongside the inhibitory peptides for Lyn, PDK1 or c-Kit. KRX-147.D103 selectively inhibited autophosphorylation of c-Kit following exposure to Stem Cell Factor (SCF) with an IC_{50} of 7 μM. SCF-induced proliferation was also inhibited. In an ex vivo assay for SCF effects on angiogenesis, 10 μM KRX-147.D103 also blocked SCF-induced vessel formation. KRX-702.H105 was found to be the most potent inhibitor of PDK1, the kinase that phosphorylates threonine 308 of Akt. This peptide thus inhibited this phosphorylation in insulin-like growth factor-stimulated DU145 prostate cancer cells. Growth of PC3 cells was also inhibited 40% by 10 μM KRX-702.H105. KRX-014.H151 was the most effective Akt inhibitor. In an in vitro kinase assay, this peptide inhibited Akt phosphorylation of its substrate GSK3. This peptide was further tested by evaluation of proliferation of the breast cancer cell line MDA-MB-231. Incubation for 3 days in the presence of 10 μM peptide resulted in 90% inhibition of proliferation. The IC_{50} value was calculated to be 3 μM. Lastly, KRX-055.G106 was found to be amongst the most active Lyn inhibitory peptides. This was used as described to evaluate cell survival and growth of prostate tumour cells and was effective with an IC_{50} value of 1.5 μM. These examples show the success of this approach in the development of new peptide inhibitors of a range of protein kinases.

2.4. Peptide inhibitors of protein kinases derived from anchoring or scaffold proteins

Additional layers of complexity in inhibition are also possible within the intact cell through compartmentalisation of protein kinases on specific anchoring proteins. In this way, protein kinases can be inhibited through their sequestration away from their preferred substrates. In this section, peptide inhibitors that can act within an intracellular context to prevent protein kinase actions are considered. Specifically, peptides derived from A-Kinase Anchoring Proteins (AKAPs) as inhibitors of cAMP-dependent protein kinase are described. In addition, the c-Jun N-terminal kinases (JNKs) can be inhibited by peptides derived from scaffold proteins in their pathway, and the mechanism of this inhibition by these peptides is also explored together with the application of JNK inhibitory peptides both in vitro and in vivo.

2.4.1. Peptides derived from A-kinase anchoring proteins (AKAPs) as inhibitors of cAMP-dependent protein kinase

The spatial and temporal activation of cAMP-dependent protein kinase in cells is controlled via several regulatory mechanisms including intracellular gradients and nanocompartments of cAMP. In addition, spatial restriction of cAMP-dependent protein kinase can be achieved through its association with A-Kinase Anchoring Proteins (AKAPs) [116,117]. AKAPs represent a large family of structurally diverse, but functionally related, proteins that are classified by their ability to interact with cAMP-dependent protein kinase. These proteins have been the subject of a number of excellent

reviews [116,118]. Rather than resembling PKI-type proteins in their interaction, AKAPs do not interact with the catalytic subunit of cAMP-dependent protein kinase but instead bind the regulatory (R) subunits RI and/or RII [116].

In most AKAPs, a 14- to 18-amino acid sequence binds to the R subunit dimers [119–122]. Peptides derived from sequences in this region have been used as effective antagonists of cAMP-dependent protein kinase anchoring in cells. The prototypic inhibitor is a 24-amino acid peptide derived from a human thyroid AKAP, Ht31 (Table 1) [118,120,123] and this inhibitor has the ability to disrupt both RI and RII subunit-mediated localisation of cAMP-dependent protein kinase [124,125].

AKAP-based peptides have been used in a range of studies evaluating the role of cAMP-dependent kinase, and in particular the requirement for AKAP binding. For example, intracellular perfusion of cultured hippocampal neurons with these peptides prevented cAMP-dependent protein kinase-mediated regulation of glutamate-induced currents [126]. Similarly, the inclusion of the Ht31 peptide during recording of skeletal muscle myotube L-type calcium channels prevented potentiation mediated by cAMP-dependent protein kinase [127]. In these studies, a mutant Ht31 peptide unable to interact with AKAPs was chosen as a negative control. To evaluate the effects that these peptides may have in intact cells, a range of approaches have been used, including their plasmid-driven overexpression and their direct delivery using the lipofectamine reagent [128]. This has been shown to block glucagon-like peptide stimulation of insulin secretion by pancreatic islet beta cells [128]. Others have used lipid modification of the peptide itself, specifically the addition of stearate. Thus, the stearated Ht31 peptide has been shown to inhibit sperm motility in a time- and concentration-dependent manner, with the control mutant peptide showing no effect [123]. Interestingly, in this example, direct inhibition of cAMP-dependent kinase activity did not mimic the AKAP-derived peptide inhibitory effects, suggesting sperm motility is a function of the R subunit of cAMP-dependent protein kinase. Other studies using the stearated Ht31 peptide or driving expression of Ht31 from a transfected vector include the evaluation of cAMP-dependent protein kinase actions in regulation of *N*-methyl-D-aspartate receptor activity [129], the translocation of aquaporin [130], β-adrenergic signalling and contraction in cardiac myocytes [131] and auditory fear memory [132]. Again, these studies show the usefulness of this peptide inhibitor in a range of cells systems and addressing important biological questions.

Structural studies have highlighted the basis for the interaction between the AKAP sequences and the RII subunit [133]. With the affinity of RII binding ranging between the various AKAP-derived peptides from 2 to 90 nM, a systematic study of multiple AKAP sequences has defined a high-affinity RII-selective AKAP-derived 17-amino acid peptide called AKAP-*IS* [134]. This sequence is shown in Table 1. This peptide was shown to interact with cAMP-dependent protein kinase inside cells and upon perfusion of hippocampal neurons led to the time-dependent run-down of α-amino-3-hydroxy-5-methyl-4-isoxazolepropionic acid (AMPA)-responsive currents [134].

A similar approach using a peptide array has defined a minimal 27mer sequence, derived from the protein kinase-binding domain of the dual-specific AKAP (D-AKAP), with similar affinity for RI and RII subunits [135]. The sequence of this peptide is shown in Table 1. An RI selective high-affinity binding peptide was also created firstly by evaluating the minimal sequence required for binding each isoform by N- and C-terminal truncations, and then using a peptide substitution array in which all 20 amino acids were substituted in each position of the D-AKAP peptide [135]. The minimal 19-amino acid sequence termed AKB(RI),RI specific is shown in Table 1. This peptide should prove useful in future studies evaluating the functions of RI localised cAMP-dependent protein kinase.

2.4.2. c-Jun N-terminal kinase (JNK) inhibitory peptides derived from the JNK pathway scaffold JNK-interacting protein (JIP)

JNK-Interacting Protein (JIP), a scaffold in the JNK pathway, was originally described as a cytosolic inhibitor of JNK actions intracellularly [136]. We have more recently characterised a peptide inhibitor of JNK derived from the minimal JNK-binding region of the scaffold protein JIP1 ([137–139], and reviewed in [140]). This 11mer peptide is shown in Table 1, and we have abbreviated its name to TI-JIP (for *T*runcated *I*nhibitory Region of *JIP*; [137]). We have shown the minimal sequence requirements for inhibition of JNK [137,138] with a K_i of 0.39 μM and that this inhibition was ATP non-competitive [138]. We have also determined structure–function activity relationships for similar peptides [137,138] and have mapped the interaction site of JNK for this peptide inhibitor [139]. The recent co-crystallisation of TI-JIP with JNK [9] confirmed this site [139] and re-emphasised the structural features revealed in our biochemical studies of TI-JIP [137]. All four residues originally identified in TI-JIP as important for mediating the inhibitory effects on JNK1 activity [137] (Arg4, Pro5, Leu8, Leu10) were shown to mediate contacts with the JNK1 protein [9].

The JIP-derived peptides selectively inhibited the kinase activity of JNK assessed in in vitro assays, and these peptides have been studied both in vitro in cultured cells and in in vivo animal models of disease. This has utilised the cell-permeable properties of a small peptide sequence derived from the HIV TAT protein (reviewed in [81]). Thus, the resulting peptides contain a short cell-permeable TAT sequence followed by a short JIP-derived peptide. An example of this sequence is *G–R–K–K–R–R–Q–R–R–R*–P–P–R–P–K–R–P–T–T–L–N–L–F–P–Q–V–P–R–S–Q–D–T as used in [141]. The cell permeable sequence is indicated in italics, and the four critical residues of TI-JIP are underlined. Table 2 briefly summarises these recent studies using these peptides in a range of disease models both in vitro and in vivo. A detailed overview of these studies has been presented in a recent review [140]. The important feature here in peptide design has again been the inclusion of D-amino acids in the retro-inverso synthesis of the peptide inhibitor to improve protease resistance

Table 2
Recent studies to evaluate efficacy of cell-permeable JNK inhibitory peptides in models of disease both in vitro and in vivo

Disease	Effect of Cell-Permeable JNK inhibitory peptides	Reference
Type 1 diabetes	Prevented β-cell death in response to IL-1 or lipoproteins	[141]
Type 2 diabetes	Improved insulin resistance; improved glucose tolerance	[172]
Stroke	Reduced brain lesion size; prevented behavioural changes; prevented death following oxygen–glucose deprivation	[173,174]
Neurotrauma	Protected against neuronal loss in secondary degeneration	[175]
Hearing loss	Prevented hair cell death after neomycin exposure; prevented acoustic trauma-induced hearing loss; did not prevent cell death after cisplatin exposure	[176,177]
Alzheimer's disease	Prevented block in long term potentiation in response to Aβ peptide; prevented apoptosis of cortical neurons	[178,179]
Asthma, eczema	Prevented eosinophil apoptosis	[180]

JNK inhibitory peptides based on the scaffold protein JIP have been increasingly used in studies in vitro and in vivo through their delivery with cell permeable peptide vector sequences.

and therefore the circulating half-life of the peptide. However, in these cases unlike that mentioned in Section 2.1.1 and 2.3.4, all residues have been used in the D-amino acid form. The inhibitory potency of this retro-inverso peptide decreased some 10-fold over the conventional L-amino acid peptide and it will be of interest to see whether more selective substitution of fewer residues might restore some of the inhibitory potency.

2.5. The promise of peptide kinase inhibitors derived from other binding partners

2.5.1. When fragments of activators act as inhibitors—the example of Akt-in

Whilst the use of inhibitory proteins has been the starting point in the design of inhibitory peptides for protein kinases, other protein partners may have the potential to inhibit activity and/or activation of a specific kinase. The proto-oncogene TCL1 has been identified as a co-activator of the kinase Akt [142], and a 15mer, Akt-*in* (Table 1), derived from TCL1 has inhibited Akt activity towards glycogen synthase kinase-3a in vitro albeit requiring high micromolar (400 μM) peptide concentrations [143]. Biochemical analyses indicated that Akt-*in* bound to the pleckstrin homology (PH) domain of Akt, thus decreasing Akt interaction with phosphatidylinositols required for activation and preventing Akt translocation to the plasma membrane [143]. Importantly, the residues involved in the interaction with Akt-*in* are divergent amongst the various PH domains of a range of signalling molecules, suggesting that specificity of actions is possible [143]. However, further specificity testing will be necessary to evaluate whether the actions of Akt-*in* are restricted to the Akt family members.

The cell-permeable protein transduction domain of TAT has been fused to Akt-*in*, thus allowing its cellular delivery. This demonstrated that Akt-*in* could inhibit platelet derived growth factor-stimulated Akt activation and direct downstream events including the phosphorylation of BAD and fork head transcription factor [143]. Importantly, the phosphorylation of the upstream PDK1 was unaffected, as were other independently regulated pathways such as p38 and ERK MAPK activation [143]. Akt-*in* also decreased cell growth and cell viability and enhanced mitochondrial depolarisation. Interestingly, Akt-*in* effects were demonstrated in many cell types, but greatest efficacy was demonstrated in cells with low TCL1 expression. This suggested that Akt-*in* was unable to efficiently compete with endogenous TCL1 [143], and that higher affinity partners acting via the same binding site may have greater effects in these cell types. The effects of Akt-*in* have also been tested in vivo following Akt-*in* injection directly into a xenograft tumour every second day for 2 weeks. This dramatically slowed tumour growth and enhanced apoptotic cell numbers [143]. Thus, Akt-*in* is an interesting lead in the development of Akt inhibitors with possible uses therapeutically in cancer treatment.

2.5.2. Cdk inhibitors based on disrupting the Cdk–cyclin interaction

Another target in the treatment of cancer is the family of cyclin-dependent kinases (Cdks) due to their critical role as cell cycle regulators. The cyclin recognition motif in the natural Cdk-inhibitory protein $p27^{KIP1}$ was used as the basis for the design and synthesis of a series of cyclic peptides [144]. Gondeau and colleagues have also recently used structural information on the interaction between Cdk2 and its activating cyclin, cyclin A, to produce a Cdk2 inhibitory peptide [145]. Their 22mer peptide, C4 as shown in Table 1, corresponds to amino acids 285 to 306 in the α-helix of cyclin A, inhibited Cdk2 activity with an IC_{50} of 1.8 μM, being competitive with respect to protein substrate binding. Again, the cell-permeable protein transduction domain of TAT was used in peptide delivery, with TAT-C4 blocking proliferation of tumour cell lines.

3. Discovery of novel peptide inhibitors

3.1. Library screening to identify novel peptide inhibitors

The screening of a variety of libraries of peptides has also allowed the discovery of peptide sequences that can inhibit protein kinases. As the following examples illustrate, these libraries can either be synthetic prepared peptides and screened biochemically or expressed in yeast or expressed and displayed on the surface of phage for subsequent screening. In such screening, different baits have also been chosen, including a full-length protein kinase or substrate fragments. These approaches are considered in turn in this section.

3.1.1. Screening with Full-length protein kinases

In any screening procedure, there are also two choices in library construction, either a random library of peptides, or a biased peptide library where residues known to be critical for

the interaction with the protein kinase are conserved at specific positions within the peptide sequence. These two approaches to library selection are considered in the following paragraphs.

The use of randomly constructed libraries has a number of potential advantages in the discovery of peptide inhibitors of protein kinases. The first is that a detailed knowledge of the protein kinase and its mode of inhibition is not required prior to initiating the screen. Interestingly, when used in the identification of substrates (rather than inhibitors) of cAMP-dependent protein kinase through the screening of a random synthetic combinatorial peptide library, this approach identified the consensus sequence of R–R–X–S [146]. This is the sequence previously identified by biochemical approaches as optimal for phosphorylation by this kinase [146]. This provides some confidence in the results of such screens due to the ultimate agreement of results of the two methods. A second advantage lies in the potential to discover new sequences that can also act as inhibitors of the protein kinase under investigation. Nishi and colleagues have used a random 15mer library expressed by bacteriophage in the search for high affinity binders and inhibitors of Src [147]. The sequencing of >100 of the bound phage showed that >60% contained the consensus sequence of G–X–X–G, and commonly this motif was repeated to G–X–X–G–X–X–G. In these sequences, X was frequently a hydrophobic amino acid such as F, V or L. A model peptide F–V–G–F–L–G–F–L–G as shown in Table 1 was tested biochemically for its effects on Src activity in vitro, and found to be inhibitory with a K_i of 24 μM. When the 3 glycine residues in this sequence were substituted with proline to produce the sequence F–V–P–F–L–P–F–L–P, the resulting K_i was 3.1 mM, thus emphasising the importance of the glycine residues in the inhibitory actions [147].

Arrays of 8mer peptide libraries on cellulose paper have also been screened, this time using a radiolabelled cGMP-dependent protein kinase 1α protein [148]. This allowed the identification of peptide sequences with high affinity of binding for this protein kinase. Iterative deconvolution of every amino acid position identified a sequence L–R–K–K–K–K–K having the highest affinity and being able to selectively inhibit cGMP-dependent protein kinase activity with a K_i of 0.8 μM in isolated enzyme assays [148]. To deliver this sequence intracellularly, peptides were synthesised with the N-terminal addition of the HIV TAT or Antennapedia membrane-permeable sequences resulting in the peptides called DT-2 or DT-3 respectively. These peptides have been used to decrease NO-induced cerebral dilation [148], inhibit reactive oxygen species generation following exposure of cardiac myocytes to acetylcholine or bradykinin [149], and implicate cGMP-dependent protein kinase in regulation of vascular tone [150] and vascular smooth muscle phenotype [151].

In contrast to the preceding examples, when some information has been available on the interaction that is the ultimate target for disruption, then all peptides in the library could include the known key amino acids. This biased screening approach has been most successfully used in the selection of SH2 domain interacting phosphotyrosine-containing peptides [152]. Nishikawa and colleagues have screened for peptides that directly inhibit the tyrosine kinase activity of ZAP-70 [153]. A tyrosine-oriented peptide library containing the sequence M–A–X–X–X–X–Y–X–X–X–X–A–K–K–K (where X = any amino acid except W, C or Y) was screened with a recombinant baculovirus expressed ZAP70–GST fusion protein [153]. Screening was performed in the presence of ATP but in the absence of Mg^{2+} to prevent peptide phosphorylation and turnover. The bound peptides were eluted and subjected to automated Edman sequencing, with the relative abundance of individual amino acids at positions N-terminal and C-terminal to the orientating tyrosine residue reflecting the relative abundance of high affinity peptides that contain these amino acids [153]. The results showed strong preference for leucine or isoleucine at all positions except the amino acid four residues towards the N-terminus (i.e., the first variable position in the library) showing preference for lysine. “Peptide 4” as shown in Table 1 was a specific and potent inhibitor of ZAP70 tyrosine kinase activity in vitro [153]. The peptide was also synthesised as a chimera with the *Drosophila* Antennapedia cell-permeable vector sequence and the effects on anti-CD3-dependent tyrosine phosphorylation in T cells evaluated and tyrosine phosphorylation of phospholipase C-γ and LAT were shown to decrease as well as interleukin-2 reporter gene expression [153]. An important finding in this study was the optimal inhibitory sequence was not equivalent to the optimal substrate sequence for ZAP-70 as previously determined by screening peptide libraries. Most notable was the divergence at the N-terminus of the peptide sequences. The inhibitor showed high affinity binding and low turnover rates, so that the slow rate of release was likely to contribute to inhibitor efficacy [153].

3.1.2. Screening with regulatory subunits

An alternative approach to screening peptide libraries for inhibitors of protein kinase activity has been to screen for peptides that interact with regulatory subunits of the kinase under investigation. An example here has been the use of Calmodulin in the screening of a random peptide phage display library [154]. This identified two major peptide classes as calcium-dependent binding partners for calmodulin. A peptide sequence from each of these classes is listed in Table 1 as “Cam peptide 1” and “Cam peptide 2”. Interestingly, these two peptides differentially inhibited Calmodulin-dependent kinase I and II but did not affect the activity of Calmodulin-dependent phosphodiesterase [154]. Therefore, despite targeting a common regulatory subunit such as calmodulin, it has been possible to identify differential inhibitors, thus suggesting that there are sufficient differences in the regions of calmodulin that interact with its targets that can be exploited in the design of specific inhibitors.

3.1.3. Screening with substrate fragments

The strategies outlined in Sections 3.1.1 and 3.1.2 have successfully identified protein kinase inhibitory peptides. However, many binding peptides identified may not be inhibitors. Instead, a peptide fragment from a specific high affinity substrate has been used to identify target peptides in screening. The rationale here has been that the identified

peptides bind the substrate and thus prevent access by the protein kinase. Perea and colleagues used this approach in screening for inhibitors of Casein Kinase 2 [155]. In this example, a random 9mer cyclic peptide phage library was screened with a target peptide based on the casein kinase 2 substrate site from the HPV-16 E7 oncoprotein. Specifically, residues 28 to 38 of this protein (L–N–D–S–S–E–E–E–D–E–I) were used in three rounds of selection, and the resulting 11 phages evaluated as blockers of the phosphorylation of the HPV-16 E7 fusion protein by casein kinase 2. The sequences of peptides from the two strongest inhibitory phages are shown in Table 1 as P1 and P15. The cyclic peptide corresponding to P15 was subsequently tested as a synthetic peptide and when included as a fusion with the cell-permeable peptide sequence at a final concentration of 100 μM inhibited casein kinase 2 phosphorylation of HPV-16 E7 by ~70% [155]. When applied to cultures of TC-1 cells, this synthetic P15 peptide activated caspase-3 and prevented tumour growth following TC-1 cell implantation [155]. This suggested that blocking casein kinase 2 actions through the targeting of its substrate could have future application in treatment of some cancer types. From the perspective of understanding protein kinase actions, it is also possible that this substrate targeting approach will provide a mechanism for selective prevention of some actions of kinases whilst leaving other actions intact.

3.2. Design of peptide inhibitors of protein kinases

The activity of tyrosine kinases such as JAK2 or the EGF-R can be negatively regulated by a family of proteins called Suppressors of Cytokine Signalling or SOCS [156]. Truncation of SOCS1 has identified regions essential for its interaction with, and inhibition of, JAK2 [157]. Recently, a 12mer peptide mimetic of SOCS-1 was described [33]. The sequence of this peptide, called Tkip, is shown in Table 1 and was developed to recognise the autophosphorylation site of JAK2. Two strategies were undertaken, one not successful but the other able to generate the inhibitory peptide. The first strategy was referred to as the complementary peptide approach as described by Villain and colleagues [158] in which hydropathic complementarity was used to drive binding of protein partners. An algorithm has been previously developed that specifies the best complementary fit [159]. This approach was used to discover binding partners for the autophosphorylation sequence of JAK2 surrounding Y1007 (i.e., ^{1001}LPQDKEYYKVKEP^{1113} where Y1007 is underlined). Notably, the peptides predicted to have the best complementary fit were not the best binding partners for the JAK2 peptide. Thus, a second approach was undertaken, and this was based on an approach originally defined by Blalock and colleagues that uses the complementary strand codons when read in the 5′ to 3′ direction [160]. The resulting peptide Tkip both bound the JAK2 autophosphorylated peptide as well as prevented JAK2 autophosphorylation and phosphorylation of the interferon-γ receptor subunit IFNGR-1, but showed specificity in actions by not inhibiting the tyrosine kinase activity of the vascular endothelial growth factor receptor or Src. However, notably, the EGF-R autophosphorylation could be inhibited by Tkip but this was consistent with the sensitivity of both JAK2 and EGF-R to SOCS mediated inhibition.

Tkip was modified by N-terminal palmitylation to increase its cell membrane permeability, then used in studies where pre-treatment with the peptide (8 μM) for 17 h completely prevented interferon-γ STAT1α phosphorylation. Evaluation of the downstream consequences showed that inhibitor pre-treatment could also inhibit interferon-γ antiviral activity and the induction of MHC Class I [33]. Subsequently, this palmitoylated Tkip peptide has been shown to inhibit both constitutive and interleukin 6-induced activation of STAT3, and to inhibit proliferation of the prostate cancer cell lines DU145 and LNCaP through slowing the movement from the G0/G1 to S-phase of the cell cycle [161]. Further structure–function analysis will be required to understand the features of Tkip critical for its inhibition.

4. Development of non-peptide, non-ATP-competitive inhibitors of protein kinases

The preceding sections have outlined an increasing number of peptide inhibitors that target protein kinases outside their ATP-binding sites. It is possible that other non-peptide small molecules can act in manner mechanistically comparable to these peptides. These may therefore provide new classes of ATP non-competitive, non-peptide inhibitors of protein kinases.

Non-peptide, ATP non-competitive kinase inhibitors have been occasionally identified in routine screening of chemical libraries. Perhaps, some of the best-known inhibitors of this type are the inhibitors of the dual specificity kinases, MEK1 and MEK2. Recent structural studies have shown these inhibitors bind a unique pocket adjacent to the ATP-binding site and that binding induced a conformational change in MEK, locking it into a closed but catalytically inactive structure [162]. Similarly, a non-ATP competitive inhibitor of the BCR-ABL tyrosine kinase has been recently described. Although its exact binding site on the kinase has yet to be reported, ON012380 differs from the widely known inhibitor imatinib (Gleevec or STI-571) by its direct competition with the protein substrate [163]. Furthermore, ON012380 was a more potent inhibitor when compared to imatinib, synergised in actions with imatinib, and could override the resistance of cells to imatinib resulting from point mutants of the Abl active site [163]. Thus, this different mode of inhibition promises the usefulness of ON012380 in the treatment of chronic myeloid leukemic patients that no longer respond to imatinib. Other non-ATP competitive inhibitors from the thiadiazolidinone as well as the thienyl and phenyl alpha-halomethyl ketone families have been identified for glycogen synthase kinase, these promising new therapeutic strategies in the treatment of Alzheimer's disease [164,165].

An alternative approach requires structural information on the site to be targeted. For example, naphthalene-based peptide substrate mimics have been used in the rational design of non-peptide inhibitors of the tyrosine kinase regions of the insulin

receptor or EGF-R [166]. Subsequently, these approaches have been extended with the use of quinoline, isoquinoline and iminochromene rings in the design of non-ATP competitive inhibitors of the Src family kinases, Lck and Src [167,168], and more recently with hydroxynapthalene and hydroxyindole derivatives as Src inhibitors [169,170]. In these latter examples, the structure of auto-inhibited Src was used as a design template in qualitative molecular modelling studies, with extensive structure–activity studies revealing functional group requirements for maximal efficacy of inhibition.

5. Conclusions and perspectives

In addition to the intense interest in the development of ATP-competitive inhibitors of protein kinases, this review has highlighted that there are many examples of peptides that can act as specific and high affinity inhibitors of protein kinases. Whilst many of these inhibitors have been based on known binding partners of the protein kinase under investigation, there are also examples of inhibitory peptides discovered through the screening of peptide libraries. The subsequent testing in protein kinase activity assays has then shown them to act as inhibitors of protein kinase activity. This latter approach now has the potential to be increasingly exploited in the search for inhibitors of protein kinases for which little information on binding partners is already available. When used in in vitro assays, such inhibitory peptides may provide clues on protein kinase regulatory mechanisms. However, when used in cellular and in vivo systems, these novel inhibitors also have the potential to reveal new biological actions of the protein kinases studied. Therefore, peptide inhibitors of protein kinases will continue to provide important tools in the study of protein kinase action.

References

[1] S.K. Hanks, A.M. Quinn, T. Hunter, The protein kinase family: conserved features and deduced phylogeny of the catalytic domains, Science 241 (1988) 42–52.
[2] G. Manning, D.B. Whyte, R. Martinez, T. Hunter, S. Sudarsanam, The protein kinase complement of the human genome, Science 298 (2002) 912–934.
[3] S. Caenepeel, G. Charydczak, S. Sudarsanam, T. Hunter, G. Manning, The mouse kinome: discovery and comparative genomics of all mouse protein kinases, Proc. Natl. Acad. Sci. U. S. A. 101 (2004) 11707–11712.
[4] P. Cohen, Protein kinases—The major drug targets of the twenty-first century? Nat. Rev., Drug Discov. 1 (2002) 309–315.
[5] P.M. Fischer, The design of drug candidate molecules as selective inhibitors of therapeutically relevant protein kinases, Curr. Med. Chem. 11 (2004) 1563–1583.
[6] P.M. Fischer, D.P. Lane, Small-molecule inhibitors of the p53 suppressor HDM2: have protein–protein interactions come of age as drug targets? Trends Pharmacol. Sci. 25 (2004) 343–346.
[7] D.R. Knighton, J.H. Zheng, L.F. Ten Eyck, V.A. Ashford, N.H. Xuong, S.S. Taylor, J.M. Sowadski, Crystal structure of the catalytic subunit of cyclic adenosine monophosphate-dependent protein kinase, Science 253 (1991) 407–414.
[8] B. Nolen, S. Taylor, G. Ghosh, Regulation of protein kinases; controlling activity through activation segment conformation, Mol. Cell 15 (2004) 661–675.
[9] Y.S. Heo, S.K. Kim, C.I. Seo, Y.K. Kim, B.J. Sung, H.S. Lee, J.I. Lee, S.Y. Park, J.H. Kim, K.Y. Hwang, Y.L. Hyun, Y.H. Jeon, S. Ro, J.M. Cho, T.G. Lee, C.H. Yang, Structural basis for the selective inhibition of JNK1 by the scaffolding protein JIP1 and SP600125, EMBO J. 23 (2004) 2185–2195.
[10] D.A. Walsh, C.D. Ashby, C. Gonzalez, D. Calkins, E.H. Fischer, E.G. Krebs, Purification and characterization of a protein inhibitor of adenosine 3′,5′-monophosphate-dependent protein kinases, J. Biol. Chem. 246 (1971) 1977–1985.
[11] C.D. Ashby, D.A. Walsh, Characterization of the interaction of a protein inhibitor with adenosine 3′,5′-monophosphate-dependent protein kinases. II. Mechanism of action with the holoenzyme, J. Biol. Chem. 248 (1973) 1255–1261.
[12] A. Szmigielski, A. Guidotti, E. Costa, Endogenous protein kinase inhibitors. Purification, characterization, and distribution in different tissues, J. Biol. Chem. 252 (1977) 3848–3853.
[13] J.G. Demaille, K.A. Peters, E.H. Fischer, Isolation and properties of the rabbit skeletal muscle protein inhibitor of adenosine 3′,5′-monophosphate dependent protein kinases, Biochemistry 16 (1977) 3080–3086.
[14] J.D. Scott, E.H. Fischer, J.G. Demaille, E.G. Krebs, Identification of an inhibitory region of the heat-stable protein inhibitor of the cAMP-dependent protein kinase, Proc. Natl. Acad. Sci. U. S. A. 82 (1985) 4379–4383.
[15] J.D. Scott, E.H. Fischer, K. Takio, J.G. Demaille, E.G. Krebs, Amino acid sequence of the heat-stable inhibitor of the cAMP-dependent protein kinase from rabbit skeletal muscle, Proc. Natl. Acad. Sci. U. S. A. 82 (1985) 5732–5736.
[16] J.D. Scott, M.B. Glaccum, E.H. Fischer, E.G. Krebs, Primary-structure requirements for inhibition by the heat-stable inhibitor of the cAMP-dependent protein kinase, Proc. Natl. Acad. Sci. U. S. A. 83 (1986) 1613–1616.
[17] H.C. Cheng, B.E. Kemp, R.B. Pearson, A.J. Smith, L. Misconi, S.M. Van Patten, D.A. Walsh, A potent synthetic peptide inhibitor of the cAMP-dependent protein kinase, J. Biol. Chem. 261 (1986) 989–992.
[18] J. Reed, V. Kinzel, H.C. Cheng, D.A. Walsh, Circular dichroic investigations of secondary structure in synthetic peptide inhibitors of cAMP-dependent protein kinase: a model for inhibitory potential, Biochemistry 26 (1987) 7641–7647.
[19] D.B. Glass, H.C. Cheng, L. Mende-Mueller, J. Reed, D.A. Walsh, Primary structural determinants essential for potent inhibition of cAMP-dependent protein kinase by inhibitory peptides corresponding to the active portion of the heat-stable inhibitor protein, J. Biol. Chem. 264 (1989) 8802–8810.
[20] J. Zheng, D.R. Knighton, L.F. ten Eyck, R. Karlsson, N. Xuong, S.S. Taylor, J.M. Sowadski, Crystal structure of the catalytic subunit of cAMP-dependent protein kinase complexed with MgATP and peptide inhibitor, Biochemistry 32 (1993) 2154–2161.
[21] D.A. Walsh, D.B. Glass, Utilization of the inhibitor protein of adenosine cyclic monophosphate-dependent protein kinase, and peptides derived from it, as tools to study adenosine cyclic monophosphate-mediated cellular processes, Methods Enzymol. 201 (1991) 304–316.
[22] J.R. Grove, P.J. Deutsch, D.J. Price, J.F. Habener, J. Avruch, Plasmids encoding PKI(1–31), a specific inhibitor of cAMP-stimulated gene expression, inhibit the basal transcriptional activity of some but not all cAMP-regulated DNA response elements in JEG-3 cells, J. Biol. Chem. 264 (1989) 19506–19513.
[23] A. Fernandez, J. Mery, M. Vandromme, M. Basset, J.C. Cavadore, N.J. Lamb, Effective intracellular inhibition of the cAMP-dependent protein kinase by microinjection of a modified form of the specific inhibitor peptide PKi in living fibroblasts, Exp. Cell Res. 195 (1991) 468–477.
[24] N.J. Lamb, J.C. Cavadore, J.C. Labbe, R.A. Maurer, A. Fernandez, Inhibition of cAMP-dependent protein kinase plays a key role in the induction of mitosis and nuclear envelope breakdown in mammalian cells, EMBO J. 10 (1991) 1523–1533.
[25] B. Yu, Y. Wang, Y. Liu, Y. Liu, X. Li, D. Wu, Z. Zong, J. Zhang, D. Yu, Protein kinase A regulates cell cycle progression of mouse fertilized eggs by means of MPF, Dev. Dyn. 232 (2005) 98–105.

[26] B. Meister, J. Fryckstedt, M. Schalling, R. Cortes, T. Hokfelt, A. Aperia, H.C. Hemmings, A.C. Nairn, M. Ehrlich, P. Greengard, Dopamine- and cAMP-regulated phosphoprotein (DARPP-32) and dopamine DA1 agonist-sensitive Na+,K+-ATPase in renal tubule cells, Proc. Natl. Acad. Sci. U. S. A. 86 (1989) 8068–8072.
[27] M.J. Lohse, J.L. Benovic, M.G. Caron, R.J. Lefkowitz, Multiple pathways of rapid beta 2-adrenergic receptor desensitization. Delineation with specific inhibitors, J. Biol. Chem. 265 (1990) 3202–3211.
[28] K.S. Murthy, G.M. Makhlouf, Interaction of cA-kinase and cG-kinase in mediating relaxation of dispersed smooth muscle cells, Am. J. Physiol. 268 (1995) C171–C180.
[29] G.D. Dalton, F.L. Smith, P.A. Smith, W.L. Dewey, Alterations in brain protein kinase A activity and reversal of morphine tolerance by two fragments of native protein kinase A inhibitor peptide (PKI), Neuropharmacology 48 (2005) 648–657.
[30] T.E. Harris, S.J. Persaud, P.M. Jones, Pseudosubstrate inhibition of cyclic AMP-dependent protein kinase in intact pancreatic islets: effects on cyclic AMP-dependent and glucose-dependent insulin secretion, Biochem. Biophys. Res. Commun. 232 (1997) 648–651.
[31] H. Tong, D. Bernstein, E. Murphy, C. Steenbergen, The role of beta-adrenergic receptor signaling in cardioprotection, FASEB J. 19 (2005) 983–985.
[32] K.S. Murthy, H. Zhou, G.M. Makhlouf, PKA-dependent activation of PDE3A and PDE4 and inhibition of adenylyl cyclase V/VI in smooth muscle, Am. J. Physiol. 282 (2002) C508–C517.
[33] L.O. Flowers, H.M. Johnson, M.G. Mujtaba, M.R. Ellis, S.M. Haider, P.S. Subramaniam, Characterization of a peptide inhibitor of Janus kinase 2 that mimics suppressor of cytokine signaling 1 function, J. Immunol. 172 (2004) 7510–7518.
[34] B.E. Kemp, E. Benjamini, E.G. Krebs, Synthetic hexapeptide substrates and inhibitors of 3′:5′-cyclic AMP-dependent protein kinase, Proc. Natl. Acad. Sci. U. S. A. 73 (1976) 1038–1042.
[35] J.R. Feramisco, E.G. Krebs, Inhibition of cyclic AMP-dependent protein kinase by analogues of a synthetic peptide substrate, J. Biol. Chem. 253 (1978) 8968–8971.
[36] H.N. Bramson, N. Thomas, R. Matsueda, N.C. Nelson, S.S. Taylor, E.T. Kaiser, Modification of the catalytic subunit of bovine heart cAMP-dependent protein kinase with affinity labels related to peptide substrates, J. Biol. Chem. 257 (1982) 10575–10581.
[37] A. Salerno, D.S. Lawrence, Covalent modification with concomitant inactivation of the cAMP-dependent protein kinase by affinity labels containing only L-amino acids, J. Biol. Chem. 268 (1993) 13043–13049.
[38] W.T. Miller, E.T. Kaiser, Probing the peptide binding site of the cAMP-dependent protein kinase by using a peptide-based photoaffinity label, Proc. Natl. Acad. Sci. U. S. A. 85 (1988) 5429–5433.
[39] C.A. O'Brian, N.E. Ward, R.M. Liskamp, D.B. de Bont, J.H. van Boom, N-myristyl–Lys–Arg–Thr–Leu–Arg: a novel protein kinase C inhibitor, Biochem. Pharmacol. 39 (1990) 49–57.
[40] N.E. Ward, C.A. O'Brian, Inhibition of protein kinase C by N-myristoylated peptide substrate analogs, Biochemistry 32 (1993) 11903–11909.
[41] C.G. Ioannides, R.S. Freedman, R.M. Liskamp, N.E. Ward, C.A. O'Brian, Inhibition of IL-2 receptor induction and IL-2 production in the human leukemic cell line Jurkat by a novel peptide inhibitor of protein kinase C, Cell. Immunol. 131 (1990) 242–252.
[42] N.E. Ward, K.R. Gravitt, C.A. O'Brian, Irreversible inactivation of protein kinase C by a peptide–substrate analog, J. Biol. Chem. 270 (1995) 8056–8060.
[43] J.H. Lee, S.K. Nandy, D.S. Lawrence, A highly potent and selective PKCalpha inhibitor generated via combinatorial modification of a peptide scaffold, J. Am. Chem. Soc. 126 (2004) 3394–3395.
[44] T. Obata, M.B. Yaffe, G.G. Leparc, E.T. Piro, H. Maegawa, A. Kashiwagi, R. Kikkawa, L.C. Cantley, Peptide and protein library screening defines optimal substrate motifs for AKT/PKB, J. Biol. Chem. 275 (2000) 36108–36115.
[45] Y. Luo, R.A. Smith, R. Guan, X. Liu, V. Klinghofer, J. Shen, C. Hutchins, P. Richardson, T. Holzman, S.H. Rosenberg, V.L. Giranda, Pseudosubstrate peptides inhibit Akt and induce cell growth inhibition, Biochemistry 43 (2004) 1254–1263.
[46] D. Graves, C. Bartleson, A. Biorn, M. Pete, Substrate and inhibitor recognition of protein kinases: what is known about the catalytic subunit of phosphorylase kinase? Pharmacol. Ther. 82 (1999) 143–155.
[47] L.B. Tabatabai, D.J. Graves, Kinetic mechanism and specificity of the phosphorylase kinase reaction, J. Biol. Chem. 253 (1978) 2196–2202.
[48] G. Pfitzer, Invited review: regulation of myosin phosphorylation in smooth muscle, J. Appl. Physiol. 91 (2001) 497–503.
[49] R.B. Pearson, L.Y. Misconi, B.E. Kemp, Smooth muscle myosin kinase requires residues on the COOH-terminal side of the phosphorylation site. Peptide inhibitors, J. Biol. Chem. 261 (1986) 25–27.
[50] K.S. Lam, J. Wu, Q. Lou, Identification and characterization of a novel synthetic peptide substrate specific for Src-family protein tyrosine kinases, Int. J. Pept. Protein Res. 45 (1995) 587–592.
[51] J. Alfaro-Lopez, W. Yuan, B.C. Phan, J. Kamath, Q. Lou, K.S. Lam, V.J. Hruby, Discovery of a novel series of potent and selective substrate-based inhibitors of p60c-src protein tyrosine kinase: conformational and topographical constraints in peptide design, J. Med. Chem. 41 (1998) 2252–2260.
[52] J.R. Kamath, R. Liu, A.M. Enstrom, Q. Lou, K.S. Lam, Development and characterization of potent and specific peptide inhibitors of p60c-src protein tyrosine kinase using pseudosubstrate-based inhibitor design approach, J. Pept. Res. 62 (2003) 260–268.
[53] L. Ramdas, N.U. Obeyesekere, G. Sun, J.S. McMurray, R.J. Budde, N-myristoylation of a peptide substrate for Src converts it into an apparent slow-binding bisubstrate-type inhibitor, J. Pept. Res. 53 (1999) 569–577.
[54] K. Parang, P.A. Cole, Designing bisubstrate analog inhibitors for protein kinases, Pharmacol. Ther. 93 (2002) 145–157.
[55] A. Ricouart, J.C. Gesquiere, A. Tartar, C. Sergheraert, Design of potent protein kinase inhibitors using the bisubstrate approach, J. Med. Chem. 34 (1991) 73–78.
[56] D. Medzihradszky, S.L. Chen, L.C. Kenyon, B.W. Gibson, Solid-phase synthesis of adenosine phosphopeptides as potential bisubstrate inhibitors of protein kinases, J. Am. Chem. Soc. 116 (1994) 9413–9419.
[57] A.C. Hines, P.A. Cole, Design, synthesis, and characterization of an ATP-peptide conjugate inhibitor of protein kinase A, Bioorg. Med. Chem. Lett. 14 (2004) 2951–2954.
[58] A. Kuznetsov, A. Uri, G. Raidaru, J. Jarv, Kinetic analysis of inhibition of cAMP-dependent protein kinase catalytic subunit by the peptide-nucleoside conjugate AdcAhxArg6, Bioorg. Chem. 32 (2004) 527–535.
[59] K. Parang, J.H. Till, A.J. Ablooglu, R.A. Kohanski, S.R. Hubbard, P.A. Cole, Mechanism-based design of a protein kinase inhibitor, Nat. Struct. Biol. 8 (2001) 37–41.
[60] S.E. Shoelson, S. Chatterjee, M. Chaudhuri, M.F. White, YMXM motifs of IRS-1 define substrate specificity of the insulin receptor kinase, Proc. Natl. Acad. Sci. U. S. A. 89 (1992) 2027–2031.
[61] A.J. Ablooglu, J.H. Till, K. Kim, K. Parang, P.A. Cole, S.R. Hubbard, R.A. Kohanski, Probing the catalytic mechanism of the insulin receptor kinase with a tetrafluorotyrosine-containing peptide substrate, J. Biol. Chem. 275 (2000) 30394–30398.
[62] B.E. Kemp, R.B. Pearson, C.M. House, Pseudosubstrate-based peptide inhibitors, Methods Enzymol. 201 (1991) 287–304.
[63] D. Mochly-Rosen, Localization of protein kinases by anchoring proteins: a theme in signal transduction, Science 268 (1995) 247–251.
[64] D. Mochly-Rosen, A.S. Gordon, Anchoring proteins for protein kinase C: a means for isozyme selectivity, FASEB J. 12 (1998) 35–42.
[65] C. House, B.E. Kemp, Protein kinase C contains a pseudosubstrate prototope in its regulatory domain, Science 238 (1987) 1726–1728.
[66] C. House, B.E. Kemp, Protein kinase C pseudosubstrate prototope: structure–function relationships, Cell. Signal. 2 (1990) 187–190.
[67] A. Ricouart, A. Tartar, C. Sergheraert, Inhibition of protein kinase C by retro-inverso pseudosubstrate analogues, Biochem. Biophys. Res. Commun. 165 (1989) 1382–1390.
[68] D.R. Alexander, J.D. Graves, S.C. Lucas, D.A. Cantrell, M.J. Crumpton, A method for measuring protein kinase C activity in permeabilized T

lymphocytes by using peptide substrates. Evidence for multiple pathways of kinase activation, Biochem. J. 268 (2) (1990) 303–308.
[69] D.R. Alexander, J.M. Hexham, S.C. Lucas, J.D. Graves, D.A. Cantrell, M.J. Crumpton, A protein kinase C pseudosubstrate peptide inhibits phosphorylation of the CD3 antigen in streptolysin-O-permeabilized human T lymphocytes, Biochem. J. 260 (1989) 893–901.
[70] T. Eichholtz, J. Alblas, M. van Overveld, W. Moolenaar, H. Ploegh, A pseudosubstrate peptide inhibits protein kinase C-mediated phosphorylation in permeabilized Rat-1 cells, FEBS Lett. 261 (1990) 147–150.
[71] S.S. Shen, W.R. Buck, A synthetic peptide of the pseudosubstrate domain of protein kinase C blocks cytoplasmic alkalinization during activation of the sea urchin egg, Dev. Biol. 140 (1990) 272–280.
[72] S.C. Ahlgren, J.D. Levine, Protein kinase C inhibitors decrease hyperalgesia and C-fiber hyperexcitability in the streptozotocin-diabetic rat, J. Neurophysiol. 72 (1994) 684–692.
[73] S.G. Rane, M.P. Walsh, J.R. McDonald, K. Dunlap, Specific inhibitors of protein kinase C block transmitter-induced modulation of sensory neuron calcium current, Neuron 3 (1989) 239–245.
[74] R. Malinow, H. Schulman, R.W. Tsien, Inhibition of postsynaptic PKC or CaMKII blocks induction but not expression of LTP, Science 245 (1989) 862–866.
[75] O. Hvalby, H.C. Hemmings, O. Paulsen, A.J. Czernik, A.C. Nairn, J.M. Godfraind, V. Jensen, M. Raastad, J.F. Storm, P. Andersen, P. Greengard, Specificity of protein kinase inhibitor peptides and induction of long-term potentiation, Proc. Natl. Acad. Sci. U. S. A. 91 (1994) 4761–4765.
[76] T. Eichholtz, D.B. de Bont, J. de Widt, R.M. Liskamp, H.L. Ploegh, A myristoylated pseudosubstrate peptide, a novel protein kinase C inhibitor, J. Biol. Chem. 268 (1993) 1982–1986.
[77] A.J. Verhoeven, J.H. Leusen, G.C. Kessels, P.M. Hilarius, D.B. de Bont, R.M. Liskamp, Inhibition of neutrophil NADPH oxidase assembly by a myristoylated pseudosubstrate of protein kinase C, J. Biol. Chem. 268 (1993) 18593–18598.
[78] T.E. Harris, S.J. Persaud, T. Saermark, P.M. Jones, A myristoylated pseudosubstrate peptide inhibitor of protein kinase C: effects on glucose- and carbachol-induced insulin secretion, Mol. Cell. Endocrinol. 121 (1996) 133–141.
[79] P.J. Bergman, K.R. Gravitt, C.A. O'Brian, An N-myristoylated protein kinase C-alpha pseudosubstrate peptide that functions as a multidrug resistance reversal agent in human breast cancer cells is not a P-glycoprotein substrate, Cancer Chemother. Pharmacol. 40 (1997) 453–456.
[80] L. Theodore, D. Derossi, G. Chassaing, B. Llirbat, M. Kubes, P. Jordan, H. Chneiweiss, P. Godement, A. Prochiantz, Intraneuronal delivery of protein kinase C pseudosubstrate leads to growth cone collapse, J. Neurosci. 15 (1995) 7158–7167.
[81] M.A. Bogoyevitch, T.S. Kendrick, D.C.H. Ng, R.K. Barr, Taking the cell by stealth or storm? Protein transduction domains (PTDs) as versatile vectors for delivery, DNA Cell Biol. 21 (2002) 879–894.
[82] I. Dominguez, M.T. Diaz-Meco, M.M. Municio, E. Berra, A. Garcia de Herreros, M.E. Cornet, L. Sanz, J. Moscat, Evidence for a role of protein kinase C zeta subspecies in maturation of *Xenopus laevis* oocytes, Mol. Cell. Biol. 12 (1992) 3776–3783.
[83] I. Dominguez, L. Sanz, F. Arenzana-Seisdedos, M.T. Diaz-Meco, J.L. Virelizier, J. Moscat, Inhibition of protein kinase C zeta subspecies blocks the activation of an NF-kappa B-like activity in *Xenopus laevis* oocytes, Mol. Cell. Biol. 13 (1993) 1290–1295.
[84] B.P. De, S. Gupta, S. Gupta, A.K. Banerjee, Cellular protein kinase C isoform zeta regulates human parainfluenza virus type 3 replication, Proc. Natl. Acad. Sci. U. S. A. 92 (1995) 5204–5208.
[85] G. Bandyopadhyay, M.L. Standaert, L. Galloway, J. Moscat, R.V. Farese, Evidence for involvement of protein kinase C (PKC)-zeta and noninvolvement of diacylglycerol-sensitive PKCs in insulin-stimulated glucose transport in L6 myotubes, Endocrinology 138 (1997) 4721–4731.
[86] S.H. Tang, G.W. Sharp, Atypical protein kinase C isozyme zeta mediates carbachol-stimulated insulin secretion in RINm5F cells, Diabetes 47 (1998) 905–912.
[87] A. Muscella, S. Greco, M.G. Elia, C. Storelli, S. Marsigliante, PKC-zeta is required for angiotensin II-induced activation of ERK and synthesis of C-FOS in MCF-7 cells, J. Cell. Physiol. 197 (2003) 61–68.
[88] M. McConkey, H. Gillin, C.R. Webster, M.S. Anwer, Cross-talk between protein kinases Czeta and B in cyclic AMP-mediated sodium taurocholate co-transporting polypeptide translocation in hepatocytes, J. Biol. Chem. 279 (2004) 20882–20888.
[89] P. Serrano, Y. Yao, T.C. Sacktor, Persistent phosphorylation by protein kinase Mzeta maintains late-phase long-term potentiation, J. Neurosci. 25 (2005) 1979–1984.
[90] D. Bonnet, K. Thiam, E. Loing, O. Melnyk, H. Gras-Masse, Synthesis by chemoselective ligation and biological evaluation of novel cell-permeable PKC-zeta pseudosubstrate lipopeptides, J. Med. Chem. 44 (2001) 468–471.
[91] B.E. Kemp, R.B. Pearson, V. Guerriero, I.C. Bagchi, A.R. Means, The calmodulin binding domain of chicken smooth muscle myosin light chain kinase contains a pseudosubstrate sequence, J. Biol. Chem. 262 (1987) 2542–2548.
[92] M. Ikebe, M. Stepinska, B.E. Kemp, A.R. Means, D.J. Hartshorne, Proteolysis of smooth muscle myosin light chain kinase. Formation of inactive and calmodulin-independent fragments, J. Biol. Chem. 262 (1987) 13828–13834.
[93] T. Itoh, M. Ikebe, G.J. Kargacin, D.J. Hartshorne, B.E. Kemp, F.S. Fay, Effects of modulators of myosin light-chain kinase activity in single smooth muscle cells, Nature 338 (1989) 164–167.
[94] T.J. Lukas, S. Mirzoeva, U. Slomczynska, D.M. Watterson, Identification of novel classes of protein kinase inhibitors using combinatorial peptide chemistry based on functional genomics knowledge, J. Med. Chem. 42 (1999) 910–919.
[95] M.E. Payne, Y.L. Fong, T. Ono, R.J. Colbran, B.E. Kemp, T.R. Soderling, A.R. Means, Calcium/calmodulin-dependent protein kinase II. Characterization of distinct calmodulin binding and inhibitory domains, J. Biol. Chem. 263 (1988) 7190–7195.
[96] R.J. Colbran, M.K. Smith, C.M. Schworer, Y.L. Fong, T.R. Soderling, Regulatory domain of calcium/calmodulin-dependent protein kinase II. Mechanism of inhibition and regulation by phosphorylation, J. Biol. Chem. 264 (1989) 4800–4804.
[97] R. Gopalakrishna, S.H. Barsky, T.P. Thomas, W.B. Anderson, Factors influencing chelator-stable, detergent-extractable, phorbol diester-induced membrane association of protein kinase C. Differences between Ca^{2+}-induced and phorbol ester-stabilized membrane bindings of protein kinase C, J. Biol. Chem. 261 (1986) 16438–16445.
[98] D. Mochly-Rosen, C.J. Henrich, L. Cheever, H. Khaner, P.C. Simpson, A protein kinase C isozyme is translocated to cytoskeletal elements on activation, Cell. Regul. 1 (1990) 693–706.
[99] D. Ron, J.H. Luo, D. Mochly-Rosen, C2 region-derived peptides inhibit translocation and function of beta protein kinase C in vivo, J. Biol. Chem. 270 (1995) 24180–24187.
[100] Z. Zhang, H, J.A. Johnson, L. Chen, N. El-Sherif, D. Mochly-Rosen, M. Boutjdir, C2 region-derived peptides of beta-protein kinase C regulate cardiac Ca^{2+} channels, Circ. Res. 80 (1997) 720–729.
[101] J.A. Johnson, M.O. Gray, C.-H. Chen, D. Mochly-Rosen, A protein kinase C translocation inhibitor as an isozyme-selective antagonist of cardiac function, J. Biol. Chem. 271 (1996) 24962–24966.
[102] M.O. Gray, J.S. Karliner, D. Mochly-Rosen, A selective epsilon-peptide protein kinase C antagonist inhibits protection of cardiac myocytes from hypoxia-induced cell death, J. Biol. Chem. 272 (1997) 30945–30951.
[103] M. Yedovitzky, D. Mochly-Rosen, J.A. Johnson, M.O. Fray, D. Ron, E. Abramovitch, E. Cerasi, R. Nesher, Translocation inhibitors define specificity of protein kinase C isoenzymes in pancreatic beta-cells, J. Biol. Chem. 272 (1997) 1417–1420.
[104] G.C. Mayne, A.W. Murray, Evidence that protein kinase Cepsilon mediates phorbol ester inhibition of calphostin C- and tumor necrosis factor-alpha-induced apoptosis in U937 histiocytic lymphoma cells, J. Biol. Chem. 273 (1998) 24115–24121.
[105] Y. Chen, A.R. Cantrell, R.O. Messing, T. Scheuer, W.A. Catterall, Specific modulation of Na+ channels in hippocampal neurons by protein kinase Cepsilon, J. Neurosci. 25 (2005) 507–513.
[106] L. Chen, H. Hahn, G. Wu, C.H. Chen, T. Liron, D. Schechtman, G. Cavallaro, L. Banci, Y. Guo, R. Bolli, G.W. Dorn, D. Mochly-Rosen, Opposing cardioprotective actions and parallel hypertrophic effects of

delta PKC and epsilon PKC, Proc. Natl. Acad. Sci. U. S. A. 98 (2001) 11114–11119.
[107] K. Inagaki, L. Chen, F. Ikeno, F.H. Lee, K. Imahashi, D.M. Bouley, M. Rezaee, P.G. Yock, E. Murphy, D. Mochly-Rosen, Inhibition of delta-protein kinase C protects against reperfusion injury of the ischemic heart in vivo, Circulation 108 (2003) 2304–2307.
[108] K. Inagaki, H.S. Hahn, G.W. Dorn, D. Mochly-Rosen, Additive protection of the ischemic heart ex vivo by combined treatment with delta-protein kinase C inhibitor and epsilon-protein kinase C activator, Circulation 108 (2003) 869–875.
[109] C.L. Murriel, E. Churchill, K. Inagaki, L.I. Szweda, D. Mochly-Rosen, Protein kinase Cdelta activation induces apoptosis in response to cardiac ischemia and reperfusion damage: a mechanism involving BAD and the mitochondria, J. Biol. Chem. 279 (2004) 47985–47991.
[110] R. Bright, A.P. Raval, J.M. Dembner, M.A. Perez-Pinzon, G.K. Steinberg, M.A. Yenari, D. Mochly-Rosen, Protein kinase C delta mediates cerebral reperfusion injury in vivo, J. Neurosci. 24 (2004) 6880–6888.
[111] M. Tanaka, R.D. Terry, G.K. Mokhtari, K. Inagaki, T. Koyanagi, T. Kofidis, D. Mochly-Rosen, R.C. Robbins, Suppression of graft coronary artery disease by a brief treatment with a selective epsilonPKC activator and a deltaPKC inhibitor in murine cardiac allografts, Circulation 110 (11 Suppl. 1) (2004) II194–II199.
[112] M. Tanaka, F. Gunawan, R.D. Terry, K. Inagaki, A.D. Caffarelli, G. Hoyt, P.S. Tsao, D. Mochly-Rosen, R.C. Robbins, Inhibition of heart transplant injury and graft coronary artery disease after prolonged organ ischemia by selective protein kinase C regulators, J. Thorac. Cardiovasc. Surg. 129 (2005) 1160–1167.
[113] M.U. Braun, D. Mochly-Rosen, Opposing effects of delta- and zeta-protein kinase C isozymes on cardiac fibroblast proliferation: use of isozyme-selective inhibitors, J. Mol. Cell. Cardiol. 35 (2003) 895–903.
[114] M. Goldenberg-Furmanov, I. Stein, E. Pikarsky, H. Rubin, S. Kasem, M. Wygoda, I. Weinstein, H. Reuveni, S.A. Ben-Sasson, Lyn is a target gene for prostate cancer: sequence-based inhibition induces regression of human tumor xenografts, Cancer Res. 64 (2004) 1058–1066.
[115] M.Y. Niv, H. Rubin, J. Cohen, L. Tsirulnikov, T. Licht, A. Peretzman-Shemer, E. Can'an, A. Tartakovsky, I. Stein, S. Albeck, I. Weinstein, M. Goldenberg-Furmanov, D. Tobi, E. Cohen, M. Laster, S.A. Ben-Sasson, H. Reuveni, Sequence-based design of kinase inhibitors applicable for therapeutics and target identification, J. Biol. Chem. 279 (2004) 1242–1255.
[116] J.J. Michel, J.D. Scott, AKAP mediated signal transduction, Annu. Rev. Pharmacol. Toxicol. 42 (2002) 235–257.
[117] W. Wong, J.D. Scott, AKAP signalling complexes: focal points in space and time, Nat. Rev., Mol. Cell Biol. 5 (2004) 959–970.
[118] M. Colledge, J.D. Scott, AKAPs: from structure to function, Trends Cell Biol. 9 (1999) 216–221.
[119] D.W. Carr, D.A. DeManno, A. Atwood, M. Hunzicker-Dunn, J.D. Scott, Follicle-stimulating hormone regulation of A-kinase anchoring proteins in granulosa cells, J. Biol. Chem. 268 (1993) 20729–20732.
[120] D.W. Carr, R.E. Stofko-Hahn, I.D. Fraser, S.M. Bishop, T.S. Acott, R.G. Brennan, J.D. Scott, Interaction of the regulatory subunit (RII) of cAMP-dependent protein kinase with RII-anchoring proteins occurs through an amphipathic helix binding motif, J. Biol. Chem. 266 (1991) 14188–14192.
[121] Z.E. Hausken, M.L. Dell'Acqua, V.M. Coghlan, J.D. Scott, Mutational analysis of the A-kinase anchoring protein (AKAP)-binding site on RII. Classification Of side chain determinants for anchoring and isoform selective association with AKAPs, J. Biol. Chem. 271 (1996) 29016–29022.
[122] S.B. Glantz, Y. Li, C.S. Rubin, Characterization of distinct tethering and intracellular targeting domains in AKAP75, a protein that links cAMP-dependent protein kinase II beta to the cytoskeleton, J. Biol. Chem. 268 (1993) 12796–12804.
[123] S. Vijayaraghavan, S.A. Goueli, M.P. Davey, D.W. Carr, Protein kinase A-anchoring inhibitor peptides arrest mammalian sperm motility, J. Biol. Chem. 272 (1997) 4747–4752.
[124] K.A. Burton, B.D. Johnson, Z.E. Hausken, R.E. Westenbroek, R.L. Idzerda, T. Scheuer, J.D. Scott, W.A. Catterall, G.S. McKnight, Type II regulatory subunits are not required for the anchoring-dependent modulation of Ca^{2+} channel activity by cAMP-dependent protein kinase, Proc. Natl. Acad. Sci. U. S. A. 94 (1997) 11067–11072.
[125] F.W. Herberg, A. Maleszka, T. Eide, L. Vossebein, K. Tasken, Analysis of A-kinase anchoring protein (AKAP) interaction with protein kinase A (PKA) regulatory subunits: PKA isoform specificity in AKAP binding, J. Mol. Biol. 298 (2000) 329–339.
[126] C. Rosenmund, D.W. Carr, S.E. Bergeson, G. Nilaver, J.D. Scott, G.L. Westbrook, Anchoring of protein kinase A is required for modulation of AMPA/kainate receptors on hippocampal neurons, Nature 368 (1994) 853–856.
[127] B.D. Johnson, T. Scheuer, W.A. Catterall, Voltage-dependent potentiation of L-type Ca2+ channels in skeletal muscle cells requires anchored cAMP-dependent protein kinase, Proc. Natl. Acad. Sci. U. S. A. 91 (1994) 11492–11496.
[128] L.B. Lester, L.K. Langeberg, J.D. Scott, Anchoring of protein kinase A facilitates hormone-mediated insulin secretion, Proc. Natl. Acad. Sci. U. S. A. 94 (1997) 14942–14947.
[129] R.S. Westphal, S.J. Tavalin, J.W. Lin, N.M. Alto, I.D. Fraser, L.K. Langeberg, M. Sheng, J.D. Scott, Regulation of NMDA receptors by an associated phosphatase-kinase signaling complex, Science 285 (1999) 93–96.
[130] E. Klussmann, K. Maric, B. Wiesner, M. Beyermann, W. Rosenthal, Protein kinase A anchoring proteins are required for vasopressin-mediated translocation of aquaporin-2 into cell membranes of renal principal cells, J. Biol. Chem. 274 (1999) 4934–4938.
[131] M.A. Fink, D.R. Zakhary, J.A. Mackey, R.W. Desnoyer, C. Apperson-Hansen, D.S. Damron, M. Bond, AKAP-mediated targeting of protein kinase a regulates contractility in cardiac myocytes, Circ. Res. 88 (2001) 291–297.
[132] M.A. Moita, R. Lamprecht, K. Nader, J.E. LeDoux, A-kinase anchoring proteins in amygdala are involved in auditory fear memory, Nat. Neurosci. 5 (2002) 837–838.
[133] M.G. Newlon, M. Roy, D. Morikis, Z.E. Hausken, V. Coghlan, J.D. Scott, P.A. Jennings, The molecular basis for protein kinase A anchoring revealed by solution NMR, Nat. Struct. Biol. 6 (1999) 222–227.
[134] N.M. Alto, S.H. Soderling, N. Hoshi, L.K. Langeberg, R. Fayos, P.A. Jennings, J.D. Scott, Bioinformatic design of A-kinase anchoring protein-in silico: a potent and selective peptide antagonist of type II protein kinase A anchoring, Proc. Natl. Acad. Sci. U. S. A. 100 (2003) 4445–4450.
[135] L.L. Burns-Hamuro, Y. Ma, S. Kammerer, U. Reineke, C. Self, C. Cook, G.L. Olson, C.R. Cantor, A. Braun, S.S. Taylor, Designing isoform-specific peptide disruptors of protein kinase A localization, Proc. Natl. Acad. Sci. U. S. A. 100 (2003) 4072–4077.
[136] M. Dickens, J.S. Rogers, J. Cavanagh, A. Raitano, Z. Xia, J.R. Halpern, M.E. Greenberg, C.L. Sawyers, R.J. Davis, A cytoplasmic inhibitor of the JNK signal transduction pathway, Science 277 (1997) 693–696.
[137] R.K. Barr, T.S. Kendrick, M.A. Bogoyevitch, Identification of the critical features of a small peptide inhibitor of JNK activity, J. Biol. Chem. 277 (2002) 10987–10997.
[138] R.K. Barr, I. Boehm, P.V. Attwood, P.M. Watt, M.A. Bogoyevitch, The critical features and the mechanism of inhibition of a kinase interaction motif-based peptide inhibitor of JNK, J. Biol. Chem. 279 (2004) 36327–36338.
[139] R.K. Barr, R.M. Hopkins, P.M. Watt, M.A. Bogoyevitch, Reverse two-hybrid screening identifies residues of JNK required for interaction with the kinase interaction motif of JNK-interacting protein-1, J. Biol. Chem. 279 (2004) 43178–43189.
[140] M.A. Bogoyevitch, Therapeutic promise of JNK ATP-noncompetitive inhibitors, Trends Mol. Med. (2005) 232–239.
[141] C. Bonny, A. Oberson, S. Negri, C. Sauser, D.F. Schorderet, Cell-permeable inhibitors of JNK: novel blockers of -cell death, Diabetes 50 (2001) 77–82.
[142] J. Laine, G. Kunstle, T. Obata, M. Sha, M. Noguchi, The protooncogene TCL1 is an Akt kinase coactivator, Mol. Cell 6 (2000) 395–407.
[143] M. Hiromura, F. Okada, T. Obata, D. Auguin, T. Shibata, C. Roume-

stand, M. Noguchi, Inhibition of Akt kinase activity by a peptide spanning the betaA strand of the proto-oncogene TCL1, J. Biol. Chem. 279 (2004) 53407–53418.
[144] M.J. Andrews, C. McInnes, G. Kontopidis, L. Innes, A. Cowan, A. Plater, P.M. Fischer, Design, synthesis, biological activity and structural analysis of cyclic peptide inhibitors targeting the substrate recruitment site of cyclin-dependent kinase complexes, Org. Biomol. Chem. 2 (2004) 2735–2741.
[145] C. Gondeau, S. Gerbal-Chaloin, P. Bello, G. Aldrian-Herrada, M.C. Morris, G. Divita, Design of a novel class of peptide inhibitors of cyclin-dependent kinase/cyclin activation, J. Biol. Chem. 280 (2005) 13793–13800.
[146] J. Wu, Q.N. Ma, K.S. Lam, Identifying substrate motifs of protein kinases by a random library approach, Biochemistry 33 (1994) 14825–14833.
[147] T. Nishi, R.J. Budde, J.S. McMurray, N.U. Obeyesekere, N. Safdar, V.A. Levin, H. Saya, Tight-binding inhibitory sequences against pp60(c-src) identified using a random 15-amino-acid peptide library, FEBS Lett. 399 (1996) 237–240.
[148] W.R. Dostmann, M.S. Taylor, C.K. Nickl, J.E. Brayden, R. Frank, W.J. Tegge, Highly specific, membrane-permeant peptide blockers of cGMP-dependent protein kinase Ialpha inhibit NO-induced cerebral dilation, Proc. Natl. Acad. Sci. U. S. A. 97 (2000) 14772–14777.
[149] T. Krieg, S. Philipp, L. Cui, W.R. Dostmann, J.M. Downey, M.V. Cohen, Peptide blockers of PKG inhibit ROS generation by acetylcholine and bradykinin in cardiomyocytes but fail to block protection in the whole heart, Am. J. Physiol. 288 (2005) H1976–H1981.
[150] M.S. Taylor, C. Okwuchukwuasanya, C.K. Nickl, W. Tegge, J.E. Brayden, W.R. Dostmann, Inhibition of cGMP-dependent protein kinase by the cell-permeable peptide DT-2 reveals a novel mechanism of vasoregulation, Mol. Pharmacol. 65 (2004) 1111–1119.
[151] N.B. Dey, K.F. Foley, T.M. Lincoln, W.R. Dostmann, Inhibition of cGMP-dependent protein kinase reverses phenotypic modulation of vascular smooth muscle cells, J. Cardiovasc. Pharmacol. 45 (2005) 404–413.
[152] W.J. Fantl, J.A. Escobedo, G.A. Martin, C.W. Turck, M. de Rosario, F. McCormick, L.T. Williams, Distinct phosphotyrosines on a growth factor receptor bind to specific molecules that mediate different signaling pathway, Cell 69 (1992) 413–423.
[153] K. Nishikawa, S. Sawasdikosol, D.A. Fruman, J. Lai, Z. Songyang, S.J. Burakoff, M.B. Yaffe, L.C. Cantley, A peptide library approach identifies a specific inhibitor for the ZAP-70 protein tyrosine kinase, Mol. Cell 6 (2000) 969–974.
[154] L.T. Nevalainen, T. Aoyama, M. Ikura, A. Crivici, H. Yan, N.H. Chua, A.C. Nairn, Characterization of novel calmodulin-binding peptides with distinct inhibitory effects on calmodulin-dependent enzymes, Biochem. J. 321 (1997) 107–115.
[155] S.E. Perea, O. Reyes, Y. Puchades, O. Mendoza, N.S. Vispo, I. Torrens, A. Santos, R. Silva, B. Acevedo, E. Lopez, V. Falcon, D.F. Alonso, Antitumor effect of a novel proapoptotic peptide that impairs the phosphorylation by the protein kinase 2 (casein kinase 2), Cancer Res. 64 (2004) 7127–7129.
[156] W.S. Alexander, D.J. Hilton, The role of suppressors of cytokine signaling (SOCS) proteins in regulation of the immune response, Annu. Rev. Immunol. 22 (2004) 503–529.
[157] H. Yasukawa, H. Misawa, H. Sakamoto, M. Masuhara, A. Sasaki, T. Wakioka, S. Ohtsuka, T. Imaizumi, T. Matsuda, J.N. Ihle, A. Yoshimura, The JAK-binding protein JAB inhibits Janus tyrosine kinase activity through binding in the activation loop, EMBO J. 18 (1999) 1309–1320.
[158] M. Villain, P.L. Jackson, M.K. Manion, W.J. Dong, Z. Su, G. Fassina, T.M. Johnson, T.T. Sakai, N.R. Krishna, J.E. Blalock, De novo design of peptides targeted to the EF hands of calmodulin, J. Biol. Chem. 275 (2000) 2676–2685.
[159] G. Fassina, G. Cassani, A. Corti, Binding of human tumor necrosis factor alpha to multimeric complementary peptides, Arch. Biochem. Biophys. 296 (1992) 137–143.
[160] J.E. Blalock, K.L. Bost, Binding of peptides that are specified by complementary RNAs, Biochem. J. 234 (1986) 679–683.
[161] L.O. Flowers, P.S. Subramaniam, H.M. Johnson, A SOCS-1 peptide mimetic inhibits both constitutive and IL-6 induced activation of STAT3 in prostate cancer cells, Oncogene 24 (2005) 2114–2120.
[162] J.F. Ohren, H. Chen, A. Pavlovsky, C. Whitehead, E. Zhang, P. Kuffa, C. Yan, P. McConnell, C. Spessard, C. Banotai, W.T. Mueller, A. Delaney, C. Omer, J. Sebolt-Leopold, D.T. Dudley, I.K. Leung, C. Flamme, J. Warmus, M. Kaufman, S. Barrett, H. Tecle, C.A. Hasemann, Structures of human MAP kinase kinase 1 (MEK1) and MEK2 describe novel noncompetitive kinase inhibition, Nat. Struct. Mol. Biol. 11 (2004) 1192–1197.
[163] K. Gumireddy, S.J. Baker, S.C. Cosenza, P. John, A.D. Kang, K.A. Robell, M.V. Reddy, E.P. Reddy, A non-ATP-competitive inhibitor of BCR-ABL overrides imatinib resistance, Proc. Natl. Acad. Sci. U. S. A. 102 (2005) 1992–1997.
[164] A. Martinez, M. Alonso, A. Castro, C. Perez, F.J. Moreno, First non-ATP competitive glycogen synthase kinase 3 beta (GSK-3beta) inhibitors: thiadiazolidinones (TDZD) as potential drugs for the treatment of Alzheimer's disease, J. Med. Chem. 45 (2002) 1292–1299.
[165] S. Conde, D.I. Perez, A. Martinez, C. Perez, F.J. Moreno, Thienyl and phenyl alpha-halomethyl ketones: new inhibitors of glycogen synthase kinase (GSK-3beta) from a library of compound searching, J. Med. Chem. 46 (2003) 4631–4633.
[166] R. Saperstein, P.P. Vicario, H.V. Strout, E. Brady, E.E. Slater, W.J. Greenlee, D.L. Ondeyka, A.A. Patchett, D.G. Hangauer, Design of a selective insulin receptor tyrosine kinase inhibitor and its effect on glucose uptake and metabolism in intact cells, Biochemistry 28 (1989) 5694–5701.
[167] T.R. Burke, B. Lim, V.E. Marquez, Z.H. Li, J.B. Bolen, I. Stefanova, I.D. Horak, Bicyclic compounds as ring-constrained inhibitors of protein-tyrosine kinase p56lck, J. Med. Chem. 36 (1993) 425–432.
[168] C.-K. Huang, F.-Y. Wu, Y.-X. Ai, Polyhydroxylated 3-(N-phenyl) carbamoyl-2-iminochromene derivatives as potent inhibitors of tyrosine kinase p60c-src, Bioorg. Med. Chem. Lett. 5 (1995) 2423–2428.
[169] T.H. Marsilje, K.L. Milkiewicz, D.G. Hangauer, The design, synthesis and activity of non-ATP competitive inhibitors of pp60(c-src) tyrosine kinase: Part 1. Hydroxynaphthalene derivatives, Bioorg. Med. Chem. Lett. 10 (2000) 477–481.
[170] K.L. Milkiewicz, T.H. Marsilje, R.P. Woodworth, N. Bifulco, M.J. Hangauer, D.G. Hangauer, The design, synthesis and activity of non-ATP competitive inhibitors of pp60(c-src) tyrosine kinase: Part 2. Hydroxyindole derivatives, Bioorg. Med. Chem. Lett. 10 (2000) 483–486.
[171] D. Mochly-Rosen, H. Khaner, J. Lopez, B.L. Smith, Intracellular receptors for activated protein kinase C. Identification of a binding site for the enzyme, J. Biol. Chem. 266 (1991) 14866–14868.
[172] H. Kaneto, Y. Nakatani, T. Miyatsuka, D. Kawamori, T.A. Matsuoka, M. Matsuhisa, Y. Kajimoto, H. Ichijo, Y. Yamasaki, M. Hori, Possible novel therapy for diabetes with cell-permeable JNK-inhibitory peptide, Nat. Med. 10 (2004) 1128–1132.
[173] T. Borsello, P.G. Clarke, L. Hirt, A. Vercelli, M. Repici, D.F. Schorderet, J. Bogousslavsky, C. Bonny, A peptide inhibitor of c-Jun N-terminal kinase protects against excitotoxicity and cerebral ischemia, Nat. Med. 9 (2003) 1180–1186.
[174] L. Hirt, J. Badaut, J. Thevenet, C. Granziera, L. Regli, F. Maurer, C. Bonny, J. Bogousslavsky, D-JNKI1, a cell-penetrating c-Jun-N-terminal kinase inhibitor, protects against cell death in severe cerebral ischemia, Stroke 35 (2004) 1738–1743.
[175] G. Tezel, X. Yang, J. Yang, M.B. Wax, Role of tumor necrosis factor receptor-1 in the death of retinal ganglion cells following optic nerve crush injury in mice, Brain Res. 996 (2004) 202–212.
[176] J. Wang, T.R. Van De Water, C. Bonny, F. de Ribaupierre, J.L. Puel, A. Zine, A peptide inhibitor of c-Jun N-terminal kinase protects against both aminoglycoside and acoustic trauma-induced auditory hair cell death and hearing loss, J. Neurosci. 23 (2003) 8596–8607.
[177] J. Wang, S. Ladrech, R. Pujol, P. Brabet, T.R. Van De Water, J.L. Puel, Caspase inhibitors, but not c-Jun NH2-terminal kinase inhibitor treatment, prevent cisplatin-induced hearing loss, Cancer Res. 64 (2004) 9217–9224.

[178] A.M. Minogue, A.W. Schmid, M.P. Fogarty, A.C. Moore, V.A. Campbell, C.E. Herron, M.A. Lynch, Activation of the c-Jun N-terminal kinase signaling cascade mediates the effect of amyloid-beta on long term potentiation and cell death in hippocampus: a role for interleukin-1beta? J. Biol. Chem. 278 (2003) 27971–27980.
[179] Q. Wang, D.M. Walsh, M.J. Rowan, D.J. Selkoe, R. Anwyl, Block of long-term potentiation by naturally secreted and synthetic amyloid beta-peptide in hippocampal slices is mediated via activation of the kinases c-Jun N-terminal kinase, cyclin-dependent kinase 5, and p38 mitogen-activated protein kinase as well as metabotropic glutamate receptor type 5, J. Neurosci. 24 (2004) 3370–3378.
[180] X. Zhang, E. Moilanen, A. Lahti, M. Hamalainen, M.A. Giembycz, P.J. Barnes, M.A. Lindsay, H. Kankaanranta, Regulation of eosinophil apoptosis by nitric oxide: role of c-Jun-N-terminal kinase and signal transducer and activator of transcription 5, J. Allergy Clin. Immunol. 112 (2003) 93–101.

THE JOURNAL OF BIOLOGICAL CHEMISTRY
Vol. 280, No. 36, Issue of September 9, pp. 31776–31782, 2005

An Electron-sharing Network Involved in the Catalytic Mechanism Is Functionally Conserved in Different Glutathione Transferase Classes*

Received for publication, March 9, 2005, and in revised form, June 13, 2005
Published, JBC Papers in Press, July 12, 2005, DOI 10.1074/jbc.M502612200

Pakorn Winayanuwattikun‡ and Albert J. Ketterman§

From the Institute of Molecular Biology and Genetics, Mahidol University, Salaya Campus, Nakhon Pathom 73170, Thailand

In *Anopheles dirus* glutathione transferase D3–3, there are electrostatic interactions between the negatively charged glutamyl α-carboxylate group of glutathione, the positively charged Arg-66, and the negatively charged Asp-100. This ionic interaction is stabilized by a network of hydrogen bonds from Ser-65, Thr-158, Thr-162, and a conserved water-mediated contact. This alternating ionic bridge interaction between negatively and positively charged residues stabilized by a network of hydrogen bonding we have named an electron-sharing network. We show that the electron-sharing network assists the glutamyl α-carboxylate of glutathione to function as a catalytic base accepting the proton from the thiol group forming an anionic glutathione, which is a crucial step in the glutathione transferase (GST) catalysis. Kinetic studies demonstrate that the mutation of electron-sharing network residues results in a decreased ability to lower the pK_a of the thiol group of glutathione. Although the residues that contribute to the electron-sharing network are not conserved in the primary sequence, structural characterizations indicate that the presence of the network can be mapped to the same region in all GST classes. A structural diversification but functional conservation suggests a significant role for the electron-sharing network in catalysis as the purpose was maintained during the divergent evolution of GSTs. This network appears to be a functionally conserved motif that contributes to the "base-assisted deprotonation" model suggested to be essential for the glutathione ionization step of the catalytic mechanism.

Glutathione transferases (GSTs,[1] EC 2.5.1.18) are a superfamily of multifunctional enzymes involved in the cellular detoxification of various physiological and xenobiotic substances (1–4). The enzyme catalyzes the nucleophilic addition of the glutathione (GSH) sulfhydryl group to electrophilic centers of such organic compounds. The glutathione conjugates formed are rendered more water soluble, thereby facilitating their eventual elimination (3–7). The catalytic strategy can be divided into steps involving binding of substrates to the enzyme active site, activation of GSH by thiol deprotonation, nucleophilic attack by the thiolate at the electrophilic center, product formation, and product release (8–11).

The cytosolic GSTs have been subdivided into at least 13 distinct evolutionary classes designated Alpha, Mu, Pi, Theta, Sigma, Zeta, Kappa, Omega, Phi, Tau, Delta, Epsilon, and Beta on the basis of their primary structure, immunological properties, and substrate specificities (3, 12–19). GSTs possess a high specificity for glutathione as the nucleophile but exhibit broad specificity with regard to structurally diverse electrophilic second substrates. Individual classes of GSTs exhibit overlapping but distinct hydrophobic substrate and ligand binding specificities while retaining a high specificity toward the thiol substrate glutathione. Hence, a step of the activation of GSH by deprotonation of the thiol group to enhance the nucleophilicity for reaction with diverse types of electrophilic centers is crucial for the enzymatic catalysis. This thiol deprotonation results from the lowering of the pK_a of the thiol group of the enzyme-bound GSH from 9.0 to between 6.0 and 6.9, which causes a 200–300-fold rate acceleration at physiological pH (6, 20).

Many of the mechanistic investigations of GSTs have emphasized the importance of a conserved tyrosine or serine residue at the glutathione binding site of certain GSTs (Tyr-8 for Pi, Tyr-9 for Alpha, Tyr-6 for Mu, and Ser-9 for Delta class) in facilitating the thiol deprotonation (10, 21–23). The hydroxyl group of this tyrosine or serine residue that is within hydrogen-bonding distance of the thiol group of enzyme-bound glutathione is considered to be required for the correct orientation and stabilization of the deprotonated thiolate anion in the active site (10, 22, 24–26).

Apart from the foregoing, several experimental observations have implicated an alternative mechanism named "base-assisted deprotonation" (25, 27). This model has been proposed on the basis of the function of the glutamyl α-carboxylate of glutathione as a catalytic base that accepts the thiol proton from the thiol group. In this regard, it has become apparent that apart from the thiol group, the α-carboxylate of the Glu residue is also a crucial functional group of the glutathione contributing to the catalytic mechanism. It has been reported that an alternative thiol substrate in which the glutamyl part of the tripeptide was decarboxylated (GABA-Cys-Gly) displayed a large decrease in the catalytic efficiency of GSTA1–1 using 1-chloro-2,4-dinitrobenzene (CDNB) as the electrophilic substrate (28). The decrease was postulated to be partially due to a raised pK_a value of the active site-bound thiol group of glutathione resulting in an inability of the enzyme to promote ionization of decarboxylated GSH. Introduction of a carboxylate in the glutathione binding site of the enzyme in a location generally occupied by the glutamyl α-carboxylate partially res-

* This work was supported in part by the Thailand Research Fund. The costs of publication of this article were defrayed in part by the payment of page charges. This article must therefore be hereby marked "*advertisement*" in accordance with 18 U.S.C. Section 1734 solely to indicate this fact.

‡ Supported by a Royal Golden Jubilee Scholarship.

§ To whom correspondence should be addressed: Institute of Molecular Biology and Genetics, Mahidol University, Salaya Campus, 25/25 Putthamonthol, Rd. 4, Salaya, Nakhon Pathom 73170, Thailand. Tel.: 66-2-800-3624 (ext. 1279); Fax: 66-2-441-9906; E-mail: frakt@mahidol.ac.th.

[1] The abbreviations used are: GST, glutathione transferase; GSH, glutathione; CDNB, 1-chloro-2,4-dinitrobenzene; adGSTD3–3, *A. dirus* GSTD3–3; FDNB, 1-fluoro-2,4-dinitrobenzene; PDB, protein data bank.

TABLE I
Steady-state kinetic parameters and pK_a values for the thiol group of GSH of wild type and mutants of adGSTD3–3 for the CDNB conjugation reaction at pH 6.5 and 25 °C

The enzyme activities were measured at varying concentrations of CDNB and GSH in 0.1 M phosphate buffer, pH 6.5. The pK_a was obtained by using 0.1 M sodium acetate buffers (from pH 5.0 to 5.5) and 0.1 M potassium phosphate buffer (from pH 6.0 to 8.5). The reaction was monitored at 340 nm, ϵ = 9600 M^{-1} cm^{-1}.

Enzyme	k_{cat}	K_m^{GSH}	K_m^{CDNB}	K_{cat}/K_m^{GSH}	k_{cat}/K_m^{CDNB}	pK_a
	s^{-1}	mM	mM	s^{-1}/mM	s^{-1}/mM	
Wild type	35.4	0.27 ± 0.05	0.14 ± 0.01	131	246	6.36 ± 0.11
S65A	29.8	1.22 ± 0.12	0.34 ± 0.06	24.5	87.2	6.89 ± 0.23
R66A	3.3	5.10 ± 0.40	0.22 ± 0.04	0.64	14.6	7.23 ± 0.18
D100A	0.6	3.52 ± 0.33	0.54 ± 0.06	0.17	1.09	7.47 ± 0.10
T158A	23.9	0.43 ± 0.02	0.13 ± 0.00	55.3	189	6.93 ± 0.23
T162A	20.6	0.44 ± 0.03	0.15 ± 0.00	46.8	162	6.96 ± 0.25
T158A/T162A	21.9	5.74 ± 0.07	0.26 ± 0.03	3.81	172	7.10 ± 0.02
T158H	61.3	1.22 ± 0.09	0.31 ± 0.01	50.1	198	6.15 ± 0.01

cued the activity lost by the deletion of the α-carboxylate from glutathione, as the ability to ionize the thiol was improved.

Recent studies in the *Anopheles dirus* GSTD3–3 (adGSTD3–3) have provided information bearing on the base-assisted deprotonation model (29). It has been demonstrated that the pK_a value of the active site-bound GSH of a mutant, where the Arg-66 that directly interacts with the glutamyl α-carboxylate was changed into alanine, was shifted ~1 pH unit toward higher pH values. The positively charged Arg-66 would provide a counter ion that helps stabilize the α-carboxylate, thereby facilitating ionization of the thiol.

Observations on the active site structure have provided a further insight into the enzyme catalysis (30). The configuration of the glutamyl α-carboxylate group of glutathione, together with the G-site residues Ser-65, Arg-66, Asp-100, Thr-158, and Thr-162 makes possible an electron-sharing network for the distribution of a charge that could be in the form of either a proton or an electron. The aim of the present study is to ascertain the validity of this proposed electron-sharing network. Our study shows that the electron-sharing network helps promote the ionization of the thiol group of GSH through the base-assisted deprotonation model.

MATERIALS AND METHODS

Site-directed Mutagenesis—The plasmid pET3a-adgstD3, previously described (31), was used to generate the mutants via PCR-based site-directed mutagenesis. The proposed residues Ser-65, Arg-66, Asp-100, Thr-158, Thr-162, and Thr-158/Thr-162 were substituted with Ala by using the mutagenic primers that have been designed according to the 5′- and 3′-sequence of the *adgstD3* wild type gene (GenBank™ accession number AF273039). Each mutant was randomly screened by restriction digestion analysis. Mutant plasmids could be distinguished from the template by digestion with the restriction enzyme corresponding to the restriction recognition site introduced by the mutagenic primers. The full-length GST coding sequences of the plasmids carrying S65A, R66A, D100A, T158A, T162A, and T158A/T162A mutations were verified by the dideoxy chain termination method.

Heterologous Expression and Purification—The proteins were expressed from the pET3a-*adgstD3* vector in *Escherichia coli* BL21 (DE3)pLysS. The cells were grown to A_{600} = 0.5, and expression was induced by addition of 0.1 mM isopropyl 1-thio-β-galactopyranoside. Following induction for 3 h, cells were collected by centrifugation and lysed using sonication. The soluble recombinant GST proteins were purified by GSTrap affinity chromatography (Amersham Biosciences) or *S*-hexylglutathione-agarose (Sigma) affinity chromatography in the case of low affinity toward the glutathione ligand. The protein concentration was determined by the Bradford method using bovine serum albumin as a standard (32). The results showed that all mutant enzymes, S65A, R66A, D100A, Thr158Ala, T162A, and T158A/T162A were successfully expressed in *E. coli* and purified by affinity chromatography.

Steady-state Kinetics—Steady-state kinetics were studied for wild type and mutant enzymes at varying concentrations of CDNB and GSH in 0.1 M phosphate buffer, pH 6.5. The reaction was monitored at 340 nm, ϵ = 9600 M^{-1} cm^{-1}. Apparent kinetic constants, k_{cat}, K_m, and k_{cat}/K_m were determined by fitting the collected data to a Michaelis-Menten equation by non-linear regression analysis using GraphPad Prism (GraphPad software, San Diego, CA).

pH Dependence of Kinetic Constants—The pH dependence of k_{cat}/K_m^{CDNB} was obtained as stated above by recording the enzymatic reaction in the following buffers: 0.1 M sodium acetate buffers (from pH 5.0–5.5) and 0.1 M potassium phosphate buffer (from pH 6.0–8.5). The control studies showed that the affinity of the enzyme toward GSH does not change in the pH range utilized. pK_a values were obtained by fitting the data to equation $y = y_{lim}/(1 + 10^{pK_a - pH})$ (10).

Fluoride/Chloride Leaving Group Substitution—The second order kinetic constants at pH 6.5 for the spontaneous reaction of GSH with CDNB and FDNB (1-fluoro-2,4-dinitrobenzene) and the catalytic center activities at pH 6.5 for adGSTD3–3 with CDNB and FDNB as cosubstrates were obtained as described previously (33).

Substrate Specificity—The specific activities of the enzymes were determined by spectrophotometer with five different substrates: CDNB, 1,2-dichloro-4-nitrobenzene, ethacrynic acid, PNPBr (*p*-nitrophenethyl bromide), and *p*-nitrobenzyl chloride as previously described (34). However, the results showed that there is no detectable activity for all recombinant enzymes toward PNPBr as a cosubstrate.

Viscosity Effect on the Kinetic Parameters—The effect of viscosity on kinetic parameters was obtained by using 0.1 M potassium phosphate buffer, pH 6.5, with varying glycerol concentrations. Viscosity values (η) at 25 °C were calculated as previously described (35).

Half-life Determination—The thermal stability assay was performed to determine half-life of the GST proteins at 45 °C. The wild type and mutant enzymes were incubated at 45 °C at the protein concentration of 1 mg/ml. The inactivation time courses were determined by withdrawing suitable aliquots at the different time points for assay of remaining activity to calculate half-life of the enzyme.

RESULTS

Steady-state kinetic constants were obtained with varying concentrations of glutathione and CDNB substrate. Michaelis-Menten kinetic analysis was performed using non-linear regression (Table I). All the mutants showed increased K_m values for glutathione, except T158A and T162A, which are third sphere residues. In particular, the mutants S65A, R66A, D100A, and T158A/T162A showed K_m increases in the range of 5–21-fold. Conversely, no significant differences were found in K_m values for CDNB substrate, except for D100A, which was ~4-fold higher, when compared with the wild type enzyme.

The mutation effects on k_{cat} values in the nucleophilic aromatic substitution reaction with CDNB were significantly decreased for R66A and D100A, ~10- and 60-fold, respectively. The remaining enzymes showed the catalytic center activity to be decreased to ~20–50% lower than wild type.

The pH dependence of k_{cat}/K_m^{CDNB} should reflect a kinetically relevant ionization of the GST·GSH complex. Therefore, an apparent pK_a value of 6.36 was determined for the wild type GST enzyme (Fig. 1). Then, to characterize the influence of the proposed electron-sharing network on GSH thiol ionization, the pK_a values for these mutant enzymes were measured by this kinetic approach (Table I). Each of the alanine mutations at the proposed network residues exhibited an increase in pK_a for the bound GSH ranging from ~0.5–1.1 pH unit higher than that found for the wild type.

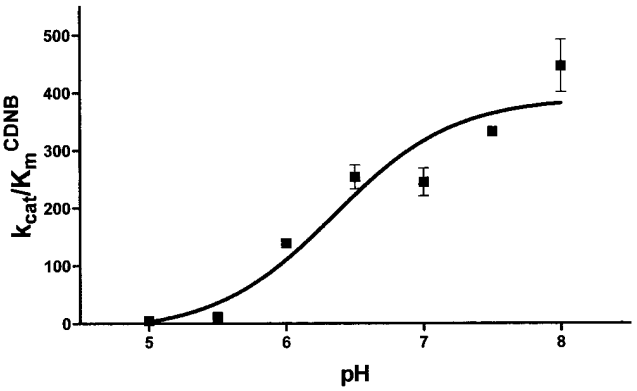

FIG. 1. **The pH dependence of kinetic parameters for CDNB-GSH conjugation of the wild type adGSTD3–3.** The *solid line* is a calculated fit of the experimental data to equation $y = y_{lim}/(1 + 10^{pK_a - pH})$. The pH values measured are within the pH 5.0–8.0 range. The pK_a value calculated is 6.36.

It is well established that the bimolecular nucleophilic substitution reactions precede through a σ-complex intermediate (36). Thus, the rate-limiting formation of a spontaneous σ-complex intermediate can be increased by substitution of chlorine in the CDNB molecule with fluorine, which is more electronegative. With regard to the results, the ratio of the catalytic rate of GSH with FDNB and CDNB was comparable with the ratio of the second-order rate constants for the spontaneous uncatalyzed reaction. That is, $k_{cat}^{FDNB}/k_{cat}^{CDNB} = 40$ is similar to $k_c^{FDNB}/k_c^{CDNB} = 47$, which indicates that the σ-complex formation is the rate-limiting step. Though the k_{cat} of the GST variants reflected different sensitivity to the nature of the leaving group, the catalytic efficiency (k_{cat}/K_m) was nearly unchanged (Table II). Therefore it appears that an alteration of the relative turnover number is a consequence of changes in binding affinity toward different substrate leaving groups rather than a reflection of the rate of σ-complex formation.

The next step was to observe the effect of viscosity on kinetic parameters to study the rate-determining step of the catalytic reaction. A decrease of the rate constant by increasing the medium viscosity should reflect the weight of diffusion events on catalysis (37). It would indicate that the rate-limiting step is related to diffusion-controlled motions of the protein or the dissociation of the product. A plot of the reciprocal of the relative catalytic constant (k_{cat}^o/k_{cat}) against the relative viscosity (η/η^o) should be linear. The slope should be equal to unity when the product release or structural transition is limited by a strictly diffusional barrier. If the slope approaches zero, either the chemistry or another non-diffusion barrier is rate-limiting. For adGSTD3–3 wild type, a plot of the inverse relative rate constant (k_{cat}^o/k_{cat}) *versus* the relative viscosity (η/η_o) gives a linear dependence with a slope (1.14 ± 0.01) very close to unity (Fig. 2). In contrast, the R66A mutant yields plots fully viscosity independent with a slope approaching zero. The other mutants, S65A, D100A, T158A, T162A, and T158A/T162A, exhibited k_{cat} values with different degrees of viscosity dependence compared with the wild type enzyme.

The activity of the enzymes toward various hydrophobic substrates revealed that the specificity or the interactions with these substrates differed (Fig. 3). This result suggests that changes in the electron-sharing network residues cause a rearrangement of the active site, resulting in changes in the topology of the active site pocket and/or the ability of the responsible residues in the active site pocket of the enzyme to interact with hydrophobic substrates by an induced-fit mechanism (26, 38).

The heat inactivation assay for adGSTD3–3 wild type was performed at different temperatures and demonstrated that the GST activity began to decrease at 45 °C (39). This temperature was used to determine half-life stabilities for the mutant enzymes. The half-life corresponds to the time of preincubation when the mutant enzymes still have 50% remaining activity. All mutant enzymes, except R66A and T162A, showed no significant difference in half-life compared with the wild type (Table III). The R66A mutant enzyme was more stable than wild type by ~60-fold. In contrast, the alanine replacement at the Thr-162 position decreased the stability of the enzyme to ~7 times lower than the wild type.

TABLE II
Effect of fluoride/chloride leaving group substitution on the rate of catalysis

The ratio of kinetic constants for the conjugation reaction catalyzing by adGSTD3–3 enzymes of GSH with CDNB and FDNB as cosubstrates was calculated at pH 6.5.

Enzyme	$k_{cat}^{FDNB}/k_{cat}^{CDNB}$	$(k_{cat}/K_m)^{FDNB}/(k_{cat}/K_m)^{CDNB}$
Wild type	2.40 ± 0.08	6.72 ± 0.34
S65A	5.28 ± 0.25	8.71 ± 1.48
R66A	5.57 ± 0.47	4.04 ± 0.77
D100A	8.40 ± 0.18	10.9 ± 0.69
T158A	2.08 ± 0.07	9.56 ± 0.68
T162A	1.77 ± 0.05	12.3 ± 0.62
T158A/T162A	1.91 ± 0.04	12.3 ± 2.77

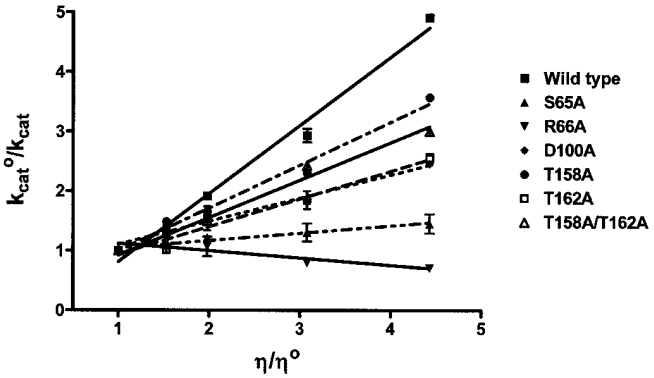

FIG. 2. **Viscosity effect on kinetic constants of wild type and mutant enzymes.** The effect of viscosity on kinetic constants was assayed by using 0.1 M potassium phosphate buffer, pH 6.5, with various glycerol concentrations. Dependence of the reciprocal of the relative turnover number (k_{cat}^o/k_{cat}) on the relative viscosity (η/η^o) for CDNB as cosubstrate with wild type (■), S65A (▲), R66A (▼), D100A (♦), T158A (●), T162A (□), and T158A/T162A (△). The experiment was performed in triplicate, and the lines were calculated by linear regression analysis. The slopes of the linear regression lines are 1.14 ± 0.01 for wild type, 0.12 ± 0.09 for S65A, −0.12 ± 0.01 for R66A, 0.37 ± 0.03 for D100A, 0.72 ± 0.02 for T158A, 0.47 ± 0.01 for T162A, and 0.63 ± 0.01 for T158A/T162A.

DISCUSSION

Comparing the six subunits of adGSTD3–3 in the crystal structure, we observed an apparent electron-sharing network consisting of an ionic bridge interaction between the negatively charged glutamyl α-carboxylate group of glutathione, positively charged Arg-66, and negatively charged Asp-100 (Fig. 4). These three functional groups appear to form a resonance motif that is stabilized by a network of hydrogen bonds between Ser-65, Thr-158, Thr-162, and a conserved water-mediated contact (Fig. 5). To test the hypothesis of this electron-sharing network involvement in enzyme catalysis, the five G-site residues forming the network, Ser-65, Arg-66, Asp-100, Thr-158, and Thr-162, were replaced with alanine.

The kinetic studies demonstrated that the mutations reduced k_{cat}, which resulted from a disruption of the electron distribution network. A dramatic decrease in enzyme activity was observed for the alanine replacements at Arg-66 and Asp-

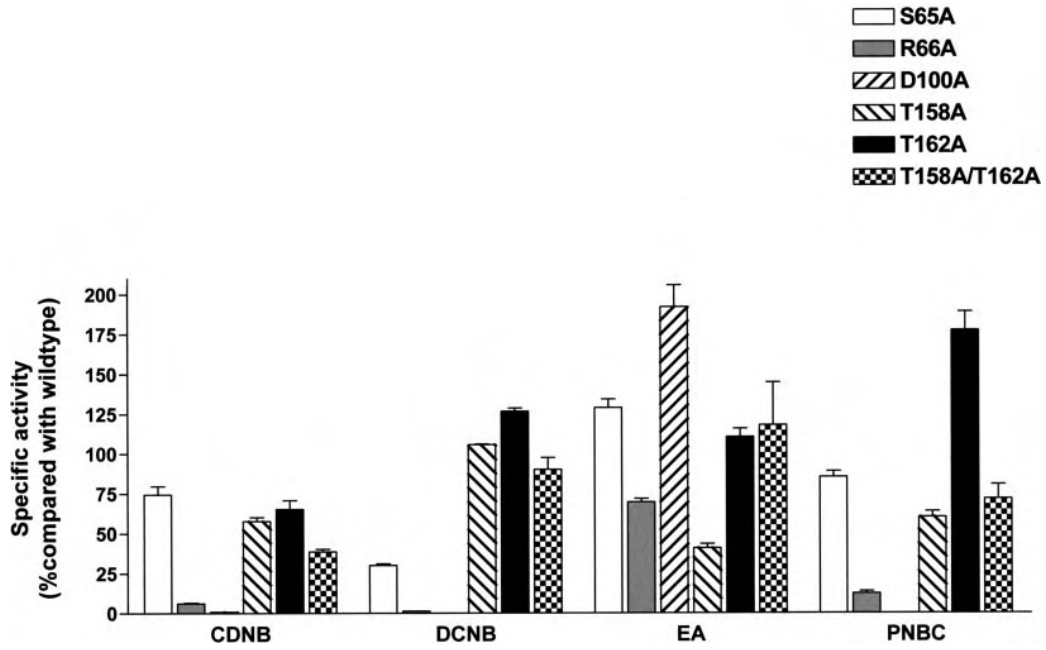

FIG. 3. **Substrate-specific activity as a percent change compared with the adGSTD3–3 (wild type).** *White column*, S65A; *gray column*, R66A; *left diagonal hatched column*, D100A; *right diagonal hatched column*, T158A; *black column*, T162A; *checked column* T158A/T162A. Four substrates were used for enzyme activity assays, *CDNB* (1-chloro-2,4-dinitrobenzene), *DCNB* (1,2-dichloro-4-nitrobenzene), *EA* (ethacrynic acid), and PNBC (*p*-nitrobenzyl chloride). The experiment was performed in triplicate, and the data are mean ± S.D.

TABLE III
Thermal stability of wild type and mutants of adGSTD3–3 at 45 °C

The wild type and mutant enzymes were incubated at 45 °C at the protein concentration of 1 mg/ml. The inactivation time courses were determined by withdrawing suitable aliquots at the different time points for assay of remaining activity to calculate half-life of the enzyme.

Enzyme	Half-life at 45 °C
	min
Wild type	2.33 ± 0.12
S65A	1.70 ± 0.08
R66A	146 ± 10.5
D100A	4.33 ± 0.26
T158A	3.05 ± 0.08
T162Ala	0.34 ± 0.02
T158A/T162A	1.18 ± 0.03

100. We propose that Arg-66 and Asp-100 are key residues in this network because they generate an ionic bridge that is critical to the function of this motif. Lesser effects were observed for the remaining positions, suggesting these results may be due to the loss from the network of several stabilizing hydrogen bonds, as the key residues are still present. The question arose whether the effect on enzyme catalysis was due to a change in the rate-limiting step of the catalytic mechanism. The pH dependence of the kinetic parameters in the binary complex was determined to observe the ionization process. A crucial property of GSTs is their ability to lower the pK_a of the thiol group of the bound GSH. The data show that the mutations caused an increase in the pK_a values for the key residues, Arg-66 and Asp-100, of ~1 pH unit. The other network position mutants, Ser-65, Thr-158, and Thr-162, gave increases in pK_a of ~0.5 pH unit when compared with the wild type. This suggests that the ionic bridge interaction and the stabilizing H-bonds of Ser-65, Thr-158, and Thr-162, as well as the water-bridge contact, are important for the ionization process. To test this concept, we engineered the wild type enzyme to introduce a more positively charged histidine into the Thr-158 position to expand the ionic bridge interaction. The k_{cat} of this mutant enzyme, T158H, is nearly two times greater and the pK_a of the bound GSH ~ 0.2 pH unit lower than the wild type (Table I).

The viscosity experiment elucidated that the rate-limiting step in the enzyme-catalyzed reaction by adGSTD3–3 is a non-physical step (Fig. 2). The mutation at Arg-66 position changed the rate-determining step from a physical to a non-physical step, which is possibly the ionization step. However, alteration of the other network residues decreased the viscosity effects to intermediate values ($0 < \text{slope} < 1$), indicating that the rate-limiting step is not strictly dependent on a diffusional barrier and that other viscosity-dependent motions or conformational changes of the mutated proteins contribute to the rate-limiting step of the catalytic reaction (37). This suggests that the structural integrity or flexibility of functionally important regions, such as this electron-sharing network, of the mutated enzymes has been altered. This idea is supported by the differences in substrate specificity, which confirm active site changes, and the differences in half-life, which confirm structural movement changes. Previously, we have observed that changing residues that form the packing of the active site wall can influence the topology of the active site, which can affect both the binding mechanism as well as the structural maintenance of the enzyme (29).

However, the stability changes also might be due to the loss/change of structure of the electron-sharing network. The Thr-158 of the electron-sharing network can form two hydrogen bonds with Ile-154 and Ala-155, a conserved loop-helix substructure of the conserved folding module (G*XX*h(S/T)*XX*Dh) (*X* is any residue and h is a hydrophobic residue) (40). The local sequence of the conserved folding module in adGSTD3–3 is G_{149}DSLTIADL$_{157}$. This conserved folding module is present in all GST classes and is composed of two structural motifs at the N-terminal region of the α6 helix. These two structural motifs are the N-capping box ((S/T)*XX*D) and the hydrophobic staple motif in which two hydrophobic residues flank the N-capping box (41–43). Previous investigations demonstrated that single point mutations of residues that formed the conserved folding module had a dramatic effect on protein stability (40–43). The α6 helix loop substructure (GST motif II)

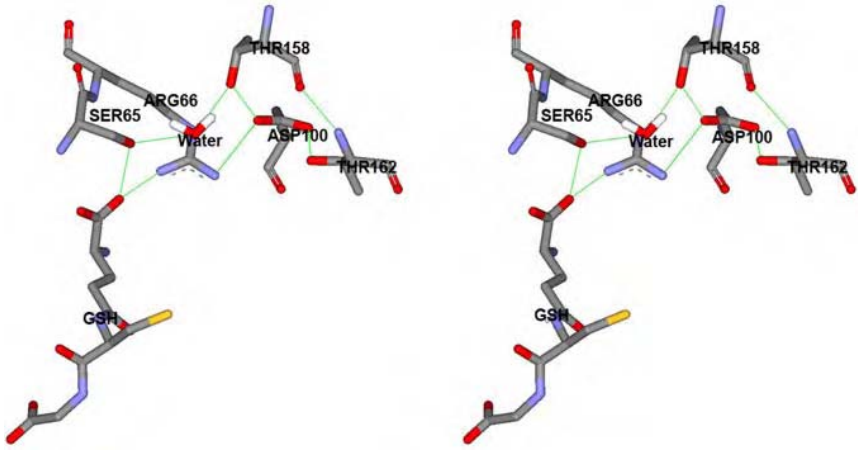

FIG. 4. **Stereo view of proposed electron-sharing network in the active site of adGSTD3–3.** The configuration of the glutamyl α-carboxylate group of glutathione together with the G-site residues Ser-65, Arg-66, Asp-100, Thr-158, and Thr-162 form an electron-sharing network. The *green line* shows the putative electron movement pathway with distances between 2.5 and 3.0 Å.

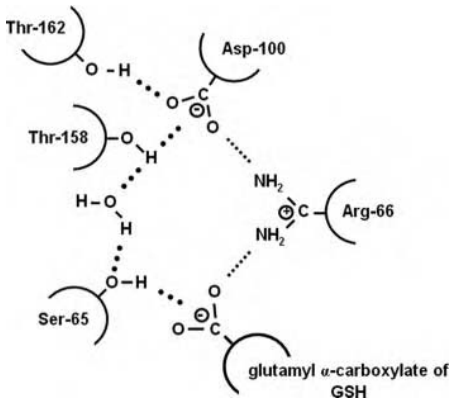

FIG. 5. **Schematic representation of the electron-sharing network in adGSTD3–3.** The proposed electron-sharing network is composed of an ionic bridge interaction between the negatively charged glutamyl α-carboxylate group of glutathione, the positively charged Arg-66, and the negatively charged Asp-100. (*dashed line*). The motif appears to be stabilized by a network of hydrogen bonds involving Ser-65, Thr-158, Thr-162, and a conserved water-mediated contact (*dotted line*).

is stabilized by a network of hydrogen bonds, and crystallographic studies indicate that these amino acid substitutions destabilized GST motif II through a partial or complete loss of the hydrogen bond network (44). Therefore the mutations in the electron-sharing network residues also appear to have an influence on the packing and/or stability of the protein because of the change to the hydrogen bond network in the motif II region.

The amino acid alignments of known Delta class GSTs show the electron-sharing network residues are identical or functionally conserved within the class. A structural observation of several available crystal structures, adGSTD3–3, adGSTD4–4, adGSTD5–5, adGSTD6–6, agGSTD1–6, and *Lc*GST, illustrate that an identical electron-sharing network is located in the same position. These equivalent residues show an acceptable range of distances between them to form the necessary ionic or hydrogen bonding. The water-mediated contact also is observed in several of the tertiary structures. Therefore, the electron-sharing network appears to be conserved in the Delta class. The question arose of whether the electron-sharing network is conserved among all GST classes or is specific to the Delta class.

A primary sequence alignment of all GST classes suggests that there is no conserved equivalent electron-sharing network. However, similar features of the electron-sharing network, that is the ionic bridge interaction between negatively and positively charged residues stabilized by a network of hydrogen bonds, can still be observed in the same region but with slightly different residue positions (Fig. 6). For example, the putative electron-sharing network in hGSTP1 consists of Arg-13, Gln-64, Ser-65, Glu-97, Asp-98, and Cys-101. Alignment of Pi class GST shows that 4 of 6 putative electron-sharing network residues are perfectly conserved in position. Previous investigations demonstrated that mutations of residues forming the putative Pi GST electron-sharing network yielded dramatic effects on the enzyme catalysis (45–48). A substitution of the charged residue at the Arg-13, Gln-64, or Asp-98 position decreased specific activity more than 95%. The decreased activities of these mutants gave a larger effect than the removal of the conserved Tyr-7 hydroxyl group, which is ~90% lower than wild type. Moreover, the k_{cat}/K_m *versus* pH profile for the D98N mutant was shifted by 0.5 pH unit in the alkaline direction. Hence, it was proposed that Asp-98 participated in proton transfer in the catalytic mechanism (48). In hGSTA1–1, the putative electron-sharing network is composed of Arg-15, Thr-68, and Glu-104. The Arg-15 and Thr-68 are strictly conserved in GST Alpha class. The mutation of Arg-15 to alanine or histidine caused a substantial reduction in the specific activity (200- or 400-fold, respectively), one order of magnitude more pronounced than the effect of the Y9F mutation (24, 49). In addition, the corresponding pK_a values of the Arg-15 mutants increase at least 0.5 pH unit when compared with the wild type (24). Mutation of the hydroxyl group that is hydrogen bonded to the α-carboxylate of the glutamate residue of glutathione (T68V) caused a shift of the pH dependence of the enzyme-catalyzed reaction ~ 1.5 pH units to more basic values as compared with the wild type (27). They also successfully mimicked the ionic bridge interaction by introducing the carboxylate group into a location generally occupied by the glutamyl α-carboxylate of hGSTA1–1. A T68E mutation increased catalytic efficiency with the decarboxylated analogue of GSH 10-fold and reduced the pK_a value of the active site-bound decarboxylated analogue of GSH by ~1 pH unit (28). For hGSTT2–2, Ser-67, Asp-104, Cys-105, and Arg-107 are proposed to be the putative electron-sharing network residues. Interestingly, Arg-107 is in hydrogen bonding distance of the main chain carbonyl of the γ-glutamyl moiety of GSH and forms an interaction with the thiol sulfur of GSH either directly or through a water molecule (38). The replacement of Arg-107 by alanine remarkably increases the apparent pK_a of the bound GSH from 6.1 to 7.8 (50, 51). Arg-107 is a crucial residue in the electron-sharing network involved in the activation of the GSH, and it is strictly conserved in the Theta class. Comparisons between GST class Pi, Alpha, Theta, and Delta indicate that the electron-sharing network residues are identical or functionally conserved even through the interclass variations of GSTs.

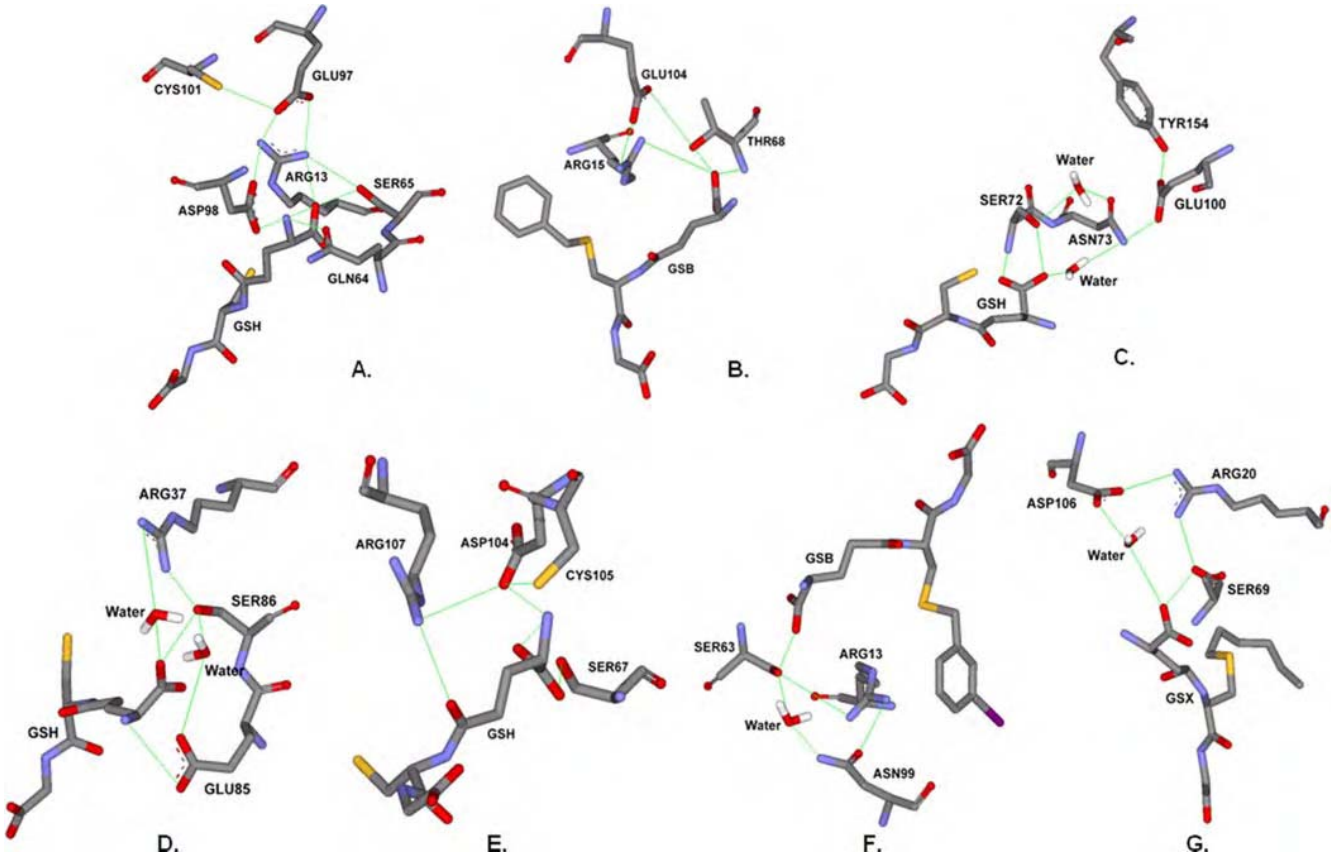

FIG. 6. **Putative electron distribution network in the other GST classes.** The electron-sharing network, which is an ionic interaction between negatively charged and positively charged residues stabilized by a network of hydrogen bonds, can be observed in the same area involving different residues in the different GST enzymes. *A*, human P_i hGSTP1–1 (PDB accession number 3GSS); *B*, human Alpha hGSTA1–1 (PDB accession number 1PKW); *C*, rat Mu rGSTM1–1 (PDB accession number 5FWG); *D*, human Omega hGSTO1–1 (PDB accession number 1EEM); *E*, human Theta hGSTT2–2 (PDB accession number 3LIR); *F*, squid Sigma GST (PDB accession number 2GSQ); and *G*, wheat Tau GSTI (PDB accession number 1GWC).The *green line* shows the putative electron movement pathway for distances between 2.5 and 3.0 Å.

Although the electron-sharing network in other GSTs has not been characterized as such and non-conservation of the primary sequences of the residues forming the network is observed, nevertheless the structural comparisons of available crystal structures suggest that the presence of the network can be mapped to the same region in all GST classes based upon the possible distances between electron-sharing atoms and mutational studies in the other classes. Therefore, it appears that the proposed electron-sharing network in all GSTs derives from two critical residues that form ionic bridge interactions between the negatively charged glutamyl α-carboxylate group of glutathione, a positively charged residue (primarily Arg) and a negatively charged residue (Glu or Asp) stabilized by hydrogen-bonding networks with surrounding residues (Ser, Thr, and/or water-mediated contact). The extent of the electron-sharing network seems to vary between GST classes. However, with regard to mutational studies in several GSTs, the electron-sharing residues share similar characteristics: changes in either of the 2 key residues, the positively and negatively charged residues forming the salt-bridge interactions, nearly abolish enzymatic activity whereas replacement of residues involved in the hydrogen-bonding network decreases activity only ~20–50%. In addition to an ionization step, which is modulated by the base-assisted deprotonation and the electron-sharing network, the catalytic rate of a GST also depends upon other processes in the catalytic mechanism, *e.g.* nucleophilic substitution, product formation, and product dissociation. However, it is reasonable to suggest that a more extensive network might correlate with an increasing catalytic rate as it has a superior ability to lower the pK_a value of bound GSH. As shown in Fig. 6, Delta and Pi class GSTs appear to have more cooperative residues in the network than Alpha class; therefore, the ability to lower the pK_a of the bound GSH for Pi (pK_a = 6.2 ± 0.1) (25) and Delta (pK_a = 6.3 ± 0.1) (29) is greater than Alpha class (pK_a = 6.7 ± 0.1) (25). However, the three enzymes exhibit similarities in catalytic activities toward CDNB substrate, Pi (k_{cat} = 34 ± 2 s^{-1}) (40), Alpha (k_{cat} = 48 ± 4 s^{-1}) (52), and Delta (k_{cat} = 35 ± 1 s^{-1}) (29). This demonstrates that additional factors in the catalytic mechanism have significant contributions to the catalytic rate and must be taken into account. One known example for such a factor is the C-terminal region of Alpha class GST, which is thought to help guide the reactants through multiple mechanisms into the transition state, resulting in an enhancement of enzymatic activity (52).

In conclusion, the present work, together with previous studies, supports the hypothesis of an electron-sharing network involved in the ionization of GSH. This network is characterized by an electrostatic interaction between negatively and positively charged amino acids stabilized by an array of hydrogen bonds. Therefore, an advantage of this type of extended network is that the electron-sharing burden is distributed among multiple residues that may be unable to fully support the function individually. This network appears to be a functionally conserved motif that contributes to the base-assisted deprotonation model suggested to be essential for the GSH ionization step of the catalytic mechanism. A structural diversification but functional conservation suggests a significant role for the electron-sharing network in catalysis as the purpose was maintained during the divergent evolution of GSTs.

REFERENCES

1. Hayes, J. D., and Pulford, D. J. (1995) *CRC Crit. Rev. Biochem. Molec. Biol.* **30,** 445–600
2. Ketterer, B. (2001) *Chem. Biol. Interact.* **138,** 27–42
3. Mannervik, B., and Danielson, U. H. (1988) *CRC Crit. Rev. Biochem.* **23,** 283–337
4. Sheehan, D., Meade, G., Foley, V. M., and Dowd, C. A. (2001) *Biochem. J.* **360,** 1–16
5. Eaton, D. L., and Bammler, T. K. (1999) *Toxicol. Sci.* **49,** 156–164
6. Armstrong, R. N. (1997) *Chem. Res. Toxicol.* **10,** 2–18
7. Jakoby, W. B., and Habig, W. H. (1980) in *Enzymatic Basis of Detoxication* (Jakoby, W. B., ed) Vol. 2, pp. 63–94, Academic Press, New York
8. Armstrong, R. N., Rife, C., and Wang, Z. (2001) *Chem. Biol. Interact.* **133,** 167–169
9. Caccuri, A. M., Ascenzi, P., Antonini, G., Parker, M. W., Oakley, A. J., Chiessi, E., Nuccetelli, M., Battistoni, A., Bellizia, A., and Ricci, G. (1996) *J. Biol. Chem.* **271,** 16193–16198
10. Caccuri, A. M., Antonini, G., Nicotra, M., Battistoni, A., Lo Bello, M., Board, P. G., Parker, M. W., and Ricci, G. (1997) *J. Biol. Chem.* **272,** 29681–29686
11. Caccuri, A. M., Lo Bello, M., Nuccetelli, M., Rossi, P., Antonini, G., Federici, G., and Ricci, G. (1998) *Biochemistry* **37,** 3028–3034
12. Ahmad, H., Wilson, D. E., Fritz, R. R., Singh, S. V., Medh, R. D., Nagle, G. T., Awasthi, Y. C., and Kurosky, A. (1990) *Arch. Biochem. Biophys.* **278,** 398–408
13. Board, P., Baker, R. T., Chelvanayagam, G., and Jermiin, L. S. (1997) *Biochem. J.* **328,** 929–935
14. Mannervik, B., Ålin, P., Guthenberg, C., Jensson, H., Tahir, M. K., Warholm, M., and Jörnvall, H. (1985) *Proc. Natl. Acad. Sci. U. S. A.* **82,** 7202–7206
15. Mannervik, B., Awasthi, Y. C., Board, P. G., Hayes, J. D., Di Ilio, C., Ketterer, B., Listowsky, I., Morgenstern, R., Muramatsu, M., Pearson, W. R., Pickett, C. B., Sato, K., Widersten, M., and Wolf, C. R. (1992) *Biochem. J.* **282,** 305–306
16. Meyer, D. J., Coles, B., Pemble, S. E., Gilmore, K. S., Fraser, G. M., and Ketterer, B. (1991) *Biochem. J.* **274,** 409–414
17. Motoyama, N., and Dauterman, W. C. (1978) *Insect. Biochem.* **8,** 337–348
18. Pemble, S. E., and Taylor, J. B. (1992) *Biochem. J.* **287,** 957–963
19. Pemble, S. E., Wardle, A. F., and Taylor, J. B. (1996) *Biochem. J.* **319,** 749–754
20. Wilce, M. C. J., and Parker, M. W. (1994) *Biochim. Biophys. Acta* **1205,** 1–18
21. Allardyce, C. S., McDonagh, P. D., Lian, L.-Y., Wolf, C. R., and Roberts, G. C. K. (1999) *Biochem. J.* **343,** 525–531
22. Kolm, R. H., Sroga, G. E., and Mannervik, B. (1992) *Biochem. J.* **285,** 537–540
23. Liu, S., Zhang, P., Ji, X., Johnson, W. W., Gilliland, G. L., and Armstrong, R. N. (1992) *J. Biol. Chem.* **267,** 4296–4299
24. Björnestedt, R., Stenberg, G., Widersten, M., Board, P. G., Sinning, I., Jones, T. A., and Mannervik, B. (1995) *J. Mol. Biol.* **247,** 765–773
25. Caccuri, A. M., Antonini, G., Board, P. G., Parker, M. W., Nicotra, M., Lo Bello, M., Federici, G., and Ricci, G. (1999) *Biochem. J.* **344,** 419–425
26. Tan, K.-L., Chelvanayagam, G., Parker, M. W., and Board, P. G. (1996) *Biochem. J.* **319,** 315–321
27. Widersten, M., Björnestedt, R., and Mannervik, B. (1996) *Biochemistry* **35,** 7731–7742
28. Gustafsson, A., Pettersson, P. L., Grehn, L., Jemth, P., and Mannervik, B. (2001) *Biochemistry* **40,** 15835–15845
29. Winayanuwattikun, P., and Ketterman, A. J. (2004) *Biochem. J.* **382,** 751–757
30. Oakley, A. J., Harnnoi, T., Udomsinprasert, R., Jirajaroenrat, K., Ketterman, A. J., and Wilce, M. C. J. (2001) *Protein Sci.* **10,** 2176–2185
31. Jirajaroenrat, K., Pongjaroenkit, S., Krittanai, C., Prapanthadara, L., and Ketterman, A. J. (2001) *Insect. Biochem. Mol. Biol.* **31,** 867–875
32. Bradford, M. M. (1976) *Anal. Biochem.* **72,** 248–254
33. Caccuri, A. M., Ascenzi, P., Lo Bello, M., Federici, G., Battistoni, A., Mazzetti, P., and Ricci, G. (1994) *Biochem. Biophys. Res. Comm.* **200,** 1428–1434
34. Habig, W. H., Pabst, M. J., and Jakoby, W. B. (1974) *J. Biol. Chem.* **249,** 7130–7139
35. Wolf, A. V., Brown, M. G., and Prentiss, P. G. (1985) *Handbook of Chemistry and Physics* (Weast, R. C., Astle, M. J., and Beyer, W. H., eds) pp. D219–D269, CRC Press, Inc., Boca Raton, FL
36. Chen, W.-J., Graminski, G. F., and Armstrong, R. N. (1988) *Biochemistry* **27,** 647–654
37. Johnson, W. W., Liu, S., Ji, X., Gilliland, G. L., and Armstrong, R. N. (1993) *J. Biol. Chem.* **268,** 11508–11511
38. Rossjohn, J., McKinstry, W. J., Oakley, A. J., Verger, D., Flanagan, J., Chelvanayagam, G., Tan, K.-L., Board, P. G., and Parker, M. W. (1998) *Structure* **6,** 309–322
39. Wongtrakul, J., Udomsinprasert, R., and Ketterman, A. (2003) *Insect Biochem. Mol. Biol.* **33,** 971–979
40. Kong, G. K. W., Polekhina, G., McKinstry, W. J., Parker, M. W., Dragani, B., Aceto, A., Paludi, D., Principe, D. R., Mannervik, B., and Stenberg, G. (2003) *J. Biol. Chem.* **278,** 1291–1302
41. Aceto, A., Dragani, B., Melino, S., Allocati, N., Masulli, M., Di Ilio, C., and Petruzzelli, R. (1997) *Biochem. J.* **322,** 229–234
42. Dragani, B., Stenberg, G., Melino, S., Petruzzelli, R., Mannervik, B., and Aceto, A. (1997) *J. Biol. Chem.* **272,** 25518–25523
43. Stenberg, G., Dragani, B., Cocco, R., Principe, D. R., Mannervik, B., and Aceto, A. (2001) *Chem. Biol. Interact.* **133,** 49–50
44. Rossjohn, J., McKinstry, W. J., Oakley, A. J., Parker, M. W., Stenberg, G., Mannervik, B., Dragani, B., Cocco, R., and Aceto, A. (2000) *J. Mol. Biol.* **302,** 295–302
45. Kong, K.-H., Inoue, H., and Takahashi, K. (1993) *Protein Eng.* **6,** 93–99
46. Manoharan, T. H., Gulick, A. M., Puchalski, R. B., Servias, A. L., and Fahl, W. E. (1992) *J. Biol. Chem.* **267,** 18940–18945
47. Manoharan, T. H., Gulick, A. M., Reinemer, P., Dirr, H. W., Huber, R., and Fahl, W. E. (1992) *J. Mol. Biol.* **226,** 319–322
48. Widersten, M., Kolm, R. H., Björnestedt, R., and Mannervik, B. (1992) *Biochem. J.* **285,** 377–381
49. Stenberg, G., Board, P. G., Carlberg, I., and Mannervik, B. (1991) *Biochem. J.* **274,** 549–555
50. Caccuri, A. M., Antonini, G., Board, P., Flanagan, J., Parker, M. W., Paolesse, R., Turella, P., Chelvanayagam, G., and Ricci, G. (2001) *J. Biol. Chem.* **276,** 5432–5437
51. Caccuri, A. M., Antonini, G., Board, P. G., Flanagan, J., Parker, M. W., Paolesse, R., Turella, P., Federici, G., Lo Bello, M., and Ricci, G. (2001) *J. Biol. Chem.* **276,** 5427–5431
52. Nilsson, L. O., Edalat, M., Pettersson, P. L., and Mannervik, B. (2002) *Biochim. Biophys. Acta* **1597,** 157–163

This paper is available online at www.jbc.org

THE JOURNAL OF BIOLOGICAL CHEMISTRY VOL. 282, NO. 3, p. 2124, January 19, 2007

VOLUME 280 (2005) PAGES 31776–31782

An electron-sharing network involved in the catalytic mechanism is functionally conserved in different glutathione transferase classes.

Pakorn Winayanuwattikun and Albert J. Ketterman

PAGES 31777–31779:

We inadvertently did not cite previously published data properly in the legends of several tables and figures. The corrected Table 1 is shown in its entirety below. The legends for Tables 2 and 3 and Figs. 2 and 3 should read as stated below.

TABLE 2. Effect of fluoride/chloride leaving group substitution on the rate of catalysis. The ratio of kinetic constants for the conjugation reaction catalyzing by adGSTD3-3 enzymes of GSH with CDNB and FDNB as co-substrates was calculated at pH 6.5. The data for wild type, S65A, and R66A have been reported previously in another format (29) and are shown here for purposes of comparison.

TABLE 3. Thermal stability of wild type and mutants of adGSTD3-3 at 45 °C. The wild type and mutant enzymes were incubated at 45 °C at the protein concentration of 1 mg/ml. The inactivation time courses were determined by withdrawing suitable aliquots at the different time points for assay of the remaining activity to calculate the half-life of the enzyme. The data for wild type, S65A, and R66A have been reported previously (29) and are shown here for purposes of comparison.

Figure 2. Viscosity effect on kinetic constants of wild-type and mutant enzymes. The effect of viscosity on kinetic constants was assayed by using 0.1 M potassium phosphate buffer, pH 6.5, with various glycerol concentrations. Dependence of the reciprocal of the relative turnover number (k_{cat}^{0}/k_{cat}) on the relative viscosity (η/η^{0}) for CDNB as cosubstrate with WT (■), S65A (▲), R66A (▼), D100A (◆), T158A (●), T162A (□), and T158A/T162A (○). The experiment was performed in triplicate. and the lines were calculated by linear regression analysis. The slopes of the linear regression lines are 1.14 ± 0.01 for wild type, 0.12 ± 0.09 for S65A, −0.12 ± 0.01 for R66A, 0.37 ± 0.03 for D100A, 0.72 ± 0.02 for T158A, 0.47 ± 0.01 for T162A, and 0.63 ± 0.01 for T158A/T162A. The data for wild type, S65A, and R66A have been reported previously (29) and are shown here for purposes of comparison.

Figure 3. Substrate-specific activity as a percent change compared with the adGSTD3-3 (wild type). The four substrates used for enzyme activity assays were: CDNB (1-chloro-2,4-dinitrobenzene), DCNB (1,2-dichloro-4-nitrobenzene), EA (ethacrynic acid), and PNBC (*p*-nitrobenzyl chloride). The experiment was performed in triplicate, and the data are mean ± S.D. The data for S65A and R66A have been reported previously (29) and are shown here for purposes of comparison.

TABLE 1

Steady-state kinetic parameters and pK_a values for the thiol group of GSH of wild type and mutants of adGSTD3-3 for the CDNB conjugation reaction at pH 6.5 and 25 °C

The enzyme activities were measured at varying concentrations of CDNB and GSH in 0.1 M phosphate buffer, pH 6.5. The pK_a value was obtained by using 0.1 M sodium acetate buffers (from pH 5.0 to 5.5) and 0.1 M potassium phosphate buffer (from pH 6.0 to 8.5). The reaction was monitored at 340 nm, $\epsilon = 9600\ M^{-1}\ cm^{-1}$.

Enzyme	k_{cat}	K_m^{GSH}	K_m^{CDNB}	k_{cat}/K_m^{GSH}	k_{cat}/K_m^{CDNB}	pK_a
	s^{-1}	mM	mM	s^{-1}/mM	s^{-1}/mM	
Wild type[a]	35.4	0.27 ± 0.05	0.14 ± 0.01	131	246	6.36 ± 0.11
S65A[a]	29.8	1.22 ± 0.12	0.34 ± 0.06	24.5	87.2	6.89 ± 0.23
R66A[a]	3.3	5.10 ± 0.40	0.22 ± 0.04	0.64	14.6	7.23 ± 0.18
D100A	0.6	3.52 ± 0.33	0.54 ± 0.06	0.17	1.09	7.47 ± 0.10
T158A	23.9	0.43 ± 0.02	0.13 ± 0.00	55.3	189	6.93 ± 0.23
T162A	20.6	0.44 ± 0.03	0.15 ± 0.00	46.8	162	6.96 ± 0.25
T158A/T162A	21.9	5.74 ± 0.07	0.26 ± 0.03	3.81	172	7.10 ± 0.02
T158H	61.3	1.22 ± 0.09	0.31 ± 0.01	50.1	198	6.15 ± 0.01

[a] The data for wild type, S65A, and R66A have been reported previously (29) and are shown here for purposes of comparison.

VOLUME 281 (2006) PAGES 38867–38870

On the processing of proghrelin to ghrelin.

Xiaorong Zhu, Yun Cao, Keith Voogd, and Donald F. Steiner

PAGE 38867:

Dr. Voogd's last name was misspelled in the author line. The correct spelling is shown above.

[6] Alternative Splicing of Glutathione S-Transferases

By JANTANA WONGSANTICHON and ALBERT J. KETTERMAN

Abstract

This chapter discusses the alternative splicing of glutathione S-transferase proteins, including current investigations of enzymatic, nonenzymatic functions, as well as structural differences between the alternatively spliced products. The data demonstrate that the different GST splice forms possess different properties, both in their catalytic function and in the effects of their protein–protein interactions.

Introduction

Alternative splicing is a potent regulatory mechanism in higher eukaryotes to generate different transcript isoforms from a single gene by differential incorporation of exons into mature mRNAs. This mechanism is often regulated in temporal patterns depending on either developmental or tissue-specific determinants. In humans, recent genomic and bioinformatic analysis indicates that approximately 35–65% of human genes are alternatively spliced (Graveley, 2001; Mironov *et al.*, 1999; Modrek and Lee, 2002; Sorek *et al.*, 2004). Generally, alternative splice events that take place in the protein-coding region will generate different primary sequences, and, therefore, the resulting proteins exhibit functional diversities. For example, in a study of the *Dscam* gene from *Drosophila melanogaster* that codes for a cell surface protein involved in neuronal connectivity, as many as 38,016 different mRNA isoforms can be generated from the single gene through alternative splicing mechanisms (Neves *et al.*, 2004; Wojtowicz *et al.*, 2004). The unique profile of *Dscam* isoforms in each individual cell type seems to specify cell identity with possible roles in the nervous system.

Glutathione S-transferases (GSTs) are ubiquitous in nature, found in most aerobic eukaryotes and prokaryotes. Cytosolic GSTs have been classified into at least 13 classes from mammals, plants, insects, parasites, fungus, as well as bacteria (Chelvanayagam *et al.*, 2001; Ketterer, 2001; Sheehan *et al.*, 2001). A vast diversity of GSTs allows the enzyme superfamily to perform various enzymatic and nonenzymatic functions. As an example, GSTs comprise a number of various isoforms that recognize at least 100 different xenobiotic chemicals (Hayes and Pulford, 1995). Alternative splicing is, therefore, only one mechanism used to generate functional heterogeneity of GSTs.

METHODS IN ENZYMOLOGY, VOL. 401

0076-6879/05 $35.00
DOI: 10.1016/S0076-6879(05)01006-2

Alternative Splicing of GSTs

Currently identified spliced transcripts of GSTs seem to share the same N-terminus that is involved in the binding and activation of glutathione. The diverse C-terminal region of the full-length GSTs is responsible for different specificities toward electrophilic hydrophobic compounds. The alternative splicing mechanism generally gives rise to functional diversities of proteins and generates the complex proteome in metazoan organisms. Consequently, the alternatively spliced GSTs may also contribute to different important physiological functions. The alternative splicing mechanism seems to take place at a comparable frequency in mammals, flies, and worms (Brett *et al.*, 2002). Therefore, it is probable that the alternative splicing mechanism for GST genes is also more prevalent than previously thought.

Mu Class

Alternative splicing was first hypothetically suggested in Mu class GSTs based on two partial transcripts from a human testis cDNA library (Ross and Board, 1993), but no further data have been obtained. However, gene structure predictions from the human genome by Ensembl automated annotation pipelines (Curwen *et al.*, 2004; Potter *et al.*, 2004), together with corresponding verifications from external identifiers, suggest alternative splicing events occur in GSTM1 and GSTM4 as illustrated in Fig. 1. In hGSTM1, there is exon skipping at exon 7, which generates two different transcript isoforms with the size of 218 and 181 amino acids. The two isoforms have protein similarity matches in the Genbank database with accession numbers of AAA59203 (Seidegård *et al.*, 1988) and AAH24005 (Strausberg *et al.*, 2002), respectively. In general, the longer transcript from most of the alternatively spliced genes is considered an ancestral form that is produced from constitutively spliced exons, whereas the shorter form arises from an exon-skipping event evolved in a later evolutionary period (Ast, 2004; Kondrashov and Koonin, 2003).

In another splicing mechanism, an alternate in-frame exon in the 3′ coding region (exon 8 or 9) each with a different 3′ UTR are brought into play in hGSTM4, which generates two different transcripts of 218 and 195 amino acids (Fig. 1B). The matching protein sequences from Genbank database are AAA57346 (Comstock *et al.*, 1993) and AAA58623 (Ross *et al.*, 1993), respectively. In fact, predicted splice variants from genomic and EST data could represent either real functional forms or perhaps noise. The noise or aberrant splicing from the prediction possibly enables the evolution of new functional forms (Lareau *et al.*, 2004). Nevertheless, when the predicted splice isoforms have corresponding sequences in public databases, this suggests an alternative splicing in these genes does occur.

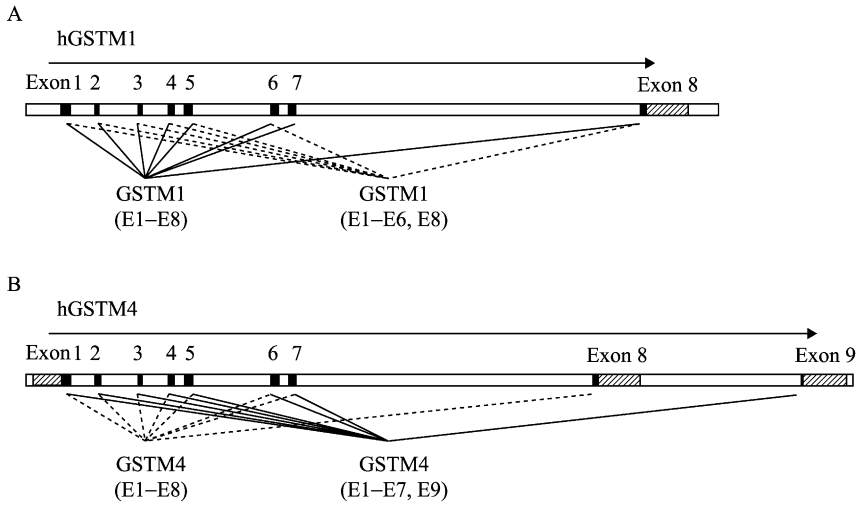

FIG. 1. Schematic diagram of predicted alternative splicing in (A) human GSTM1 and (B) GSTM4. The shaded boxes indicate untranslated regions (UTR), whereas solid boxes are coding regions.

Omega Class

A recent study of the genomic organization of Ov-GST3, classified as an omega class GST, from the human parasitic nematode *Onchocerca volvulus* revealed three different alternatively spliced transcripts (Kampkötter *et al.*, 2003). The differential splicing of exons 4–6 (Fig. 2) generates splicing transcripts of OvGST3-1, OvGST3-2, and OvGST3-3 with sizes of 145, 239, and 198 amino acids, respectively. An investigation of the genomic DNA organization and reverse transcriptase-polymerase chain reaction (RT-PCR) was performed to verify the existence of all three isoforms as functional transcripts. Among the three *O. volvulus* GSTs, OvGST1–OvGST3, OvGST3 was shown to be the stress-responsive transcript that was significantly up-regulated under toxic oxidant stimulation (Liebau *et al.*, 2000). Variable alternatively spliced transcripts of these particular filarial GSTs might confer advantages for the parasitic defense against different environmental stress, as well as serving as host immune effector molecules.

Sigma Class

In an annotation and phylogeny study of the *Anopheles gambiae* genome, an alternatively spliced gene from this Dipteran species was

identified (Ding *et al.*, 2003). The resulting transcripts were classified as sigma class GSTs by a comparative analysis of the *Drosophila melanogaster* and *Anopheles gambiae* genomes. The genomic organization in Fig. 3 shows the two splicing products of GSTS1-1 and GSTS1-2 with the sizes of 200 and 195 amino acids, respectively. However, functional studies of these two isoforms still need to be performed.

Delta Class

Perhaps the best-characterized alternatively spliced GSTs are from an orthologous delta class gene in the Anopheline mosquitoes, *Anopheles gambiae* or *Anopheles dirus* (Pongjaroenkit *et al.*, 2001; Ranson *et al.*, 1998). Investigations of the genomic organization (Fig. 4), as well as the putative splice sites (Table I), demonstrate the splicing mechanism in the *An. gambiae aggst1*α gene and the *An. dirus adgst1AS1* gene is highly conserved. However, an investigation of the *Drosophila* genome reveals no such mechanism in any of the cytosolic GSTs, even though the two Diptera, *Anopheles gambiae* and *Drosophila melanogaster*, diverged only approximately 250 million years ago with considerable similarities in their proteomes (Zdobnov *et al.*, 2002). It is thought that *Anopheles gambiae* and

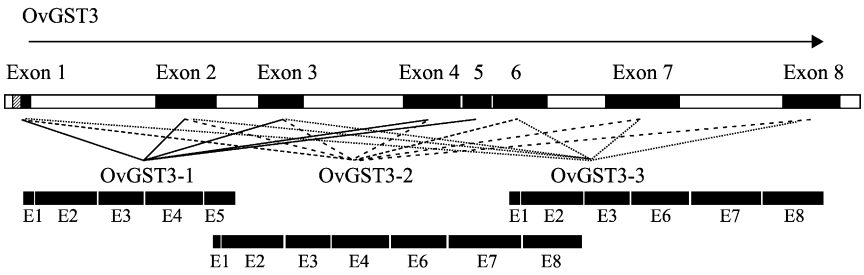

FIG. 2. Schematic diagram of alternative splicing in an Omega class GST from *O. volvulus*. The shaded box indicates a UTR region, whereas solid boxes are coding regions.

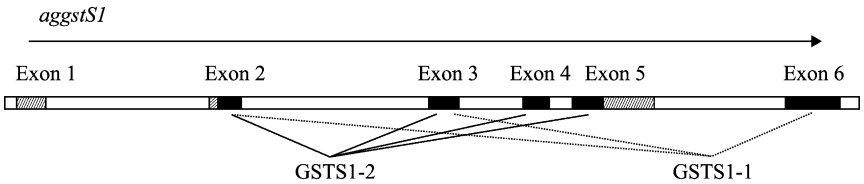

FIG. 3. Schematic diagram of the alternative splicing in a Sigma class GST from *An. gambiae*. The shaded boxes indicate UTR regions whereas solid boxes are coding regions.

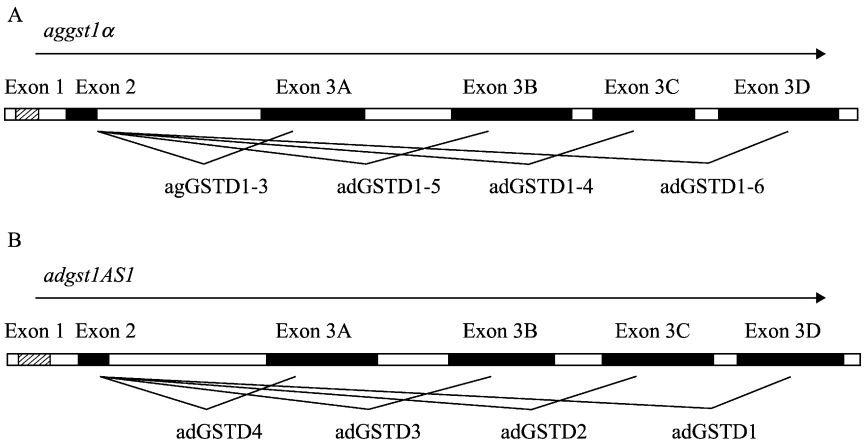

FIG. 4. Schematic diagram of orthologous alternative splicing in a gene member of Delta class GSTs from (A) *An. gambiae* and (B) *An. dirus*. The shaded box indicates 5′ UTR region, whereas solid boxes are coding regions.

TABLE I
THE EXON COMPOSITION AND SPLICE SITES OF ALTERNATIVE TRANSCRIPTS COMPARED BETWEEN THE *AN. GAMBIAE AGGST1A* GENE AND THE *AN. DIRUS ADGST1AS1* GENE (PONGJAROENKIT *ET AL.*, 2001; RANSON *ET AL.*, 1998)

Gene	Exon composition consensus	5′ Splice site (exon/intron) AG/GTRAGT	3′ Splice site (intron/exon) Y_nNYAG/NN
aggst1α	exon1. . .exon2	TG/GTGAGT	CCCCAG/AA
	exon2. . .exon3A	AG/GTAGGT	AAAG/CT
	exon2. . .exon3B		CCTAG/AT
	exon2. . .exon3C		TTTGTAG/CT
	exon2. . .exon3D		TTTTCTAG/CT
adgst1AS1	exon1. . .exon2	CG/GTGAGT	CTCGCAG/AA
	exon2. . .exon3A	AG/GTAAGT	TTTAAAG/CT
	exon2. . .exon3B		CCCTCAG/AT
	exon2. . .exon3C		TCCGCAG/CT
	exon2. . .exon3D		ATTACAG/CT

(R = A or G, Y = C or T, N = A, C, G, or T).

Anopheles dirus have diverged in the last 2 or 3 million years. This suggests that the alternative splicing has recently occurred and is being conserved in the very close evolutionarily related species for physiologically important reasons. Each alternative transcript shares the same exon 2 at the

N-terminus, which is about one fifth of the entire protein, demonstrating a significant role of this domain for glutathione binding. In addition to genomic investigation, each alternatively spliced product was confirmed by RT-PCR to determine the coding sequences and predicted spliced sites. A comparison of the *aggst1*α and *adgst1AS1* genes reveals an identical exon/intron arrangement (Fig. 4). Comparing coding regions between these orthologous genes shows high nucleotide identities ranging between 80–90%, although the size and sequence of the introns vary (Pongjaroenkit *et al.*, 2001).

Structural Impact of Spliced Variants

The spliced variants of the Anopheline GSTs are mainly used for discussion in this and the following section because of the advantages of available structural and functional information over alternatively spliced GSTs from other classes.

Primary Sequences

The primary amino acid sequence alignment of *An. gambiae* and *An. dirus* alternatively spliced GSTs (Fig. 5A) suggests these two species are highly evolutionarily related, although *An. gambiae* is found in Africa and *An. dirus* in South East Asia. Amino acid comparisons of GST splicing products from the two mosquito species show greater than 60% identity (Fig. 5B). Comparisons between species orthologous isoforms showed higher identity than between splicing isoforms within a species, which suggests that the conservation of each splicing isoform might possess a distinctive function or response to different kinds of xenobiotic compounds.

Tertiary Structures

Currently, there are three available crystal structures of the Anopheline GST spliced products: adgstD3, adgstD4, and recently aggstD1-6 (Chen *et al.*, 2003; Oakley *et al.*, 2001). These three GST isoforms represent three of the four splice products from the orthologous genes and possess overall sequence identities greater than 60%. The tertiary structures are incredibly similar (Fig. 6), although the active site conformations are different, as shown in Fig. 7. Active site topologies of adgstD3 and aggstD1-6 are nearly identical, because not only do their amino acid sequences share 80% identity and 90% similarity but also the amino acid residues that form the active site pocket share 95% identity. This means that only 2 of the 44 amino acid residues that make up the pocket are different. In addition, the two different residues are functionally conserved, changing Thr158 and

A

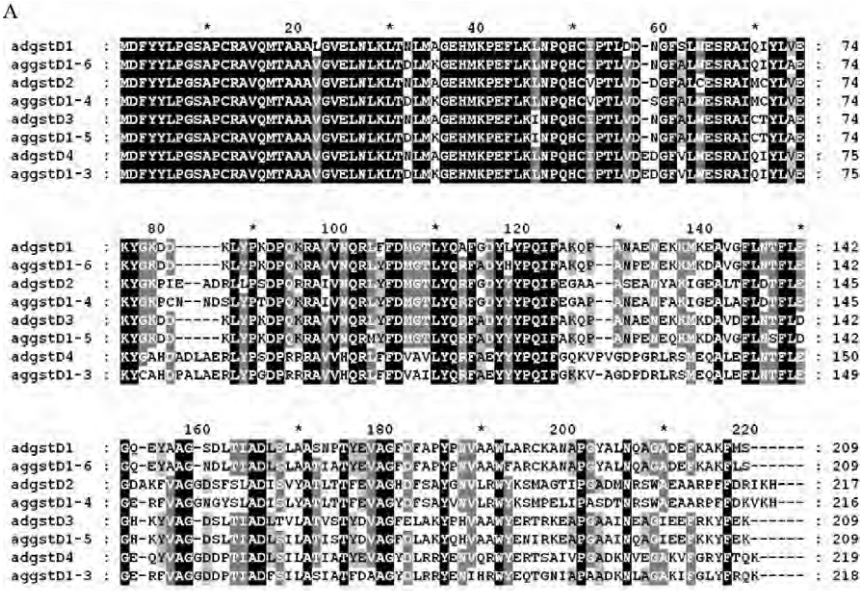

B

	aggstD1-6	adgstD2	aggstD1-4	adgstD3	aggstD1-5	adgstD4	aggstD1-3
adgstD1	**91%** **95%**	61% 73%	62% 74%	77% 87%	76% 86%	63% 73%	60% 72%
aggstD1-6		61% 75%	65% 75%	80% 90%	82% 91%	65% 76%	63% 76%
adgstD2			**85%** **91%**	63% 78%	61% 79%	62% 74%	59% 71%
aggstD1-4				62% 78%	63% 80%	59% 74%	60% 74%
adgstD3					**92%** **97%**	64% 78%	61% 77%
aggstD1-5						64% 77%	63% 77%
adgstD4							**86%** **92%**

FIG. 5. An amino acid sequence comparison of alternatively spliced delta class GSTs from *An. dirus* and *An. gambiae*. (A) Sequence alignment. (B) Matrix table of percent identities (top line) and percent similarities (bottom line). Percent identities of orthologous splicing transcripts are shown in bold. (Genbank accession numbers are adgstD1 AF273041; adgstD2 AF273038; adgstD3 AF273039; adgstD4 AF273040; aggstD1-3 AAC79992; aggstD1-4 AAC79994; aggstD1-5 AAC79993; and aggstD1-6 AAC79995.)

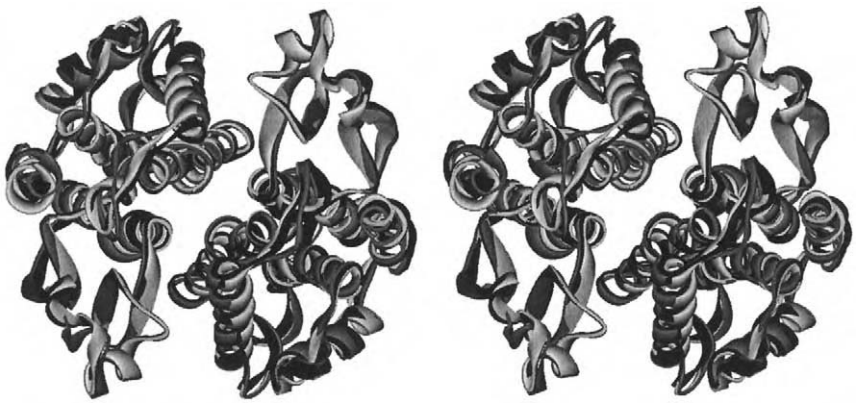

FIG. 6. Stereo view of a structural superimposition of splicing products of *Anopheles dirus* adgstD3 (black), *Anopheles dirus* adgstD4 (grey), and *Anopheles gambiae* aggstD1-6 (white). *An. dirus* adgstD3 and adgstD4 as well as *An. gambiae* aggstD1-6 have Protein Data Bank accession numbers 1JLV, 1JLW, and 1PN9, respectively.

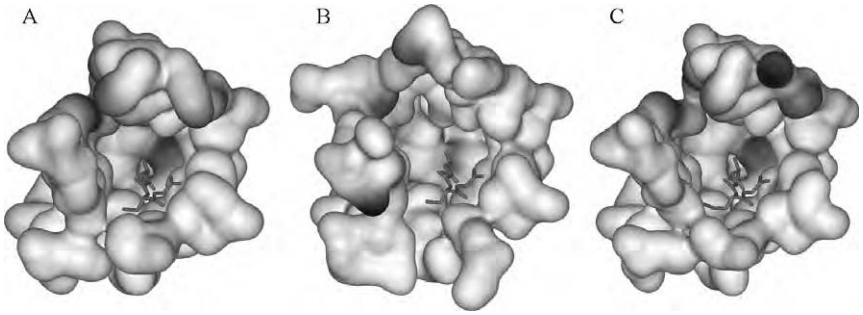

FIG. 7. Active site topology of the splicing products from (A) *Anopheles dirus* adgstD3, (B) *Anopheles dirus* adgstD4, and (C) *Anopheles gambiae* aggstD1-6. The three tertiary structures were superimposed to illustrate active sites in an identical view. Ball and stick representations show the glutathione (or S-hexyl glutathione for aggstD1-6) in the active site pocket.

Tyr206 in adgstD3 to Ser158 and Phe207 in adgstD1-6, respectively. The active site pocket of adgstD4 enzyme is apparently more unique because of the diverse amino acid residues used to form the active site. The distinct active site topology provides diverse enzyme specificity toward xenobiotics and insecticides. Anopheline delta class GSTs, as well as epsilon class, have been implicated in detoxication particularly in insecticide resistance (Ortelli *et al.*, 2003; Prapanthadara *et al.*, 2000; Ranson *et al.*, 1997).

Intersubunit Interaction

Structural investigations of available crystal structures of Anopheline alternatively spliced GSTs demonstrate several dimeric interactions along the subunit interfaces. Amino acid residues involved in the intersubunit interactions in *An. gambiae* aggstD1-6 structure are similar to *An. dirus* adgstD3, although they are not orthologous enzymes; therefore, no representation is shown here. The intersubunit interactions of the observed structures involve two main locations: the center of the twofold axis and both ends of the twofold axis.

Intersubunit Interaction in the Center of the Twofold Axis

TOP REGION. There is an ionic interaction across the dimer interface at the top of the twofold axis of adgstD4 with E116 from one subunit and R134 of the other subunit but absent in the equivalent residues in adgstD3 (Fig. 8A).

MIDDLE REGION. Hydrophobic interactions are prevalent in the middle of the dimeric structure primarily by a counterpart aromatic residue (Y98 in adgstD3, F104 in adgstD4) from both subunits that hook around each other with an offset pi–pi interaction in a ''clasp-like'' arrangement (Fig. 8B). There are also several hydrophobic residues (A67, L97, and M101 in adgstD3; A68, L103, and V107 in adgstD4) involved generating a lock-and-key motif by surrounding the aromatic ''clasp'' residues (which form the ''key''). However, this motif is particularly different from that demonstrated in alpha/mu/pi GST classes (Hornby *et al.*, 2002; Sayed *et al.*, 2000; Stenberg *et al.*, 2000), in which the lock-and-key motif is formed at either end of the twofold axis. In addition, a unique feature of the delta GST is that the ''key'' residue itself also acts as the ''lock'' for the other subunit. The lock-and-key ''clasp'' interaction is highly conserved in other nonalternatively spliced delta class GSTs such as adgstD5, adgstD6, and LcGST from *Lucilia cuprina*.

BOTTOM REGION. An ionic interaction is not only present in the top region, but also the bottom region in the center of the twofold axis with E75 in adgstD4 interacting with R96 from the other subunit. This interaction is also present in adgstD3 with E74 interacting with R90 from the other subunit (Fig. 8C).

Intersubunit Interaction at Either End of the Twofold Axis. There is an additional ionic interaction for adgstD4 at either end of the twofold axis with R94 from one subunit interacting with D57 and D59 from the other subunit (Fig. 8D). This interaction is absent for the equivalent residues of adgstD3.

The alternatively spliced adgstD3 and adgstD4 seem to possess differences in the dimeric interface such that there are two additional ionic interactions that occur at the dimer interface of adgstD4 but do not occur

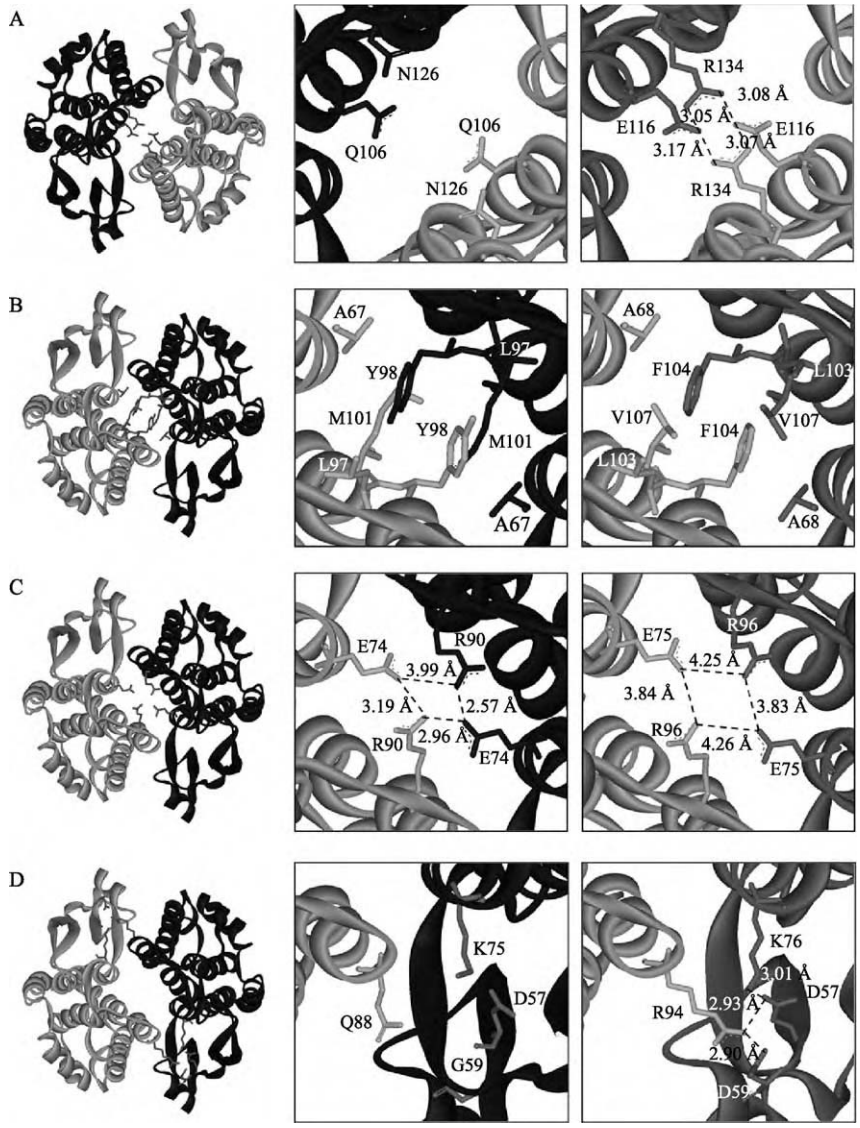

FIG. 8. Dimeric interactions along the subunit interface compared between adgstD3 (left boxes) and adgstD4 (right boxes). The structural representations in B, C, and D were horizontally rotated by 180° for a better view.

in the equivalent positions in adgstD3. The role of ionic interactions in proteins is generally to stabilize the tertiary and quaternary structures. This is supported by previous thermal stability experiments that showed the half-life at 45° to be 3.8 and 12.9 min for adgstD3 and adgstD4, respectively (Wongsantichon *et al.*, 2003; Wongtrakul *et al.*, 2003).

Functional Impact of Splicing

Substrate Specificity

All Anopheline GST spliced isoforms are able to catalyze the common CDNB substrate with different catalytic efficiencies. Table II shows kinetic properties of all four spliced isoforms from the *An. dirus* adgst1AS1 gene and two of the spliced isoforms from the *An. gambiae* aggst1α gene. Kinetic characteristics of each spliced variant are diverse in either affinity toward substrates (K_m) or turn over number (k_{cat}). Available kinetic information for aggstD1-6 and aggstD1-5 are also shown to compare their catalytic properties with the orthologous *An. dirus* enzymes, adgstD1 and adgstD3, respectively. Although amino acid identities of orthologous GSTs from both Anopheline species are greater than 90%, the enzymes display catalytic differences. Moreover, crystal structure shows the active site residues in adgstD1-6 and adgstD3 to be nearly identical. As discussed in the previous section, the 44 active site residues differ by only two functionally conserved amino acids. However, the kinetic data show the enzymes possess very different kinetic properties, illustrating a continuing evolution of the GSTs after species divergence.

Because of a major role of GST enzymes in detoxication processes, many electrophilic hydrophobic compounds have been used to characterize

TABLE II
KINETIC PARAMETERS OF ALTERNATIVELY SPLICED DELTA CLASS GSTS FROM *AN. DIRUS* AND *AN. GAMBIAE*. (JIRAJAROENRAT *ET AL.*, 2001; KETTERMAN *ET AL.*, 2001; RANSON *ET AL.*, 1997)

Enzyme	V_{max} (μmol/min/mg)	k_{cat} (s^{-1})	K_m (m*M*)		k_{cat}/K_m (mM^{-1} S^{-1})	
			GSH	CDNB	GSH	CDNB
adgstD1	12.9 ± 0.63	5.0	0.86 ± 0.18	0.10 ± 0.03	6	48
adgstD2	63.9 ± 3.50	25.9	1.30 ± 0.15	0.21 ± 0.03	20	121
adgstD3	67.5 ± 1.97	26.9	0.40 ± 0.05	0.10 ± 0.01	67	269
adgstD4	40.3 ± 1.89	16.9	0.83 ± 0.08	0.52 ± 0.07	20	32
aggstD1-5	83.51	40.47	0.822	0.099	49	410
aggstD1-6	348.35	136.2	0.807	0.123	120	792

TABLE III
SUBSTRATE SPECIFICITY OF ALTERNATIVELY SPLICED DELTA CLASS GSTs FROM *AN. DIRUS* AND *AN. GAMBIAE*. (RANSON *ET AL.*, 1997; UDOMSINPRASERT *ET AL.*, 2004)

	Specific activity (μmol/min/mg of protein)			
Enzyme	CDNB (1 m*M*)	DCNB (1 m*M*)	PNPB (0.1 m*M*)	DDTase[a] activity
adgstD1	6.54 ± 0.53	0.070 ± 0.002	nd	0.95
adgstD2	45.1 ± 3.41	0.177 ± 0.006	0.047 ± 0.010	1.87 ± 0.82
adgstD3	67.5 ± 1.97	0.312 ± 0.023	nd	2.66 ± 0.29
adgstD4	41.8 ± 1.40	0.042 ± 0.011	0.023 ± 0.002	7.50 ± 1.68
aggstD1-5	56.44 ± 8.71	0.326 ± 0.035	<0.15	4.80 ± 0.09
aggstD1-6	195.14 ± 11.95	0.636 ± 0.026	<0.15	7.71 ± 0.72

[a] The DDTase activity is expressed as nmol DDE formation/mg of enzyme protein. CDNB, 1-chloro 2,4-dinitrobenzene; DCNB, 1,2-chloro 4-nitrobenzene; PNPB, *p*-nitrophenethyl bromide; PNBC, *p*-nitrobenzyl chloride. Nd, no detectable activity.

catalytic specificities of the enzymes. Table III demonstrates that all four alternatively spliced GSTs from *Anopheles dirus*, as well as aggstD1-5 and adgstD1-6 from *Anopheles gambiae*, possess various specificities toward the substrates tested. There is almost negligible activity toward PNPB, a specific substrate for theta class GSTs; hence, these alternatively spliced GSTs do not evidently belong to the theta class as initially classified before the complete *Anopheles gambiae* and *Drosophila melanogaster* genomes became available.

DDTase activity was also investigated because of its potential role in insecticide resistance and was found to be elevated in resistant insect strains (Ortelli *et al.*, 2003; Prapanthadara *et al.*, 1995). Most of the alternatively spliced Anopheline GSTs are able to metabolize DDT to different extents. Noticeably, whereas aggstD1-6 possesses the greatest DDTase activity, the orthologous *An. dirus* enzyme adgstD1 possesses the lowest. Therefore, a high primary sequence identity does not correlate with catalytic properties of the enzymes. Moreover, the nearly identical active site pockets of adgstD3 and aggstD1-6 do not correlate with substrate specificities.

Permethrin inhibition of CDNB activity shows that adgstD2, adgstD3, and adgstD4 possess similar affinities (K_i) in the range of 9–53 μM, and each alternatively spliced isoform displays different types of inhibition kinetics (Jirajaroenrat *et al.*, 2001). The types of inhibition in adgstD2, adgstD3, and adgstD4 are uncompetitive, noncompetitive, and competitive, respectively. Dissimilar inhibition patterns imply that permethrin interacts differently with the individual isoforms and possibly with different binding sites on each isoform.

Regulation of the JNK Pathway

Studies of mammalian GST Pi and Mu revealed that several GSTs were involved in the regulation of signaling pathways by protein–protein interactions. For example, mammalian GST Pi was first demonstrated to inhibit JNK (c-Jun N-terminal kinase, a member of the mitogen activated stress kinase family-MAPK) activity in a dose-dependent manner (Adler *et al.*, 1999), and the JNK inhibition was suggested to occur by a direct interaction of GST Pi to the C-terminal of JNK (Wang *et al.*, 2001). Mammalian GST Mu was shown to inhibit ASK1 (Apoptosis Signal-regulating Kinase 1, a member of the mitogen-activated stress kinase family-MAPKKK) activity by binding of the C-terminus of GST Mu to the N-terminus of ASK1 (Cho *et al.*, 2001). This suggests that different GST classes can possibly interact with different stress kinase proteins in the MAP kinase pathway.

A study of the interactions of the four alternatively spliced delta class GSTs from *Anopheles dirus* to components of the Diptera JNK pathway revealed that individual isoforms differentially interact with *Drosophila* HEP (Hemipterous, upstream activator of JNK and a member of the mitogen-activated stress kinase family-MAPKK) and *Drosophila* JNK (Udomsinprasert *et al.*, 2004). HEP and JNK seemed to have effects on GST activity by inhibiting activities of adgstD2, adgstD3, and adgstD4 to various extents. The activity of adgstD1 could only be inhibited by HEP, but not JNK. Furthermore, all four alternatively spliced GSTs also had effects on the protein kinase activities. The adgstD2, adgstD3, and adgstD4 increased the ability of JNK to phosphorylate Jun (a substrate for JNK), whereas adgstD1 inhibited JNK activity by 50% in the presence of HEP, JNK, and Jun. Without Jun in the reaction, effects of individual GST isoforms on JNK and HEP phosphorylation also were observed, because JNK is a substrate for HEP and HEP is a substrate for JNK. Results showed that adgstD2 and adgstD3 can increase phosphorylation of both JNK and HEP, whereas adgstD1 and adgstD4 inhibit the phosphorylation of HEP but not JNK. This suggests that the different alternatively spliced isoforms of GST can act as positive and negative regulators of the JNK signaling pathway. The different protein–protein interactions between the alternatively spliced GSTs and components of the JNK pathway might be significant in regulation of the stress kinase proteins in response to stress and under normal conditions for maintenance of basal activity.

Conclusion

Alternative splicing is one mechanism used in the GST superfamily to increase the diversity of isoforms that can metabolize a broad spectrum of compounds and perform nonenzymatic functions such as a regulatory role

in a signal transduction pathway. The data from the splice forms show that not only are the amino acid residues in the active site pocket significant to the catalytic function of the enzymes, but residues outside the active site pocket also are crucial for catalytic efficiencies and determining substrate specificities. These data again highlight the functional diversity of the GST splice forms. Other than the enzymatic and nonenzymatic properties, discussed herein, alternative splicing mechanisms of GSTs that have taken place during the course of evolution might have significant roles in additional functions that still remain to be explained.

Acknowledgments

This work was supported by the Thailand Research Fund (TRF). JW was supported by a Royal Golden Jubilee (RGJ) scholarship.

References

Adler, V., Yin, Z., Fuchs, S. Y., Benezra, M., Rosario, L., Tew, K. D., Pincus, M. R., Sardana, M., Henderson, C. J., Wolf, C. R., Davis, R. J., and Ronai, Z. (1999). Regulation of JNK signaling by GSTp. *EMBO J.* **18,** 1321–1334.

Ast, G. (2004). How did alternative splicing evolve? *Nat. Rev. Genet.* **5,** 773–782.

Brett, D., Pospisil, H., Valcárcel, J., Reich, J., and Bork, P. (2002). Alternative splicing and genome complexity. *Nat. Genet.* **30,** 29–30.

Chelvanayagam, G., Parker, M. W., and Board, P. G. (2001). Fly fishing for GSTs: A unified nomenclature for mammalian and insect glutathione transferases. *Chem. Biol. Interact.* **133,** 256–260.

Chen, L., Hall, P. R., Zhou, X. E., Ranson, H., Hemingway, J., and Meehan, E. J. (2003). Structure of an insect d-class glutathione S-transferase from a DDT-resistant strain of the malaria vector *Anopheles gambiae*. *Acta Cryst. D.* **59,** 2211–2217.

Cho, S.-G., Lee, Y. H., Park, H.-S., Ryoo, K., Kang, K. W., Park, J., Eom, S.-J., Kim, M. J., Chang, T.-S., Choi, S.-Y., Shim, J., Kim, Y., Dong, M.-S., Lee, M.-J., Kim, S. G., Ichijo, H., and Choi, E.-J. (2001). Glutathione *S*-transferase Mu modulates the stress-activated signals by suppressing apoptosis signal-regulating kinase 1. *J. Biol. Chem.* **276,** 12749–12755.

Comstock, K. E., Johnson, K. J., Rifenbery, D., and Henner, W. D. (1993). Isolation and analysis of the gene and cDNA for a human Mu class glutathione S-transferase, GSTM4. *J. Biol. Chem.* **268,** 16958–16965.

Curwen, V., Eyras, E., Andrews, T. D., Clarke, L., Mongin, E., Searle, S. M. J., and Clamp, M. (2004). The Ensembl automatic gene annotation system. *Genome Res.* **14,** 950.

Ding, Y., Ortelli, F., Rossiter, L. C., Hemingway, J., and Ranson, H. (2003). The *Anopheles gambiae* glutathione transferase supergene family: Annotation, phylogeny and expression profiles. *BMC Genomics* **4,** 35–50.

Graveley, B. R. (2001). Alternative splicing: Increasing diversity in the proteomic world. *Trends Genet.* **17,** 100–107.

Hayes, J. D., and Pulford, D. J. (1995). The glutathione S-transferase supergene family: Regulation of GST and the contribution of the isoenzymes to cancer chemoprotection and drug resistance. *CRC Crit. Rev. Biochem. Molec. Biol.* **30,** 445–600.

Hornby, J. A. T., Codreanu, S. G., Armstrong, R. N., and Dirr, H. W. (2002). Molecular recognition at the dimer interface of a class Mu glutathione transferase: Role of a hydrophobic interaction motif in dimer stability and protein function. *Biochemistry* **41,** 14238–14247.

Jirajaroenrat, K., Pongjaroenkit, S., Krittanai, C., Prapanthadara, L., and Ketterman, A. J. (2001). Heterologous expression and characterization of alternatively spliced glutathione *S*-transferases from a single *Anopheles* gene. *Insect Biochem. Mol. Biol.* **31,** 867–875.

Kampkötter, A., Volkmann, T. E., de Castro, S. H., Leiers, B., Klotz, L.-O., Johnson, T. E., Link, C. D., and Henkle-Dührsen, K. (2003). Functional analysis of the glutathione S-transferase 3 from *Onchocerca volvulus* (Ov-GST-3): A parasite GST confers increased resistance to oxidative stress in *Caenorhabditis elegans*. *J. Mol. Biol.* **325,** 25–37.

Ketterer, B. (2001). A bird's eye view of the glutathione transferase field. *Chem. Biol. Interact.* **138,** 27–42.

Ketterman, A. J., Prommeenate, P., Boonchauy, C., Chanama, U., Leetachewa, S., Promtet, N., and Prapanthadara, L. (2001). Single amino acid changes outside the active site significantly affect activity of glutathione S-transferases. *Insect Biochem. Mol. Biol.* **31,** 65–74.

Kondrashov, F. A., and Koonin, E. V. (2003). Evolution of alternative splicing: Deletions, insertions and origin of functional parts of proteins from intron sequences. *Trends Genet.* **19,** 115–119.

Lareau, L. F., Green, R. E., Bhatnagar, R. S., and Brenner, S. E. (2004). The evolving roles of alternative splicing. *Curr. Opin. Struct. Biol.* **14,** 273–282.

Liebau, E., Eschbach, M.-L., Tawe, W., Sommer, A., Fischer, P., Walter, R. D., and Henkle-Dührsen, K. (2000). Identification of a stress-responsive *Onchocerca volvulus* glutathione S-transferase (*Ov*-GST-3) by RT-PCR differential display. *Mol. Biochem. Parasitol.* **109,** 101–110.

Mironov, A. A., Fickett, J. W., and Gelfand, M. S. (1999). Frequent alternative splicing of human genes. *Genome Res.* **9,** 1288–1293.

Modrek, B., and Lee, C. (2002). A genomic view of alternative splicing. *Nat. Genet.* **30,** 13–19.

Neves, G., Zucker, J., Daly, M., and Chess, A. (2004). Stochastic yet biased expression of multiple *Dscam* splice variants by individual cells. *Nat. Genet.* **36,** 240–246.

Oakley, A. J., Harnnoi, T., Udomsinprasert, R., Jirajaroenrat, K., Ketterman, A. J., and Wilce, M. C. J. (2001). The crystal structures of glutathione S-transferases isozymes 1–3 and 1–4 from *Anopheles dirus* species B. *Protein Science* **10,** 2176–2185.

Ortelli, F., Rossiter, L. C., Vontas, J., Ranson, H., and Hemingway, J. (2003). Heterologous expression of four glutathione transferase genes genetically linked to a major insecticide-resistance locus from the malaria vector *Anopheles gambiae*. *Biochem. J.* **373,** 957–963.

Pongjaroenkit, S., Jirajaroenrat, K., Boonchauy, C., Chanama, U., Leetachewa, S., Prapanthadara, L., and Ketterman, A. J. (2001). Genomic organization and putative promotors of highly conserved glutathione S-transferases originating by alternative splicing in *Anopheles dirus*. *Insect Biochem. Mol. Biol.* **31,** 75–85.

Potter, S. C., Clarke, L., Curwen, V., Keenan, S., Mongin, E., Searle, S. M. J., Stabenau, A., Storey, R., and Clamp, M. (2004). The Ensembl analysis pipeline. *Genome Res.* **14,** 934–941.

Prapanthadara, L., Ketterman, A. J., and Hemingway, J. (1995). DDT-resistance in *Anopheles gambiae* giles from Zanzibar Tanzania based on increased DDT-dehydrochlorinase activity of glutathione S-transferases. *Bull. Entomol. Res.* **85,** 267–274.

Prapanthadara, L., Promtet, N., Koottathep, S., Somboon, P., and Ketterman, A. J. (2000). Isoenzymes of glutathione S-transferase from the mosquito Anopheles dirus species B: The purification, partial characterization and interaction with various insecticides. *Insect Biochem. Mol. Biol.* **30,** 395–403.

Ranson, H., Collins, F., and Hemingway, J. (1998). The role of alternative mRNA splicing in generating heterogeneity within the *Anopheles gambiae* class I glutathione S-transferase family. *Proc. Natl. Acad. Sci. USA* **95,** 14284–14289.

Ranson, H., Prapanthadara, L., and Hemingway, J. (1997). Cloning and characterization of two glutathione S-transferases from a DDT-resistant strain of *Anopheles gambiae*. *Biochem. J.* **324,** 97–102.

Ross, V. L., and Board, P. G. (1993). Molecular cloning and heterologous expression of an alternatively spliced human Mu class glutathione S-transferase transcript. *Biochem. J.* **294,** 373–380.

Sayed, Y., Wallace, L. A., and Dirr, H. W. (2000). The hydrophobic lock-and-key intersubunit motif of glutathione transferase A1–1: Implications for catalysis, ligandin function and stability. *FEBS Lett.* **465,** 169–172.

Seidegård, J., Vorachek, W. R., Pero, R. W., and Pearson, W. R. (1988). Hereditary differences in the expression of the human glutathione transferase active on *trans*-stilbene oxide are due to a gene deletion. *Proc. Natl. Acad. Sci. USA* **85,** 7293–7297.

Sheehan, D., Meade, G., Foley, V. M., and Dowd, C. A. (2001). Structure, function and evolution of glutathione transferases: Implications for classification of non-mammalian members of an ancient enzyme superfamily. *Biochem. J.* **360,** 1–16.

Sorek, R., Shamir, R., and Ast, G. (2004). How prevalent is functional alternative splicing in the human genome. *Trends Genet.* **20,** 68–71.

Stenberg, G., Abdalla, A.-M., and Mannervik, B. (2000). Tyrosine 50 at the subunit interface of dimeric human glutathione transferase P1–1 is a structural key residue for modulating protein stability and catalytic function. *Biochem. Biophys. Res. Comm.* **271,** 59–63.

Strausberg, R. L., Feingold, E. A., Grouse, L. H., Derge, J. G., Klausner, R. D., Collins, F. S., Wagner, L., Shenmen, C. M., Schuler, G. D., Altschul, S. F., Zeeberg, B., Buetow, K. H., Schaefer, C. F., Bhat, N. K., Hopkins, R. F., Jordan, H., Moore, T., Max, S. I., Wang, J., Hsieh, F., Diatchenko, L., Marusina, K., Farmer, A. A., Rubin, G. M., Hong, L., Stapleton, M., Soares, M. B., Bonaldo, M. F., Casavant, T. L., Scheetz, T. E., Brownstein, M. J., Usdin, T. B., Toshiyuki, S., Carninci, P., Prange, C., Raha, S. S., Loquellano, N. A., Peters, G. J., Abramson, R. D., Mullahy, S. J., Bosak, S. A., Mcewan, P. J., McKernan, K. J., Malek, J. A., Gunaratne, P. H., Richards, S., Worley, K. C., Hale, S., Garcia, A. M., Gay, L. J., Hulyk, S. W., Villalon, D. K., Muzny, D. M., Sodergren, E. J., Lu, X. H., Gibbs, R. A., Fahey, J., Helton, E., Ketteman, M., Madan, A., Rodrigues, S., Sanchez, A., Whiting, M., Madan, A., Young, A. C., Shevchenko, Y., Bouffard, G. G., Blakesley, R. W., Touchman, J. W., Green, E. D., Dickson, M. C., Rodriguez, A. C., Grimwood, J., Schmutz, J., Myers, R. M., Butterfield, Y. S. N., Kryzywinski, M. I., Skalska, U., Smailus, D. E., Schnerch, A., Schein, J. E., Jones, S. J. M., and Marra, M. A. (2002). Generation and initial analysis of more than 15,000 full-length human and mouse cDNA sequences. *Proc. Natl. Acad. Sci. USA* **99,** 16899–16903.

Udomsinprasert, R., Bogoyevitch, M. A., and Ketterman, A. J. (2004). Reciprocal regulation of glutathione *S*-transferase spliceforms and the *Drosophila* c-Jun N-terminal Kinase pathway components. *Biochem. J.* **383,** 483–490.

Wang, T., Arifoglu, P., Ronai, Z., and Tew, K. D. (2001). Glutathione *S*-transferase P1-1 (GSTP1-1) inhibits c-Jun N-terminal kinase (JNK1) signaling through interaction with the C terminus. *J. Biol. Chem.* **276,** 20999–21003.

Wojtowicz, W. M., Flanagan, J. J., Millard, S. S., Zipursky, S. L., and Clemens, J. C. (2004). Alternative splicing of *Drosophila* Dscam generates axon guidance receptors that exhibit isoform-specific homophilic binding. *Cell* **118,** 619–633.

Wongsantichon, J., Harnnoi, T., and Ketterman, A. J. (2003). A sensitive core region in the structure of glutathione S-transferases. *Biochem. J.* **373,** 759–765.

Wongtrakul, J., Sramala, I., and Ketterman, A. (2003). A non-active site residue, cysteine 69, of glutathione S-transferase adGSTD3-3 has a role in stability and catalytic function. *Protein Peptide Lett.* **10,** 375–385.

Zdobnov, E. M., von Mering, C., Letunic, I., Torrents, D., Suyama, M., Copley, R. R., Christophides, G. K., Thomasova, D., Holt, R. A., Subramanian, G. M., Mueller, H. M., Dimopoulos, G., Law, J. H., Wells, M. A., Birney, E., Charlab, R., Halpern, A. L., Kokoza, E., Kraft, C. L., Lai, Z. W., Lewis, S., Louis, C., Barillas-Mury, C., Nusskern, D., Rubin, G. M., Salzberg, S. L., Sutton, G. G., Topalis, P., Wides, R., Wincker, P., Yandell, M., Collins, F. H., Ribeiro, J., Gelbart, W. M., Kafatos, F. C., and Bork, P. (2002). Comparative genome and proteome analysis of *Anopheles gambiae* and *Drosophila melanogaster*. *Science* **298,** 149–159.

Further Reading

Prapanthadara, L., Koottathep, S., Promtet, N., Hemingway, J., and Ketterman, A. J. (1996). Purification and characterization of a major glutathione S-transferase from the mosquito *Anopheles dirus* (species B). *Insect Biochem. Mol. Biol.* **26,** 277–285.

[7] Disruption of the Glutathione Transferase Pi Class Genes

By COLIN J. HENDERSON and C. ROLAND WOLF

Abstract

Glutathione transferases are a multi-gene family of enzymes responsible for the metabolism of a wide range of both endogenous and exogenous substrates. These polymorphic enzymes, which form part of an adaptive response to chemical and oxidative stress, are widely distributed and ubiquitously expressed and are subject to regulation by a number of structurally unrelated chemicals. One of these enzymes, GST P, has been the focus of much research in recent years in relation to its involvement in the etiology of disease, particularly cancer. As part of our research efforts into GST P, we have developed a mouse line that lacks this enzyme and have used this model to investigate the consequences of the absence of GST P on tumorigenesis, drug metabolism, and toxicity.

Introduction

Glutathione Transferases

Glutathione transferases, historically referred to as glutathione S-transferases, hence the common abbreviation GST, are a family of dimeric enzymes involved in phase II detoxification reactions (EC 2.5.1.18).

METHODS IN ENZYMOLOGY, VOL. 401 0076-6879/05 $35.00

DOI: 10.1016/S0076-6879(05)01007-4

Identification, characterization and structure of a new Delta class glutathione transferase isoenzyme

Rungrutai UDOMSINPRASERT*[1], Saengtong PONGJAROENKIT†[1], Jantana WONGSANTICHON*, Aaron J. OAKLEY‡, La-aied PRAPANTHADARA§, Matthew C. J. WILCE‡ and Albert J. KETTERMAN*[2]

*Institute of Molecular Biology and Genetics, Mahidol University, Salaya Campus, 25/25 Putthamonthol Road 4, Salaya, Nakon Pathom 73170, Thailand, †Department of Biology, Faculty of Science, Maejo University, Chiangmai 50290, Thailand, and ‡Department of Pharmacology/Crystallography Centre, University of Western Australia, Crawley 6009, Australia, and §Research Institute for Health Sciences, Chiangmai University, Chiangmai 50200, Thailand

The insect GST (glutathione transferase) supergene family encodes a varied group of proteins belonging to at least six individual classes. Interest in insect GSTs has focused on their role in conferring insecticide resistance. Previously from the mosquito malaria vector *Anopheles dirus*, two genes encoding five Delta class GSTs have been characterized for structural as well as enzyme activities. We have obtained a new Delta class GST gene and isoenzyme from *A. dirus*, which we name adGSTD5-5. The adGSTD5-5 isoenzyme was identified and was only detectably expressed in *A. dirus* adult females. A putative promoter analysis suggests that this GST has an involvement in oogenesis. The enzyme displayed little activity for classical GST substrates, although it possessed the greatest activity for DDT [1,1,1-trichloro-2,2-bis-(*p*-chlorophenyl)ethane] observed for Delta GSTs. However, GST activity was inhibited or enhanced in the presence of various fatty acids, suggesting that the enzyme may be modulated by fatty acids. We obtained a crystal structure for adGSTD5-5 and compared it with other Delta GSTs, which showed that adGSTD5-5 possesses an elongated and more polar active-site topology.

Key words: *Anopheles dirus*, crystal structure, Delta class glutathione transferase, enzyme characterization, glutathione transferase gene, regulatory element.

INTRODUCTION

The insect GST (glutathione transferase) (EC 2.5.1.18) supergene family encodes a diverse set of proteins belonging to at least six individual classes (Delta, Epsilon, Sigma, Theta, Zeta, Omega and several unclassified genes) [1]. Interest in insect GSTs has focused on their role in conferring insecticide resistance [2] and in protecting against cellular damage by oxidative stress [3]. Many resistant insects are associated with elevated levels of GST activity [4]. In *Anopheles dirus*, two genes encoding five GST isoenzymes from the Delta class have been acquired previously and characterized for structural as well as enzyme activities [5–8]. To this end, we have identified a new Delta class GST isoenzyme from *Anopheles dirus* species B, which we named adGSTD5-5 (in insect GST nomenclature, 'D' refers to the Delta class and '5-5' refers to the homodimeric isoenzyme [9,10]). The availability of the *A. dirus* genome sequence has also enabled a putative promoter prediction, which suggests that this GST is involved in developmental-stage regulation. Moreover, the adGSTD5-5 enzyme was expressed and studied for structural as well as functional characteristics. The crystal structure of adGSTD5-5 was also obtained. Our data therefore reveal an overview of an evolutionarily conserved enzyme from gene to protein function.

MATERIALS AND METHODS

Genomic isolation of *gstD5*

A. dirus genomic library construction and screening was performed as described previously [7]. Using lower stringency hybridization, the presence of another GST gene was revealed on the phage clone of *adgst1AS1*. The recombinant phage clone 8A.2 was sequenced further until the complete sequence of 15 694 bp for the insert was obtained (GenBank® accession number AF251478).

adGSTD5-5 expression construct

The mRNAs were isolated from the fourth instar larvae, pupae, male and female adults by using TRIzol® reagent (Invitrogen) as described in the manufacturer's instructions. First-strand cDNA was synthesized by using Superscript II reverse transcriptase (Gibco BRL) and the oligo(dT)$_{15}$ primer 5′-GGCGGTCGACATATG(dT)$_{15}$-3′ (Proligo Singapore Pty), as described in the instruction manual. The N-terminus primer (5′-CACGCCG**CATATG**ACGACGGTGCTGTACTATC-3′) and C-terminus primer (5′-CGCCGTCGA**CATATG**CTACTGCTTCAACTTCGA-3′) were designed from the N-terminus and C-terminus of the amino acid coding region. The initial codon (ATG) and stop codon (TAG) are underlined, and the NdeI recognition site also incorporated in both primers is shown in bold. The PCR amplification (35 cycles of 94 °C for 1 min, 60 °C for 30 s and 72 °C for 1 min, and then a final extension step at 72 °C for 7 min) was performed on a PE system 2400 (PerkinElmer). The PCR product was purified from gel by GENECLEAN® II kit (BIO 101, La Jolla, CA, U.S.A.) following the manufacturer's instructions. The purified PCR product was digested with NdeI, and ligated into pET3a (Novagen) at the NdeI site. The ligated reaction was transformed into *Escherichia coli* DH5α cells. Then the recombinant clones were sequenced in both directions. Finally, the recombinant clones were transformed into *E. coli* BL21(DE3)pLysS competent cells for protein expression. The expression and purification of the recombinant enzyme was performed as described previously [11].

Abbreviations used: AP-1, activator protein 1; CDNB, 1-chloro-2,4-dinitrobenzene; DDT, 1,1,1-trichloro-2,2-bis-(*p*-chlorophenyl)ethane; GST, glutathione transferase; RMSD, root mean square deviation.

[1] These authors contributed equally to this work.

[2] To whom correspondence should be addressed (email frakt@mahidol.ac.th).

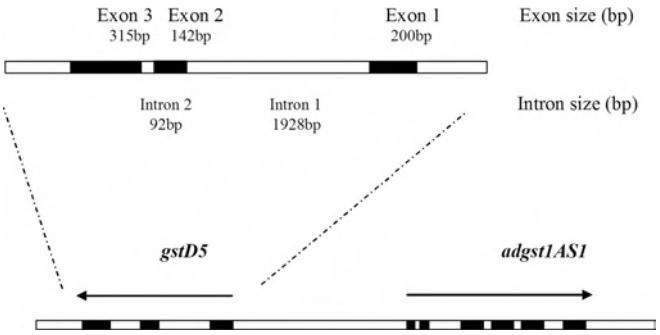

Figure 1 ***adgst1AS1*** **and** ***gstD5*** **gene organization of 8A.2 clone**

The *gstD5* gene is located 4620 bp upstream, with the opposite orientation to *adgst1AS1*. The 15694 bp genomic sequence has GenBank® accession number AF251478.

Characterization of the recombinant adGSTD5-5 enzyme

GST assay

Steady-state kinetics were studied for adGSTD5-5 at varying concentrations of CDNB (1-chloro-2,4-dinitrobenzene) and GSH in 0.1 M phosphate buffer, pH 6.5. The reaction was monitored at 340 nm, $\varepsilon = 9600\ M^{-1} \cdot cm^{-1}$. Apparent kinetic parameters, k_{cat}, K_m and k_{cat}/K_m were determined by fitting the collected data to a Michaelis–Menten equation by non-linear regression analysis using GraphPad Prism (GraphPad software, San Diego, CA, U.S.A.) [8,12]. The cumene hydroperoxide assay was performed by the method of Wendel [13]. The inhibition studies were performed using the GST assay conditions of 3 mM CDNB and 10 mM GSH (except for adGSTD2-2 and adGSTD6-6, where 15 mM GSH was used) in the absence and presence of various concentrations of inhibitors. Inhibitor solutions were diluted appropriately to maintain a constant concentration of organic solvent, if used, when the inhibitor concentration was varied. Protein quantification was determined by the method of Bradford [14] using the Bio-Rad reagent with BSA as the standard protein.

Crystallization

Culture trays (Flow Laboratories, McLean, VA, U.S.A.) sealed with petroleum jelly and siliconized coverslips (Hampton Research, Laguna Niguel, CA, U.S.A.) were used to grow crystals by the hanging-drop vapour-diffusion method. The well contained a 1 ml solution containing 1.6–2 M Li_2SO_4, 1 mM $CuCl_2$ and 100 mM sodium phosphate buffer, pH 6.5–7.5. A 1 μl aliquot of protein (13.1 mg/ml), 1 μl of 10 mM glutathione sulphonic acid and 1 μl of well solution were applied to the bipyramidal crystals (0.1–0.2 mm) that appeared within 24 h of setting up the tray.

Data collection

Crystals were transferred to artificial mother liquor containing 20 % (v/v) glycerol before snap-freezing at 100 K using an Oxford Cryo-Cooler. Data were collected using a Mar345 Image Plate system (marresearch GmbH, Norderstedt, Germany) with Cu-Kα X-rays from a Rigaku Ru-200 rotating anode generator equipped with Ni-focusing mirrors.

Structure solution and refinement

The adGST1-6 (adGSTD6-6) monomer solved at 2.15 Å (1 Å = 0.1 nm) resolution (Protein Date Bank code 1V2A) was used as a search model for molecular replacement using Molrep [15]. All structure refinement was performed using CNS (Crystallography and NMR System) [16] and model building in O [17]. A random selection of 5 % of reflections was chosen as a Free-R set to test the validity of various refinement steps. Alignment of adGSTD5-5 with adGSTD3-3 and adGSTD4-4 was performed using Deep View Swiss-PdbViewer version 3.7 (http://www.expasy.org/spdbv/) to obtain the RMSD (root mean square deviation) of the α-carbon backbone [18]. The Figures were created with Accelrys DS ViewerPro 5.0.

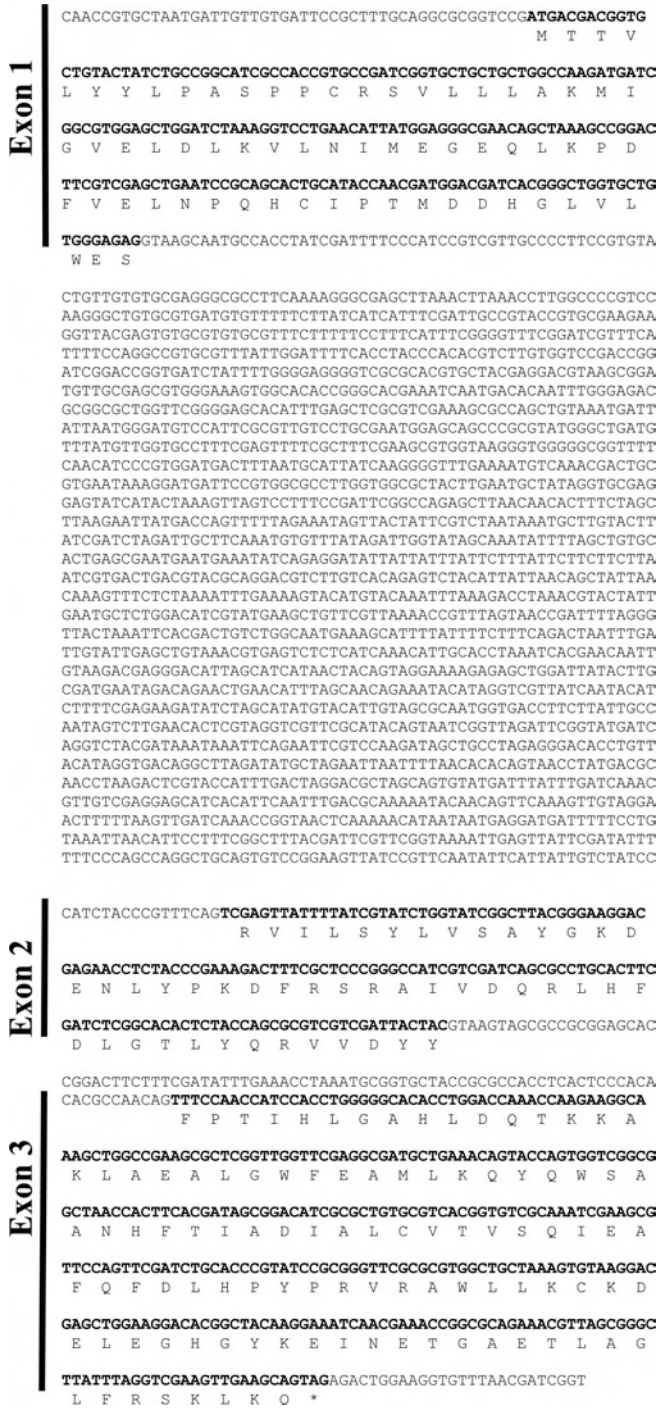

Figure 2 **The** ***gstD5*** **gene organization is composed of three coding regions that code for one GST protein**

The coding sequence is shown in bold, with the translated amino acid sequence below. The last codon of exon 1 is split, with the last base of the codon in exon 2.

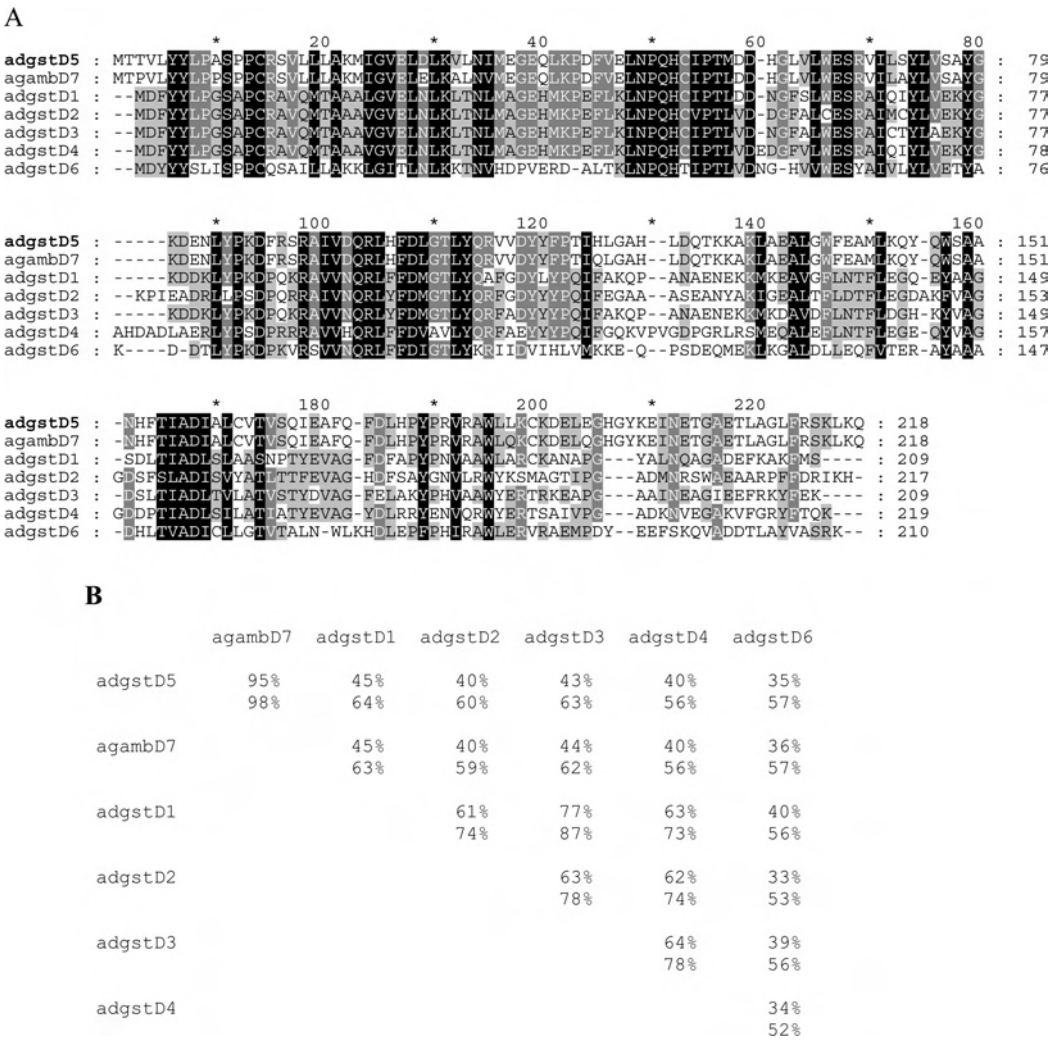

Figure 3 Amino acid sequence comparison of *A. dirus* adGSTD5-5 and the orthologous enzyme of AgGSTD7 from *A. gambiae* (agambD7) and five previously obtained *A. dirus* Delta GSTs using GeneDoc version 2.6

The sequences are adGSTD1-1, adGSTD2-2, adGSTD3-3, adGSTD4-4 and adGSTD6-6 (GenBank® accession numbers AF273041, AF273038, AF273039, AF273040 and AY014406 respectively [6,8]). (**A**) The dashes indicate gaps in the sequence. Black shading indicates 100 % conserved residues for the seven sequences, dark grey indicates 80 % conserved, and light grey indicates 60 % conserved. (**B**) Matrix table of percentage amino acid identities (top value) and percentage amino acid similarities (bottom value) for the sequences aligned in (**A**).

RESULTS AND DISCUSSION

Genomic organization and isolation of cDNA of *adgstD5*

A BLAST analysis of the 15 694 bp complete sequence of phage clone 8A.2 revealed a new GST gene, *adgstD5*, from the malaria vector *A. dirus*. This gene was named *adgstD5* for *A. dirus* GST class Delta protein coding sequence 5. The *adgstD5* gene is located upstream and is in reverse orientation to the *adgst1AS1* gene (Figure 1). Previously, we had a partial sequence for the phage insert, which suggested that the second gene was downstream, as well as possibly of the same Delta class GST as *adgst1AS1* and therefore was called *gst1-5* for insect GST class one enzyme five [7]. The derived amino acid sequence of the three coding exons is shown in Figure 2. The BLAST analysis yielded the highest identity to aggst1-7 (now referred to as gstD7), the product of the *aggst1β* gene of *Anopheles gambiae* [19]. The percentage amino acid identity for these two enzymes is 95 % and the percentage similarity is 98 % (Figure 3). The two mosquito malaria vectors *A. dirus* and *A. gambiae* have been diverged for several million years, the first in Southeast Asia and the second in Africa. The high degree of sequence conservation between the two *Anopheles* species suggests that this GST isoenzyme has a role in the metabolism of a compound that is a common metabolic product or a significant component in the environment in many living cells. A comparison with the available *A. gambiae* genome data shows that the adGSTD5 protein has 29–45 % amino acid identity with other Delta GSTs and 9–36 % with GSTs from the remaining classes. The percentage amino acid similarity to the Delta GSTs is 49–66 %. Therefore this GST is most like the Delta class GSTs; however, this gene encodes a singular GST protein with marginal amino acid identity with other Delta class GSTs.

Putative promoters of *adgstD5*

Previously, intronless GST genes have been reported in *Drosophila*; however, later introns were identified, as well as a 5′ untranslated region exon [20]. Our data of the exon composition of *adgstD5* define only the coding region. An additional possible 5′ and 3′ splice site were identified by BCM Gene Finder [21]. This suggests a possible 5′ splice site (TG/**GT**GGTT) and 3′ splice site

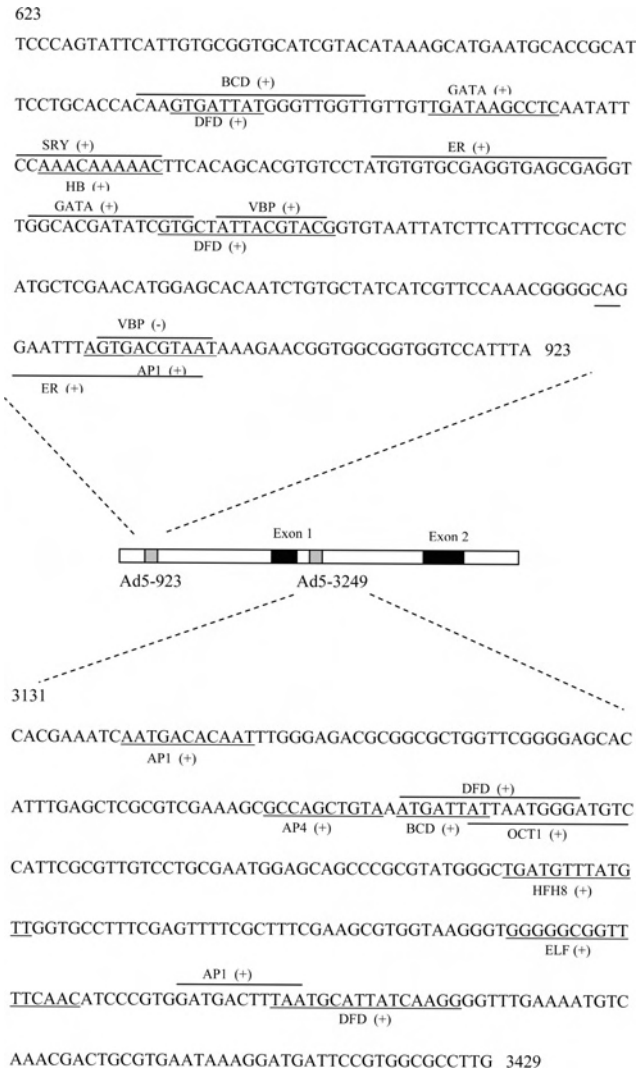

Figure 4 Sequence of two putative promoters of *gstD5* (Ad5-923 and Ad5-3429)

Potential transcription-factor-binding sites were mapped on the region of these two putative promoters by the MatInspector program. BCD, bicoid; ELF, grainyhead protein of *Drosophila*; ER, oestrogen receptor; HFH8, forkhead domain protein; SRY, sex-determining region Y; VBP, vitellogenin-binding protein. The binding site of each potential transcription factor is underlined or overlined. The (+) indicates the binding site on the sense strand, while (−) indicates the binding site on the antisense strand.

(TTGC**AG**/GC) (bold indicates the usually conserved splice site codon cleavage points) 771 bp and 11 bp upstream of exon 1 respectively. This implies that there is an exon that may be a 5′ untranslated region. Analysis also revealed two putative promoters, Ad5-923 and Ad5-3429, which may be defined as regulatory promoters of *adgstD5*, and are required to fulfil the core promoter activity in specific physiological circumstances (Figure 4).

Ad5-923 contains several binding sites for developmentally regulated transcription factors, such as hunchback, *Dfd*, AP-1 (activator protein 1) and GATA-1 (Figure 4). Also of interest are several binding sites of oestrogen receptor and oestrogen-dependent protein (oestrogen-receptor- and vitillogenin-binding protein) and maternal-effect protein in Ad5-923. It has been reported that there is an oestrogen-like compound in another arthropod, the ovary of shrimp (*Parapenaeus fissurus*) [22]. Searching the *Drosophila* genome database for an oestrogen receptor sequence yielded one sequence (CG 7404 gene product) on chromosome 3, that was distinct from the ecdysone receptor gene which is located on chromosome 2. BLAST analysis of the CG 7404 gene product provided the highest score to an oestrogen-related receptor β (41 % identity and 53 % similarity). These data imply that oestrogen-like compounds in insects may function in a similar way to vertebrate oestrogen. It is possible that the type of transcription factor binding sites detected in Ad5-293 may have contributed to the specific expression of Adgst5 mRNA in adult female mosquitoes.

Oocyte development in female mosquitoes involves lipid synthesis at extra-ovarian sites, such as the fat body, transfer and then incorporation into oocytes [23,24]. In *Aedes aegypti*, the dry weight of oocytes consists of 35 % lipids, 80 % of which has been transported from fat body [23,24]. The accumulation and transport of the lipid reserves in adult female mosquitoes would create an oxidative stress burden that could be alleviated by increased GST expression. The presence of an oestrogen-response element upstream of the *GSTA* gene was proposed to have a possible role in sexually maturing female plaice oocyte development [25]. The authors suggested that the enormous mobilization of lipids during lipovitellin synthesis in females presents a specific requirement of a GST-mediated detoxification mechanism to deal with lipid peroxidation, since up to 50 % of total fish egg lipid is composed of polyunsaturated fatty acids originating from the mother [25]. Ad5-923 contained both the oestrogen-response element and a vitellogenin-binding-protein element, which suggests that *adgstD5* might be involved in oogenesis, as was proposed for the fish GST.

Currently, the number of genes known to be regulated by elements outside the 5′ flanking region is constantly increasing. These intronic regulators often direct cell-type-specific or developmentally regulated gene expression [26]. Ad5-3429 is located within the intron, and contains several binding sites for factors that are reported to be involved in embryo or tissue development; that is, bicoid, HFH8, Elf, oct, *dfd* and AP-1 (Figure 4). This putative promoter therefore may be involved in developmental-stage regulation.

Expression and characterization of the recombinant adGSTD5-5 enzyme

Induction of the *E. coli* culture gave a high yield of recombinant adGSTD5-5 protein expression (250–300 mg/l of *E. coli* culture). However, adGSTD5-5 had a very weak affinity for GST-affinity chromatography medium compared with other GST isoenzymes from *A. dirus*, so the final yield of purified GST was low (1–3 mg/l of *E. coli* culture).

The characterization of the recombinant adGSTD5-5 was intrinsically problematic, as the enzyme possessed low detectable activities, suggesting the enzyme possessed very different substrate specificities compared with the other *A. dirus* GSTs. The adGSTD5-5 enzyme had an intermediate specific activity in GSH conjugation with the classical GST substrate CDNB. The K_m for GSH was the lowest observed for all six *A. dirus* GSTs (Table 1), suggesting the highest affinity binding to GSH. An estimated V_{max} of 167 μmol/min per mg and K_m of 14.9 mM are given only for purposes of comparison, as the data was collected well below the K_m value owing to CDNB solubility limits. The fairly high K_m for CDNB indicated low-affinity binding for this substrate. Cumene hydroperoxide activity was measured for adGSTD5-5 and also, for comparison, adGSTD4-4. The adGSTD5-5 activity of 0.293 ± 0.004 μmol/min per mg of protein (mean $\pm$ S.D.) was 6-fold greater than the 0.050 ± 0.009 μmol/min per mg of protein determined for adGSTD4-4. Our study of a range of compounds shown previously to be substrates for cytosolic GSTs

Table 1 Kinetic parameters of *A. dirus* GSTs

The data for adGSTD1-1, adGSTD2-2, adGSTD3-3, adGSTD4-4 and adGSTD6-6 have been reported previously [6,8,11].

			CDNB		GSH	
Isoenzyme	V_{max} (μmol/min per mg)	k_{cat} (s^{-1})	K_m (mM)	k_{cat}/K_m ($mM^{-1} \cdot s^{-1}$)	K_m (mM)	k_{cat}/K_m ($mM^{-1} \cdot s^{-1}$)
adGSTD5-5	167 ± 48	69	14.9 ± 4.9	5	0.21 ± 0.01	400
adGSTD1-1	12.9 ± 0.6	5.03	0.10 ± 0.03	48.4	0.86 ± 0.2	5.86
adGSTD2-2	63.9 ± 3.50	25.9	0.21 ± 0.03	121	1.30 ± 0.15	20
adGSTD3-3	67.5 ± 1.97	26.9	0.10 ± 0.01	269	0.40 ± 0.05	67
adGSTD4-4	40.3 ± 1.89	16.9	0.52 ± 0.67	32	0.83 ± 0.08	20
adGSTD6-6	2.2 ± 0.3	0.9	5.3 ± 0.8	0.2	1.8 ± 0.4	0.5

Table 2 Inhibition study of CDNB activity

The CDNB activity was measured in the absence and presence of the respective compound at the concentration given. The data presented represent the means ± S.D. for at least three independent experiments. ND, not detected.

		Inhibition (%)					
Compound	Concentration (mM)	adGSTD5-5	adGSTD1-1	adGSTD2-2	adGSTD3-3	adGSTD4-4	adGSTD6-6
Dichloroacetic acid	0.5	16.84 ± 3.22	ND	ND	ND	ND	ND
Cumene hydroperoxide	2.5	37.17 ± 1.19	30.36 ± 9.53	60.44 ± 2.15	28.94 ± 4.82	29.53 ± 3.77	28.27 ± 2.56
p-Nitrobenzyl chloride	1.0	33.40 ± 6.07	43.38 ± 5.17	37.60 ± 3.67	55.36 ± 1.84	49.77 ± 1.35	9.52 ± 1.98
p-Nitrophenyl bromide	0.1	35.72 ± 1.50	24.30 ± 14.52	17.28 ± 0.88	33.39 ± 3.78	31.33 ± 3.10	3.17 ± 3.85
Ethacrynic acid	0.1	84.67 ± 0.71	100 ± 0	99.57 ± 0.59	98.31 ± 0.10	100 ± 0	86.36 ± 1.65
	0.01	55.22 ± 0.66	99.46 ± 1.54	94.88 ± 1.32	81.61 ± 0.76	85.49 ± 1.58	57.73 ± 3.09
	0.001	40.28 ± 3.16	81.88 ± 4.14	64.16 ± 3.74	37.95 ± 1.99	46.45 ± 3.39	37.55 ± 1.40
S-Hexylglutathione	0.1	71.98 ± 1.76	94.93 ± 0.65	97.08 ± 0.92	67.84 ± 1.10	76.91 ± 0.26	64.14 ± 3.58
	0.01	24.87 ± 3.93	63.18 ± 3.21	75.44 ± 0.61	32.07 ± 1.58	20.09 ± 1.24	35.03 ± 2.46
Permethrin	0.01	35.56 ± 1.68	20.37 ± 1.90	27.36 ± 5.45	35.87 ± 1.87	47.73 ± 3.08	11.70 ± 1.87
Deltamethrin	0.01	40.15 ± 2.17	11.01 ± 7.51	30.72 ± 3.53	35.28 ± 3.05	49.30 ± 2.37	15.87 ± 5.29
λCyhalothrin	0.01	39.96 ± 1.19	21.88 ± 10.66	29.11 ± 2.88	26.38 ± 1.73	40.50 ± 1.40	23.26 ± 5.58

Table 3 DDTase activity of the recombinant GST isoenzymes from *A. dirus*

The DDTase activity is expressed as nmol of DDE (dichlorodiphenyldichloroethylene) formation/mg of enzyme protein. The CDNB specific activity is in μmol/min per mg of protein.

Isoenzyme	DDTase activity	CDNB activity	DDTase/CDNB
adGSTD5-5	78.77 ± 13.19	19.2	4.11
adGSTD1-1	<1.0	12.2	–
adGSTD2-2	1.87 ± 0.82	39.7	0.05
adGSTD3-3	2.66 ± 0.29	64.6	0.04
adGSTD4-4	7.50 ± 1.68	38.3	0.20
adGSTD6-6	1.28 ± 0.22	1.37	0.93

from the classes described previously, including 1,2-dichloro-4-nitrobenzene, *p*-nitrophenethyl bromide and ethacrynic acid, revealed that there was no detectable activity with these known GST substrates, even at 10-fold increased enzyme concentration compared with that used in the CDNB assay. Nevertheless, adGSTD5-5 did interact with these substrates as well as pyrethroid insecticides, as shown by inhibition of CDNB activity (Table 2). Intriguingly, only adGSTD5-5 was inhibited by dichloroacetic acid, which is the specific substrate for Zeta class GSTs in dechlorination of dichloroacetic acid to glyoxylic acid [27–31]. However, this dechlorination activity was undetectable for adGSTD5-5. Despite low GSH-conjugating activity, adGSTD5-5 possessed the greatest DDT [1,1,1-trichloro-2,2-bis-(*p*-chlorophenyl)ethane] dehydrochlorination activity of the six recombinant GSTs that we have currently obtained (Table 3). The DDTase activity was 11–62-fold different among the five

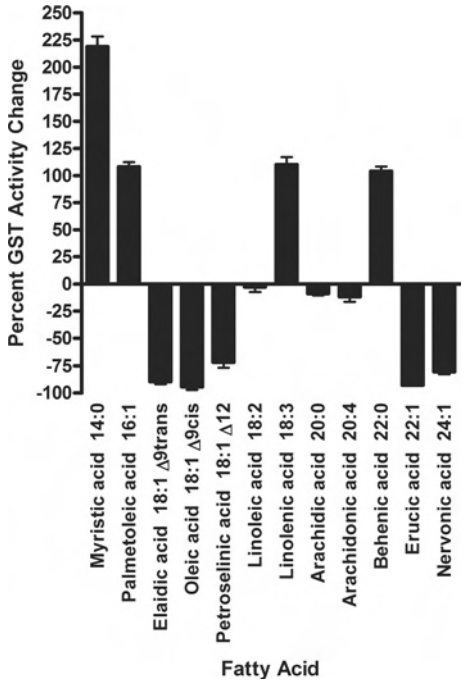

Figure 5 Fatty acid effects on adGSTD5-5 CDNB activity

The final concentration of fatty acids tested was 50 μM in the standard CDNB assay. Data show the changed enzyme activity for CDNB in the presence of the respective fatty acid, where negative values show inhibition and positive values show activation relative to the absence of any fatty acid.

Table 4 X-ray data reduction statistics

Values in parentheses refer to the highest resolution bin (2.59–2.50 Å).

Parameter	Value
R-factor (%)	7.8 (39.6)
$I/\sigma I$	12.9 (2.6)
Number of observations	37582 (3682)
Number of unique observations	9605 (963)
Multiplicity	3.9 (3.8)
Completeness (%)	95.6 (97.9)

Table 5 Model statistics

Values in parentheses refer to the highest resolution bin (2.66–2.50 Å).

Parameter	Value
R-factor	0.233 (0.351)
R-free	0.265 (0.407)
Non-hydrogen atoms in model:	
Protein	1732
Glutathione sulphonic acid	23
Water	44
Cu^{2+} ions	3
Mean B-factor	45.5
B-factor from Wilson plot	41.8
RMSD from ideal values	
Bond lengths	0.007 Å
Bond angles	1.4°
Dihedral angles	20.8°
Improper angles	0.82°

A. dirus GSTs, and adGSTD1-1 had no detectable activity (Table 3). A ratio of DDTase/CDNB activity showed that the adGSTD5-5 enzyme possessed a 4–100-fold greater DDT substrate preference compared with the other GSTs. Altogether, these data illustrate that adGSTD5-5 displays catalytic properties distinct from the insect GST isoenzymes defined previously. Two additional classes of soluble GSTs, Omega and Zeta, were also described recently with unusual enzymatic activities in a variety of organisms, including mammals [32–34]. This suggests that gene rearrangement in combination with structural evolution presumably constitutes an evolutionary function of the GST enzymes operating in Nature [35]. The mechanism of catalysis and the residues involved are yet to be investigated for adGSTD5-5.

Various mammalian GST isoforms have been shown to be highly active in conjugating toxic lipid alkenals and purine and pyrimidine alkenals, all of which are believed to arise in cells as a consequence of oxidative processes [36,37]. Interestingly, adGSTD5-5 contained the putative regulatory elements involved in detoxification of lipid peroxidation. Therefore we investigated the role of heterologously expressed adGSTD5-5 involved in detoxification of potentially deleterious fatty acid metabolites by assaying the effect of polyunsaturated fatty acids on GSH conjugation with CDNB. Our data demonstrated adGSTD5-5 interaction with several fatty acids (Figure 5). An interesting observation was that, although several fatty acids appeared to have little effect on CDNB activity, the others tested either inhibited activity by 72–94 % or enhanced activity by 104–219 %. This fatty acid interaction yielding various effects on adGSTD5-5 implies that adGSTD5-5 may have a physiological role in protection against oxidative stress as reported previously for GST Alpha class isoenzymes that appear to be involved in the signalling mechanisms of apoptosis [38].

Structural determination of the adGSTD5-5 enzyme

Molecular replacement was successful with the solution corresponding to the highest peak in the rotation function (5.97σ) and translation function (13.82σ) as shown in Table 4. The initial model (R-factor = 0.526, R-free = 0.515) was subjected to rigid body, positional and temperature-factor refinement, reducing the R-factor to 0.466 (R-free = 0.485). Sigma-A weighted $2F_o$-F_c and F_o-F_c electron density maps calculated from this model revealed a molecule in the G-site not present in the model. This was clearly a glutathione sulphonic acid molecule. Six cycles of positional refinement, B-factor refinement and model building were performed in which the amino acid sequence of the model was changed from that of adGSTD6-6 to adGSTD5-5. The final model includes amino acid residues 2–215, one glutathione sulphonic acid molecule and 44 water molecules. Statistics for this model are given in Table 5. The adGSTD5-5 structure obtained for this study is shown in Figure 6 (Protein Data Bank accession number 1R5A).

The tertiary structure obtained from crystallographic analysis showed the adGSTD5-5 protein to possess the canonical GST structure (Figure 7). The physiologically relevant state of the protein is a dimer, which is present in the crystal owing to a 2-fold symmetry operation. The overall structure is broadly similar to that of previously determined Delta class GST structures [5].

Figure 6 Stereo view of adGSTD5-5

The view is looking down on the 2-fold axis into the active site, with the glutathione sulphonic acid shown as a ball-and-stick figure. The co-ordinates for the tertiary structure have been deposited in the Protein Data Bank under the accession code 1R5A.

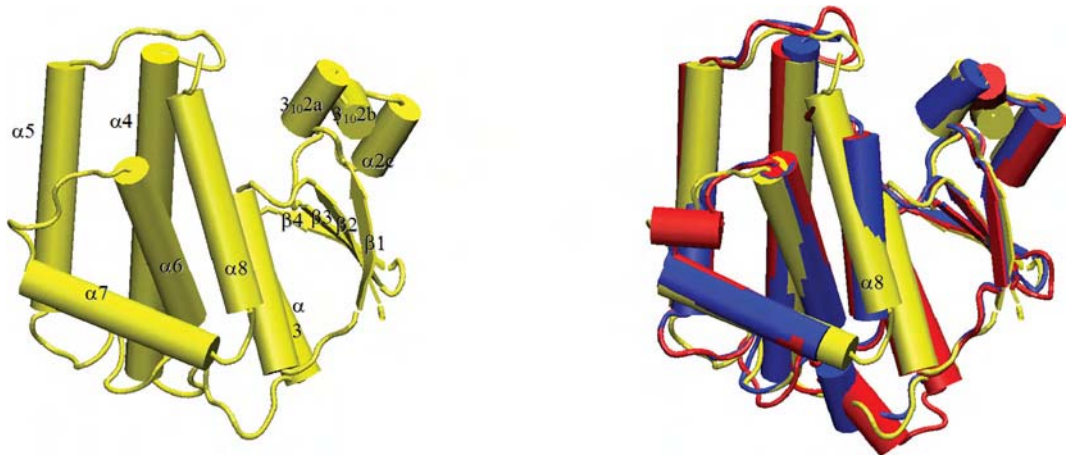

Figure 7 Cartoon representation of adGSTD5-5

Cylinders represent helices, arrows represent strands, and lines represent random coil. Left: adGSTD5-5, with secondary structure elements labelled. Right: Aligned *Anopheles* GSTs. adGSTD3-3 is in blue, adGSTD4 is in red, and adGSTD5-5 is in yellow.

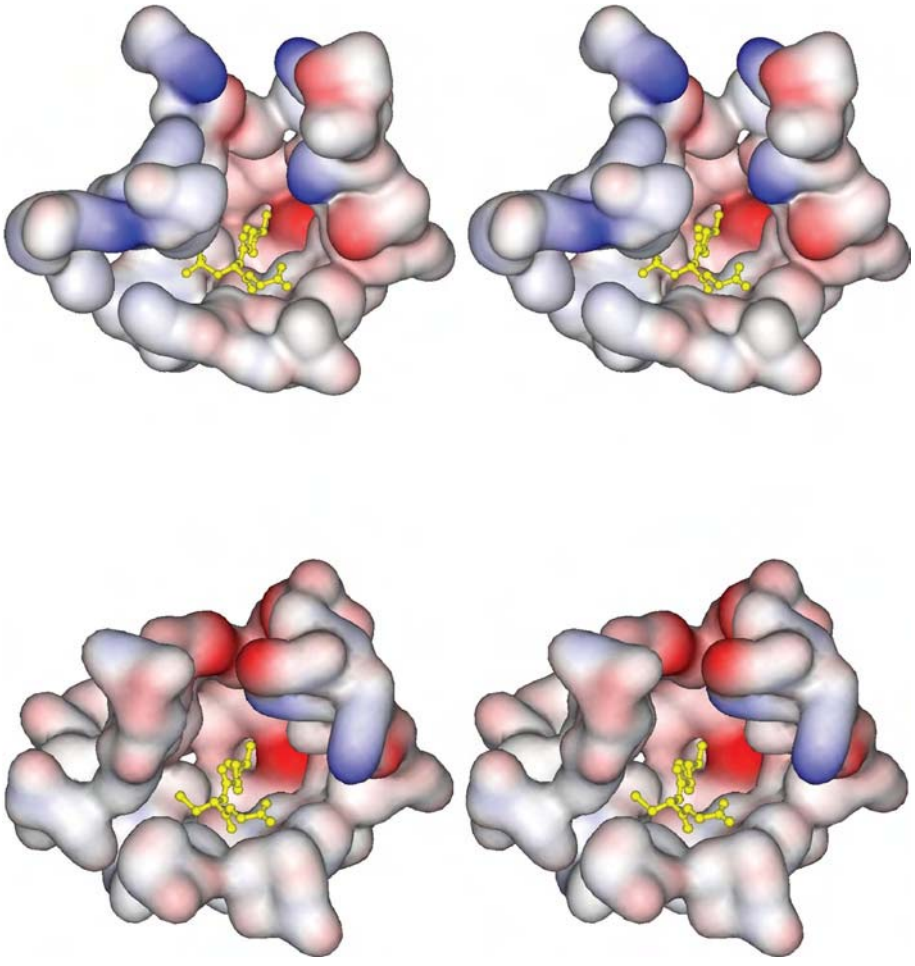

Figure 8 Stereo views of the electrostatic potential surface of the active-site pockets of adGSTD5-5 and adGSTD3-3

The two tertiary structures were aligned to illustrate the same view of the active site. The top panel shows adGSTD5-5, and the bottom panel shows adGSTD3-3. A yellow ball-and-stick representation shows the GSH in the pocket.

The G-site is formed mostly by residues from the N-terminal thioredoxin domain. Like other Delta class GSTs, a serine residue (Ser^{11}) appears to be responsible for activating the GSH thiol residue in catalysis. However, in the absence of direct evidence such as site-directed mutagenesis, it is possible that a nearby serine, cysteine or tyrosine residue may be the major catalytic

residue. The presence of a histidine residue (His^{119}) was unexpected: GST H-sites normally being lined with hydrophobic residues. A water molecule sits in the H-site and is hydrogen-bonded to $His^{119}N\varepsilon2$. An alignment of the adGSTD5-5 tertiary structure with these two *A. dirus* GSTs, adGSTD3-3 and adGSTD4-4 (Protein Data Bank accession numbers 1JLV and 1JLW respectively), illustrates the conserved nature of GST tertiary structure. adGSTD5-5 possessed an RMSD of 1.42 Å and 1.25 Å for the α-carbon alignment with adGSTD3-3 and adGSTD4-4 respectively. There are significant differences between the packing of helix $\alpha8$ of adGSTD5-5 with the rest of the protein. As a result, this helix is closer to the C-terminal domain compared with other insect GST isoenzymes (Figure 7). This can be attributed to the replacement of packing residues in adGSTD5-5 by smaller amino acids. As such, the overall shape of the H-site is different in adGSTD5-5 compared with the adGSTD3-3 and adGSTD4-4 isoenzymes. A comparison of adGSTD5-5 and adGSTD3-3 showed 47% identity in the 43 amino acids that make up the active-site pocket with an average RMSD of 0.616 Å for the identical amino acid residues. However, the shape of the two active-site pockets seems to be quite distinct, with the adGSTD5-5 pocket appearing to be elongated (Figure 8). In comparison, the adGSTD5-5 pocket also appears to be more polar, with an increase in both positive and negative charges that contributes to distinct orientations of GSH and substrate binding. These structurally unique features of adGSTD5-5, especially in the vicinity of the active site and the C-terminus, may define the substrate repertoire for this particular GST, whereby it displays an unusual enzymatic property. These results suggest that there is considerable structural plasticity in the active site of Delta class GSTs, and that their catalytic activities may not be restricted to hydrophobic co-substrates.

Conclusion

The adGSTD5-5 isoenzyme was identified and only detectably expressed in *A. dirus* adult females. A high degree of sequence conservation of this gene across several million years of divergent evolution between two Anopheline malaria vector species suggests that this GST isoenzyme performs an important function. A putative promoter analysis suggests that this GST has an involvement in oogenesis and in developmental-stage regulation. The enzyme displayed little activity for classical GST substrates, although it possessed the greatest activity for DDT, 10-fold, observed for Delta GSTs. However enzyme activity was increased or decreased by fatty acid interaction, suggesting that the GST activity may be modulated by fatty acids. A tertiary structure comparison revealed differences in active-site composition, with an elongated and more polar active-site topology.

This work was supported by the Thailand Research Fund, and R.U. was supported by a Royal Golden Jubilee Scholarship.

REFERENCES

1 Ding, Y., Ortelli, F., Rossiter, L. C., Hemingway, J. and Ranson, H. (2003) The *Anopheles gambiae* glutathione transferase supergene family: annotation, phylogeny and expression profiles. BMC Genomics **4**, 35–50

2 Vontas, J. G., Small, G. J. and Hemingway, J. (2001) Glutathione S-transferases as antioxidant defence agents confer pyrethroid resistance in *Nilaparvata lugens*. Biochem. J. **357**, 65–72

3 Zou, S., Meadows, S., Sharp, L., Jan, L. Y. and Jan, Y. N. (2000) Genome-wide study of aging and oxidative stress response in *Drosophila melanogaster*. Proc. Natl. Acad. Sci. U.S.A. **97**, 13726–13731

4 Prapanthadara, L., Hemingway, J. and Ketterman, A. J. (1993) Partial purification and characterization of glutathione S-transferases involved in DDT resistance from the mosquito *Anopheles gambiae*. Pestic. Biochem. Physiol. **47**, 119–133

5 Oakley, A. J., Harnnoi, T., Udomsinprasert, R., Jirajaroenrat, K., Ketterman, A. J. and Wilce, M. C. J. (2001) The crystal structures of glutathione S-transferases isozymes 1–3 and 1–4 from *Anopheles dirus* species B. Protein Sci. **10**, 2176–2185

6 Jirajaroenrat, K., Pongjaroenkit, S., Krittanai, C., Prapanthadara, L. and Ketterman, A. J. (2001) Heterologous expression and characterization of alternatively spliced glutathione *S*-transferases from a single *Anopheles* gene. Insect Biochem. Mol. Biol. **31**, 867–875

7 Pongjaroenkit, S., Jirajaroenrat, K., Boonchauy, C., Chanama, U., Leetachewa, S., Prapanthadara, L. and Ketterman, A. J. (2001) Genomic organization and putative promoters of highly conserved glutathione S-transferases originating by alternative splicing in *Anopheles dirus*. Insect Biochem. Mol. Biol. **31**, 75–85

8 Udomsinprasert, R. and Ketterman, A. J. (2002) Expression and characterization of a novel class of glutathione S-transferase from *Anopheles dirus*. Insect Biochem. Mol. Biol. **32**, 425–433

9 Mannervik, B., Awasthi, Y. C., Board, P. G., Hayes, J. D., Di Ilio, C., Ketterer, B., Listowsky, I., Morgenstern, R., Muramatsu, M., Pearson, W. R. et al. (1992) Nomenclature for human glutathione transferases. Biochem. J. **282**, 305–306

10 Chelvanayagam, G., Parker, M. W. and Board, P. G. (2001) Fly fishing for GSTs: a unified nomenclature for mammalian and insect glutathione transferases. Chem. Biol. Interact. **133**, 256–260

11 Ketterman, A. J., Prommeenate, P., Boonchauy, C., Chanama, U., Leetachewa, S., Promtet, N. and Prapanthadara, L. (2001) Single amino acid changes outside the active site significantly affect activity of glutathione S-transferases. Insect Biochem. Mol. Biol. **31**, 65–74

12 Prapanthadara, L., Koottathep, S., Promtet, N., Hemingway, J. and Ketterman, A. J. (1996) Purification and characterization of a major glutathione S-transferase from the mosquito *Anopheles dirus* (species B). Insect Biochem. Mol. Biol. **26**, 277–285

13 Wendel, A. (1981) Glutathione peroxidase. Methods Enzymol. **77**, 325–333

14 Bradford, M. M. (1976) A rapid and sensitive method for the quantitation of microgram quantities of protein utilizing the principle of protein-dye binding. Anal. Biochem. **72**, 248–254

15 Vagin, A. and Teplyakov, A. (2000) An approach to multi-copy search in molecular replacement. Acta Crystallogr. Sect. D Biol. Crystallogr. **56**, 1622–1624

16 Brunger, A. T., Adams, P. D., Clore, G. M., DeLano, W. L., Gros, P., Gross-Kunstleve, R. W., Jiang, J. S., Kuszewski, J., Nilges, M., Pannu, N. S. et al. (1998) Crystallography & NMR system: a new software suite for macromolecular structure determination. Acta Crystallogr. Sect. D Biol. Crystallogr. **54**, 905–921

17 Jones, T. A., Zou, J. Y., Cowan, S. W. and Kjeldgaard, M. (1991) Improved methods for building protein models in electron density maps and the location of errors in these models. Acta Crystallogr. Sect. A Found. Crystallogr. **47**, 110–119

18 Guex, N. and Peitsch, M. C. (1997) SWISS-MODEL and the Swiss-PdbViewer: an environment for comparative protein modeling. Electrophoresis **18**, 2714–2723

19 Ranson, H., Collins, F. and Hemingway, J. (1998) The role of alternative mRNA splicing in generating heterogeneity within the *Anopheles gambiae* class I glutathione S-transferase family. Proc. Natl. Acad. Sci. U.S.A. **95**, 14284–14289

20 Lougarre, A., Bride, J. M. and Fournier, D. (1999) Is the insect glutathione S-transferase I gene family intronless? Insect Mol. Biol. **8**, 141–143

21 Smith, R., Wiese, B., Wojzynski, M., Davison, D. and Worley, K. (1996) BCM search launcher – an integrated interface to molecular biology data base search and analysis services available on the World Wide Web. Genome Res. **6**, 454–462

22 Jeng, S. S., Wan, W. C. and Chang, C. F. (1978) Existence of an estrogen-like compound in the ovary of the shrimp *Parapenaeus fissurus*. Gen. Comp. Endocrinol. **36**, 211–214

23 Ziegler, R. and Ibrahim, M. M. (2001) Formation of lipid reserves in fat body and eggs of the yellow fever mosquito, *Aedes aegypti*. J. Insect Physiol. **47**, 623–627

24 Briegel, H., Gut, T. and Lea, A. O. (2003) Sequential deposition of yolk components during oogenesis in an insect, *Aedes aegypti* (Diptera: Culicidae). J. Insect Physiol. **49**, 249–260

25 Leaver, M. J., Wright, J. and George, S. G. (1997) Structure and expression of a cluster of glutathione S-transferase genes from a marine fish, the plaice (*Pleuronectes platessa*). Biochem. J. **321**, 405–412

26 Warnecke, C., Willich, T., Holzmeister, J., Bottari, S. P. and Fleck, E. (1999) Efficient transcription of the human angiotensin II type 2 receptor gene requires intronic sequence elements. Biochem. J. **340**, 17–24

27 Anderson, W. B., Board, P. G., Gargano, B. and Anders, M. W. (1999) Inactivation of glutathione transferase zeta by dichloroacetic acid and other fluorine-lacking α-haloalkanoic acids. Chem. Res. Toxicol. **12**, 1144–1149

28 Tong, Z., Board, P. G. and Anders, M. W. (1998) Glutathione transferase zeta catalyses the oxygenation of the carcinogen dichloroacetic acid to glyoxylic acid. Biochem. J. **331**, 371–374

29 Tzeng, H.-F., Blackburn, A. C., Board, P. G. and Anders, M. W. (2000) Polymorphism- and species-dependent inactivation of glutathione transferase zeta by dichloroacetate. Chem. Res. Toxicol. **13**, 231–236

30 Thom, R., Dixon, D. P., Edwards, R., Cole, D. J. and Lapthorn, A. J. (2001) The structure of a Zeta class glutathione S-transferase from *Arabidopsis thaliana*: characterisation of a GST with novel active-site architecture and a putative role in tyrosine catabolism. J. Mol. Biol. **308**, 949–962
31 Polekhina, G., Board, P. G., Blackburn, A. C. and Parker, M. W. (2001) Crystal structure of maleylacetoacetate isomerase/glutathione transferase zeta reveals the molecular basis for its remarkable catalytic promiscuity. Biochemistry **40**, 1567–1576
32 Board, P. G., Coggan, M., Chelvanayagam, G., Easteal, S., Jermiin, L. S., Schulte, G. K., Danley, D. E., Hoth, L. R., Griffor, M. C., Kamath, A. V. et al. (2000) Identification, characterization, and crystal structure of the omega class glutathione transferases. J. Biol. Chem. **275**, 24798–24806
33 Anders, M. W., Anderson, W. B., Tzeng, H.-F. and Board, P. G. (2001) Glutathione transferase zeta: novel xenobiotic substrates and enzyme inactivation. Chem. Biol. Interact. **133**, 211–216
34 Board, P., Baker, R. T., Chelvanayagam, G. and Jermiin, L. S. (1997) Zeta, a novel class of glutathione transferases in a range of species from plants to humans. Biochem. J. **328**, 929–935
35 Parker, M. W., McKinstry, W. J., Oakley, A. J., Polekhina, G., Rossjohn, J., Chelvanayagam, G., Board, P. G., Di Ilio, C., Caccuri, A. M., Ricci, G. and Lo Bello, M. (2001) Evolution of functional diversity as observed through structural studies of glutathione transferases. Chem. Biol. Interact. **133**, 8–12
36 Berhane, K., Widersten, M., Engström, Å., Kozarich, J. W. and Mannervik, B. (1994) Detoxication of base propenals and other α,β-unsaturated aldehyde products of radical reactions and lipid peroxidation by human glutathione transferases. Proc. Natl. Acad. Sci. U.S.A. **91**, 1480–1484
37 Ishikawa, T., Esterbauer, H. and Sies, H. (1986) Role of cardiac glutathione transferase and of the glutathione S-conjugate export system in biotransformation of 4-hydroxynonenal in the heart. J. Biol. Chem. **261**, 1576–1581
38 Yang, Y., Cheng, J.-Z., Singhal, S. S., Saini, M., Pandya, U., Awasthi, S. and Awasthi, Y. C. (2001) Role of glutathione *S*-transferases in protection against lipid peroxidation: overexpression of hGSTA2–2 in K562 cells protects against hydrogen peroxide induced apoptosis and inhibits JNK and caspase 3 activation. J. Biol. Chem. **276**, 19220–19230

Received 6 December 2004/14 February 2005; accepted 17 February 2005
Published as BJ Immediate Publication 17 February 2005, DOI 10.1042/BJ20042015

Available online at www.sciencedirect.com
SCIENCE DIRECT®
Insect Biochemistry and Molecular Biology 35 (2005) 197–205
Reprint 13
Insect Biochemistry and Molecular Biology
www.elsevier.com/locate/ibmb

Intra-subunit residue interactions from the protein surface to the active site of glutathione S-transferase AdGSTD3–3 impact on structure and enzyme properties

Jeerang Wongtrakul[a], Issara Sramala[b], La-aied Prapanthadara[a], Albert J. Ketterman[b,*]

[a]*Research Institute for Health Sciences, Chiang Mai University, P.O. Box 80 CMU, Thailand 50200*
[b]*Institute of Molecular Biology & Genetics, Mahidol University, Salaya campus, 25/25 Putthamonthol Road 4, Salaya, Nakon Pathom 73170, Thailand*

Received 16 August 2004; received in revised form 12 November 2004; accepted 17 November 2004

Abstract

Structural residues are one of the major factors that modulate the catalytic specificity as well as having a role in stability of the glutathione S-transferases (GST). To understand how residues remote from the active site can affect enzymatic properties, four mutants, His144Ala, Val147Leu, Val147Ala and Arg96Ala, were generated. The selected residues appear to be in a putative intra-subunit interaction pathway from the exterior Asp150 to the active site Arg66 of AdGSTD3–3. The analysis of the four mutants suggested that the interaction formed between Asp150 and His144 is required for the packing of the hydrophobic core in domain 2. Mutations of both Asp150 and His144 impacted upon enzymatic properties. Two Val147 mutants also showed contribution to packing and support of the N-capping box motif by demonstrating shorter half-lives. The planar guanidinium of Arg96 is in a stacked geometry with the face of the aromatic ring of Phe140 in a cation-π interaction. The Arg96 also interacts with several other residues one of which, Asp100, is in the active site. These interactions restrict movement of the residues in this region and as the data demonstrates when Arg96 is changed have dramatic impact on stability and enzyme properties. These findings indicate the significance of the roles played by residue interactions which can cause conformational changes and thereby influence the catalytic activity and stability of an enzyme.

Keywords: Glutathione S-transferase; Structure; Molecular dynamics simulation; Enzyme specificity

1. Introduction

Glutathione S-transferases (EC 2.5.1.18; GSTs) are a family of enzymes involved in cellular detoxification by catalyzing the nucleophilic attack of glutathione (GSH) on the electrophilic center of a number of toxic compounds and xenobiotics such as insecticides (Booth et al., 1961). Besides their detoxification roles, GSTs are also involved in the modulation of signal transduction, ion channels and the storage of nitric oxide (Adler et al., 1999; Cho et al., 2001; Dulhunty et al., 2001; Lo Bello et al., 2001; Wang et al., 2001). Cytosolic GSTs have been grouped into at least 13 distinct classes, namely alpha, mu, pi, theta, sigma, kappa, omega, beta, phi, tau, zeta, delta and epsilon on the basis of immunological and structural properties (Sawicki et al., 2003; Sheehan et al., 2001). GSTs consist of identical or structurally related subunits. Each subunit, approximately 25 kDa, consists of two domains and contains an active site consisting of a G-site (GSH binding site) and an H-site (hydrophobic substrate binding site). The G-site is formed primarily by the N-terminal domain, which is structurally related to thioredoxin. The H-site is formed by the amino acids in the

Abbreviations: GST, glutathione S-transferase; GSH, glutathione; G-site, glutathione binding site; H-site, hydrophobic substrate binding site; CDNB, 1-chloro-2, 4-dinitrobenzene

*Corresponding author. Tel.: +66 2800 3624 8x1279; fax: +66 2441 9906.
E-mail addresses: frakt@mahidol.ac.th, albertketterman@yahoo.com (A.J. Ketterman).

0965-1748/$ - see front matter © 2004 Elsevier Ltd. All rights reserved.
doi:10.1016/j.ibmb.2004.11.003

region of the α4-helix to α8-helix. Whereas, the structure of the G-site is well conserved among GSTs, the H-site varies widely in different classes, leading to differences in substrate specificity (Armstrong, 1997). In addition, GSTs also possess a ligand binding site that is located in either part of the substrate binding site or at the dimer interface (Lyon and Atkins, 2002; Sayed et al., 2000).

Structural residues are one of the major factors that modulate the catalytic specificity as well as having a role in stability of the GSTs. Several of these residues have been identified as being located at the subunit interface, intra-domain interface and the N-terminus of helix 6 (Dragani et al., 1997; Luo et al., 2002; Xiao et al., 1999). In alpha class GST the interaction of Arg69 and Gln100 with the active site residue Arg15 appeared to control signaling across the subunits. A mutation of Arg69 to Ala resulted in a disruption of the signaling. Intra-subunit interactions have also been shown to be important in rGSTM1-1 where Arg77 in helix 3 forms inter-domain hydrogen bonds with Asp97 and Glu100 in helix 4 and with Tyr154 in helix 6, and thereby plays an important role in stabilizing the monomer (Luo et al., 2002). Recent work on an insect delta class GST (AdGSTD3–3) proposed that Asp150, located in the loop before helix 6, may contribute to the catalytic efficiency of the enzyme through an intra-subunit interaction with several residues in the interior of the protein that affects the active site (Wongtrakul et al., 2003b). Asp150 forms an ionic interaction with His144 (another residue in the loop between helix 5 and helix 6). As a result, the interaction appeared to stabilize the loop of residues 142–155 between helix 5 and 6. In addition, two conserved hydrophobic residues within the loop, Val147 and Ala148, also have van der Waal contact with neighboring residues in the hydrophobic core that support Arg96 in helix 4. Therefore, the movement of Arg96 residue may then influence Arg66 in the active site. The hypothesized residues positions and interactions are based upon observations of the available crystal structure for this protein (Protein Data Bank accession number 1JLV; (Oakley et al., 2001). To test this hypothesis, the roles of the three residues in the proposed pathway, His144, Val147 and Arg96, were studied further by means of site-directed mutagenesis. Two mutants, Asp150Ser and Asp150Tyr, demonstrated maximum changes in catalytic efficiency and the least stability (Wongtrakul et al., 2003b). Molecular dynamics simulations also were performed to characterize interactions in this region. Previously we have reported this delta class (insect class 1) GST enzyme as adGST 1–3, which had been named according to the insect GST nomenclature in use. However, to be in alignment with a proposed universal GST nomenclature we have renamed the enzyme AdGSTD3–3 (Chelvanayagam et al., 2001). Where the 'D' refers to the GST delta class and the subunit number remains the same since the subunits were enumerated as they were initially discovered. The double number, GSTD3–3 for example, signifies the enzyme is a homodimer.

2. Materials and methods

2.1. Site-directed mutagenesis

The plasmid pET3a containing AdGSTD3–3 coding sequence has previously been constructed (Jirajaroenrat et al., 2001). The construct was used as a DNA template in a PCR reaction according to Quick Change™ site-directed mutagenesis described by Stratagene. The following oligonucleotides R96A-f: 5′ CAGAAGCGCG-CCG TC**GTTAAC**CAG**GCG**CTGTACTCGACATG 3′, H144A-f: 5′ CTGAACACCTTCCTGGACGGG**GC-CAAGTACGTGG**CG 3′, V147A-f: 5′ CTGGACGGG-CACAAGTAC**GCTGCAG**GCGACAGTCTGACG 3′ V147L-f: 5′ CTGGACGGGCACAAGTA**CTTAG**CG-GGCACAGTCTGACG 3′ were used as mutagenic primers for the mutants along the proposed pathway. The changed nucleotide residues are shown in bold type and the additional recognition sites for restriction endonucleases are underlined. The recombinant plasmids were randomly screened by restriction analysis then the nucleotide sequences of the plasmids carrying the mutations were verified by full-length sequencing in both directions using a Bigdye™ terminator cycle sequencing kit (Perkin Elmer).

2.2. Protein expression and purification

The protein expression and purification were carried out as previously described (Wongsantichon et al., 2003). After affinity purification the wild type and mutant enzymes were homogeneous as judged by SDS–PAGE. The protein concentration was determined by the method of Bradford using bovine serum albumin as the standard protein (Bradford, 1976).

2.3. Kinetic studies

The GST activity assays were performed as previously described (Prapanthadara et al., 1996). Thermal stability was measured as a function of time. All the wild type and mutant enzymes were incubated (0.1 mg/ml in 0.1 M potassium phosphate pH 6.5 containing 5 mM DTT and 1 mM EDTA) at 45 °C and aliquots were assayed for activity in the standard 1-chloro-2, 4-dinitrobenzene (CDNB) assay at different time-points.

2.4. Molecular dynamics simulation

Several one-nanosecond molecular dynamics trajectories of AdGSTD3–3 in complex with GSH were

generated. Gromac 3.0 (http://www.gromacs.org) with Gromacs force fields was used throughout the study. Initial coordinates of AdGSTD3–3 at 1.75 Å resolution (Protein Data Bank accession number 1 JLV) were from the X-ray crystal structure of the complex with GSH (Oakley et al., 2001). Residue Asp 150 was replaced with serine and tyrosine residues using Deepview Swiss-PdbViewer software (http://www.expasy.org/spdbv/). The file was then converted into (.GRO) format. The protein was immersed in a cubic box full of water molecules. Na^+ ions sufficient to neutralize the systems were added by replacing some of the water molecules to minimize the protein–ion electrostatic interaction. A temperature of 300 K was used for the minimization and molecular dynamics simulation. Molecular dynamics simulation was performed in an isobaric (NPT) ensemble. First a steepest descent energy minimization was performed without restraints to eliminate initial contacts of the protein atoms. Then a molecular dynamics simulation was performed with positional restraint on the protein atoms to let water and ions move freely in the system. Finally, an unrestrained molecular dynamics simulation was performed for 1 ns. The crystal structure and simulated structures were visualized either by DS ViewerPro 5.0 (Accelrys Inc) or Deepview Swiss-PdbViewer v3.5b4.

3. Results

The residues involved in the intra-subunit interaction characterized in this study are shown in Fig. 1. All the recombinant protein variants of the studied region were successfully expressed in *Escherichia.coli* and purified. Table 1 summarizes the kinetic constants for GSH-CDNB conjugation. Disruption of the ionic interaction by the substitution of His144 with Ala resulted in a 15% increase of k_{cat}, similar to the replacement of Asp150 with Ser, Tyr and Ala which ranged from 10% to 25% increase compared to the wild type. In addition, the K_m^{GSH} of His144Ala was approximately 1.3-fold larger than that of the wild type. It also possessed a similar K_m^{GSH} value compared to Asp150Ala mutant. In contrast, the His144 mutation scarcely affects the K_m^{CDNB} ,whereas all the Asp150 mutations significantly decreased the values. The Val147Ala mutant displayed a 1.5-fold decrease in catalytic efficiency with CDNB when compared with the wild type. An even greater effect with both GSH and CDNB was seen with Val147Leu. The replacement of Arg96 to Ala greatly affects the catalytic properties of AdGSTD3–3. For example, the k_{cat}, K_m^{GSH} and K_m^{CDNB} are 1.8-, 9.5- and 2.9-fold more than that of the wild type, respectively. In addition, the k_{cat}/K_m toward both GSH and CDNB substrates is 5.1-and 1.5-fold less than that of the wild type.

The specific activities of wild type AdGSTD3–3 and the variant enzymes were determined with five alternative substrates; 1-chloro-2, 4-dinitrobenzene, 1,2-dichloro-4-nitrobenzene (DCNB), 4-nitrobenzyl chloride, 4-nitrophenethyl bromide and ethacrynic acid. The substrates chosen have been reported to be preferred by different GST classes: CDNB—general substrate; DCNB—mu class; 4-nitrobenzyl chloride—rat theta

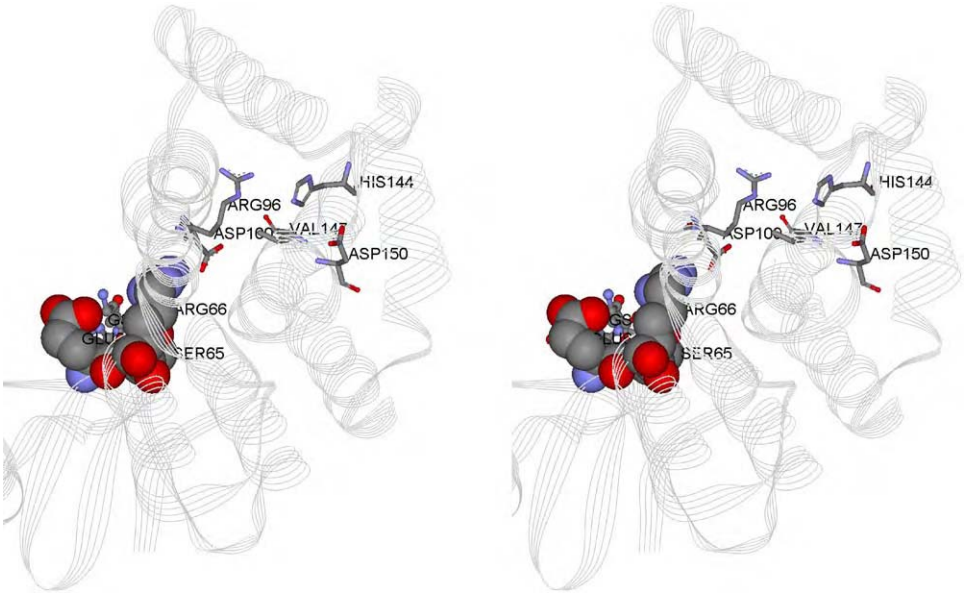

Fig. 1. Stereo view of the residues that are involved in a putative intra-subunit interaction in AdGSTD3–3. The figure shows a ribbon structure of one subunit of AdGSTD3–3 with several residues, His144, Asp150, Val147, Arg96 and Asp100 that appear to impact structurally upon Arg66. The active site residues, Glu64, Ser65 and Arg66 are shown in CPK. The substrate GSH, is shown in ball and stick form.

Table 1
Kinetic constants for the enzymes with residue changes along the proposed pathway of interaction

Enzymes	V_{max}	k_{cat}	GSH		CDNB	
			K_m	k_{cat}/K_m	K_m	k_{cat}/K_m
AdGSTD3-3[a]	63.6±6.2	25.2	0.29±0.03	86.9	0.13±0.01	194
Asp150Ser[a]	70.2±1.0	27.8	0.17±0.02	160	0.07±0.01	391
Asp150Tyr[a]	74.2±6.8	29.5	0.21±0.02	141	0.09±0.01	327
Asp150Ala[a]	80.2±7.0	31.7	0.33±0.02	96.7	0.08±0.02	382
His144Ala	73.7±3.3	29.1	0.37±0.06	79.5	0.14±0.01	205
Val147Ala	63.0±1.7	24.9	0.26±0.03	96.1	0.19±0.01	131
Val147Leu	54.4±1.2	21.6	0.34±0.04	63.6	0.20±0.04	105
Arg96Ala	118±7.0	46.8	2.75±0.12	17.0	0.38±0.06	125

Note: The units are: V_{max}: μmol/min/mg, K_m: mM, $k$cat: s^{-1}, k_{cat}/K_m: /mM/s. The data are mean±standard deviation from at least 3 independent experiments. The activity was measured in 0.1 M potassium phosphate, pH 6.5, 25–27 °C.
[a]From (Wongtrakul et al., 2003).

Table 2
Specific activity towards five different substrates for the enzymes with residue changes along the proposed pathway of interaction

Enzyme	CDNB (1 mM)	DCNB (1 mM)	4-nitrobenzyl chloride (0.1 mM)	4-nitrophenethyl bromide (0.1 mM)	Ethacrynic acid (0.2 mM)
AdGSTD3-3[a]	57.2±3.2	0.248±0.003	0.135±0.013	0.019±0.007	0.087±0.010
Asp150Ser[a]	64.7±5.5	0.249±0.005	0.142±0.009	0.070±0.008	0.126±0.016
Asp150Tyr[a]	63.9±3.7	0.289±0.003	0.173±0.020	0.067±0.013	0.100±0.016
Asp150Ala[a]	68.9±3.8	0.284±0.009	0.111±0.004	0.021±0.004	0.050±0.017
His144Ala	59.0±4.4	0.229±0.013	0.106±0.008	0.010±0.001	0.056±0.007
Val147Ala	68.8±2.0	0.243±0.005	0.135±0.018	0.018±0.004	0.101±0.014
Val147Leu	62.6±4.4	0.225±0.009	0.104±0.005	0.013±0.001	0.053±0.010
Arg96Ala	66.3±4.1	0.212±0.003	0.060±0.006	<0.005	0.045±0.006

The units are μmol/min/mg of protein. The data are mean±standard deviation from at least 3 independent experiments. The substrate concentration used were 1 mM CDNB, 1 mM DCNB (1,2-dichloro-4-nitrobenzene), 0.1 mM 4-nitrobenzyl chloride, 0.1 mM 4-nitrophenethyl bromide and 0.2 mM ethacrynic acid.
[a]From (Wongtrakul et al., 2003).

class; 4-nitrophenethyl bromide–human theta class and ethacrynic acid—pi class (Mannervik and Danielson, 1988; Hayes and Pulford, 1995). The results are compiled in Table 2. The single mutation that produced the most pronounced difference in specific activity is the Arg96Ala mutation, which decreased the specific activities for the substrates excluding CDNB. The Val147Ala mutation showed no changes in the specific activities for the same set of substrates. For His144Ala and Val147-Leu, both mutations displayed small decreases in activities for the substrates. All the mutations showed little effect on the activity with the CDNB substrate.

An inhibition study of CDNB activity was performed using different compounds such as the hydrophobic substrates, pyrethroid insecticides and a GSH analog (Table 3). The residues studied showed only small effects for these compounds on the inhibition of CDNB activity. A result of interest was Arg96Ala which was still inhibited by 4-nitrophenethyl bromide although it no longer possessed any detectable activity for this as a substrate. It was observed that His144Ala, Val147Ala and Val147Leu mutants had a shorter half-life at 45 °C of approximately 50% compared to the wild type enzyme (Fig. 2). Therefore, both residues 144 and 147 significantly affect the packing of the hydrophobic core in domain 2. Surprisingly, the Arg96Ala was more stable with a half-life of approximately 187 min. Clearly the residue is involved in structural maintenance.

The models of Asp150 mutants from our previous results demonstrated conformational changes in domain 2 as shown by changes in several parameters such as helical dihedral angles and residue movement (Wongtrakul et al., 2003b). Therefore, molecular dynamics simulations of Asp150Ser and Asp150Tyr were performed to obtain a clearer understanding of the changes in the catalytic efficiency and the stability of the enzyme. The AdGSTD3-3 at position 150 was changed to Ser and Tyr residues. After the energy minimization and positional restraint, the system was simulated for 1000 ps. The fluctuation of the system was also monitored using the AdGSTD3–3 structure. The four control values were obtained by using the coordinates of AdGSTD3–3 after a 1000 ps MD simulation as starting coordinates, then performing four separate simulations

Table 3
Inhibition of CDNB activity of the enzymes with residue changes along the proposed pathway of interaction

Percent inhibition								
Enzyme	4-NBC 1 mM	CuOOH 2.5 mM	DCNB 1 mM	4-NPB 0.1 mM	Deltamethrin 0.01 mM	Permethrin 0.01 mM	EA 0.001 mM	S-hexyl 0.01 mM
Wild type	50.6±2.9	43.3±3.6	53.3±5.8	40.1±7.4	65.4±7.1	51.1±7.4	35.3±4.3	21.7±6.8
His144Ala	43.9±5.1	27.0±5.7	40.4±1.8	23.6±5.8	44.2±8.8	38.8±8.0	32.7±5.1	23.0±3.8
Val147Ala	40.8±7.5	50.6±2.0	42.4±4.2	19.5±7.3	59.5±2.5	53.1±7.0	27.8±2.6	10.8±4.4
Val147Leu	47.9±3.0	41.5±2.6	54.3±6.3	31.4±5.8	66.1±3.6	49.0±2.3	23.0±2.8	24.2±6.4
Arg96Ala	30.8±8.0	48.1±5.0	35.9±4.2	27.3±4.1	88.6±3.4	65.5±8.6	29.1±8.1	14.7±1.4

The data are mean±standard deviation for at least 3 independent experiments. Inhibition assays were performed using standard GST assay in the presence of 4-NBC, 4-nitrobenzyl chloride; CuOOH, cumene hydroperoxide; DCNB, 1,2-dichloro-4-nitrobenzene; 4-NPB, 4-nitrophenethyl bromide; deltamethrin, permethrin; EA, ethacrynic acid and S-hexyl glutathione.

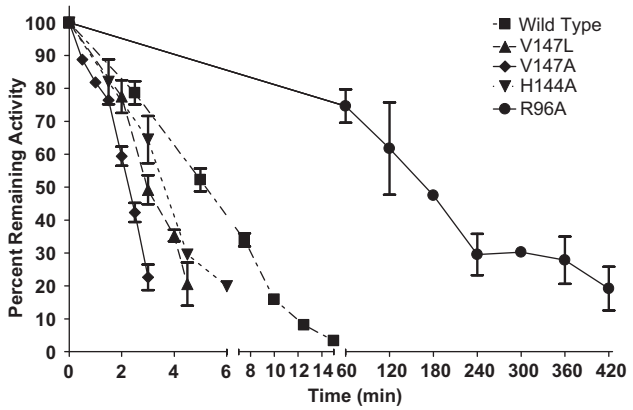

Fig. 2. Half-life time course at 45° for the enzymes with residue changes along the proposed pathway of interaction. Data plotted are means±standard deviations for three independent experiments.

for 200 ps with four different random seed numbers. Then the four sets of values were averaged and shown in Table 4.

The root mean square deviation (RMSD) indicates the difference between the protein structures obtained from the simulation and the original crystal structure. The RMSD were calculated from the alpha carbons of each GST peptide backbone. All of the simulations of wild type, Asp150Ser and Asp150Tyr reached a structural equilibrium after approximately 500 ps. All the simulations are characterized by a small deviation from the crystal structure, with an RMSD value of 0.8–1.6 Å over the time 500–1000 ps (Table 4). The radius of gyration which reflects the evolution of the overall shape of the protein was analyzed. For each of the simulations, the protein reached a structural equilibrium at similar values of the radius of gyration, very close to the value for the native state (approximately 20 Å). The total potential, electrostatic and van der Waals energies of wild type, Asp150Ser and Asp150Tyr showed similar fluctuations compared to the four controls. It was found that helix 2 and several loops that link GST helices showed a high mobility. This result was observed with a study in pi class where helix 2 was found to undergo extensive movement (Stella et al., 1999). Center of gravity analysis of our simulations shows changes in the structures do occur. This parameter measures the movement of the center of mass of the dimeric GST. It was found that the locations of Asp150 residue relative to the center of gravity in wild type and Asp150Tyr are similar at 0 and 1000 ps time points. Interestingly, Asp150Ser demonstrated different coordinates suggesting that it had different conformations at 0 and 1000 ps. The structural coordinates of the time point that showed maximum changes in center of gravity of Asp150Ser was generated and superimposed with the structure of the wild type at 1000 ps. It was found that the alpha carbon backbone of Asp150, Val147 and Val148 were shifted approximately 3 and 1.5 Å, respectively. In addition, the loop before helix 6 also faces the opposite direction compared to the wild type (Fig. 3). In the wild type protein, interaction between His144 and Asp150 appeared to be preserved in the MD simulation and even strengthened with an increased dipole–dipole interaction from His144 to the Asp150 backbone carbonyl oxygen (Fig. 3). In the mutant proteins the possible hydrogen bond formation from His144 to the O atom of the hydroxyl group of serine or tyrosine was not observed possibly due to packing rearrangements. In the simulation the distance was sometimes up to 7.28 Å from the His 144 to OH of Serine (Asp150Ser mutant) or 6.98 Å from the His 144 to OH of Tyr (Asp150Tyr mutant). Therefore, the results from the simulations support the proposed pathway.

4. Discussion

Characterization of Asp150 mutant enzymes from our previous work demonstrated that the mutation appeared to affect a sensitive region of the tertiary

Table 4
Analysis of the 1000 ps molecular dynamics simulations of the AdGSTD3-3 Asp-150 mutants

Parameters	Control	AdGSTD3-3	Asp150Ser	Asp150Tyr
Total energy	(−715306)–(−711620)	(−716836)–(−713671)	(−715379)–(−712271)	(−715602)–(−712129)
RMSD	0.827–1.309	1.092–1.586	1.003–1.496	0.917–1.307
Radius of gyration	20.179–20.5707	20.1483–20.5125	19.9965–20.33	20.0664–20.3439
Electrostatic energy	(−290.895)–(−55.26)	(−297.438)–(−97.6813)	(−186.964)–(−59.5189)	(−193.972)–(−53.3244)
Van der Waals energy	(−144.053)–(−54.368)	(−138.135)–(−50.1937)	(−136.97)–(−58.1716)	(−168.352)–(−86.9131)
Center of gravity (Cg)		(*X*, *Y*, *Z*)	(*X*, *Y*, *Z*)	(*X*, *Y*, *Z*)
Position changes of residue 150 relative to the Cg at 0 and 1000 ps		0 ps: 7.200, −10.890, 19.854 1000 ps: −0.0357, −14.348, 17.156	0 ps: −6.294, −11.370, 17.850 1000 ps: 1.258, −6.041, 21.229	0 ps: −5.389, −11.006, 19.102 1000 ps: −5.235, −12.744, 17.765
Maximum changes in Cg compared with the wild type			$X = 5.8$ Å ($T = 673$ ps) $Y = 9.6$ Å ($T = 940$ ps) $Z = 6.1$ Å ($T = 937$ ps)	$X = 7.6$ Å ($T = 855$ ps) $Y = 3.6$ Å ($T = 781$ ps) $Z = 4.6$ Å ($T = 972$ ps)

The units are: total energy: kJ/mol, RMSD: Å, radius of gyration: Å, electrostatic energy and Van der Waals energy: kJ/mol.

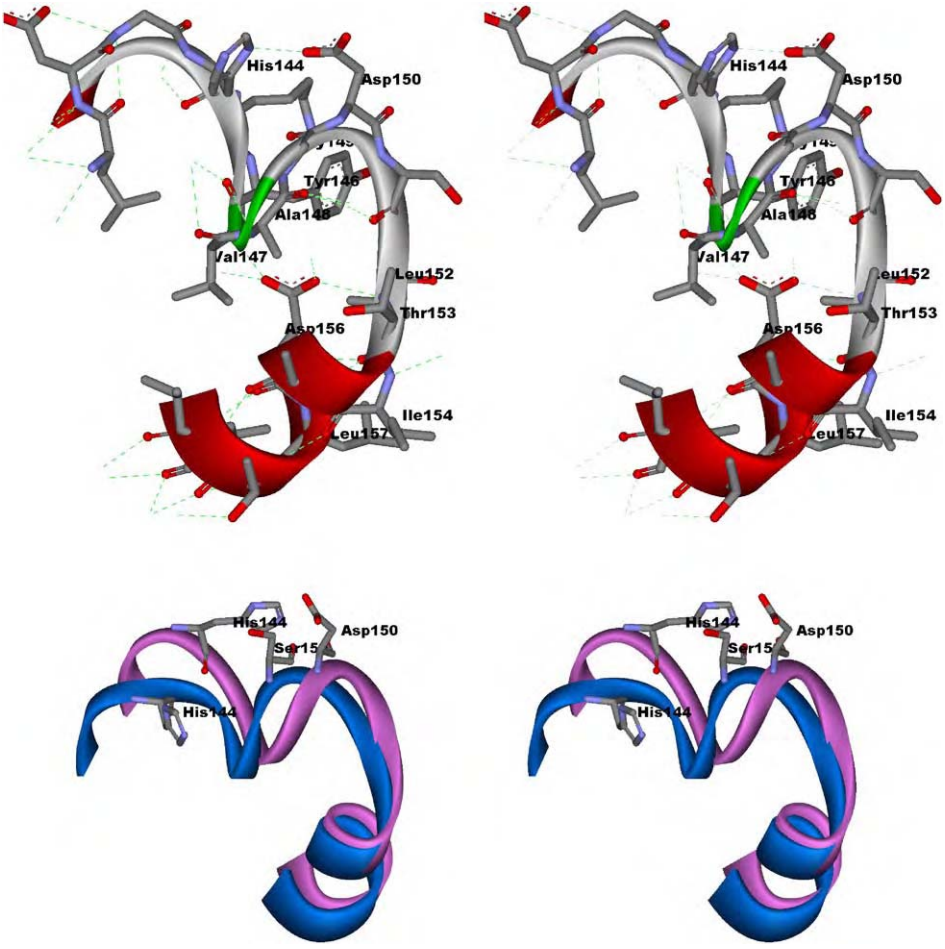

Fig. 3. Stereo view of the interhelical loop region in AdGSTD3–3. The top panel shows the N-capping box and hydrophobic staple motifs in AdGSTD3–3. H-bonds are shown as green dashed lines. The bottom panel shows the superimposition between Asp150Ser (blue) and wild type AdGSTD3–3 (purple) using the time point that showed maximum changes in the center of gravity compared with the wild type at 1000 ps.

structure resulting in changes in substrate specificity and stability (Wongtrakul et al., 2003b). In addition differing conformational changes were observed from Asp150 static models, e.g. dihedral angles of the helices, residue movements, etc. It was proposed that the mutation would affect neighboring residues that support two

important structural motifs, the N-capping box and the hydrophobic staple motif located in the loop before helix 6. Both motifs play a major role in the folding and stability of GSTs (Stenberg et al., 2000; Dragani et al., 1997; Cocco et al., 2001; Aceto et al., 1997). Therefore, the neighboring residue position Val147 was further studied after changing it to Ala and Leu. It was found that the mutations do affect the stability and catalytic activity of AdGSTD3–3 which support the hypothesis. Several studies have demonstrated that a mutation of a residue near an N-capping box decreases the stability of the GST. In GSTP1-1, Gly146 (Gly149 equivalent residue in AdGSTD3–3) which is a conserved residue found in all GSTs was shown to support the stability and refolding. This residue is located in a bend of the long loop before helix 6 with no specific contact with other parts of the molecule but only with neighboring residues that support the N-capping box motif. The mutation of Gly146 to Val lead to a substantial change of the backbone conformation (Kong et al., 2003). In addition, a Phe151Leu study in pi class also demonstrated a shorter half-life at 50 °C (Lin et al., 2003). Phe151 (Ile154 equivalent residue in AdGSTD3–3) is located at the N-terminus of helix 6. An analysis of tertiary structure suggested that the mutation produced a cavity in the core and destabilized the structure. Therefore, our study provides additional evidence of other neighboring residues that affect the N-capping box motif which leads to activity and stability changes in the enzyme.

In addition, two pathways were proposed, an intra- and an inter-subunit route of Asp150 residue interaction to the active site (Wongtrakul et al., 2003b).This study mainly focused on the intra-subunit interaction. Mutations of positions His144Ala, Val147Ala and Val147Leu between Asp150 and the catalytic residues in the active site were generated. The variant proteins all had shorter half-lives compared to the wild type enzyme of approximately 50%. The ionic interaction between Asp150 and His144 is required for the packing of the hydrophobic core in domain 2. Disruption of this ionic interaction formed by both residues made the loop before helix 6 more flexible. The residues on the loop would therefore pack in the hydrophobic core with greater movement compared to the wild type thereby giving the His144Ala protein a shorter half-life at 45 °C. Residue 147 is positioned in the hydrophobic core of domain 2 and contributes to packing so that the Val147Leu showed a slight variation in structure demonstrating a change in the stability and substrate activity when compared to the wild type. In addition, a decrease in core residue volume with Ala substitution also lead to losses in hydrophobic stabilization and favorable van der Waals interactions that occur as a result of the tighter packing in the core. Val147Ala possessed a shorter half-life compared to Val147Leu suggesting that the reduction of the size and hydrophobicity of the interior side-chain resulted in creating internal cavities thereby reducing the stability of the enzyme. Val147 and Ala148 appear to be conserved hydrophobic residues found in delta class GSTs e.g. Ala148 in *L. cuprina* and Ala148, Ala149 in *D. melanogaster*. Both residues are also conserved across AdGST isoenzymes, Ala147 and Ala148 in AdGSTD1-1, Val151 and Ala152 in AdGSTD2-2, Val155 and Ala156 in AdGSTD4-4. Val147 is equivalent to Ile144 and Leu148 in pi and alpha class, respectively. This residue was reported to have an important role in the stability of the final structure of the protein (Cocco et al., 2001; Dragani et al., 1997). In AdGSTD3–3, the amide NH of Val147 directly formed a hydrogen bond with Asp156 which is the N-capping box residue. This interaction is specific and required for stabilization of the long loop preceding helix 6 which is strictly conserved in GST classes (Aceto et al., 1997).

For the Arg96Ala enzyme, the mutation dramatically increased the stability of the enzyme to 187 min. The effect may be due to residue interactions at the subunit interface. However, the crystal structure of AdGSTD3–3 shows the main chain of Arg96 interacts with residues near the active site in its own subunit to support the active site structure. The amino side chain of Arg96 is in close contact, 3.6 Å, with the aromatic ring of Phe140 in helix 5, in a cation-π interaction (Fig. 4). The planar guanidinium of Arg is in a parallel or stacked geometry with the face of the aromatic ring. In addition, strengthening this geometry the Arg side chain NE atom hydrogen bonds to the carbonyl of Val147 which thus yields an energetically favorable configuration (Ma and Dougherty, 1997). The Arg96 also interacts with several other residues one of which, Asp100, is in the active site (Fig. 4). These interactions with Arg96 would restrict movement of the residues in this region and as the data demonstrates, when Arg96 is changed, yield different obtainable conformations that impact on stability and enzyme properties.

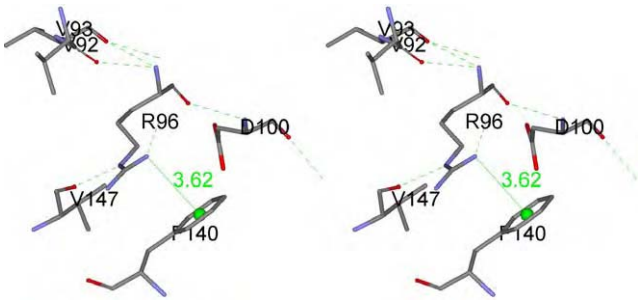

Fig. 4. Stereo view of residues interacting with Arg96. The dotted lines represent hydrogen bonds. The planar guanidinium of Arg96 is shown stacked with the face of the aromatic ring of Phe140. The sphere is the centroid of the benzene ring of Phe140 with the distance to the NH1 atom of Arg96 shown.

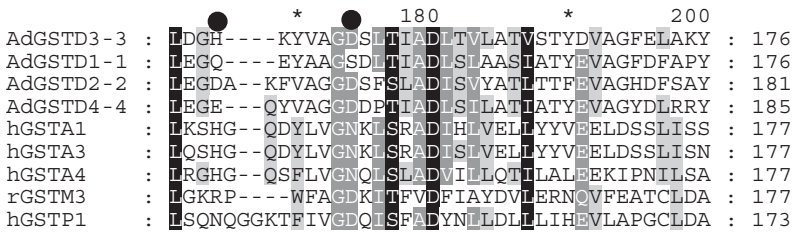

Fig. 5. Alignment of topologically equivalent amino acid residues of GSTs from different classes. Residue numbering for each sequence is shown at the right. Black, dark gray and light gray shadings represent 100%, 80% and 60% sequence similarity respectively. The sequences have the following Genbank accession numbers. AdGSTD3–3 (AAG38505.1), AdGSTD1-1 (AF273041_1), AdGSTD2-2 (AAG38504.1), AdGSTD4-4 (AAG38506.1), hGSTA1 (P08263), hGSTA3 (Q16772), hGSTA4 (AAD27704), rGSTM3 (P08009), hGSTP1 (P09211). His 144 and Asp 150 residues of AdGSTD3–3 are marked as black dots.

Based on the results from molecular dynamics simulations, the location of Asp150 relative to the center of gravity was changed during the simulation. The loop before helix 6 also faced a different direction compared to the wild type structure. In addition, Val147 and Ala148 had a slight movement in the alpha carbon backbone. The results from the simulations therefore support the static models (Wongtrakul et al., 2003a) by demonstrating a different conformation at the same position which is in the domain 2 region located adjacent to both the N-capping box and hydrophobic staple motifs.

An alignment of the topologically equivalent region of several classes of GSTs shows that both His144 and Asp150 are not widely conserved (Fig. 5). However, examination of the crystal structures for these proteins at the equivalent positions in the tertiary structure show there are residues present that form hydrogen bonds across the random coil loop to stabilize it. For example, in the delta GST AdGSTD4-4 (formerly AdGST1-4) Glu152 hydrogen bonds to the backbone nitrogen of Gly158, whereas in human pi GST the Asn136 side chain hydrogen bonds to the carbonyl backbone oxygen of both Phe142 and Gly145. In human alpha GST1-1 multiple hydrogen bonds form across the equivalent loop region from His143 to the carbonyl oxygen of Tyr147, the backbone nitrogen of Asp146 to the oxygen of the side chain of Asn151 and the side chain oxygen OD1 of Asp157 to the backbone nitrogen of Leu148. Therefore, although the residues in the region vary, this preserved functional stabilization of the random coil loop suggests relatively important structural contributions from the loop need to be maintained.

In the present study, the effects of residue interaction can be detected at every mutation in the proposed pathway as assessed by changes in kinetic properties and the stability. Mutations of both Asp150 and His144 impacted upon enzymatic properties. Differences in kinetic parameters were also detected when Val147 was mutated to Ala and Leu. The effect was greater when Arg96 was replaced with Ala. The mutant showed marked differences in every kinetic parameter. Therefore, the pathway of residue interaction in AdGSTD3–3 is likely to occur by Asp150 influencing specificity and catalysis through affects on the active site Arg66 from Arg96 with contributions from His144 and Val147.

In summary, the results described here show that the ionic interaction between Asp150 and His144 impacts on catalysis of AdGSTD3–3 via intra-subunit interactions of multiple residues. In addition, a change of Asp150 and the alterations in volume of the hydrophobic core may bring about secondary effects altering the stability of the enzyme by influencing the N-capping box region. These findings indicate the significance of the roles played by residue interactions which can cause conformational changes and thereby influence the catalytic activity and stability of an enzyme.

Acknowledgements

This work was supported by the Thailand Research Fund (TRF) to J.W.

References

Aceto, A., Dragani, B., Melino, S., Allocati, N., Masulli, M., Di Ilio, C., Petruzzelli, R., 1997. Identification of an N-capping box that affects the α6-helix propensity in glutathione S-transferase superfamily proteins: a role for an invariant aspartic residue. Biochem. J. 322, 229–234.

Adler, V., Yin, Z., Fuchs, S.Y., Benezra, M., Rosario, L., Tew, K.D., Pincus, M.R., Sardana, M., Henderson, C.J., Wolf, C.R., Davis, R.J., Ronai, Z., 1999. Regulation of JNK signaling by GSTp. EMBO J 18, 1321–1334.

Armstrong, R.N., 1997. Structure, catalytic mechanism, and evolution of the glutathione transferases. Chem. Res. Toxicol. 10, 2–18.

Booth, J., Boyland, E., Sims, P., 1961. An enzyme from rat liver catalysing conjugations with glutathione. Biochem. J. 79, 516–524.

Bradford, M.M., 1976. A rapid and sensitive method for the quantitation of microgram quantities of protein utilizing the principle of proteindye binding. Anal. Biochem. 72, 248–254.

Chelvanayagam, G., Parker, M.W., Board, P.G., 2001. Fly fishing for GSTs: a unified nomenclature for mammalian and insect glutathione transferases. Chem. Biol. Interact. 133, 256–260.

Cho, S.-G., Lee, Y.H., Park, H.-S., Ryoo, K., Kang, K.W., Park, J., Eom, S.-J., Kim, M.J., Chang, T.-S., Choi, S.-Y., Shim, J., Kim,

Y., Dong, M.-S., Lee, M.-J., Kim, S.G., Ichijo, H., Choi, E.-J., 2001. Glutathione S-transferase Mu modulates the stress-activated signals by suppressing apoptosis signal-regulating kinase 1. J. Biol. Chem. 276, 12749–12755.

Cocco, R., Stenberg, G., Dragani, B., Principe, D.R., Paludi, D., Mannervik, B., Aceto, A., 2001. The folding and stability of human alpha class glutathione transferase A1-1 depend on distinct roles of a conserved N-capping box and hydrophobic staple motif. J. Biol. Chem. 276, 32177–32183.

Dragani, B., Stenberg, G., Melino, S., Petruzzelli, R., Mannervik, B., Aceto, A., 1997. The conserved N-capping box in the hydrophobic core of glutathione S-transferase P1–1 is essential for refolding. Identification of a buried and conserved hydrogen bond important for protein stability. J. Biol. Chem. 272, 25518–25523.

Dulhunty, A., Gage, P., Curtis, S., Chelvanayagam, G., Board, P., 2001. The glutathione transferase structural family includes a nuclear chloride channel and a ryanodine receptor calcium release channel modulator. J. Biol. Chem. 276, 3319–3323.

Hayes, J.D., Pulford, D.J., 1995. The glutathione S-transferase supergene family: regulation of GST and the contribution of the isoenzymes to cancer chemoprotection and drug resistance. CRC Crit. Rev. Biochem. Molec. Biol. 30, 445–600.

Jirajaroenrat, K., Pongjaroenkit, S., Krittanai, C., Prapanthadara, L., Ketterman, A.J., 2001. Heterologous expression and characterization of alternatively spliced glutathione S-transferases from a single *Anopheles* gene. Insect Biochem. Molec. Biol. 31, 867–875.

Kong, G.K.W., Polekhina, G., McKinstry, W.J., Parker, M.W., Dragani, B., Aceto, A., Paludi, D., Principe, D.R., Mannervik, B., Stenberg, G., 2003. Contribution of glycine 146 to a conserved folding module affecting stability and refolding of human glutathione transferase P1-1. J. Biol. Chem. 278, 1291–1302.

Lin, H.J., Johansson, A.-S., Stenberg, G., Materi, A.M., Park, J.M., Dai, A., Zhou, H., Gim, J.S.Y., Kau, I.H., Hardy, S.I., Parker, M.W., Mannervik, B., 2003. Naturally occurring Phe151Leu substitution near a conserved folding module lowers stability of glutathione transferase P1–1. Biochim. Biophys. Acta 1649, 16–23.

Lo Bello, M., Nuccetelli, M., Caccuri, A.M., Stella, L., Parker, M.W., Rossjohn, J., McKinstry, W.J., Mozzi, A.F., Federici, G., Polizio, F., Pedersen, J.Z., Ricci, G., 2001. Human glutathione transferase P1-1 and nitric oxide carriers: a new role for an old enzyme. J. Biol. Chem. 276, 42138–42145.

Luo, J.-K., Hornby, J.A.T., Wallace, L.A., Chen, J., Armstrong, R.N., Dirr, H.W., 2002. Impact of domain interchange on conformational stability and equilibrium folding of chimeric class μ glutathione transferases. Protein Sci. 11, 2208–2217.

Lyon, R.P., Atkins, W.M., 2002. Kinetic characterization of native and cysteine 112-modified glutathione S-transferase A1-1: reassessment of nonsubstrate ligand binding. Biochemistry 41, 10920–10927.

Ma, J.C., Dougherty, D.A., 1997. The cation-p interaction. Chem. Rev. 97, 1303–1324.

Mannervik, B., Danielson, U.H., 1988. Glutathione transferases—structure and catalytic activity. CRC Crit. Rev. Biochem. 23, 283–337.

Oakley, A.J., Harnnoi, T., Udomsinprasert, R., Jirajaroenrat, K., Ketterman, A.J., Wilce, M.C.J., 2001. The crystal structures of glutathione S-transferases isozymes 1–3 and 1–4 from *Anopheles dirus* species B. Protein Sci. 10, 2176–2185.

Prapanthadara, L., Koottathep, S., Promtet, N., Hemingway, J., Ketterman, A.J., 1996. Purification and characterization of a major glutathione S-transferase from the mosquito *Anopheles dirus* (species B). Insect Biochem. Molec. Biol. 26, 277–285.

Sawicki, R., Singh, S.P., Mondal, A.K., Beneš, H., Zimniak, P., 2003. Cloning, expression and biochemical characterization of one epsilon-class (GST-3) and ten delta-class (GST-1) glutathione S-transferases from *Drosophila melanogaster*, and identification of additional nine members of the epsilon class. Biochem. J. 370, 661–669.

Sayed, Y., Wallace, L.A., Dirr, H.W., 2000. The hydrophobic lock-and-key intersubunit motif of glutathione transferase A1-1: implications for catalysis, ligandin function and stability. FEBS Lett. 465, 169–172.

Sheehan, D., Meade, G., Foley, V.M., Dowd, C.A., 2001. Structure, function and evolution of glutathione transferases: implications for classification of non-mammalian members of an ancient enzyme superfamily. Biochem. J. 360, 1–16.

Stella, L., Nicotra, M., Ricci, G., Rosato, N., Di Iorio, E.E., 1999. Molecular dynamics simulations of human glutathione transferase P1-1: analysis of the induced-fit mechanism by GSH binding. Proteins 37, 1–9.

Stenberg, G., Dragani, B., Cocco, R., Mannervik, B., Aceto, A., 2000. A conserved "hydrophobic staple motif" plays a crucial role in the refolding of human glutathione transferase P1-1. J. Biol. Chem. 275, 10421–10428.

Wang, T., Arifoglu, P., Ronai, Z., Tew, K.D., 2001. Glutathione *S*-transferase P1-1 (GSTP1-1) inhibits c-Jun N-terminal kinase (JNK1) signaling through interaction with the C terminus. J. Biol. Chem. 276, 20999–21003.

Wongsantichon, J., Harnnoi, T., Ketterman, A.J., 2003. A sensitive core region in the structure of glutathione S-transferases. Biochem. J. 373, 759–765.

Wongtrakul, J., Sramala, I., Ketterman, A., 2003a. A non-active site residue, cysteine 69, of glutathione S-transferase adGSTD3–3 has a role in stability and catalytic function. Protein Peptide Lett. 10, 375–385.

Wongtrakul, J., Udomsinprasert, R., Ketterman, A., 2003b. Non-active site residues Cys69 and Asp150 affected the enzymatic 53 properties of glutathione *S*-transferase AdGSTD3–3. Insect Biochem. Molec. Biol. 33, 979.

Xiao, B., Singh, S.P., Nanduri, B., Awasthi, Y.C., Zimniak, P., Ji, X., 1999. Crystal structure of a murine glutathione S-transferase in complex with a glutathione conjugate of 4-hydroxynon-2-enal in one subunit and glutathione in the other: evidence of signaling across the dimer interface. Biochemistry 38, 11887–11894.

Reprint 14

Available online at www.sciencedirect.com

SCIENCE DIRECT®

Biochimica et Biophysica Acta 1697 (2004) 89–101

BIOCHIMICA ET BIOPHYSICA ACTA

BBA

www.bba-direct.com

Review

Targeting the JNK MAPK cascade for inhibition: basic science and therapeutic potential

Marie A. Bogoyevitch[a,b,*], Ingrid Boehm[a], Aaron Oakley[c], Albert J. Ketterman[d], Renae K. Barr[a]

[a] *Cell Signalling Laboratory, Biochemistry and Molecular Biology, School of Biomedical and Chemical Sciences, University of Western Australia, Crawley, WA 6009, Australia*

[b] *Western Australian Institute for Medical Research (WAIMR), Australia*

[c] *Crystallography Centre, University of Western Australia, Nedlands 6907, Perth, Australia*

[d] *Institute of Molecular Biology and Genetics, Mahidol University, Salaya Campus, Nakhon Pathom 73170, Thailand*

Received 29 September 2003; accepted 12 November 2003

Abstract

The c-Jun N-terminal protein kinases (JNKs) form one subfamily of the mitogen-activated protein kinase (MAPK) group of serine/threonine protein kinases. The JNKs were first identified by their activation in response to a variety of extracellular stresses and their ability to phosphorylate the N-terminal transactivation domain of the transcription factor c-Jun. One approach to study the function of the JNKs has included in vivo gene knockouts of each of the three JNK genes. Whilst loss of either JNK1 or JNK2 alone appears to have no serious consequences, their combined knockout is embryonic lethal. In contrast, the loss of JNK3 is not embryonic lethal, but rather protects the adult brain from glutamate-induced excitotoxicity. This latter example has generated considerable enthusiasm with JNK3, considered an appropriate target for the treatment of diseases in which neuronal death should be prevented (e.g. stroke, Alzheimer's and Parkinson's diseases). More recently, these gene knockout animals have been used to demonstrate that JNK could provide a suitable target for the protection against obesity and diabetes and that JNKs may act as tumour suppressors. Considerable effort is being directed to the development of chemical inhibitors of the activators of JNKs (e.g. CEP-1347, an inhibitor of the MLK family of JNK pathway activators) or of the JNKs themselves (e.g. SP600125, a direct inhibitor of JNK activity). These most commonly used inhibitors have demonstrated efficacy for use in vivo, with the successful intervention to decrease brain damage in animal models (CEP-1347) or to ameliorate some of the symptoms of arthritis in other animal models (SP600125). Alternative peptide-based inhibitors of JNKs are now also in development. The possible identification of allosteric modifiers rather than direct ATP competitors could lead to inhibitors of unprecedented specificity and efficacy.

Keywords: c-Jun N-terminal kinase; CEP-1347; SP600125; JNK-interacting protein; Peptide inhibitor; Cell-permeable peptide

1. Introduction

The c-Jun N-terminal protein kinases (JNKs) are a family of serine/threonine protein kinases of the mitogen-activated protein kinase (MAPK) group. More broadly, JNKs are members of the CMGC family of protein kinases of the recently described human kinome (see Ref. [1]). These protein kinases act within a multi-tiered protein kinase cascade as depicted in Fig. 1. The mammalian JNKs were first described biochemically following their activation in response to a variety of environmental stresses [2,3], thus they have been also called ''stress-activated protein kinases'' or SAPKs. However, it is now also recognised that the JNKs are activated following the exposure of a variety of cells to cytokines and growth factors (e.g. as

Abbreviations: CEP-1347, Cephalon Incorporated library compound number 1347; ERK, extracellular signal regulated kinase; IC_{50}, concentration of compound to achieve 50% inhibition; IB, islet brain protein; JIP, JNK-interacting protein; JNK, c-Jun N-terminal kinase; K_i, inhibitory constant; KIM, kinase interaction motif; JSAP, JNK/SAPK-associated protein; MAPK, mitogen-activated protein kinase; MEKK, MAP kinase kinase kinase; MKK, MAPK kinase; MLK, mixed lineage kinase; SAPK, stress-activated protein kinase; SP600125, Signal Pharmaceuticals library compound number 600125; TI-JIP, truncated inhibitory region of JIP

* Corresponding author. Cell Signalling Laboratory, Biochemistry and Molecular Biology (M310), School of Biomedical and Chemical Sciences, University of Western Australia, 35 Stirling Highway, Crawley, WA 6009, Australia. Tel.: +61-8-9380-1348; fax: +61-8-9380-1148.

E-mail address: marieb@cyllene.uwa.edu.au (M.A. Bogoyevitch).

1570-9639/$ - see front matter © 2003 Elsevier B.V. All rights reserved.
doi:10.1016/j.bbapap.2003.11.016

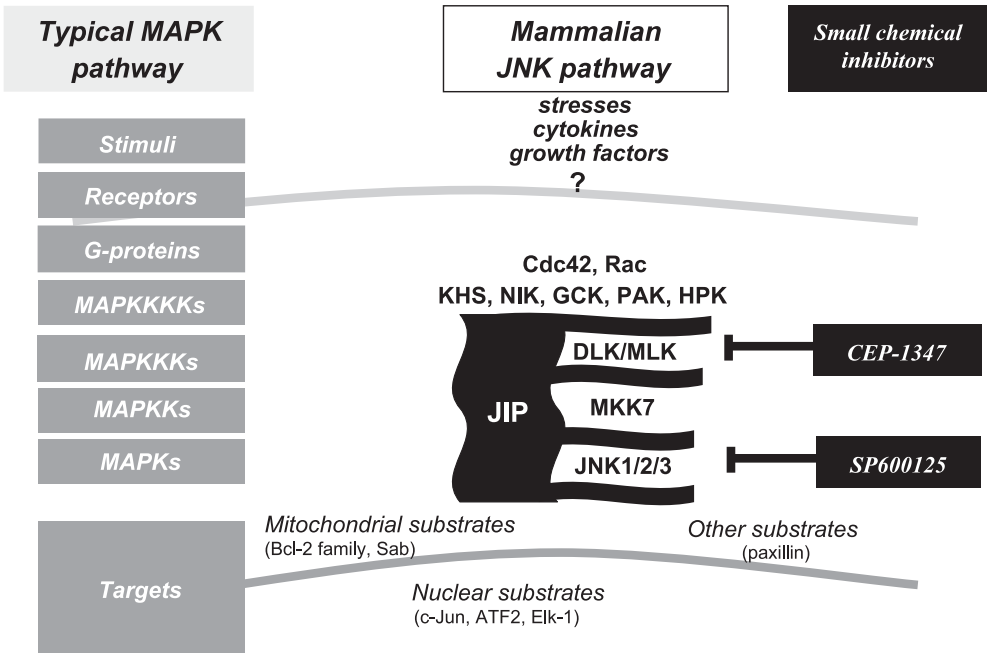

Fig. 1. Organisation of the JNK pathway. A typical MAPK pathway highlights the similarity in organisation shared by these pathways, where a stimulus interacts with its receptor and leads to the activation of small G proteins. The protein kinase cascade that is subsequently activated is composed of up to four tiers of kinases, culminating in activation of the specific MAPKs. In the specific example of the mammalian JNK pathway, diversity in signalling is seen with multiple different kinases at the various levels of the pathway. JNKs are in fact the products of three different genes, yielding the protein products JNK1, JNK2 and JNK3. These protein kinases phosphorylate a variety of target proteins including nuclear substrates, mitochondrial substrates, and substrates at other locations such as paxillin. Two small chemical inhibitors of this pathway have been recently described. Whilst CEP-1347 inhibits the MLK in the pathway, SP600125 directly inhibits JNK.

reviewed in Ref. [4]). In this way, JNKs can serve as critical mediators of a variety of extracellular stimuli.

As their name suggests, the JNKs have also been characterised by their ability to associate with and phosphorylate regulatory sites in the N-terminus of the transcription factor c-Jun [5]. However, ongoing studies indicate that JNKs can phosphorylate a variety of additional transcription factors (such as ATF-2, Elk-1, NFAT and p53) [6–9]. Furthermore, JNKs can play a wider intracellular role through their phosphorylation of non-nuclear proteins. For example, an important role for the JNKs has been suggested in the regulation of apoptosis. Here JNKs directly phosphorylate substrates localised to the mitochondria such as the Bim-related members of the Bcl2 family and lead to Bax-dependent apoptosis [10]. These examples serve to illustrate that signals from JNKs can diverge and regulate events in multiple intracellular compartments. This is shown schematically in Fig. 1.

In mammals, there are three JNK genes (*Jnk*1, *Jnk*2 and *Jnk*3), each on a different chromosome (in humans, 10q11.1–11.2, 5q35.3 and 4q21–q22.1, respectively) [1]. Each mammalian JNK gene can be subjected to alternative splicing, such that the three genes are predicted to give rise to at least 10 different JNK proteins [11]. Whilst the precise differences between the 10 JNK protein products have not been clearly defined, at least one study has demonstrated that the isoforms differentially recognise and phosphorylate their transcription factor substrates [11]. More recently, JNK2 spliceforms have been shown to have higher constitutive activity that correlates with primary glial tumour formation [12]. A JNK homologue has also been described in *Drosophila* [13,14] and a human JNK isoform [15] was shown to functionally complement deficiencies in a distantly related SAPK, p38 Hog, in *Saccharomyces cerevisiae* [15]. This conservation is also apparent in the upstream components of the JNK pathway (Refs. [16–20] and reviewed in Ref. [21]). Thus, the JNK signalling module has been proposed to play important biological roles in diverse eukaryotic species.

In the following sections, this review considers the roles that JNKs may play in mammalian systems, with particular emphasis on the targeting of JNKs or their upstream activators for therapeutic intervention. We begin with the initial approaches to understanding JNK function in which JNK genes have been eliminated either alone or in combination. We then consider small chemical inhibitors and small peptide inhibitors of JNKs. Whilst there is little published data on the in vivo effects of these JNK inhibitors, it is clear that a number of pharmaceutical companies are now exploring the therapeutic potential of JNK inhibitors through in vitro and in vivo studies, with evidence that some inhibitors are already being taken into clinical trials.

2. Gene knockout studies reveal the potential physiological or pathophysiological roles of JNK and the JNK pathway

In the initial absence of effective chemical inhibitors, the selective disruption of JNK genes or genes encoding JNK pathway components has provided an effective approach in evaluating the potential therapeutic benefits of inhibiting JNK. Taking the simplest situation first, that of the genetically tractable organism *Drosophila*, the loss of the single JNK gene (*Basket*) or upstream JNK activators such as *Hemipterous*), has demonstrated the requirement during mid-embryogenesis for both dorsal and thorax closure (for a review see Ref. [21]). This suggests that, at least in the processes of development, JNK can regulate tissue morphogenesis and polarity. The added advantage here is that the study of *Drosophila* has revealed the mechanisms underlying the morphological phenomenon. Specifically, the JNK signalling pathway regulates the expression of the transforming growth factor-β-like gene, *decapentaplegic* in cells of the leading epidermal edge during dorsal closure [21]. Similar approaches are also possible in other simple multicellular eukaryotes such as the nematode worm, *Caenorhabditis elegans*, with the identification of the genes for a JNK protein (*Jnk*-1) and the upstream activator (*Jkk*-1). These function in type-D GABAergic motoneurons to coordinate locomotion [22]. The situation in *C. elegans* however is more complex with four additional JNK genes C49C3.10, T07A9.3, Y51B9A.9, ZC416.4 as described on the KinBase website (see http://kinase.com). The multiple genes for JNK highlights the complexity of signalling that is likely, even in this relatively simple multi-cellular organism, and suggests that the different JNK isoforms could play specific roles in multicellular organisms.

Of particular interest has been the study of JNK functions in mammalian systems. It has been possible to study this contribution through the selective disruption of the JNK pathway at the level of JNK, further downstream (e.g. by targeting substrates such as c-Jun), or further upstream (e.g. by targeting regulators of the pathway, such as the MAPK kinases). All three approaches have been undertaken. c-Jun has been specifically targeted by gene disruption (*c-Jun* −/− as used in Refs. [23–26], or conditional gene targeting using Cre/LoxP-mediated recombination as used in Refs. [27,28]). An alternative approach has altered the c-Jun product to produce a non-phosphorylatable mutant (c-JunAA in which serine 63 and serine 73 of the transactivation domain are changed to alanine) [29,30]. However, these changes can only evaluate the contribution of signalling via c-Jun. Given that many other JNK substrates are likely, as shown in Fig. 1, this approach cannot provide a complete understanding of the different roles of JNK. Conversely, the disruption of upstream events in the JNK pathway is likely to give a better idea of the complexity of the signalling events associated with the JNK pathway. However, the redundancy of these kinases (e.g. two MAPK kinases, MKK4 and MKK7, act directly on JNK) as well as the potential for kinases further upstream to also act as modulators of other pathways (e.g. MLK3 can modulate both JNK and p38 pathways, Ref. [31]) has made this analysis difficult. Here we restrict our discussion to those studies that have directly targeted the genes for JNK.

Evaluating the contribution of JNK is complicated by the need to study each of the mammalian JNKs encoded by three separate genes—*Jnk*1 (on chromosome 14 of mouse or 10 of human), *Jnk*2 (on chromosome 11 of mouse or 5 of human), and *Jnk*3 (on chromosome 5 of mouse or 4 of human) and the resulting 10 alternatively spliced protein products. The apparent restriction of JNK3 protein expression to the brain, and to a lesser extent the heart and testes, has made it a good initial target to study the effects of selective gene disruption. Thus, the disruption of *Jnk*3 was not associated with any obvious abnormal phenotype and these animals were born normally. Furthermore, these *Jnk*3 −/− mice were protected from kainic acid-induced seizures that, in wild-type mice, were associated with 60% death rates from continuous tonic–clonic convulsions [32]. At the cellular level, *Jnk*3 disruption protected the hippocampal cells from glutamate-induced excitotoxicity. This observation was consistent with previous inferences of the mechanisms of neurotoxicity arising from potent induction of c-Jun and sustained activity of the AP-1 transcription factor. Similar phenotypic changes in excitotoxicity did not accompany the loss of *Jnk*1 or *Jnk*2 genes. These studies support approaches to selectively target JNK3 in the prevention of the neurotoxicity associated with excess excitatory amino acid release. JNK3 has been suggested to be a good target in the treatment of the acute ischaemia of stroke as well as the chronic loss of neurons in neurodegenerative diseases such as Parkinson's and Alzheimer's diseases.

In contrast to the expression pattern of JNK3, the expression of JNK1 and JNK2 proteins is not tissue-restricted. It has therefore taken greater efforts and more complex studies to understand the roles of these two JNK isoforms in physiological or pathophysiological processes. In the first studies to evaluate *Jnk*1 −/− and *Jnk*2 −/− mice, the loss of either JNK isoform was shown to alter T cell differentiation [33–35]. For example, the loss of JNK1 resulted in T cells that hyperproliferated, showed less activation-induced apoptosis, and differentiated preferentially into helper cell T_H2 antigen-presenting cells [34]. JNK2 was required for interferon production by T_H1 cells and efficient T cell activation and apoptosis [33,35]. Thus, these studies support a role for JNKs in T cell differentiation [36]. Because the inappropriate regulation of T cells underlies many autoimmune diseases, attention has been directed to the inhibition of JNKs in diseases such as rheumatoid arthritis (see Section 3).

*Jnk*1 −/− and *Jnk*2 −/− mice have further implicated these two JNK isoforms in important physiological events other than T cell differentiation. For example, a closer inspection of *Jnk*1 −/− brain tissue has shown hypo-

phosphorylated microtubule-associated proteins MAP2 and MAP1B together with compromised microtubule assembly. Thus, in addition to potential regulatory roles through cytokine loops and transcription factor activity, there is direct phosphorylation-dependent regulation of microtubule assembly by JNK1 [37]. Using *Jnk*1 −/− mice, Jimenez et al. [38] have also implicated JNK1 signalling in the inhibition of neovascularization by thrombospondin-1, whereas more recently, *Jnk*1 −/− mice have been shown to be significantly protected from obesity-induced insulin resistance [39]. These observations highlight a very broad range of important JNK1-regulated events in vivo. Whilst these studies support the selective targeting of JNK1, for example in the treatment of type 2 diabetes, they also suggest a potential for unwanted side-effects.

The specific roles of JNK2 have been similarly explored in *Jnk*2 −/− mice, although at this point in time there are fewer published studies using these animals. Some of the first studies have shown the requirement for JNK2 in the optimal induction of interferon-α_1 and -β transcription following infection of murine embryonic fibroblasts with vesicular stomatitis virus [40]. Whilst this implicates JNK2 in the activation of innate immune responses, it also emphasises that JNKs can play pivotal roles in the regulation of gene expression. In more recent studies, roles specifically for JNK2 as a mediator of inflammatory responses have been explored. Thus, in a passive collagen-induced arthritis model, the *Jnk*2 −/− animals showed modestly decreased joint damage (cartilage erosion and proteoglycan depletion) but little effect on inflammation, leading to a conclusion that JNK2 was not the sole mediator of arthritic changes [41]. This emphasises that in many tissues in which JNK1 and JNK2 are co-expressed, they may have redundant or at least overlapping roles. Thus, both isoforms may need to be inhibited for maximal therapeutic benefit [41].

In contrast to the above studies in which the loss of either JNK1 or JNK2 has enabled studies of phenotypic changes in the adult animal, the loss of JNK1 and JNK2 in combination has been shown to be embryonically lethal. This failure to complete embryonic development has been attributed to an apparent increase in apoptosis of the forebrain and decreases in apoptosis in the lateral edges of the hindbrain prior to neural tube closure [42]. Thus, JNK1 and JNK2 would appear to have both pro-apoptotic and anti-apoptotic roles in the development of the brain.

More detailed studies have been recently undertaken with mice retaining a single allele of either *Jnk*1 or *Jnk*2. This has revealed, in the *Jnk*1 −/− *Jnk*2 −/+ animals, that JNKs may also play a role in closure of the optic fissure, a process that resembles the dorsal and thorax closure processes in *Drosophila* [43]. In mammals, this process appears to require the expression of bone morphogenic protein-4 that is the functional ortholog of the *Drosophila decapentaplegic* (as described earlier in this section). This leads, via a cytokine cascade, to the expression of a paired-like homeobox transcription factor, Pax2. JNK therefore appears to play a conserved role in morphogenetic processes during embryonic development in insects and mammals.

Despite these advances in our understanding of JNK function that highlight JNKs as suitable targets for therapeutic intervention, there are additional complications that cannot be ignored. For example, in a mouse model of multi-stage skin tumorigenesis, JNK1 deficiency enhanced tumour burden, whereas JNK2 deficiency inhibited tumorigenesis [44,45]. These observations, together with suggestions that under some conditions, the JNK pathway may provide tumour suppression in mice [46] as well as in humans [47–53], could raise alarm about the possible therapeutic targeting of JNK. These studies do hint at the complexity of the processes. However, the long-term loss of the JNK pathway, particularly throughout the entire life of an organism (including its embryonic development), does not accurately model the acute therapeutic inhibition of JNK. For example, acute JNK inhibition would be appropriate in the treatment of stroke. Alternatively, when considering the need for more chronic administration (e.g. in treating patients with Alzheimer's or Parkinson's diseases), JNK inhibition would only be initiated in the later years of these patients' lives. The changes that can accompany long-term loss of JNK are most clearly illustrated in the recent microarray analysis undertaken on primary embryonic cells prepared from wild-type, *Jnk*1 −/− and *Jnk*2 −/− mice [54]. In addition to anticipated results that the selective loss of JNK1 or JNK2 could lead to differences in gene expression following exposure to known JNK pathway activators, obvious differences in the gene expression patterns were noted prior to this treatment. Specifically, of the 558 genes tested, eight genes were overexpressed in the *Jnk*2 −/− cells, suggesting that JNK2 usually suppresses their expression. At least three genes were increased in expression in the *Jnk*1 −/− cells, suggesting that JNK1 negatively regulates these genes under normal conditions, whereas the expression of 22 genes was decreased in *Jnk*1 −/− or *Jnk*2 −/− conditions. This latter result suggested that JNK1 or JNK2 usually act positively in controlling the expression of these genes. It is therefore likely that more extensive array analysis of animals targeted for loss of the JNK expression will reveal further complexities of the phenotypic changes.

In parallel to these studies, other approaches to inhibit expression of JNKs such as antisense techniques and the more recently adopted RNA-mediated interference approaches should accelerate discoveries of the cellular events mediated by JNKs. These studies will provide information on whether JNKs are suitable (i.e. "drugable") targets. For therapeutic use, a JNK inhibitor that can be readily administered to patients at the time of their disease diagnosis, is now needed. In the following three sections, we therefore review the use of three inhibitors of either the JNK pathway or the JNKs.

3. CEP-1347, a semisynthetic inhibitor of the MLK protein kinases in the JNK cascade

CEP-1347 (shown in Fig. 2(a)), originally called KT7515 (or 3,9 bis[(ethylthio)methyl]-K252a), was identified in a medicinal chemistry approach directed to retain the desirable properties of the naturally occurring compound K252a whilst minimising any undesirable effects [55]. Specifically, a series of 3,9-disubstituted [(alkylthio)methyl]- and (alkoxymethyl)-K252a derivatives were tested for an enhanced neurotrophic response. This was specifically evaluated by the survival of cholinergic neurons in spinal neuron cultures and their maintenance of choline acetyl transferase activity. At the same time, the aim was to also reduce biochemical properties that limited its use as a therapeutic agent. For example, for a compound to be ultimately used in neuronal applications, it was considered important to have low inhibitory activity towards the high affinity nerve growth factor-receptor, *trk* [55]. CEP-1347 met these initial criteria, and was also demonstrated to have decreased ability to inhibit protein kinase C, cAMP-dependent protein kinase and myosin light chain kinase [55].

The link between CEP-1347 and the JNK signalling pathway was made soon after this initial description. The study by Maroney et al. [56] at Cephalon Incorporated demonstrated that, in the absence of trophic support, the death of cultured rat embryonic neurons was accompanied by 4-fold increases in JNK activity. CEP-1347 both rescued the neurons and prevented JNK activation at similar low concentrations, the IC_{50} for the inhibition of these events being approximately 20 nM. Thus, it was proposed that CEP-1347 acted at some point of the JNK pathway, and would provide a suitable compound to test in further studies on neuronal cell death.

Most of the subsequent 40 or so studies using CEP-1347 in the last 5 years have focused on its use in the prevention of apoptosis. Most have effectively used CEP-1347 in vitro and in vivo in models of neuronal cell death and neurodegenerative diseases. A complete overview of these papers is beyond the scope of this review, and the reader is directed to an excellent recent summary of these works [57].

There are additional indications that the use of CEP-1347 will find broader application. For example, in experimental models of pancreatitis, CEP-1347 pretreatment (given at doses up to 60 mg/kg body weight, injected intravenously, up to 4 h prior to the caerulein to induce pancreatitis) was effective in lowering the JNK activation associated with this disease state, decreasing pancreatic oedema, and decreasing the histological severity of the pancreatitis [58]. Curiously, other markers of pancreatitis, namely increased serum lipase or amylase, were not affected by the CEP-1347 treatment [58]. It remains unclear whether this reflects the inability of CEP-1347 to completely abolish JNK activity under the conditions of its use, or more likely that JNK-independent

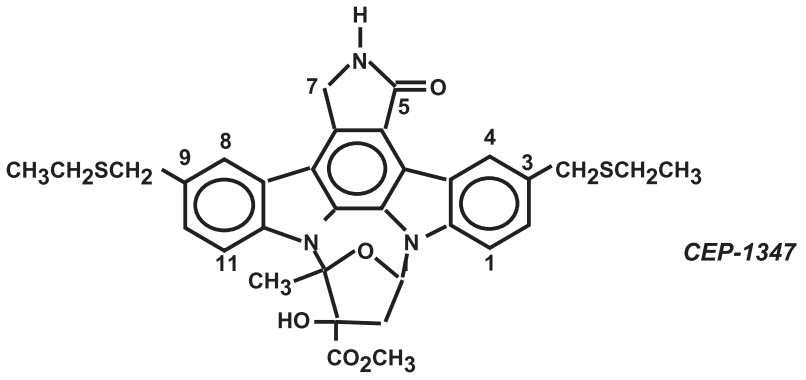

CEP-1347

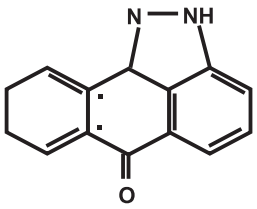

SP600125

Fig. 2. Chemical inhibitors of the JNK pathway. (a) CEP-1347, originally called KT7515, was identified in series of 3,9-disubstituted [(alkylthio)methyl]- and (alkoxymethyl)-K252a derivatives [55]. This compound is a 3,9 bis[(ethylthio)methyl] substituted K252a, and the positions of carbons 3 and 9 as defined in the parent K252a compound are indicated. These substitutions allowed the desirable neurotrophic properties of the naturally occurring compound K252a to be retained, whilst decreasing the inhibitory activity towards protein kinase C, cAMP-dependent protein kinase, and myosin light chain kinase [55]. (b) SP600125, (anthra[1,9-cd]pyrazol-6(2H)-one), was identified by screening of a proprietary diversity library. SP600125, acted as a reversible ATP-competitive inhibitor of equal potency towards three JNK gene products, JNK1, JNK2 and JNK3. Specifically, IC_{50} values calculated for JNK1, JNK2 and JNK3 were 40, 40 and 90 nM, respectively [63].

signalling pathways regulate the secretory disturbance in this disease state. Similarly, CEP-1347 has been shown to dose-dependently attenuate the transforming growth factor β-induced modulation of lung fibroblasts to myofibroblasts, thus suggesting that CEP-1347 might find ultimate therapeutic application in preventing the fibrogenic process of pulmonary fibrosis [59]. CEP-1347 has also implicated JNKs in the regulation of the production of the cytokine, RANTES, by human bronchial epithelial cells following their exposure to influenza virus [60]. Furthermore, CEP-1347 promises to be of great use in evaluating the contribution of the JNK pathway in signal transduction mechanisms. For example, pretreatment of cells prior to the exposure to ultraviolet radiation prevented the usual phosphorylation of Serine 36 of the p66 isoform of the intracellular adaptor protein Shc [61]. This phosphorylation of p66 Shc has been previously implicated in the cell death response to oxidative damage, so that these latter observations again support a potential use for CEP-1347 as a modulator of cell death in response to stress.

This increasing use raises the question of how CEP-1347 acts to inhibit JNK activation, i.e. what is the direct biochemical target of CEP-1347 in the signalling events leading to JNK activation? The initial study by Maroney et al. [56] showed that CEP-1347 acted upstream in the JNK pathway because pretreatment with CEP-1347 inhibited JNK activity in Cos-7 cells subjected to stress with ultraviolet irradiation, osmotic shock, or exposure to tunicamycin. Interestingly, CEP-1347 was not effective in inhibiting the ability of MAP kinase kinase kinase (MEKK) to activate JNK, suggesting that CEP-1347 acted either at events more membrane proximal than MEKK, or in a parallel, non-MEKK-dependent pathway [56]. When this was later examined in more detail, CEP-1347 significantly inhibited JNK activation following transfection of Cos7 cells with constitutively active small G-proteins (Rac1QL or cdc42QL), MAPKKKKs (KHS, GCK, NIK) as well as certain MAPKKKs (MLK1, MLK2, MLK3, DLK, LZK) but not other MAPKKKs (e.g. MEKK1 and MEKK5) or other MAPKKs (e.g. MKK4 and MKK7) [62]. This suggested that CEP-1347 acted to inhibit events upstream of MKK4/7 and most likely at the level of MAPKKKs including kinases known as the mixed lineage kinases (MLKs). Indeed the MLKs were shown to be inhibited in vitro, with CEP-1347 being a direct competitive inhibitor of ATP with a K_i of 17 ± 2 nM.

The results with CEP-1347 therefore appear promising, but more rigorous testing is needed to determine that inhibiting the upstream components in the JNK pathway is desirable. First, other MEKK-dependent routes for JNK activation are not affected by CEP-1347. In these situations, CEP-1347 would not be effective in preventing JNK activation, and thus would not be a useful compound to prevent JNK-mediated cell death. Secondly, MLKs have the potential to affect additional targets and signalling proteins. For example, as acknowledged by Maroney et al. [62], multiple proteins including β-tubulin, prohibitin, dynamin and members of the KIP3 family have been found to associate with MLKs. Whilst the nature of these associations remains unclear, the question will remain whether the therapeutic efficacy of CEP-1347 reflects only its attenuation of JNK activation. In the following section, further studies aimed at identifying direct JNK inhibitors are described.

4. SP600125, an anthrapyrazolone ATP-competitive inhibitor of JNK MAPK

More recently, there has been attention directed towards inhibiting JNK MAPK rather than the upstream components of the pathway. Presumably this targeting could produce greater specificity of effects. Fig. 2(b) shows the chemical structure of SP600125 (i.e. anthra[1,9-cd]pyrazol-6-(2H)-one). This anthrapyrazole was identified in high throughput screening of a proprietary chemical library held by Celgene for direct inhibitors of JNK activity [63]. Anthrapyrazoles have not been previously reported as kinase inhibitors; however, the presence of nitrogens within the highly planar, fused-ring structure of SP600125 is consistent with features of other known kinase inhibitors [63]. One disadvantage conferred by such a ring structure is its poor solubility in water (only 0.0012 ng/ml) as originally described by Bennett et al. [63]. However, its solubility can be enhanced in the presence of dimethylsulfoxide. Stock solutions of 20 mM concentration are possible and allow its use at micromolar concentrations in cell culture applications as described in the following paragraphs. Further chemical modification studies have also been undertaken to define the critical features of SP600125 required for its inhibition of JNK. These have shown that N-alkyl substitution lowered inhibitory activity, whereas a chlorine added at position 8 produced a more potent analog [63]; it may thus be possible to further enhance the solubility of SP600125-derivatives whilst retaining or improving the ability to inhibit JNK.

SP600125 acted as a reversible ATP-competitive inhibitor of equal potency towards three JNK gene products, JNK1, JNK2 and JNK3. Specifically, IC_{50} values calculated for JNK1, JNK2 and JNK3 were 40, 40 and 90 nM, respectively [63]. For some applications, an inhibitor with this ability to interfere with all JNK isoforms will be expected to be desirable, but again it should be noted that the results of JNK gene knockout studies have suggested isoform specific roles (see earlier discussion in Section 2). This suggests that the discovery of new compounds (or SP600125 derivatives) showing isoform selectivity would be highly desirable.

Testing the specificity of SP600125 in in vitro assays with some 16 other purified protein kinases showed 300-fold selectivity of inhibition of the extracellular signal regulated kinases (ERKs) and p38 MAPKs, the closest kinase relatives of the JNKs [63]. SP600125 also showed

some ability to inhibit kinases upstream in the JNK pathway and p38 pathways. Specifically, MKK4 and MKK7 were inhibited with IC_{50} values of 0.4 and 5.1 μM, respectively. Whilst this inhibition of these JNK pathway components would likely enhance strategies to target JNK activities for inhibition, it should be noted that the p38 MAPK pathway components, MKK3 and MKK6 were inhibited with IC_{50} values of 1.5 and 1.0 μM, respectively. This creates a situation in which the use of higher concentrations of SP600125 may have broader effects than initially anticipated. Further work is therefore required to evaluate the specificity of SP600125 towards a broader range of kinases. This is now becoming increasingly possible with a number of commercial suppliers of recombinant active protein kinases, and many academic labs also developing such valuable resources. However, for potential clinical applications, the biological effects following SP600125 exposure will most likely dictate whether this compound is an attractive lead compound for ultimate use in the clinic.

The first studies using SP600125 in vitro and in vivo were published in 2001 (see Ref. [64] and the commentary in Ref. [65]). Since then, the use of SP600125 has been increasingly popular, and likely arises from two reasons. First, the ability to study the contribution of JNK signalling to biological processes has been restricted to the introduction of active or dominant-negative JNK pathway components into cells, most routinely by transfection. Whilst this has provided a good body of information on the potential of JNK pathways to play critical roles in mammalian cells, the process of transfection alters the cell for many hours to days prior to the experimental test. This is clearly a disadvantage, and contrasts with the chemical inhibitors that can be rapidly applied to cells either in vitro or in vivo to dissect the contributions of the ERK and p38 MAPK pathways. For example, PD98059 and UO126 target the activity of MEK1/MEK2 in the ERK MAPK pathway [66], whereas SB203580 and related pyridinylimidazole compounds directly inhibit p38 MAPK (as reviewed in Refs. [67,68]). The use of MAPK pathway inhibitors has greatly accelerated the understanding of these pathways. The second reason for the popularity of SP600125 (even when a compound such as CEP-1347 has been reported) likely lies in the commercial release of SP600125 but not CEP-1347. This could explain why, in comparison to the 37 studies using CEP-1347 since 1998, there have already been more than 60 reports of the use of the now commercially available SP600125 since 2001, with more than 40 in the first 6 months of 2003 alone.

In presenting an overview of the biology revealed through the use of SP600125, we begin with the first reports of its biological efficacy by Han et al. [64]. These studies translated their observations in isolated fibroblast-like synoviocytes into an animal model for rheumatoid arthritis (an adjuvant arthritis model induced in Lewis rats). SP600125 (30 mg/kg/day) was given by subcutaneous injection 8 days after the initiation of the arthritis-initiating adjuvant injections so that it preceded the expected onset of arthritis-like symptoms (including paw swelling, bone changes, joint inflammation and damage) by approximately 2 days. Treatment continued until day 14. This 6-day SP600125 treatment strategy was shown to modestly decrease swelling, provide a modest anti-inflammatory effect, but have a marked protective effect on joint destruction with significantly less joint damage and remodelling than in the vehicle-treated controls [64]. This suggests, as might be expected, that the complex disease phenotype observed in rheumatoid arthritis is the end result of a number of signal transduction pathways. Supporting this contention, suppression of NF-κB in this model was associated with prominent anti-inflammatory effects but no changes in bone destruction (as reviewed in Ref. [69]). In contrast, the JNK pathway would appear to be associated with regulation of genes such as collagenase 3 that contribute to the remodelling process [64]. Similarly, the use of SP600125 has implicated JNK as a regulator of the expression of 92 kDa type IV collagenase [70].

More recently, there have been many other studies that have used SP600125 to evaluate the potential contribution of JNK activity to a range of biochemical and biological events. Commonly, JNKs have been implicated in the regulation of cytokine expression. For example, JNKs appear to negatively regulate the production of interleukin-12 following lipopolysaccharide challenge of macrophages [71]. Conversely, fibroblast production of RANTES requires JNK activity [72] as does connective tissue growth factor production by lung fibroblasts [73]. More complex roles for JNK have been similarly revealed with the use of SP600125 in models of wound healing [74], cell cycle arrest by flurbiprofen [75], and neurotoxicity in Alzheimer's disease [76]. Similarly, recent studies with SP600125 have shown the inhibition of long-term potentiation by interleukin-1 [77], regulation of cell migration through JNK-dependent phosphorylation of paxillin [78] and JNK-dependent release of the mitochondrial protein Smac [79]. As more laboratories adopt the use of SP600125, it is likely that the list of biological processes potentially mediated by JNKs will continue to grow.

5. Peptide inhibitors of JNK MAPK

Most drug discovery programs focused on the development of protein kinase inhibitors have, in general, concentrated on the design or screening of small organic compounds that are competitive inhibitors of the ATP-binding site of their protein kinase of interest. This can prove to be a successful strategy as discussed in the previous examples of the JNK pathway inhibitor CEP-1347 (Section 3) and the direct JNK inhibitor SP600125 (Section 4). Within the broader context of other protein kinase inhibitors, the use of an ATP-like molecule as an inhibitor is clearly demonstrated by the biological efficacy of STI-571 (also called Gleevec) that was first described to inhibit the

kinase activity of the Bcr-Abl fusion protein in Chronic Myeloid Leukemia [80]. In this example, the STI-571 inhibitor occupies the ATP binding site, recognising a distinct inactive conformation of the activation loop of Abl, thus providing direct competitive inhibition and allosteric control of the kinase activity [80]. Furthermore, taking the examples of widely used p38 MAPK inhibitors as an example, it is clear that the compound SB203580 and related pyridinylimidazole compounds, act as ATP competitive inhibitors with direct confirmation that the inhibitor occupies the ATP-binding site coming from the co-crystallisation of the kinase and the inhibitor [67]. The specificity of inhibition of SB203580 towards p38-α and p38-β (but not related p38s γ and δ, ERKs or JNKs) again reinforces the idea that ATP-competitive inhibitors can be specific. In this example, the substitution of three amino acids in JNK1, p38-γ and p38-δ was sufficient to allow the mutant kinases to be sensitive to SB203580 [81]. Thus, specific kinase inhibitors can be found that can take advantage of altered conformations of active and inactive kinases as well as subtle sequence variations in the ATP-binding site of the kinases even within closely related members of one family.

One potential disadvantage of an ATP-competitive inhibitor could be that the usually high endogenous levels of ATP might effectively reduce the efficacy of an ATP-competitive inhibitor. This has been observed with SP600125, where competition with high intracellular concentrations of ATP has been one of the reasons used to explain an increase in IC_{50} for JNK inhibition from 0.2 μM in vitro to 5–10 μM intracellularly [63]. As an alternative to competitive binding to the ATP-binding site, it remains possible that compounds that target either peptide substrate binding sites, or other allosteric regulatory sites could be inhibitors of protein kinases. Theoretically this would broaden the range of possible target sites, and have the added advantage that the inhibitor would not need to compete with the high intracellular ATP concentrations.

At least two mechanisms other than ATP-binding site competition may be useful in the consideration of inhibitors of JNK MAPKs. First is the possibility that competition with a protein kinase's second substrate (i.e. its protein/peptide substrate) could provide a specific mechanism of inhibition. Thus, non-phosphorylatable substrate analogues could have the potential to compete with binding and phosphorylation reactions. This is the basis on which a number of dominant-negative mutants of kinases in signalling pathways have been designed. Probably the first reported success of using a substrate-based peptide inhibitor came from the pioneering work of Feramisco and Krebs [82] in which a peptide substrate (LRRASLG) of cAMP-dependent protein kinase was modified so that the phosphorylated serine residue was replaced with an alanine. This produced a potent inhibitor of cAMP-dependent protein kinase [82]. Similar approaches used with cAMP-dependent protein kinases could yield a peptide inhibitors with in vitro K_i values ranging from 4 nM to 150 μM [83], demonstrating that the correct choice of peptide can provide potent kinase inhibitory molecules.

In the case of JNK, this use of substrate-based protein/peptide mutants has been exploited with the expression of a c-Jun mutant that cannot be phosphorylated in its transactivation/regulatory domain by JNK (i.e. S63 → A, S73 → A c-Jun double mutant) as described in Section 2. However, we have shown a peptide-based strategy based on this approach is not effective in in vitro inhibition of previously activated JNK. Specifically, when peptide sequences immediately surrounding the Serine 63 and Serine 73 were tested alone or in combination, no significant inhibition of JNK was noted (Fig. 3). At least one possible reason for the discrepancy between the efficacy of full-length c-Jun S → A mutants, and the S → A mutant c-Jun based 11mer peptides likely lies in the use of additional kinase-interaction motifs (KIMs) in substrates such as c-Jun [84]. In our assay, an 11mer peptide based on the KIM of c-Jun was not an effective inhibitor of activated JNK (Fig. 3). However, it has been recently reported that a peptide based on the motif of c-Jun that interacts with JNK (the so-called δ-domain which includes the KIM and extends beyond this sequence, i.e. sequence ILKQSMTLNLADPVGSLKPHLRAKN) can act as an inhibitor of JNK phosphorylation of c-Jun both in vitro and in cells [85]. The reason for the differences between the studies may lie in the exact lengths of the two peptides, and that higher concentrations of peptides (i.e. >100 μM in Ref. [85] versus <2 μM in Fig. 3) might afford better inhibition both in vitro and in cells.

The second possibility to identify new JNK inhibitors entertains the idea that allosteric modulation of JNK activity might be possible. Here the aim would be to identify inhibitors (either peptides or small chemical non-peptides) that are neither competitive with ATP, nor with the peptide substrate. To date, a peptide inhibitor which may act in this manner has been described by two groups that have independently characterised a peptide sequence derived from a non-substrate JNK-interacting protein (JIP).

In a two-hybrid screen to identify novel JNK binding partners, a novel JIP was identified [86]. This was named JIP1, with three mammalian members of this family now recognised (JIP1, JIP2 and JIP3) [87–89]. These have been given the alternative names of Islet Brain Protein-1 (IB1) and IB2 due to their tissue expression pattern (i.e. high expression in the pancreatic islets and brain Refs. [90–92]) or JSAP1 to indicate the association with JNK/stress-activated protein-associated protein [93]. An intriguing observation of the original study was the ability of JIP1 to inhibit JNK activity [86]. There are at least two possible explanations for this observation. First, some studies have attributed the ability of JIP overexpression to inhibit JNK activity in mammalian cells to its ability to retain JNK in the cytoplasm [86]. Thus, if active JNK is unable to enter the nucleus, this would impair its ability to phosphorylate and activate its transcription factor substrates such as c-Jun. Supporting this idea, Fan et al. [94] have shown that

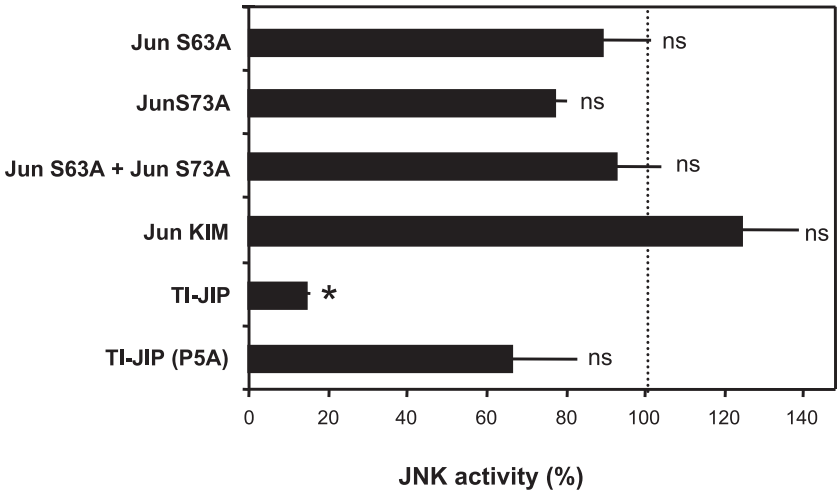

Fig. 3. Peptide inhibitors of JNK. Our laboratory has recently explored the use of peptide inhibitors of JNK [96]. In our in vitro assay for inhibitors of JNK, we incubated JNK1 immunoprecipitated from osmotically shocked Cos cells with the peptide inhibitor of choice (final concentration 1700 nM), 1 μCi [γ-^{32}P]-ATP and 10 μg GST-c-Jun (1–135) as a substrate [96]. All peptides tested have been synthesized using the Pepset multipin synthesis technology of Mimotopes (Melbourne, Australia). Here we show that peptides based entirely on the c-Jun sites of phosphorylation (peptides labelled as Jun S63A (sequence: SDLLTAPDVGL), Jun S73A (sequence: LLKKAAPELER) or a combination of these two peptides, i.e. Jun S63A + Jun S73A) are only marginally effective as inhibitors of JNK (previously unpublished observations). Similarly, the KIM of Jun (sequence: ILKQSMTLNLA) is only marginally effective as a JNK inhibitor, when compared to the almost complete inhibition recorded for the KIM of the scaffold protein JIP (TI-JIP, sequence: RPKPRTTLNLF). However, the simple substitution of the second proline in the JIP KIM (TI-JIP P5A, sequence: RPKRATTLNLF) abolishes the inhibition of JNK, thus suggesting that this proline is essential for the JNK inhibitory activity of the 11mer peptide.

overexpressed JIP1 blocked the phosphorylation of nuclear substrates such as c-Jun and ATF2 but not non-nuclear substrates such as Bcl-2/Bcl-$X_{(L)}$. A second possibility is that, although a scaffold should enhance the formation of active pathway complexes, its overexpression would result in excess scaffold. Each scaffold molecule could then bind a separate pathway component rather than all components of the pathway in a regulated complex, thereby effectively disrupting the regulated complex. However, a third possibility should also be considered. Two independent groups have recently described small peptides derived from JIP that can act as inhibitors of JNK [95,96]. The approaches taken to identify these JIP-derived peptides and to demonstrate their efficacy as JNK inhibitors are described in the following paragraphs.

By sequence comparison between two isoforms of the JIP/IB scaffold proteins, JIP1/IB1 and JIP2/IB2, Bonny et al. [95] identified a minimal conserved domain of 18–20 amino acids. The conserved 20 amino acid sequence from JIP1/IB1 (sequence: RPKRPTTLNLFPQVPRSQDT) was first tested in transfection studies, in which it prevented apoptotic death induced by interleukin-1 [95]. This simple test demonstrated the biological efficacy of the short peptide sequence. It showed that the actions of JIPs, when overexpressed even as full-length proteins, may not result from aberrant scaffolding or sequestering JNKs in the cytosol because this peptide was not a scaffold or a cytosolic anchor. Similarly, our recent study [96] has shown that a short peptide sequence (sequence: GPGTGSGDTYRPKRPTTLNLF) identified through similarity with the JNK-binding domain of c-Jun, overlapped partially with the sequence described by Bonny et al. This peptide was a direct inhibitor of the activity of JNK1 in vitro, without inhibiting ERK or p38 MAPKs under similar conditions [96]. Furthermore, the shorter sequence (RPKRPTTLNLF) was also an effective direct inhibitor, with an essential requirement for each of four residues within this 11 amino acid sequence (specifically R4, P5, L8 and L10) [96]. We have called this peptide TI-JIP as it represents the truncated inhibitory region of JIP. The specific and direct interaction of the peptide inhibitor with JNK rather than the c-Jun substrate suggests that these peptides target an area not directly in the active site of the kinase. Potential sites for this interaction include the common docking domain of ERK and similar sites of p38 MAPKs [97,98]. Using the information on this published p38 MAPK interaction with the substrate peptide, pepMEF2A (KPDLRVVIPP), or a peptide derived from the MKK3 protein (pepMKK3b, sequence: KKDRISC) it is possible to model the shorter peptide inhibitor (RPKRPTTLNLF) bound to the JNK3 structure as shown in Fig. 4. From this model, it appears that the peptide inhibitor acts at a site remote from the active site, possibly acting as an allosteric modulator.

Taking these observations a step further, the direct and acute delivery of a 20 amino JNK-inhibitor peptide has been achieved through its coupling to a cell-permeable peptide sequence of10 amino acids derived from the human immunodeficiency virus TAT protein [95]. This final sequence was *GRKKKRRQRRPP***RPKRPTTLNLFPQVPRSQDT** in which the underlined proline residues have been introduced between the vector (shown in italics) and inhibitor sequence

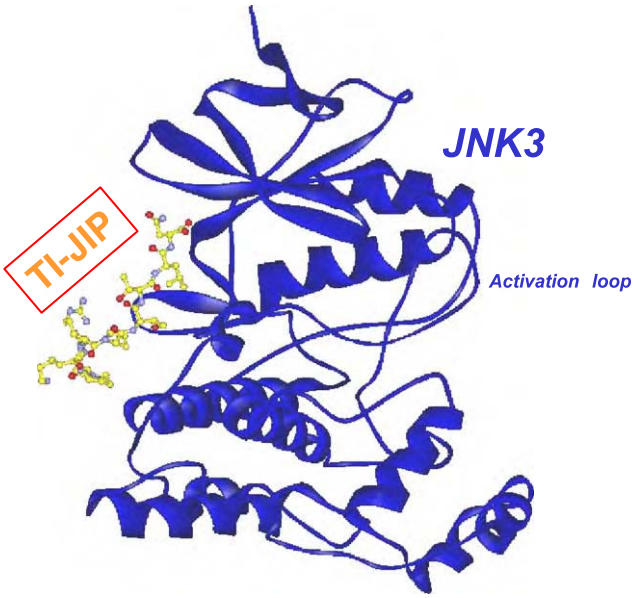

Fig. 4. Model of interaction of TI-JIP with JNK. Based on the identified binding site for peptides pepMEF2A (sequence: KPDLRVVIPP) and pepMKK3b (sequence: KKDLRISC) with p38 MAPK as reported by Chang et al. [98], a model is presented for the interaction site of TI-JIP with JNK MAPK. The TI-JIP peptide is shown in ball-and-stick representation, and JNK in the blue ribbon diagram. The activation loop for JNK is indicated, and suggests that the mode of action of TI-JIP, if this is the binding site, could be through an allosteric mechanism.

(shown in bold). This is a strategy being increasingly used for the delivery of peptides or full-length proteins to cells in vitro or even in vivo [99,100]. Further modifications were made, such that an all-D retro-inverso peptide (i.e. a peptide synthesised in the reverse sequence from D-amino acids rather than L-amino acids) improved intracellular stability of the peptide. However, it should also be noted that this change decreased the efficacy of inhibition of JNK activity by almost 15- to 20-fold, suggesting that it may be difficult to improve the delivery, stability and inhibitory efficacy simultaneously. Despite the lower efficacy, the TAT-conjugated retro-inverso peptide could inhibit IL1-stimulated apoptosis for up to 2 weeks [95]. These studies thus demonstrate that peptide-derived inhibitors for JNK activity are now available. It will be interesting to see whether these lead to new concepts relating to the modulation of JNK activity, through the identification of the sites on JNK bound by the peptide inhibitors. Alternatively, their delivery into cells may provide new insights into JNK-regulated processes with the possible extension in the future to in vivo studies.

6. Conclusions and perspectives on the therapeutic applications of JNK inhibitors

Given the intense interest in the JNK signalling pathway (with more than 3800 PubMed citation hits since their discovery in 1991), it hardly surprising that effective chemical inhibitors of the JNKs are highly sought after both by the academic research community and the pharmaceutical industry. Whilst CEP-1347 and SP600125 have been the subject of peer-reviewed studies as described in Sections 3 and 4 of this review, the published information on their efficacy in clinical trials remains limited. Cephalon has been directing attention towards treatment of Alzheimer's disease and Parkinson's disease. According to web resources, Cephalon has commenced enrolment of patients in a randomized, double-blind, placebo-controlled, dose-finding Phase II/III clinical trial for CEP-1347 as an orally active JNK pathway inhibitor, anticipating participation by approximately 800 patients with early stage Parkinson's disease at as many as 65 sites in the USA and Canada. Even less information is currently available on the trials by Celgene, however there again have been web press releases confirming that their lead JNK inhibitors have completed Phase I clinical trials.

As highlighted in a recent review, there would appear to be more than 16 disclosed compounds listed in patent applications in the last 3 years by scientists at companies including Aventis, Esai, Hoffman-LaRoche, Merck, Takeda and Vertex [101]. The efficacy of these in vitro has been demonstrated, although no published information is yet available. With the selective targeting of protein kinases becoming a therapeutic reality with the clinical use of small molecule inhibitors such as STI-571, it will be of great interest to see just how many of these JNK inhibitor compounds progress to clinical trials, which specific diseases are to be targeted, and whether desired therapeutic outcomes can be achieved without unwanted side-effects.

Acknowledgements

The work by the authors on peptide inhibitors of JNK has been supported by a Discovery Project Grant by the Australian Research Council, and the Neurotrauma Program of WAIMR. In addition, I. Boehm acknowledges the support of a School of Biomedical and Chemical Sciences Scholarship, and R.K. Barr acknowledges the support by a Hackett at UWA Postgraduate Student Scholarship and a Woodside Neurotrauma PhD Excellence Award.

References

[1] G. Manning, D.B. Whyte, R. Martinez, T. Hunter, S. Sudarsanam, The protein kinase complement of the human genome, Science 298 (2002) 1912–1934.
[2] J.M. Kyriakis, J. Avruch, pp54 microtubule-associated protein 2 kinase. A novel serine/threonine protein kinase regulated by phosphorylation and stimulated by poly L-lysine, J. Biol. Chem. 265 (1990) 17355–17363.
[3] J.M. Kyriakis, P. Banerjee, E. Nikolakaki, T. Dai, E.A. Rubie, M.F. Ahmad, J. Avruch, J.R. Woodgett, The stress-activated protein kinase subfamily of c-Jun kinases, Nature 369 (1994) 156–160.

[4] H. Ichijo, From receptors to stress-activated MAP kinases, Oncogene 18 (1999) 6087–6093.
[5] B. Dérijard, M. Hibi, I.-H. Wu, T. Barrett, B. Su, T. Deng, M. Karin, R.J. Davis, JNK1: a protein kinase stimulated by UV light and Ha-Ras that binds and phosphorylates the c-Jun activation domain, Cell 76 (1994) 1025–1037.
[6] S. Gupta, D. Campbell, B. Dérijard, R.J. Davis, Transcription factor ATF2 regulation by the JNK signal transduction pathway, Science 267 (1995) 389–393.
[7] S.-H. Yang, P.R. Yates, A.J. Whitmarsh, R.J. Davis, A.D. Sharrocks, The Elk-1 ETS-domain transcription factor contains a mitogen-activated protein kinase targeting motif, Mol. Cell. Biol. 18 (1998) 710–720.
[8] C.W. Chow, M. Rincon, J. Cavanagh, M. Dickens, R.J. Davis, Nuclear accumulation of NFAT4 opposed by the JNK signaling pathway, Science 278 (1997) 1638–1641.
[9] T. Buschmann, O. Potapova, A. Bar-Shira, V.N. Ivanov, S.Y. Fuchs, S. Henderson, V.A. Fried, T. Minamoto, D. Alarcon-Vargas, M.R. Pincus, W.A. Gaarde, N.J. Holbrook, Y. Shiloh, Z. Ronai, Jun NH_2-terminal kinase phosphorylation of p53 on Thr-81 is important for p53 stabilization and transcriptional activities in response to stress, Mol. Cell. Biol. 21 (2001) 2743–2754.
[10] K. Lei, R.J. Davis, JNK phosphorylation of Bim-related members of the Bcl2 family induces Bax-dependent apoptosis, Proc. Natl. Acad. Sci. U. S. A. 100 (2003) 2432–2437.
[11] S. Gupta, T. Barrett, A.J. Whitmarsh, J. Cavanagh, H.K. Sluss, B. Dérijard, R.J. Davis, Selective interaction of JNK protein kinase isoforms with transcription factors, EMBO J. 15 (1996) 2760–2770.
[12] H. Tsuiki, M. Tnani, I. Okamoto, L.C. Kenyon, D.R. Emlet, M. Holgado-Madruga, I.S. Lanham, C.J. Joynes, K.T. Vo, A.J. Wong, Constitutively active forms of c-*Jun* NH_2-terminal kinase are expressed in primary gial tumors, Cancer Res. 63 (2003) 250–255.
[13] H.K. Sluss, Z. Han, T. Barrett, R.J. Davis, Y.T. Ip, A JNK signal transduction pathway that mediates morphogenesis an immune response in *Drosophila*, Genes Dev. 10 (1996) 2745–2758.
[14] J.R. Riesgo-Escovar, M. Jenni, A. Fritz, E. Hafen, The Drosophila Jun-N-terminal kinase is required for cell morphogenesis but not for DJun-dependent cell fate specification in the eye, Genes Dev. 10 (1996) 2759–2768.
[15] Z. Galcheva-Gargova, B. Dérijard, I.-H. Wu, R.J. Davis, An osmosensing signal transduction pathway in mammalian cells, Science 265 (1994) 806–808.
[16] Y.-C. Su, J.E. Treisman, E.Y. Skolnik, The *Drosophila* Ste20-related kinase misshapen is required for embryonic dorsal closure and acts through a JNK MAPK module on an evolutionarily conserved signaling pathway, Genes Dev. 12 (1998) 2371–2380.
[17] B. Stronach, N. Perrimon, Activation of the JNK pathway during dorsal closure in *Drosophila* requires the mixed lineage kinase, *slipper*, Genes Dev. 16 (2002) 377–387.
[18] J.A. Botella, I.A. Baines, D.D. Williams, D.C.I. Goberhan, C.G. Proud, C. Wilson, The *Drosphila* cell shape regulator c-Jun N-terminal kinase also functions as a stress-activated protein kinase, Insect Biochem. Mol. Biol. 31 (2001) 839–847.
[19] T. Igaki, H. Kanda, Y. Yamamoto-Goto, H. Kanuka, E. Kuranaga, T. Aigaki, M. Miura, Eiger, a TNF superfamily ligand that triggers the *Drosophila* JNK pathway, EMBO J. 21 (2002) 3009–3018.
[20] H.-W. Chen, M.J. Marinissen, S.-W. Oh, X. Chen, M. Melnick, N. Perrimon, J.S. Gutkind, S.X. Huo, CKA, a novel multidomain protein, regulates the JUN N-terminal Kinase signal transduction pathway in *Drosophila*, Mol. Cell. Biol. 22 (2002) 1792–1803.
[21] B.E. Stronach, N. Perrimon, Stress signaling in *Drosophila*, Oncogene 18 (1999) 6172–6182.
[22] M. Kawasaki, N. Hisamoto, Y. Iino, M. Yamamoto, J. Ninomiya-Tsuji, K. Matsumoto, A *Caenorhabditis elegans* JNK signal transduction pathway regulates coordinated movement via type-D GABAergic motor neurons, EMBO J. 18 (1999) 3604–3615.
[23] F. Hilberg, A. Aguzzi, N. Howells, E.F. Wagner, c-Jun is essential for normal mouse development and hepatogenesis, Nature 365 (1993) 179–181.
[24] R. Wisdom, R.S. Johnson, C. Moore, c-Jun regulates cell cycle progression and apoptosis by distinct mechanisms, EMBO J., (1999) 188–197.
[25] M. Palmada, S. Kanwal, N.J. Rutkoski, C. Gustafson-Brwon, R.S. Johnson, R. Wisdom, B.D. Carter, c-*Jun* is essential for sympathetic neuronal death induced by NGF withdrawal but not by p75 activation, J. Cell Biol. 158 (2002) 453–461.
[26] E. Passegue, W. Jochum, A. Behrens, R. Ricci, E.F. Wagner, Jun B can substitute for c-Jun in mouse development and cell proliferation, Nat. Genet. 30 (2002) 158–166.
[27] A. Behrens, J. Haigh, F. Mechta-Grigoriou, A. Nagy, M. Yaniv, E.F. Wagner, Impaired intervertebral disc formation in the absence of Jun, Development 130 (2003) 103–109.
[28] R. Zenz, H. Scheuch, P. Martin, C. Frank, R. Eferl, L. Kenner, M. Sibilia, E.F. Wagner, c-Jun regulates eyelid closure and skin tumor development through EGFR signaling, Dev. Cell 4 (2003) 879–889.
[29] J.P. David, K. Sabapathy, O. Hoffmann, M.H. Idarraga, E.F. Wagner, JNK1 modulates osteoclastogenesis through both c-Jun phosphorylation dependent and -independent mechanisms, J. Cell. Sci. 115 (2002) 4317–4325.
[30] A. Behrens, W. Jochum, M. Sibilia, E.F. Wagner, Oncogenic transformation by ras and fos is mediated by c-Jun N-terminal phosphorylation, Oncogene 19 (2000) 2657–2663.
[31] L.A. Tibbles, Y.L. Ing, F. Kiefer, N. Iscove, J.R. Woodgett, N. Lassam, MLK-3 activates the SAPK/JNK and p38/RK pathways via SEK1 and MKK3, EMBO J. 15 (1996) 521–533.
[32] D.D. Yang, C.-Y. Kuan, A.J. Whitmarsh, M. Rincon, T.S. Zheng, R.J. Davis, P. Rakic, R.A. Flavell, Absence of excitotoxicity induced apoptosis in the hippocampus of mice lacking the Jnk3 gene, Nature 389 (1997) 865–870.
[33] D.D. Yang, D. Conze, A.J. Whitmarsh, T. Barrett, R.J. Davis, M. Rincon, R.A. Flavell, Differentiation of $CD4^+$ cells to Th1 cells requires MAP kinase JNK2, Immunity 9 (1998) 575–585.
[34] C. Dong, D.D. Yang, M. Wysk, A.J. Whitmarsh, R.J. Davis, R.A. Flavell, Defective T cell differentiation in the absence of Jnk1, Science 282 (1998) 2092–2095.
[35] K. Sabapathy, Y. Hu, T. Kallunki, M. Schreiber, J.P. David, W. Jochum, E.F. Wagner, M. Karin, JNK2 is required for efficient T-cell activation and apoptosis but not for normal lymphocyte development, Curr. Biol. 9 (1999) 116–125.
[36] C. Dong, D.D. Yang, C. Tournier, A.J. Whitmarsh, J. Xu, R.J. Davis, R.A. Flavell, JNK is required for effector T-cell function but not for T-cell activation, Nature 405 (2000) 91–94.
[37] L. Chang, Y. Jones, M.H. Ellisman, S.B. Goldstein, M. Karin, JNK1 is required for maintenance of neuronal microtubules and controls phosphorylation of microtubule-associated proteins, Dev. Cell 4 2003.
[38] B. Jimenez, O.V. Volpert, F. Reiher, L. Chang, A. Munoz, M. Karin, N. Bouck, c-Jun N-terminal kinase activation is required for the inhibition of vascularization by thrombospondin-1, Oncogene 20 (2001) 3443–3448.
[39] J. Hirosumi, G. Tuncman, L. Chang, C.Z. Gorgun, K.T. Uysal, K. Maeda, M. Karin, G.S. Hotamisligil, A central role for JNK in obesity and insulin resistance, Nature 420 (2002) 333–336.
[40] W.-M. Chu, D. Ostertag, Z.-W. Li, L. Chang, Y. Chen, Y. Hu, B. Williams, J. Perrault, M. Karin, JNK2 and IKKβ are required for activating the innate response to viral infection, Immunity 11 (1999) 721–731.
[41] Z. Han, L. Chang, Y. Yamanishi, M. Karin, G.S. Firestein, Joint damage and inflammation in c-Jun N-terminal Kinase 2 knockout mice with passive murine collagen-induced arthritis, Arthritis Rheum. 46 (2002) 818–823.
[42] C.Y. Kuan, D.D. Yang, D.R. Samanta Roy, R.J. Davis, P. Rakic, R.A. Flavell, The Jnk1 and Jnk2 protein kinases are required for

regional specific apoptosis during early brain development, Neuron 22 (1999) 667–676.
[43] C.R. Weston, A. Wong, J.P. Hall, M.E.P. Goad, R.A. Flavell, R.J. Davis, JNK initiates a cytokine cascade that causes Pax2 expression and closure of the optic fissure, Genes Dev. 17 (2003) 1271–1280.
[44] N. Chen, M. Nomura, Q.-B. She, W.-Y. Ma, A.M. Bode, L. Wang, R.A. Flavell, Z. Dong, Suppression of skin tumorigenesis in c-Jun NH_2-terminal kinase-2-deficient mice, Cancer Res. 61 (2001) 3908–3912.
[45] Q.-B. She, N. Chen, A.M. Bode, R.A. Flavell, Z. Dong, Deficiency of c-Jun-NH_2-terminal kinase-1 in mice enhances skin tumor development by 12-*O*-tetradecanoylphorbol-13-acetate, Cancer Res. 62 (2002) 1343–1348.
[46] N.J. Kennedy, H.K. Sluss, S.N. Jones, D. Bar-Sagi, R.A. Flavell, R.J. Davis, Suppression of Ras-stimulated transformation by the JNK signal transduction pathway, Genes Dev. 17 (2003) 629–637.
[47] D.H. Teng, W.L. Perry, J.K. Hogan, M. Baumgard, R. Bell, S. Berry, T. Davis, D. Frank, C. Frye, T. Hattier, R. Hu, S. Jammulapati, T. Janecki, A. Leavitt, J.T. Mitchell, R. Pero, D. Sexton, M. Schroeder, P.H. Su, B. Swedlund, J.M. Kyriakis, J. Avruch, P. Bartel, A.K. Wong, S.V. Tavtigian, et al, Human mitogen-activated protein kinase kinase 4 as a candidate tumor suppressor, Cancer Res. 57 (1997) 4177–4182.
[48] G.H. Su, W. Hilgers, M.C. Shekher, D.J. Tang, C.J. Yeo, R.H. Hruban, S.E. Kern, Alterations in pancreatic, biliary, and breast carcinomas support MKK4 as a genetically targeted tumor suppressor gene, Cancer Res. 58 (1998) 2339–2342.
[49] B.A. Yoshida, Z. Dubauskas, M.A. Chekmareva, T.R. Christiano, W.M. Stadler, C.W. Rinker-Schaeffer, Mitogen-activated protein kinase kinase 4/stress-activated protein/Erk kinase 1 (MKK4/SEK1), a prostate cancer metastasis suppressor gene encoded by human chromosome 17, Cancer Res. 59 (1999) 5483–5487.
[50] H.L. Kim, D.J. Vander Griend, X. Yang, D.A. Benson, Z. Dubauskas, B.A. Yoshida, M.A. Chekmareva, Y. Ichikawa, M.H. Sokoloff, P. Zhan, T. Karrison, A. Lin, W.M. Stadler, T. Ichikawa, M.A. Rubin, C.W. Rinker-Schaeffer, Mitogen-activated protein kinase kinase 4 metastasis suppressor gene expression is inversely related to histological pattern in advancing human prostatic cancers, Cancer Res. 61 (2001) 2833–2837.
[51] S. Yoshida, K. Fukino, H. Harada, H. Nagai, I. Imoto, J. Inazawa, H. Takahashi, A. Teramoto, M. Emi, The c-Jun NH_2-terminal kinase3 (JNK3) gene: genomic structure, chromosomal assignment, and loss of expression in brain tumors, J. Hum. Genet. 46 (2001) 182–187.
[52] S.D. Yamada, J.A. Hickson, Y. Hrobowski, D.J. Vander Griend, D. Benson, A. Montag, T. Karrison, D. Huo, J. Rutgers, S. Adams, C.W. Rinker-Schaeffer, Mitogen-activated protein kinase kinase 4 (MKK4) acts as a metastasis suppressor gene in human ovarian carcinoma, Cancer Res. 62 (2002) 6717–6723.
[53] K.S. Chae, B.K. Ryu, M.G. Lee, D.S. Byun, S.G. Chi, Expression and mutation analyses of MKK4, a candidate tumour suppressor gene encoded by chromosome 17p, in human gastric adenocarcinoma, Eur. J. Cancer 38 (2002) 2048–2057.
[54] N. Chen, Q.-B. She, A.M. Bode, Z. Dong, Differential gene expression profiles in *Jnk*1- and *Jnk*2-deficient murine fibroblast cells, Cancer Res. 62 (2002) 1300–1340.
[55] M. Kaneko, Y. Saito, H. Saito, T. Matsumoto, Y. Matsuda, J.L. Vaught, C.A. Dionne, T.S. Angeles, M.A. Glicksman, N.T. Neff, D.P. Rotella, J.C. Kauer, J.P. Mallamo, R.L. Hudkins, C. Murakata, Neurotrophic 3,9-bis[(alkylthio)methyl]- and -bis(alkoxymethyl)-K-252a derivatives, J. Med. Chem. 40 (1997) 1863–1869.
[56] A.C. Maroney, M.A. Glicksman, A.N. Basma, K.M. Walton, E. Knight, C.A. Murphy, B.A. Bartlett, J.P. Finn, T. Angeles, Y. Matsuda, N.T. Neff, C.A. Dionne, Motoneuron apoptosis is blocked by CEP-1347 (KT 7515), a novel inhibitor of the JNK signaling pathway, J. Neurosci. 18 (1998) 104–111.
[57] M.S. Saporito, R.L. Hudkins, A.C. Maroney, Discovery of CEP-1347/KT-7515, an inhibitor of the JNK/SAPK pathway for the treatment of neurodegenerative diseases, Prog. Med. Chem. 40 (2002) 23–62.
[58] A.C.C. Wagner, L. Mazzucchelli, M. Miller, A.M. Camoratto, B. Goke, CEP-1347 inhibits caerulein-induced rat pancreatic JNK activation and ameliorates caerulein pancreatitis, Am. J. Physiol.: Gasterointest. Liver Physiol. 278 (2000) G165–G172.
[59] S. Hashimoto, Y. Gon, I. Takeshita, K. Matsumoto, S. Maruoka, T. Horie, Transforming growth factor-b1 induces phenotypic modulation of human lung fibroblasts to myofibroblasts through a c-Jun NH_2-terminal kinase-dependent pathway, Am. J. Respir. Crit. Care Med. 163 (2001) 152–157.
[60] K. Kujime, S. Hashimoto, Y. Gon, K. Shimizu, T. Horie, p38 mitogen-activated protein kinase and c-*Jun* NH_2-terminal kinase regulate RANTES production by influenza virus-infected human bronchial epithelial cells, J. Immunol., (2000) 3222–3228.
[61] S. Le, T.J. Connors, A.C. Maroney, c-Jun N-terminal kinase specifically phosphorylates p66ShcA at Serine 63 in response to ultraviolet radiation, J. Biol. Chem. 276 (2001) 48332–48336.
[62] A.C. Maroney, J.P. Finn, T.J. Connors, J.T. Durkin, T. Angeles, G. Gessner, Z. Xu, S.L. Meyer, M.J. Savage, L.A. Greene, R.W. Vaught, J.L. Vaught, CEP-1347 (KT7515), a semisynthetic inhibitor of the mixed lineage kinase family, J. Biol. Chem. 276 (2001) 25302–25308.
[63] B.L. Bennett, D.T. Sasaki, B.W. Murray, E.C. O'Leary, S.T. Sakata, W. Xu, J.C. Leisten, A. Motiwala, S. Pierce, Y. Satoh, S.S. Bhagwat, A.M. Manning, D.W. Anderson, SP600125, and anthrapyrazolone inhibitor of Jun N-terminal kinase, Proc. Natl. Acad. Sci. U. S. A. 98 (2001) 13681–13686.
[64] Z. Han, D.L. Boyle, L. Chang, B. Bennett, M. Karin, L. Yang, A.M. Manning, G.S. Firestein, c-Jun N-terminal kinase is required for metalloproteinase expression and joint destruction in inflammatory arthritis, J. Clin. Invest. 108 (2001) 73–81.
[65] M.P. Vincenti, C.E. Brinckerhoff, The potential of signal transduction inhibitors for the treatment of arthritis: is it all just JNK? J. Clin. Invest. 108 (2001) 181–183.
[66] M.F. Favata, K.Y. Horiuchi, E.J. Manos, A.J. Daulerio, D.A. Stradley, W.S. Feeser, D.E. Van Dyk, W.J. Pitts, R.A. Earl, F. Hobbs, R.A. Copeland, R.L. Magolda, P.A. Scherle, J.M. Trzaskos, Identification of a novel inhibitor of mitogen-activated protein kinase kinase, J. Biol. Chem. 273 (1998) 18623–18632.
[67] F.G. Salituro, U.A. Germann, K.P. Wilson, G.W. Bemis, T. Fox, M.S.S. Su, Inhibitors of p38 MAP kinase: therapeutic intervention in cytokine-mediated diseases, Curr. Med. Chem. 6 (1999) 807–823.
[68] J.C. Lee, S. Kumar, D.E. Griswold, D.C. Underwood, B.J. Votta, J.L. Adams, Inhibition of p38 MAP kinse as a therapeutic strategy, Immunopharmacology 47 (2000) 185–201.
[69] P.P. Tak, G.S. Firestein, NF-κB: a key role in inflammatory diseases, J. Clin. Invest. 107 (2001) 7–11.
[70] M. Shin, C. Yan, D. Boyd, An inhibitor of c-*Jun* amino terminal kinase (SP600125) represses c-Jun activation, DNA-binding and PMA-inducible 92-kDa type IV collagenase expression, Biochim. Biophys. Acta 1589 (2002) 311–316.
[71] M. Utsugi, K. Dobashi, T. Ishizuka, K. Endou, J. Hamuro, Y. Murata, T. Nakazawa, M. Mori, c-Jun N-terminal kinase negatively regulates lipopolysaccharide-induced IL-12 production in human macrophages: role of mitogen-activated protein kinase in glutathione redox regulation of IL-12 production, J. Immunol. 171 (2003) 628–635.
[72] M. Meguro, F. Nishimura, H. Ohyama, S. Takashiba, Y. Murayama, S. Matsushita, Ligation of IFN-gamma-induced HLA-DR molecules on fibroblasts induces RANTES expression via c-Jun N-terminal kinase (JNK) pathway, Cytokine 22 (2003) 107–115.
[73] M. Utsugi, K. Dobashi, T. Ishizuka, K. Masubuchi, Y. Shimizu, T. Nakazawa, M. Mori, c-Jun-NH_2-terminal kinase mediates expression of connective tissue growth factor induced by transforming growth

factor-beta1 in human lung fibroblasts, Am. J. Respir. Cell Mol. Biol. 28 (2003) 754–761.
[74] D. Javelaud, J. Laboureau, E. Gabison, F. Verrecchia, A. Mauviel, Disruption of basal JNK activity differentially affects key fibroblast functions important for wound healing, J. Biol. Chem. 278 (2003) 24624–24628.
[75] S. Grosch, I. Tegeder, K. Schilling, T.J. Maier, E. Niederberger, G. Geisslinger, Activation of c-Jun-N-terminal-kinase is crucial for the induction of a cell cycle arrest in human colon carcinoma cells caused by flurbiprofen enantiomers, FASEB J. 17 (2003) 1316–1318.
[76] C.A. Marques, U. Keil, A. Bonert, B. Steiner, C. Haass, W.E. Muller, A. Eckert, Neurotoxic mechanisms caused by the Alzheimer's disease-linked swedish amyloid precursor protein mutation: oxidative stress, caspases, and the JNK pathway, J. Biol. Chem. 278 (30) (2003) 28294–28302.
[77] B.P. Curran, H.J. Murray, J.J. O'Connor, A role for c-Jun N-terminal kinase in the inhibition of long-term potentiaion by interleukin-1β and long-term depression in the rate dentate gyrus in vitro, Neuroscience 118 (2003) 347–357.
[78] C. Huang, Z. Rajfur, C. Borchers, M.D. Schaller, K. Jacobson, JNK phosphorylates paxillin and regulates cell migration, Nature 424 (2003) 219–223.
[79] D. Chauhan, G. Li, T. Hideshima, K. Podar, C. Mitsiades, N. Mitsiades, N. Munshi, S. Kharbanda, K.C. Anderson, JNK-dependent release of mitochondrial protein, Smac, during apoptosis in multiple myeloma (MM) cells, J. Biol. Chem. 278 (2003) 17593–17596.
[80] T. Schindler, W. Bornmann, P. Pellicena, W.T. Miller, B. Clarkson, J. Kuriyan, Structural mechanism for STI-571 inhibition of Abelson tyrosine kinase, Science 289 (2000) 1938–1942.
[81] R.J. Gum, M.M. McLaughlin, S. Kumar, Z. Wang, M.J. Bower, J.C. Lee, J.L. Adams, G.P. Livi, E.J. Goldsmith, P.R. Young, Acquisition of sensitivity of stress-activated protein kinases to the p38 inhibitor, SB 203580, by alteration of one or more amino acids within the ATP binding pocket, J. Biol. Chem. 273 (1998) 15605–15610.
[82] J.R. Feramisco, E.G. Krebs, Inhibition of cyclic AMP-dependent protein kinase by analogues of a synthetic peptide substrate, J. Biol. Chem. 253 (1978) 8968–8971.
[83] D.A. Walsh, D.B. Glass, Utilization of the inhibitor protein of adenosine cyclic monophosphate-dependent protein kinase, and peptides derived from it, as tools to study adenosine cyclic monophosphate-mediated cellular processes, Methods Enzymol. 201 (1991) 304–316.
[84] C. Dunn, C. Wiltshire, A. MacLaren, D.A. Gillespie, Molecular mechanism and biological functions of c-Jun N-terminal kinase signalling via the c-Jun transcription factor, Cell. Signal. 14 (2002) 585–593.
[85] D. Holzberg, C.G. Knight, O. Dittrich-Breiholz, H. Schneider, A. Dorrie, E. Hoffmann, K. Resch, M. Kracht, Disruption of the c-JUN–JNK complex by a cell-permeable peptide containing the c-JUN δdomain induces apoptosis and affects a distinct set of IL1-induced inflammatory genes, J. Biol. Chem. 278 (2003) 40213–40223.
[86] M. Dickens, J.S. Rogers, J. Cavanagh, A. Raitano, Z. Xia, J.R. Halpern, M.E. Greenberg, C.L. Sawyers, R.J. Davis, A cytoplasmic inhibitor of the JNK signal transduction pathway, Science 277 (1997) 693–696.
[87] A.J. Whitmarsh, J. Cavanagh, C. Tournier, J. Yasuda, R.J. Davis, A mammalian scaffold complex that selectively mediates MAP kinase activation, Science 281 (1998) 1671–1674.
[88] J. Yasuda, A.J. Whitmarsh, J. Cavanagh, M. Sharma, R.J. Davis, The JIP group of mitogen-activated protein kinase scaffold proteins, Mol. Cell. Biol. 19 (1999) 7245–7254.
[89] N. Kelkar, S. Gupta, M. Dickens, R.J. Davis, Interaction of a mitogen-activated protein kinase signaling module with the neuronal protein JIP3, Mol. Cell. Biol. 20 (2000) 1030–1043.
[90] C. Bonny, P. Nicod, G. Waeber, IB1, a JIP-related nuclear protein present in insulin-secreting cells, J. Biol. Chem. 273 (1998) 1843–1846.
[91] V. Mooser, A. Maillard, C. Bonny, M. Steinmann, P. Shaw, D.P. Yarnall, D.K. Burns, D.F. Schorderet, P. Nicod, G. Waeber, Genomic organization, fine-mapping, and expression of the human islet-brain 1 (IB1)-Jun–amino-terminal kinase interacting protein-1 (JIP-1) gene, Genomics 55 (1999) 202–208.
[92] J. Schoorlemmer, M. Goldfarb, Fibroblast growth factor homologous factors and the islet brain-2 scaffold protein regulate activation of a stress-activated protein kinase, J. Biol. Chem. 277 (2002) 49111–49119.
[93] M. Ito, K. Yoshioka, M. Akechi, S. Yamashita, N. Takamatsu, K. Sugiyama, M. Hibi, Y. Nakabeppu, T. Shiba, K.-I. Yamamoto, JSAP1, a novel Jun N-terminal protein kinase (JNK)-binding protein that functions as a scaffold factor in the JNK signaling pathway, Mol. Cell. Biol. 19 (1999) 7539–7548.
[94] M. Fan, M. Goodwin, T. Vu, C. Brantley-Finley, W.A. Gaarde, T.C. Chambers, Vinblastine-induced phosphorylation of Bcl-2 and Bcl-XL is mediated by JNK and occurs in parallel with inactivation of the Raf-1/MEK/ERK cascade, J. Biol. Chem. 275 (2000) 29980–29985.
[95] C. Bonny, A. Oberson, S. Negri, C. Sauser, D.F. Schorderet, Cell-permeable inhibitors of JNK: novel blockers of β-cell death, Diabetes 50 (2001) 77–82.
[96] R.K. Barr, T.S. Kendrick, M.A. Bogoyevitch, Identification of the critical features of a small peptide inhibitor of JNK activity, J. Biol. Chem. 277 (2002) 10987–10997.
[97] T. Tanoue, M. Adachi, T. Moriguchi, E. Nishida, A conserved docking motif in MAP kinases common to substrates, activators and regulators, Nat. Cell Biol. 2 (2000) 110–116.
[98] C.I. Chang, B.E. Xu, R. Akella, M.H. Cobb, E.J. Goldsmith, Crystal structures of MAP kinase p38 complexed to the docking sites on its nuclear substrate MEF2A and activator MKK3b, Mol. Cell 9 (2002) 1241–1249.
[99] M. Becker-Hapak, S.S. McAllister, S.F. Dowdy, TAT-mediated protein transduction into mammalian cells, Methods 24 (2001) 247–256.
[100] M.A. Bogoyevitch, T.S. Kendrick, D.C.H. Ng, R.K. Barr, Taking the cell by stealth or storm? Protein transduction domains (PTDs) as versatile vectors for delivery, DNA Cell Biol. 21 (2002) 879–894.
[101] A.M. Manning, R.J. Davis, Targeting JNK for therapeutic benefit: from JUNK to gold, Nat. Rev., Drug Discov. 2 (2003) 554–565.